ANALYSE DER EFFEKTE VON MIKROPLASTIKPARTIKELN AUF ZELLULÄRER EBENE

DISSERTATION

zur Erlangung des akademischen Grades einer

Doktorin der Naturwissenschaften (Dr. rer. nat.)

in der Bayreuther Graduiertenschule für Mathematik und Naturwissenschaften (BayNAT)

der Universität Bayreuth

vorgelegt von
Julia Jasiński
aus Bautzen

Bayreuth, 2023

Die vorliegende Arbeit wurde in der Zeit von Juni 2019 bis März 2023 in Bayreuth am Lehrstuhl Biomaterialien unter Betreuung von Herrn Professor Dr. Thomas Scheibel angefertigt.

Vollständiger Abdruck der von der Bayreuther Graduiertenschule für Mathematik und Naturwissenschaften (BayNAT) der Universität Bayreuth genehmigten Dissertation zur Erlangung des akademischen Grades einer Doktorin der Naturwissenschaften (Dr. rer. nat).

Form der Dissertation: Kumulative Dissertation

Dissertation eingereicht: 17. März 2023

Zulassung durch das Leitungsgremium: 03.April 2023

Wissenschaftliches Kolloquium: 26. Oktober 2023

Amtierender Direktor: Prof. Dr. Jürgen Köhler

Prüfungsausschuss:

Prof. Dr. Thomas Scheibel	(Gutachter)
Prof. Dr. Holger Kress	(Gutachter)
Prof. Dr. Seema Agarwal	(Vorsitz)
Prof. Dr. Heike Feldhaar	

Für meine Familie und Freunde

Inhaltsverzeichnis

Abbildungsverzeichnis

Tabellenverzeichnis

Zusammenfassung

Plastik ist aus unserer heutigen Gesellschaft nicht mehr wegzudenken. Ob elektronische Technik, Autoreifen, Kleidung oder Verpackungsmaterial, überall sind Kunststoffe enthalten. Dabei ist seit einigen Jahrzehnten nicht nur das Problem der Umweltverschmutzung mit Makroplastik, sondern auch Mikroplastik bekannt. Mikroplastik kann dabei aus Abrieb oder Bewitterung durch Umwelteinflüsse von größeren Plastikfragmenten entstehen. Über die Nahrung oder die Atemluft können Mikroplastikpartikel in den Organismus gelangen. Verschiedene Studien zeigten bereits eine Akkumulation von Mikroplastikpartikeln in diversen Organen, wobei nach wie vor nicht klar ist, wie lange Polymerpartikel im Körper verbleiben, unter welchen Voraussetzungen sie wieder ausgeschieden werden können und welche Effekte sie im Organismus hervorrufen. Da Mikroplastik sehr komplex ist, konnten die Auswirkungen noch nicht vollständig erfasst werden. Es ist bekannt, dass eine Aufnahme und daraus resultierende Effekte von der Form (Sphären vs. Fasern vs. Fragmente), der Zusammensetzung (reines Polymer vs. dem Vorhandensein von Additiven), oder auch dem Vorhandensein einer Eco-Corona abhängig sein können. Insbesondere Bakterien, organische Materialien, oder auch Umweltgifte können an der Mikroplastikoberfläche adsorbieren und somit in den Organismus gelangen, wo sie unterschiedliche, bis heute nicht geklärte Effekte auslösen können. Um die Auswirkungen von Mikroplastik abbilden zu können, sind derzeit noch Modelle notwendig. Dafür wurden in der vorliegenden Arbeit sphärische Polymerpartikel und murine Zelllinien verwendet. In diesem Zusammenhang wurden Modellpartikel, namentlich Celluloseacetat (CA) und fluoreszierende Polystyrol (PS) selbst hergestellt, andere zugekauft.

In einer ersten Studie wurden die Interaktionen von murinen Makrophagen (J774A.1, ImKC) und Epithelzellen (STC-1, BNL CL.2) mit gut charakterisierten PS Partikeln unterschiedlicher Größe (0,2- 6,0 µm) untersucht. Es wurde erwartet, dass Makrophagen die Partikel aktiv aufnehmen, was in dieser Studie bestätigt werden konnte. Epithelzellen beider untersuchter Zelllinien nahmen Mikropartikel nicht in signifikanter Zahl auf. Anzeichen für zellulären Stress sowie Auswirkungen auf die Zellproliferation wurden bei Zellpopulationen mit hoher Partikel-Zellinteraktion beobachtet.

In einer zweiten Studie lag der Fokus auf der Ausbildung einer Protein-Corona unter definierten Laborbedingungen an PS Partikeln, um den Einfluss dieser auf Partikel-Zellinteraktionen und die Aufnahme in zwei Epithelzelllinien zu untersuchen. Um die Bildung einer Protein-Corona zu steuern, wurden die Partikel mit Modellproteinen vorbeschichtet und anschließend in serumhaltigem Zellmedium inkubiert. Dabei konnte gezeigt werden, dass die Partikelhistorie einen signifikanten Einfluss auf die Zusammensetzung der Protein-Corona und damit auf

die Interaktion der Partikel mit Zellen hat.

In einer dritten Studie wurden die Oberflächeneigenschaften und die chemische Zusammensetzung von zwei handelsüblichen, nominell identischen PS Mikropartikeln, die häufig in Effektstudien verwendet werden, charakterisiert. Es ließen sich deutliche Unterschiede im Monomergehalt, dem ζ-Potential und der Oberflächenladungsdichten identifizieren. Zellen, die Partikeln ausgesetzt waren, die ein stärker ausgeprägtes ζ-Potenzial und einen höheren Monomergehalt aufwiesen, zeigten eine höhere Partikelinteraktion und daraus folgend einen Rückgang des Zellstoffwechsels und der Proliferation, insbesondere bei höheren Partikelkonzentrationen.

In einer vierten Studie wurden Mikropartikel aus konventionellen Polymeren wie PS, Polyethylen (PE), Polyvinylchlorid (PVC) und biologisch basierten Polymeren wie Polymilchsäure (PLA) und CA verwendet, um die Aufnahme verschiedener Polymerpartikel und deren zellulären Effekte auf Makrophagen und Epithelzellen zu analysieren. Die Mikropartikel wiesen eine geringe Differenz im Durchmesser auf, was einen Vergleich der zellulären Wirkungen in Abhängigkeit vom Polymertyp ermöglicht. Trotz der unterschiedlichen Partikeleigenschaften wurde die Aufnahme von Polymerpartikeln durch Makrophagen beobachtet, während Epithelzellen nur PS Partikel aufnahmen. Dabei spielte insbesondere für Makrophagen das ζ-Potential der Mikropartikel und die daraus resultierende Zusammensetzung der Protein-Corona eine entscheidende Rolle für die Aufnahme.

In einer fünften Studie lag der Fokus auf der Verteilung von PS Partikeln während der Zellteilung in murinen Makrophagen und der Analyse der Exkretion der Partikel. Die Verteilung während der Zellteilung scheint zufällig zu sein und es wurde keine aktive Exkretion von Partikeln beobachtet. Um den intrazellulären Verbleib der Partikel zu analysieren wurden bestimmte Organelle auf eine Ko-Lokalisation untersucht. Während alle Partikel, unabhängig von ihrer Größe, eine Ko-Lokalisation mit dem Zytoplasma zeigten, wurden kleinere Partikel in Verbindung mit Endosomen und dem endoplasmatischen Retikulum gefunden.

In einer letzten Teilarbeit sollten Leberzellsphäroide angezüchtet, sowie deren Interaktion mit PS Partikeln untersucht werden. Hierbei sollten zusätzlich neue PS Partikel für die Verwendung in verschiedenen Zellkulturmodellen etabliert werden. Bezüglich der Oberflächeneigenschaften und der Partikel-Zellinteraktion wurden Unterschiede zu den kommerziell erwerbbaren Partikeln festgestellt. Dabei zeigte sich auch eine Translokation der Mikropartikel in den Sphäroiden, was die Notwendigkeit der Verwendung von 3D Zellmodellen in der Mikroplastikforschung unterstreicht.

Summary

It is impossible to imagine today's society without plastic. Whether electronic technology, car tyres, clothing or packaging material, plastics are everywhere. For several decades, not only the problem of environmental pollution with macroplastics but also microplastics has been known. Microplastics can result from larger plastic fragments by abrasion or weathering due to environmental influences. Microplastic particles can enter the organism through food or the air we breathe. Various studies have shown an accumulation of microplastic particles in various organs, although it is still not clear how long polymer particles remain in the body, under what conditions they can be excreted again, and what effects they cause in the organism. Since microplastics are very complex, it has not yet been possible to fully assess their effects. It is known that uptake and effects can depend on the shape (spheres vs. fibers vs. fragments), the composition (pure polymer vs. the presence of additives), or even the presence of an eco-corona. In particular, bacteria, organic materials, or environmental toxins can adsorb on the microplastic surface and thus enter the organism, where they can trigger various effects that have not yet been clarified. To be able to depict the effects of microplastics, models are currently still necessary. For this purpose, spherical polymer particles and murine cell lines were used in the present thesis. Some model particles, namely cellulose acetate (CA) and fluorescent polystyrene (PS) were directly produced, others purchased.

In a first study, the interactions of murine macrophages (J774A.1, ImKC) and epithelial cells (STC-1, BNL CL.2) with well-characterized PS particles of different sizes (0.2- 6.0 µm) were investigated. Macrophages were expected to actively engulf the particles, which was confirmed in this study. Epithelial cells of both investigated cell lines did not take up microparticles in significant numbers. Indications of cellular stress as well as effects on cell proliferation were observed in cell populations with high particle-cell interaction.

In a second study, the focus was on the formation of a protein corona under defined laboratory conditions on PS particles to investigate its influence on particle-cell interactions and uptake in two epithelial cell lines. To control the formation of a protein corona, the particles were pre-coated with model proteins and then incubated in a serum-containing cell medium. It was shown that particle history has a significant influence on the composition of the protein corona and thus on the interaction of the particles with cells.

In a third study, the surface properties and chemical composition of two commercially available, nominally identical PS microparticles, which are frequently used in effect studies, were characterized. Significant differences in monomer content, ζ-potential, and surface charge density could be identified. Cells exposed to particles that had a more pronounced ζ-potential

and higher monomer content showed higher particle interactions and consequent decrease in cell metabolism and proliferation, especially at higher particle concentrations.
In a fourth study, microparticles of conventional polymers such as PS, polyethylene (PE), poly(vinyl chloride) (PVC), and biologically based polymers such as poly(lactic acid) (PLA) and CA were used to analyze the uptake of different polymer particles and their cellular effects on macrophages and epithelial cells. The microparticles have a narrow size range, which allows a comparison of cellular effects depending on the polymer type. Despite the different particle properties, the uptake of polymer particles by macrophages was observed, whereas epithelial cells only took up PS particles. Especially for macrophages, the ζ-potential and the resulting protein corona composition of the microparticles played a decisive role in the uptake.
In a fifth study, the focus was on the distribution of PS particles during cell division in murine macrophages and the analysis of the excretion of the particles. The distribution during cell division appears to be random, and no active excretion of particles was observed. To analyze the intracellular fate of the particles, specific organelles were examined regarding co-localization. While all particles, regardless of size, showed co-localization with the cytoplasm, smaller particles were found associated with endosomes and the endoplasmic reticulum.
In a sixth project, liver cell spheroids were grown and the interaction with PS particles was investigated. In addition, new PS particles should be developed for use in various cell culture models. With regard to surface properties and particle-cell interactions, differences were found compared to commercially available particles. A translocation of the microparticles in the spheroids was observed, which underlines the necessity of using 3D cell models in microplastic research.

1 Einleitung

1.1 Plastik und Mikroplastik

Plastik ist aus der heutigen Welt nicht mehr wegzudenken. Ob in technischen Geräten, Reifen, Kosmetikartikeln, Verpackungen oder auch Kleidung, all diese Gegenstände bestehen komplett oder teilweise aus Plastik. Und das hat verschiedene gute Gründe. Materialien aus Plastik sind vergleichsweise billig, leicht, wenig Wärme- und elektrisch leitfähig, beständig gegenüber chemischer, biologischer und physikalischer Zersetzung, und vergleichsweise einfach herzustellen [1–6]. Die Entdeckung und Herstellung von Bakelit, dem ersten vollsynthetischen Plastik, durch Leo Hendrick Baekeland im Jahre 1907 stellt einen wichtigen Meilenstein für industriell produzierte Kunststoffe dar [2, 6–8]. Seit den 1930 - 1940er Jahren sind die auch heute noch hauptsächlich verwendeten Plastikarten, Polystyrol (PS), Polymethylmethacrylat (PMMA) und Polyolefine, industriell im großen Maßstab herstellbar [8, 9]. Seitdem steigt sowohl der Bedarf als auch die Produktion an Plastik jährlich [3, 8–11]. Im Jahr 2020 wurden weltweit 367 Millionen Tonnen Plastik produziert [11]. Für Europa waren die meistproduzierten Plastikarten dabei Polypropylen (PP), Polyethylene (PE) und Polyvinylchlorid (PVC) [11].
Aber was ist Plastik eigentlich? „Plastik“, aus dem Griechischen *plastikos* was „formbar“ bedeutet, ist die gängige Bezeichnung für eine Vielzahl von synthetischen oder künstlichen Polymeren [8, 9]. Laut ISO-Definition ist Plastik *„Material, das als wesentlichen Bestandteil ein hochmolekulares Polymer enthält und das in einem bestimmten Stadium seiner Verarbeitung zu Fertigerzeugnissen durch Fließen geformt werden kann“* [12, 13]. Damit fallen alle synthetischen Polymere mit zugesetzten Additiven, sowie stark veränderte natürliche Polymere unter die Definition Plastik [13]. Biologisch basierte, weniger veränderte Polymere, z.B. gefärbte Naturfasern wie Wolle oder Baumwolle, sind damit per Definition kein Plastik, sondern natürliche Polymere. Weitere natürliche Polymere sind z.B. Proteine und Polysaccharide wie Seide, Cellulose, Alginat oder Agar (Abb. 1) [8, 13]. Konventionelles Plastik basiert auf Erdöl, allerdings ist seit einigen Jahren auch so genanntes „Bioplastik“ verfügbar, welches auch als Biokunstoff bekannt ist, und entweder biologisch abbaubar ist und/oder auf nachwachsenden Rohstoffen basiert [14–19]. Beispielhaft für auf biologischen Monomeren basierende Polymere sind dabei Polymilchsäure (PLA) oder Polybutylensuccinat (PBS). Davon zu unterscheiden ist biobasiertes Plastik, welches auf natürlichen Polymeren basiert. Dazu zählen Stärke (und ihre Derivate), Cellulose (und ihre Derivate) oder Polyhydroxyalkanoate (PHA) [15, 17, 18, 20].

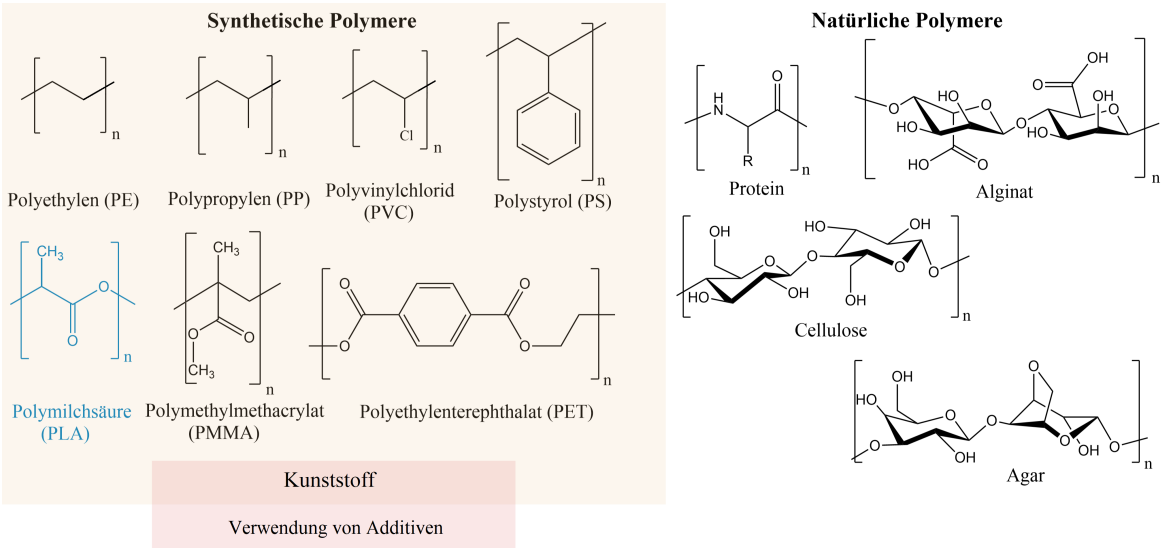

Abbildung 1: Darstellung der chemischen Strukturen einiger ausgewählter synthetischer und natürlicher Polymere. Synthetische Polymere werden oft mit Additiven, wie Weichmachern, Farbpartikeln oder Flammschutzmitteln, versetzt und als Kunststoffe („Plastik “) bezeichnet. Die hier dargestellten synthetischen Polymere sind typische Grundbausteine für petrolbasierte, konventionelle Kunststoffe. Eine Ausnahme stellt PLA dar, welches sowohl auf nachwachsenden Rohstoffen basiert als auch biologisch abbaubar ist und damit als Biokunststoff bezeichnet wird. Protein: R= Rest (Aminosäure).

Bioabbaubares Plastik wird mit Hilfe von Mikroorganismen (Bakterien, Hefen und Pilzen) zuerst fragmentiert, durch spezielle Enzyme in die entsprechenden Monomere zersetzt und anschließend assimiliert, sodass nach vollständigem Abbau lediglich Wasser, Kohlenstoffdioxid und Biomasse verbleiben [15–21]. Biokunststoffe haben in den letzten Jahren immer mehr an Bedeutung gewonnen, denn konventionelles Plastik hat einen gewaltigen Nachteil: durch seine große Widerstandsfähigkeit ist es nicht einfach abbaubar, sondern muss verbrannt oder recycelt werden [8, 22–25]. Allerdings sind nicht alle Polymerarten gleich gut zum Recyceln geeignet, und die Verwendung von Additiven erschwert dies zusätzlich [22, 25–27]. Zusammen mit dem geringen Preis und der einfachen Verfügbarkeit führt es oft dazu, dass Plastikartikel durch ungeeignete Entsorgung, sei dies unbeabsichtigt beispielsweise durch veraltete Mülldeponien oder beabsichtigt durch beispielsweise simples Entsorgen in der Natur, in der Umwelt landen [25, 28–30]. Allerdings steigt der Anteil an recyceltem und für die Energiegewinnung genutztem Plastik stetig [11, 18]. So erhöhte sich der Anteil von recyceltem Plastik im Zeitraum von 2006-2020 in der EU um 177 %, der Anteil von zur Energiegewinnung genutzten Plastik um 77 % und der Anteil des Plastikmülls, der auf der Abfalldeponie landete, verringerte sich um 46 % [11].

Nichtsdestotrotz bestand viele Jahre, und besteht noch heute, ein Problem mit der geeigneten Entsorgung. So gelangen jedes Jahr Millionen Tonnen an Plastikmüll in die Umwelt [25, 27,

31, 32]. Neben direkten Einflüssen durch große, mit dem bloßen Augen erkennbaren, Plastikstücken (= Makroplastik) ist seit den 1970er Jahren das Thema Plastikverschmutzung der Meere bekannt und hat durch verschiedene neue Erkenntnisse an Bedeutung gewonnen [13, 32–36]. Dabei wurde von Thompson *et al.* 2004 das erste Mal von Mikroplastik als mikroskopisch kleinem Plastikmüll gesprochen [35, 37]. Hier haben sich die ersten Studien ebenfalls auf die Einflüsse auf die marine Umgebung bezogen [30, 35, 38–46]. Heute wird Mikroplastik als Plastik mit einer Größe zwischen 5 mm und 0,1 µm charakterisiert [13, 42, 47, 48]. Andere Definitionen gehen von einer Größe zwischen 1 mm und 1 µm aus [6, 13, 38]. Damit wird Mikroplastik von Makroplastik (> 5 mm) und Nanoplastik (1- 100 nm, beziehungsweise < 1 µm) abgegrenzt [6, 13, 49]. Der Begriff Mikroplastik inkludiert verschiedene Formen. So wird zwischen sphärischen Partikeln, Fasern, Fragmenten, Schäumen und Filmen unterschieden (Abb. 2) [6, 13, 50–54].

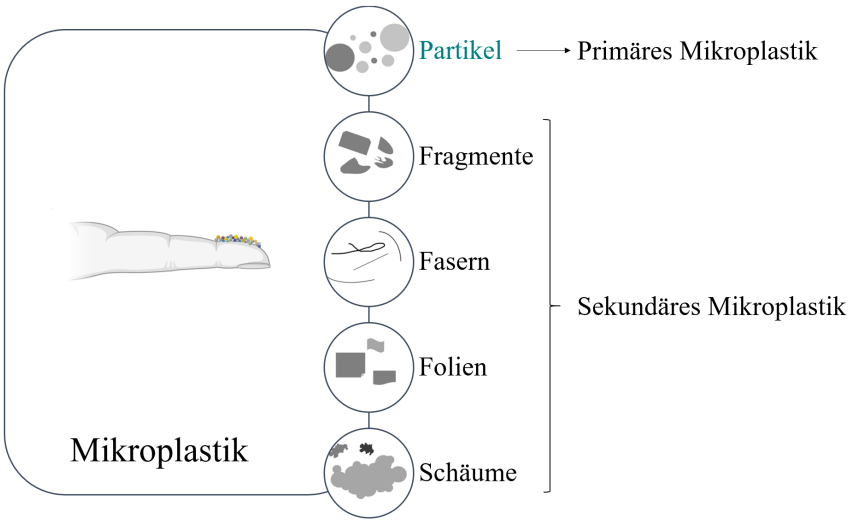

Abbildung 2: Schematische Darstellung der unterschiedlichen Formen von Mikroplastik. Die Unterteilung von Mikroplastik erfolgt anhand der Form (Partikel, Fragmente, Fasern, Folien oder Schäume) und anhand des Ursprungs (primäres vs. sekundäres Mikroplastik). Dabei fallen Partikel häufig in die Gruppe des primären Mikroplastiks, die anderen Formen entstehen meist durch Abrieb oder Verwitterung von größeren Plastikteilen und fallen in die Gruppe des sekundären Mikroplastiks. Die in der vorliegenden Arbeit hauptsächlich verwendeten Mikroplastikpartikel wurden farblich hervorgehoben.

Aber Mikroplastik ist nicht gleich Mikroplastik, es wird auch anhand seiner Herkunft differenziert. Primäres Mikroplastik sind demnach Mikroplastikpartikel, welche in dieser Größe produziert wurden (Abb. 3 (1)) [3, 37, 39, 55, 56]. Dem gegenüber steht sekundäres Mikroplastik, welches durch Bewitterung in der Umwelt (beispielsweise durch UV-Strahlung) oder Abreibung entstandene Plastikfragmente umfasst (Abb. 3 (2)) [37, 39, 40, 47, 56]. Browne *et*

al., zeigten dabei ebenfalls auf, dass beispielsweise auch der Abrieb von Kleidung durch Waschen in der Waschmaschine Mikrofasern verursacht [55, 57–59]. Diese resultieren ebenfalls, abhängig von der Filtration des Waschwassers und dem Kleidungsstoff, in Mikroplastikfasern [55, 58, 59]. Derzeit kann davon ausgegangen werden, dass primäres Mikroplastik hauptsächlich aus sphärischen Partikeln besteht, während sekundäres Mikroplastik aus verschiedenen Formen zusammengesetzt ist [13, 39, 60]. Trotz vieler Jahre intensiver Forschung sind die Auswirkungen auf die verschiedenen Ebenen in der Umwelt nach wie vor großteils nicht geklärt.

1.2 Auswirkungen von Mikroplastik auf die Umwelt

1.2.1 Umwelt, Tiere und Modellorganismen

Um die Bedrohungen unseres Planeten einordnen zu können und daraus die Grenzen festzulegen, innerhalb derer die Menschheit sicher agieren kann, wurde das Konzept der *planetary boundaries* (planetare Grenzen) von Rockström *et al.* 2009 eingeführt [61–63]. Dabei werden neben dem Klimawandel, der Übersäuerung der Ozeane, dem stratosphärischen Ozonabbau, der atmosphärischen Aerosolbelastung, dem Süßwasserverbrauch, der Landnutzungsänderung, den biochemischen Strömungen von Phosphor und Stickstoff, der biosphärischen Integrität (unterteilt in genetische und funktioneller Diversität), auch chemische Verschmutzung, beziehungsweise neuartige Verbindungen, als Bedrohungen eingeordnet [61–63]. Galten nach Steffen *et al.*, 2015 noch der Verlust der genetischen Diversität und der Stickstoffströmung als Hauptbedrohung, wurden durch Persson *et al.*, 2022 zusätzlich der Verlust der funktionellen Diversität, die Phosphorströmung und neuartige Verbindungen als Hochrisiko für den Planeten dargestellt [63, 64]. Unter den Bereich der neuartigen Verbindungen fallen neben radioaktive Substanzen und Schwermetallen auch eine weiter Bereich an organischen Verbindungen, wie beispielsweise Kunststoffe. Damit wurde im Jahr 2022 Plastikverschmutzung als eine von vielen Bedrohungen für den Planeten beschrieben, nach Persson *et al.* sogar als die mit dem höchsten Risiko [61–64].

Als erste Publikation über die Gefahr der Plastikverschmutzung in der marinen Umwelt gilt Carpenter und Smith *et al.* aus dem Jahr 1972 [33, 65]. Seitdem steigen die wissenschaftlichen Bemühungen den Einfluss von Plastik in der Umwelt zu analysieren. Dabei konnten neueste Erkenntnisse die Auswirkungen der Plastikverschmutzung in der Umwelt aufzeigen. Über Wind, Regen und Meeresströmungen verteilt sich Mikroplastik auch in die entlegensten Gebiete, was darin resultiert, dass nahezu überall, auch in Gebieten, die weit entfernt von menschlicher Zivilastion liegen, Mikroplastik gefunden werden konnte [66–68]. Diese Gebiete umfassen sowohl Meere [41, 44, 47, 50, 69, 70], Flüsse und Seen [71–76], Böden [65,

77–79] als auch Schnee [80–84], Meeresböden [43, 45, 85, 86] und, ganz allgemein, die Luft [87–91]. Die Mikroplastik-Konzentration unterscheidet sich dabei stark, je nachdem, wo die Analysen vorgenommen wurden. So wurde in der Themse eine Mikroplastik-Konzentration von 22-297 Partikel pro Liter identifiziert [92]. Allerdings erschwert das Fehlen einer standardisierten Methodik der Probenname eine eindeutige Aussage. So beschrieben Lindeque *et al.*, dass bei der Verwendung eines Netzes mit 100 µm Maschenweite zur Probenentnahme 2,5-fach mehr Mikroplastik gefunden wurde als bei der Verwendung eines Netzes mit 333 µm Maschenbreite [93]. Außerdem wird darauf hingewiesen, dass die Mikroplastik-Konzentration in der Umwelt unterschätzt werden könnte und bei über 3700 Mikroplastikpartikeln/m^3 liegt [93]. Zusätzlich muss erwähnt werden, dass bei den wenigen umfassenden Erhebungen, die es derzeit gibt, zusätzlich unterschiedliche Maßstäbe (beispielsweise Anzahl der Partikel oder Gewicht der Partikel) und unterschiedliche Einheiten (wie l, m^3, km^2) verwendet werden, was zu nicht miteinander vergleichbaren Informationen aus aller Welt führt [94]. Einmal in der Umwelt, können Pathogene (wie Bakterien), persistente organische Schadstoffe (engl. *persistent organic pollutants*, POPs) oder Schwermetalle an der Oberfläche des Mikroplastiks adsorbieren (Abb. 3 (3)) [95–100]. POPs kommen in Oberflächengewässern und Sedimenten vor und adsorbieren natürlicherweise an organischen Phasen wie beispielsweise Sedimenten oder anderen partikulären Stoffen [101]. Beispiele für diese Schadstoffe (POPs) sind polychlorierte Biphenyle (PCBs), polyaromatische Kohlenwasserstoffe (PAHs), chlororganische Pestizide (z. B. DDT, HCH), polybromierte Diphenylether (PBDEs), aber auch Pharmazeutika wie Antibiotika und Anti-Depressiva [100–103], wobei viele nachweislich toxisch oder karzinogen sind [104–108]. Pathogene wie Bakterien können dabei einen Bakterienfilm („Biofilm“), auf der Mikroplastikoberfläche ausbilden, wobei die hydrophobe Mikroplastikoberfläche die Biofilmbildung stimuliert [97, 109–113]. Die Ansiedlung von Bakterien führt potentiell zur biologischen Degradation der Polymere, wodurch es wiederum zur Freisetzung von Plastik-assoziierten Chemikalien kommt [111, 112, 114, 115]. Da durch die UV-Strahlen Mikroplastik teilweise zerfällt und sich daraus resultierend die Oberfläche und die Polarität erhöht, begünstigt die Alterung des Mikroplastiks ebenfalls die Biofilmbildung [112, 116–118]. Zusammengenommen führt die Biofilmbildung zu einer Veränderung der Plastikoberfläche und damit zum vertikalen Transport des Mikroplastiks, also beispielsweise dem Absinken in einem marinen System, wodurch es für marine Organismen verfügbar wird [97, 112, 118, 119]. Zusätzlich kann Mikroplastik durch sein hohes Oberflächen/Volumen-Verhältnis diverse Schadstoffe oder Pathogene effizient sorbieren und konzentrieren, sowie als Transportmittel für die Selbigen agieren, was die Gefahr durch Mikroplastik erhöht [99, 102, 120, 121]. Interessanterweise differenzieren die

Polymerarten in der Effizienz der Sorption verschiedener hydrophober organischer Verbindungen, wobei PS in Studien 8-200 Mal mehr PAHs sorbierte als PE oder PP [100, 102, 122]. PS zeigt dabei eine mesoporische Oberfläche und amorphe Polymerketten, während PE als nicht-porös beschrieben wird [100, 123]. Somit hängt die Effizienz der Sorption unterschiedlicher POPs von der molekularen Struktur und der Zusammensetzung des Mikroplastiks ab [100, 102, 103].

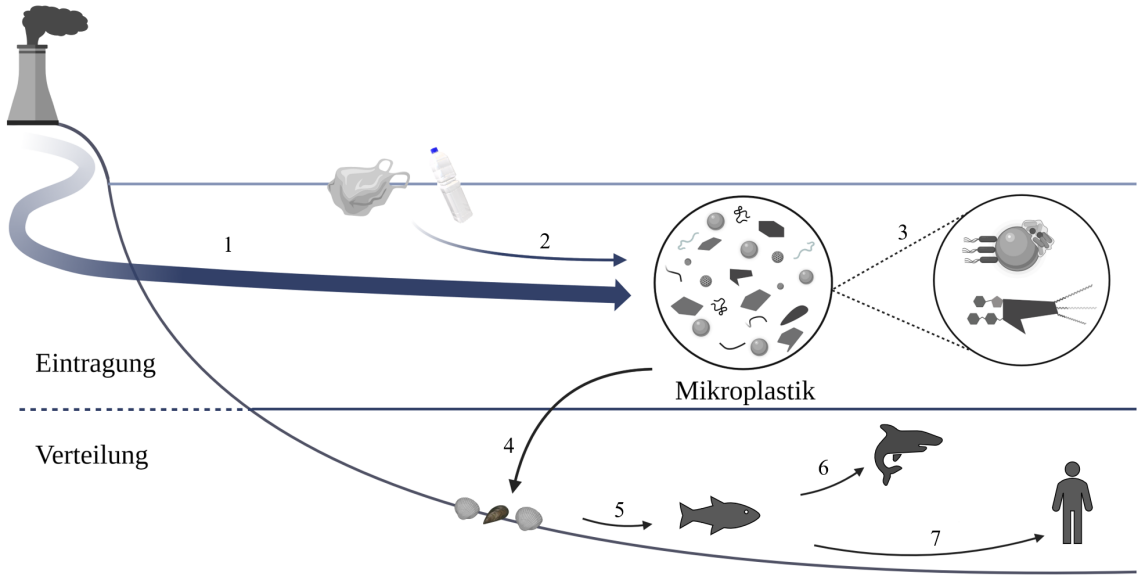

Abbildung 3: Schematische Darstellung der Eintragungs- (1-3) und Verteilungswege (4-7) von Mikroplastik in der Umwelt. Durch unsachgemäße Entsorgung gelangen kleine Plastikpartikel in die Umwelt (= primäres Mikroplastik, 1). Des Weiteren kann Makroplasik durch Verwitterung, UV-Strahlung, mechanischen Abrieb, etc., in Mikroplastik zerfallen (= sekundäres Mikroplastik, 2). In der Umwelt können Pathogene, wie beispielsweise Bakterien, und Schadstoffe an der Oberfläche der Mikroplastikpartikel adsorbieren (3). Diese Mikroplastikpartikel können von verschiedenen Organismen, wie beispielsweise marinen Filtrierern (Muscheln, Phytoplankton ...) aufgenommen werden und somit in die Nahrungskette gelangen (4). Einmal in der Nahrungskette, akkumuliert das Mikroplastik in den unterschiedlichen Organismen (5). So wurde in Organismen, die weiter oben in der Nahrungskette stehen, eine höhere Konzentration an Mikroplastik gefunden (6). Auch Menschen nehmen, durch verschiedene Eintragungswege wie dem Verzehr von bestimmten Lebensmitteln, beispielsweise Fisch, oder aber auch durch Einatmen, Mikroplastik auf (7).

Durch die Verteilung des Mikroplastiks in der Umwelt kann dieses von verschiedenen Organismen aufgenommen werden und somit in die Nahrungskette gelangen [7, 40, 124–126]. Dieser Prozess wird auch als trophische Verteilung bezeichnet [94, 127, 128]. In der marinen Umwelt gelangen Mikroplastikpartikel meist durch so genannte Filtrierer (Muscheln, Schwämme, Plankton, ...), welche ihre Nahrung undifferenziert aufnehmen, in die Nahrungskette (Abb. 3 (4)) [94, 124, 127, 129, 130]. Durch das Fressen dieser, in der Nahrungskette am Anfang ste-

henden, Filtrierer können die Mikroplastikpartikel auch in andere Organismen aufgenommen werden (Abb. 3 (5)) [127, 130, 131]. Andere Organismen können durch Verwechslung oder basierend auf sensorischen, wie beispielsweise visuellen oder olfaktorischen, Signalen ebenfalls Mikroplastik aufnehmen [130, 132–135]. Generell nehmen pelagische Organismen wie Zooplankton oder Phytoplankton eher weniger dichtes und damit schwimmendes Plastik (PE, PP) auf, während benthische Organismen wie Würmer oder Mollusken eher dichteres Plastik (PS, PVC) aufnehmen, da dieses eher zu Boden sinkt und somit für diese Organismen verfügbar wird [40, 118, 129, 136–138]. Dabei kann Mikroplastik im Laufe der Zeit immer weiter in den jeweiligen Organismen akkumulieren. Thompson *et al.*, und Andrady *et al.*, zeigten allerdings, dass verschiedene marine Organismen in der Lage sind, ungewollte Materialien wie Sediment oder Partikel auszuscheiden, ohne dass diese Schäden verursachten [39, 124, 139]. So konnte gezeigt werden, dass Ringelwürmer (Annelida) und Wenigborster (Oligochaeta) Mikroplastik mit anderen Fäkalien ausschieden [35, 124]. Größere Säugetiere wie Wale oder andere weiter oben in der Nahrungskette stehende Organismen, zeigen durch die zunehmende Akkumulation des Mikroplastik in der Nahrungskette die höchsten Konzentration an Mikroplastik (Abb. 3 (6)) [94, 130, 138, 140, 141]. Mikroplastik wird neben der marinen Umgebung aber auch in der terrestrischen Umgebung, also beispielsweise Böden, gefunden. Die hier gefundenen Mikroplastikpartikel werden über Wind und Regen oder Schnee, illegale Abfallablagerungen, Klärschlamm und Abwasser oder die landwirtschaftliche Verwendung von Plastikfolien zum Mulchen eingebracht [68, 142–144]. Dabei könnten Böden nach O'Connor *et al.*, die größte Ansammlung von Mikroplastik in der Umwelt aufweisen [68, 145]. Trotzdem ist vergleichsweise wenig über die Effekte auf terrestrische Lebewesen bekannt. Zusätzlich zu der Akkumulation des Mikroplastiks in der Nahrungskette steigt auch die Gefahr durch die Aufnahme verschiedener Pathogene oder Umweltgifte, für welche Mikroplastik als Transporter dienen können [94, 146–148]. Dabei stellt der Mensch keine Ausnahme dar (Abb. 3 (7)) [124, 148–150]. Auch wir nehmen Mikroplastik, beispielsweise durch den Verzehr verschiedener Lebensmittel wie Fisch, diverse Meeresfrüchte, Bier oder Honig auf [124, 148–152]. Da Mikroplastik auch in der Luft gefunden wird, welches aus dem Abrieb von Kleidung mit hohem Anteil an synthetischen Materialien, oder auch durch den Abrieb von Autoreifen entsteht, kann davon ausgegangen werden, dass wir ebenfalls täglich Mikroplastik einatmen [88, 153, 154]. In verschiedenen Feldstudien an marinen Organismen wurden hauptsächlich Fasern und Fragmente im Verdauungstrakt der Tiere gefunden, während nur selten sphärische Partikel identifiziert werden konnten [128, 155, 156]. Die Effekte des Mikroplastiks auf Zooplankton sind dabei am besten untersucht und umfassen die Verstopfung des Verdauungstraktes, die

Verringerung des Appetits und die Beeinträchtigung der Nahrungsaufnahme, woraus Unterernährung, langsames Wachstum und teilweise Tod resultierten [124, 157, 158]. Für Fische wurde beschrieben, dass größere Mikroplastikteile im Magen stecken und damit zu einer Hungerperiode der Fische führen können [159]. Allerdings wurden keine signifikanten Beeinträchtigungen auf die Fitness beschrieben [159]. Die genauen Wirkmechanismen des Mikroplastiks und die daraus resultierenden toxischen Reaktionen in den unterschiedlichen Organismen sind nicht bekannt. Die realen von Mikroplastik-induzierten Effekte auf verschiedene Organismen sind ein sehr komplexes System, in das viele verschiedene Faktoren, wie beispielsweise die Alterung des Plastiks, das Vorhandensein und die Zusammensetzung eines Biofilms, die Polymerart des Plastiks, das Vorhandensein von Additiven, etc., einwirken [137, 156]. Aus diesem Grund ist es sehr schwer, alle Faktoren gleichzeitig zu erfassen, weshalb oft Modellorganismen wie Muscheln, Zebrafische oder Mäuse, und Modellmikroplastik in kontrollierten Studien verwendet werden. Die Ergebnisse dieser Tierstudien konnten bisher keine eindeutigen Auswirkungen aufzeigen. Verschiedene Laborstudien an Muscheln zeigten, dass Mikroplastik, wenn es auf die Kiemenoberfläche trifft, über das Kiemenepithel assimiliert oder in den Mund und das Verdauungssystem transportiert werden kann [160–162]. Allerdings werden nicht alle über die Kiemen aufgenommene Partikel weiter in den Organismus gelangen, denn Muscheln sind in der Lage, nicht nahrhafte Partikel (beispielsweise Steine) auszuscheiden [162–164]. Es ist derzeit nicht geklärt, wie genau zwischen nahrhaften und nicht-nahrhaften Partikeln unterschieden wird, da auch bei Mikroplastik Unterschiede in der Aufnahme festgestellt wurden. Neben Brate *et al.*, die beschrieben, dass gealterte PE Partikel eher aufgenommen werden als ungealterte [165], konnten verschiedene Studien neben der verabreichten Mikroplastikkonzentration, die Größe, Form und Farbe des Mikroplastiks als Selektionsfaktoren identifizieren [129, 166–168]. Im Hinblick auf die Toxizität von Mikroplastik in Muscheln wurden verschiedene Effekte konstatiert, welche histologische Veränderungen des Verdauungstraktes, reduzierte Filteraktivität, neurotoxische Effekte und verschiedene Entzündungsreaktionen umfassen [160, 162, 165, 169]. Beispielsweise zeigten Wang *et al.*, anhand von PS Partikeln, dass in Muscheln Entzündungsreaktionen und Einflüsse auf den Energiemetabolismus hervorgerufen werden können [170]. Green *et al.*, zeigten beispielsweise die Effekte von PE Fragmenten in Miesmuscheln (*Mytilus edulis*) und identifizierten eine Reduktion der Anzahl sowie der Bindungsstärke der Byssusfäden [156, 171]. Als Modellorganismus für aquatische Organismen werden Zebrafische (*Danio rerio*) verwendet, für welche die Akkumulation von PS in verschiedenen Organen (Darm, Leber und Kiemen) beschrieben wurde [172–175]. Daraus resultierten Veränderungen auf Organebene, welche für den Darm eine verringerte Integrität der Epithelbarriere, mehr Entzündungs-

reaktionen, oxidativen Stress und Veränderungen des Darmmikrobioms umfassten (vergleiche Kapitel 1.2.2 Auswirkungen auf Organebene) [172–175]. In der Leber der Zebrafische wurden metabolische Veränderungen auf der Enzymebene und oxidativer Stress hervorgerufen [172–175]. Lei *et al.*, verglichen verschiedenen Polymerpartikeln (Polyamid (PA), PE, PP, PVC und PS) und konnten Schäden im Darm von Zebrafischen feststellen [176]. Bei keiner der Studien wurden direkte, Polymer-induzierte toxische Effekte festgestellt, die unmittelbar zum Tod der Tiere führten [175, 177–180]. Für terrestrische Organismen gelten unter anderem Mäuse (*Mus musculus*) als Modellorganismen. Hier wurden nach der oralen Gabe von Mikroplastik mit der Nahrung ebenfalls Akkumulationen in diversen Organen, wie dem Darm, der Leber und den Nieren, und Veränderungen in diesen (Veränderungen in der Zusammensetzung des Darmmikrobioms, metabolische Veränderungen und Entzündungsreaktionen), beobachtet [158, 181–183] (siehe Kapitel 1.2.2 Auswirkungen auf Organebene). Für Kompostwürmer (*Eisenia fetida*) wurde gezeigt, dass durch die Interaktion und Aufnahme von Mikroplastik aus dem Boden das Mikrobiom der Organismen zerstört, das oxidative Stresslevel anstieg, sowie das Wachstum einiger Individuen gehemmt wurde [184–187]. Da der Boden als am stärksten mit Mikroplastik kontaminiert gilt, ist es gerade für die Untersuchung von Kompostwürmern und anderen im Boden lebenden Organismen von besonderer Bedeutung, die Interaktion zwischen Mikroplastik und Mikroorganismen, sowie Mikroplastik und Umweltschadstoffen (wie oben beschrieben) nicht außer Acht zu lassen, um damit die Effekte auf diese Organismen besser evaluieren zu können [156].

Zusätzlich dazu besteht ebenfalls die Möglichkeit, dass dem Plastik zugesetzte Additive, wie Weichmacher (z.B. Phthalate), Stabilisatoren (z.B. Alkylphenole) oder Monomere (z.B. Bisphenol A, Styrol) aus dem Plastik in die Umwelt gelangen, welche hier wiederum einen Einfluss haben [101, 188, 189]. So begünstigen Verdauungsflüssigkeiten die Auswaschung von sorbierten Schadstoffen [100, 190]. Je länger die aufgenommenen Mikroplastikpartikel dabei im Organismus verbleiben, desto höher ist die Wahrscheinlichkeit, dass die interagierenden Schadstoffe in das Körpergewebe übergehen [100, 191]. Viele Gruppen postulieren daraus, dass die beobachteten schädlichen Effekte hauptsächlich aus der Desorption von Schwermetallen und anderen Umweltgiften, welche durch Mikroplastik einfacher und in höherer Konzentration in die Organismen gelangen, sowie den Additiven, welche den Plastikartikeln oft zugesetzt werden, resultieren [160, 177, 183, 192–194]. Um die Auswirkungen auf den Organismus besser einschätzen zu können, müssen die Effekte auf der Organebene genauer betrachtet werden.

1.2.2 Auswirkungen auf Organebene

Die nachfolgenden Auswirkungen von Mikroplastik auf die Organebene wurden am Beispiel von Mäusen beschrieben, da diese die am besten untersuchten Säugetiere sind. Die Verwendung von Mäusen und Ratten als Modellorganismen zeigen, dass die orale Aufnahme von Mikroplastik, meist über die Nahrung, zu einer Aufnahme durch den Darm, genauer die Darmgefäßbarriere, in das Lymphsystem und den Blutkreislauf führt (Abb. 4 (1)) [175, 195, 196]. Dabei stellt der Dünndarm den wichtigsten adsorptiven Teil des Magen-Darm-Traktes dar. Neben der Aufnahme von Wasser, Nährstoffen und anderen Verbindungen dient er ebenfalls als eine Schutzbarriere für den Organismus [197, 198]. Das gastrointestinale Epithel wird aus mehreren Zelltypen gebildet, beispielsweise Enterozyten, Becherzellen, enteroendokrinen Zellen oder M-Zellen [198–200]. Enterozyten sind durch spezielle Zell-Zell-Kontakte, so genannte Tight Junctions, verbunden und bilden die epitheliale Schicht, während Becherzellen durch Schleimsezernierung diese schützen [198, 201, 202]. M-Zellen sind im Dünndarm mit Peyer-Plaques assoziiert und spielen eine wichtige Rolle für das Immunsystem, genauer gesagt für das Schleimhaut-assoziierte lymphatische Gewebe (engl. *mucosa associated lymphoid tissue*, MALT) [203–205]. Dabei nehmen M-Zellen auf der Darminnenseite (apikale Seite) Antigene, wie Bakterien, Viren oder auch Makromoleküle, auf und geben sie auf der gegenüberliegenden, basalen Seite an die Zellen den adaptiven Immunsystems ab [203–205]. Somit können auch kleinere Partikel über M-Zellen durch die Darmwand in das lymphatische System gelangen [198, 206–208]. Über das lymphatische System werden Antigene, darunter beispielsweise auch Plastikpartikel, in die Leber und Gallenblase transportiert, wobei einige Partikel anschließend zusammen mit der Galle in den Darm zurückgeführt werden und mit den Fäkalien ausgeschieden werden [198, 207, 209]. Neben der Aufnahme durch M-Zellen werden Aufnahmewege durch Enterozyten (via Endozytose, vergleiche Abschnitt 1.3.1.1 Aufnahmewege von Zellen), dem Durchdringen von intrazellulären Zwischenräumen und der Persorption (über Lücken, welche aus dem Verlust von Enterozyten entstehen) diskutiert [210, 211]. Bei allen Aufnahmewegen scheint die Größe der Partikel die wichtigste Rolle zu spielen, da kleinere Partikel eher über Endozytose aufgenommen oder über intrazelluläre Routen in das Lymphsystem gelangen können [212–214]. Die genauen Schwellenwerte für eine Aufnahme von Mikroplastik über die Darmwand sind jedoch noch unklar [212–214]. Bei größeren Partikeln besteht die Gefahr, dass diese durch mechanische Einwirkungen die Darmwand verletzen, ähnlich wie es für Zooplankton beschrieben wurde [215]. Allerdings führen nach Wright *et al.* nur unrealistisch hohe Konzentrationen von Mikroplastik, oder die Verwendung von Partikeln mit adsorbierten POPs und anderen Schadstoffen, zu einer Entzündung der Darmschleimhaut und akuten Beeinträch-

tigung der Lebensfähigkeit der Organismen [175, 214]. Des Weiteren wird davon ausgegangen, dass der Hauptteil der aufgenommenen Mikroplastikpartikel nicht die Darmwand durchdringt, da für 2 µm Latexpartikel beschrieben wurde, dass lediglich 0,04- 0,3 % der Partikel das Epithel durchquerten [101, 214, 216]. Es ist jedoch auch bekannt, dass das Durchbrechen des Darmepithels einfacher ist, wenn Zellbarrieren defekt sind, beispielsweise bei entzündlichen Darmerkrankungen wie Colitis Ulcerosa oder Morbus Chron [101, 217–219]. Zusätzlich zu der oralen Aufnahme von Mikroplastik, welche hauptsächlich für Fasern beschrieben wurde, ist die respiratorische Aufnahme über die Alveolen der Lunge bekannt (Abb. 4 (2)) [89, 211, 214, 220, 221]. Die Alveolen bestehen aus zwei Arten von Alveolarepithelzellen, auch Pneumozyten genannt, sowie Alveolarmakrophagen [222, 223]. Pneumozyten des Typs I bilden eine möglichst dünne Basallamina aus, welche als Blut-Luft-Schranke bezeichnet wird [222, 223]. Pneumozyten Typ II sind für die Produktion eines Flüssigkeitsfilms zuständig, um die Alveolen zu stabilisieren und zusätzlich die darunter liegende Epithelschicht zu schützen [214, 222–225]. Durch den Flüssigkeitsfilm werden beispielsweise auch größere Partikel an dem Durchdringen der Blut-Luft-Schranke gehindert [214, 221, 226]. Kleinere Partikel können jedoch, wie für den Verdauungstrakt beschrieben, durch Endozytose oder intrazelluläre Wege tiefer in das Lungengewebe eindringen und auch die Blut-Luft-Schranke durchdringen [214, 226]. Die Funktion der Alveolarmakrophagen ist unter anderem die Aufnahme von Staub, wobei auch Plastikpartikel über verschiedene zelluläre Aufnahmewege (vergleiche 1.3.1.1 Aufnahmewege von Zellen) in die Makrophagen aufgenommen werden [214, 221].

Einmal in den Blutkreislauf gelangt werden die Mikroplastikpartikel in Organe, wie die Leber, Galle oder die Nieren, transportiert [175, 193, 227, 228]. Diese Organe sind an der Transformation und Ausscheidung von (Schad-)Stoffen beteiligt (Abb. 4). Allerdings scheinen sich die inerten, synthetischen Polymerpartikel nicht oder nur schlecht transformieren und abbauen zu lassen, wodurch es zu einer Akkumulation in diesen Organen kommt [175, 193, 227, 228]. Die Akkumulation wurde ebenfalls in den Organen, die mit den Plastikpartikeln in Berührung kommen und eine Barriere darstellen, also der Lunge und dem Darm, beschrieben [175, 193, 227, 228]. Hier akkumulierten vor allem größere Partikel, die diese Barriere nicht durchdringen konnten [175, 193, 227, 228]. Neben der Partikelgröße spielen weitere Eigenschaften der Mikroplastikpartikel, wie beispielsweise Hydrophobizität oder Morphologie, eine wichtige Rolle bei der Aufnahme, Akkumulation und Eliminierung der Partikel [175, 211–214]. Zu den pathologischen Veränderungen des Darms, induziert durch die Akkumulation des Mikroplastiks, gehören die verminderte Schleimsekretion, eine Störung der Darmbarriere, Darmentzündungen und eine Störung des Darmmikrobioms [158, 175, 181, 182, 229–231]. Die Störungen des

Darmmikrobioms umfassen sowohl die Veränderung der mikrobiellen Diversität und damit auch der mikrobiellen Zusammensetzung [181, 182, 211]. Dabei war nach der oralen Gabe von PS Partikeln das Auftreten von Bakterien der Phyla *Actinobacteria*, α-, γ-*Proteobacteria* und *Firmicutes* signifikant verringert [181, 182]. Im Gegensatz dazu beschrieben Luo *et al.*, dass die orale Gabe von PS Partikeln keinen signifikanten Unterschied im Vorkommen von Bakterien der Phyla *Firmicutes*, *Proteobacteria* und *Bacteriodetes* ergab, jedoch *Actinobacteria* und *Epsilonbacteraeota* signifikant vermehrt vorkamen [229]. Durch die unterschiedlichen Ergebnisse kann keine eindeutige Aussage darüber erfolgen, welchen genauen Einfluss PS Partikel auf die Zusammensetzung des Darmmikrobioms haben. Für PE Partikel wurden signifikant vermehrt *Firmicutes*, *Malainabacteria* und *Actinobacteria* gefunden [175, 230, 232].

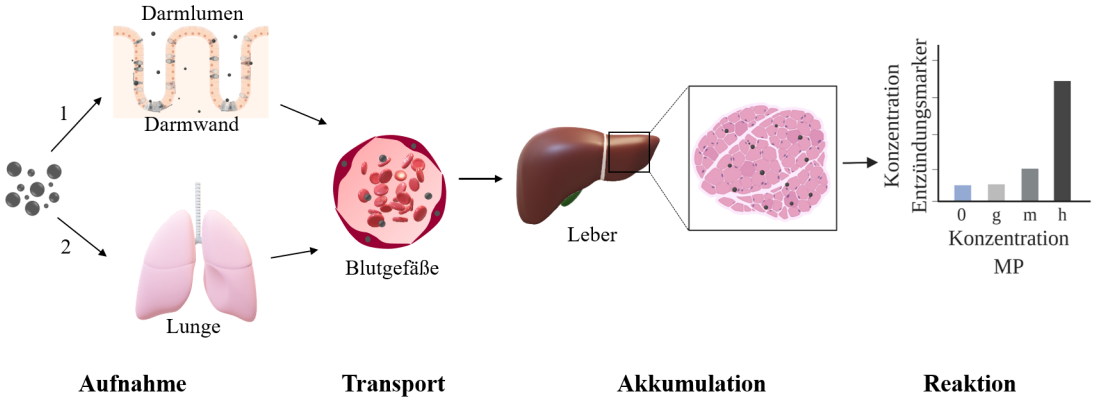

Abbildung 4: Schematische Darstellung der Akkumulation von Mikroplastik in Organen. Die Aufnahme kann über die Nahrung (oral, 1) oder über das Einatmen (respiratorisch, 2) erfolgen. Durch dünne Barrieren, wie beispielsweise bei Defekten in der Darmwand oder der Blut-Luft-Schranke der Alveolen können kleine Partikel in den Blutkreislauf gelangen. Hier werden die Partikel durch den Körper transportiert und akkumulieren in verschieden Organen, wie der Leber, den Nieren oder auch dem Darm. Die Akkumulation der Partikel kann zu Entzündungsreaktionen führen, wobei Reaktionen oft als abhängig von der Mikroplastikkonzentration beschrieben werden.

Im Vergleich dazu wurde in Zebrafischen die Veränderungen im Darmmikrobiom mit dem reduzierten Vorkommen von verschiedenen Bakterien der Bakterienphyla *Bacterioidetes* und *Proteobacteria* und dem vermehrten Vorkommen von Bakterien des Phylums *Firmicutes* beschrieben [158, 174, 233, 234]. Die Zusammensetzung des Darmmikrobioms ist von großer Bedeutung und ist dafür zuständig, dass diverse physiologische und biochemische Funktionen, wie beispielsweise die Adsorption von Nährstoffen, aufrecht erhalten werden können [158, 233, 235–237]. Das Darmmikrobiom unterscheidet sich zwischen verschiedenen Tierarten, so stellen in Zebrafischen *Proteobacteria* und *Fusobacteria* die Mehrheit der Bakterien dar [158, 238]. Dahingegen findet man in Mäusen und Menschen hauptsächlich *Firmicutes* und *Bac-*

terioidetes [158, 238, 239]. Es ist bekannt, dass verschiedene Umweltgifte wie Antibiotika, Pestizide oder Schwermetalle zu einer Veränderung im Darmmikrobiom führen können, was in physiologischer Dysfunktion und dem Auftreten diverser Erkrankungen (Entzündungsreaktionen, Veränderungen im Energiemetabolismus, Glucose- und Fettsäurestoffwechsel oder Übergewicht) resultiert [158, 173, 233, 237, 240]. Aus diesen Gründen ist das Darmmikrobiom ein wichtiger Indikator für die toxikologische Einordnung verschiedener Stoffe [158, 234]. Zu den dokumentierten Lebererkrankungen gehören Entzündungen und Lipidakkumulationen, Veränderungen des Lipidprofils, sowie Fettstoffwechselstörungen [158, 175, 227–230]. Die Erkrankungen der Lunge umfassen neben Verletzungen, Entzündungen auch verstärkte Asthmasymptome [89, 241, 242]. In den untersuchten Organen, in denen Entzündungsreaktionen detektiert wurden, wurden auch Veränderungen in der Anzahl, Funktion, enzymatischen Aktivität und oxidativen Stressreaktion von Immunzellen detektiert (Immunotoxizität) [158, 175, 211, 227–230, 243]. Dabei ist bekannt, dass die Immunotoxizität Einfluss auf das Darmmikrobiom hat (und umgekehrt), sowie dass das Darmmikrobiom und die Beeinträchtigungen der Epithelschichten in Wechselwirkung stehen [211]. In Laborexperimenten mit Mäusen wurden hauptsächlich sphärische PS und PE Modellpartikel verwendet. Allerdings konnten diese Resultate oft nur bei sehr hoher, in der Umwelt unrealistischer, Konzentration erreicht werden. Andere Gruppen zeigten keine negativen Effekte, abhängig von der Mikroplastikkonzentration und dem Polymer [175, 198, 244, 245]. Durch die Ergebnisse von Experimenten an Fischen ist bekannt, dass die Akkumulation von an Mikroplastik adsorbierten POPs im Gewebe, wie dem Fettgewebe, oder die Freisetzung von Additiven im Organismus und daraus resultierende Entzündungsreaktionen möglich sind [101, 175, 193, 232]. Allgemein sind die Auswirkungen von komplexeren Mikroplastiksystemen in Mäusen derzeit noch nicht gut erforscht.

1.3 Experimentelle Modelle in der Mikroplastikforschung auf zellulärer Ebene

Um das komplexe Mikroplastik-Thema analysierbar zu machen, müssen sowohl biologische als auch partikuläre Modelle verwendet werden. Im Folgenden werden zelluläre Modelle und Partikelmodelle näher betrachtet.

1.3.1 Zelluläre Aufnahmemechanismen

Die zelluläre Aufnahme (Endozytose) stellt einen zentralen Baustein in der Immunantwort und der Aufrechterhaltung des Immunsystems dar [246–250]. Bei eukaryotischen Zellen wird zwischen vier Mechanismen (rezeptorvermittelt (Clathrin), Caveolae, Phagozytose und Ma-

kropinozytose) unterschieden [246–251]. Dabei haben unterschiedliche Zelltypen unterschiedliche Möglichkeiten zur Zellaufnahme [246, 248, 250]. Epithelzellen sind für die Ausbildung von Membranen (Epithel) und damit einer Schutzbarriere, sowie der Produktion von Sekreten zuständig [252–254]. Zusätzlich transportieren Epithelzellen bestimmte Stoffe, beispielsweise Nährstoffe im Darm, von ihrer apikalen (dem Lumen zugewandten) zu ihrer basalen Seite und damit in darunterliegende Gewebe [252, 255–257]. Epithelzellen nehmen Stoffe über Clathrin- (Rezeptor)-vermittelte Endozytose oder Makropinozytose auf [255–257]. Dabei ist die Clathrin-vermittele Endozytose der häufigste Mechanismus der Endozytose [248, 250, 256–258]. Nach der Bindung eines Liganden, beispielsweise Wachstumsfaktoren, Proteine und Metabolite, an den entsprechenden Rezeptor, welcher auf der Zellmembran repräsentiert ist, wird die Einstülpung der Zellmembran durch das Protein Clathrin gefördert (Abb. 5) [246, 248, 250, 251, 259, 260].

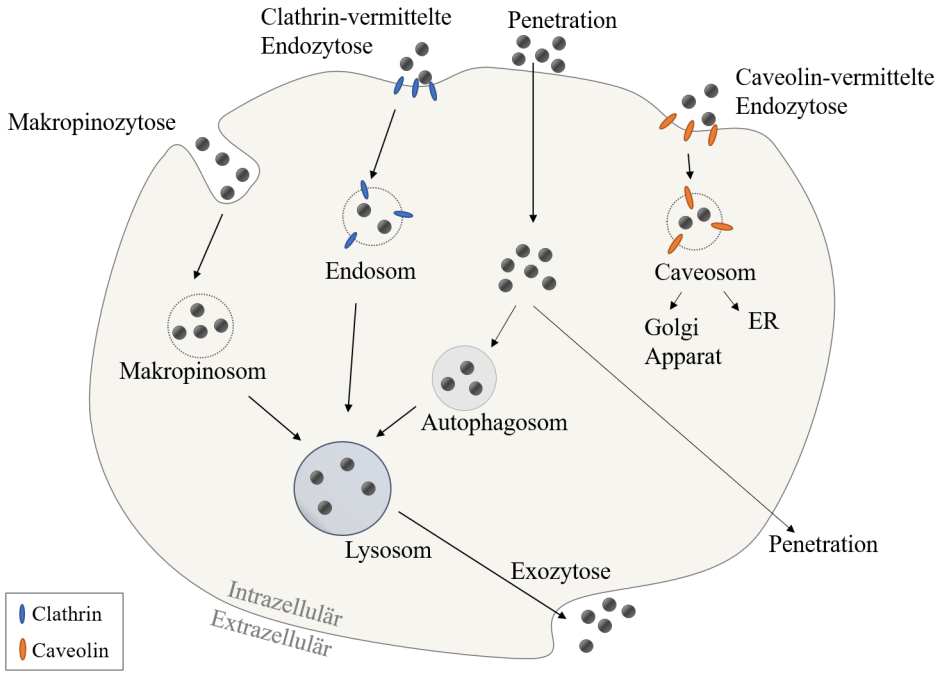

Abbildung 5: Schematische Darstellung der Endozytosewege von partikulären Stoffen. Nach der Makropinozytose bildet sich ein Makropinosom, welches anschließend mit Lysosomen fusioniert. Bei der Clathrin-vermittelten Endzytose werden Vesikel der Zellmembran mit Hilfe des Proteins Clathrin abgeschnürt. Die resultierenden Vesikel werden über Endosomen transportiert, welche mit Lysosomen fusionieren. Nanopartikel können die Zellmembran auch direkt durchdringen (Penetration). Intrazellulär können sie entweder direkt wieder die Zellmembran penetrieren oder werden in Autophagosomen gebündelt und ebenfalls zu Lysosomen transportiert. Caveolin-vermittelte Aufnahme führt zur Bildung von Caveosomen, welche entweder zum Golgi Apparat oder dem Endoplasmatischen Retikulum (ER) transportiert werden. Die Exozytose, also Freisetzung in den extrazellulären Raum, erfolgt fast ausschließlich über Lysosomen, welche mit der Zellmembran fusionieren.

Die so entstandenen, clathrinbeschichteten Vesikel haben einen Durchmesser von ca. 100 nm und werden intrazellulär zu Endosomen transportiert, welche anschließend mit Lysosomen fusionieren [246, 248, 250, 251, 259, 260]. Lysosomen (0,1- 1,2 µm in Durchmesser) sind Zellorganellen mit saurem pH-Wert (pH 4,5- 5) und enthalten Verdauungsenzyme, wie Nukleasen, Lipasen oder Hydrolasen [261–263]. Im Gegensatz zur Clathrin-vermittelten Endocytose kann die extrazelluläre Flüssigkeit und darin gelöste Stoffe meistens unspezifisch (ohne die Beteiligung von Rezeptoren) in das Zellinnere via Makropinozytose gelangen (Abb. 5) [248, 250, 264]. Dabei werden ebenfalls Vesikel aus der Zellmembran abgeschnürt, so genannte Makropinosomen, welche einen Durchmesser von ca. 150 nm haben [248, 250, 264]. Auch diese Vesikel werden zu Lysosomen transportiert [248, 250]. Spezifisch für glatte Muskelzellen, Fibroblasten, Adipozyten, Pneumozyten Typ I und Endothelzellen ist die Aufnahme via Caveolen (Abb. 5) [246, 248, 250, 265, 266]. Caveolen sind flaschenförmige Einstülpungen auf der Zellmembranoberfläche und bilden, wenn sie in die Zelle abgeschnürt werden, ca. 50-100 nm große Vesikel, sogenannte Caveosomen [246, 248, 250, 265, 266]. Caveosomen werden anschließend zum Golgi Apparat oder das Endoplasmatische Retikulum (ER) transportiert. Diese Art der Aufnahme wird beispielsweise für den Transport von Albumin und die Internalisierung des Insulinrezeptors verwendet [246, 248, 250, 265]. Des weiteren können gelöste Stoffe die Zellmembran durchdringen (Penetration, Abb. 5), was jedoch nicht als Endozytoseweg zählt. Intrazellulär werden diese Stoffe entweder in Autophagsomen gepackt und zu Lysosomen transportiert oder können die Zelle durch passive Penetration der Zellmembran wieder verlassen [267]. Einen besonderen Stellenwert im Immunsystem nehmen Phagozyten (Fresszellen), beispielsweise Makrophagen und neutrophile Granulozyten, ein [268–270]. Sie sind in der Lage Mikroorganismen, kleinere Partikel, tote Zellen und Zelltrümmer aufzunehmen und damit für den Körper unschädlich zu machen (Abb. 6) [268–271]. Epithelzellen, Fibroblasten und Endothelzellen sind ebenfalls in der Lage zur Phagozytose, auch wenn hierbei keine Mikroorganismen aufgenommen werden, sondern apoptotische (tote) Zellen aus dem System entfernt werden [268–271]. Die Internalisierung via Phagozytose setzt die Bindung an Membranrezeptoren der Zelloberfläche voraus (Abb. 6 (1)) [269, 270, 272]. Zu diesen Rezeptoren gehören Mannoserezeptoren, Fcγ-Rezeptoren, Fresszellen- (*scavenger*) Rezeptoren und Komplementrezeptoren [268–270, 273–275]. Allgemein interagieren Mustererkennungsrezeptoren (engl. *pattern recognition receptors*, PRRs), welche Scavenger-Rezeptoren inkludieren, mit so genannten Pathogen-assoziierten molekularen Mustern (engl. *pathogen-associated molecular patterns*, PAMPs) [268, 276–278]. Diese PAMPs sind charakteristisch für Mikroorganismen und ermöglichen damit eine Erkennung durch das Immunsystem [268–270, 276, 278]. Zusätz-

lich werden tote, körpereigene Zellen oder deren Bestandteile über die Bindung von diversen polyanionischen Liganden an *scavenger*-Rezeptoren erkannt [273, 279, 280]. Weiterhin können bakterielle Peptidoglykane oder auf der Oberfläche von Mikroorganismen präsentiere Mannose über Mannoserezeptoren binden und damit identifiziert werden [268, 274, 281, 282].

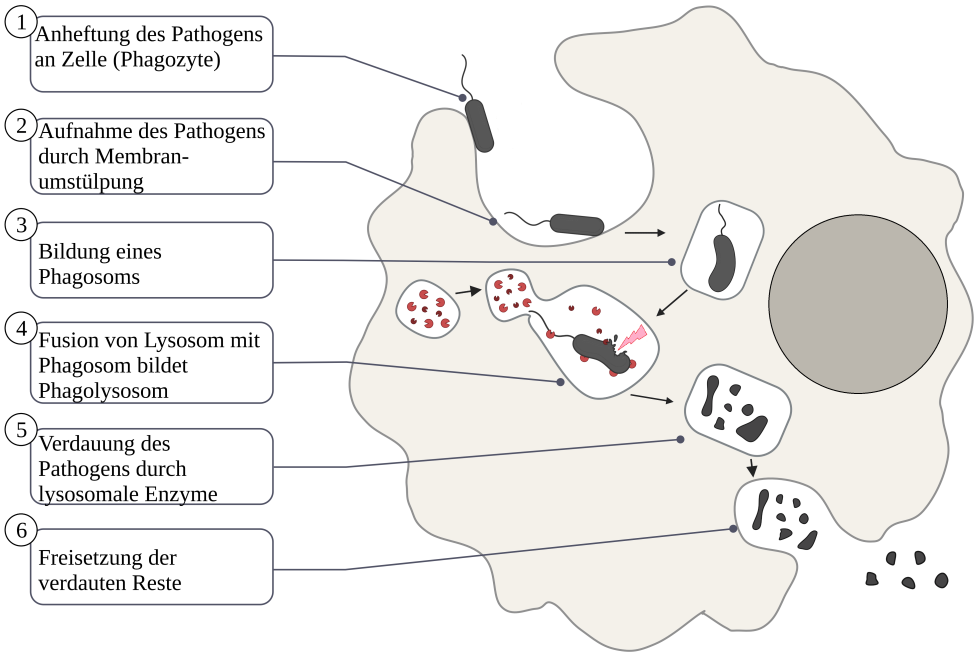

Abbildung 6: Schematische Darstellung der Phagozytose und Autophagie von Pathogenen, wie Bakterien. Pathogene werden über Chemotaxis erkannt und adhärieren an der Zelloberfläche spezialisierter Zellen (Phagozyten, 1). Durch Einstülpungen der Zellmembran werden Pathogene in die Zelle aufgenommen (2) und bilden im nächsten Schritt ein so genanntes Phagosom, welches das Pathogen enthält (3). Das Phagosom fusioniert mit speziellen Zellstrukturen, den so genannten Lysosomen, wodurch sich das Phagolysosom bildet (4). Durch die lysosomalen Enzyme werden die Pathogene verdaut und damit unschädlich gemacht (5). Die Reste werden über Exozytose wieder aus der Zelle frei gesetzt (6).

Die Erkennung von Pathogenen, krankhaften Zellen, wie beispielsweise Krebszellen, oder toten Zellen wird durch das Vorhandensein von Opsoninen vereinfacht [270, 283–285]. Opsonine sind extrazelluläre Proteine, spezifischer gesagt Komplementfaktoren oder Antikörper, die an der Oberfläche der „Zielzellen“ binden und damit für die Phagozytose markieren [270, 283–285]. Sie bilden zusätzlich eine Verbindung zwischen den Phagozyten und Zielzellen aus, binden also an den entsprechenden Oberflächenrezeptor der Phagozyten, wobei Komplementfaktoren über Komplementrezeptoren und Antikörpern, wie Immunglobulin G (IgG), an Fcγ-Rezeptoren gebunden werden [268, 270, 272, 275, 284, 286, 287]. Da es essentiell ist, dass Opsonine nur an körperfremde Zellen oder kranke körpereigene Zellen binden und diese für die Phagozytose markieren, binden einige Opsonine ebenfalls an PAMPs [288–291]. Wenn Opsonine körperei-

gene Zellen für Phagozyten sichtbar machen, binden sie an sogenannte Phosphatidylserine, welche von toten, gestressten oder sterbenden Zellen exprimiert werden [271, 277, 288, 292]. Es ist bekannt, dass die Opsonierung, das heißt die Belegung der Oberfläche der Zielzellen mit Opsoninen, essentiell für die Erkennung von Nanopartikeln durch Makrophagen ist, da ohne die Opsonine keine Internalisierung der Nanopartikel erfolgt [292–294].

Nach der Erkennung der Zielzellen verformt sich die Zellmembran der Phagozyten um das Pathogen (Abb. 6 (2)) [268, 270, 272, 295]. Diese Einstülpung führt zur Aufnahme in die Phagozyten und der Bildung eines Phagosoms (Abb. 6 (3)) [268, 270, 272, 295, 296]. Die Internalisierung der Zielzellen wird von der Polymerisation von Aktinfilamenten gesteuert und ist damit Aktin-abhängig [250, 268, 270, 272, 296, 297]. Das Phagosom wird intrazellulär transportiert, bis es mit einem Lysosom fusioniert, woraus die Bildung eines Phagolysosoms resultiert (Abb. 6 (4)) [268, 270, 298, 299]. Die im Lysosom enthaltenen Enzyme führen, nach der Fusionierung zu einem Phagolysosom, zur Herabsetzung des pH-Wertes und der Zersetzung (Hydrolyse) der Pathogene, Fremdstoffe oder toter Zellen (Abb. 6 (5)) [262, 263, 270, 300]. Für die Verdauung von Mikroorganismen werden im Phagolysosom eine Kombination von oxidativen und nicht-oxidativen Prozessen genutzt [270, 301–304]. Der auch als respiratorischer Burst bezeichnete oxidative Prozess umfasst dabei die nicht-mitochondriale Produktion von reaktiver Sauerstoffspezies (engl. *reactive oxygen species*, ROS) [270, 301, 302, 305–308]. Die Freisetzung von Enzymen, wie Lysozym oder Defensinen, beschreiben den nicht-oxidativen Prozess [270, 301, 302, 304]. Die so verdauten Reste werden zur Zellmembran des Phagozyten transportiert, mit dieser fusioniert und damit in den extrazellulären Raum freigesetzt („Exozytose“) [270, 302].

Experimentell lassen sich die Aufnahmemechanismen durch Inhibition der jeweiligen Mechanismen unterscheiden. So depolymerisiert beispielsweise Cytochalasin D Aktinfilamente und inhibiert somit die Aktin-abhängigen Internalisierungsmechanismen Phagozytose und Makropinozytose [250, 268, 297, 309, 310]. Für die Hemmung der Clathrin-vermittelten Aufnahme wird Chlorpromazinhydrochlorid verwendet, da es den Verlust von Clathrinen indiziert, während Nystatin und Filipin die Ausbildungen von Caveolae und damit die Aufnahme über Calvolae-vermittelte Endozytose inhibiert [250, 311–313]. Basierend auf diesen Experimenten ist bekannt, dass humane Lungenepithelzellen (Zelllinie A549) PS Partikel mit einer Größe von 40 nm über Clathrin- und Caveolin-vermittelte Endozytose aufnehmen, während größere Partikel (1 µm) nicht internalisiert werden konnten [250]. Liu *et al.*, zeigten ebenfalls, dass Leukozyten verschiedene Endozytosemechanismen nutzen, abhängig von der Partikelgröße. So wurden PS Partikel mit einem Durchmesser von 50 nm über Clathrin- und Caveolin-

vermittelte Endozytose aufgenommen, während 500 nm große Partikel über Makropinozytose internalisiert werden [267]. Die Internalisierung von 5 µm großen Partikeln konnte dabei nicht beschrieben werden [267]. Murine Makrophagen waren hingegen in der Lage, PS Partikel mit einem Durchmesser größer als 1 µm mittels Aktin-abhängiger Endozytose (Phagozytose oder Makropinozytose) aufzunehmen [250, 297, 314]. Zusätzlich konnten durch die Inhibition der Aktin-abhängigen Endozytosemechanismen die Aufnahme von 1 und 2 µm Partikeln nicht vollständig inhibiert werden [297]. Ebenso wurde die Aufnahme von 40 nm PS Partikel mittels Phagozytose, Makropinozytose oder Clathrin-vermitteltet beschrieben [250, 315]. Diese Ergebnisse deuten darauf hin, dass Makrophagen verschiedene Aufnahmewege für die gleichen Partikel nutzen [250, 297, 316]. Gleichzeitig wurde beschrieben, dass die Aufnahmemechanismen von der Zelllinie abhängig sind, da sich auch die Aufnahmewege in verschiedenen Epithelzelllinien unterscheiden [250, 257, 315, 317].

Bei Makrophagen spielt zusätzlich die Polarisierung eine entschiedene Rolle. So ist bekannt, dass die klassisch aktivierten M1 Makrophagen Entzündungsstoffe, beispielsweise Zytokine, Interleukin (IL)-1β, induzierbare Stickstoffoxid-Synthase (iNOS) oder Tumornekrose Fakror (TNF)-α, sekretieren, sowie Pathogene und zerstörtes Gewebe aufnehmen und damit dem System entziehen können [318–320]. Danach werden M1 zu alternativ aktivierten M2 Makrophagen, welche entzündungshemmende Stoffe wie IL-10, IL1Ra, oder Arginase 1 (Arg1) sekretieren um die Entzündungsreaktion abklingen zu lassen und in die Phase der Wundheilung überzugehen [318–321]. Neben der Sekretion von Wachstumsfaktoren können M2 Makrophagen auch die Geweberegeneration oder Angiogenese unterstützen [319, 321, 322]. M1 Makrophagen wären prädestiniert für die Partikelaufnahme, allerdings stehen diesbezüglich Studien noch aus. Antonios *et al.*, konnten jedoch zeigen, dass M1 Makrophagen durch die Inkubation mit PMMA Partikeln hervorgerufen werden [320]. Dabei sekretierten unpolarisierte, M0 Makrophagen durch die Partikelinkubation TNF-α, welches die Polarisation zu M1 Makrophagen induzierte [320]. Ähnliche Ergebnisse wurden für die Inkubation mit PE Partikeln gezeigt [323]. Im Gegensatz dazu konnten Stock *et al.* keinen Einfluss auf die Polarisierung von Makrophagen bei der Inkubation mit PS Partikeln zeigen [198].

1.3.2 Mehrdimensionale Zellmodelle

2D Zellmonolayer können nicht vollständig die natürliche Zellumgebung abbilden [324–327]. *In vivo* bilden Zell-Zell-Kontakte sowie Zell-(Extrazellulär)-Matrix Interaktionen die Grundlage für Gewebestrukturen [324, 325, 327]. Für eine bessere Abbildung der natürlichen Umgebung sorgt die Verwendung von 3D-Zellkultur, zumal Zellen hier in einer 3D Umgebung kultiviert

werden können [324–326, 328]. Dies spielt insbesondere in der Krebsforschung eine große Rolle, da für Tumormodelle sogenannte Sphäroide oder Organoide verwendet werden [324–326, 329]. Dabei sind Sphäroide als 3D Zellcluster definiert, welche keine 3D Matrix brauchen und sich, abhängig von der Zelllinie, selbstständig durch Zell-Zell-Kontakte ausbilden [324–326]. Sphäroide besitzen einen optimalen Größenbereich, welcher bei maximal 350 µm liegt [330]. Bei zunehmender Größe ist das Wachstum durch einen Diffusionsgradienten gehemmt, welcher zu einem Mangel an Nährstoffen im Kern des Sphäroids führt (= nekrotischer Kern) [330, 331]. Die Bildung von Sphäroiden kann im hängendem Tropfen (engl. *hanging drop*), auf Gerüstbasis, auf nicht-adhärenter Oberfläche oder rotierender Kultur erfolgen [327, 328, 332]. Im Gegensatz dazu sind Organoide meist aus Stammzellen gebildete komplexere Zellcluster, die eine spezifische Umgebung benötigen. Sie können jedoch die parentalen Organe besser abbilden als einfachere Sphäroide und werden oft als Mini-Organe bezeichnet [333–336]. Bei Organoiden können spezifisch Proteine mittels Immunofluoreszenzfärbung angefärbt und damit die entsprechenden Entwicklungsstadien der parentalen Organe nachgewiesen werden (Abb. 7) [329, 333, 334, 336–338]. Anwendung finden Sphäroide hauptsächlich in der Tumor- und Krebsforschung, sie können jedoch auch verwendet werden, um Toxizität von bestimmten Materialien im Vergleich zu 2D Monolayern besser zu analysieren [324, 332]. Bisher liegen wenig Daten zu Mikroplastik und dessen Einfluss in 3D Zellkulturmodellen vor. So beschrieben Hua *et al.* den Einfluss von 1 und 10 µm PS Partikeln auf Organoide, welche die menschliche Großhirnrinde im Embryonalstadium nachahmten, und zeigten einen signifikanten Einfluss der Mikroplastikpartikel auf die Strukturierung des Nervengewebes [339]. Die Verwendung von Leberorganoiden zeigten nach der Inkubation mit 1 µm PS Partikeln erhöhte oxidative Stressreaktion, sowie Hepatotoxizität und Leberveränderungen, welche laut den Autoren gegebenenfalls zu Krebs führen können [340]. Die Analyse des Einflusses von Mikroplastikfasern in Organoiden der Atemwege belegte in erster Linie keine direkte Toxizität, allerdings wurden Fasern teilweise in Organoide eingebunden, was zu Langzeitfolgen in Lungenepithelzellen führen könnte [341, 342]. Für intestinale Organoide wurde die Akkumulation von 50 nm PS Partikeln in spezifischen Zelltypen, wie den Goblet Zellen oder endokrinen Zellen, nachgewiesen, während andere Zellen in den Organoiden weniger Nanopartikelakkumulation zeigten [343]. Das demonstriert, dass mit Hilfe der mehrdimensionalen Zellmodelle weitere Lücken in der Mikroplastikforschung zwischen *in vivo* und *in vitro* Ergebnissen geschlossen werden können.

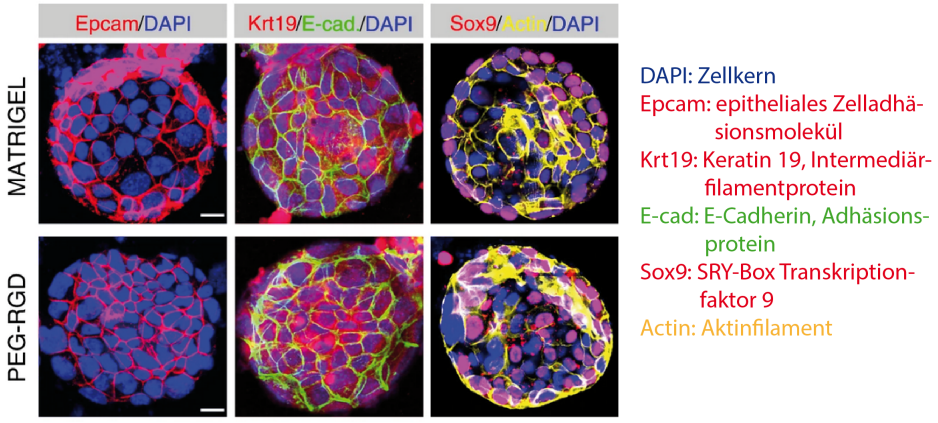

Abbildung 7: Mikroskopische Aufnahmen von Leberorganoiden. Immunfärbung von Leberorganoid aus Leber-Primärzellen auf unterschiedlichen Oberflächen (Matrigel oder PEG-RGD-Hydrogel) mit morphologischen und zellspezifischen Markern wie dargestellt. Marker wie *Epcam*, *E-Cad*, *Krt19*, und *Sox9* zeigen den Vorläufer-Phänotyp, und damit das Vorhandensein von noch nicht vollständig differenzierten Hepatozyten an. Skalenbalken: 50 µm. Nachdruck mit freundlicher Genehmigung des Verlags. Modifiziert nach Sorrentino, G., Rezakhani, S., Yildiz, E., Nuciforo, S., Heim, M. H., Lutolf, M. P., Schoonjans, K. Mechano-modulatory synthetic niches for liver organoid derivation (2020). *Nature Commununications* **11**, 3416. Copyright (2020) Springer Nature.

1.3.3 (Mikro-)Partikel

1.3.3.1 Partikel als Modell für zelluläre Effektstudien

Für die Analyse des Effektes von Plastikpartikeln *in vitro* und *in vivo* wurden hauptsächlich PS und PE Partikel verschiedener Größen verwendet [344, 345]. Für Effektstudien, welche die Auswirkungen von Partikeln untersuchten, wurden neben Metall- auch Stärkepartikel verwendet [344–347]. Die Unterscheidung zwischen Nano- und Mikropartikel erfolgt anhand der Größe, wobei Nanopartikel als Materialien mit einer Größe zwischen 1-100 nm definiert sind, bei Nanotubes kann die axiale Dimension größer ausfallen [346–348]. In den verschiedenen Studien hatten Nanopartikel häufig einen größeren Einfluss als Mikropartikel [345, 346, 348, 349]. Dabei wird postuliert, dass dies einerseits am größeren Oberflächen/Volumen-Verhältnis der Nanopartikel liegt, andererseits an der Aggregatbildung [247, 345, 346, 348, 349]. Außerdem können kleine Partikel schneller und in einer größeren Anzahl von Phagozyten aufgenommen werden, jedoch auch von Epithelzellen oder anderen Nicht-Phagozyten [247, 344–346]. Yang *et al.* beschrieben für Nanopartikel, dass die Bildung von ROS und damit oxidativem Stress die Hauptquelle von Partikel-induzierter Zytotoxizität darstellt [350]. Die ROS-Bildung war bei Vergleichsstudien zwischen Nano- und Mikropartikeln nicht eindeutig bei einer der beiden Größen erhöht [175, 351–355]. Bei Nanopartikeln wurde zudem eine andere intrazelluläre Verteilung beobachtet [247, 346, 356]. Beispielsweise wurden Nanopartikel im Zellkern gefunden, was für Mikropartikel nicht der Fall war [247, 356]. Zusätzlich korrelierte die Bildung von

intranuklearen Protein Clustern, ausgelöst durch die Aufnahme von Siliciumdioxid Nanopartikeln, mit der Inhibierung der Replikation sowie der Zellteilung [247, 356]. Liang *et al.* haben auch die Bedeutung der Analyse der Effekte der gleichzeitigen Inkubation mit Nano- und Mikropartikeln (PS) in Mäusen unterstrichen, da diese Kombination nicht nur näher an den Umweltbedingungen ist, sondern auch zu einer Dysfunktion der Darmbarriere führte [357]. Bei *in vitro* Studien mit verschiedenen Zelllinien und Polymermikropartikeln wurden keine oder nicht-signifikante zytotoxischen Effekte in physiologischen (der Umwelt vorkommenden) Konzentrationen nachgewiesen [175, 358]. Lediglich in sehr hohen Konzentrationen wurden eine vermehrte ROS-Produktion, sowie erhöhte zelluläre Entzündungsmarker identifiziert [175, 198, 358–361].

1.3.3.2 Herstellung von Modell-Polymermikropartikeln

Mikropartikel können, neben den bereits erwähnten Polymeren, aus verschiedenen Materialien wie Glas oder Keramiken bestehen [362–364]. Für Polymermikropartikeln besteht ein großes Anwendungsinteresse, beispielsweise in Druckertinten, in der Chromatografie (wie Hochleistungsflüssigkeitschromatographie oder Gel-Permeations-Chromatographie), oder auch der Kalibrierung von Instrumenten [365, 366]. Polymermikropartikel werden auch in der Biomedizin, beispielsweise beim Transport von Wirkstoffen (*drug delivery*) oder der *in vivo* Bildgebung verwendet [367–370]. Dabei werden je nach Anwendung verschiedene Eigenschaften, wie zum Beispiel unterschiedliche Größen, Größenverteilungen, Porosität, Oberflächenmodifizierung, etc., vorausgesetzt [368, 371, 372]. Die gewünschten Eigenschaften sowie das Polymer bestimmen dabei die Herstellungsmethode der Mikropartikel. Die gängigen Herstellungsmethoden der partikelformenden, heterogenen Polymerisation umfassen die Emulsions-, Suspensions-, Präzipitations- und Dispersionspolymerisation [365, 368, 373, 374]. Neben der heterogenen Polymerisation gibt es noch die Möglichkeit, fertig synthetisierte Polymere zu Partikeln zu verarbeiten, beispielsweise mittels Sprühtrocknung, Lösungsmittelverdampfung in Emulsion oder Fällung, das heißt der Zugabe eines Nicht-Lösungsmittels [368, 375, 376]. Diese als zweiter Weg beschriebene Methode wird häufig auch für die Herstellung von Mikropartikeln aus natürlichen Polymeren verwendet [368, 369, 376]. Jede der genannten heterogenen Polymerisationsmethoden deckt einen gewissenen Größenbereich der resultierenden Polymerpartikel ab [368]. So werden für Emulsionspolymerisation Partikel mit einem Durchmesser von 0,05-0,4 µm erreicht, mittels Dispersionspolymerisation Größen zwischen 0,1-15 µm, für Präzipitationspolymerisation 0,1-5 µm und mittels Suspensionspolymerisation können Partikel mit einem Durchmesser zwischen 5-1000 µm hergestellt werden [365, 368, 377–385]. Methoden anhand der oben beschriebenen zweiten Route der Partikelherstellung nach der Polymerisation wei-

sen eine deutlich größere Varianz im Partikeldurchmesser auf [368]. In der hier vorliegenden Arbeit wurden Partikel mittels Präzipitationspolymerisation sowie, für natürliche Polymere, Lösungsmittelverdampfung und Membran-Emulgierung (engl. *pre-mix membrane emulsification*) hergestellt. Mittels Präzipitationspolymerisation können gleichmäßige Mikropartikel ohne Verwendung von Stabilisatoren hergestellt werden, allerdings ist eine Mindestkonzentration erforderlich und diese Methode ist nur für wenige Monomere geeignet (Abb. 8 I) [383, 386–388]. Im ersten Schritt (Initiation) liegen die funktionalisierten Monomere oder Polymervorstufen getrennt voneinander vor [386, 387, 389]. Bei der photoinduzierten Präzipitationspolymerisation werden durch die Verwendung von Licht (hν) Monomere oder Polymervorstufen chemisch verbunden (Photoklick-Reaktion) und bilden Polymerketten aus (Oligomerbildung) [386, 387, 389]. Diese Polymerketten verbinden sich über die Zeit wiederum mit anderen Polymerketten und bilden so Polymerknäuel aus (Nukleation), aus denen sich dann bei Erreichen einer kritischen Konzentration Partikel bilden (Partikelwachstum) (Abb. 8 I) [386, 387, 389]. Diese Polymerisationsmethode erfordert neben einem vernetzbarem Monomer einen Initiator wie 2,2'-Azoisobutyronitril (AIBN) und ein Reaktionsmedium [368, 386, 387, 389, 390].

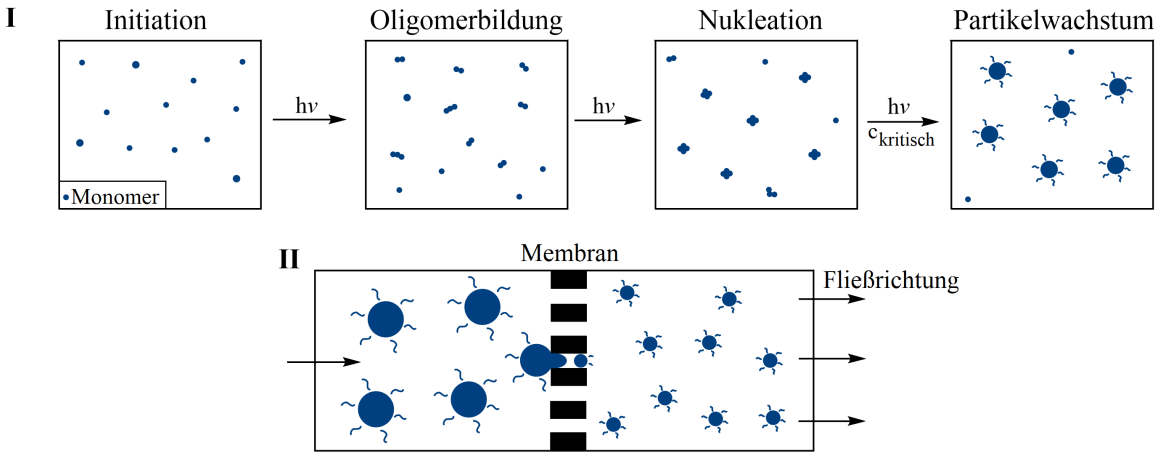

Abbildung 8: Schematische Darstellungen der Synthese von Mikropartikeln mittels Präzipitationspolymerisation (I), oder *pre-mix membrane emulsification* (II). I: Die Monomere liegen im ersten Schritt (Initiation) getrennt voneinander vor. Durch die Verwendung von Licht (hν) werden die Monomere chemisch verbunden und bilden Polymerketten aus (Oligomerbildung), welche im weiteren Verlauf der Reaktion verlängert und verstrickt werden (Nukleation). Bei Erreichen einer kritischen Konzentration kommt es zur Partikelbildung (Partikelwachstum). Da die Polymerpartikel bei einer bestimmten Konzentration ausfallen, wird diese Art der Partikelherstellung als Präzipitationspolymerisation bezeichnet. II: Bei der Herstellung mittels Membran-Emulgierung (engl. *pre-mix membrane emulsification*) werden die Polymere vorgemixt (engl. (*pre-mix*)) und durch mehrmalige Filtration in die gewünschte Partikelgröße gebracht.

Dabei stellt die Verwendung des richtigen Reaktionsmediums den kritischer Teil dar, denn dieses muss gleichzeitig als Lösungsmittel für den Initiator, die Monomere und die gebildeten Oligomere dienen, zusätzlich jedoch als nahezu Theta- (θ)- Lösungsmittel für die polymeren Ketten nach der Nukleation ausfallen [383, 386, 389–391]. Dabei sollen die Polymerketten, beziehungsweise Polymerpartikel, aus der Lösung ausfallen, um separate Partikel zu erhalten [389]. Als θ-Lösungsmittel werden Lösungsmittel bezeichnet, in denen das gelöste Polymer an der Grenze seiner Löslichkeit ist und sich wie eine ideale Kette verhält, beispielsweise für PS Cyclohexan, *trans*-Decalin und Acetonitril (ACN) [383, 386, 391–394]. Allerdings sind diese Lösungsmittel nicht für alle Polymere geeignet, und es können auch nicht alle Polymerpartikel über Präzipitationspolymerisation hergestellt werden [383, 386, 390]. Die Partikelgröße kann vergleichsweise einfach über die eingesetzte Monomerkonzentration (je höher desto größere Partikel), die Initiatorkonzentration (je geringer desto größer die Partikel), oder auch der Lösungsmittelzusammensetzung kontrolliert werden [383, 386, 395, 396]. Zusätzlich können Mikropartikeleigenschaften wie die Porosität der Partikel über die Verwendung des Lösungsmittels gesteuert werden [389, 391]. So zeigte die Verwendung von ACN keine Porosität in resultierenden Poly-Divinylbenzol (DVB) Partikeln, während eine Addition von Toluol zu porösen poly-DVB-Mikropartikeln führte [391]. Die Herstellung von Nano-und Mikropartikeln mittels Lösungsmittelverdampfung (engl. *solvent evaporation*) ist hauptsächlich aus der pharmazeutischen Anwendung für die Einkapselung von Wirkstoffen bekannt [397–401]. Dabei handelt es sich um einen zweistufigen Prozess, bei dem zuerst die Emulgierung einer Polymerlösung erfolgt, welche den Wirkstoff enthält, gefolgt von der Partikelhärtung durch Lösungsmittelverdampfung und Polymerfällung [376, 398–401]. Das gewünschte Polymer muss durch Verwendung eines, mit Wasser nicht-mischbaren, meist organischen Lösungsmittels wie Methylenchlorid oder Chloroform in Lösung gebracht werden [376, 398–401]. Diese organische Lösung wird anschließend mit einer wässrigen Lösung dispergiert, welche mit einem Emulgator, beispielsweise Polyvinylalkohol oder Methylcellulose, versetzt wurde [398–401]. Während der Emulgierung wird die Polymerlösung durch Scherkräfte in Mikrotröpfchen aufgebrochen, was entweder durch einen Homogenisator, Ultraschall oder Mixer realisiert wird [376, 398–401]. Dieser erste Schritt bestimmt hauptsächlich die Größenverteilung der resultierenden Partikel [400]. Im zweiten Schritt, der Verdampfung des organischen Lösungsmittels, härten die gebildeten Mikrotröpfchen aus und können anschließend durch Filtration und Trocknung geerntet werden [376, 400]. Reste von Emulgatoren oder nicht-eingekapseltem Wirkstoff können durch Waschen entfernt werden. Der zweite Schritt bestimmt dabei die Partikelmorphologie und hat einen entscheidenden Einfluss auf die Wirkstofffreisetzung [376, 400]. Die

Lösungsmittelverdampfung ist eine gängige Methode, um PLA oder PLGA Partikel herzustellen [376, 400–402]. Bei der Membran-Emulgierung (*pre-mix membrane emulsification*) werden Polymere zusammen mit Stabilisatoren vorgemixt [403–407]. Dabei bildet beispielsweise eine Wasser-Methanol-Emulsion ein Nicht-Lösungsmittel, in dem sich die Partikel bilden können ohne das Polymer zu lösen [403–407]. Durch mehrmalige Filtration werden die Polymere in die gewünschte Partikelgröße gebracht (Abb. 8 II) [403–407]. Die Partikelgröße wird hierbei durch die Filtergröße, aber auch über die Konzentration und dem eingesetzten Volumen des Nicht-Lösungsmittels, beispielsweise Methanol, bestimmt [405, 406].

1.3.3.3 Einfluss von (Nano-)Partikeleigenschaften auf zelluläre Aufnahme

Für die zelluläre, Rezeptor-induzierte Partikelaufnahme müssen Partikel, wie zuvor für Pathogene beschrieben, ebenfalls von Zellmembranrezeptoren erkannt werden. Als Rezeptoren der Zelloberfläche wurden dabei hauptsächlich Integrine identifiziert, da bei Mäusen, die kein Integrin exprimierten (Integrin-*knock-out* Mäuse) die Phagozytose, sowie zelluläre Entzündungsreaktionen reduziert waren [408]. Somit interagieren die Integrine der Zellmembran mit an der Partikeloberfläche gebundenen Proteinen [408, 409].

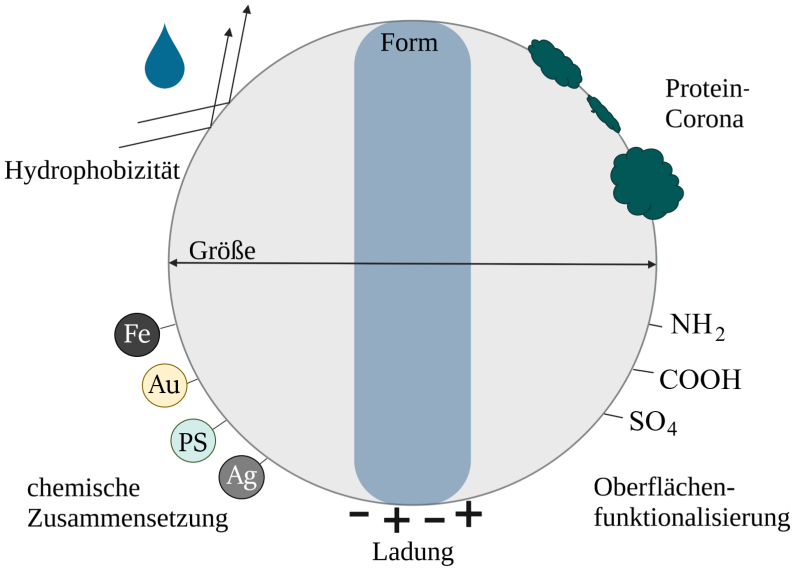

Abbildung 9: Schematische Darstellung der für die zellulären Interaktion wichtigen Partikelcharakteristiken. Zu den wichtigsten Partikeleigenschaften gehören neben der chemischen Zusammensetzung, Größe, Form und einer Corona auch die Oberflächenfunktionalisierung und -ladung. Die chemische Zusammensetzung bezieht sich auf das Material des Partikels (Fe: Eisen, Au: Gold, PS: Polystyrol, Ag: Silber). Die Oberflächenfunktionalisierung beschreibt das Einbringen von funktionellen Gruppen wie Amin- (NH_2), Carboxyl- (COOH) oder Sulfatgruppen (SO_4). Bestimmte Partikeleigenschaften bedingen sich oft gegenseitig, beispielsweise kann die Oberflächenfunktionalisierung nicht nur die Ladung bestimmen, sondern auch die Hydrophobizität oder die Zusammensetzung der Protein-Corona verändern.

Der Fokus der zellulären Aufnahme lag in den letzten Jahren auf Nanopartikeln, da diese vermehrt Anwendung als Wirkstoffsysteme in der Medizin finden [410–412]. Dementsprechend sind hauptsächlich Eigenschaften der Nanopartikel auf die zelluläre Aufnahme bekannt (Abb. 9). Zu diesen Partikeleigenschaften zählt der Partikeldurchmesser, wobei generell gilt, dass kleine Partikel schneller und vermehrt aufgenommen werden [296, 411–416]. Für Makrophagen ist zusätzlich bekannt, dass eine Partikelgröße von 2-3 µm der optimale Durchmesser für die Phagozytose darstellt [296, 414, 416]. Bezüglich der Partikelform wurde beschrieben, dass Stäbchen einfacher aufgenommen werden als Sphären, allerdings nur bei einem Durchmesser kleiner als 3 µm. Ab 3 µm wurden von verschiedenen Zelltypen Sphären bevorzugt [411, 412, 417, 418]. Interessanterweise wurden bei anorganischen Materialien stets Sphären bevorzugt aufgenommen [296, 419]. Von Leclerc *et al.* wurde beschrieben, dass PS Partikel, welche eine carboxylierte Oberflächenfunktionalisierung (-COOH) trugen, von Makrophagen besser aufgenommen wurden als PS Partikel mit einer Aminogruppe (-NH_2) [297]. Des Weiteren ist für die Oberflächenmodifizierung bekannt, dass IgG-beschichtete Partikel besser [420, 421], und mit Polyethylenglykol beschichtete (=PEGylierte) Partikel schlechter aufgenommen werden [412, 422, 423]. Durch die Oberflächenmodifizierung wird auch gezielt Ladung auf die Partikeloberfläche eingebracht und kann somit verändert werden. Die Ladung der Partikeloberfläche spielt eine wichtige Rolle, da stärker geladene Partikel eher aufgenommen werden als schwach oder nicht geladene Partikel (Tab. 1) [413, 416, 424, 425]. Die positive Oberflächenladung der meisten Nanopartikel korreliert mit einer höheren zellulären Aufnahme und einer größeren Zytotoxizität in nicht-phagozytischen Zellen [426]. Dagegen werden anionische Partikel von Phagozyten besser aufgenommen (Tab. 1) [426]. Die Oberflächenladung bestimmt ebenfalls den Aufnahmemechanismus. So beschrieben Harush-Frenkel *et al.*, dass positiv geladene PEGylierte PLA Partikel eine schnelle Aufnahme über den Clathrin-vermittelten Weg zeigen, während negativ geladene Partikel eine geringere Aufnahmerate aufwiesen und über einen anderen Endozytose-Weg aufgenommen wurden (Tab. 1) [427]. Außerdem verursachen positiv geladene Partikel eine unspezifische Adhäsion an der Zellmembran, die negativ und nahezu neutral geladenen Partikel verringern jedoch die unspezifische Adsorption und begünstigen spezifische Zellerkennung und Internalisierung, beispielsweise über Liganden-vermittelte Aufnahme [422, 428]. Neben der Internalisierung kann die Partikelladung auch die Verteilung im Körper und in den Zellen beeinflussen (Tab. 1). So wurden negativ oder neutral geladene Partikel nach kurzer Inkubationszeit (eine Stunde nach respiratorischer Gabe) in Lymphknoten gefunden, während bei positiv geladenen Partikeln die pulmonale lymphatische Translokation inhibiert war [429, 430]. Weiterhin wurden positiv geladene Nanopartikel im

Zytoplasma und Zellkern gefunden, während sie, im Vergleich zu negativ geladenen Partikeln, nicht in den Endosomen gefunden wurden [431–433].

Tabelle 1: Tabellarische Gegenüberstellung des Einflusses der Partikeloberflächenladung auf die zelluläre Interaktion und Internalisierung (Aufnahme), sowie auf die intrazelluläre und pulmonale Translokation.

	kationische Partikel	Quellen
Aufnahme	höhere Internalisierungsrate in nicht-Phagozyten	[426]
	Clathrin-vermittelte Endozytose	[422, 427, 428]
	unspezifische Zellmembraninteraktion	[422, 428]
Translokation	im Zytoplasma und Zellkern, nicht in Endosomen	[431–433]
	in der Blutbahn	[429, 430]

	anionische Partikel	Quellen
Aufnahme	bessere Internalisierung in Phagozyten	[426]
	Liganden-vermittelte Endozytose	[422, 427, 428]
	spezifische Adhäsion	[422, 428]
Translokation	in Endosomen	[431–433]
	in den Lymphknoten	[429, 430]

Verschiedene Studien zeigten auch, dass hydrophobe Partikel besser aufgenommen werden als Partikel aus hydrophilem Material [412, 413, 422, 434, 435]. Zu den mechanischen Eigenschaften ist bekannt, dass harte Partikel besser aufgenommen als weiche [436]. Mahmoudi *et al.* zeigten, dass unterschiedliche Zelllinien die gleiche Art von Nanopartikel unterschiedlich aufnehmen, was zusätzlich die Zelllinienabhängigkeit bei der Aufnahme unterstreicht [437]. Dies wurde ebenfalls von dem Ergebnis von Lunov *et al.* bestätigt, bei dem die beiden als Phagozyten zählenden Zelltypen Makrophagen und Monozyten verglichen wurden. Hierbei zeigte sich, dass Makrophagen carboxylierte PS Partikel präferieren, während Monozyten eher PS-NH_2 aufnahmen [438].

Das Vorhandensein von Serum, wie es beispielsweise im Wachstumsmedium in der Zellkultur verwendet wird, scheint die Nanopartikel-Aufnahme in nicht-phagozytischen Zellen zu verringern, erhöht sie aber in phagozytischen Zellen [426]. Damit liefert die Ausbildung und Zusammensetzung einer Protein-Corona, entsprechend Treuel *et al.* eine ungefähr 5 nm dicke Schicht um die Partikel, eine der wichtigsten Oberflächeneigenschaften, die die Partikel-Zellinteraktion (PZI) beeinflusst [439–441]. Grundsätzlich lagern sich in einer biologischen Umgebung biologische Stoffe an der Partikeloberfläche an [442, 443]. Dies geschieht über elektrostatische Wechselwirkungen wie van-der-Waals Wechselwirkungen und Wasserstoffbrücken [444, 445]. Je nach

biologischer Umgebung unterscheidet sich die Zusammensetzung dieser Partikel-Corona, so werden sich beispielsweise in Proteinlösungen Proteine anlagern und in der Umwelt organische Stoffe, Pestizide, Schadstoffe, etc. (Abb. 10). Historisch gesehen begann die Analyse der Partikel-Corona mit der Protein-Corona an Nanopartikeln, was dazu führt, dass diese am besten erforscht ist [443, 446]. Mit dem zunehmendem Nachweis von Partikeln in der Umwelt wurde der Begriff der Umwelt-Corona etabliert, bei der die Adsorption natürlicher organischer Stoffe (*natural organic matter*, NOM), eine große Rolle spielt [443, 446, 447]. Später wurde neben NOM und Proteinen die Adsorption von Pestiziden und POPs untersucht und der Begriff der Eco-Corona eingeführt (Abb. 10) [443, 446, 448, 449].

Für die Ausbildung und dem Aufbau der Protein-Corona gibt es verschiedene Modelle, meistens wird aber zwischen einer harten (engl. *hard corona*, innere Schicht) und weichen (engl. *soft corona*, äußere Schicht) Corona unterschieden (Abb. 10, Multilayer Modell) [447, 450–455]. Dabei besteht die harte Corona aus Proteinen mit hoher Bindungsaffinität zur Partikeloberfläche, wohingegen die weiche Corona aus Proteinen mit weniger starker Bindungsaffinität zu Partikeloberfläche besteht [447, 452, 454, 455]. Diese Proteine haben eine stärkere Bindungsaffinität zu den Proteinen der harten Corona [447, 452, 454, 455]. Allerdings ist das Vorhandensein einer Multi- oder Monolayer Protein-Corona kontrovers diskutiert [455]. Beim Monolayer-Modell wird nur eine Schicht (= Monolayer) aus Protein auf der Partikeloberfläche ausgebildet. Diese Monolayer wurden hauptsächlich bei kleinen Nanopartikeln (unter 10 nm) beschrieben, bei größeren Nanopartikeln wurden weitgehend Multilayer ausgebildet [452, 453, 455–457]. Zusätzlich hat das Nanopartikel-Material auf die Ausbildung einer Mono- oder Multilayer Protein-Corona einen großen Einfluss, da bei Gold- und Polymerpartikeln hauptsächlich Monolayer beschrieben wurden, bei anderen organischen (nicht aus Kunststoff bestehenden) Nanopartikeln hingegen Multilayer [455]. Allgemein wird die Ausbildung der Protein-Corona mit dem sogenannten Vroman-Effekt erklärt [447, 450, 454, 455, 458]. Der Vroman-Effekt wurde auf flachen Oberflächen beschrieben und bezeichnet die zeitabhängige Änderung in der Zusammensetzung der Protein-Corona [447, 450, 454, 458, 459]. Dabei adsorbieren Proteine, die in einer hohen Konzentration im jeweiligen Medium vorkommen, schneller in der frühen Phase [447, 450, 454, 458, 459]. Diese werden im Verlauf durch weniger häufig vorkommenden Proteinen ersetzt, welche aber eine höhere Bindungsaffinität zur Oberfläche haben [447, 450, 454, 458, 459]. Während dieser Serie an komplizierten Adsorptions- und Desorptionsstufen bleibt die Anzahl an an der Oberfläche adsorbierten Proteinen konstant [447, 450, 454, 458, 459]. Dieses, vergleichsweise alte Modell, wurde 2015 durch Docter *et al.* durch ein neueres Modell ergänzt [447].

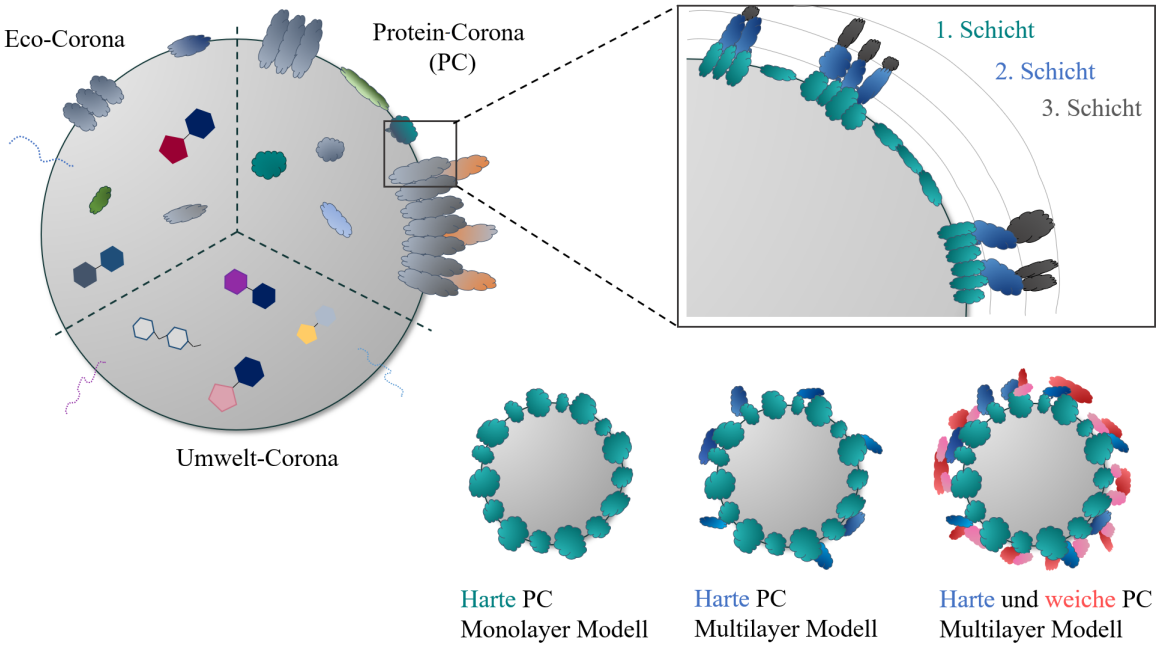

Abbildung 10: Schematische Darstellung der Ausbildungen von Coronae um Partikel und verschiedener Modelle der Protein-Corona. Historisch wurde zuerst an der Adsorption von Proteinen auf der Partikeloberfläche und der Ausbildung einer Protein-Corona geforscht. In den nachfolgenden Jahren verlagerte sich die Forschung auf die Analyse der sogenannten Umwelt-Corona, bestehend aus natürlichen organischen Stoffen (NOM) und der Eco-Corona, bestehend aus Proteinen, NOMs, Pestiziden oder persistenten organischen Schadstoffen (POP). Für die Ausbildung der Protein-Corona werden verschiedene Modelle diskutiert. Generell besteht die Protein-Corona aus mehreren Schichten (beispielsweise Schicht 1-3). Es wird zwischen einer harten Corona (Monolayer oder Multilayer, blau) und einer weichen Corona (rot) unterschieden.

In diesem Modell ist die Evolution der Protein-Corona als deutlich schneller, innerhalb 30 Sekunden, und die zeitliche Veränderung in der Zusammensetzung der Corona wird eher als quantitativ als qualitativ (verglichen zum alten Modell) beschrieben [447, 454]. Als Vorlage für dieses Modell haben unter anderem die Ergebnisse von Tenzer *et al.* gedient. Hier bildete sich die Protein-Corona auf der Basis von humanen Plasma auf PS und Silika Nanopartikeln sehr schnell aus, und anschließend unterschieden sich die Proteine, welche die Protein-Corona bildeten, nicht mehr [460]. Lediglich die quantitative Zusammensetzung änderte sich [460].
Wie bereits oben beschrieben erlaubt die Adsorption von bestimmten Proteinen (= Opsonine) eine einfachere Erkennung von Makrophagen, andere dagegen (= Dysopsonine) erschweren diese. Als Opsonine gelten Fibrinogen, IgG und Komplementfaktoren [461–463], während humanes Serumalbumin (HSA), bovines Serumalbumin (BSA) und Apolipoproteine als Dysopsonine bekannt sind [463, 464]. Dobrovolskaia *et al.* zeigten, dass die Adsorption von Opsoninen an der Nanopartikeloberfläche einerseits die Bindung an Zellrezeptoren verbessert, anderer-

seits die Repulsion der negativ geladenen Nanopartikel von der ebenfalls negativ geladenen Zellmembran reduzieren kann, was zu mehr PZI führen kann [465]. Zusätzlich beeinflusst die Oberflächenladung und -funktionalisierung der Nanopartikel deren Protein-Corona Zusammensetzung [439, 440, 447, 466]. So zeigten Fleischer *et al.*, dass durch die Anwesenheit von fetalem Kälberserum (engl. *fetal calf serum*, FCS) im Medium die PZI von kationischen PS Nanopartikeln erhöht, während die PZI von anionischen PS-Nanopartikeln verringert war [439, 466]. Interessanterweise zeigten Fleischer *et al.* hier, dass BSA, der Hauptbestandteil von FCS, einer Strukturänderung in der Sekundärstruktur nach Bindung an kationischen PS Nanopartikeln unterliegt, was für anionische PS Nanopartikel nicht der Fall war [439, 467]. Durch die Änderung in der Sekundärstruktur von BSA wurden kationische PS Nanopartikel über den Scavenger-Rezeptor aufgenommen, während anionische PS Nanopartikel über die Bindung des Albumin-Rezeptors auf der Zellmembran interagierten [439, 468]. Weiterhin kann beispielsweise die PEGylierung der Partikeloberfläche die Adsorption von BSA inhibieren, was wiederum Einfluss auf die PZI hat [444]. Die Anzahl an adsorbierten Proteinen an der Partikeloberfläche ist bei hydrophoben Oberflächen größer und allgemein ist die Adsorption und Desorption abhängig von Hydrophobizität [450]. Weitere Faktoren, die die Zusammensetzung der Protein-Corona beeinflussen sind Inkubationszeit und -temperatur, Oberflächenmorphologie und -topografie sowie das Verhältnis zwischen Partikelkonzentration und Medium [447]. Die Datenlage zum Verhalten der Protein-Corona bei Überführung von einem in ein anderes Medium, beispielsweise wenn Partikel aus der Umwelt in einen Organismus gelangen und mit Speichel, Magensäure oder Blut in Kontakt kommen, ist nach wie vor unklar. Dabei stellt sich die Frage, ob die Original-Corona stabil erhalten bleibt oder substanziellen Änderungen unterliegt [447, 469, 470]. Derzeit wird davon ausgegangen, dass die Corona je nach Umgebung bestimmten Änderungen unterliegt, die Original-Corona jedoch teilweise erhalten bleibt und damit Informationen über die vergangenen Stationen erhalten bleiben [447, 451, 469]. Die Protein-Corona beeinflusst auch die Verteilung von Nanopartikeln im Körper oder in einzelnen Zellen [430, 471–474]. So können opsonierte Nanopartikel schneller von Phagozyten aufgenommen und transportiert werden, wodurch sie eher in Leber und Milz akkumulieren [462, 472, 475]. Im Vergleich dazu werden Partikel, die Dysopsonine an ihrer Oberfläche adsorbieren, weniger von Phagozyten erkannt und aufgenommen, was dazu führt, dass die länger im Blutkreislauf zirkulieren [472, 476, 477]. Die Adsorption von Proteinen kann auch zu Agglomeration von Nanopartikeln und damit veränderter Verfügbarkeit für PZI führen [474, 478]. Derzeit fehlen Daten zur Zusammensetzung und Auswirkung einer Protein-Corona an Mikroplastikpartikeln. Man kann von einem Unterschied zwischen Mikro- und Nanopartikeln

ausgehen, da signifikante Unterschiede in der Protein-Corona Zusammensetzung bereits ab 10 nm Größenunterschied gefunden wurden [479].

2 Zielsetzung

Trotz zunehmender Verbreitung von Mikroplastik in der Umwelt sind Aussagen über mögliche schädigende Wirkungen auf verschiedene Organismen derzeit noch nicht möglich, z.B. nach der Aufnahme über Nahrung, Trinkwasser oder Atemluft. Schon bei einer einfachen Translokation durch den Verdauungstrakt kommen die Mikroplastikpartikel mit den dortigen Gewebezellen, insbesondere den Barriere-bildenden Epithelzellen, in Kontakt [175, 232]. Durch aktive oder passive zelluläre Aufnahme und dem Durchdringen der entsprechenden Gewebeschichten können sie anschließend im gesamten Körper verteilt werden [227, 228]. Als Bestandteil des Immunsystems sind Makrophagen, welche entweder im Körper patrouillieren oder in bestimmten Organen ansässig und spezialisiert sind, prädestiniert für die Aufnahme von Mikroplastikpartikeln. Durch die Aufnahme von Makrophagen könnten auch Mikroplastikpartikel weiter in verschiedene Organe transportiert werden [243, 323]. Damit sind die Anreicherung im Körper und entsprechend induzierte Langzeitwirkungen denkbar [228, 361]. In der vorliegenden Arbeit wurden die Interaktion, Aufnahme und intrazellulärer Verteilung von Mikroplastikpartikeln mit murinen Zelllinien untersucht. Dabei wurden Epithelzelllinien aus dem Darm und der Leber, sowie Makrophagenzelllinien aus dem Aszites und der Leber verwendet (Abb. 11).

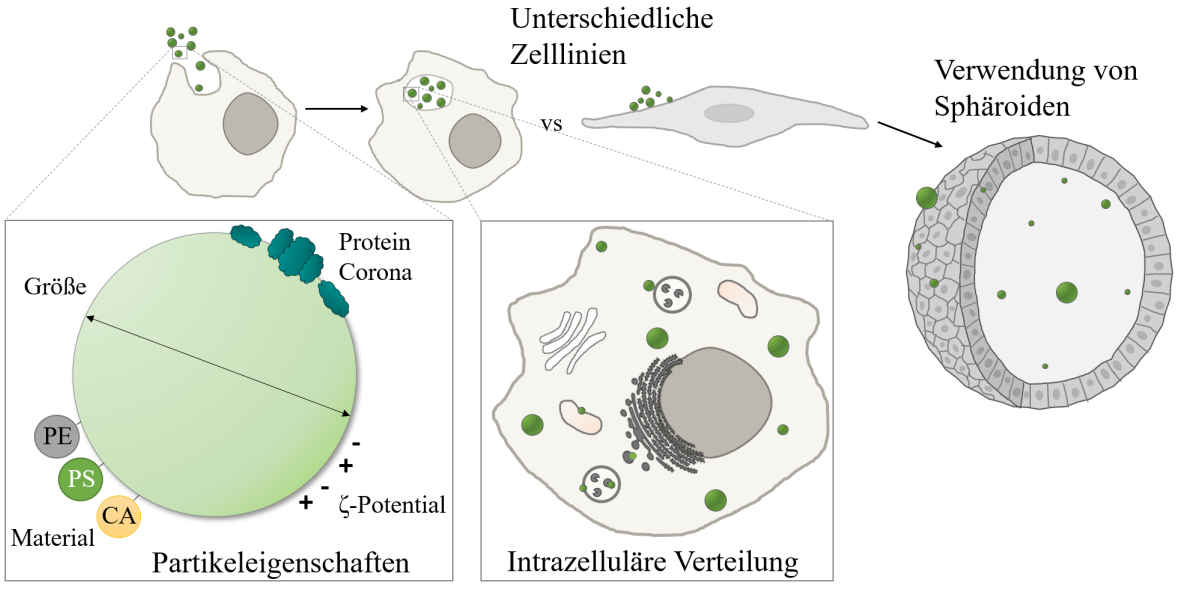

Abbildung 11: Ziel der vorliegenden Arbeit war die Analyse der Partikel-Zellinteraktion in Abhängigkeit verschiedener Partikeleigenschaften und unterschiedlicher Zelllinien. Zusätzlich wurde die intrazelluläre Verteilung, sowie Verteilung an Tochterzellen, von PS Partikeln verschiedener Größe bei Fresszellen (Makrophagen) untersucht. Aus Epithelzellen wurden Sphäroide entwickelt, welche als mehrdimensionale Zellmodelle für die Analyse der Partikelinteraktion dienten.

In einer Studie sollten die zelluläre Aufnahme und zellschädigenden Auswirkungen von PS Partikeln verschiedener Größe untersucht werden, wobei sowohl größen- als auch zelllinienabhängige Effekte analysiert werden sollten. Des Weiteren wurde die Auswirkung der Verwendung von nominell gleichen PS Partikeln zweier Hersteller auf die zelluläre Interaktion mit Makrophagen miteinander verglichen. Neben reinen Partikeln sollte der Einfluss einer artifiziellen, kontrollierten Protein-Corona auf PS Partikeln verschiedener Größe untersucht werden. In der Umwelt findet man neben PS Partikeln auch andere Polymerpartikel. Aus diesem Grund sollten zusätzlich zu PS Partikeln Mikropartikel aus verschiedenen Polymerarten analysiert und deren zelluläre Aufnahme, sowie zelluläre Effekte identifiziert werden. Neben der Aufnahme ist es von großer Wichtigkeit, auch die Freisetzung von Mikropartikeln aus Zellen zu untersuchen. Mikropartikel, die nicht zeitnah wieder freigesetzt werden, sondern in den Zellen für einen längeren Zeitraum verbleiben, sollten bezüglich einer möglichen Ko-Lokalisation mit ausgewählten Zellorganellen untersucht und damit der intrazelluläre Verbleib der Partikel identifiziert werden. Um die zellulären Effekte von nicht-toxischen Partikeln zu identifizieren sollten als Referenzmaterial Celluloseacetat Partikel hergestellt werden. Die Effekte dieser Referenzpartikel sollten in einer Studie mit den zellulären Effekten anderer Polymerpartikel verglichen werden.

Da 2D-Zellkultur nur ein stark vereinfachtes Modellsystem widerspiegelt, sollten zusätzlich erste Versuche bezüglich der Partikelinteraktion an Sphäroiden aus Leberepithelzellen durchgeführt werden, um ein besseres Verständnis für das Verhalten von Mikroplastik in mehrdimensionalen Zellkulturmodellen zu entwickeln.

3 Synopsis

Die vorliegende Arbeit umfasst drei Publikationen und zwei Manuskripte, welche in Abschnitt 5 aufgelistet sind. Die erste Publikation wurde als Erstautorin verfasst und befasst sich mit der Aufnahme und den zellulären Effekten von PS Partikeln unterschiedlicher Größe bei Inkubation mit vier Modellzelllinien (Teilarbeit I). Die Auswirkungen unterschiedlicher Oberflächen, hervorgerufen durch unterschiedliche Herstellungsmethoden oder dem Aufbringen einer kontrollierten Protein-Corona, wurden in zwei weiteren Teilarbeiten untersucht (Teilarbeit II und III). Außerdem wurde die intrazelluläre Verteilung und Freisetzung unterschiedlich großer PS Partikel in Makrophagen in einer Teilarbeit untersucht (Teilarbeit V, Manuskript). Eine weitere Teilarbeit befasst sich mit der Aufnahme und den Effekten unterschiedlicher Polymermikropartikel in Modellzelllinien (Teilarbeit IV, Manuskript). In einer letzten Teilarbeit wurden fluoreszierende Mikropartikel mit einer neuen Methode hergestellt und ihre Verwendbarkeit für zelluläre Studien analysiert, wobei neben 2D-Zellkultur auch Sphäroide aus Epithelzellen verwendet wurden (Teilarbeit VI, nicht als Veröffentlichung geplant).
Nachfolgend werden wichtige von mir erzielte Ergebnisse der einzelnen Teilarbeiten dargestellt, diskutiert und in Verbindung zueinander gebracht. Die jeweiligen Eigenanteile sind in Abschnitt 6 aufgeführt.

3.1 Herstellung von Modell-Mikropartikeln

Seit vielen Jahren sind verschiedene Methoden bekannt, um Mikropartikel herzustellen. Dabei bestimmen verschiedene Eigenschaften die Herstellungsmethode, unter anderem die angestrebte Partikelgröße oder das Vorhandensein von Oberflächenmodifizierungen, sowie das Material. Hier werden zwei Methoden vorgestellt, welche im Rahmen der Arbeit weiterentwickelt wurden, um Celluloseacetat und Polystyrol Mikropartikel mit gewünschten Eigenschaften herzustellen.

3.1.1 Herstellung von Celluloseacetat Partikeln

Celluloseacetat (CA) ist als biologisch basiertes, nicht toxisches Material in der Literatur beschrieben [480–482] und sollte aus diesem Grund als Referenzmaterial für verschiedene Toxizitätsstudien hergestellt werden. Hierbei wurde analysiert, ob das Material, beispielsweise PS oder PE, potentiell toxisch ist, oder ob eine zelluläre Reaktion durch eine Inkubation mit Partikeln als Fremdkörper verursacht wird. Da CA bereits als Polymer vorliegt, war keine Synthese des Polymers notwendig, es musste jedoch für die Herstellung gelöst werden. Für die Herstellung von CA Mikropartikeln wurde einerseits das Verfahren der Lösungsmittelver-

dampfung (engl. *solvent evaporation*) auf Basis eines Patentes von Wagenknecht verwendet [483]. Diese Methode führte zu vergleichsweise großen Partikeln mit ca. 20 µm in Durchmesser (Abb. 12). Da diese erreichte Größe jedoch nicht für Zellstudien geeignet war, sollten Mikropartikel mit einer Größe kleiner als 10 µm hergestellt werden.

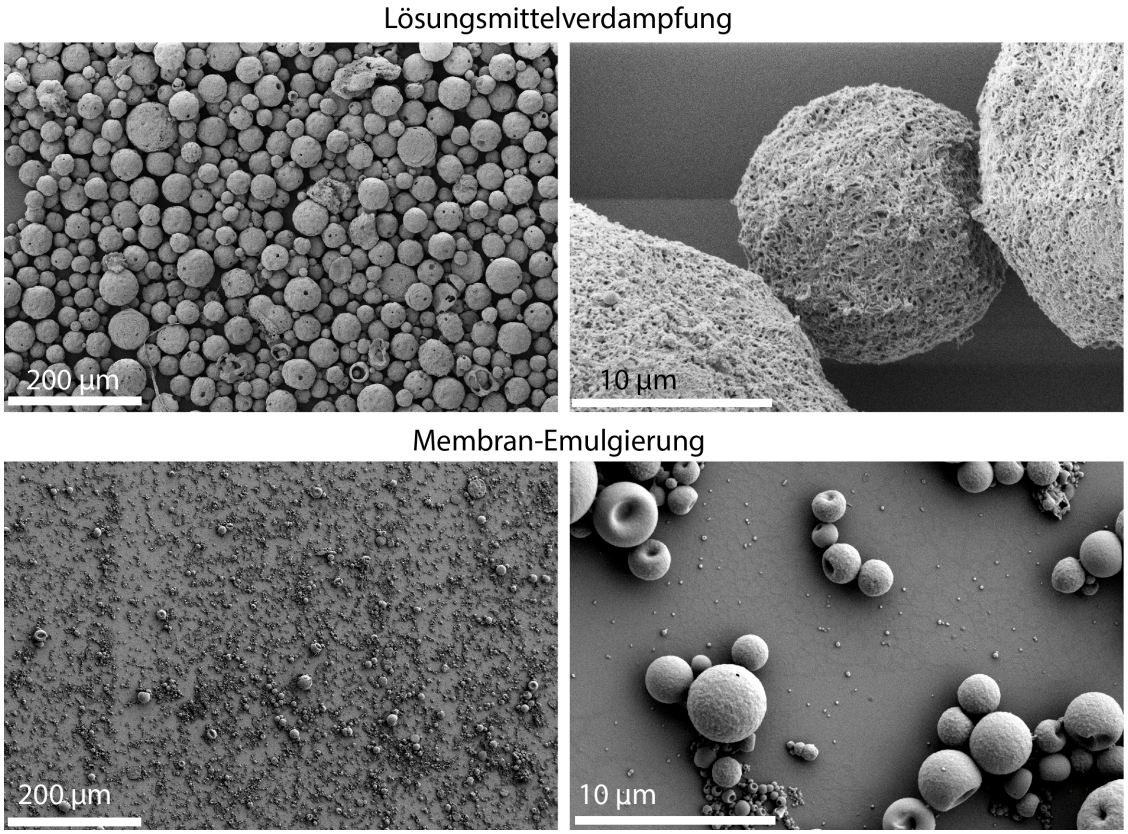

Abbildung 12: Rasterelektronische Aufnahmen von Celluloseacetat Partikeln, welche mittels Lösungsmittelverdampfung (*solvent evaporation*) oder Membran-Emulgierung (engl. *pre-mix membrane emulsification*) hergestellt wurden. Skalenbalken wie angegeben.

Für die Herstellung kleinerer CA Mikropartikel wurde eine Membran-Emulgierung, als eine Art der Emulsionspolymerisation, verwendet (Abb. 12). Diese Methode wurde bisher für andere biobasierte Polymere wie PLA verwendet, jedoch nicht für CA. Das Protokoll für die CA Mikropartikelherstellung ist an eine Veröffentlichung von Sawalha *et al.* angelehnt, welche PLA Mikropartikel mit dieser Methode herstellten [405]. Das Protokoll wurde durch die Verwendung von Ethylacetat anstelle von Dichlormethan als Lösungsmittel für CA angepasst. Die resultierenden CA Partikel hatten einen deutlich geringeren Durchmesser von ungefähr 2-3 µm. Verwendung fanden die Partikel, welche mittels *solvent evaporation* hergestellt wurden und einen größeren Partikeldurchmesser aufwiesen, in einer Studie am Modellorganismus *Daphnia magna*, welche eine Kooperation mit Michael Schwarzer und Julian Brehm (Lehrstuhl Tierökologie I, Universität Bayreuth) war (Veröffentlichung VIII, nicht Teil der Dissertation).

Die Mikropartikel, welche mittels *pre-mix membrane emulsification* hergestellt wurden, wurden für Zellstudien in Veröffentlichung IV verwendet.

3.1.2 Herstellung von fluoreszierenden Partikeln mittel NITEC

Für verschiedene Analysen werden fluoreszierende Partikel benötigt. Darunter fallen auch die Detektion und Quantifizierung der Partikel-Zellinteraktion, die Lokalisierung von Partikeln in Zellen und bestimmten Zellkompartimenten (Organellen). Allerdings sind nicht alle Polymermikropartikel mit einer Fluoreszenzmarkierung kommerziell erwerbbar. Aus diesem Grund wurden fluoreszierende Mikropartikel im Rahmen einer Kooperation mit Dr. Laura Delafresnaye (Soft Matter Materials Group, Prof. Dr. Christopher Barner-Kowollik, Queensland University of Technology, Brisbane, Australien) hergestellt (Abb. 3.1.2). Ziel war die Etablierung einer Polymerpartikelbibiliothek, welche definierte Oberflächeneigenschaften aufweisen und mit Photoklick-Reaktion (Präzipitationspolymerisation) hergestellt werden können.

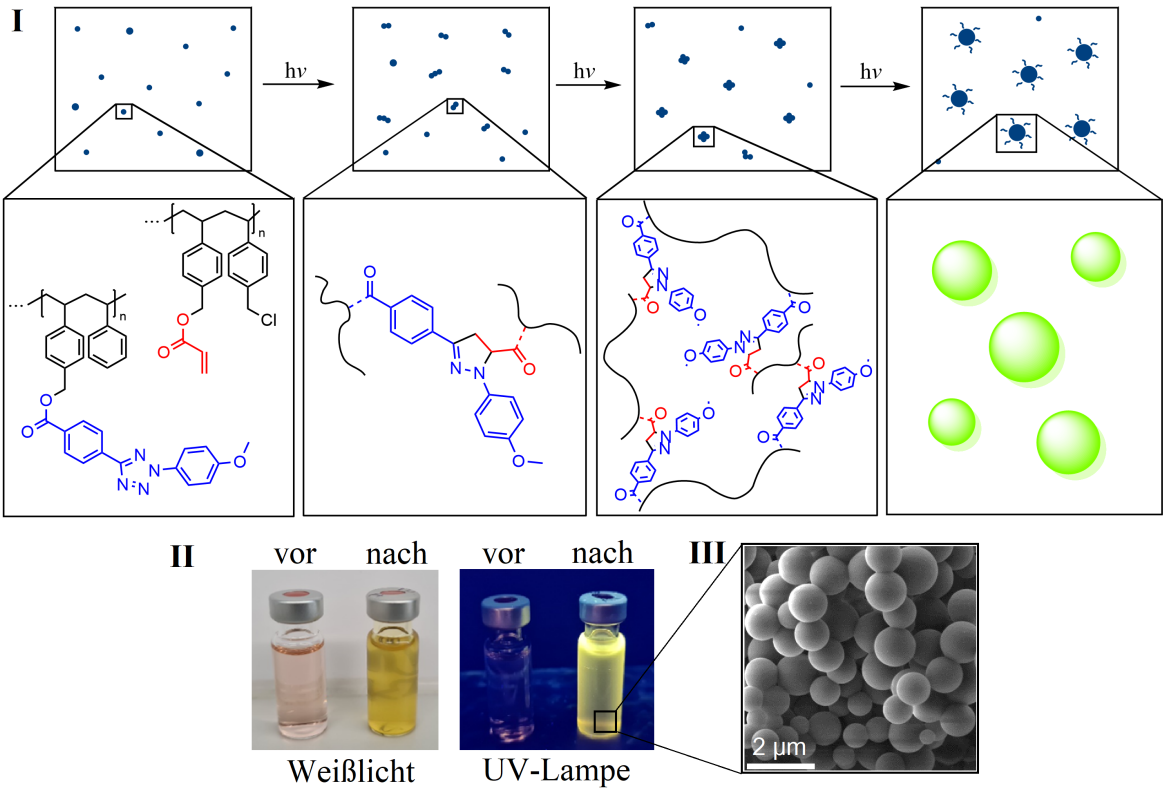

Abbildung 13: Herstellung von inhärent fluoreszierenden PS Partikeln mittels Photopolymerisation, genauer einer NITEC Reatkion. I: schematische Darstellung der Partikelsynthese der Vorpolymere Polystyrol-Tetrazol (blau) und Polystyrol-Acrylat (rot) mittels Photopolymerisation bei gleichzeitiger Partikelsynthese (Präzipitationspolymerisation). II: fotografische Aufnahmen der Reaktionsgefäße vor und nach Photopolymerisation in Weißlicht und unter einer UV-Lampe (λ_{ex}= 365 nm), welche die Fluoreszenz der Partikel zeigt. III: rasterelektronenmikroskopische Aufnahme der resultierenden PS Partikel. Skalenbalken wie angegeben.

Zu Beginn sollten PS Mikropartikel, aber auch PMMA und PE Mikropartikel als reine Polymermikropartikel ohne Oberflächenmodifizierung hergestellt werden. Allerdings war nur die Produktion von PS Partikeln erfolgreich und die Produktion der anderer Polymerpartikel ist noch Bestand aktueller Forschungsarbeiten. Im Folgenden werden die PS Partikel weiter beschrieben . Dabei wurden zuerst Vorpolymere (*pre-polymers*, Polystyrol-Tetrazol und Polystyrol-Acrylat) mittels RAFT-Polymerisation synthetisiert, wobei diese Polymerisation eine einfache und gute Kontrolle über das Molekulargewicht der Polymere erlaubt. Die anschließende Nutzung einer NITEC-Reaktion sorgte für die Synthese des Polymers (Polystyrol-basiertes Copolymer) mit inhärenter Fluoreszenz (= Photopolymerisation) und gleichzeitige Partikelsynthese (= Präzipitationspolymerisation) (Abb. 3.1.2). Dabei war die Herstellung von PS Partikel im Größenbereich von 200- 500 nm bereits am der Soft Matter Materials Group der QUT etabliert und musste durch Veränderungen im Verhältnis der beiden Vorpolymere, sowie der Reaktionszeit für die Produktion von Partikeln mit einem Durchmesser von mehr als 1 µm etabliert werden. Die resultierenden Partikel hatten einen Durchmesser von ungefähr 1,5 µm und zeigten Fluoreszenz bei Anregung mit 365 nm (Abb. 3.1.2) und konnten in Teilarbeit VI, sowohl für die Analyse der Partikel-Zellinteraktionen, als auch für die Analyse in Leberzellsphäroiden verwendet werden.

3.2 Was beeinflusst die zelluläre Interaktion und Internalisierung von Modell-Mikroplastikpartikeln?

3.2.1 Größen- und Zelllinienabhängigkeit

Die Partikelaufnahme in Zellen wurde bereits für bestimmte Zellarten und -linien, sowie unterschiedliche Polymerpartikel mit unterschiedlichen Größen und Oberflächenmodifizierungen beschrieben. Dabei wurden aber selten die gleichen Zelllinien, Partikelgrößen oder Modifizierungen verwendet, was einen eindeutigen Vergleich zwischen bestimmten Zell- und Polymerarten sehr erschwert. Es fehlen also Studien, die einen einheitlichen Vergleich zwischen Polymeren, Partikeldurchmessern und Zelllinien ermöglichen.

In der vorliegenden Arbeit wurden vier Zelllinien verwendet. Dabei wurden zwei Arten von Makrophagen genutzt: J774A.1 als „patrouillierende “ Makrophagen aus dem Aszites und die residenten Lebermakrophagen ImKC. Zusätzlich wurden Leberepithel- (BNL CL.2) und Darmepithelzellen (STC-1) verwendet. In einer ersten Studie wurden fluoreszierende PS Partikel ohne Oberflächenmodifizierung (pristin) mit unterschiedlicher Größe (0,2 - 6 µm), aber in enger Größenverteilung, hinsichtlich ihrer zellulären Interaktion, Internalisierung und Effekte auf Zellproliferation und -metabolismus untersucht. Die Internalisierung der Partikel wurde quali-

tativ mittels Elektronen- und Fluoreszenzmikroskopie bestimmt. Die Partikel-Zellinteraktion (PZI) konnte mit Hilfe von Durchflusszytometrie quantifiziert werden, allerdings ist hier zu beachten, dass mit dieser Methode nicht zwischen internalisierten Partikeln und Partikeln, die an der Zellmembran haften (ohne Internalisierung) zu unterscheiden ist.

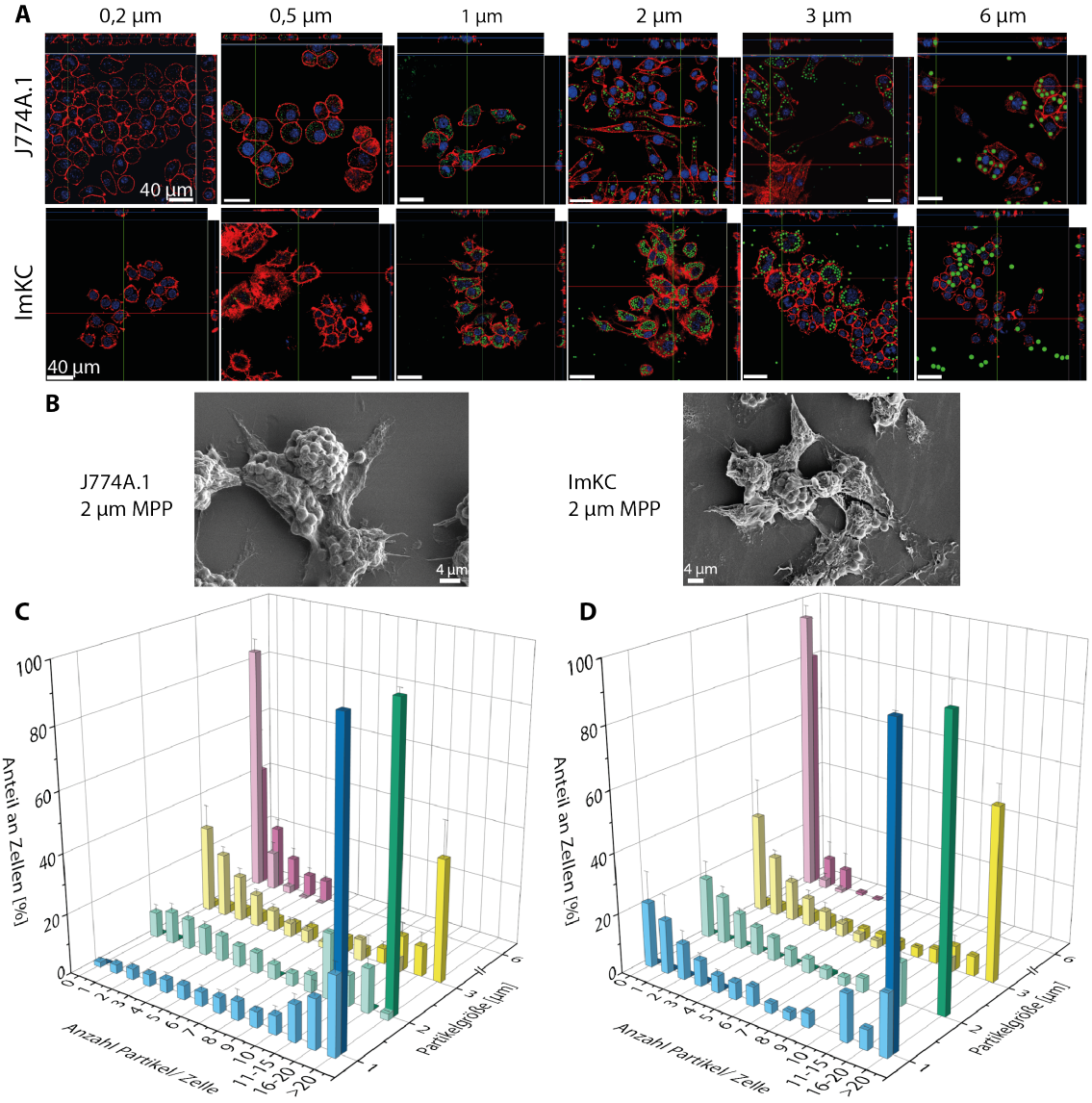

Abbildung 14: Partikelaufnahme in Makrophagen (J774A.1 und ImKC) von PS Partikeln mit unterschiedlichem Durchmesser (0,2 - 6 µm). Die Partikelaufnahme konnte mittels Fluoreszenzmikroskopie (CLSM, A) und Elektronenmikroskopie (B) analysiert werden. Für die fluoreszenzmikroskopischen Aufnahmen wurden das Zytoskellet (rot) und die Zellkerne (blau) gefärbt, während die PS Partikel eine grüne Fluoreszenz aufwiesen. Skalenbalken wie angegeben. Die Quantifizierung der Partikel-Zellinteraktion konnte für 1- 6 µm Partikel mittels Durchflusszytometrie erfolgen (C: J774A.1, D: ImkC). Dabei wurde für die jeweilige Partikelgröße zwei Partikelkonzentrationen (hell: gering, dunkel: hoch) verwendet. Nachdruck mit freundlicher Genehmigung des Verlags. Modifiziert nach Rudolph, J., Voelkl, M., Jérôme, V., Scheibel, T., & Freitag, R. Noxic Effects of Polystyrene Microparticles on Murine Macrophages and Epithelial Cells. *Scientific Reports* **11**, 15702 (2021). Copyright (2021) Springer Nature.

Durch einen Schreibfehler („Quantitative analysis of MPP uptake“ anstatt „Quantitative analysis of MPP interaction “) im ersten Manuskript (Rudolph, Völkl *et al.*, 2021) im Absatz „Material und Methoden “ (S. 11), in dem sich fälschlicherweise auf eine quantitativen Analyse der Partikelaufnahme mittels Durchflusszytometrie, statt der durchgeführten quantitativen Analyse der Partikelinteraktion bezogen wurde, könnte der Eindruck gewonnen werden, dass eine Quantifizierung der Aufnahme stattfand. Des Weiteren scheinen im Manuskript ausgewählte Stellen (Abschnitt „Conclusion “ auf S. 10, Abschnitt „Abstract “ auf S. 1) eine Quantifizierung der Aufnahme zu implizieren, welche jedoch, wie bereits erwähnt, nicht stattfand. Durch die qualitative Analyse der Partikelaufnahme mittels konfokaler Mikroskopie konnte jedoch abgeleitet werden, dass die für Phagozytose spezialisierten Makrophagen einen, im Vergleich zu Epithelzellen, größeren Bereich an Partikelgrößen aufnehmen können (0,2 - 6 µm), sowie eine größere Zahl an Partikeln internalisieren (Abb. 14 A und B). Für eine quantitative Aussage müssten allerdings zusätzliche Aufnahmen quantitativ ausgewertet werden. Bei Epithelzellen zeigten sich starke Unterschiede, da Darmepithelzellen maximal 0,2 µm Partikel internalisierten, während in Leberepithelzellen auch Partikel bis zu einer Größe von 3 µm internalisiert wurden. In dieser Studie wurde die PZI erstmalig mittels Durchflusszytometrie quantifiziert. Dadurch konnten teilweise große Unterschiede in der Verteilung der interagierenden Partikel zwischen den beiden Makrophagenzelllinien identifiziert werden (Abb. 14 C und D). Für beide Makrophagen wurde beobachtet, dass kleinere Partikel (1 und 2 µm) vermehrt mit Zellen interagierten, wohingegen 6 µm Partikel die geringste PZI zeigten. Dies kann mit der Größe von Bakterien erklärt werden, welche normalerweise eine Größe von maximal 4 µm besitzen, wodurch die 6 µm Partikel eher unattraktiv für Partikelaufnahme sein könnten [484]. Zusätzlich zeigten ImKC Zellen für alle Mikropartikel (1 - 6 µm) eine geringe PZI, während J774A.1 Zellen jeweils mit deutlich mehr Partikeln interagierten. In J774A.1 Makrophagen wurde neben der erhöhten Anzahl der interagierenden Partikeln pro Zelle auch eine vermehrte, totale Anzahl an Zellen gefunden, welche generell mit Partikeln interagierten. Anders gesagt gab es in ImKC Makrophagen mehr Zellen, die keine PZI zeigte. Dies könnte in der ursprünglichen Umgebung der beiden Zelllinien begründet sein, da J774A.1 wandernde Makrophagen sind, während ImKC Zellen spezialisierte Makrophagen aus der Leber sind, welche dort ansässig sind. Dabei könnten ImKC Zellen auf die Aufnahme von kleineren Partikeln spezialisiert sein [485, 486]. In beiden Zelllinien gab es jedoch immer ein paar Zellen, welche keine oder deutlich weniger Partikel aufnahmen, wohingegen andere Zellen zur gleichen Zeit 10 oder mehr Partikel aufgenommen hatten. Diese Unterschiede wurden auch in weiteren Studien beobachtet, konnten jedoch nie komplett erklärt werden und wurden teilweise in Teilarbeit V durch die

Untersuchung mit polarisierten Makrophagen adressiert. Die durch Inkubation mit bakteriellem Lipopolysaccharid (LPS) oder Interleukin (IL)-4 zu M1, beziehungsweise M2 polarisierten Makrophagen zeigten mitunter starke Unterschiede in der Partikelaufnahme. Dabei wiesen M1 Makrophagen eine erhöhte PZI auf, während M2 Makrophagen eine geringere PZI indizierten. Basierend auf diesen Ergebnissen könnte eine veränderte Polarisierung, aber auch eine andere Aktivierung von einigen Makrophagen zu den Unterschieden in der Partikelinteraktion führen. Auch hier konnten teilweise große Unterschiede zwischen den beiden Makrophagenzelllinien identifiziert werden, welche durch deren unterschiedlich schnellen Zellmetabolismus/ Zellteilungsrate begründet sein könnte.
Wie bereits beschrieben konnten ebenfalls für die beiden verwendeten Epithelzelllinien Unterschiede festgestellt werden. Bei STC-1 Zellen konnte mittels mikroskopischer Methoden die Anheftung von nicht-aufgenommenen Partikeln ($\geq$ 0,5 µm) an der Zelloberfläche beobachtet werden. Die Aufnahme von 0,2 µm Partikeln könnte mittels Endozytose erfolgen, was mit der Literatur übereinstimmt [487, 488]. Im Gegensatz dazu konnten Leberepithelzellen auch größere Partikel aufnehmen, obwohl sie in der Literatur als nicht-fähig für Phagozytose beschrieben werden [489, 490]. Hier wurden als Aufnahmemechanismus Makropinozytose angenommen, welche für die Aufnahme von partikulärem Material bekannt ist [268, 426]. Zusammenfassend ist die Partikelaufnahme in Epithelzellen meist auf molekulare Transportmechanismen begrenzt, während Makrophagen mit Hilfe von Phagozytose einen großen Bereich an Partikeldurchmessern internalisieren können. Zusätzlich wurde der Einfluss der Partikelkonzentration auf die PZI untersucht, wobei mehr Partikel eine erhöhte Partikelinteraktion bedeutete, was für alle Zelllinien bestätigt werden konnte. Trotz der hohen Aufnahme durch die Makrophagen konnte eine Verringerung der metabolischen Aktivität nur bei sehr hohen Mikroplastik-Konzentrationen gemessen werden, während bei Epithelzellen keine negativen Auswirkungen beobachtet wurden.

3.2.2 Einfluss einer artifiziellen Protein-Corona

Anschließend sollte der Einfluss einer kontrollierten Proteinbeschichtung von Partikeln auf die zelluläre Interaktion mit Epithelzellen untersucht werden. Dafür wurden PS Partikel (0,2 und 3 µm im Durchmesser) mit ausgewählten Modellproteinen (BSA, Myoglobin, β-Lactoglobulin, Lysozym und Fibrinogen) beschichtet. Die Beschichtung wurde mittels SDS-PAGE bestätigt und eine Veränderung des ζ-Potentials nach der Proteinbeschichtung bestimmt (Abb. 15 A). Hierbei unterschieden sich die Werte des ζ-Potentials teilweise stark, abhängig von der Proteinbeschichtung. So führte beispielsweise die Beschichtung mit Lysozym zu einem positiven

ζ-Potential (+10 mV für 0,2 µm und +13 mV für 3 µm). Diese Unterschiede wurden nach der Inkubation mit serumhaltigen Zellmedium fast ausgeglichen und befanden sich in einem ähnlichen Bereich (0,2 µm: ca. -20 mV, 3 µm: ca. -35 mV). Die Angleichung des ζ-Potentials konnte als erster Hinweis für eine Interaktion der Serumproteine mit der erstgebildeten Proteinschicht verstanden werden. Allerdings ist unbekannt, ob es sich um eine Verdrängung der Modellproteine durch Serumproteine handelt oder ob sich Serumproteine als zweite Schicht um die erste Proteinschicht (Modellproteine) legen, wodurch sich das ζ-Potential angleicht.

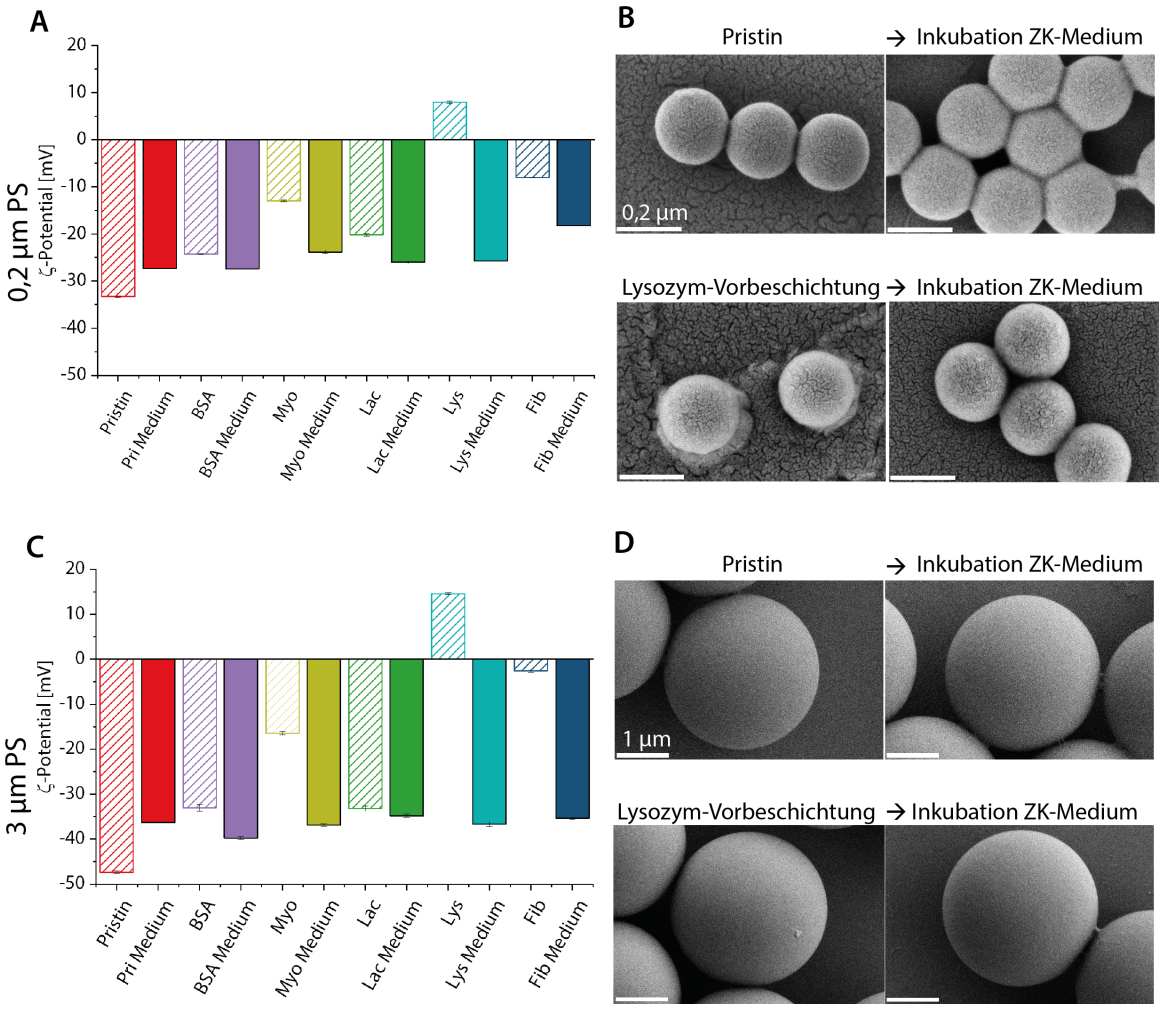

Abbildung 15: Analyse der Oberflächeneigenschaften nach von 0,2 (A,B) und 3 µm (C,D) PS Partikeln vor und nach der Inkubation mit ausgewählten Modellproteinen, sowie nach der Inkubation in Zellkulturmedium (ZK-Medium). A, C: Analyse des ζ-Potentials, B, D: Analyse mittels Rasterelektronenmikroskopie am Beispiel von Lysozym. Skalenbalken wie angegeben. Nachdruck mit freundlicher Genehmigung des Verlags. Modifiziert nach Jasinski, J., Wilde, M., Voelkl, M., Jérôme, V., Froehlich, T., Freitag, R., & Scheibel, T. Tailor-Made Protein Corona Formation on Polystyrene Microparticles and its Effect on Epithelial Cell Uptake. *ACS Applied Materials & Interfaces* **14**, 47277-47287 (2022). Copyright (2022) American Chemical Society.

Eine mikroskopische Untersuchung mittels REM konnte keine Unterschiede zwischen den unterschiedlichen Proteinbeschichtungen feststellen. Jedoch konnten nach der Beschichtung mit beispielsweise Lysozym rauere Stellen auf der Partikeloberfläche beobachtet werden, welche als Proteinaggregate verstanden werden können (Abb. 15 B, D). Nach der zusätzlichen Inkubation in serumhaltigen Zellmedium konnte eine ausgeprägtere Schicht um die Partikel, insbesondere zwischen den Partikeln, beobachtet werden, was einen Hinweis auf eine zusätzliche Beschichtung mit Serumproteinen sein kann (Abb. 15 B). Hinweise auf die Unterschiede in der Adsorption der Modellproteine auf einer PS Oberfläche konnten auch mittels QCM-D (engl. *quartz crystal microbalance with dissipation monitoring*, Quarzkristall-Mikrowaage mit Dissipationsüberwachung) gefunden werden. Dabei wurde anstatt einer Partikeloberfläche ein PS Film auf die QCM-Chips aufgebracht, um eine homogene Beschichtung der Chipoberfläche zu gewährleisten. Eine Inkubation mit Modellproteinen zeigte keine signifikanten Unterschiede in der Adsorption der einzelnen Modellproteine auf der PS-Oberfläche. Einzig Lysozym bildete eine Ausnahme, da hier eine signifikant geringere Adsorption identifiziert wurde. Die Inkubation in Zellkulturmedium, welches zusätzliche Proteine enthält, zeigte große Unterschiede in der Zusammensetzung der Protein-Corona, abhängig von der Vorbeschichtung mit einem Modellprotein. Diese Protein-Corona Zusammensetzung auf 3 µm Partikeln konnte mittels Flüssigchromatographie mit Massenspektrometrie-Kopplung (LC-MS/MS) quantifiziert werden. Als Kontrollpartikel dienten Partikel, welche in Wasser statt in einer Modellproteinlösung inkubiert wurden („pristin“). Dabei konnten alle Modellproteine aus der Vorbeschichtung nach der Inkubation in Zellkulturmedium in der Protein-Corona detektiert werden. Die Modellproteine BSA und Lysozym bildeten dabei jeweils das am häufigsten vorkommende Protein der Protein-Corona, während sowohl bei den anderen Modellprotein-Vorbeschichtungen als auch bei der Kontrolle Hämoglobin (Untereinheit β) am häufigsten vorkam. Da BSA eines der Hauptproteine des verwendeten Rinderserums ist, ist die Häufung von BSA in der Protein-Corona auf eine Addition der beiden verwendeten Systeme (Modellprotein und Rinderserum) zurückzuführen. Die Unterschiede in den Daten für Lysozym in der Adsorption auf PS mittels QCM-D und der Häufigkeit in der Protein-Corona, welche mit LC-MS/MS analysiert wurde, kann durch die Unterschiede der beiden Methoden erklärt werden. Dabei ist LC-MS/MS eine hoch sensitive Methode für die Proteinidentifikation. Des Weiteren lässt sich die Proteinadsorption auf Filmen, wie sie in der QCM-D Messung verwendet wurden, nicht eins zu eins auf die von Partikeln übertragen [491, 492].

Anschließend wurde die PZI bei Epithelzellen in Abhängigkeit von der kontrollierten und charakterisierten Protein-Corona untersucht. Dabei wurde die PZI mittels Durchflusszytome-

trie quantifiziert, während die zelluläre Aufnahme mittels konfokaler Mikroskopie qualitativ untersucht wurde (Abb. 16). Die Epithelzelllinien wurden bereits in einer vorherigen Teilarbeit verwendet (vergleiche 3.2.1 Größen-und Zelllinienabhängigkeit). Hier zeigten die Darmepithelzellen (STC-1) lediglich eine Aufnahme von 0,2 µm pristinen PS Partikeln, während Leberepithelzellen (BNL CL.2) pristine Partikel bis zu einer Größe von 3 µm internalisierten. Es konnte mittels konfokaler Mikroskopie insbesondere für Myoglobin-vorbeschichtete 3 µm Partikel eine Aufnahme in STC-1 Zellen beobachtet werden, was für pristine Partikel oder die anderen Modellproteine nicht der Fall war. In BNL CL.2 Zellen wurden keine Unterschiede in der Aufnahme beobachtet, da alle Modellprotein-vorbeschichteten Partikel aufgenommen wurden. Bezüglich der Partikel-Zellinteraktion zeigten BSA-beschichtete Partikel eine sehr ähnliche Interaktion wie pristine Partikel. In beiden Zelllinien zeigten Fibrinogen- und β-Lactoglobulin-vorbeschichtete Partikel eine, im Vergleich zu pristinen Partikeln, geringere zelluläre Interaktion. Im Vergleich dazu zeigten Lysozym-beschichtete Partikel mit die höchste zelluläre Interaktion. Da Lysozym das einzige, bei neutralem pH, positiv geladene Protein ist, führt die Vorbeschichtung mit Lysozym von Partikeln zum einzigen positiven ζ-Potenzial, das der Proteinladung folgt. Die Verwendung von LC-MS/MS zeigte eine hohe Affinität von Lysozym für PS im Vergleich zu Serumproteinen und eine hohe Partikel-Proteininteraktion im Vergleich zu den anderen, neutral oder negativ geladenen Modellproteinen. Es ist bekannt, dass Lysozym-beschichtete Goldnanopartikel von murinen Fibroblastenzellen durch Clathrin-abhängige Endozytose internalisiert werden [493], was die zelluläre Interaktion mit Lysozym-beschichteten Partikeln bestätigt. Allerdings ist dieser Endozytoseweg nicht für die verwendeten 3 µm Partikel beschrieben. Fibrinogen stellte sich ebenfalls als auffälliges Protein dar, da hier die zelluläre Interaktion signifikant verringert war. Dabei wurden bei Fibrinogen-vorbeschichteten Partikeln eine Aggregatbildung beobachtet, welche die Verfügbarkeit für die zelluläre Interaktion verringert haben könnte. Für keine der vorbeschichteten Partikel wurden zellschädigende Effekte identifiziert, auch unter Verwendung unterschiedlicher Konzentrationen (vergleiche 3.2.1 Größen- und Zelllinienabhängigkeit). Zusammenfassend gab es in Abhängigkeit der Vorbeschichtung mit Modellproteinen signifikante Unterschiede, insbesondere in der Partikel-Zellinteraktion.

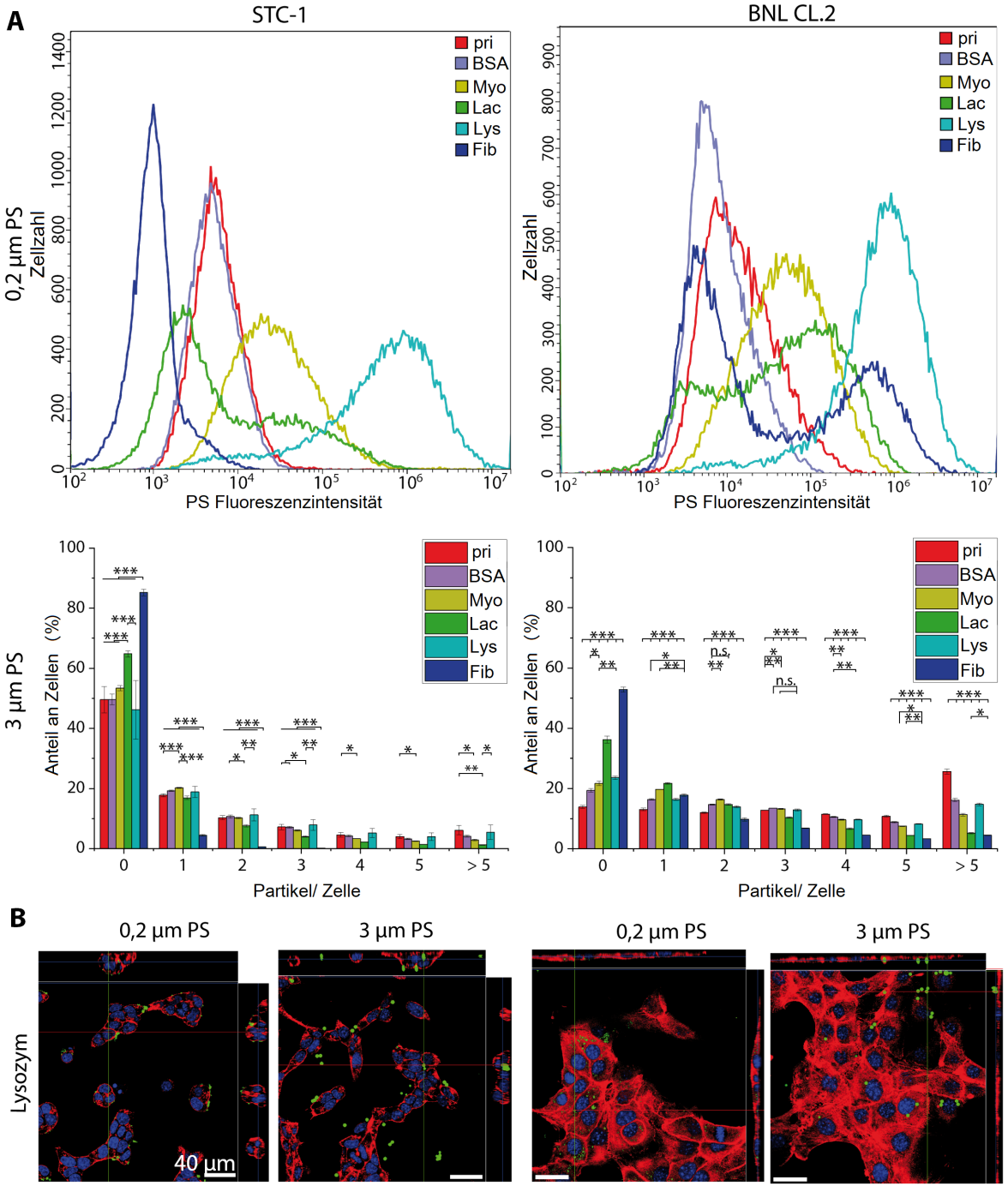

Abbildung 16: Analyse der Partikel-Zellinteraktion von 0,2 und 3 µm PS Partikeln mit murinen Epithelzellen in Abhängigkeit ihrer Vorbeschichtung mit ausgewählten Modellproteinen. A: Analyse mittels Durchflusszytometrie. Für 3 µm Partikel konnte eine Quantifizierung der PZI erfolgen. B: Aufnahmeanalyse mittels konfokaler Mikroskopie. Das Zytoskelett wird in rot, die Zellkerne in blau und die PS Partikel in grün dargestellt. Skalenbalken wie angegeben. Nachdruck mit freundlicher Genehmigung des Verlags. Modifiziert nach Jasinski, J., Wilde, M., Voelkl, M., Jérôme, V., Froehlich, T., Freitag, R., & Scheibel, T. Tailor-Made Protein Corona Formation on Polystyrene Microparticles and Its Effect on Epithelial Cell Uptake. *ACS Applied Materials & Interfaces* **14**, 47277-47287 (2022). Copyright (2022) American Chemical Society.

3.2.3 Physikochemische Eigenschaften von Polymer-identischen Partikeln

In den meisten Studien über den Einfluss von Mikroplastikpartikeln auf die zelluläre Aufnahme und deren Effekte wurden Partikel anhand ihrer Größe, Form oder Polymertyp unterschieden. Allerdings traten widersprüchliche Ergebnisse zwischen den unterschiedlichen Studien auf, obwohl die gleichen Arten von Partikeln verwendet wurden. In einer weiteren Studie sollten nun zwei nominell gleiche PS Partikel miteinander bezüglich deren Aufnahme und zellulären Effekte in den Makrophagenzelllinien J774A.1 und ImKC verglichen werden. Die Partikel hatten einen Durchmesser von 3 µm und wiesen keine Oberflächenmodifizierung auf. Sie wurden von PolyScienes (Polysciences Inc., Warrington, PA, USA; P-MPP) und Micromod (Micromod Partikeltechnologie GmbH, Rostock, Deutschland; M-MPP) bezogen. In ersten Analysen zu den physikochemischen Eigenschaften zeigten sich große Unterschiede (Abb. 17). So konnte mittels Rasterelektronenmikroskopie bei P-MPP eine strukturierte Oberfläche identifiziert werden, während die Partikeloberfläche von M-MPP glatter erschien (Abb. 17 I A). Bei der Bestimmung des ζ-Potentials zeigten sich ebenfalls große Unterschiede, da P-MPP in allen untersuchten Medien (KCl und Zellkulturmedium) mit -80,3 $\pm$ 0,7 mV (gewaschen in KCl) und -28,6 $\pm$ 0,1 mV (DMEM) ein deutlich stärker negativeres Potential aufwies als M-MPP unter den gleichen Bedingungen (-0,7 $\pm$ 0,2 mV in KCl und -1,5 $\pm$ 0,0 mV in DMEM) (Abb. 17 I B). Diese Differenzen blieben unabhängig vom pH-Wert bestehen, was mittels einer ζ-Potentialmessung während einer pH Titration gezeigt werden konnte (Abb. 17 I C). Weitere Analysen der physikochemischen Eigenschaften mittels NMR und CP-AFM konnten zeigen, dass P-MPP einen kleinen Anteil von negativ-geladenen Sulfatgruppen und eine gleichmäßige Verteilung der negativen Ladung auf der Partikeloberfläche besitzt. Im Gegensatz dazu konnten neutral-geladene Benzoesäureestereinheiten und heterogen verteilte Ladung auf der Oberfläche von M-MPP identifiziert werden. Die unterschiedlichen Herstellungsmethoden der beiden PS Partikel waren eine mögliche Erklärung für diese Differenzen. Dabei konnte für P-MPP das Vorhandensein von Sulfatgruppen auf einen Initiator, welcher für die radikalische Polymerisation notwendig ist, zurückgeführt werden. Dahingegen wurde das Vorhandensein von einem geringen Anteil an Carboxylgruppen in M-MPP auf Oxidationsprozesse während der Polymerisation zurückgeführt. Zusätzlich wurde die Präsenz eines neutral-geladenen Tensids bei M-MPP vermutet. Diese Unterschiede in den physikochemischen Eigenschaften der eigentlich „gleichen“ Partikel führten zu komplett unterschiedlichen Aufnahmeverhalten bei Makrophagen, welche auch die Unterschiede in vorherigen Publikationen erklären könnte (Abb. 17 II).

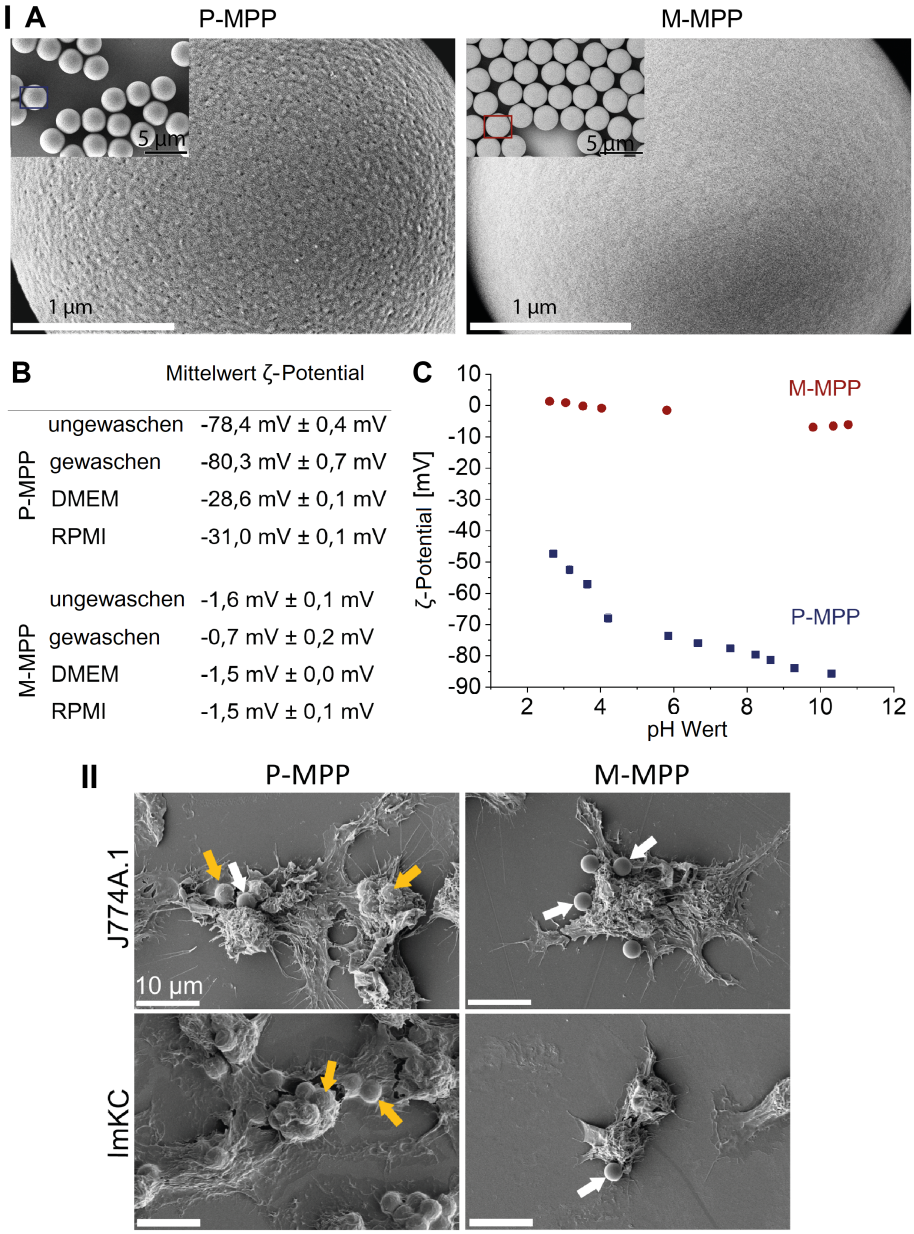

Abbildung 17: Vergleich der Partikel zweier Hersteller (PolySciences (P-MPP), Micromod (M-MPP)) in Hinblick auf ihre physikochemischen Eigenschaften (I) und Partikel-Zellinteraktion (II). I: Analyse mittels Rasterelektronenmikroskopie (REM) (A), und mittels Messungen des ζ-Potenials in verschiedenen Medien (B und C). Für die ζ-Potenialmessungen bei pH 6 wurden die Partikel ungewaschen und nach Waschen mit Wasser, sowie nach der Inkubation in Zellkulturmedium (DMEM und RPMI, mit 10 % FCS) analysiert (B). Für die Messungen bei unterschiedlichen pH-Werten wurde eine pH-Titration durchgeführt (C). II: Analyse der PZI der beiden Partikel in zwei Makrophagenzelllinien (J774A.1 und ImKC) mittels REM. Aufgenommene Partikel wurden mit orangenen Pfeilen, nicht aufgenommene Partikel mit weißen Pfeilen hervorgehoben. Skalenbalken wie angegeben. Nachdruck mit freundlicher Genehmigung des Verlags. Modifiziert nach Ramsperger, A.F.R.M., Jasinski, J., Voelkl, M., Witzmann, T., Meinhart, M., Jérôme, V., Kretschmer, W.P., Freitag, R., Senker, J., Fery, A., Kress, H., Scheibel, T. & Laforsch, C. Supposedly Identical Microplastic Particles Substantially Differ in Their Material Properties Influencing Particle-Cell Interactions and Cellular Responses. *Journal of Hazardous Materials* **425**, 127961 (2022). Copyright (1969) Elsevier.

So zeigten beide Makrophagenzelllinien eine starke Partikelinternalisierung bei P-MPP, während nur wenige M-MPP mit den Zellen interagierten. Diese Unterschiede konnten durch die prominentere Oberfläche bei P-MPP, sowie dem stärker geladenen ζ-Potential erklärt werden. Dabei könnte die Phagozytose einerseits direkt durch die Partikeloberfläche beeinflusst werden, da beispielsweise Bakterien bei neutralem pH ebenfalls ein ζ-Potential von -22 mV aufweisen und die Phagozytose bei Partikeln mit einer rauen Oberfläche deutlich erhöht war. So wurde bereits beschrieben, dass das ζ-Potential einen Einfluss auf die PZI hat, was mit unseren Beobachtungen übereinstimmt [426, 494]. Des Weiteren kann die Phagozytose aber auch indirekt durch das Vorhandensein einer unterschiedlichen Protein-Corona um die Partikel beeinflusst werden. Dabei könnten Proteine aus dem Zellkulturmedium unterschiedlich mit den jeweiligen Partikeloberflächen interagieren und damit verschieden zusammengesetzte Protein-Coronae hervorrufen, welche anschließend unterschiedlich mit der Zelloberfläche interagieren [448, 451, 460]. Dies wurde bisher jedoch nur für Nanopartikel beschrieben, wobei sich bei Mikropartikeln die Aufnahmemechanismen von denen von Nanopartikeln unterscheiden, und damit noch nicht bekannt ist, inwieweit sich die Ergebnisse von Nano- auf Mikropartikel übertragen lassen. Interessanterweise waren die oben beschriebenen Unterschiede in der PZI bei serum-freier Kultivierung und Partikelinkubation fast verschwunden. Generell war hier eine etwas geringere Partikelaufnahme erkennbar, allerdings wurden ebenfalls Micromod Partikel von beiden Makrophagenzelllinien aufgenommen (Abb. 18). Daraus leitete sich die Hypothese ab, dass Serumproteine des Zellkulturmediums anders an der M-MPP Oberfläche adsorbieren als an der von P-MPP. Hier würde es Serumproteine bei M-MPP geben, welche die PZI reduzieren und/oder Serumproteine bei P-MPP geben, welche die PZI stark erhöhen. Bei der Analyse der Protein-Corona mittels LC-MS/MS stellten sich Unterschiede in der Proteinadsorption dar (Tab. 2). So waren bei P-MPP in Medium mit Serum deutlich mehr Proteine identifizierbar, und das am häufigsten vorkommende Protein war Hämoglobin (fetal subunit β). Dahingegen war BSA das am häufigsten vorkommende Protein bei M-MPP. Proteine wie Cathelidicin 2 (Cath2), Komplementfaktor B und Komplementkomponente 3 (Komplement C3) wurden ausschließlich in P-MPP Proben gefunden. Dabei ist Cath2 (Calcium-abhängiges) als Zelladhäsionsprotein bekannt, wobei ebenfalls von Coorens *et al.* eine erhöhte PZI von Cath2-behandelten PS Partikeln in RAW Makrophagen beschrieben wurde [495]. Allerdings muss angemerkt werden, dass dies ausschließlich für equines Cath2 beschrieben wurde, nicht aber für Cath2 aus anderen Organismen wie Hühnern. Zudem erfolgte hier die Inkubation in serumhaltigem Medium, was eine Interaktion mit bovinen Proteinen zu Folge hatte, wodurch eine eindeutige Aussage zum Einfluss von Cath2 auf die PZI nicht möglich ist.

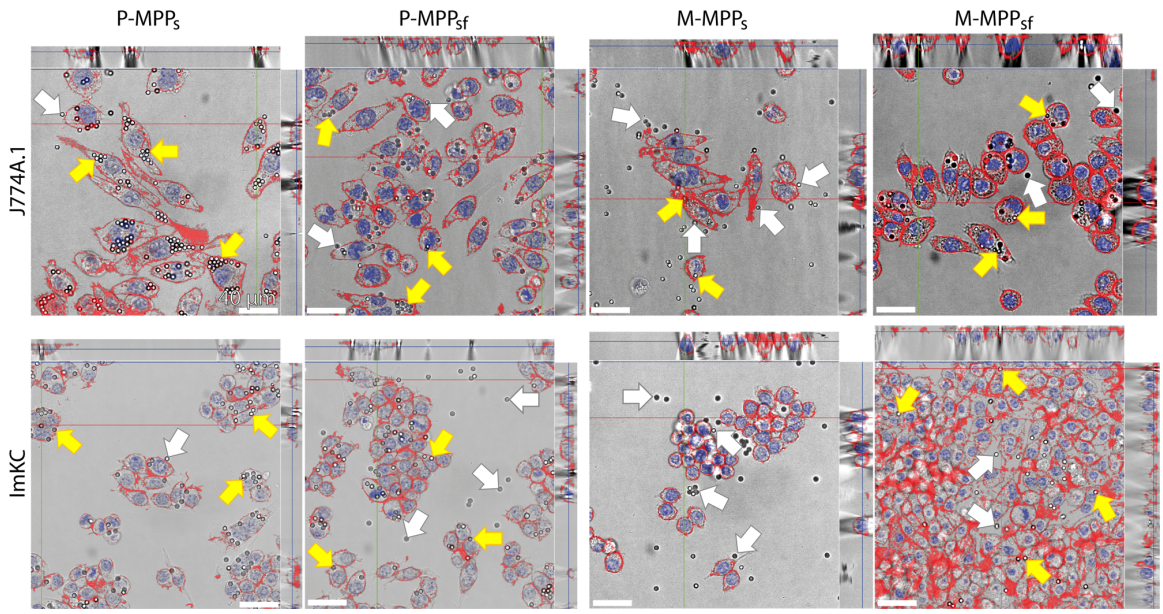

Abbildung 18: Aufnahme von Partikeln der beiden Partikelhersteller, PolySciences (P-MPP) und Micromod (M-MPP), in Makrophagen in serum-freien (sf) und serum-haltigem (s) Medium. Freie, nicht-aufgenommene Partikel sind beispielhaft mit weißen Pfeilen gekennzeichnet, während aufgenommene Partikel mit gelben Pfeilen angezeigt werden. Die Analyse erfolgte mittels Fluoreszenzmikroskopie, wofür das Zytoskellet mit Rhodamin-Phalloidin (rot) und die Zellkerne mittels DAPI (blau) angefärbt wurden. Für die Identifikation der nichtfluoreszierenden Partikel wurde zusätzlich Hellfeld verwendet. Skalenbalken wie angegeben.

Das Protein Komplement C3, welches in P-MPP, jedoch nicht in M-MPP gefunden wurde, ist ein bekanntes Opsonin und erleichtert die Erkennung durch Immunzellen wie Makrophagen [496, 497]. Komplementfaktor B, sowie Komplement C3, sind Proteine des alternativen Komplementweges und damit Bestandteil des adaptativen Immunsystems, welches Pathogene opsoniert und damit aus dem System entfernt [498, 499]. Dieser Aufnahmeweg wird durch die Bindung von C3b an Pathogenen ausgelöst, wobei das Protein C3b aus C3 entsteht [498, 499]. Dieser Aufnahmeweg wäre neben Pathogenen auch für Partikel denkbar, wobei C3b an die Partikeloberfläche binden könnte. BSA wurde als Hauptprotein in der Protein-Corona von M-MPP identifiziert. Es ist in der Literatur bekannt, dass BSA als Dysopsonin agiert und die zelluläre Aufnahme inhibiert oder verringert [413]. Allerdings kann das Vorhandensein von BSA nicht der einzige Grund für die verringerte Aufnahme von M-MPP sein, da bei Inkubation der P-MPP mit BSA (Vorbeschichtung mit BSA, siehe vorheriger Abschnitt) keine verringerte Aufnahme für Makrophagen und Epithelzellen gefunden werden konnte. Dabei sollte jedoch bedacht werden, dass die Proteine aus dem Serum bovine Proteine sind und nicht zwangsläufig mit den Zellmembranrezeptoren der murinen Zellen interagieren müssen. Trotzdem könnten die aufgeführten Proteine ein Grund für die vermehrte Aufnahme von P-

MPP sein, was einen indirekten Einfluss der physikochemischen Partikeleigenschaften auf die PZI unterstreicht.

Tabelle 2: Quantitative Analyse der Zusammensetzung der Protein-Corona mittels LC-MS/MS. 3 µm PS Partikel der Hersteller PolySciences (P-MPP) und Micromod (M-MPP) wurden in Zellkulturmedium (mit 10 % FCS) inkubiert. Der emPAI-Wert, der eine Abschätzung der Proteinhäufigkeit ermöglicht, ist in Klammern angegeben. Besonders erwähnte Proteine wurden in orange hervorgehoben.

P-MPP	M-MPP
Hämoglobin fetal subunit β (2,99)	BSA (2,78)
BSA (2,76)	Hämoglobin subunit α (1,08)
Serotransferrin (1,34)	Hämoglobin fetal subunit β (1,0)
Hämoglobin subunit α (1,08)	Serotransferrin (0,85)
α-2-HS-Glykoprotein (0,96)	α-2-HS-Glykoprotein (0,78)
Cathelicidin-2 (0,73)	Apolipoprotein A-I (0,64)
Apolipoprotein A-I (0,45)	α-1-Antiproteinase (0,5)
α-1-Antiproteinase (0,38)	
Fetuin-B (0,3)	
Gelsolin (0,21)	
Keratin, Typ II cytoskeletal (0,13)	
α-fetoprotein (0,11)	
Lactotransferrin (0,1)	
α-2-Makroglobulin (0,09)	
Komplementfaktor B (0,09)	
Komplement C3 (0,08)	

3.2.4 Unterschiede zwischen verschiedenen Polymerpartikeln

Neben Partikelgröße und Oberflächenmodifikation wurde auch das Material als entscheidender Faktor für die zelluläre Interaktion mit Partikeln in der Literatur beschrieben [494, 500]. Nachdem gezeigt werden konnte, dass die Vorbeschichtung von PS Partikeln einen Einfluss auf die Protein-Corona in serum-haltigem Medium und daraus resultierend die PZI hat (3.2.2 Einfluss einer artifiziellen Protein-Corona), sollten nun unterschiedliche Polymerpartikel auf ihr Verhalten mit Zelllinien untersucht werden. Als Kontrolle dienten PS Partikel, da hier die Interaktion bereits aus vorangegangenen Studien bekannt ist. Neben erdölbasierten Partikeln (PE, PS, PVC) wurden auch biobasierte (PLA und CA) Polymermikropartikel verwendet, wobei CA als nicht-zytotoxisch gilt, und eventuell auftretende zelluläre Effekte auf die Interaktion der Zellen mit Partikeln an sich und weniger auf das Material zurückgeführt werden können. Die CA Partikel wurden mittels Membran-Emulgierung selbst hergestellt (3.1.1 Herstellung von Celluloseacetat Partikeln). Die Analyse der Partikeleigenschaften erfolgte mittels REM, DLS und der Bestimmung des ζ-Potentials (Abb. 19).

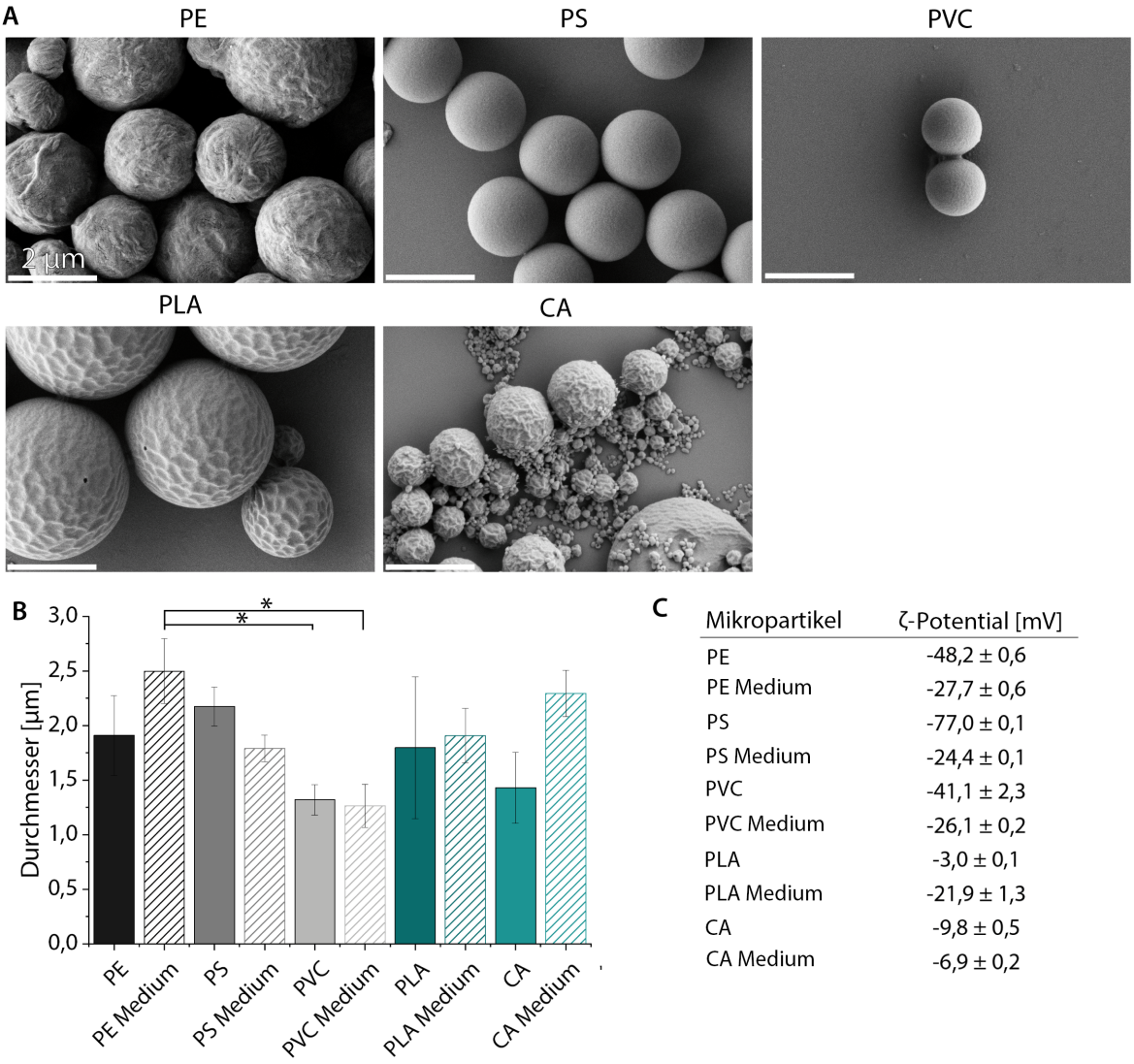

C

Mikropartikel	ζ-Potential [mV]
PE	-48,2 ± 0,6
PE Medium	-27,7 ± 0,6
PS	-77,0 ± 0,1
PS Medium	-24,4 ± 0,1
PVC	-41,1 ± 2,3
PVC Medium	-26,1 ± 0,2
PLA	-3,0 ± 0,1
PLA Medium	-21,9 ± 1,3
CA	-9,8 ± 0,5
CA Medium	-6,9 ± 0,2

Abbildung 19: Analyse der Partikeleigenschaften ausgewählter Polymermikropartikel mittels REM, DLS und ζ-Potentialmessungen. Als Polymermikropartikel dienten erdölbasierte Polymere (PE, PS und PVC), sowie biobasierte Polymere (PLA und CA). A: Elektronenmikroskopische Aufnahme der Mikropartikel. Skalenbalken wie angegeben. B und C: DLS und ζ-Potentialmessungen von pristinen und in Zellkulturmedium inkubierten („Medium“) Mikropartikeln. Nachdruck mit freundlicher Genehmigung des Verlags. Modifiziert nach Jasinski, J., Voelkl, M., Wilde, M., Jérôme, V., Fröhlich, T., Freitag, R. & Scheibel, T. Influence of the Polymer Type of a Microplastic Challenge on the Reaction of Murine Cells. *Journal of Hazardous Materials* **465**, 133280 (2024). Copyright (1969) Elsevier.

Hier konnten für PE, PLA und CA auffälligere Oberflächenmorphologien im Vergleich zu PS und PVC beobachtet werden (Abb. 19 A). Alle Partikel wiesen auch nach der Inkubation in Zellmedium einen hydrodynamischen Radius unter 2,5 µm auf (Abb. 19 B), womit von einer ähnlichen Größe der Partikel auch unter Zellkulturbedingungen ausgegangen werden kann. Die Analyse des ζ-Potentials zeigte große Unterschiede der pristinen Partikel (-77 mV für PS bis -3 mV für PLA), wobei die Inkubation in serumhaltigem Zellmedium die großen Unterschiede

jedoch fast vollständig ausglich (-28 mV bis -22 mV) (Abb. 19 C). Diese Angleichung wird möglicherweise durch die Adsorption der Serumproteine auf der Partikeloberfläche hervorgerufen. Die Ausnahme bildet CA, da hier auch nach der Inkubation in Zellmedium das ζ-Potential bei -7 mV lag. Die PZI wurde mittels konfokaler Mikroskopie untersucht, da hier auch zwischen aufgenommenen und mit der Oberfläche interagierenden Partikeln unterschieden werden kann (Abb. 20). Für Makrophagen (J774A.1 und ImKC) konnte für alle Polymerpartikel eine Internalisierung beobachtet werden, wobei CA eine leicht geringere Aufnahme zeigte. Zieht man hier das ζ-Potential von CA heran, welches im Vergleich zu den anderen Polymerpartikeln auch in Zellkulturumgebung vergleichsweise gering ist, stimmen diese Beobachtungen mit denen aus 3.2.3 (Physikochemische Eigenschaften von scheinbar gleichen Partikeln) überein. Auch da zeigten die PS Partikel mit dem geringeren ζ-Potential eine verringerte zelluläre Aufnahme. Damit konnte die Bedeutung des ζ-Potential von Partikeln für die PZI herausgestellt werden. Daraus lässt sich folgern, dass weniger das Polymer oder Material an sich für die PZI verantwortlich ist, sondern vielmehr dessen Oberfläche, oder spezifischer das ζ-Potential. PLA Partikel wiesen dabei eine höhere Verteilung der Partikelgröße auf als vorher mittels REM und DLS erkennbar war. Nichtsdestotrotz konnten auch für vergleichsweise große (ca. 10 µm) Partikel eine Aufnahme in den beiden Makrophagenzelllinien beobachtet werden. Das unterstreicht, dass Makrophagen mittels Phagozytose auch größere partikuläre Materialien aufnehmen können. Die Epithelzelllinien (STC-1 und BNL CL.2) wiesen eine geringere Partikelaufnahme im Vergleich zu Makrophagen auf, was mit der Beobachtung der ersten Studie (3.2.1 Größen- und Zelllinienabhängigkeit) übereinstimmt. Dabei konnte für STC-1 (Darmepithelzellen) lediglich eine sehr geringe Aufnahme von PS Partikeln beobachtet werden, auch wenn STC-1 Zellen mit allen Polymerpartikeln Interaktionen aufwiesen. Für BNL CL.2 (Leberepithelzellen) konnte neben der Aufnahme von PS Partikeln, welche die Ergebnisse der ersten Studie (3.2.1 Größen- und Zelllinienabhängigkeit) unterstreichen, auch eine Internalisierung von PE und CA Partikeln gefunden werden.

Mit Hilfe von LC-MS/MS ließen sich die an die Partikeloberfläche gebundenen Proteine identifizieren. Hier konnten wir die Adsorption von Serumproteinen an der Oberfläche der Polymerpartikel bestätigen, und bei allen Polymermikropartikeln war BSA das am häufigsten vorkommende Protein in der Protein-Corona. Durch die Kategorisierung der gefundenen Proteine anhand ihrer Beteiligung an biologischen Prozessen oder molekularbiologischen Funktionen ließen sich Unterschiede feststellen. PE und PS Mikropartikel wiesen eine ähnliche Proteinzusammensetzung, insbesondere hinsichtlich der Proteine, die am Sauerstofftransport, der Zelladhäsion oder der zellulären Mobilität beteiligt sind, auf.

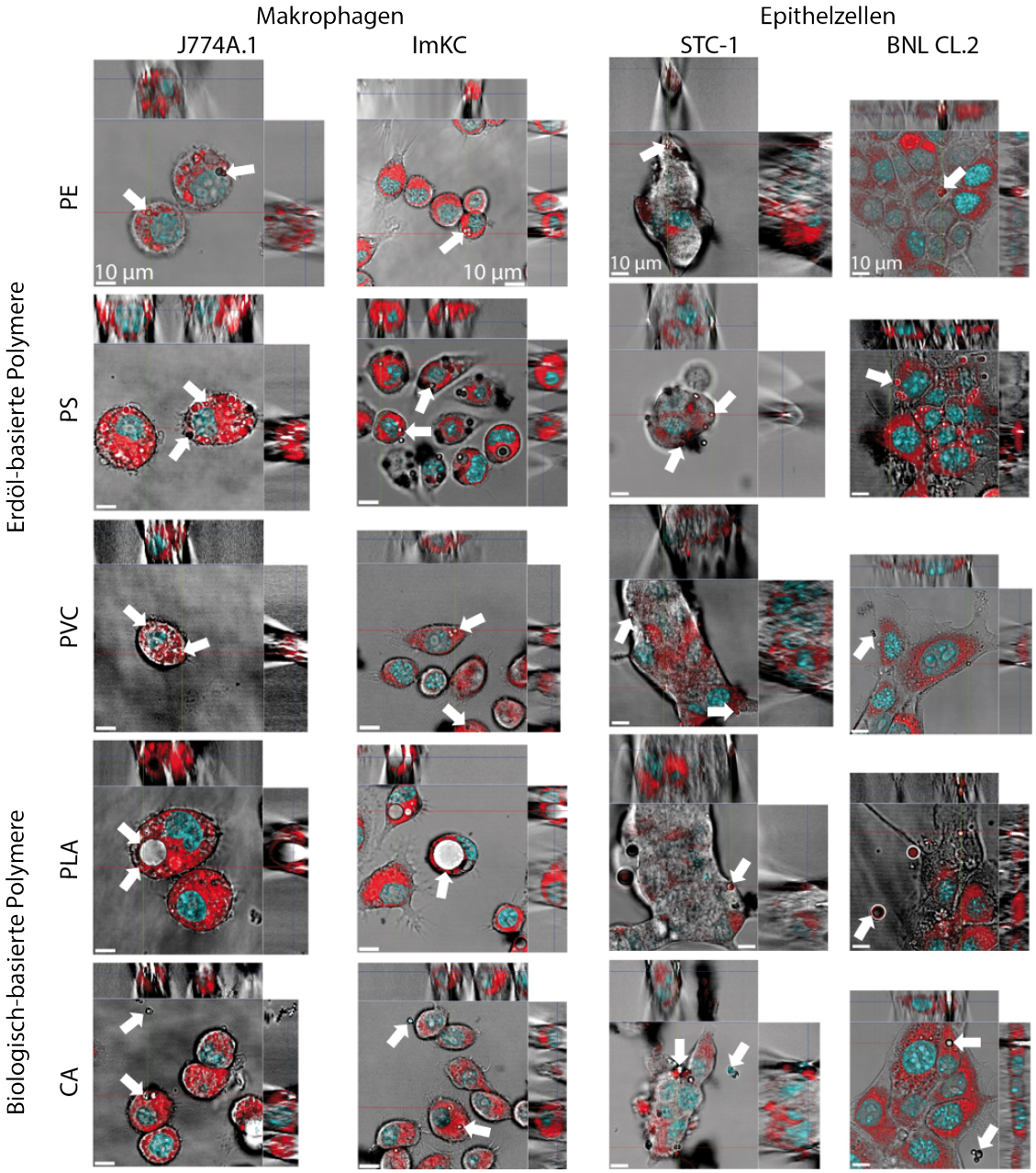

Abbildung 20: Mikroskopische Analyse der Partikelaufnahme ausgewählter Polymermikropartikel in murinen Makrophagen (J774A.1 und ImKC). Partikel wurden beispielhaft mit weißen Pfeilen gekennzeichnet. Die Analyse erfolgte mittels Fluoreszenzmikroskopie (CLSM), wofür das Zytoskelett mit Rhodamin-Phalloidin (rot) und die Zellkerne mittels DAPI (blau) angefärbt wurden. Für die Identifikation der nicht-fluoreszierenden Partikel wurde zusätzlich Hellfeld verwendet. Skalenbalken wie angegeben. Nachdruck mit freundlicher Genehmigung des Verlags. Modifiziert nach Jasinski, J., Voelkl, M., Wilde, M., Jérôme, V., Fröhlich, T., Freitag, R. & Scheibel, T. Influence of the Polymer Type of a Microplastic Challenge on the Reaction of Murine Cells. *Journal of Hazardous Materials* **465**, 133280 (2024). Copyright (1969) Elsevier.

Der Hauptunterschied zwischen PE und PS Mikropartikeln bestand in der Quantität von Transporterproteinen, welche häufiger in der Protein-Corona von PE zu finden sind; sowie

nicht-charakterisierten Proteinen, die in PS Partikeln häufiger vorkommen. Bemerkenswert ist, dass Proteine, die am Immunsystem und an der Aktivierung der Immunantwort beteiligt sind, hauptsächlich an PS Partikeln zu finden sind, während CA Mikropartikel die geringste Menge dieser Proteine in der Protein-Corona aufweisen. Im Gegensatz dazu wiesen CA Partikel die größte Menge an Ionen- und Metalltransportproteinen auf. Die geringere Anzahl an Immunsystem-assoziierten Proteinen in der Protein-Corona von CA Partikeln kann, neben dem ζ-Potential, ein weiterer Grund für eine geringere zelluläre Aufnahme sein, insbesondere bei Immunzellen wie Makrophagen. Makrophagen können sowohl Krankheitserreger als auch bestimmte Stoffe durch Phagozytose aufnehmen, einem spezialisierten und Rezeptor-vermittelten Aufnahmemechanismus [268, 501, 502]. Dabei können an der Partikeloberfläche adsorbierte Serumproteine, d.h. Opsonine wie Fetuin a oder Komplement C3, mit den Zellmembranrezeptoren interagieren und die Phagozytose von Mikropartikeln durch Makrophagen initiieren [503, 504], wie es bereits für P-MPP in Abschnitt 3.2.3 (Physikochemische Eigenschaften von scheinbar gleichen Partikeln) beschrieben wurde. So könnten PS Partikel aufgrund der höheren Anzahl von Opsoninen in ihrer Protein-Corona in größerer Zahl oder leichter aufgenommen werden als CA Partikel. PVC und PLA Partikel wiesen eine große Menge an Proteinen auf, die an der zellulären Adhäsion und der zellulären Mobilität beteiligt sind, welche die Interaktion mit den Zelllinien erklären könnten. Die zelluläre Interaktion mit den unterschiedlichen Polymerpartikeln hatte keinen toxischen Einfluss auf Zellen, wie eine Analyse mittels MTT indizierte. Damit konnte gezeigt werden, dass ein potentiell toxischer Einfluss von Mikropartikeln nicht von den Polymeren an sich hervorgerufen wird. Allerdings war der Einfluss der biobasierten Partikel auf die ROS-Produktion bei Makrophagen erhöht im Vergleich zu erdölbasierten Partikeln. Bei Epithelzellen führte die Inkubation mit den biobasierten Partikeln im Vergleich zu erdölbasierten Partikeln nur zu einer leichten Erhöhung der ROS-Produktion. Hierbei ist zu beachten, dass Epithelzellen, im Gegensatz zu Makrophagen keine oder eine deutlich geringere Aufnahme der biobasierten Partikeln aufwiesen. Eine mögliche Hypothese hierzu ist, dass biobasierte Partikel in Makrophagen, beispielsweise durch lysosomale Enzyme oder eine pH-Wert Veränderung, angegriffen werden, und die freigesetzten Monomere oder Oligomere einen Einfluss auf die zelluläre Entwicklung haben. Allerdings konnte dies bisher weder be- noch widerlegt werden. Zusammenfassend unterstreichen diese Ergebnisse die Hypothese, dass die Oberflächeneigenschaften des Mikropartikels für die zelluläre Interaktion eine wichtigere Rolle spielt als der Polymertyp an sich.

3.3 Wie verhalten sich Mikroplastikpartikel in Zellen?

In der Literatur wie auch in der vorliegenden Arbeit wurde die Aufnahme von Mikropartikeln in verschiedenen Zelllinien beobachtet. Es konnte bis jetzt noch keine zelluläre Freisetzung von Mikropartikeln gezeigt werden, allerdings schon von Nanopartikeln [485, 505]. Des Weiteren wurden verschiedene zelluläre Effekte in Hinblick auf die mitochondriale Aktivität oder DNA-Integrität nach der Inkubation mit Mikroplastikpartikeln beschrieben, welche eine Ko-Lokalisierung nahelegen [506, 507]. Dadurch ergibt sich die Frage nach dem Verbleib der Mikropartikel nach der zellulären Aufnahme. Genauso unklar ist das Verhalten von aufgenommenen Mikropartikeln bei der Zellteilung und die eventuelle Verteilung an Tochterzellen. Für die Analyse des intrazellulären Verbleibs der Mikropartikel wurde eine Fluoreszenzfärbung von ausgewählten Organellen (Mitochondrien, Endoplasmatisches Retikulum (ER), Golgi Apparat, frühe und späte Endosomen, sowie Lysosomen) durchgeführt. Dabei wurden Mitochondrien aufgrund der beschriebenen mitochondrialien Effekte nach einer Inkubation mit Mikropartikeln ausgewählt. Der Golgi-Apparat und das ER wurden untersucht, da sie Teil der intrazellulären Transportmaschinerie sind und als Endpunkt nach der Caveolin-vermittelten Aufnahme beschrieben wurden [267]. Der Transport nach der Endozytose erfolgt über Vesikel wie Endosomen, welche eine hierarchische Alterung über frühe Endosomen und späte Endosomen durchlaufen [508, 509]. Späte Endosomen fusionieren anschließend mit Lysosomen [508, 509]. Aus diesem Grund wurden diese beiden Organellen, Endosomen und Lysosomen, untersucht. Zusätzlich wurde das komplette Zytoplasma als Kontrolle für die Internalisierung der Partikel angefärbt (Abb. 21). Für eine einfachere Partikel-Lokalisation in Zellen wurden fluoreszierende PS Partikel verwendet. Eine Untersuchung der Größenabhängigkeit in der Ko-Lokalisation mit Zellorganellen wurde durch die Verwendung von unterschiedlich großen (0,2, 0,5 und 3 µm) Partikeln realisiert. Alle aufgenommenen Partikel konnten im Zytoplasma gefunden werden (Abb. 21). Interessanterweise wurde für 3 µm Partikel trotz einer Internalisierung keine Gelbfärbung mit dem Zytoplasma gefunden, wie es bei den kleineren Partikel der Fall war und was auf eine Ko-Lokalisation schließen lässt. Dies lässt sich durch eine Verdrängung des Zytoplasmas erklären, wodurch eine ungefärbte Höhle im Zytoplasma zurückbleibt. Abhängig von der Partikelgröße wurden ebenfalls einzelne Partikel im Endoplasmatischen Retikulum (0,2 und 0,5 µm, Abb. 21 A) oder in frühen und späten Endosomen (0,5 µm) gefunden (Abb. 21 B). Unabhängig von der Größe wurden keine Partikel in Mitochondrien, Lysosomen und dem Golgi Apparat beobachtet. Daher konnte die zuvor beschriebene mitochondriale Schädigung nicht auf einem direkten Kontakt zwischen den Mitochondrien und den Partikeln zurückgeführt werden. Für die 3 µm Partikel ist aufgrund des im Vergleich zu den Organellen

großen Partikeldurchmessers eine Lokalisierung mit Organellen nicht zu erwarten. Eine Exozytose von Goldnanopartikeln (2-40 nm) über Lysosomen wurde in der Literatur beschrieben [485, 505]. Koval und Preiter zeigten eine Translokation von 0,2 bis 0,75 µm IgG-PS Partikeln in Lysosomen. Größere Partikel (1 µm) wurden jedoch nicht in den Lysosomen gefunden [420, 510]. Da hier keine Partikel in den Lysosomen gefunden wurden, könnte man davon ausgehen, dass keine Exozytose von Partikeln zu erwarten ist. Um einen möglichen Exozytoseweg besser abschätzen zu können, wurden zusätzlich Endosomen durch eine Antikörperfärbung gegen EEA1 (frühe Endosomen) und Rab7 (späte Endosomen) untersucht. EEA1 (engl. *early endosome antigen 1*) ist ausschließlich in frühen Endosomen lokalisiert und spielt durch die Vermittlung von Membranfusionen eine wichtige Rolle im endosomalen Transport [511]. Das Protein Rab7 (engl. *ras-related protein Rab-7*), wurde vorwiegend in späten Endosomen gefunden und ist am Transport von Endosomen von frühen zu späten endozytischen Zellkompartimenten beteiligt [512]. Für 0,5 µm Partikel wurde in den späten Endosomen für beide Zelllinien eine Translokation beobachtet (Abb. 21). Dem hierarchischen endozytischen Weg folgend sollten die kleinen Partikel, wenn sie die späten Endosomen erreicht haben, auch in den Lysosomen zu finden sein [513]. Allerdings muss bedacht werden, dass Rab7-Proteine nicht nur in den späten Endosomen, sondern auch in den späten Phagosomen und Makropinosomen exprimiert werden [513–516]. Dies ist auch bei EEA1 der Fall, sodass die EEA1-Färbung des frühen Endosoms auch die Färbung des frühen Phagosoms oder Makropinosoms darstellen kann [513, 516]. Da die zelluläre Aufnahme bei beiden Zelllinien hauptsächlich auf Phagozytose beruht [517], könnte dies ein Hinweis darauf sein, dass 0,5 µm große Partikel im frühen und/oder späten Phagosom lokalisiert sein könnten. Zusammen mit der fehlenden Lokalisierung in den Lysosomen könnte dies bedeuten, dass die Partikel nach dem Phagosom kein Phagolysosom bilden [420, 510, 515]. Folgt man der Annahme, dass die frühen und späten Phagosomen zusätzlich zu den Endosomen gefärbt werden, könnte dies die Unterschiede in der Lokalisierung der 0,2 µm und 0,5 µm Partikeln erklären. Hier werden kleine Partikel wie 0,2 µm PS Partikel über einen anderen endozytischen Weg aufgenommen (z. B. Clathrin- oder Calveolin-vermittelter Weg), als 0,5 µm Partikel die möglicherweise durch Phagozytose oder Makropinozytose aufgenommen wurden [268, 517] und in ein Phagosom oder Makropinosom verpackt werden. Da 0,2 µm Partikel möglicherweise über Clathrin- oder Calveolin-vermittelte Wege anstelle von Phagozytose oder Makropinozytose aufgenommen wurden, wird kein Phagosom/Makropinosom gebildet und daher auch keine Ko-Lokalisation festgestellt [268, 517, 518]. Lysosomen sind dafür bekannt, dass sie an der Beseitigung von Krankheitserregern beteiligt sind, weshalb eine Ko-Lokalisierung mit PS Partikeln nach der Aufnahme vermutet

wurde [261, 519, 520]. Die fehlende Ko-Lokalisierung mit Lysosomen könnte darauf zurückzuführen sein, dass die Zellen die Partikel nicht als Bedrohung oder Krankheitserreger erkennen, welcher entfernt werden muss.

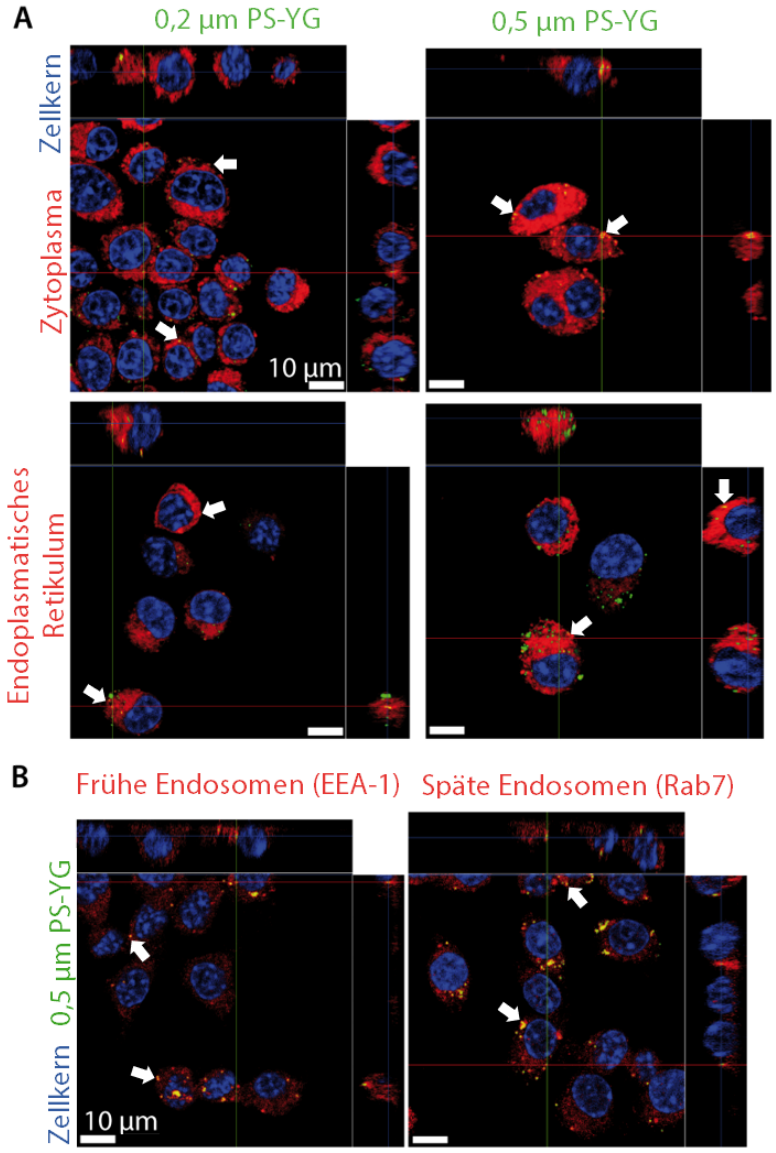

Abbildung 21: Ko-Lokalisation von PS Partikeln unterschiedlicher Größe (0,2 und 0,5 µm) mit ausgewählten Zellorganellen in murinen Makrophagen (ImKC). A: Ko-Lokalisation im Zytoplasma und dem Endoplasmatischen Retikulum. B: Ko-Lokalisierung von 0,5 µm Partikeln mit Endosomen. Frühe und späte Endosomen wurden mit Antikörpern angefärbt (EEA-1 bzw. Rab7). Die jeweiligen Organellen sind in rot dargestellt. Zusätzlich wurden die Zellkerne mittels HOECHST (blau) gefärbt. Die PS Partikel weisen eine grüne Fluoreszenz auf. Eine Ko-Lokalisation wird durch eine gleichzeitige Färbung (Gelbfärbung) zwischen den rot gefärbten Organellen und grün fluoreszierenden Partikeln angezeigt, hervorgehoben durch weiße Pfeile. Skalenbalken wie angegeben. Nachdruck mit freundlicher Genehmigung des Verlags. Modifiziert nach Jasinski, J., Völkl, M., Hahn, J., Jérôme, V., Freitag, R., & Scheibel, T. Polystyrene Microparticle Distribution After Ingestion by Murine Macrophages. *Journal of Hazardous Materials*, **457**, 131796 (2023). Copyright (1969) Elsevier.

Es wurden Unterschiede zwischen den Makrophagen-Zelllinien festgestellt, da nur wenige 0,5 µm große Partikel in den späten Endosomen/Phagosomen in J774A.1-Zellen und keine in den frühen Endosomen/Phagosomen gefunden wurden. Im Gegensatz dazu wurden in ImKC sowohl in frühen als auch in späten Endosomen 0,5 µm große Partikel identifiziert. Dies könnte durch den Phänotyp der Zellen erklärt werden, da die Geschwindigkeit der Phagosomenreifung vom Aktivierungsstatus der Makrophagen abhängt [521]. Hier zeigten die M1-Makrophagen eine langsamere Phagosomenreifung im Vergleich zu M0- und M2-Makrophagen. Es kann davon ausgegangen werden, dass Mikroplastikpartikel in Makrophagen über Phagozytose aufgenommen und anschließend in Phagosomen abgeschnürt werden. Die Geschwindigkeit und das Ausmaß der Phagosomenreifung kann je nach Aktivierungsstatus der Makrophagen unterschiedlich sein [521]. Wie in dieser Teilarbeit durch Matthias Völkl gezeigt, wiesen nichtaktivierte (M0) ImKC mehr CD80 (M1-Marker) auf als J774A.1. Dies könnte die Kinetik der Phagosomenreifung beeinflussen. Bei ImKC-Zellen könnte diese Reifung langsamer sein, sodass eine Ko-Lokalisierung der Partikel im frühen und späten Endosom sichtbar ist. In J774A.1 reifen die Phagosomen schneller, was zu einer vergangenen und nicht mehr nachweisbaren Ko-Lokalisierung mit dem frühen Endosom/frühen Phagosom führen würde. Generell sind die Ko-Lokalisationsergebnisse mit Vorsicht zu interpretieren, da wir nur einen Zeitpunkt analysiert haben (nach einer 15-stündigen Inkubation) und die Möglichkeit besteht, dass die Partikel entweder die Organellen noch nicht erreicht haben oder bereits außerhalb der Organellen transportiert wurden. Hier wäre eine kinetische Analyse erforderlich, um die intrazellulären Wege aufzudecken. Daneben wurde das Verhalten der Partikel während der Zellteilung, sowie eine mögliche Partikelfreisetzung mittels Zeitraffer-Mikroskopie an lebenden Zellen (engl. *live-cell time-lapse microscopy*) analysiert (Abb. 22). Die Beobachtung der zellulären Aufnahme zeigte starke Unterschiede innerhalb einer Zellpopulation. So wurden Zellen beobachtet, die viele Partikel aufnahmen, während andere Zellen keine Partikel internalisierten. Dies war bereits anhand mikroskopischer Analysen, beispielsweise der konfokalen Mikroskopie in der ersten Studie (3.2.1 Größen- und Zelllinienabhängigkeit), zu beobachten und unterstreicht diese Ergebnisse. Durch eine Untersuchung mit M1 und M2 gezielt polarisierten Makrophagen war es möglich, eine Teilerklärung dafür zu liefern. Dabei waren M1 polarisierte Makrophagen deutlich effektiver in der Partikelaufnahme als unpolarisierte oder M2 polarisierte Makrophagen. Für die Zellteilung konnte gezeigt werden, dass die Verteilung der Partikel an die Tochterzellen zufällig und nicht symmetrisch abläuft. Eine Halbierung der Partikel bei der Zellteilung wurde nicht gezeigt. Das konnte beispielsweise in Abb. 22 mit roten Kreisen hervorgehoben gezeigt werden.

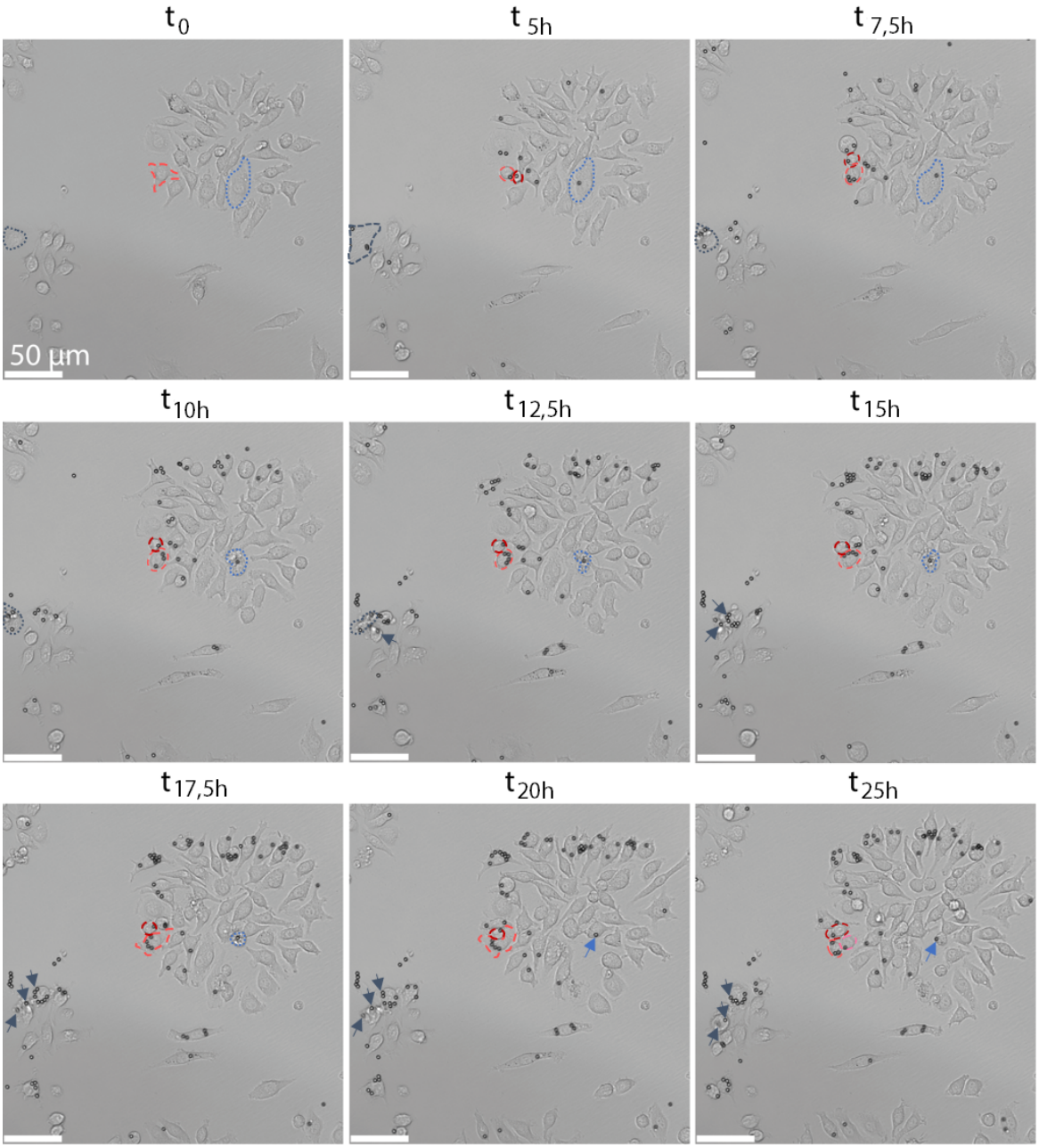

Abbildung 22: Analyse der Aufnahme und Freisetzung, sowie der Verteilung während der Zellteilung von 3 µm PS Partikeln in murinen Makrophagen (ImKC) über 25 Stunden. Die Partikelverteilung während der Zellteilung wurde mit roten Umkreisungen markiert. Blaue Markierungen zeigen apoptotische Zellen (blaue Umkreisung) mit aufgenommenen Partikeln, wobei die durch die Apoptose freigesetzen Partikel durch die Nachbarzellen aufgenommen (blaue Pfeile) werden. Skalenbalken wie angegeben. Nachdruck mit freundlicher Genehmigung des Verlags. Modifiziert nach Jasinski, J., Völkl, M., Hahn, J., Jérôme, V., Freitag, R., & Scheibel, T. Polystyrene Microparticle Distribution After Ingestion by Murine Macrophages. *Journal of Hazardous Materials*, **457**, 131796 (2023). Copyright (1969) Elsevier.

Eine Zelle mit vier aufgenommenen Partikeln resultierte in zwei Tochterzellen, wobei eine Tochterzelle drei Partikel und die andere Tochterzelle einen Partikel enthielt. Dies wurde

zusätzlich durchflusszytometrisch quantifiziert und bestätigt. Mittels Zeitraffer-Mikroskopie konnte keine aktive Freisetzung der Partikel beobachtet werden. Allerdings wurden bei Zelltod die von der entsprechenden Zelle internalisierten Partikel, wie alle Zellbestandteile, freigesetzt (Abb. 22 blaue Kreise). Diese können dann von Nachbarzellen, ebenfalls wie alle anderen Zellbestandteile, aufgenommen werden. Auch dies konnte mittels Zeitraffer-Mikroskopie (Abb. 22 blaue Pfeile) gezeigt werden. Da nur wenige Partikel in bestimmten Organellen (Endoplasmatisches Retikulum, Endosomen) gefunden wurden, kann angenommen werden, dass die Partikel nicht aktiv in bestimmten Organellen angereichert werden. Während die Partikel durch den Zelltod freigesetzt wurden, wurde keine aktive Exozytose beobachtet. Benachbarte Zellen nahmen die freigesetzten Partikel zusammen mit Zelltrümmern wieder auf. Daher kann präsumiert werden, dass die aufgenommenen Partikel nicht in großer Zahl freigesetzt werden, was zu einer Akkumulation führt und somit potenzielle Langzeiteffekte möglich sind.

3.4 Wie verhalten sich Modell-Polymermikropartikel in 3D Zellsystemen?

2D-Zellkulturen können nicht alle mechanischen und biochemischen Signale, die *in vivo* vorhanden sind, originalgetreu nachbilden [327, 522]. So überwiegen bei 2D-Zellkulturen die Wechselwirkungen von Zelle zu Plastik und nicht die entscheidenden Wechselwirkungen von Zelle zu Zelle und Zelle zu extrazellulärer Matrix (EZM) [522, 523]. Um eine realistischere Einordnung der Interaktion mit Mikroplastik zu erhalten, wurden im letzten Teilprojekt multizelluläre Sphäroide aus Leberepithelzellen gezüchtet. Sphäroide bilden sich durch Aggregation und Selbstorganisation von Zellen, wenn eine Oberfläche fehlt an welcher sie anheften können. Die Selbstorganisation ahmt dabei natürliche Prozesse nach, die während der Embryogenese, Morphogenese und Organogenese ablaufen [522, 524]. Sphäroide können in einem Größenbereich von bis zu 700 µm die architektonischen und funktionellen Merkmale von natürlichem Gewebe imitieren [330, 522]. In diesem Teilprojekt wurden selbst hergestellte PS Partikeln mit definierter Oberfläche verwendet (siehe 3.1.2 Herstellung von fluoreszierenden Partikeln mittels NITEC), und deren Anwendung in 2D und 3D Zellkultur untersucht. Dabei war die definierte Oberfläche besonders wichtig, da in 3.2.3 (Physikochemische Eigenschaften von scheinbar gleichen Partikeln) bereits gezeigt wurde, dass kommerzielle Partikel Unterscheide aufweisen und nicht zwangsläufig vergleichbar sind. Da bereits in den vorangegangenen Teilstudien gezeigt wurde, dass das ζ-Potential eines der wichtigsten Oberflächencharakteristika für die zelluläre Interaktion ist, wurde dieses auch für die selbst hergestellten Partikel bestimmt. Dies lag mit -24,1 $\pm$ 3,7 mV in KCl, beziehungsweise -17,8 $\pm$ 1,2 mV in Zellmedium, über dem der kommerziell erwerbbaren PS Partikel. Allerdings waren die Unterschiede

unter Zellkulturbedingungen nicht signifikant. Die Untersuchung der Partikel-Zellinteraktion wurde mit den bereits vorher verwendeten Zelllinien (J774A.1, ImKC, STC-1 und BNL CL.2) durchgeführt, um die Ergebnisse mit denen aus 3.2.1 (Größen- und Zelllinienabhängigkeit) vergleichen zu können (Abb. 23 2D Monolayer). Dabei konnten Unterschiede zu kommerziellen PS Partikel aufgezeigt werden, da auch in STC-1 Zellen eine Internalisierung der Partikel festgestellt wurde. Kommerzielle PS Partikel mit diesem Durchmesser (2 µm) zeigten keine Internalisierung in STC-1 Zellen. Für die anderen Zelllinien wurde, analog zu den kommerziellen PS Partikel, eine Internalisierung beobachtet. Für die 3D Zellkultur, also die Bildung und Analyse von Sphäroiden, wurden die Epithelzellen weiter verwendet. STC-1 (Darmepithel-) Zellen zeigten jedoch keine Sphäroidbildung, wohingegen für BNL CL.2 (Leberepithel-) Zellen Sphäroide sowohl mittels der *liquid overlay* Technik, als auch mit nicht-adhäsiven Hydrogelen gezüchtet werden konnten.

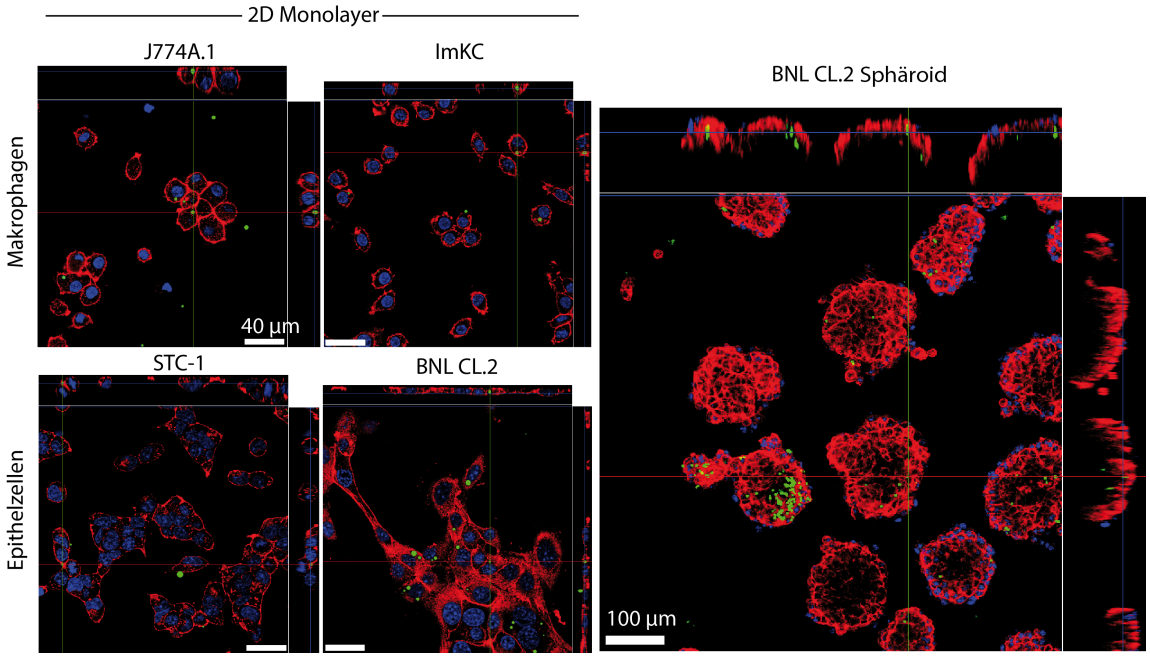

Abbildung 23: Zelluläre Interaktion von selbst hergestellten PS Partikeln in 2D Zellmonolayern (Makrophagen J774A.1 und ImKC, sowie Epithelzellen STC-1 und BNL CL.2). Zusätzlich wurden aus BNL CL.2 Epithelzellen Sphäroide auf Methylcellulose gezüchtet (3D) und mit PS Partikeln inkubiert. Für die Analyse mittels Fluoreszenzmikroskopie wurden das Aktinzytoskellets (rot) und die Zellkerne (blau) gefärbt, während die Partikel eine grüne Fluoreszenz aufweisen. Skalenbalken wie angegeben.

Bei der *liquid overlay* Technik wird die Anheftung von Zellen an Gewebekulturplatten gehemmt und gleichzeitig die Zell-Zell-Aggregation gefördert [522, 525]. Dabei werden die Zellen in einer Suspension auf flache Gewebekulturschalen mit wenig haftenden Oberflächen wie Agarose ausgesät. Die resultierenden Sphäroide waren jedoch sehr groß (ca. 500- 1000 µm)

und eher flach. Alternativ wurden nicht-adhäsive, 12%-ige Methylcellulose-Hydrogele verwendet, welche die EZM imitieren sollen [526, 527]. Die resultierenden Sphäroide waren deutlich kleiner (100- 200 µm) und zeigten eine sphärische Form, allerdings führte die hohe Viskosiät des Hydrogels teilweise zu einer ungleichmäßigen Verteilung auf der Kulturplatte und daher zu inhomogenen Sphäroiden. Die Inkubation der selbst hergestellten PS Partikel mit Lebersphäroiden zeigte eine Translokation der Partikel in den Sphäroiden (Abb. 23 BNL CL.2 Sphäroid). Bereits in 2D wurde für BNL CL.2 Zellen eine Aufnahme der Partikel beschrieben. Daher wäre eine Translokation der Partikel durch die zelluläre Aufnahme der Epithelzellen denkbar, welche die Partikel in das Sphäroidinnere exkretieren. Allerdings konnte bis jetzt nicht abschließend geklärt werden, ob die Partikel nicht auch zufällig im Sphäroid gefunden wurden und beispielsweise die Zellen um die Partikel herum gewachsen sind. Dies könnte unter Anderem mittels Zeitraffer-Mikroskopie (*live-cell time-lapse microscopy*) untersucht werden. Nichtsdestotrotz unterstreicht die Translokation auch in Sphäroiden die vielfältige Anwendbarkeit der mittels NITEC-Reaktion hergestellten PS Partikel.

4 Literatur

1. Ozdemir, M., Yurteri, C. U. & Sadikoglu, H. Physical Polymer Surface Modification Methods and Applications in Food Packaging Polymers. *Critical Reviews in Food Science and Nutrition* **39,** 457–477 (1999).
2. Halden, R. U. Plastics and Health Risks. *Annual Review of Public Health* **31,** 179–194 (2010).
3. Leslie, H. Review of Microplastics in Cosmetics. *IVM Institute for Environmental Studies* (2014).
4. Fernqvist, F., Olsson, A. & Spendrup, S. What's in It for Me? Food Packaging and Consumer Responses, a Focus Group Study. *British Food Journal* **117,** 1122–1135 (2015).
5. Jabeen, N., Majid, I. & Nayik, G. A. Bioplastics and Food Packaging: A Review. *Cogent Food & Agriculture* **1,** 1117749 (2015).
6. Frias, J. & Nash, R. Microplastics: Finding a Consensus on the Definition. *Marine Pollution Bulletin* **138,** 145–147 (2019).
7. Thompson, R. C., Swan, S. H., Moore, C. J. & Vom Saal, F. S. Our Plastic Age. *Philosophical Transactions of the Royal Society B: Biological Sciences* **364,** 1973–1976 (2009).
8. Geyer, R. in *Mare Plasticum- The Plastic Sea* 31–47 (Springer, 2020).
9. Gilbert, M. in *Brydson's Plastics Materials* 1–18 (Elsevier, 2017).
10. Drzyzga, O. & Prieto, A. Plastic Waste Management, a Matter for the 'Community'. *Microbial Biotechnology* **12,** 66 (2019).
11. Plastics Europe. *Plastics - the Facts 2021* `https://plasticseurope.org/knowledge-hub/plastics-the-facts-2021/`. online; Zugriff am 14.03.2022. 2021.
12. International Organization for Standardization. *Plastics - Vocabulary (ISO 472:2013)* `https://www.iso.org/obp/ui/#iso:std:iso:472:ed-4:v1:en`. online; Zugriff am 14.03.2022. 2013.
13. Hartmann, N. B., Huffer, T., Thompson, R. C., Hassellöv, M., Verschoor, A., Daugaard, A. E., Rist, S., Karlsson, T., Brennholt, N., Cole, M., Herrling, M. P., Hess, M. C., Ivleva, N. P., L, L. A. & Wagner, M. Are We Speaking the Same Language? Recommendations for a Definition and Categorization Framework for Plastic Debris. *Environmental Science & Technology* **53,** 1039–1047 (2019).
14. Aminabhavi, T., Balundgi, R. & Cassidy, P. A Review on Biodegradable Plastics. *Polymer-Plastics Technology and Engineering* **29,** 235–262 (1990).
15. Huang, J.-C., Shetty, A. S. & Wang, M.-S. Biodegradable Plastics: A Review. *Advances in Polymer Technology* **10,** 23–30 (1990).
16. Hawkins, G. in *Accumulation* 63–81 (Routledge, 2013).
17. Havstad, M. R. in *Plastic Waste and Recycling* 97–129 (Elsevier, 2020).
18. Ghosh, K. & Jones, B. H. Roadmap to Biodegradable Plastics— Current State and Research Needs. *ACS Sustainable Chemistry & Engineering* **9,** 6170–6187 (2021).
19. Filiciotto, L. & Rothenberg, G. Biodegradable Plastics: Standards, Policies, and Impacts. *ChemSusChem* **14,** 56–72 (2021).
20. Kabasci, S. in *Plastic Waste and Recycling* 67–96 (Elsevier, 2020).
21. Greene, J. P. *Sustainable Plastics: Environmental Assessments of Biobased, Biodegradable, and Recycled Plastics* (John Wiley & Sons, 2014).

22. Henshaw, J. M., Han, W. & Owens, A. D. An Overview of Recycling Issues for Composite Materials. *Journal of Thermoplastic Composite Materials* **9,** 4–20 (1996).

23. Aguado, J., Serrano, D. & San Miguel, G. European Trends in the Feedstock Recycling of Plastic Wastes. *Global Nest Journal* **9,** 12–19 (2007).

24. Verma, R., Vinoda, K., Papireddy, M. & Gowda, A. Toxic Pollutants from Plastic Waste- A Review. *Procedia Environmental Sciences* **35,** 701–708 (2016).

25. Idumah, C. I. & Nwuzor, I. C. Novel Trends in Plastic Waste Management. *SN Applied Sciences* **1,** 1–14 (2019).

26. Brar, L. S. & Elsayed, K. Analysis and Optimization of Cyclone Separators with Eccentric Vortex Finders Using Large Eddy Simulation and Artificial Neural Network. *Separation and Purification Technology* **207,** 269–283 (2018).

27. Vanapalli, K. R., Sharma, H. B., Ranjan, V. P., Samal, B., Bhattacharya, J., Dubey, B. K. & Goel, S. Challenges and Strategies for Effective Plastic Waste Management during and Post COVID-19 Pandemic. *Science of The Total Environment* **750,** 141514 (2021).

28. Agamuthu, P. Challenges in Sustainable Management of Construction and Demolition Waste. *Waste Management & Research* **26,** 491–492 (2008).

29. Carr, S. A., Liu, J. & Tesoro, A. G. Transport and Fate of Microplastic Particles in Wastewater Treatment Plants. *Water Research* **91,** 174–182 (2016).

30. Prata, J. C., Silva, A. L. P., Da Costa, J. P., Mouneyrac, C., Walker, T. R., Duarte, A. C. & Rocha-Santos, T. Solutions and Integrated Strategies for the Control and Mitigation of Plastic and Microplastic Pollution. *International Journal of Environmental Research and Public Health* **16,** 2411 (2019).

31. Li, W. C., Tse, H. & Fok, L. Plastic Waste in the Marine Environment: A Review of Sources, Occurrence and Effects. *Science of the Total Environment* **566,** 333–349 (2016).

32. Derraik, J. G. The Pollution of the Marine Environment by Plastic Debris: A Review. *Marine Pollution Bulletin* **44,** 842–852 (2002).

33. Carpenter, E. J. & Smith Jr, K. Plastics on the Sargasso Sea Surface. *Science* **175,** 1240–1241 (1972).

34. Wong, C., Green, D. R. & Cretney, W. J. Quantitative Tar and Plastic Waste Distributions in the Pacific Ocean. *Nature* **247,** 30–32 (1974).

35. Thompson, R. C., Olsen, Y., Mitchell, R. P., Davis, A., Rowland, S. J., John, A. W., McGonigle, D. & Russell, A. E. Lost at Sea: Where Is All the Plastic? *Science* **304,** 838–838 (2004).

36. Andrady, A. L. & Neal, M. A. Applications and Societal Benefits of Plastics. *Philosophical Transactions of the Royal Society B: Biological Sciences* **364,** 1977–1984 (2009).

37. Wang, J., Zheng, L. & Li, J. A Critical Review on the Sources and Instruments of Marine Microplastics and Prospects on the Relevant Management in China. *Waste Management & Research* **36,** 898–911 (2018).

38. Browne, M. A., Galloway, T. & Thompson, R. Microplastic- An Emerging Contaminant of Potential Concern? *Integrated Environmental Assessment and Management* **3,** 559–561 (2007).

39. Andrady, A. L. Microplastics in the Marine Environment. *Marine Pollution Bulletin* **62,** 1596–1605 (2011).

40. Cole, M., Lindeque, P., Halsband, C. & Galloway, T. S. Microplastics as Contaminants in the Marine Environment: A Review. *Marine Pollution Bulletin* **62,** 2588–2597 (2011).

41. Zarfl, C., Fleet, D., Fries, E., Galgani, F., Gerdts, G., Hanke, G. & Matthies, M. Microplastics in Oceans. *Marine Pollution Bulletin* **62,** 1589–1591 (2011).

42. Wright, S. L., Thompson, R. C. & Galloway, T. S. The Physical Impacts of Microplastics on Marine Organisms: A Review. *Environmental Pollution* **178,** 483–492 (2013).

43. Woodall, L. C., Sanchez-Vidal, A., Canals, M., Paterson, G. L., Coppock, R., Sleight, V., Calafat, A., Rogers, A. D., Narayanaswamy, B. E. & Thompson, R. C. The Deep Sea is a Major Sink for Microplastic Debris. *Royal Society Open Science* **1,** 140317 (2014).

44. Galloway, T. S., Cole, M. & Lewis, C. Interactions of Microplastic Debris Throughout the Marine Ecosystem. *Nature Ecology & Evolution* **1,** 1–8 (2017).

45. Zhang, D., Liu, X., Huang, W., Li, J., Wang, C., Zhang, D. & Zhang, C. Microplastic Pollution in Deep-Sea Sediments and Organisms of the Western Pacific Ocean. *Environmental Pollution* **259,** 113948 (2020).

46. Amelia, T. S. M., Khalik, W. M. A. W. M., Ong, M. C., Shao, Y. T., Pan, H.-J. & Bhubalan, K. Marine Microplastics as Vectors of Major Ocean Pollutants and Its Hazards to the Marine Ecosystem and Humans. *Progress in Earth and Planetary Science* **8,** 1–26 (2021).

47. Moore, C. J. Synthetic Polymers in the Marine Environment: A Rapidly Increasing, Long-Term Threat. *Environmental Research* **108,** 131–139 (2008).

48. Vert, M., Doi, Y., Hellwich, K.-H., Hess, M., Hodge, P., Kubisa, P., Rinaudo, M. & Schué, F. Terminology for Biorelated Polymers and Applications (IUPAC Recommendations 2012). *Pure and Applied Chemistry* **84,** 377–410 (2012).

49. Gigault, J., Ter Halle, A., Baudrimont, M., Pascal, P.-Y., Gauffre, F., Phi, T.-L., El Hadri, H., Grassl, B. & Reynaud, S. Current Opinion: What Is a Nanoplastic? *Environmental Pollution* **235,** 1030–1034 (2018).

50. Hidalgo-Ruz, V., Gutow, L., Thompson, R. C. & Thiel, M. Microplastics in the Marine Environment: A Review of the Methods Used for Identification and Quantification. *Environmental Science & Technology* **46,** 3060–3075 (2012).

51. Lusher, A., Welden, N., Sobral, P. & Cole, M. Sampling, Isolating and Identifying Microplastics Ingested by Fish and Invertebrates. *Analytical Methods* **9,** 1346–1360 (2017).

52. Frias, J., Pagter, E., Nash, R., O'Connor, I., Carretero, O., Filgueiras, A., Viñas, L., Gago, J., Antunes, J., Bessa, F., Sobral, P., Goruppi, A., Tirelli, V., Pedrotti, M. L., Suaria, G., Aliani, S., Lopes, C., Raimundo, J., Caetano, M. & Gerdts, G. Standardised Protocol for Monitoring Microplastics in Sediments. Deliverable 4.2. *JPI-Oceans BASEMAN Project,* 24–37 (2018).

53. Kooi, M. & Koelmans, A. A. Simplifying Microplastic via Continuous Probability Distributions for Size, Shape, and Density. *Environmental Science & Technology Letters* **6,** 551–557 (2019).

54. Waldschläger, K. & Schüttrumpf, H. Infiltration Behavior of Microplastic Particles with Different Densities, Sizes, and Shapes—from Glass Spheres to Natural Sediments. *Environmental Science & Technology* **54,** 9366–9373 (2020).

55. Napper, I. E. & Thompson, R. C. Release of Synthetic Microplastic Plastic Fibres from Domestic Washing Machines: Effects of Fabric Type and Washing Conditions. *Marine Pollution Bulletin* **112,** 39–45 (2016).

56. Barrick, A., Champeau, O., Chatel, A., Manier, N., Northcott, G. & Tremblay, L. A. Plastic Additives: Challenges in Ecotox Hazard Assessment. *PeerJ* **9,** e11300 (2021).

57. Zubris, K. A. V. & Richards, B. K. Synthetic Fibers as an Indicator of Land Application of Sludge. *Environmental Pollution* **138,** 201–211 (2005).

58. Browne, M. A., Crump, P., Niven, S. J., Teuten, E., Tonkin, A., Galloway, T. & Thompson, R. Accumulation of Microplastic on Shorelines Woldwide: Sources and Sinks. *Environmental Science & Technology* **45,** 9175–9179 (2011).

59. De Falco, F., Di Pace, E., Cocca, M. & Avella, M. The Contribution of Washing Processes of Synthetic Clothes to Microplastic Pollution. *Scientific Reports* **9,** 1–11 (2019).

60. Fendall, L. S. & Sewell, M. A. Contributing to Marine Pollution by Washing Your Face: Microplastics in Facial Cleansers. *Marine Pollution Bulletin* **58,** 1225–1228 (2009).

61. Rockström, J., Steffen, W., Noone, K., Persson, Å., Chapin III, F. S., Lambin, E., Lenton, T. M., Scheffer, M., Folke, C., Schellnhuber, H. J., Nykvist, B., de Wit, C. A., Hughes, T., van der Leeuw, S., Rodhe, H., Sörlin, S., Snyder, P. K., Costanza, R., Svedin, U., Falkenmark, M., Karlberg, L., Corell, R. W., Fabry, V. J., Hansen, J., Walker, B., Liverman, D., Richardson, K., Crutzen, P. & Foley, J. Planetary Boundaries: Exploring the Safe Operating Space for Humanity. *Ecology and Society* **14** (2009).

62. Rockström, J., Steffen, W., Noone, K., Persson, Å., Chapin, F. S., Lambin, E. F., Lenton, T. M., Scheffer, M., Folke, C., Schellnhuber, H. J., Nykvist, B., de Wit, C. A., Hughes, T., van der Leeuw, S., Rodhe, H., Sörlin, S., Snyder, P. K., Costanza, R., Svedin, U., Falkenmark, M., Karlberg, L., Corell, R. W., Fabry, V. J., Hansen, J., Walker, B., Liverman, D., Richardson, K., Crutzen, P. & Foley, J. A. A Safe Operating Space for Humanity. *Nature* **461,** 472–475 (2009).

63. Steffen, W., Richardson, K., Rockström, J., Cornell, S. E., Fetzer, I., Bennett, E. M., Biggs, R., Carpenter, S. R., De Vries, W., De Wit, C. A., Folke, C., Gerten, D., Heinke, J., Mace, G. M., Persson, L. M., Ramanathan, V., Reyers, B. & Sörlin, S. Planetary Boundaries: Guiding Human Development on a Changing Planet. *Science* **347,** 1259855 (2015).

64. Persson, L., Carney Almroth, B. M., Collins, C. D., Cornell, S., de Wit, C. A., Diamond, M. L., Fantke, P., Hassellöv, M., MacLeod, M., Ryberg, M. W., Søgaard Jørgensen, P., Villarrubia-Gómez, P., Wang, Z. & Hauschild, M. Z. Outside the Safe Operating Space of the Planetary Boundary for Novel Entities. *Environmental Science & Technology* (2022).

65. Do Sul, J. A. I. & Costa, M. F. The Present and Future of Microplastic Pollution in the Marine Environment. *Environmental Pollution* **185,** 352–364 (2014).

66. Horton, A. A. & Dixon, S. J. Microplastics: An Introduction to Environmental Transport Processes. *Wiley Interdisciplinary Reviews: Water* **5,** e1268 (2018).

67. Evangeliou, N., Grythe, H., Klimont, Z., Heyes, C., Eckhardt, S., Lopez-Aparicio, S. & Stohl, A. Atmospheric Transport Is a Major Pathway of Microplastics to Remote Regions. *Nature Communications* **11,** 1–11 (2020).

68. Waldschläger, K., Lechthaler, S., Stauch, G. & Schüttrumpf, H. The Way of Microplastic through the Environment–Application of the Source-Pathway-Receptor Model. *Science of the Total Environment* **713,** 136584 (2020).

69. Lusher, A. L., Burke, A., O'Connor, I. & Officer, R. Microplastic Pollution in the Northeast Atlantic Ocean: Validated and Opportunistic Sampling. *Marine Pollution Bulletin* **88,** 325–333 (2014).

70. Everaert, G., De Rijcke, M., Lonneville, B., Janssen, C., Backhaus, T., Mees, J., van Sebille, E., Koelmans, A., Catarino, A. I. & Vandegehuchte, M. B. Risks of Floating Microplastic in the Global Ocean. *Environmental Pollution* **267,** 115499 (2020).

71. Wagner, M., Scherer, C., Alvarez-Muñoz, D., Brennholt, N., Bourrain, X., Buchinger, S., Fries, E., Grosbois, C., Klasmeier, J., Marti, T., Rodriguez-Mozaz, S., Urbatzka, R., Vethaak, A. D., Winther-Nielsen, M. & Reifferscheid, G. Microplastics in Freshwater Ecosystems: What We Know and What We Need to Know. *Environmental Sciences Europe* **26,** 1–9 (2014).

72. Dris, R., Imhof, H., Sanchez, W., Gasperi, J., Galgani, F., Tassin, B. & Laforsch, C. Beyond the Ocean: Contamination of Freshwater Ecosystems with (Micro-) Plastic Particles. *Environmental Chemistry* **12,** 539–550 (2015).

73. Li, J., Liu, H. & Chen, J. P. Microplastics in Freshwater Systems: A Review on Occurrence, Environmental Effects, and Methods for Microplastics Detection. *Water Research* **137,** 362–374 (2018).

74. Rezania, S., Park, J., Din, M. F. M., Taib, S. M., Talaiekhozani, A., Yadav, K. K. & Kamyab, H. Microplastics Pollution in Different Aquatic Environments and Biota: A Review of Recent Studies. *Marine Pollution Bulletin* **133,** 191–208 (2018).

75. Sun, J., Dai, X., Wang, Q., van Loosdrecht, M. C. & Ni, B.-J. Microplastics in Wastewater Treatment Plants: Detection, Occurrence and Removal. *Water Research* **152,** 21–37 (2019).

76. Stanton, T., Johnson, M., Nathanail, P., MacNaughtan, W. & Gomes, R. L. Freshwater Microplastic Concentrations Vary through Both Space and Time. *Environmental Pollution* **263,** 114481 (2020).

77. Rillig, M. C. Microplastic in Terrestrial Ecosystems and the Soil? *Environmental Science & Technology* **46,** 6453–6454 (2012).

78. Rillig, M. C., Ingraffia, R. & de Souza Machado, A. A. Microplastic Incorporation intoSsoil in Agroecosystems. *Frontiers in Plant Science* **8,** 1805 (2017).

79. Townsend, K. R., Lu, H.-C., Sharley, D. J. & Pettigrove, V. Associations Between Microplastic Pollution and Land Use in Urban Wetland Sediments. *Environmental Science and Pollution Research* **26,** 22551–22561 (2019).

80. Obbard, R. W., Sadri, S., Wong, Y. Q., Khitun, A. A., Baker, I. & Thompson, R. C. Global Warming Releases Microplastic Legacy Frozen in Arctic Sea Ice. *Earth's Future* **2,** 315–320 (2014).

81. Peeken, I., Primpke, S., Beyer, B., Gütermann, J., Katlein, C., Krumpen, T., Bergmann, M., Hehemann, L. & Gerdts, G. Arctic Sea Ice Is an Important Temporal Sink and Means of Transport for Microplastic. *Nature Communications* **9,** 1–12 (2018).

82. Parolini, M., Antonioli, D., Borgogno, F., Gibellino, M. C., Fresta, J., Albonico, C., De Felice, B., Canuto, S., Concedi, D., Romani, A., Rosio, E., Gianotti, V., Laus, M., Ambrosini, R. & Cavallo, R. Microplastic Contamination in Snow from Western Italian Alps. *International Journal of Environmental Research and Public Health* **18,** 768 (2021).

83. Pastorino, P., Pizzul, E., Bertoli, M., Anselmi, S., Kušće, M., Menconi, V., Prearo, M. & Renzi, M. First Insights into Plastic and Microplastic Occurrence in Biotic and Abiotic Compartments, and Snow from a High-Mountain Lake (Carnic Alps). *Chemosphere* **265,** 129121 (2021).

84. Zhang, Y., Gao, T., Kang, S., Allen, S., Luo, X. & Allen, D. Microplastics in Glaciers of the Tibetan Plateau: Evidence for the Long-Range Transport of Microplastics. *Science of The Total Environment* **758,** 143634 (2021).

85. Van Cauwenberghe, L., Vanreusel, A., Mees, J. & Janssen, C. R. Microplastic Pollution in Deep-Sea Sediments. *Environmental Pollution* **182,** 495–499 (2013).

86. La Daana, K. K., Johansson, C., Frias, J., Gardfeldt, K., Thompson, R. C. & O'Connor, I. Deep Sea Sediments of the Arctic Central Basin: A Potential Sink for Microplastics. *Deep Sea Research Part I: Oceanographic Research Papers* **145,** 137–142 (2019).

87. Syafei, A. D., Nurasrin, N. R., Assomadi, A. F. & Boedisantoso, R. Microplastic Pollution in the Ambient Air of Surabaya, Indonesia. *Current World Environment* **14,** 290 (2017).

88. Gasperi, J., Wright, S. L., Dris, R., Collard, F., Mandin, C., Guerrouache, M., Langlois, V., Kelly, F. J. & Tassin, B. Microplastics in Air: Are We Breathing It In? *Current Opinion in Environmental Science & Health* **1,** 1–5 (2018).

89. Prata, J. C. Airborne Microplastics: Consequences to Human Health? *Environmental Pollution* **234,** 115–126 (2018).

90. Amato-Lourenço, L. F., dos Santos Galvão, L., de Weger, L. A., Hiemstra, P. S., Vijver, M. G. & Mauad, T. An Emerging Class of Air Pollutants: Potential Effects of Microplastics to Respiratory Human Health? *Science of the Total Environment* **749,** 141676 (2020).

91. Zhang, Q., Zhao, Y., Du, F., Cai, H., Wang, G. & Shi, H. Microplastic Fallout in Different Indoor Environments. *Environmental Science & Technology* **54,** 6530–6539 (2020).

92. Horton, A. A., Svendsen, C., Williams, R. J., Spurgeon, D. J. & Lahive, E. Large Microplastic Particles in Sediments of Tributaries of the River Thames, UK–Abundance, Sources and Methods for Effective Quantification. *Marine Pollution Bulletin* **114,** 218–226 (2017).

93. Lindeque, P. K., Cole, M., Coppock, R. L., Lewis, C. N., Miller, R. Z., Watts, A. J., Wilson-McNeal, A., Wright, S. L. & Galloway, T. S. Are We Underestimating Microplastic Abundance in the Marine Environment? A Comparison of Microplastic Capture with Nets of Different Mesh-Size. *Environmental Pollution* **265,** 114721 (2020).

94. Carbery, M., O'Connor, W. & Palanisami, T. Trophic Transfer of Microplastics and Mixed Contaminants in the Marine Food Web and Implications for Human Health. *Environment International* **115,** 400–409 (2018).

95. Teuten, E. L., Rowland, S. J., Galloway, T. S. & Thompson, R. C. Potential for Plastics to Transport Hydrophobic Contaminants. *Environmental Science & Technology* **41,** 7759–7764 (2007).

96. Frias, J., Sobral, P. & Ferreira, A. M. Organic Pollutants in Microplastics from Two Beaches of the Portuguese Coast. *Marine Pollution Bulletin* **60,** 1988–1992 (2010).

97. Zettler, E. R., Mincer, T. J. & Amaral-Zettler, L. A. Life in the Plastisphere": Microbial Communities on Plastic Marine Debris. *Environmental Science & Technology* **47,** 7137–7146 (2013).

98. McCormick, A., Hoellein, T. J., Mason, S. A., Schluep, J. & Kelly, J. J. Microplastic Is an Abundant and Distinct Microbial Habitat in an Urban River. *Environmental Science & Technology* **48,** 11863–11871 (2014).

99. Brennecke, D., Duarte, B., Paiva, F., Caçador, I. & Canning-Clode, J. Microplastics as Vector for Heavy Metal Contamination from the Marine Environment. *Estuarine, Coastal and Shelf Science* **178,** 189–195 (2016).

100. Fred-Ahmadu, O. H., Bhagwat, G., Oluyoye, I., Benson, N. U., Ayejuyo, O. O. & Palanisami, T. Interaction of Chemical Contaminants with Microplastics: Principles and Perspectives. *Science of the Total Environment* **706,** 135978 (2020).

101. Bouwmeester, H., Hollman, P. C. & Peters, R. J. Potential Health Impact of Environmentally Released Micro-and Nanoplastics in the Human Food Production Chain: Experiences from Nanotoxicology. *Environmental Science & Technology* **49,** 8932–8947 (2015).

102. Rochman, C. M., Hoh, E., Hentschel, B. T. & Kaye, S. Long-Term Field Measurement of Sorption of Organic Contaminants to Five Types of Plastic Pellets: Implications for Plastic Marine Debris. *Environmental Science & Technology* **47,** 1646–1654 (2013).

103. Wang, W. & Wang, J. Different Partition of Polycyclic Aromatic Hydrocarbon on Environmental Particulates in Freshwater: Microplastics in Comparison to Natural Sediment. *Ecotoxicology and Environmental Safety* **147,** 648–655 (2018).

104. Mastrangelo, G., Fadda, E. & Marzia, V. Polycyclic Aromatic Hydrocarbons and Cancer in Man. *Environmental Health Perspectives* **104,** 1166–1170 (1996).

105. Cogliano, V. J. Assessing the Cancer Risk from Environmental PCBs. *Environmental Health Perspectives* **106,** 317–323 (1998).

106. Boström, C.-E., Gerde, P., Hanberg, A., Jernström, B., Johansson, C., Kyrklund, T., Rannug, A., Törnqvist, M., Victorin, K. & Westerholm, R. Cancer Risk Assessment, Indicators, and Guidelines for Polycyclic Aromatic Hydrocarbons in the Ambient Air. *Environmental Health Perspectives* **110,** 451–488 (2002).

107. Cohn, B. A., Wolff, M. S., Cirillo, P. M. & Sholtz, R. I. DDT and Breast Cancer in Young Women: New Data on the Significance of Age at Exposure. *Environmental Health Perspectives* **115,** 1406–1414 (2007).

108. Lim, J.-e., Nam, C., Yang, J., Rha, K. H., Lim, K.-M. & Jee, S. H. Serum Persistent Organic Pollutants (POPs) And Prostate Cancer Risk: A Case-Cohort Study. *International Journal of Hygiene and Environmental Health* **220,** 849–856 (2017).

109. Pompilio, A., Piccolomini, R., Picciani, C., D'Antonio, D., Savini, V. & Di Bonaventura, G. Factors Associated with Adherence to and Biofilm Formation on Polystyrene by *Stenotrophomonas maltophilia*: The Role of Cell Surface Hydrophobicity and Motility. *FEMS Microbiology Letters* **287,** 41–47 (2008).

110. Sanni, O., Chang, C.-Y., Anderson, D. G., Langer, R., Davies, M. C., Williams, P. M., Williams, P., Alexander, M. R. & Hook, A. L. Bacterial Attachment to Polymeric Materials Correlates with Molecular Flexibility and Hydrophilicity. *Advanced Healthcare Materials* **4,** 695–701 (2015).

111. Nauendorf, A., Krause, S., Bigalke, N. K., Gorb, E. V., Gorb, S. N., Haeckel, M., Wahl, M. & Treude, T. Microbial Colonization and Degradation of Polyethylene and Biodegradable Plastic Bags in Temperate Fine-Grained Organic-Rich Marine Sediments. *Marine Pollution Bulletin* **103,** 168–178 (2016).

112. Rummel, C. D., Jahnke, A., Gorokhova, E., Kühnel, D. & Schmitt-Jansen, M. Impacts of Biofilm Formation on the Fate and Potential Effects of Microplastic in the Aquatic Environment. *Environmental Science & Technology Letters* **4,** 258–267 (2017).

113. Wu, X., Pan, J., Li, M., Li, Y., Bartlam, M. & Wang, Y. Selective Enrichment of Bacterial Pathogens by Microplastic Biofilm. *Water Research* **165,** 114979 (2019).

114. Sabev, H. A., Barratt, S. R., Greenhalgh, M., Handley, P. & Robson, G. Biodegradation and Biodeterioration of Man-Made Polymeric Materials. *Fungi in Biogeochemical Cycles,* 212–235 (2006).

115. Shah, A. A., Hasan, F., Hameed, A. & Ahmed, S. Biological Degradation of Plastics: A Comprehensive Review. *Biotechnology Advances* **26,** 246–265 (2008).

116. Feldman, D. Polymer Weathering: Photo-Oxidation. *Journal of Polymers and the Environment* **10,** 163–173 (2002).

117. Andrady, A. L. in *Marine Anthropogenic Litter* 57–72 (Springer, 2015).

118. Long, M., Moriceau, B., Gallinari, M., Lambert, C., Huvet, A., Raffray, J. & Soudant, P. Interactions between Microplastics and Phytoplankton Aggregates: Impact on Their Respective Fates. *Marine Chemistry* **175,** 39–46 (2015).

119. Fazey, F. M. & Ryan, P. G. Biofouling on Buoyant Marine Plastics: An Experimental Study into the Effect of Size on Surface Longevity. *Environmental Pollution* **210,** 354–360 (2016).

120. Hartmann, N. B., Rist, S., Bodin, J., Jensen, L. H., Schmidt, S. N., Mayer, P., Meibom, A. & Baun, A. Microplastics as Vectors for Environmental Contaminants: Exploring Sorption, Desorption, and Transfer to Biota. *Integrated Environmental Assessment and Management* **13,** 488–493 (2017).

121. Caruso, G. Microplastics as Vectors of Contaminants. *Marine Pollution Bulletin* **146,** 921–924 (2019).

122. Lee, H., Shim, W. J. & Kwon, J.-H. Sorption Capacity of Plastic Debris for Hydrophobic Organic Chemicals. *Science of the Total Environment* **470,** 1545–1552 (2014).

123. Seidensticker, S., Grathwohl, P., Lamprecht, J. & Zarfl, C. A Combined Experimental and Modeling Study to Evaluate pH-Dependent Sorption of Polar and Non-polar Compounds to Polyethylene and Polystyrene Microplastics. *Environmental Sciences Europe* **30,** 1–12 (2018).

124. Cole, M., Lindeque, P., Fileman, E., Halsband, C., Goodhead, R., Moger, J. & Galloway, T. S. Microplastic Ingestion by Zooplankton. *Environmental Science & Technology* **47,** 6646–6655 (2013).

125. Guzzetti, E., Sureda, A., Tejada, S. & Faggio, C. Microplastic in Marine Organism: Environmental and Toxicological Effects. *Environmental Toxicology and Pharmacology* **64,** 164–171 (2018).

126. Wang, W., Gao, H., Jin, S., Li, R. & Na, G. The Ecotoxicological Effects of Microplastics on Aquatic Food Web, from Primary Producer to Human: A Review. *Ecotoxicology and Environmental Safety* **173,** 110–117 (2019).

127. Farrell, P. & Nelson, K. Trophic Level Transfer of Microplastic: *Mytilus edulis* (L.) To *Carcinus maenas* (L.) *Environmental Pollution* **177,** 1–3 (2013).

128. Setälä, O., Fleming-Lehtinen, V. & Lehtiniemi, M. Ingestion and Transfer of Microplastics in the Planktonic Food Web. *Environmental Pollution* **185,** 77–83 (2014).

129. Browne, M. A., Dissanayake, A., Galloway, T. S., Lowe, D. M. & Thompson, R. C. Ingested Microscopic Plastic Translocates to the Circulatory System of the Mussel, *Mytilus edulis* (L.) *Environmental Science & Technology* **42,** 5026–5031 (2008).

130. Nelms, S. E., Galloway, T. S., Godley, B. J., Jarvis, D. S. & Lindeque, P. K. Investigating Microplastic Trophic Transfer in Marine Top Predators. *Environmental Pollution* **238,** 999–1007 (2018).

131. Eriksson, C. & Burton, H. Origins and Biological Accumulation of Small Plastic Particles in Fur Seals from Macquarie Island. *AMBIO: A Journal of the Human Environment* **32,** 380–384 (2003).

132. Hoarau, L., Ainley, L., Jean, C. & Ciccione, S. Ingestion and Defecation of Marine Debris by Loggerhead Sea Turtles, *Caretta caretta*, from By-Catches in the South-West Indian Ocean. *Marine Pollution Bulletin* **84,** 90–96 (2014).

133. De Sá, L. C., Luís, L. G. & Guilhermino, L. Effects of Microplastics on Juveniles of the Common Goby (*Pomatoschistus microps*): Confusion with Prey, Reduction of the Predatory Performance and Efficiency, and Possible Influence of Developmental Conditions. *Environmental Pollution* **196,** 359–362 (2015).

134. Neves, D., Sobral, P., Ferreira, J. L. & Pereira, T. Ingestion of Microplastics by Commercial Fish off the Portuguese Coast. *Marine Pollution Bulletin* **101,** 119–126 (2015).

135. Savoca, M. S., Wohlfeil, M. E., Ebeler, S. E. & Nevitt, G. A. Marine Plastic Debris Emits a Keystone Infochemical for Olfactory Foraging Seabirds. *Science Advances* **2,** e1600395 (2016).

136. Hurley, R. R., Woodward, J. C. & Rothwell, J. J. Ingestion of Microplastics by Freshwater Tubifex Worms. *Environmental Science & Technology* **51,** 12844–12851 (2017).

137. De Sá, L. C., Oliveira, M., Ribeiro, F., Rocha, T. L. & Futter, M. N. Studies of the Effects of Microplastics on Aquatic Organisms: What Do We Know and Where Should We Focus Our Efforts in the Future? *Science of the Total Environment* **645,** 1029–1039 (2018).

138. Franzellitti, S., Canesi, L., Auguste, M., Wathsala, R. H. & Fabbri, E. Microplastic Exposure and Effects in Aquatic Organisms: A Physiological Perspective. *Environmental Toxicology and Pharmacology* **68,** 37–51 (2019).

139. Thompson, R. C. Plastic Debris in the Marine Environment: Consequences and Solutions. *Marine Nature Conservation in Europe* **193,** 107–115 (2006).

140. Fossi, M. C., Panti, C., Guerranti, C., Coppola, D., Giannetti, M., Marsili, L. & Minutoli, R. Are Baleen Whales Exposed to the Threat of Microplastics? A Case Study of the Mediterranean Fin Whale (*Balaenoptera physalus*). *Marine Pollution Bulletin* **64,** 2374–2379 (2012).

141. Frias, J. P., Otero, V. & Sobral, P. Evidence of Microplastics in Samples of Zooplankton from Portuguese Coastal Waters. *Marine Environmental Research* **95,** 89–95 (2014).

142. Chae, Y. & An, Y.-J. Current Research Trends on Plastic Pollution and Ecological Impacts on the Soil Ecosystem: A Review. *Environmental Pollution* **240,** 387–395 (2018).

143. Büks, F. & Kaupenjohann, M. Global Concentrations of Microplastics in Soils- A Review. *Soil* **6,** 649–662 (2020).

144. He, D., Bristow, K., Filipović, V., Lv, J. & He, H. Microplastics in Terrestrial Ecosystems: A Scientometric Analysis. *Sustainability* **12,** 8739 (2020).

145. O'Connor, D., Pan, S., Shen, Z., Song, Y., Jin, Y., Wu, W.-M. & Hou, D. Microplastics Undergo Accelerated Vertical Migration in Sand Soil Due to Small Size and Wet-Dry Cycles. *Environmental Pollution* **249,** 527–534 (2019).

146. Kelly, B. C., Ikonomou, M. G., Blair, J. D., Morin, A. E. & Gobas, F. A. Food Web Specific Biomagnification of Persistent Organic Pollutants. *Science* **317,** 236–239 (2007).

147. Oliveira, M., Ribeiro, A., Hylland, K. & Guilhermino, L. Single and Combined Effects of Microplastics and Pyrene on Juveniles (0+ Group) Of the Common Goby *Pomatoschistus microps* (Teleostei, Gobiidae). *Ecological Indicators* **34,** 641–647 (2013).

148. Rochman, C. M., Tahir, A., Williams, S. L., Baxa, D. V., Lam, R., Miller, J. T., Teh, F.-C., Werorilangi, S. & Teh, S. J. Anthropogenic Debris in Seafood: Plastic Debris and Fibers from Textiles in Fish and Bivalves Sold for Human Consumption. *Scientific Reports* **5,** 1–10 (2015).

149. Ziccardi, L. M., Edgington, A., Hentz, K., Kulacki, K. J. & Kane Driscoll, S. Microplastics as Vectors for Bioaccumulation of Hydrophobic Organic Chemicals in the Marine Environment: A State-Of-The-Science Review. *Environmental Toxicology and Chemistry* **35,** 1667–1676 (2016).

150. Barboza, L. G. A., Vethaak, A. D., Lavorante, B. R., Lundebye, A.-K. & Guilhermino, L. Marine Microplastic Debris: An Emerging Issue for Food Security, Food Safety and Human Health. *Marine Pollution Bulletin* **133,** 336–348 (2018).

151. Liebezeit, G. & Liebezeit, E. Synthetic Particles as Contaminants in German Beers. *Food Additives & Contaminants: Part A* **31,** 1574–1578 (2014).

152. Karbalaei, S., Hanachi, P., Walker, T. R. & Cole, M. Occurrence, Sources, Human Health Impacts and Mitigation of Microplastic Pollution. *Environmental Science and Pollution Research* **25,** 36046–36063 (2018).

153. Vianello, A., Jensen, R. L., Liu, L. & Vollertsen, J. Simulating Human Exposure to Indoor Airborne Microplastics Using a Breathing Thermal Manikin. *Scientific Reports* **9,** 1–11 (2019).

154. Zhang, Q., Xu, E. G., Li, J., Chen, Q., Ma, L., Zeng, E. Y. & Shi, H. A Review of Microplastics in Table Salt, Drinking Water, and Air: Direct Human Exposure. *Environmental Science & Technology* **54,** 3740–3751 (2020).

155. Mohsen, M., Wang, Q., Zhang, L., Sun, L., Lin, C. & Yang, H. Microplastic Ingestion by the Farmed Sea Cucumber *Apostichopus japonicus* in China. *Environmental Pollution* **245,** 1071–1078 (2019).

156. Weis, J. S. Improving Microplastic Research. *AIMS Environmental Science* **6,** 326–340 (2019).

157. Lee, K.-W., Shim, W. J., Kwon, O. Y. & Kang, J.-H. Size-Dependent Effects of Micro Polystyrene Particles in the Marine Copepod *Tigriopus japonicus*. *Environmental Science & Technology* **47,** 11278–11283 (2013).

158. Lu, L., Luo, T., Zhao, Y., Cai, C., Fu, Z. & Jin, Y. Interaction between Microplastics and Microorganism as Well as Gut Microbiota: A Consideration on Environmental Animal and Human Health. *Science of the Total Environment* **667,** 94–100 (2019).

159. Rummel, C. D., Löder, M. G., Fricke, N. F., Lang, T., Griebeler, E.-M., Janke, M. & Gerdts, G. Plastic Ingestion by Pelagic and Demersal Fish from the North Sea and Baltic Sea. *Marine Pollution Bulletin* **102,** 134–141 (2016).

160. Von Moos, N., Burkhardt-Holm, P. & Köhler, A. Uptake and Effects of Microplastics on Cells and Tissue of the Blue Mussel *Mytilus edulis* L. After an Experimental Exposure. *Environmental Science & Technology* **46,** 11327–11335 (2012).

161. Beyer, J., Green, N. W., Brooks, S., Allan, I. J., Ruus, A., Gomes, T., Bråte, I. L. N. & Schøyen, M. Blue Mussels (*Mytilus edulis* spp.) As Sentinel Organisms in Coastal Pollution Monitoring: A Review. *Marine Environmental Research* **130,** 338–365 (2017).

162. Li, J., Lusher, A. L., Rotchell, J. M., Deudero, S., Turra, A., Bråte, I. L. N., Sun, C., Hossain, M. S., Li, Q., Kolandhasamy, P. & Shi, H. Using Mussel as a Global Bioindicator of Coastal Microplastic Pollution. *Environmental Pollution* **244,** 522–533 (2019).

163. Ward, J. E. & Shumway, S. E. Separating the Grain from the Chaff: Particle Selection in Suspension-and Deposit-Feeding Bivalves. *Journal of Experimental Marine Biology and Ecology* **300,** 83–130 (2004).

164. Santana, M. F., Moreira, F. T., Pereira, C. D., Abessa, D. & Turra, A. Continuous Exposure to Microplastics Does Not Cause Physiological Effects in the Cultivated Mussel *Perna perna*. *Archives of Environmental Contamination and Toxicology* **74,** 594–604 (2018).

165. Bråte, I. L. N., Blázquez, M., Brooks, S. J. & Thomas, K. V. Weathering Impacts the Uptake of Polyethylene Microparticles from Toothpaste in Mediterranean Mussels (*M. galloprovincialis*). *Science of the Total Environment* **626,** 1310–1318 (2018).

166. Revel, M., Lagarde, F., Perrein-Ettajani, H., Bruneau, M., Akcha, F., Sussarellu, R., Rouxel, J., Costil, K., Decottignies, P., Cognie, B., Châtel, A. & Mouneyrac, C. Tissue-Specific Biomarker Responses in the Blue Mussel *Mytilus* spp. Exposed to a Mixture of Microplastics at Environmentally Relevant Concentrations. *Frontiers in Environmental Science* **7,** 33 (2019).

167. Ward, J. E., Zhao, S., Holohan, B. A., Mladinich, K. M., Griffin, T. W., Wozniak, J. & Shumway, S. E. Selective Ingestion and Egestion of Plastic Particles by the Blue Mussel (*Mytilus edulis*) And Eastern Oyster (*Crassostrea virginica*): Implications for Using Bivalves as Bioindicators of Microplastic Pollution. *Environmental Science & Technology* **53,** 8776–8784 (2019).

168. Li, J., Wang, Z., Rotchell, J. M., Shen, X., Li, Q. & Zhu, J. Where Are We? Towards an Understanding of the Selective Accumulation of Microplastics in Mussels. *Environmental Pollution* **286,** 117543 (2021).

169. Avio, C. G., Cardelli, L. R., Gorbi, S., Pellegrini, D. & Regoli, F. Microplastics Pollution after the Removal of the Costa Concordia Wreck: First Evidences from a Biomonitoring Case Study. *Environmental Pollution* **227,** 207–214 (2017).

170. Wang, C., Hou, M., Shang, K., Wang, H. & Wang, J. Microplastics (Polystyrene) Exposure Induces Metabolic Changes in the Liver of Rare Minnow (*Gobiocypris rarus*). *Molecules* **27,** 584 (2022).

171. Green, D. S., Colgan, T. J., Thompson, R. C. & Carolan, J. C. Exposure to Microplastics Reduces Attachment Strength and Alters the Haemolymph Proteome of Blue Mussels (*Mytilus edulis*). *Environmental Pollution* **246,** 423–434 (2019).

172. Lu, Y., Zhang, Y., Deng, Y., Jiang, W., Zhao, Y., Geng, J., Ding, L. & Ren, H. Uptake and Accumulation of Polystyrene Microplastics in Zebrafish (*Danio rerio*) And Toxic Effects in Liver. *Environmental Science & Technology* **50,** 4054–4060 (2016).

173. Chen, L., Hu, C., Lai, N. L.-S., Zhang, W., Hua, J., Lam, P. K., Lam, J. C. & Zhou, B. Acute Exposure to Pbdes at an Environmentally Realistic Concentration Causes Abrupt Changes in the Gut Microbiota and Host Health of Zebrafish. *Environmental Pollution* **240,** 17–26 (2018).

174. Qiao, R., Sheng, C., Lu, Y., Zhang, Y., Ren, H. & Lemos, B. Microplastics Induce Intestinal Inflammation, Oxidative Stress, and Disorders of Metabolome and Microbiome in Zebrafish. *Science of the Total Environment* **662,** 246–253 (2019).

175. Yong, C. Q. Y., Valiyaveettil, S. & Tang, B. L. Toxicity of Microplastics and Nanoplastics in Mammalian Systems. *International Journal of Environmental Research and Public Health* **17,** 1509 (2020).

176. Lei, L., Wu, S., Lu, S., Liu, M., Song, Y., Fu, Z., Shi, H., Raley-Susman, K. M. & He, D. Microplastic Particles Cause Intestinal Damage and Other Adverse Effects in Zebrafish *Danio rerio* and Nematode *Caenorhabditis elegans*. *Science of the Total Environment* **619,** 1–8 (2018).

177. Rainieri, S., Conlledo, N., Larsen, B. K., Granby, K. & Barranco, A. Combined Effects of Microplastics and Chemical Contaminants on the Organ Toxicity of Zebrafish (*Danio rerio*). *Environmental Research* **162,** 135–143 (2018).

178. Mak, C. W., Yeung, K. C.-F. & Chan, K. M. Acute Toxic Effects of Polyethylene Microplastic on Adult Zebrafish. *Ecotoxicology and Environmental Safety* **182,** 109442 (2019).

179. Qiao, R., Lu, K., Deng, Y., Ren, H. & Zhang, Y. Combined Effects of Polystyrene Microplastics and Natural Organic Matter on the Accumulation and Toxicity of Copper in Zebrafish. *Science of the Total Environment* **682,** 128–137 (2019).

180. Bhagat, J., Zang, L., Nishimura, N. & Shimada, Y. Zebrafish: An Emerging Model to Study Microplastic and Nanoplastic Toxicity. *Science of The Total Environment* **728,** 138707 (2020).

181. Lu, L., Wan, Z., Luo, T., Fu, Z. & Jin, Y. Polystyrene Microplastics Induce Gut Microbiota Dysbiosis and Hepatic Lipid Metabolism Disorder in Mice. *Science of the Total Environment* **631,** 449–458 (2018).

182. Jin, Y., Lu, L., Tu, W., Luo, T. & Fu, Z. Impacts of Polystyrene Microplastic on the Gut Barrier, Microbiota and Metabolism of Mice. *Science of the Total Environment* **649,** 308–317 (2019).

183. Wang, J., Peng, C., Li, H., Zhang, P. & Liu, X. The Impact of Microplastic-Microbe Interactions on Animal Health and Biogeochemical Cycles: A Mini-Review. *Science of The Total Environment* **773,** 145697 (2021).

184. Cao, D., Wang, X., Luo, X., Liu, G. & Zheng, H. Effects of Polystyrene Microplastics on the Fitness of Earthworms in an Agricultural Soil. *IOP Conference Series: Earth and Environmental Science* **61,** 012148 (2017).

185. Rodríguez-Seijo, A., da Costa, J. P., Rocha-Santos, T., Duarte, A. C. & Pereira, R. Oxidative Stress, Energy Metabolism and Molecular Responses of Earthworms (*Eisenia fetida*) Exposed to Low-Density Polyethylene Microplastics. *Environmental Science and Pollution Research* **25,** 33599–33610 (2018).

186. Wang, J., Coffin, S., Sun, C., Schlenk, D. & Gan, J. Negligible Effects of Microplastics on Animal Fitness and Hoc Bioaccumulation in Earthworm *Eisenia fetida* in Soil. *Environmental Pollution* **249,** 776–784 (2019).

187. Chen, Y., Liu, X., Leng, Y. & Wang, J. Defense Responses in Earthworms (*Eisenia fetida*) Exposed to Low-Density Polyethylene Microplastics in Soils. *Ecotoxicology and Environmental Safety* **187,** 109788 (2020).

188. Sajiki, J. & Yonekubo, J. Leaching of Bisphenol a (BPA) To Seawater from Polycarbonate Plastic and Its Degradation by Reactive Oxygen Species. *Chemosphere* **51,** 55–62 (2003).

189. Teuten, E. L., Saquing, J. M., Knappe, D. R., Barlaz, M. A., Jonsson, S., Björn, A., Rowland, S. J., Thompson, R. C., Galloway, T. S., Yamashita, R., Ochi, D., Watanuki, Y., Moore, C., Viet, P. H., Tana, T. S., Prudente, M., Boonyatumanond, R., Zakaria, M. P., Akkhavong, K., Ogata, Y., Hirai, H., Iwasa, S., Mizukawa, K., Hagino, Y., Imamura, A., Saha, M. & Takada, H. Transport and Release of Chemicals from Plastics to the Environment and to Wildlife. *Philosophical Transactions of the Royal Society B: Biological Sciences* **364,** 2027–2045 (2009).

190. Chua, E. M., Shimeta, J., Nugegoda, D., Morrison, P. D. & Clarke, B. O. Assimilation of Polybrominated Diphenyl Ethers from Microplastics by the Marine Amphipod, *Allorchestes compressa*. *Environmental Science & Technology* **48,** 8127–8134 (2014).

191. Voparil, I. M. & Mayer, L. M. Dissolution of Sedimentary Polycyclic Aromatic Hydrocarbons into the Lugworm's (*Arenicola marina*) Digestive Fluids. *Environmental Science & Technology* **34,** 1221–1228 (2000).

192. Rochman, C. M., Hoh, E., Kurobe, T. & Teh, S. J. Ingested Plastic Transfers Hazardous Chemicals to Fish and Induces Hepatic Stress. *Scientific Reports* **3,** 1–7 (2013).

193. Deng, Y., Zhang, Y., Qiao, R., Bonilla, M. M., Yang, X., Ren, H. & Lemos, B. Evidence That Microplastics Aggravate the Toxicity of Organophosphorus Flame Retardants in Mice (*Mus musculus*). *Journal of Hazardous Materials* **357,** 348–354 (2018).

194. Mu, X., Qi, S., Liu, J., Yuan, L., Huang, Y., Xue, J., Qian, L., Wang, C. & Li, Y. Toxicity and Behavioral Response of Zebrafish Exposed to Combined Microplastic and Bisphenol Analogues. *Environmental Chemistry Letters* **20,** 41–48 (2022).

195. Banerjee, A. & Shelver, W. L. Micro-and Nanoplastic-Mediated Pathophysiological Changes in Rodents, Rabbits, and Chickens: A Review. *Journal of Food Protection* **84,** 1480–1495 (2021).

196. An, R., Wang, X., Yang, L., Zhang, J., Wang, N., Xu, F., Hou, Y., Zhang, H. & Zhang, L. Polystyrene Microplastics Cause Granulosa Cells Apoptosis and Fibrosis in Ovary through Oxidative Stress in Rats. *Toxicology* **449,** 152665 (2021).

197. Martínez, C., González-Castro, A., Vicario, M. & Santos, J. Cellular and Molecular Basis of Intestinal Barrier Dysfunction in the Irritable Bowel Syndrome. *Gut and Liver* **6,** 305 (2012).

198. Stock, V., Böhmert, L., Lisicki, E., Block, R., Cara-Carmona, J., Pack, L. K., Selb, R., Lichtenstein, D., Voss, L., Henderson, C. J., Zabinsky, E., Sieg, H., Braeuning, A. & Lampen, A. Uptake and Effects of Orally Ingested Polystyrene Microplastic Particles *In Vitro* and *In Vivo*. *Archives of Toxicology* **93,** 1817–1833 (2019).

199. Cheng, H. & Leblond, C. Origin, Differentiation and Renewal of the Four Main Epithelial Cell Types in the Mouse Small Intestine V. Unitarian Theory of the Origin of the Four Epithelial Cell Types. *American Journal of Anatomy* **141,** 537–561 (1974).

200. Jones, B. D., Ghori, N. & Falkow, S. *Salmonella typhimurium* Initiates Murine Infection by Penetrating and Destroying the Specialized Epithelial M Cells of the Peyer's Patches. *The Journal of Experimental Medicine* **180,** 15–23 (1994).

201. Dauca, M., Bouziges, F., Colin, S., Kedinger, M., Keller, M., Schilt, J., Simon-Assmann, P. & Haffen, K. Development of the Vertebrate Small Intestine and Mechanisms of Cell Differentiation. *International Journal of Developmental Biology* **34,** 205–218 (2003).

202. Takahashi, T. & Shiraishi, A. Stem Cell Signaling Pathways in the Small Intestine. *International Journal of Molecular Sciences* **21,** 2032 (2020).

203. Kernéis, S., Bogdanova, A., Kraehenbuhl, J.-P. & Pringault, E. Conversion by Peyer's Patch Lymphocytes of Human Enterocytes into M Cells That Transport Bacteria. *Science* **277,** 949–952 (1997).

204. Kraehenbuhl, J.-P. & Neutra, M. R. Epithelial M Cells: Differentiation and Function. *Annual Review of Cell and Developmental Biology* **16,** 301–332 (2000).

205. Hathaway, L. & Kraehenbuhl, J. The Role of M Cells in Mucosal Immunity. *Cellular and Molecular Life Sciences* **57,** 323–332 (2000).

206. Pappo, J. & Ermak, T. Uptake and Translocation of Fluorescent Latex Particles by Rabbit Peyer's Patch Follicle Epithelium: A Quantitative Model for M Cell Uptake. *Clinical and Experimental Immunology* **76,** 144 (1989).

207. Jani, P., McCarthy, D. & Florence, A. Nanosphere and Microsphere Uptake via Peyer's Patches: Observation of the Rate of Uptake in the Rat after a Single Oral Dose. *International Journal of Pharmaceutics* **86,** 239–246 (1992).

208. Shakweh, M., Besnard, M., Nicolas, V. & Fattal, E. Poly (Lactide-Co-glycolide) Particles of Different Physicochemical Properties and Their Uptake by Peyer's Patches in Mice. *European Journal of Pharmaceutics and Biopharmaceutics* **61,** 1–13 (2005).

209. Galloway, T. S. in *Marine Anthropogenic litter* 343–366 (Springer, 2015).

210. Powell, J. J., Faria, N., Thomas-McKay, E. & Pele, L. C. Origin and Fate of Dietary Nanoparticles and Microparticles in the Gastrointestinal Tract. *Journal of Autoimmunity* **34,** J226–J233 (2010).

211. Hirt, N. & Body-Malapel, M. Immunotoxicity and Intestinal Effects of Nano-and Microplastics: A Review of the Literature. *Particle and Fibre Toxicology* **17,** 1–22 (2020).

212. Jani, P., Halbert, G. W., Langridge, J. & Florence, A. T. Nanoparticle Uptake by the Rat Gastrointestinal Mucosa: Quantitation and Particle Size Dependency. *Journal of Pharmacy and Pharmacology* **42,** 821–826 (1990).

213. Doyle-McCullough, M., Smyth, S., Moyes, S. & Carr, K. Factors Influencing Intestinal Microparticle Uptake *In Vivo*. *International Journal of Pharmaceutics* **335,** 79–89 (2007).

214. Wright, S. L. & Kelly, F. J. Plastic and Human Health: A Micro Issue? *Environmental Science & Technology* **51,** 6634–6647 (2017).

215. Wang, Y., Mao, Z., Zhang, M., Ding, G., Sun, J., Du, M., Liu, Q., Cong, Y., Jin, F., Zhang, W. & Wang, J. The Uptake and Elimination of Polystyrene Microplastics by the Brine Shrimp, *Artemia parthenogenetica*, and Its Impact on Its Feeding Behavior and Intestinal Histology. *Chemosphere* **234,** 123–131 (2019).

216. Carr, K. E., Smyth, S. H., McCullough, M. T., Morris, J. F. & Moyes, S. M. Morphological Aspects of Interactions between Microparticles and Mammalian Cells: Intestinal Uptake and Onward Movement. *Progress in Histochemistry and Cytochemistry* **46,** 185–252 (2012).

217. Schmidt, C., Lautenschlaeger, C., Collnot, E.-M., Schumann, M., Bojarski, C., Schulzke, J.-D., Lehr, C.-M. & Stallmach, A. Nano-and Microscaled Particles for Drug Targeting to Inflamed Intestinal Mucosa- A First *In Vivo* Study in Human Patients. *Journal of Controlled Release* **165,** 139–145 (2013).

218. Yan, Z., Liu, Y., Zhang, T., Zhang, F., Ren, H. & Zhang, Y. Analysis of Microplastics in Human Feces Reveals a Correlation between Fecal Microplastics and Inflammatory Bowel Disease Status. *Environmental Science & Technology* (2021).

219. Zheng, H., Wang, J., Wei, X., Chang, L. & Liu, S. Proinflammatory Properties and Lipid Disturbance of Polystyrene Microplastics in the Livers of Mice with Acute Colitis. *Science of The Total Environment* **750,** 143085 (2021).

220. Geiser, M., Schurch, S. & Gehr, P. Influence of Surface Chemistry and Topography of Particles on Their Immersion into the Lung's Surface-Lining Layer. *Journal of Applied Physiology* **94,** 1793–1801 (2003).

221. Ruge, C. A., Kirch, J. & Lehr, C.-M. Pulmonary Drug Delivery: From Generating Aerosols to Overcoming Biological Barriers- Therapeutic Possibilities and Technological Challenges. *The Lancet Respiratory Medicine* **1,** 402–413 (2013).

222. Kotton, D. N., Ma, B. Y., Cardoso, W. V., Sanderson, E. A., Summer, R. S., Williams, M. C. & Fine, A. Bone Marrow-Derived Cells as Progenitors of Lung Alveolar Epithelium. *Development* **128,** 5181–5188 (2001).

223. Knudsen, L. & Ochs, M. The Micromechanics of Lung Alveoli: Structure and Function of Surfactant and Tissue Components. *Histochemistry and Cell Biology* **150,** 661–676 (2018).

224. Bardales, R. H., Xie, S.-S., Schaefer, R. & Hsu, S.-M. Apoptosis Is a Major Pathway Responsible for the Resolution of Type II Pneumocytes in Acute Lung Injury. *The American Journal of Pathology* **149,** 845 (1996).

225. Daniels, C. B. & Orgeig, S. Pulmonary Surfactant: The Key to the Evolution of Air Breathing. *Physiology* **18,** 151–157 (2003).

226. Kreyling, W. G., Semmler-Behnke, M., Seitz, J., Scymczak, W., Wenk, A., Mayer, P., Takenaka, S. & Oberdörster, G. Size Dependence of the Translocation of Inhaled Iridium and Carbon Nanoparticle Aggregates from the Lung of Rats to the Blood and Secondary Target Organs. *Inhalation Toxicology* **21,** 55–60 (2009).

227. Deng, Y., Zhang, Y., Lemos, B. & Ren, H. Tissue Accumulation of Microplastics in Mice and Biomarker Responses Suggest Widespread Health Risks of Exposure. *Scientific Reports* **7,** 1–10 (2017).

228. Yang, Y.-F., Chen, C.-Y., Lu, T.-H. & Liao, C.-M. Toxicity-Based Toxicokinetic/ Toxicodynamic Assessment for Bioaccumulation of Polystyrene Microplastics in Mice. *Journal of Hazardous Materials* **366,** 703–713 (2019).

229. Luo, T., Wang, C., Pan, Z., Jin, C., Fu, Z. & Jin, Y. Maternal Polystyrene Microplastic Exposure during Gestation and Lactation Altered Metabolic Homeostasis in the Dams and Their F1 and F2 Offspring. *Environmental Science & Technology* **53,** 10978–10992 (2019).

230. Li, B., Ding, Y., Cheng, X., Sheng, D., Xu, Z., Rong, Q., Wu, Y., Zhao, H., Ji, X. & Zhang, Y. Polyethylene Microplastics Affect the Distribution of Gut Microbiota and Inflammation Development in Mice. *Chemosphere* **244,** 125492 (2020).

231. Choi, Y. J., Park, J. W., Kim, J. E., Lee, S. J., Gong, J. E., Jung, Y.-S., Seo, S. & Hwang, D. Y. Novel Characterization of Constipation Phenotypes in ICR Mice Orally Administrated with Polystyrene Microplastics. *International Journal of Molecular Sciences* **22,** 5845 (2021).

232. Deng, Y., Yan, Z., Shen, R., Wang, M., Huang, Y., Ren, H., Zhang, Y. & Lemos, B. Microplastics Release Phthalate Esters and Cause Aggravated Adverse Effects in the Mouse Gut. *Environment International* **143,** 105916 (2020).

233. Jin, Y., Xia, J., Pan, Z., Yang, J., Wang, W. & Fu, Z. Polystyrene Microplastics Induce Microbiota Dysbiosis and Inflammation in the Gut of Adult Zebrafish. *Environmental Pollution* **235,** 322–329 (2018).

234. Qiao, R., Deng, Y., Zhang, S., Wolosker, M. B., Zhu, Q., Ren, H. & Zhang, Y. Accumulation of Different Shapes of Microplastics Initiates Intestinal Injury and Gut Microbiota Dysbiosis in the Gut of Zebrafish. *Chemosphere* **236,** 124334 (2019).

235. Sekirov, I., Russell, S. L., Antunes, L. C. M. & Finlay, B. B. Gut Microbiota in Health and Disease. *Physiological Reviews* (2010).

236. Tremaroli, V. & Bäckhed, F. Functional Interactions between the Gut Microbiota and Host Metabolism. *Nature* **489,** 242–249 (2012).

237. Jin, Y., Wu, S., Zeng, Z. & Fu, Z. Effects of Environmental Pollutants on Gut Microbiota. *Environmental Pollution* **222,** 1–9 (2017).

238. Rawls, J. F., Mahowald, M. A., Ley, R. E. & Gordon, J. I. Reciprocal Gut Microbiota Transplants from Zebrafish and Mice to Germ-Free Recipients Reveal Host Habitat Selection. *Cell* **127,** 423–433 (2006).

239. Eckburg, P. B., Bik, E. M., Bernstein, C. N., Purdom, E., Dethlefsen, L., Sargent, M., Gill, S. R., Nelson, K. E. & Relman, D. A. Diversity of the Human Intestinal Microbial Flora. *Science* **308,** 1635–1638 (2005).

240. Jakobsson, H. E., Jernberg, C., Andersson, A. F., Sjölund-Karlsson, M., Jansson, J. K. & Engstrand, L. Short-Term Antibiotic Treatment Has Differing Long-Term Impacts on the Human Throat and Gut Microbiome. *PloS One* **5,** e9836 (2010).

241. Lu, K., Lai, K. P., Stoeger, T., Ji, S., Lin, Z., Lin, X., Chan, T. F., Fang, J. K.-H., Lo, M., Gao, L., Qiu, C., Chen, S., Chen, G., Li, L. & Wang, L. Detrimental Effects of Microplastic Exposure on Normal and Asthmatic Pulmonary Physiology. *Journal of Hazardous Materials* **416,** 126069 (2021).

242. Li, Y., Shi, T., Li, X., Sun, H., Xia, X., Ji, X., Zhang, J., Liu, M., Lin, Y., Zhang, R., Zheng, Y. & Tang, J. Inhaled Tire-Wear Microplastic Particles Induced Pulmonary Fibrotic Injury via Epithelial Cytoskeleton Rearrangement. *Environment International* **164,** 107257 (2022).

243. Palaniappan, S., Sadacharan, C. M. & Rostama, B. Polystyrene and Polyethylene Microplastics Decrease Cell Viability and Dysregulate Inflammatory and Oxidative Stress Markers of MDCK and L929 Cells *In Vitro*. *Exposure and Health* **14,** 75–85 (2022).

244. Shim, W. J., Hong, S. H. & Eo, S. E. Identification Methods in Microplastic Analysis: A Review. *Analytical Methods* **9,** 1384–1391 (2017).

245. Rafiee, M., Dargahi, L., Eslami, A., Beirami, E., Jahangiri-Rad, M., Sabour, S. & Amereh, F. Neurobehavioral Assessment of Rats Exposed to Pristine Polystyrene Nanoplastics upon Oral Exposure. *Chemosphere* **193,** 745–753 (2018).

246. Conner, S. D. & Schmid, S. L. Regulated Portals of Entry into the Cell. *Nature* **422,** 37–44 (2003).

247. Unfried, K., Albrecht, C., Klotz, L.-O., Von Mikecz, A., Grether-Beck, S. & Schins, R. P. Cellular Responses to Nanoparticles: Target Structures and Mechanisms. *Nanotoxicology* **1,** 52–71 (2007).

248. Doherty, G. J. & McMahon, H. T. Mechanisms of Endocytosis. *Annual Review of Biochemistry* **78,** 857–902 (2009).

249. Hillaireau, H. & Couvreur, P. Nanocarriers' Entry into the Cell: Relevance to Drug Delivery. *Cellular and Molecular Life Sciences* **66,** 2873–2896 (2009).

250. Kuhn, D. A., Vanhecke, D., Michen, B., Blank, F., Gehr, P., Petri-Fink, A. & Rothen-Rutishauser, B. Different Endocytotic Uptake Mechanisms for Nanoparticles in Epithelial Cells and Macrophages. *Beilstein Journal of Nanotechnology* **5,** 1625–1636 (2014).

251. Schmid, S. L. Clathrin-Coated Vesicle Formation and Protein Sorting: An Integrated Process. *Annual Review of Biochemistry* **66,** 511–548 (1997).

252. Lu, L. & Walker, W. A. Pathologic and Physiologic Interactions of Bacteria with the Gastrointestinal Epithelium. *The American Journal of Clinical Nutrition* **73,** 1124S–1130S (2001).

253. Lambrecht, B. N. & Hammad, H. The Airway Epithelium in Asthma. *Nature Medicine* **18,** 684–692 (2012).

254. Ganesan, S., Comstock, A. T. & Sajjan, U. S. Barrier Function of Airway Tract Epithelium. *Tissue Barriers* **1,** e24997 (2013).

255. Matter, K. & Mellman, I. Mechamisms of Cell Polarity: Sorting and Transport in Epithelial Cells. *Current Opinion in Cell Biology* **6,** 545–554 (1994).

256. Mostov, K. E., Verges, M. & Altschuler, Y. Membrane Traffic in Polarized Epithelial Cells. *Current Opinion in Cell Biology* **12,** 483–490 (2000).

257. Stearns, R. C., Paulauskis, J. D. & Godleski, J. J. Endocytosis of Ultrafine Particles by A549 Cells. *American Journal of Respiratory Cell and Molecular Biology* **24,** 108–115 (2001).

258. Kirchhausen, T., Owen, D. & Harrison, S. C. Molecular Structure, Function, and Dynamics of Clathrin-Mediated Membrane Traffic. *Cold Spring Harbor Perspectives in Biology* **6,** a016725 (2014).

259. Brodsky, F. M., Chen, C.-Y., Knuehl, C., Towler, M. C. & Wakeham, D. E. Biological Basket Weaving: Formation and Function of Clathrin-Coated Vesicles. *Annual Review of Cell and Developmental Biology* **17,** 517–568 (2001).

260. Schmid, E. M., Ford, M. G. J., Burtey, A., Praefcke, G. J. K., Peak-Chew, S.-Y., Mills, I. G., Benmerah, A. & McMahon, H. T. Role of the AP2 β-Appendage Hub in Recruiting Partners for Clathrin-Coated Vesicle Assembly. *PLoS Biology* **4,** e262 (2006).

261. De Duve, C. The Lysosome. *Scientific American* **208,** 64–73 (1963).

262. Appelqvist, H., Wäster, P., Kågedal, K. & Öllinger, K. The Lysosome: From Waste Bag to Potential Therapeutic Target. *Journal of Molecular Cell Biology* **5,** 214–226 (2013).

263. Lawrence, R. E. & Zoncu, R. The Lysosome as a Cellular Centre for Signalling, Metabolism and Quality Control. *Nature Cell Biology* **21,** 133–142 (2019).

264. Schmid, E. M. & McMahon, H. T. Integrating Molecular and Network Biology to Decode Endocytosis. *Nature* **448,** 883–888 (2007).

265. Rothberg, K. G., Heuser, J. E., Donzell, W. C., Ying, Y.-S., Glenney, J. R. & Anderson, R. G. Caveolin, a Protein Component of Caveolae Membrane Coats. *Cell* **68,** 673–682 (1992).

266. Parton, R. G. & Simons, K. The Multiple Faces of Caveolae. *Nature Reviews Molecular Cell Biology* **8,** 185–194 (2007).

267. Liu, L., Xu, K., Zhang, B., Ye, Y., Zhang, Q. & Jiang, W. Cellular Internalization and Release of Polystyrene Microplastics and Nanoplastics. *Science of The Total Environment* **779,** 146523–146535 (2021).

268. Aderem, A. & Underhill, D. M. Mechanisms of Phagocytosis in Macrophages. *Annual Review of Immunology* **17,** 593–623 (1999).

269. Underhill, D. M. & Ozinsky, A. Phagocytosis of Microbes: Complexity in Action. *Annual review of Immunology* **20,** 825 (2002).

270. Flannagan, R. S., Jaumouillé, V. & Grinstein, S. The Cell Biology of Phagocytosis. *Annual Review of Pathology: Mechanisms of Disease* **7,** 61–98 (2012).

271. Roos, A., Xu, W., Castellano, G., Nauta, A. J., Garred, P., Daha, M. R. & van Kooten, C. Mini-Review: A Pivotal Role for Innate Immunity in the Clearance of Apoptotic Cells. *European Journal of Immunology* **34,** 921–929 (2004).

272. Richards, D. M. & Endres, R. G. The Mechanism of Phagocytosis: Two Stages of Engulfment. *Biophysical Journal* **107,** 1542–1553 (2014).

273. Epstein, J., Eichbaum, Q., Sheriff, S. & Ezekowitz, R. A. B. The Collectins in Innate Immunity. *Current Opinion in Immunology* **8,** 29–35 (1996).

274. Stahl, P. D. & Ezekowitz, R. A. B. The Mannose Receptor Is a Pattern Recognition Receptor Involved in Host Defense. *Current Opinion in Immunology* **10,** 50–55 (1998).

275. Joshi, T., Butchar, J. P. & Tridandapani, S. Fcγ Receptor Signaling in Phagocytes. *International Journal of Hematology* **84,** 210–216 (2006).

276. Janeway Jr, C. A. The Immune System Evolved to Discriminate Infectious Nonself from Noninfectious Self. *Immunology Today* **13,** 11–16 (1992).

277. Bianchi, M. E. DAMPs, PAMPs and Alarmins: All We Need to Know about Danger. *Journal of Leukocyte Biology* **81,** 1–5 (2007).

278. Kumar, H., Kawai, T. & Akira, S. Pathogen Recognition by the Innate Immune System. *International Reviews of Immunology* **30,** 16–34 (2011).

279. Peiser, L., Mukhopadhyay, S. & Gordon, S. Scavenger Receptors in Innate Immunity. *Current Opinion in Immunology* **14,** 123–128 (2002).

280. Cheng, C., Hu, Z., Cao, L., Peng, C. & He, Y. The Scavenger Receptor SCARA1 (CD204) Recognizes Dead Cells through Spectrin. *Journal of Biological Chemistry* **294,** 18881–18897 (2019).

281. Ezekowitz, R., Sastry, K., Bailly, P. & Warner, A. Molecular Characterization of the Human Macrophage Mannose Receptor: Demonstration of Multiple Carbohydrate Recognition-like Domains and Phagocytosis of Yeasts in Cos-1 Cells. *The Journal of Experimental Medicine* **172,** 1785–1794 (1990).

282. Allen, L. & Aderem, A. Molecular Definition of Distinct Cytoskeletal Structures Involved in Complement-and Fc Receptor-Mediated Phagocytosis in Macrophages. *The Journal of Experimental Medicine* **184,** 627–637 (1996).

283. Winkelstein, J. A. Opsonins: Their Function, Identity, and Clinical Significance. *The Journal of Pediatrics* **82,** 747–753 (1973).

284. Ehlenberger, A. G. & Nussenzweig, V. The Role of Membrane Receptors for C3B and C3d in Phagocytosis. *The Journal of Experimental Medicine* **145,** 357–371 (1977).

285. Moghimi, S. M. & Patel, H. M. Serum Opsonins and Phagocytosis of Saturated and Unsaturated Phospholipid Liposomes. *Biochimica et Biophysica Acta (BBA) - Biomembranes* **984,** 384–387 (1989).

286. Carroll, M. C. The Role of Complement and Complement Receptors in Induction and Regulation of Immunity. *Annual Review of Immunology* **16,** 545 (1998).

287. Ravetch, J. V. & Bolland, S. IGg Fc Receptors. *Annual Review of Immunology* **19,** 275 (2001).

288. Wu, Y., Tibrewal, N. & Birge, R. B. Phosphatidylserine Recognition by Phagocytes: A View to a Kill. *Trends in Cell Biology* **16,** 189–197 (2006).

289. Fuentes, A.-L., Millis, L., Vapenik, J. & Sigola, L. Lipopolysaccharide-Mediated Enhancement of Zymosan Phagocytosis by RAW 264.7 Macrophages Is Independent of Opsonins, Laminarin, Mannan, and Complement Receptor 3. *journal of Surgical Research* **189,** 304–312 (2014).

290. Merle, N. S., Noe, R., Halbwachs-Mecarelli, L., Fremeaux-Bacchi, V. & Roumenina, L. T. Complement System Part II: Role in Immunity. *Frontiers in Immunology* **6,** 257 (2015).

291. Jun, J.-I. & Lau, L. F. CCN1 Is an Opsonin for Bacterial Clearance and a Direct Activator of Toll-like Receptor Signaling. *Nature Communications* **11,** 1–15 (2020).

292. Liu, D., Liu, F. & Song, Y. K. Recognition and Clearance of Liposomes Containing Phosphatidylserine Are Mediated by Serum Opsonin. *Biochimica et Biophysica Acta (BBA) - Biomembranes* **1235,** 140–146 (1995).

293. Frank, M. M. & Fries, L. F. The Role of Complement in Inflammation and Phagocytosis. *Immunology Today* **12,** 322–326 (1991).

294. Papini, E., Tavano, R. & Mancin, F. Opsonins and Dysopsonins of Nanoparticles: Facts, Concepts, and Methodological Guidelines. *Frontiers in Immunology* **11,** 567365 (2020).

295. Griffin Jr, F. M., Griffin, J. A., Leider, J. E. & Silverstein, S. C. Studies on the Mechanism of Phagocytosis. I. Requirements for Circumferential Attachment of Particle-Bound Ligands to Specific Receptors on the Macrophage Plasma Membrane. *The Journal of Experimental Medicine* **142,** 1263–1282 (1975).

296. Paul, D., Achouri, S., Yoon, Y.-Z., Herre, J., Bryant, C. E. & Cicuta, P. Phagocytosis Dynamics Depends on Target Shape. *Biophysical Journal* **105,** 1143–1150 (2013).

297. Leclerc, L., Boudard, D., Pourchez, J., Forest, V., Sabido, O., Bin, V., Palle, S., Grosseau, P., Bernache, D. & Cottier, M. Quantification of Microsized Fluorescent Particles Phagocytosis to a Better Knowledge of Toxicity Mechanisms. *Inhalation Toxicology* **22,** 1091–1100 (2010).

298. Griffiths, G., Hoflack, B., Simons, K., Mellman, I. & Kornfeld, S. The Mannose 6-Phosphate Receptor and the Biogenesis of Lysosomes. *Cell* **52,** 329–341 (1988).

299. Vieira, O. V., Bucci, C., Harrison, R. E., Trimble, W. S., Lanzetti, L., Gruenberg, J., Schreiber, A. D., Stahl, P. D. & Grinstein, S. Modulation of Rab5 and Rab7 Recruitment to Phagosomes by Phosphatidylinositol 3-Kinase. *Molecular and Cellular Biology* **23,** 2501–2514 (2003).

300. Desjardins, M., Huber, L. A., Parton, R. G. & Griffiths, G. Biogenesis of Phagolysosomes Proceeds through a Sequential Series of Interactions with the Endocytic Apparatus. *The Journal of Cell Biology* **124,** 677–688 (1994).

301. Smith, J. A. Neutrophils, Host Defense, and Inflammation: A Double-Edged Sword. *Journal of Leukocyte Biology* **56,** 672–686 (1994).

302. Nathan, C. Neutrophils and Immunity: Challenges and Opportunities. *Nature Reviews Immunology* **6,** 173–182 (2006).

303. Urban, C. F., Lourido, S. & Zychlinsky, A. How Do Microbes Evade Neutrophil Killing? *Cellular Microbiology* **8,** 1687–1696 (2006).

304. Johnson, M. B., Ball, L. M., Daily, K. P., Martin, J. N., Columbus, L. & Criss, A. K. Opa+ *Neisseria gonorrhoeae* Exhibits Reduced Survival in Human Neutrophils via Src Family Kinase-Mediated Bacterial Trafficking into Mature Phagolysosomes. *Cellular Microbiology* **17,** 648–665 (2015).

305. Babior, B. M. The Respiratory Burst of Phagocytes. *The Journal of Clinical Investigation* **73,** 599–601 (1984).

306. De Groote, M. A., Ochsner, U. A., Shiloh, M. U., Nathan, C., McCord, J. M., Dinauer, M. C., Libby, S. J., Vazquez-Torres, A., Xu, Y. & Fang, F. C. Periplasmic Superoxide Dismutase Protects *Salmonella* From Products of Phagocyte NADPH-Oxidase and Nitric Oxide Synthase. *Proceedings of the National Academy of Sciences* **94,** 13997–14001 (1997).

307. Banerjee, R., Anguita, J., Roos, D. & Fikrig, E. Cutting Edge: Infection by the Agent of Human Granulocytic Ehrlichiosis Prevents the Respiratory Burst by Down-Regulating $gp91^{phox}$. *The Journal of Immunology* **164,** 3946–3949 (2000).

308. Mantegazza, A. R., Savina, A., Vermeulen, M., Pérez, L., Geffner, J., Hermine, O., Rosenzweig, S. D., Faure, F. & Amigorena, S. NADPH Oxidase Controls Phagosomal pH and Antigen Cross-Presentation in Human Dendritic Cells. *Blood, The Journal of the American Society of Hematology* **112,** 4712–4722 (2008).

309. Cooper, J. A. Effects of Cytochalasin and Phalloidin on Actin. *Journal of Cell Biology* **105,** 1473–1478 (1987).

310. Fenteany, G. & Glogauer, M. Cytoskeletal Remodeling in Leukocyte Function. *Current Opinion in Hematology* **11,** 15–24 (2004).

311. Christian, A., Haynes, M., Phillips, M. & Rothblat, G. Use of Cyclodextrins for Manipulating Cellular Cholesterol Content. *Journal of Lipid Research* **38,** 2264–2272 (1997).

312. Ivanov, A. I. Pharmacological Inhibition of Endocytic Pathways: Is It Specific Enough to Be Useful? *Exocytosis and Endocytosis,* 15–33 (2008).

313. McMahon, H. T. & Boucrot, E. Molecular Mechanism and Physiological Functions of Clathrin-Mediated Endocytosis. *Nature Reviews Molecular Cell Biology* **12,** 517–533 (2011).

314. Iversen, T.-G., Skotland, T. & Sandvig, K. Endocytosis and Intracellular Transport of Nanoparticles: Present Knowledge and Need for Future Studies. *Nano Today* **6,** 176–185 (2011).

315. Dos Santos, T., Varela, J., Lynch, I., Salvati, A. & Dawson, K. A. Effects of Transport Inhibitors on the Cellular Uptake of Carboxylated Polystyrene Nanoparticles in Different Cell Lines. *PloS One* **6,** e24438 (2011).

316. Jiang, L. Q., Wang, T. Y., Webster, T. J., Duan, H.-J., Qiu, J. Y., Zhao, Z. M., Yin, X. X. & Zheng, C. L. Intracellular Disposition of Chitosan Nanoparticles in Macrophages: Intracellular Uptake, Exocytosis, and Intercellular Transport. *International Journal of Nanomedicine* **12,** 6383 (2017).

317. Kato, T., Yashiro, T., Murata, Y., Herbert, D. C., Oshikawa, K., Bando, M., Ohno, S. & Sugiyama, Y. Evidence That Exogenous Substances Can Be Phagocytized by Alveolar Epithelial Cells and Transported into Blood Capillaries. *Cell and Tissue Research* **311,** 47–51 (2003).

318. Fadok, V., McDonald, P., Bratton, D. & Henson, P. Regulation of Macrophage Cytokine Production by Phagocytosis of Apoptotic and Post-apoptotic Cells. *Biochemical Society Transactions* **26,** 653–656 (1998).

319. Arnold, L., Henry, A., Poron, F., Baba-Amer, Y., Van Rooijen, N., Plonquet, A., Gherardi, R. K. & Chazaud, B. Inflammatory Monocytes Recruited after Skeletal Muscle Injury Switch into Antiinflammatory Macrophages to Support Myogenesis. *The Journal of Experimental Medicine* **204,** 1057–1069 (2007).

320. Antonios, J. K., Yao, Z., Li, C., Rao, A. J. & Goodman, S. B. Macrophage Polarization in Response to Wear Particles *In Vitro*. *Cellular & Molecular Immunology* **10,** 471–482 (2013).

321. Xie, W., Fu, X., Tang, F., Mo, Y., Cheng, J., Wang, H. & Chen, X. Dose-Dependent Modulation Effects of Bioactive Glass Particles on Macrophages and Diabetic Wound Healing. *Journal of Materials Chemistry B* **7,** 940–952 (2019).

322. Kodelja, V., Müller, C., Tenorio, S., Schebesch, C., Orfanos, C. E. & Goerdt, S. Differences in Angiogenic Potential of Classically vs Alternatively Activated Macrophages. *Immunobiology* **197,** 478–493 (1997).

323. Zhao, L., Shi, W., Hu, F., Song, X., Cheng, Z. & Zhou, J. Prolonged Oral Ingestion of Microplastics Induced Inflammation in the Liver Tissues of C57BL/6J Mice through Polarization of Macrophages and Increased Infiltration of Natural Killer Cells. *Ecotoxicology and Environmental Safety* **227,** 112882 (2021).

324. Costa, E. C., Moreira, A. F., de Melo-Diogo, D., Gaspar, V. M., Carvalho, M. P. & Correia, I. J. 3D Tumor Spheroids: An Overview on the Tools and Techniques Used for Their Analysis. *Biotechnology Advances* **34,** 1427–1441 (2016).

325. Lee, D., Pathak, S. & Jeong, J.-H. Design and Manufacture of 3D Cell Culture Plate for Mass Production of Cell-Spheroids. *Scientific Reports* **9,** 1–8 (2019).

326. Białkowska, K., Komorowski, P., Bryszewska, M. & Miłowska, K. Spheroids as a Type of Three-Dimensional Cell Cultures- Examples of Methods of Preparation and the Most Important Application. *International Journal of Molecular Sciences* **21,** 6225 (2020).

327. Shao, C., Chi, J., Zhang, H., Fan, Q., Zhao, Y. & Ye, F. Development of Cell Spheroids by Advanced Technologies. *Advanced Materials Technologies* **5,** 2000183 (2020).

328. Foty, R. A Simple Hanging Drop Cell Culture Protocol for Generation of 3D Spheroids. *Journal of Visualized Experiments,* e2720 (2011).

329. Sorrentino, G., Rezakhani, S., Yildiz, E., Nuciforo, S., Heim, M. H., Lutolf, M. P. & Schoonjans, K. Mechano-Modulatory Synthetic Niches for Liver Organoid Derivation. *Nature Communications* **11,** 3416 (2020).

330. Singh, S. K., Abbas, S., Saxena, A. K., Tiwari, S., Sharma, L. K. & Tiwari, M. Critical Role of Three-Dimensional Tumorsphere Size on Experimental Outcome. *BioTechniques* **69,** 333–338 (2020).

331. Ryu, N.-E., Lee, S.-H. & Park, H. Spheroid Culture System Methods and Applications for Mesenchymal Stem Cells. *Cells* **8,** 1620 (2019).

332. Desai, P. K., Tseng, H. & Souza, G. R. Assembly of Hepatocyte Spheroids Using Magnetic 3D Cell Culture for CYP450 Inhibition/Induction. *International Journal of Molecular Sciences* **18,** 1085 (2017).

333. Eglen, R. M. & Reisine, T. Human iPS Cell-Derived Patient Tissues and 3D Cell Culture Part 2: Spheroids, Organoids, and Disease Modeling. *Slas Technology: Translating Life Sciences Innovation* **24,** 18–27 (2019).

334. Subramanian, A., Sidhom, E.-H., Emani, M., Vernon, K., Sahakian, N., Zhou, Y., Kost-Alimova, M., Slyper, M., Waldman, J., Dionne, D., Nguyen, L. T., Weins, A., Marshall, J. L., Rosenblatt-Rosen, O., Regev, A. & Greka, A. Single Cell Census of Human Kidney Organoids Shows Reproducibility and Diminished Off-Target Cells after Transplantation. *Nature Communications* **10,** 1–15 (2019).

335. Berishvili, E., Casiraghi, F., Amarelli, C., Scholz, H., Piemonti, L., Berney, T. & Montserrat, N. Mini-Organs Forum: How to Advance Organoid Technology to Organ Transplant Community. *Transplant International* **34,** 1588–1593 (2021).

336. Sarvestani, S. K., Signs, S., Hu, B., Yeu, Y., Feng, H., Ni, Y., Hill, D. R., Fisher, R. C., Ferrandon, S., DeHaan, R. K., Stiene, J., Cruise, M., Hwang, T. H., Shen, X., Spence, J. R. & Huang, E. H. Induced Organoids Derived from Patients with Ulcerative Colitis Recapitulate Colitic Reactivity. *Nature Communications* **12,** 1–18 (2021).

337. Guan, Y., Xu, D., Garfin, P. M., Ehmer, U., Hurwitz, M., Enns, G., Michie, S., Wu, M., Zheng, M., Nishimura, T., Sage, J. & Peltz, G. Human Hepatic Organoids for the Analysis of Human Genetic Diseases. *JCI Insight* **2** (2017).

338. Rios, A. C. & Clevers, H. Imaging Organoids: A Bright Future Ahead. *Nature Methods* **15,** 24–26 (2018).

339. Hua, T., Kiran, S., Li, Y. & Sang, Q.-X. A. Microplastics Exposure Affects Neural Development of Human Pluripotent Stem Cell-Derived Cortical Spheroids. *Journal of Hazardous Materials* **435,** 128884 (2022).

340. Cheng, W., Li, X., Zhou, Y., Yu, H., Xie, Y., Guo, H., Wang, H., Li, Y., Feng, Y. & Wang, Y. Polystyrene Microplastics Induce Hepatotoxicity and Disrupt Lipid Metabolism in the Liver Organoids. *Science of The Total Environment* **806,** 150328 (2022).

341. Winkler, A., Santo, N., Madaschi, L., Cherubini, A., Rusconi, F., Rosso, L., Tremolada, P., Lazzari, L. & Bacchetta, R. Lung Organoids and Microplastic Fibers: A New Exposure Model for Emerging Contaminants. *bioRxiv* (2021).

342. Winkler, A. S., Cherubini, A., Rusconi, F., Santo, N., Madaschi, L., Pistoni, C., Moschetti, G., Sarnicola, M. L., Crosti, M., Rosso, L., Tremolada, P., Lazzari, L. & Baccetta, R. Human Airway Organoids and Microplastic Fibers: A New Exposure Model for Emerging Contaminants. *Environment International* **163,** 107200 (2022).

343. Hou, Z., Meng, R., Chen, G., Lai, T., Qing, R., Hao, S., Deng, J. & Wang, B. Distinct Accumulation of Nanoplastics in Human Intestinal Organoids. *Science of The Total Environment,* 155811 (2022).

344. Dobrovolskaia, M. A., Aggarwal, P., Hall, J. B. & McNeil, S. E. Preclinical Studies to Understand Nanoparticle Interaction with the Immune System and Its Potential Effects on Nanoparticle Biodistribution. *Molecular Pharmaceutics* **5,** 487–495 (2008).

345. Martin, L. M., Gan, N., Wang, E., Merrill, M. & Xu, W. Materials, Surfaces, and Interfacial Phenomena in Nanoplastics Toxicology Research. *Environmental Pollution* **292,** 118442 (2022).

346. Hoshyar, N., Gray, S., Han, H. & Bao, G. The Effect of Nanoparticle Size on *In Vivo* Pharmacokinetics and Cellular Interaction. *Nanomedicine* **11,** 673–692 (2016).

347. Kumar, V., Sharma, N. & Maitra, S. *In Vitro* and *In Vivo* Toxicity Assessment of Nanoparticles. *International Nano Letters* **7,** 243–256 (2017).

348. Nel, A., Xia, T., Madler, L. & Li, N. Toxic Potential of Materials at the Nanolevel. *Science* **311,** 622–627 (2006).

349. Duffin, R., Tran, L., Brown, D., Stone, V. & Donaldson, K. Proinflammogenic Effects of Low-Toxicity and Metal Nanoparticles *In Vivo* and *In Vitro*: Highlighting the Role of Particle Surface Area and Surface Reactivity. *Inhalation Toxicology* **19,** 849–856 (2007).

350. Yang, H., Liu, C., Yang, D., Zhang, H. & Xi, Z. Comparative Study of Cytotoxicity, Oxidative Stress and Genotoxicity Induced by Four Typical Nanomaterials: The Role of Particle Size, Shape and Composition. *Journal of Applied Toxicology* **29,** 69–78 (2009).

351. Nair, S., Sasidharan, A., Divya Rani, V., Menon, D., Nair, S., Manzoor, K. & Raina, S. Role of Size Scale of Zno Nanoparticles and Microparticles on Toxicity toward Bacteria and Osteoblast Cancer Cells. *Journal of Materials Science: Materials in Medicine* **20,** 235–241 (2009).

352. Sabbioni, E., Fortaner, S., Farina, M., Del Torchio, R., Olivato, I., Petrarca, C., Bernardini, G., Mariani-Costantini, R., Perconti, S., Di Giampaolo, L., Gornati, R. & Di Giocchino, M. Cytotoxicity and Morphological Transforming Potential of Cobalt Nanoparticles, Microparticles and Ions in Balb/3T3 Mouse Fibroblasts: An *In Vitro* Model. *Nanotoxicology* **8,** 455–464 (2014).

353. Sahu, D., Kannan, G., Tailang, M. & Vijayaraghavan, R. *In Vitro* Cytotoxicity of Nanoparticles: A Comparison between Particle Size and Cell Type. *Journal of Nanoscience* **2016** (2016).

354. Wang, L., Huang, X., Sun, W., Too, H. Z., Laserna, A. K. C. & Li, S. F. Y. A Global Metabolomic Insight into the Oxidative Stress and Membrane Damage of Copper Oxide Nanoparticles and Microparticles on Microalga Chlorella vulgaris. *Environmental Pollution* **258,** 113647 (2020).

355. Chang, M.-C., Tang, C.-M., Lin, Y.-H., Liu, H.-C., Wang, T.-M., Lan, W.-C., Cheng, R.-H., Lin, Y.-R., Chang, H.-H. & Jeng, J.-H. Toxic Mechanisms of Roth801, Canals, Microparticles and Nanoparticles of ZnO on MG-63 Osteoblasts. *Materials Science and Engineering: C* **119,** 111635 (2021).

356. Chen, M. & von Mikecz, A. Formation of Nucleoplasmic Protein Aggregates Impairs Nuclear Function in Response to SiO_2 Nanoparticles. *Experimental Cell Research* **305,** 51–62 (2005).

357. Liang, B., Zhong, Y., Huang, Y., Lin, X., Liu, J., Lin, L., Hu, M., Jiang, J., Dai, M., Wang, B., Zhang, B., Meng, H., Lelaka, J. J. J., Sui, H., Yang, X. & Huang, Z. Underestimated Health Risks: Polystyrene Micro-and Nanoplastics Jointly Induce Intestinal Barrier Dysfunction by Ros-Mediated Epithelial Cell Apoptosis. *Particle and Fibre Toxicology* **18,** 1–19 (2021).

358. Paul, M. B., Stock, V., Cara-Carmona, J., Lisicki, E., Shopova, S., Fessard, V., Braeuning, A., Sieg, H. & Böhmert, L. Micro-and Nanoplastics- Current State of Knowledge with the Focus on Oral Uptake and Toxicity. *Nanoscale Advances* **2,** 4350–4367 (2020).

359. Schirinzi, G. F., Pérez-Pomeda, I., Sanchís, J., Rossini, C., Farré, M. & Barceló, D. Cytotoxic Effects of Commonly Used Nanomaterials and Microplastics on Cerebral and Epithelial Human Cells. *Environmental Research* **159,** 579–587 (2017).

360. Hesler, M., Aengenheister, L., Ellinger, B., Drexel, R., Straskraba, S., Jost, C., Wagner, S., Meier, F., von Briesen, H., Büchel, C., Wick, P., Buerki-Thurnerr, T. & Kohl, Y. Multi-Endpoint Toxicological Assessment of Polystyrene Nano-and Microparticles in Different Biological Models *In Vitro*. *Toxicology in Vitro* **61,** 104610 (2019).

361. Dong, C.-D., Chen, C.-W., Chen, Y.-C., Chen, H.-H., Lee, J.-S. & Lin, C.-H. Polystyrene Microplastic Particles: *In Vitro* Pulmonary Toxicity Assessment. *Journal of Hazardous Materials* **385,** 121575 (2020).

362. Hoehne, M., Samuel, F., Dong, A., Wurth, C., Mahler, H.-C., Carpenter, J. F. & Randolph, T. W. Adsorption of Monoclonal Antibodies to Glass Microparticles. *Journal of Pharmaceutical Sciences* **100,** 123–132 (2011).

363. Vakifahmetoglu, C., Zeydanli, D., Ozalp, V. C., Borsa, B. A. & Soraru, G. D. Hierarchically Porous Polymer Derived Ceramics: A Promising Platform for Multidrug Delivery Systems. *Materials & Design* **140,** 37–44 (2018).

364. Yadavali, S., Jeong, H.-H., Lee, D. & Issadore, D. Silicon and Glass Very Large Scale Microfluidic Droplet Integration for Terascale Generation of Polymer Microparticles. *Nature Communications* **9,** 1–9 (2018).

365. Kawaguchi, S. & Ito, K. Dispersion Polymerization. *Polymer Particles* **175,** 299–328 (2005).

366. Barner, L. Synthesis of Microspheres as Versatile Functional Scaffolds for Materials Science Applications. *Advanced Materials* **21,** 2547–2553 (2009).

367. Klibanov, A. L. Targeted Delivery of Gas-Filled Microspheres, Contrast Agents for Ultrasound Imaging. *Advanced Drug Delivery Reviews* **37,** 139–157 (1999).

368. Kawaguchi, H. Functional Polymer Microspheres. *Progress in Polymer Science* **25,** 1171–1210 (2000).

369. Sinha, V., Singla, A. K., Wadhawan, S., Kaushik, R., Kumria, R., Bansal, K. & Dhawan, S. Chitosan Microspheres as a Potential Carrier for Drugs. *International Journal of Pharmaceutics* **274,** 1–33 (2004).

370. Freiberg, S. & Zhu, X. Polymer Microspheres for Controlled Drug Release. *International Journal of Pharmaceutics* **282,** 1–18 (2004).

371. Singh, C., Purohit, S., Singh, M. & Pandey, B. Design and Evaluation of Microspheres: A Review. *Journal of Drug Delivery Research* **2,** 18–27 (2013).

372. Hossain, K. M. Z., Patel, U. & Ahmed, I. Development of Microspheres for Biomedical Applications: A Review. *Progress in Biomaterials* **4,** 1–19 (2015).

373. Lok, K. P. & Ober, C. K. Particle Size Control in Dispersion Polymerization of Polystyrene. *Canadian Journal of Chemistry* **63,** 209–216 (1985).

374. Arshady, R. Suspension, Emulsion, and Dispersion Polymerization: A Methodological Survey. *Colloid and Polymer Science* **270,** 717–732 (1992).

375. Hou, W.-H. & Lloyd, T. B. A New Technique for Preparing Monodisperse Polymer Particles. *Journal of Applied Polymer Science* **45,** 1783–1788 (1992).

376. O'Donnell, P. B. & McGinity, J. W. Preparation of Microspheres by the Solvent Evaporation Technique. *Advanced Drug Delivery Reviews* **28,** 25–42 (1997).

377. Winslow, F. & Matreyek, W. Particle Size in Suspension Polymerization. *Industrial & Engineering Chemistry* **43,** 1108–1112 (1951).

378. Vanderhoff, J. W. *Mechanism of Emulsion Polymerization* in *Journal of Polymer Science: Polymer Symposia* **72** (1985), 161–198.

379. Tseng, C., Lu, Y., El-Aasser, M. & Vanderhoff, J. Uniform Polymer Particles by Dispersion Polymerization in Alcohol. *Journal of Polymer Science Part A: Polymer Chemistry* **24,** 2995–3007 (1986).

380. Landfester, K., Schork, F. J. & Kusuma, V. A. Particle Size Distribution in Mini-Emulsion Polymerization. *Comptes Rendus Chimie* **6,** 1337–1342 (2003).

381. Chern, C. Emulsion Polymerization Mechanisms and Kinetics. *Progress in Polymer Science* **31,** 443–486 (2006).

382. Kotoulas, C. & Kiparissides, C. A Generalized Population Balance Model for the Prediction of Particle Size Distribution in Suspension Polymerization Reactors. *Chemical Engineering Science* **61,** 332–346 (2006).

383. Li, G. L., Möhwald, H. & Shchukin, D. G. Precipitation Polymerization for Fabrication of Complex Core–Shell Hybrid Particles and Hollow Structures. *Chemical Society Reviews* **42,** 3628–3646 (2013).

384. Chaudhary, V. & Sharma, S. Suspension Polymerization Technique: Parameters Affecting Polymer Properties and Application in Oxidation Reactions. *Journal of Polymer Research* **26,** 1–12 (2019).

385. Lovell, P. A. & Schork, F. J. Fundamentals of Emulsion Polymerization. *Biomacromolecules* **21,** 4396–4441 (2020).

386. Zhang, H. Controlled/"Living" Radical Precipitation Polymerization: A Versatile Polymerization Technique for Advanced Functional Polymers. *European Polymer Journal* **49,** 579–600 (2013).

387. Hooker, J. P., Delafresnaye, L., Barner, L. & Barner-Kowollik, C. With Polymer Photoclicks to Fluorescent Microspheres. *Materials Horizons* **6,** 356–363 (2019).

388. Zhang, R., Gao, R., Gou, Q., Lai, J. & Li, X. Precipitation Polymerization: A Powerful Tool for Preparation of Uniform Polymer Particles. *Polymers* **14,** 1851 (2022).

389. Pardeshi, S. & Singh, S. K. Precipitation Polymerization: A Versatile Tool for Preparing Molecularly Imprinted Polymer Beads for Chromatography Applications. *RSC Advances* **6,** 23525–23536 (2016).

390. Goh, E. C. & Stöver, H. D. Cross-Linked Poly (Methacrylic Acid-Co-poly (Ethylene Oxide) Methyl Ether Methacrylate) Microspheres and Microgels Prepared by Precipitation Polymerization: A Morphology Study. *Macromolecules* **35,** 9983–9989 (2002).

391. Li, W.-H. & Stöver, H. D. Porous Monodisperse Poly (Divinylbenzene) Microspheres by Precipitation Polymerization. *Journal of Polymer Science Part A: Polymer Chemistry* **36,** 1543–1551 (1998).

392. Brochard, F. & De Gennes, P. Dynamical Scaling for Polymers in Theta Solvents. *Macromolecules* **10,** 1157–1161 (1977).

393. Adam, M. & Delsanti, M. Viscosity and Longest Relaxation Time of Semi-dilute Polymer Solutions: II. Theta Solvent. *Journal de Physique* **45,** 1513–1521 (1984).

394. Terao, K. & Mays, J. W. On-Line Measurement of Molecular Weight and Radius of Gyration of Polystyrene in a Good Solvent and in a Theta Solvent Measured With a Two-Angle Light Scattering Detector. *European Polymer Journal* **40,** 1623–1627 (2004).

395. Yoshimatsu, K., Reimhult, K., Krozer, A., Mosbach, K., Sode, K. & Ye, L. Uniform Molecularly Imprinted Microspheres and Nanoparticles Prepared by Precipitation Polymerization: The Control of Particle Size Suitable for Different Analytical Applications. *Analytica Chimica Acta* **584,** 112–121 (2007).

396. Hooker, J. P., Feist, F., Delafresnaye, L., Barner, L. & Barner-Kowollik, C. Precisely Controlled Microsphere Design via Visible-Light Cross-Linking of Functional Prepolymers. *Advanced Functional Materials* **30,** 1905399 (2020).

397. Bodmeier, R. & McGinity, J. W. The Preparation and Evaluation of Drug-Containing Poly (DL-Lactide) Microspheres Formed by the Solvent Evaporation Method. *Pharmaceutical Research* **4,** 465–471 (1987).

398. Beck, L. R., Cowsar, D. R., Lewis, D. H., Cosgrove Jr, R. J., Riddle, C. T., Lowry, S. L. & Epperly, T. A New Long-Acting Injectable Microcapsule System for the Administration of Progesterone. *Fertility and Sterility* **31,** 545–551 (1979).

399. Arshady, R. Microspheres and Microcapsules, a Survey of Manufacturing Techniques: Part III: Solvent Evaporation. *Polymer Engineering & Science* **30,** 915–924 (1990).

400. Rosca, I. D., Watari, F. & Uo, M. Microparticle Formation and Its Mechanism in Single and Double Emulsion Solvent Evaporation. *Journal of Controlled Release* **99,** 271–280 (2004).

401. Krishna Sailaja, A. & Jyothika, M. A Review on Microcapsules. *CIBTech Journal of Pharmaceutical Sciences* **4,** 26–33 (2014).

402. Si, W., Yang, Q., Zong, Y., Ren, G., Zhao, L., Hong, M. & Xin, Z. Toward Understanding the Effect of Solvent Evaporation on the Morphology of PLGA Microspheres by Double Emulsion Method. *Industrial & Engineering Chemistry Research* **60,** 9196–9205 (2021).

403. Suzuki, K., Shuto, I. & Hagura, Y. Characteristics of the Membrane Emulsification Method Combined with Preliminary Emulsification for Preparing Corn Oil-In-Water Emulsions. *Food Science and Technology International* **2,** 43–47 (1996).

404. Vladisavljević, G. T., Shimizu, M. & Nakashima, T. Preparation of Monodisperse Multiple Emulsions at High Production Rates by Multi-Stage Premix Membrane Emulsification. *Journal of Membrane Science* **244,** 97–106 (2004).

405. Sawalha, H., Purwanti, N., Rinzema, A., Schroën, K. & Boom, R. Polylactide Microspheres Prepared by Premix Membrane Emulsification- Effects of Solvent Removal Rate. *Journal of Membrane Science* **310,** 484–493 (2008).

406. Nazir, A., Schroën, K. & Boom, R. Premix Emulsification: A Review. *Journal of Membrane Science* **362,** 1–11 (2010).

407. Ma, G. Microencapsulation of Protein Drugs for Drug Delivery: Strategy, Preparation, and Applications. *Journal of Controlled Release* **193,** 324–340 (2014).

408. Zaveri, T. D., Dolgova, N. V., Lewis, J. S., Hamaker, K., Clare-Salzler, M. J. & Keselowsky, B. G. Macrophage Integrins Modulate Response to Ultra-High Molecular Weight Polyethylene Particles and Direct Particle-Induced Osteolysis. *Biomaterials* **115,** 128–140 (2017).

409. Zhang, C., Jugold, M., Woenne, E. C., Lammers, T., Morgenstern, B., Mueller, M. M., Zentgraf, H., Bock, M., Eisenhut, M., Semmler, W. & Kiessling, F. Specific Targeting of Tumor Angiogenesis by RGD-Conjugated Ultrasmall Superparamagnetic Iron Oxide Particles Using a Clinical 1.5-T Magnetic Resonance Scanner. *Cancer Research* **67,** 1555–1562 (2007).

410. Sun, C., Lee, J. S. & Zhang, M. Magnetic Nanoparticles in MR Imaging and Drug Delivery. *Advanced Drug Delivery Reviews* **60,** 1252–1265 (2008).

411. Salatin, S., Maleki Dizaj, S. & Yari Khosroushahi, A. Effect of the Surface Modification, Size, and Shape on Cellular Uptake of Nanoparticles. *Cell Biology International* **39,** 881–890 (2015).

412. Behzadi, S., Serpooshan, V., Tao, W., Hamaly, M. A., Alkawareek, M. Y., Dreaden, E. C., Brown, D., Alkilany, A. M., Farokhzad, O. C. & Mahmoudi, M. Cellular Uptake of Nanoparticles: Journey inside the Cell. *Chemical Society Reviews* **46,** 4218–4244 (2017).

413. Tabata, Y. & Ikada, Y. Effect of the Size and Surface Charge of Polymer Microspheres on Their Phagocytosis by Macrophage. *Biomaterials* **9,** 356–362 (1988).

414. Champion, J. A., Walker, A. & Mitragotri, S. Role of Particle Size in Phagocytosis of Polymeric Microspheres. *Pharmaceutical Research* **25,** 1815–1821 (2008).

415. Gaumet, M., Gurny, R. & Delie, F. Localization and Quantification of Biodegradable Particles in an Intestinal Cell Model: The Influence of Particle Size. *European Journal of Pharmaceutical Sciences* **36,** 465–473 (2009).

416. Kettler, K., Veltman, K., van De Meent, D., van Wezel, A. & Hendriks, A. J. Cellular Uptake of Nanoparticles as Determined by Particle Properties, Experimental Conditions, and Cell Type. *Environmental Toxicology and Chemistry* **33,** 481–492 (2014).

417. Champion, J. A. & Mitragotri, S. Role of Target Geometry in Phagocytosis. *Proceedings of the National Academy of Sciences* **103,** 4930–4934 (2006).

418. Doshi, N. & Mitragotri, S. Macrophages Recognize Size and Shape of Their Targets. *PloS One* **5,** e10051 (2010).

419. Lu, Z., Qiao, Y., Zheng, X. T., Chan-Park, M. B. & Li, C. M. Effect of Particle Shape on Phagocytosis of CdTe Quantum Dot-Cystine Composites. *MedChemComm* **1,** 84–86 (2010).

420. Koval, M., Preiter, K., Adles, C., Stahl, P. D. & Steinberg, T. H. Size of IgG-Opsonized Particles Determines Macrophage Response during Internalization. *Experimental Cell Research* **242,** 265–273 (1998).

421. Monteiro-Riviere, N. A., Samberg, M. E., Oldenburg, S. J. & Riviere, J. E. Protein Binding Modulates the Cellular Uptake of Silver Nanoparticles into Human Cells: Implications for *In Vitro* to *In Vivo* Extrapolations? *Toxicology Letters* **220,** 286–293 (2013).

422. Mao, Z., Zhou, X. & Gao, C. Influence of Structure and Properties of Colloidal Biomaterials on Cellular Uptake and Cell Functions. *Biomaterials Science* **1,** 896–911 (2013).

423. Kurtz-Chalot, A., Villiers, C., Pourchez, J., Boudard, D., Martini, M., Marche, P. N., Cottier, M. & Forest, V. Impact of Silica Nanoparticle Surface Chemistry on Protein Corona Formation and Consequential Interactions with Biological Cells. *Materials Science and Engineering: C* **75,** 16–24 (2017).

424. Gilberti, R. M., Joshi, G. N. & Knecht, D. A. The Phagocytosis of Crystalline Silica Particles by Macrophages. *American Journal of Respiratory Cell and Molecular Biology* **39,** 619–627 (2008).

425. Gratton, S. E., Ropp, P. A., Pohlhaus, P. D., Luft, J. C., Madden, V. J., Napier, M. E. & DeSimone, J. M. The Effect of Particle Design on Cellular Internalization Pathways. *Proceedings of the National Academy of Sciences* **105,** 11613–11618 (2008).

426. Fröhlich, E. The Role of Surface Charge in Cellular Uptake and Cytotoxicity of Medical Nanoparticles. *International Journal of Nanomedicine* **7,** 5577 (2012).

427. Harush-Frenkel, O., Debotton, N., Benita, S. & Altschuler, Y. Targeting of Nanoparticles to the Clathrin-Mediated Endocytic Pathway. *Biochemical and Biophysical Research Communications* **353,** 26–32 (2007).

428. Sunderland, C. J., Steiert, M., Talmadge, J. E., Derfus, A. M. & Barry, S. E. Targeted Nanoparticles for Detecting and Treating Cancer. *Drug Development Research* **67,** 70–93 (2006).

429. Choi, H. S., Ashitate, Y., Lee, J. H., Kim, S. H., Matsui, A., Insin, N., Bawendi, M. G., Semmler-Behnke, M., Frangioni, J. V. & Tsuda, A. Rapid Translocation of Nanoparticles from the Lung Airspaces to the Body. *Nature Biotechnology* **28,** 1300–1303 (2010).

430. Liu, Q., Guan, J., Qin, L., Zhang, X. & Mao, S. Physicochemical Properties Affecting the Fate of Nanoparticles in Pulmonary Drug Delivery. *Drug Discovery Today* **25,** 150–159 (2020).

431. Yue, Z.-G., Wei, W., Lv, P.-P., Yue, H., Wang, L.-Y., Su, Z.-G. & Ma, G.-H. Surface Charge Affects Cellular Uptake and Intracellular Trafficking of Chitosan-Based Nanoparticles. *Biomacromolecules* **12,** 2440–2446 (2011).

432. Chen, X., Liu, Y., Wang, L., Liu, Y., Zhang, W., Fan, B., Ma, X., Yuan, Q., Ma, G. & Su, Z. Enhanced Humoral and Cell-Mediated Immune Responses Generated by Cationic Polymer-Coated PLA Microspheres with Adsorbed HbsAg. *Molecular Pharmaceutics* **11,** 1772–1784 (2014).

433. Song, C., Zhang, X., Wei, W. & Ma, G. Principles of Regulating Particle Multiscale Structures for Controlling Particle-Cell Interaction Process. *Chemical Engineering Science* **232,** 116343 (2021).

434. Ahsan, F., Rivas, I. P., Khan, M. A. & Suárez, A. I. T. Targeting to Macrophages: Role of Physicochemical Properties of Particulate Carriers—Liposomes and Microspheres—on the Phagocytosis by Macrophages. *Journal of Controlled Release* **79,** 29–40 (2002).

435. Faraasen, S., Vörös, J., Csúcs, G., Textor, M., Merkle, H. P. & Walter, E. Ligand-Specific Targeting of Microspheres to Phagocytes by Surface Modification with Poly (L-Lysine)-Grafted Poly (Ethylene Glycol) Conjugate. *Pharmaceutical Research* **20,** 237–246 (2003).

436. Beningo, K. A. & Wang, Y.-l. Fc-Receptor-Mediated Phagocytosis Is Regulated by Mechanical Properties of the Target. *Journal of Cell Science* **115,** 849–856 (2002).

437. Mahmoudi, M., Saeedi-Eslami, S. N., Shokrgozar, M. A., Azadmanesh, K., Hassanlou, M., Kalhor, H. R., Burtea, C., Rothen-Rutishauser, B., Laurent, S., Sheibani, S. & Vali, H. Cell "Vision": Complementary Factor of Protein Corona in Nanotoxicology. *Nanoscale* **4,** 5461–5468 (2012).

438. Lunov, O., Syrovets, T., Loos, C., Beil, J., Delacher, M., Tron, K., Nienhaus, G. U., Musyanovych, A., Mailander, V., Landfester, K. & Simmet, T. Differential Uptake of Functionalized Polystyrene Nanoparticles by Human Macrophages and a Monocytic Cell Line. *ACS Nano* **5,** 1657–1669 (2011).

439. Fleischer, C. C. & Payne, C. K. Nanoparticle–Cell Interactions: Molecular Structure of the Protein Corona and Cellular Outcomes. *Accounts of Chemical Research* **47,** 2651–2659 (2014).

440. Treuel, L., Brandholt, S., Maffre, P., Wiegele, S., Shang, L. & Nienhaus, G. U. Impact of Protein Modification on the Protein Corona on Nanoparticles and Nanoparticle-Cell Interactions. *ACS Nano* **8,** 503–513 (2014).

441. Gräfe, C., Weidner, A., vd Lühe, M., Bergemann, C., Schacher, F. H., Clement, J. H. & Dutz, S. Intentional Formation of a Protein Corona on Nanoparticles: Serum Concentration Affects Protein Corona Mass, Surface Charge, and Nanoparticle-Cell Interaction. *The International Journal of Biochemistry & Cell Biology* **75,** 196–202 (2016).

442. Lynch, I. & Dawson, K. A. Protein-Nanoparticle Interactions. *Nano-Enabled Medical Applications,* 231–250 (2008).

443. Wheeler, K. E., Chetwynd, A. J., Fahy, K. M., Hong, B. S., Tochihuitl, J. A., Foster, L. A. & Lynch, I. Environmental Dimensions of the Protein Corona. *Nature Nanotechnology* **16,** 617–629 (2021).

444. Galdino, F. E., Picco, A. S., Sforca, M. L., Cardoso, M. B. & Loh, W. Effect of Particle Functionalization and Solution Properties on the Adsorption of Bovine Serum Albumin and Lysozyme onto Silica Nanoparticles. *Colloids and Surfaces B: Biointerfaces* **186,** 110677 (2020).

445. Li, X., He, E., Xia, B., Liu, Y., Zhang, P., Cao, X., Zhao, L., Xu, X. & Qiu, H. Protein Corona-Induced Aggregation of Differently Sized Nanoplastics: Impacts of Protein Type and Concentration. *Environmental Science: Nano* **8,** 1560–1570 (2021).

446. Hadjidemetriou, M. & Kostarelos, K. Evolution of the Nanoparticle Corona. *Nature Nanotechnology* **12,** 288–290 (2017).

447. Docter, D., Westmeier, D., Markiewicz, M., Stolte, S., Knauer, S. & Stauber, R. The Nanoparticle Biomolecule Corona: Lessons Learned–Challenge Accepted? *Chemical Society Reviews* **44,** 6094–6121 (2015).

448. Saavedra, J., Stoll, S. & Slaveykova, V. I. Influence of Nanoplastic Surface Charge on Eco-Corona Formation, Aggregation and Toxicity to Freshwater Zooplankton. *Environmental Pollution* **252,** 715–722 (2019).

449. Fadare, O. O., Wan, B., Liu, K., Yang, Y., Zhao, L. & Guo, L.-H. Eco-Corona vs Protein Corona: Effects of Humic Substances on Corona Formation and Nanoplastic Particle Toxicity in *Daphnia magna*. *Environmental Science & Technology* **54,** 8001–8009 (2020).

450. Cedervall, T., Lynch, I., Lindman, S., Berggård, T., Thulin, E., Nilsson, H., Dawson, K. A. & Linse, S. Understanding the Nanoparticle-Protein Corona Using Methods to Quantify Exchange Rates and Affinities of Proteins for Nanoparticles. *Proceedings of the National Academy of Sciences* **104,** 2050–2055 (2007).

451. Lundqvist, M., Stigler, J., Elia, G., Lynch, I., Cedervall, T. & Dawson, K. A. Nanoparticle Size and Surface Properties Determine the Protein Corona with Possible Implications for Biological Impacts. *Proceedings of the National Academy of Sciences* **105,** 14265–14270 (2008).

452. Casals, E., Pfaller, T., Duschl, A., Oostingh, G. J. & Puntes, V. Time Evolution of the Nanoparticle Protein Corona. *ACS Nano* **4,** 3623–3632 (2010).

453. Winzen, S., Schoettler, S., Baier, G., Rosenauer, C., Mailaender, V., Landfester, K. & Mohr, K. Complementary Analysis of the Hard and Soft Protein Corona: Sample Preparation Critically Effects Corona Composition. *Nanoscale* **7,** 2992–3001 (2015).

454. Corbo, C., Molinaro, R., Parodi, A., Toledano Furman, N. E., Salvatore, F. & Tasciotti, E. The Impact of Nanoparticle Protein Corona on Cytotoxicity, Immunotoxicity and Target Drug Delivery. *Nanomedicine* **11,** 81–100 (2016).

455. Latreille, P.-L., Le Goas, M., Salimi, S., Robert, J., De Crescenzo, G., Boffito, D. C., Martinez, V. A., Hildgen, P. & Banquy, X. Scratching the Surface of the Protein Corona: Challenging Measurements and Controversies. *ACS Nano* **16,** 1689–1707 (2022).

456. Wang, H., Shang, L., Maffre, P., Hohmann, S., Kirschhöfer, F., Brenner-Weiß, G. & Nienhaus, G. U. The Nature of a Hard Protein Corona Forming on Quantum Dots Exposed to Human Blood Serum. *Small* **12,** 5836–5844 (2016).

457. Carril, M., Padro, D., Del Pino, P., Carrillo-Carrion, C., Gallego, M. & Parak, W. J. *In Situ* Detection of the Protein Corona in Complex Environments. *Nature Communications* **8,** 1–5 (2017).

458. Mahmoudi, M., Lynch, I., Ejtehadi, M. R., Monopoli, M. P., Bombelli, F. B. & Laurent, S. Protein- Nanoparticle Interactions: Opportunities and Challenges. *Chemical Reviews* **111,** 5610–5637 (2011).

459. Vroman, L. Protein-Nanoparticle Interactionseffect of Adsorbed Proteins on the Wettability of Hydrophilic and Hydrophobic Solids. *Nature* **196,** 476–477 (1962).

460. Tenzer, S., Docter, D., Kuharev, J., Musyanovych, A., Fetz, V., Hecht, R., Schlenk, F., Fischer, D., Kiouptsi, K., Reinhardt, C., Landfester, K., Schild, H., Maskos, M., Knauer, S. K. & Stauber, R. H. Rapid Formation of Plasma Protein Corona Critically Affects Nanoparticle Pathophysiology. *Nature Nanotechnology,* 772–781 (2013).

461. Ishida, T., Harashima, H. & Kiwada, H. Interactions of Liposomes with Cells *In Vitro* and *In Vivo*: Opsonins and Receptors. *Current Drug Metabolism* **2,** 397–409 (2001).

462. Owens III, D. E. & Peppas, N. A. Opsonization, Biodistribution, and Pharmacokinetics of Polymeric Nanoparticles. *International Journal of Pharmaceutics* **307,** 93–102 (2006).

463. Monopoli, M. P., Walczyk, D., Campbell, A., Elia, G., Lynch, I., Baldelli Bombelli, F. & Dawson, K. A. Physical- Chemical Aspects of Protein Corona: Relevance to *In Vitro* and *In Vivo* Biological Impacts of Nanoparticles. *Journal of the American Chemical Society* **133,** 2525–2534 (2011).

464. Camner, P., Lundborg, M., Låstbom, L., Gerde, P., Gross, N. & Jarstrand, C. Experimental and Calculated Parameters on Particle Phagocytosis by Alveolar Macrophages. *Journal of Applied Physiology* **92,** 2608–2616 (2002).

465. Dobrovolskaia, M. A., Patri, A. K., Zheng, J., Clogston, J. D., Ayub, N., Aggarwal, P., Neun, B. W., Hall, J. B. & McNeil, S. E. Interaction of Colloidal Gold Nanoparticles with Human Blood: Effects on Particle Size and Analysis of Plasma Protein Binding Profiles. *Nanomedicine: Nanotechnology, Biology and Medicine* **5,** 106–117 (2009).

466. Fleischer, C. C. & Payne, C. K. Nanoparticle Surface Charge Mediates the Cellular Receptors Used by Protein-Nanoparticle Complexes. *The Journal of Physical Chemistry B* **116,** 8901–8907 (2012).

467. Hollóczki, O. & Gehrke, S. Nanoplastics Can Change the Secondary Structure of Proteins. *Scientific Reports* **9,** 1–7 (2019).

468. Fleischer, C. C. & Payne, C. K. Secondary Structure of Corona Proteins Determines the Cell Surface Receptors Used by Nanoparticles. *The Journal of Physical Chemistry B* **118,** 14017–14026 (2014).

469. Monopoli, M. P., Åberg, C., Salvati, A. & Dawson, K. A. Biomolecular Coronas Provide the Biological Identity of Nanosized Materials. *Nature Nanotechnology* **7,** 779–786 (2012).

470. Mahmoudi, M., Abdelmonem, A. M., Behzadi, S., Clement, J. H., Dutz, S., Ejtehadi, M. R., Hartmann, R., Kantner, K., Linne, U., Maffre, P., Metzler, S., Moghadam, M. K., Pfeiffer, C., Rezaei, M., Ruiz-Lozano, P., Serpooshan, V., Shokrgozar, M. A., Nienhaus, U. G. & Parak, W. J. Temperature: The "Ignored" Factor at the Nanobio Interface. *ACS Nano* **7,** 6555–6562 (2013).

471. Nagayama, S., Ogawara, K.-i., Fukuoka, Y., Higaki, K. & Kimura, T. Time-Dependent Changes in Opsonin Amount Associated on Nanoparticles Alter Their Hepatic Uptake Characteristics. *International Journal of Pharmaceutics* **342,** 215–221 (2007).

472. Aggarwal, P., Hall, J. B., McLeland, C. B., Dobrovolskaia, M. A. & McNeil, S. E. Nanoparticle Interaction with Plasma Proteins as It Relates to Particle Biodistribution, Biocompatibility and Therapeutic Efficacy. *Advanced Drug Delivery Reviews* **61,** 428–437 (2009).

473. Lesniak, A., Fenaroli, F., Monopoli, M. P., Åberg, C., Dawson, K. A. & Salvati, A. Effects of the Presence or Absence of a Protein Corona on Silica Nanoparticle Uptake and Impact on Cells. *ACS Nano* **6,** 5845–5857 (2012).

474. Mirshafiee, V., Kim, R., Mahmoudi, M. & Kraft, M. L. The Importance of Selecting a Proper Biological Milieu for Protein Corona Analysis *In Vitro*: Human Plasma versus Human Serum. *The International Journal of Biochemistry & Cell Biology* **75,** 188–195 (2016).

475. Gref, R., Domb, A., Quellec, P., Blunk, T., Müller, R., Verbavatz, J.-M. & Langer, R. The Controlled Intravenous Delivery of Drugs Using PEG-Coated Sterically Stabilized Nanospheres. *Advanced Drug Delivery Reviews* **16,** 215–233 (1995).

476. Moghimi, S. M., Muir, I., Illum, L., Davis, S. S. & Kolb-Bachofen, V. Coating Particles with a Block Co-polymer (Poloxamine-908) Suppresses Opsonization but Permits the Activity of Dysopsonins in the Serum. *Biochimica et Biophysica Acta (BBA) - Molecular Cell Research* **1179,** 157–165 (1993).

477. Göppert, T. & Müller, R. Adsorption Kinetics of Plasma Proteins on Solid Lipid Nanoparticles for Drug Targeting. *International Journal of Pharmaceutics* **302,** 172–186 (2005).

478. Li, X., He, E., Jiang, K., Peijnenburg, W. J. & Qiu, H. The Crucial Role of a Protein Corona in Determining the Aggregation Kinetics and Colloidal Stability of Polystyrene Nanoplastics. *Water Research* **190,** 116742 (2021).

479. Tenzer, S., Docter, D., Rosfa, S., Wlodarski, A., Kuharev, J., Rekik, A., Knauer, S. K., Bantz, C., Nawroth, T., Bier, C., Sirirattanapan, J., Mann, W., Treuel, L., Zellner, R., Maskos, M., Schild, H. & Stauber, R. H. Nanoparticle Size Is a Critical Physicochemical Determinant of the Human Blood Plasma Corona: A Comprehensive Quantitative Proteomic Analysis. *ACS Nano* **5,** 7155–7167 (2011).

480. Thomas, W., McGrath, L., Baarson, K., Auletta, C., Daly, I. & McConnell, R. Subchronic Oral Toxicity of Cellulose Acetate in Rats. *Food and chemical toxicology* **29,** 453–458 (1991).

481. Mayer, J. M., Elion, G. R., Buchanan, C. M., Sullivan, B. K., Pratt, S. D. & Kaplan, D. L. Biodegradable Blends of Cellulose Acetate and Starch: Production and Properties. *Journal of Macromolecular Science, Part A: Pure and Applied Chemistry* **32,** 775–785 (1995).

482. Chen, Y., Qiu, Y., Chen, W. & Wei, Q. Electrospun Thymol-Loaded Porous Cellulose Acetate Fibers with Potential Biomedical Applications. *Materials Science and Engineering: C* **109,** 110536 (2020).

483. Wagenknecht, W., Fanter, C. & Loth, F. *Verfahren zur Herstellung von sphärischen Mikropartikeln auf Celluloseacetat-Basis* `https://patents.google.com/patent/EP0750007B1/de?oq=EP0750007B1`. Patent EP0750007. 1996.

484. Kowalski, W., Bahnfleth, W. P. & Whittam, T. Filtration of Airborne Microorganisms: Modeling and Prediction. *ASHRAE Transactions* **105,** 4–17 (1999).

485. Sadauskas, E., Wallin, H., Stoltenberg, M., Vogel, U., Doering, P., Larsen, A. & Danscher, G. Kupffer Cells Are Central in the Removal of Nanoparticles from the Organism. *Particle and Fibre Toxicology* **4,** 1–7 (2007).

486. Wang, Z.-Y., Burlak, C., Klaunig, J. E. & Kamendulis, L. M. Development of a Cytokine-Producing Immortalized Murine Kupffer Cell Line. *Cytokine* **70,** 165–172 (2014).

487. Shah, B., Kona, S., Gilbertson, T. A. & Nguyen, K. T. Effects of Poly-(Lactide-Co-glycolide) Nanoparticles on Electrophysiological Properties of Enteroendocrine Cells. *Journal of Nanoscience and Nanotechnology* **11,** 3533–3542 (2011).

488. Kamakura, R., Raza, G. S., Prasannan, A., Walkowiak, J. & Herzig, K.-H. Dipeptidyl Peptidase-4 and GLP-1 Interplay in STC-1 and GLUtag Cell Lines. *Peptides* **134,** 170419 (2020).

489. Shang, L., Nienhaus, K. & Nienhaus, G. U. Engineered Nanoparticles Interacting with Cells: Size Matters. *Journal of Nanobiotechnology* **12,** 1–11 (2014).

490. Attia, M. F., Anton, N., Akasov, R., Chiper, M., Markvicheva, E. & Vandamme, T. F. Biodistribution and Toxicity of X-Ray Iodinated Contrast Agent in Nano-Emulsions in Function of Their Size. *Pharmaceutical Research* **33,** 603–614 (2016).

491. Aguilar, K. C., Tello, F., Bierhalz, A. C., Romo, M. G. G., Flores, H. E. M. & Grosso, C. R. Protein Adsorption onto Alginate-Pectin Microparticles and Films Produced by Ionic Gelation. *Journal of Food Engineering* **154,** 17–24 (2015).

492. Rahmati, M. & Mozafari, M. Protein Adsorption on Polymers. *Materials Today Communications* **17,** 527–540 (2018).

493. Lee, Y. & Geckeler, K. E. Cytotoxicity and Cellular Uptake of Lysozyme-Stabilized Gold Nanoparticles. *Journal of Biomedical Materials Research Part A* **100,** 848–855 (2012).

494. Musyanovych, A., Dausend, J., Dass, M., Walther, P., Mailänder, V. & Landfester, K. Criteria Impacting the Cellular Uptake of Nanoparticles: A Study Emphasizing Polymer Type and Surfactant Effects. *Acta Biomaterialia* **7,** 4160–4168 (2011).

495. Coorens, M., Scheenstra, M. R., Veldhuizen, E. J. & Haagsman, H. P. Interspecies Cathelicidin Comparison Reveals Divergence in Antimicrobial Activity, Tlr Modulation, Chemokine Induction and Regulation of Phagocytosis. *Scientific Reports* **7,** 1–11 (2017).

496. Van Lookeren Campagne, M., Wiesmann, C. & Brown, E. J. Macrophage Complement Receptors and Pathogen Clearance. *Cellular Microbiology* **9,** 2095–2102 (2007).

497. Heesters, B. A., Chatterjee, P., Kim, Y.-A., Gonzalez, S. F., Kuligowski, M. P., Kirchhausen, T. & Carroll, M. C. Endocytosis and Recycling of Immune Complexes by Follicular Dendritic Cells Enhances B Cell Antigen Binding and Activation. *Immunity* **38,** 1164–1175 (2013).

498. Lambris, J. D. The Multifunctional Role of C3, the Third Component of Complement. *Immunology Today* **9,** 387–393 (1988).

499. Thurman, J. M. & Holers, V. M. The Central Role of the Alternative Complement Pathway in Human Disease. *The Journal of Immunology* **176,** 1305–1310 (2006).

500. Stock, V., Laurisch, C., Franke, J., Dönmez, M. H., Voss, L., Böhmert, L., Braeuning, A. & Sieg, H. Uptake and Cellular Effects of PE, PP, PET and PVC Microplastic Particles. *Toxicology in Vitro* **70,** 105021 (2021).

501. Brown, E. J. Complement Receptors, Adhesion, and Phagocytosis. *Infectious Agents and Disease* **1,** 63–70 (1992).

502. García-García, E. & Rosales, C. Signal Transduction During Fc Receptor-Mediated Phagocytosis. *Journal of Leukocyte Biology* **72,** 1092–1108 (2002).

503. Wang, H., Zhang, M., Bianchi, M., Sherry, B., Sama, A. & Tracey, K. J. Fetuin (α2-HS-Glycoprotein) Opsonizes Cationic Macrophagedeactivating Molecules. *Proceedings of the National Academy of Sciences* **95,** 14429–14434 (1998).

504. Ricklin, D., Reis, E. S., Mastellos, D. C., Gros, P. & Lambris, J. D. Complement Component C3- The "Swiss Army Knife" of Innate Immunity and Host Defense. *Immunological Reviews* **274,** 33–58 (2016).

505. Oh, N. & Park, J.-H. Surface Chemistry of Gold Nanoparticles Mediates Their Exocytosis in Macrophages. *ACS Nano* **8,** 6232–6241 (2014).

506. Wu, B., Wu, X., Liu, S., Wang, Z. & Chen, L. Size-Dependent Effects of Polystyrene Microplastics on Cytotoxicity and Efflux Pump Inhibition in Human Caco-2 Cells. *Chemosphere* **221,** 333–341 (2019).

507. Liu, T., Hou, B., Wang, Z. & Yang, Y. Polystyrene Microplastics Induce Mitochondrial Damage in Mouse GC-2 Cells. *Ecotoxicology and Environmental Safety* **237,** 113520 (2022).

508. Scott, C. C., Vacca, F. & Gruenberg, J. *Endosome Maturation, Transport and Functions* in *Seminars in cell & Developmental Biology* **31** (2014), 2–10.

509. Podinovskaia, M. & Spang, A. The Endosomal Network: Mediators and Regulators of Endosome Maturation. *Endocytosis and Signaling,* 1–38 (2018).

510. De Chastellier, C. & Thilo, L. Phagosome Maturation and Fusion with Lysosomes in Relation to Surface Property and Size of the Phagocytic Particle. *European Journal of Cell Biology* **74,** 49–62 (1997).

511. Christoforidis, S., McBride, H. M., Burgoyne, R. D. & Zerial, M. The Rab5 Effector EEA1 is a Core Component of Endosome Docking. *Nature* **397,** 621–625 (1999).

512. Hyttinen, J. M., Niittykoski, M., Salminen, A. & Kaarniranta, K. Maturation of Autophagosomes and Endosomes: A Key Role for Rab7. *Biochimica et Biophysica Acta (BBA)-Molecular Cell Research* **1833,** 503–510 (2013).

513. Vieira, O. V., Botelho, R. J. & Grinstein, S. Phagosome Maturation: Aging Gracefully. *Biochemical Journal* **366,** 689–704 (2002).

514. Bohdanowicz, M. & Grinstein, S. Vesicular Traffic: A Rab SANDwich. *Current Biology* **20,** R311–R314 (2010).

515. Mukherjee, K., Khatua, B. & Mandal, C. Sialic Acid-Siglec-E Interactions during *Pseudomonas aeruginosa* Infection of Macrophages Interferes with Phagosome Maturation by Altering Intracellular Calcium Concentrations. *Frontiers in Immunology* **11,** 332 (2020).

516. Lee, H.-J., Woo, Y., Hahn, T.-W., Jung, Y. M. & Jung, Y.-J. Formation and Maturation of the Phagosome: A Key Mechanism in Innate Immunity against Intracellular Bacterial Infection. *Microorganisms* **8,** 1298 (2020).

517. Uribe-Querol, E. & Rosales, C. Phagocytosis: Our Current Understanding of a Universal Biological Process. *Frontiers in Immunology* **11,** 1066 (2020).

518. Egami, Y. Molecular Imaging Analysis of Rab GTPases in the Regulation of Phagocytosis and Macropinocytosis. *Anatomical Science International* **91,** 35–42 (2016).

519. Settembre, C., Fraldi, A., Medina, D. L. & Ballabio, A. Signals From the Lysosome: A Control Centre for Cellular Clearance and Energy Metabolism. *Nature Reviews Molecular Cell Biology* **14,** 283–296 (2013).

520. Zhang, Z., Yue, P., Lu, T., Wang, Y., Wei, Y. & Wei, X. Role of Lysosomes in Physiological Activities, Diseases, and Therapy. *Journal of Hematology & Oncology* **14,** 1–39 (2021).

521. Canton, J. Phagosome Maturation in Polarized Macrophages. *Journal of Leukocyte Biology* **96,** 729–738 (2014).

522. Achilli, T.-M., Meyer, J. & Morgan, J. R. Advances in the Formation, Use and Understanding of Multi-Cellular Spheroids. *Expert Opinion on Biological Therapy* **12,** 1347–1360 (2012).

523. Kleinman, H. K., Philp, D. & Hoffman, M. P. Role of the Extracellular Matrix in Morphogenesis. *Current Opinion in Biotechnology* **14,** 526–532 (2003).

524. Kunz-Schughart, L. A., Schroeder, J. A., Wondrak, M., Van Rey, F., Lehle, K., Hofstaedter, F. & Wheatley, D. N. Potential of Fibroblasts to Regulate the Formation of Three-Dimensional Vessel-like Structures from Endothelial Cells *in Vitro*. *American Journal of Physiology-Cell Physiology* **290,** C1385–C1398 (2006).

525. Nagelkerke, A., Bussink, J., Sweep, F. C. & Span, P. N. Generation of Multicellular Tumor Spheroids of Breast Cancer Cells: How to Go Three-Dimensional. *Analytical Biochemistry* **437,** 17–19 (2013).

526. Thirumala, S., Gimble, J. M. & Devireddy, R. V. Methylcellulose Based Thermally Reversible Hydrogel System for Tissue Engineering Applications. *Cells* **2,** 460–475 (2013).

527. Delplace, V., Pickering, A. J., Hettiaratchi, M. H., Zhao, S., Kivijärvi, T. & Shoichet, M. S. Inverse Electron-Demand Diels-Alder Methylcellulose Hydrogels Enable the Co-Delivery of Chondroitinase ABC and Neural Progenitor Cells. *Biomacromolecules* **21,** 2421–2431 (2020).

5 Publikationen und Manuskripte

∗ gleichberechtigte Co-Autorenschaft

I. **Rudolph, J.***, Völkl, M.*, Jérôme, V., Scheibel, T., & Freitag, R. Noxic Effects of Polystyrene Microparticles on Murine Macrophages and Epithelial Cells. *Scientific Reports*, **11** (1), 1-16 (2021). doi: https://doi.org/10.1038/s41598-021-95073-9

II. Ramsperger, A. F. R. M.*, **Jasinski, J.***, Völkl, M.*, Witzmann, T., Meinhart, M., Jérôme, V., Kretschmer, W. P., Freitag, R., Senker, J., Fery, A., Kress, H., Scheibel., T. & Laforsch, C. Supposedly Identical Microplastic Particles Substantially Differ in Their Material Properties Influencing Particle-Cell Interactions and Cellular Responses. *Journal of Hazardous Materials*, **425**, 127961 (2022). doi: https://doi.org/10.1016/j.jhazmat.2021.127961

III. **Jasinski, J.**, Wilde, M. V., Völkl, M., Jérôme, V., Fröhlich, T., Freitag, R. & Scheibel, T. Tailor-Made Protein Corona Formation on Polystyrene Microparticles and Its Effect on Epithelial Cell Uptake. *ACS Applied Materials & Interfaces*, **14** (41), 47277-47287 (2022). doi: https://doi.org/10.1021/acsami.2c13987

IV. **Jasinski, J.**, Völkl, M., Wilde, M. V., Jérôme, V., Fröhlich, T., Freitag, R., & Scheibel, T. Influence of the Polymer Type of a Microplastic Challenge on the Reaction of Murine Cells. *Journal of Hazardous Materials*, **465**, 133280 (2024). doi: https://doi.org/10.1016/j.jhazmat.2023.133280

V. **Jasinski, J.***, Völkl, M.*, Hahn, J., Jérôme, V., Freitag, R. & Scheibel, T. Polystyrene Microparticle Distribution After Ingestion by Murine Macrophages. *Journal of Hazardous Materials*, **457**, 131796 (2023). doi: https://doi.org/10.1016/j.jhazmat.2023.131796

Publikationen und Manuskripte, welche nicht Teil der Dissertation sind

VI. Riedl, S., A., B.*, Völkl, M.*, Holzinger, A., **Jasinski, J.**, Jérôme, V., Scheibel, T., Feldhaar, H. & Freitag, R. *In Vitro* Cultivation of Primary Intesintal Cells from *Eisenia fetida* as Basis for Ecotoxicological Studies. *Ecotoxicology*, **31**(2), 221-233 (2022). doi: https://doi.org/10.1007/s10646-021-02495-2

VII. Schwarzer, M., Brehm, J., Vollmer, M., **Jasinski, J.**, Xu, C., Zainuddin, S., Fröhlich, T., Schott, M., Greiner, A., Scheibel. T., & Laforsch, C. Shape, Size, and Polymer Dependent Effects of Microplastics on *Daphnia magna*. *Journal of Hazardous Materials* **426**, 128136 (2022). doi: https://doi.org/10.1016/j.jhazmat.2021.128136

VIII. Völkl, M., Jérôme, V., Weig, A., **Jasinski, J.**, Meides, N., Strohriegl, P., Scheibel, T., & Freitag, R. Pristine and Artificially-Aged Polystyrene Microplastic Particles Differ in Regard to Cellular Response. *Journal of Hazardous Materials*, **435**, 128955 (2022). doi: https://doi.org/10.1016/j.jhazmat.2022.128955

IX. Mondellini, S., Schwarzer, M., Völkl, M., **Jasinski, J.**, Jérôme, V., Scheibel, T., Freitag, R., & Laforsch, C. Size Dependent Uptake and Trophic Transfer of Microplastics in Unicellular Freshwater Eukaryotes. *in preparation*

6 Darstellung des Eigenanteils und Teilarbeiten

6.1 Teilarbeit I

Noxic Effects of Polystyrene Microparticles on Murine Macrophages and Epithelial Cells

Autoren: **Julia Rudolph***, Matthias Völkl*, Valérie Jérôme, Thomas Scheibel und Ruth Freitag

∗ gleichberechtigte Co-Autorenschaft

Die Konzeptionierung sowie alle Experimente dieser Teilarbeit wurden zu gleichen Teilen von Matthias Völkl und mir durchgeführt. Dabei wurde die Partikelanalyse mittels DLS und ζ-Potentialmessungen, sowie die qualitativen und quantitativen Analysen der zellulären Interaktion und Aufnahme mittels Rasterelektronenmikroskopie, Konfokalmikroskopie und Durchflusszytometrie von mir durchgeführt und ausgewertet. Zusätzlich wurde der Resazurin Assay von mir durchgeführt und ausgewertet. Daten zu den zellulären Effekten (Zytotoxizität) wurden von Matthias Völkl erhoben. Das Manuskript wurde von mir zusammen mit Matthias Völkl verfasst. Valérie Jérôme, Thomas Scheibel und Ruth Freitag waren an der Konzeptionierung, wissenschaftlichen Diskussionen und der Fertigstellung des Manuskripts beteiligt.

Der Artikel wurde am 03.08.2021 im Journal *Scientific Reports* veröffentlicht.

Nachdruck unter freundlicher Genehmigung des Verlags. Rudolph, J., Völkl, M., Jérôme, V., Scheibel, T. & Freitag, R. Noxic Effects of Polystyrene Microparticles on Murine Macrophages and Epithelial Cells. *Scientific Reports* **11**, 15702 (2021).

www.nature.com/scientificreports

scientific reports

Check for updates

OPEN

Noxic effects of polystyrene microparticles on murine macrophages and epithelial cells

Julia Rudolph[1,7], Matthias Völkl[2,7], Valérie Jérôme[2], Thomas Scheibel[1,3,4,5,6]✉ & Ruth Freitag[2,4]✉

Microplastic (MP) contamination has been identified as an ecological problem with an increasing impact on everyday life. Yet, possible effects of MP at the cellular level are still poorly understood. Here, the interaction of murine macrophages (J774A.1, ImKC) and epithelial cells (STC-1, BNL CL.2) with well-characterized poly(styrene) MP particles (MPP) of varying sizes (0.2–6.0 µm) was studied. Macrophages are expected to actively engulf particles which could be confirmed in this study, while epithelial cells are found in tissues with direct contact with ingested or inhaled MPP. Here, the epithelial cells from both investigated cell lines did not ingest MPP in significant numbers. Concomitantly, no cytotoxic effects nor any influence on cellular proliferation were observed. Cells from the two macrophage cell lines showed high ingestion of MPP of all sizes, but cytotoxic effects were observed only for one of them (ImKC) and only at MPP concentrations above 250 µg/mL. Indications of cellular stress as well as effects on cell proliferation were observed for cell populations with high particle cell interactions.

Large-scale industrial plastic production started in the nineteen-fifties, initially using waste material from the chemical industry as the basis for the production of polyvinyl chloride (PVC)[1–3]. Low production costs, properties like durability, ductility, and lightweight have promoted the increasing use of plastic. Over eight billion tons of plastic have been produced since the beginning, and roughly 80% of the produced plastic is assumed to have accumulated in the environment [4]. Over 10 million tons of plastic waste enter the oceans per year[5], and the latest results indicate that the contamination of the terrestrial environment by plastics may be 4–23 times higher[6–8]. Due to (photo-)chemical, mechanical, and/or biological degradation, larger plastic residues tend to disintegrate into smaller particles[9], so-called microplastic (MP) and nanoplastic. MP is defined as plastic fragments with a size between 0.1 µm and 5 mm[10] and can today be found in all investigated environmental compartments[11–15]. MP has been shown to enter the food chain and to have an impact on the fitness of several species[16–19].

One of the major microplastic entry points into organisms is the ingestion of contaminated food[20,21]. Ingested MPP then migrate through the gastrointestinal tract, where they may interact with the resident tissues and cause gut toxicity (e.g. inflammation of the gut lining). As a consequence, an impairment of the gut-vascular barrier can develop, and MPP then gain access to the liver via the portal vein[22,23]. Effects have in particular been shown in the presence of submicron and nanoparticles, i.e. particles with a diameter < 1 µm. In one study, polystyrene (PS) particles < 0.3 µm were found in the liver, spleen, blood, and bone marrow of rats after 10 days of feeding[24], while particles with a diameter of 0.1 µm were uptaken with a 15- to 250-fold higher frequency by intestinal tissue compared to larger particles (≥ 0.5 µm)[25].

Once foreign matter enters the body, among the first responders at the cellular level are cells of the immune system. Macrophages are specialized in engulfing foreign particular matter via phagocytosis[26]. In this context, exudate and resident macrophages can be differentiated[27] Exudate macrophages are found in the bloodstream, patrolling the whole body ready to reach local inflammation sites[28], while resident macrophages are confined to a specific tissue[29]. The latter are usually specialized in cell morphology and function[30]. Foreign particulate matter acts as a stimulus to activate macrophages. Macrophages, once activated, prime the immune system in

[1]Department of Biomaterials, Faculty of Engineering Sciences, University of Bayreuth, Bayreuth, Germany. [2]Department of Process Biotechnology, Faculty of Engineering Sciences, University of Bayreuth, Bayreuth, Germany. [3]Bayreuth Center for Colloids and Interfaces (BZKG), Universität Bayreuth, Bayreuth, Germany. [4]Bayreuth Center for Molecular Biosciences (BZMB), Universität Bayreuth, Bayreuth, Germany. [5]Bayreuth Center for Material Science (BayMAT), Universität Bayreuth, Bayreuth, Germany. [6]Bavarian Polymer Institute (BPI), Universität Bayreuth, Bayreuth, Germany. [7]These authors contributed equally: Julia Rudolph and Matthias Völkl. ✉email: thomas.scheibel@bm.uni-bayreuth.de; ruth.freitag@uni-bayreuth.de

MPP size (µm)	ζ-potential (mV)				
	KCl	10% FCS	RPMI 1640	$DMEM_{Lonza}$	$DMEM_{ATCC}$
0.2	− 47.4 ± 0.3	− 26.7 ± 0.3	− 26.3 ± 0.1	− 26.9 ± 0.2	− 26.0 ± 0.2
0.5	− 52.8 ± 0.2	− 25.2 ± 0.1	− 26.2 ± 0.1	− 25.2 ± 0.1	− 24.6 ± 0.2
1.0	− 66.1 ± 0.1	− 27.9 ± 0.1	− 29.2 ± 0.5	− 26.4 ± 0.0	− 25.0 ± 0.1
2.0	− 76.7 ± 0.3	− 29.9 ± 0.2	− 30.7 ± 0.1	− 29.3 ± 0.2	− 27.7 ± 0.4
3.0	− 79.0 ± 0.6	− 31.1 ± 0.3	− 29.6 ± 0.4	− 30.3 ± 0.2	− 28.6 ± 0.2
6.0	− 85.4 ± 1.4	− 10.1 ± 0.7	− 11.7 ± 0.2	− 12.7 ± 0.4	− 11.3 ± 0.3

Table 1. ζ-potential analysis of differently sized PS-MPP. MPP were incubated in 1 mM KCl or pre-incubated overnight in growth media (DMEM or RPMI) or 10% (v/v) FCS in 1 × DPBS. The ζ-potential was measured in 1 mM KCl (pH 6). Data represent mean ± SD, n = 3.

various directions, which inter alia tags them as suitable test cells for cytotoxicity assays[31]. The response of macrophages to stimulation ranges from induced cell proliferation, secretion of reactive oxygen species (ROS)[32,33] and interferon-α and -β[34], to delayed hypersensitivity. Phagocytosis goes along with higher oxygen uptake and enhanced production of ROS, known as respiratory burst[35,36]. An increase in ROS resulting from MP ingestion has been already shown in vivo for different organisms[37,38], however, cells grown in vitro seemed to be less affected[39,40]. At physiological levels, ROS function as "redox messengers" in intracellular signaling and regulation, whereas an excess of ROS induces cell death by promoting the intrinsic apoptotic pathway[41].

Whereas phagocytosis is a mechanism for the uptake of larger particles (size ≥ 0.5 µm) and is observed only in specialized cell types like macrophages[42–45], a second endocytotic uptake mechanism, namely pinocytosis can be performed by most cell types. Pinocytosis refers to the uptake of fluids or small particles (< 0.5 µm). Some cells can also take up larger particles (1–5 µm) by macropinocytosis[46]. For a given particle, the uptake mechanism depends on the particle size as well as on its interaction with (specific) receptors to the cellular membrane and in consequence on the cell type[42,44,47]. It has been shown that a given macrophage cell line uses different uptake mechanisms for particles of different sizes. For example, Geiser et al. showed that nanoparticles (0.078 µm in diameter) were ingested using nonphagocytic mechanisms, whereas 0.2 µm and 1 µm particles were ingested by phagocytic mechanisms[48].

Direct effects of MMP on cells are considerably less well studied than their effects on the fitness of entire organisms. Olivier et al. observed cytotoxic effects on murine macrophages (J774A.1) and fibroblasts (L929) for 0.45 and 3.53 µm PS particles at concentrations above 500 µg/mL[49]. Hwang et al. identified cytotoxic effects of 3 µm PS particles at 1000 µg/mL on human dermal fibroblasts[50]. Stock et al. showed a reduced viability of Caco-2 cells, a human epithelial cell line, in the presence of 1 µm PS particles[51]. In most of these studies, MPP were mainly classified by polymer type, particle shape, and size[52–54]. A few studies emphasized the importance of the particle surface for cellular uptake and toxicity[55–58]. In this context, the so-called protein corona, i.e. the highly dynamic protein layer, which forms on the surface of any particle placed in a protein-containing solution, such as whole blood or plasma[59–61], influences the physicochemical surface properties of MPP like surface charge and roughness[62,63] and in turn, the cellular uptake[56,62–65].

Although the particle size is widely recognized as decisive for cellular uptake, few comparative investigations using a series of MPP of a defined and narrow size distribution have been performed so far. Moreover, a clear understanding of how cells from the primary line of defense of the body (i.e. macrophages as part of the immune system and barrier-forming epithelial cells) react to exposure to MPP is largely lacking. In this work, we analyzed the impact of MPP on four murine model cell lines, two macrophage types (J774A.1 from ascites as an example for exudate macrophages and ImKC as an example for hepatic resident macrophages, i.e. Kupffer cells), one intestinal (STC-1) and one hepatic epithelial cell line (BNL Cl.2). Six batches of graded PS particles, each with narrow size distribution and covering a range from 0.2 to 6.0 µm were used. Besides uptake, the impact of the particles on cell metabolism and proliferation was investigated.

Results and discussion

ζ-Potential of MPP. The ζ-potential of MPP is assumed to influence cellular uptake[58,66,67]. Therefore, the ζ-potentials of all MPP were measured in 1 mM KCl (pH 6) and after incubation in the different growth media or fetal calf serum (FCS) diluted in DPBS (Table 1).

The ζ-potential decreased with increasing MPP diameter from − 47.4 ± 0.3 mV for 0.2 µm particles to − 85.4 ± 1.4 mV for 6 µm particles in KCl. In growth medium and FCS, the ζ-potential was higher and the pronounced difference observed as a function of the particle size after incubation in KCl solution was not observed in this case. Instead, all ζ-potentials fell in the range between − 10 and − 30 mV. Similar effects of incubation in cell culture media on the ζ-potential have been observed previously[67,68]. Since the effect of FCS-containing culture media on the ζ-potential was similar to that of 10% FCS in DPBS, we assume that the observed effects are mainly due to a corona formed on the MPP by proteins from FCS rather than culture medium-specific components. Since all culture media used in our study contained FCS, we expect similar protein coronae for all MPP once they had come into contact with the cell culture media during the experiments. In consequence, all MPP are expected to show similar surface properties, and their reaction with different cell lines can be compared directly.

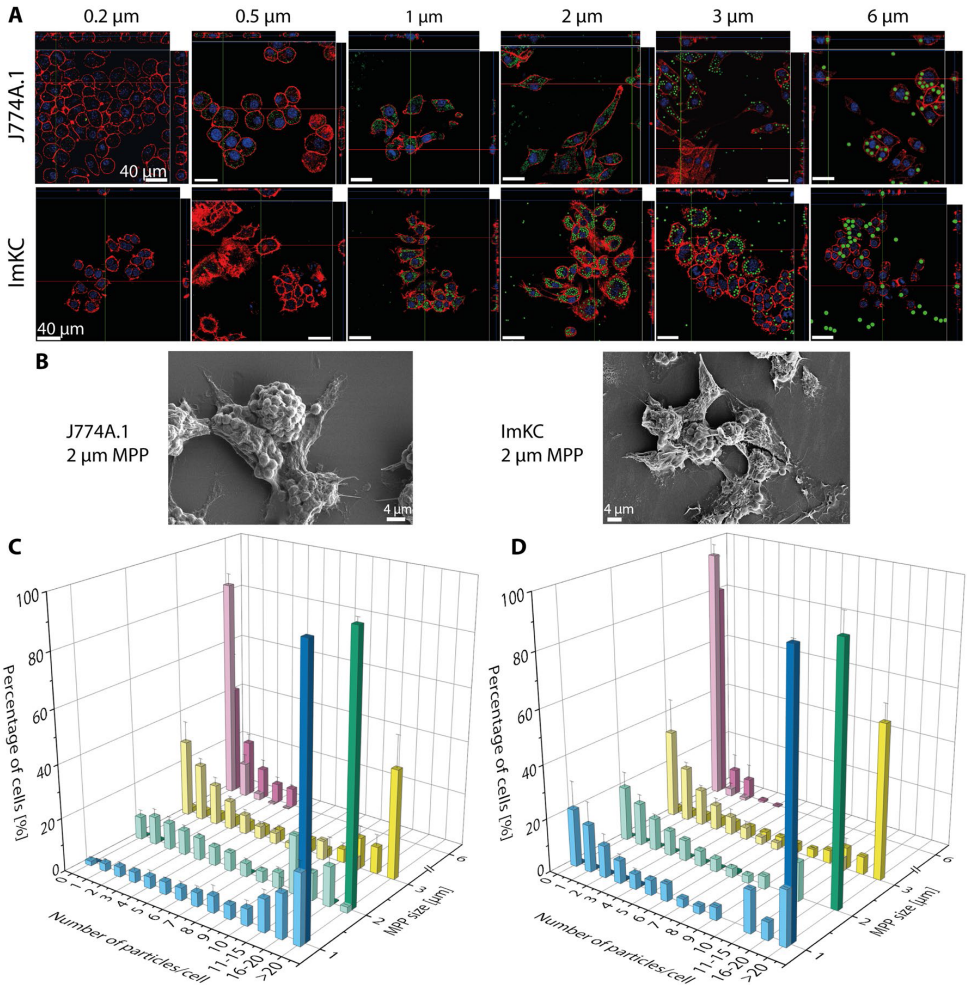

Figure 1. Analysis of size-dependent uptake of PS-MPP by J774A.1 and ImKC macrophages. Analysis was performed using confocal laser scanning microscopy (CLSM, **A**), scanning electron microscopy (SEM, **B**), and flow cytometry (**C**, **D**). (**A**) Size and number of added particles per cell: 0.2 µm: 750,000, 0.5 µm: 48,000, 1 µm: 2000, 2 µm: 700, 3 µm: 200, 6 µm: 25. Actin filaments were stained with rhodamine-phalloidin (red), nuclei were stained with DAPI (blue); FITC-fluorescent MPP are shown in green. Scale bars: 40 µm. (**B**) Representative SEM images are shown for each cell line in the presence of 2 µm MPP. Additional images are shown in Supplementary Fig. S2. Scale bars: 4 µm. (**C**,**D**) Results of flow cytometry measurements of J774A.1 (**C**) and ImKC (**D**). Shown are the percentage of cells in correspondence to the number of interacting particles per cell and the size of the particles. Light colors represent low concentration, dark colors the high concentration of MPP (see Table 2). Note that no data was available for 0.2 and 0.5 µm particles due to lacking resolution of the flow cytometer. The calculation of the number of interacting particles per cell is based on the fluorescence intensity of the particles (histograms, Supplementary Fig. S1). Data represent mean ± SD, n = 3.

MPP uptake by macrophages and epithelial cells depends on particle size. MPP ingestion by the macrophage cells as a function of MPP size was analyzed using confocal laser scanning microscopy (CLSM) and scanning electron microscopy (SEM) (Fig. 1A,B, Supplementary Fig. S2). Flow cytometry was used to statistically quantify the interaction between MPP and macrophages (Fig. 1C,D) using two different concentrations (low concentration: lc, high concentration: hc, Table 2) of fluorescent PS-MPP (Supplementary Fig. S1).

According to these data, ingestion of MPPs of all sizes was observed for both macrophage cell lines. J774A.1 cells seemed to ingest more MPP per cell than the ImKC cells. Using flow cytometry, in the case of the micron-sized particles, the numbers of MPP interacting per cell were obtained based on the fluorescence intensity (Supplementary Fig. S1). No direct quantification was possible for the submicron-sized particles (0.2 and 0.5 µm). However, in that case, a concentration depended shift was detected in fluorescence intensity for the whole cell

Particle size	Low concentration (particles/cell)	High concentration (particles/cell)
0.2 µm	10	100,000
0.5 µm	10	10,000
1 µm	10	1000
2 µm	10	400
3 µm	10	100
6 µm	2	25

Table 2. Overview of MPP concentrations used for proliferation tests, flow cytometry, and ROS assays. For all particle sizes, a low and high concentration, depending on the particle size, was applied. Low concentration = < 1% coverage of the plate; medium concentration = 1–10% coverage of the plate; high concentration = 20–30% coverage of the plate.

population (Supplementary Fig. S1). For J774A.1 (Fig. 1C), high interaction rates were observed for MPP sizes between 1 and 3 µm. Increasing MPP concentrations resulted in a rising number of particle-cell interactions (PCI). In contrast, the majority of the J774A.1 cells did not interact with particles of 6 µm, and the 6 µm-MPP were in fact the only ones where no differences could be observed for low and high MPP concentrations. This effect may be related to the natural function of macrophages. Most air- and water-borne bacteria have a size between 1 and 4 µm[69]. Due to their "oversize", 6 µm MPP become less attractive for ingestion. The ingestion of particles has in principle been reported for sizes up to 10 µm for J774A.1, but particle surface modifications with e.g. IgG or carboxyl groups were necessary in such cases, and ingestion rates were still rather low[43,68,70–72]. For the liver macrophage cell line ImKC, a similar trend as for J774A.1 was observed. The general tendency for particle uptake was lower, but a significant ($p < 0.05$) decrease in MPP-cell interactions was found only for 1 μm_{lc} MPP. As liver macrophages, ImKC cells are expected to be more specialized towards internalizing small particles[73,74].

In case of the intestinal epithelial cells (STC-1), no uptake of MPP larger than 0.2 µm was observed using CLSM and SEM (Fig. 2A,B, Supplementary Fig. S2). Larger MPP merely interacted with the cellular surface, which was detectable with both microscopic methods. This is corroborated by flow cytometry analysis (Fig. 2C,D). While there was no size effect, the MPP-cell-interactions increased slightly at higher concentrations. The lacking ingestion of particles above 0.2 µm and the low MPP interaction with STC-1 is consistent with previous studies focusing on nanoparticles, where particles with sizes of up to 0.12 µm were ingested by STC-1 cells via endocytosis[75,76].

The hepatic epithelial cells (BNL CL.2) did take up MPP < 6 µm (Fig. 2A,B, and Supplementary Fig. S2), albeit at numbers smaller than the macrophages. BNL CL.2 cells have been described as non-phagocytotic[77,78], but the ingestion of micron-sized particles could in principle also take place by macropinocytosis[42,46]. As recently described, hepatic epithelial cells can take up apoptotic or necrotic cells, since clearance of such cells is substantial to sustain tissue homeostasis[79]. Quantification of the interaction using flow cytometry data (Fig. 2D), corroborated again the CSLM and SEM measurements. At low concentrations, 1–3 µm-sized MPP, showed nearly no interaction with the cells. In contrast, MPP-cell interactions could be detected at high concentrations. In case of the 6 µm-MPP, almost no interactions took place with BNL CL.2 cells independent of the concentration. As shown in Fig. 2D, there are significant differences in the uptake behavior of the two cell lines. The intestinal epithelial cells (STC-1 cells) did not interact with particles even at high concentrations, while the liver epithelial cells (BNL CL.2 cells) showed internalization and higher interaction rates in particular at elevated MPP concentrations.

Analysis of MPP effects on metabolic activity (MTT assay). Uptake and accumulation of MPP in intracellular compartments could have a detrimental effect on cellular metabolism. The dose–response of macrophages and epithelial cells to MPP treatment was analyzed using an MTT assay (mitochondrial activity). Cells were incubated with increasing concentrations of 0.2–6 µm MPP, and the metabolic activity, i.e., MTT conversion by cellular oxidoreductases, was analyzed after 24 and 72 h of incubation (Fig. 3).

In epithelial cells, no negative metabolic effects were observed, no matter which concentration, MPP size, or incubation time was considered. This correlates well with the above-shown low tendency for MPP uptake. MPP merely attached to the cellular surface did not appear to affect cellular metabolism. Macrophages showed reduced metabolic activity, albeit only at MPP concentrations above 250 µg/mL after 24 h of incubation. These effects seemed to be related to the MPP size, since the reduction in metabolic activity was the highest for MPPs with 0.5–3 µm diameter, while 0.2 and 6 µm sized MPPs showed little to no effects over the concentration range tested. This result might be due to different uptake mechanisms for differently sized particles. Particles with diameters between 0.5 and 3 µm are mainly taken up via phagocytosis[55,80], which is an energy-dependent process[81], and this might explain the lower metabolic activity for cells with high phagocytic activity. In case of the 6 µm particles, on the other hand, we had previously observed no tendency for uptake. In consequence, a pronounced effect on the metabolic activity would have been surprising and was indeed not observed. Uptake of 0.2 µm sized particles seems to be part of a less energy-intensive uptake mechanism, which in consequence is less of a burden on the metabolism.

Noticeably, for 2 and 3 µm MPP in the low concentration range (10–37.5 µg/mL), we also detected a slight, but significant ($p < 0.05$) increase in metabolic activity (compared to non-treated cells) for ImKC cells. A similar trend was observed for J774A.1 cells after incubation with 2 µm MPP. This might be related to a hormetic response,

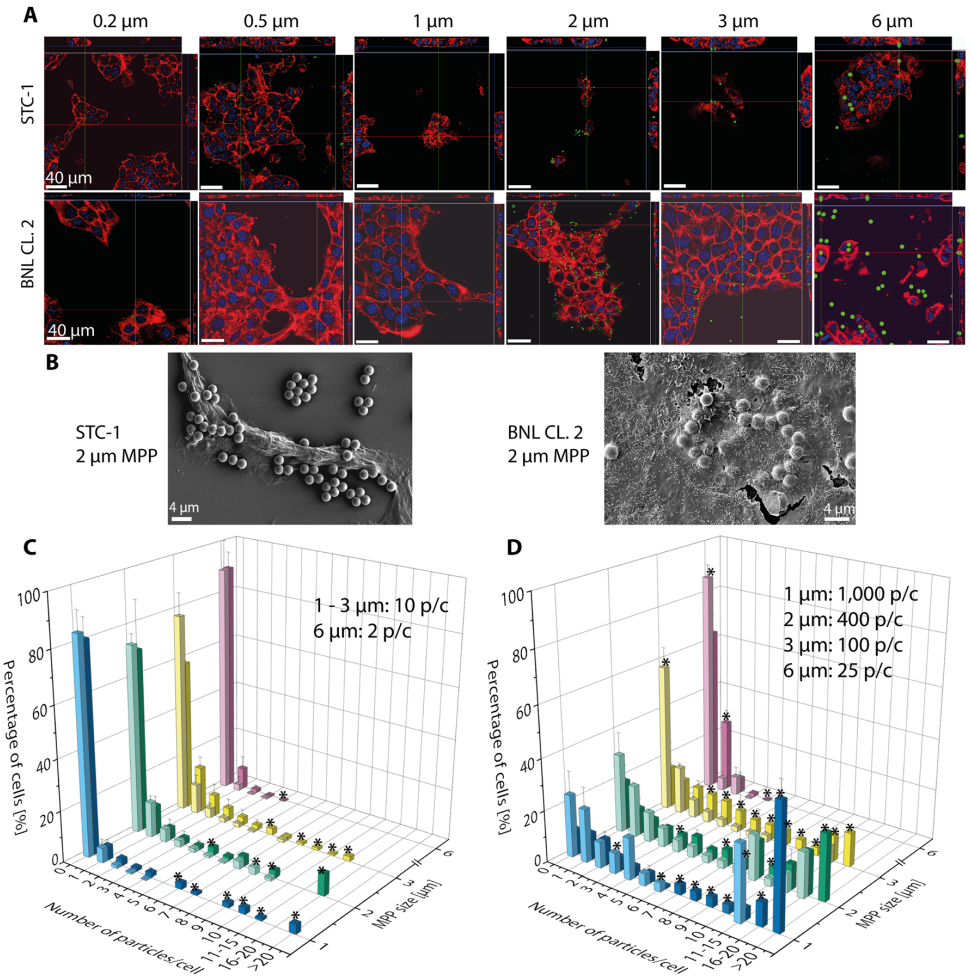

Figure 2. Analysis of the particle uptake by the epithelial cells (STC-1, BNL CL.2) as a function of size and concentration. Analysis was performed using confocal laser scanning microscopy (CLSM, **A**), scanning electron microscopy (SEM, **B**), and flow cytometry (**C**,**D**). (**A**) Size and number of added particles per cell: 0.2 µm: 750,000, 0.5 µm: 48,000, 1 µm: 2000, 2 µm: 700, 3 µm: 200, 6 µm: 25. Actin filaments were stained with rhodamine-phalloidin (red), nuclei were stained with DAPI (blue); FITC-fluorescent MPP are shown in green. Scale bars: 40 µm. (**B**) Representative SEM images are shown for each cell line in the presence of 2 µm MPP. Additional images are shown in Supplementary Fig. S2. Scale bars: 4 µm. (**C**,**D**) Results of flow cytometry measurements of STC-1 (light color) and BNL CL.2 (dark color) at low (**C**) and high (**D**) particle concentrations. The added number of particles per cell are given in the graph as p/c. No data are available for 0.2 and 0.5 µm particles due to lacking resolution of the flow cytometer. Data represent mean ± SD, n = 3. Stars represent statistically significant data points ($p < 0.05$) between both cell lines. For better clarity, no differentiation of significance level is shown.

which leads to a stimulation of the cellular metabolism in response to mild stress[82]. As recently published, such a response can be detected using the MTT assay[83]. An extension of the contact time between cells and particles (i.e., 72 h incubation) induces a drop in the metabolic activity already at concentrations of 10–100 µg/mL for both macrophage cell lines. ImKC seemed to be more sensitive than J774A.1.

Our results underline the importance of analyzing the size effects of MPP using preparations with narrow size distributions, as slight differences in size, e.g. between 0.2 and 0.5 µm, already lead to divergent metabolic responses. Our data further indicated the importance of MPP interaction/uptake, since both macrophage cell lines only showed a reduced metabolic response in the presence of particles between 0.5 and 3 µm, with high PCI.

Effects of MPP size and concentration on the induction of intracellular ROS. ROS generation was analyzed after incubation of the cells with MPP of different sizes at low and high concentrations. For this

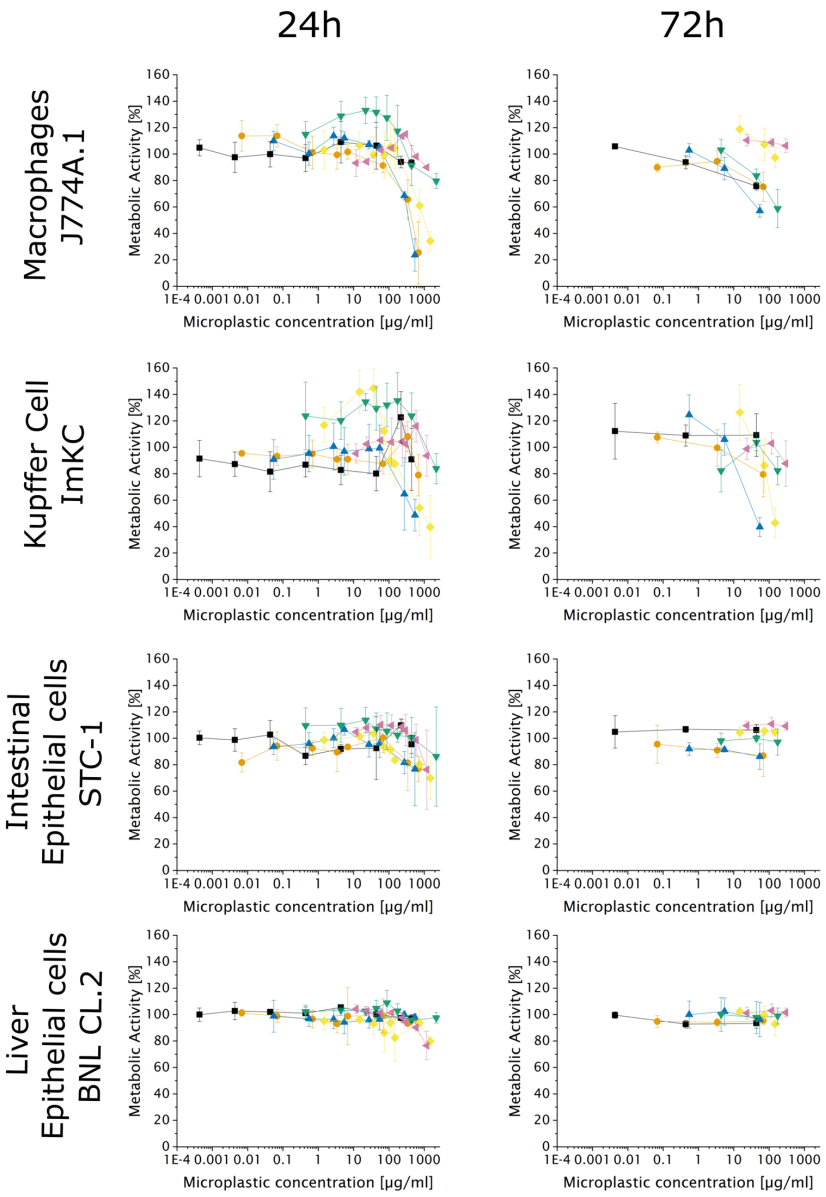

Figure 3. Cell metabolic activity after 24 h and 72 h in the presence of MPP. The metabolic activity was determined using the MTT assay in correlation to cells without particles acting as negative control. Data represent mean ± SD, n = 3 biological replicates. Particle sizes: black square = 0.2 µm, orange circle = 0.5 µm, blue triangle = 1 µm, green down-pointing triangle = 2 µm, yellow diamond = 3 µm, purple left-pointing triangle = 6 µm.

purpose, the fluorescence resulting from oxidation of DCFDA by intracellular ROS was detected using flow cytometry (Fig. 4). In one out of four cell lines, namely ImKC, MPP concentration and size showed a tendency for higher ROS generation (Fig. 4), while the other three cell lines showed no enhanced ROS production (Supplementary Fig. S3). This finding is in line with work from other groups, also based on the study of entire cell populations in contact with MPP, i.e. these studies as well showed no statistically significant change in ROS production after MP treatment[39,40]. As an exception, the ImKC cells, i.e. cells from the resident liver macrophage cell line, showed a slight, but significant concentration-dependent rise in ROS. This increase was most pronounced

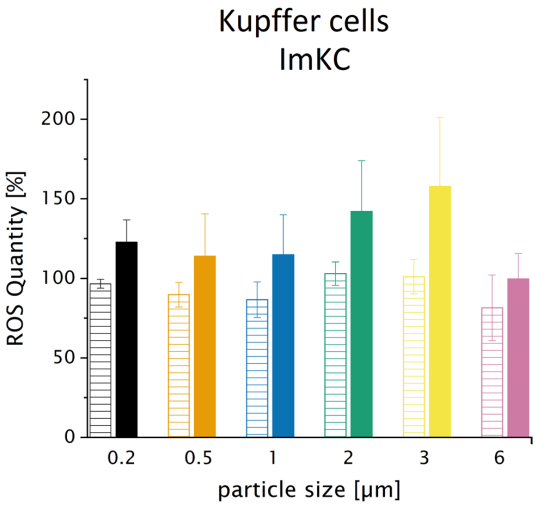

Figure 4. The appearance of reactive oxygen species upon increasing particle concentrations for ImKC macrophages. ROS of the whole cell population treated with an increasing particle concentration (striped bars = low concentration; full bars = high concentration). Quantity is represented in relation to a negative control without particles (100%). Data represent mean ± SD, n = 3.

in the presence of 1–3 µm MPP. It is known that Kupffer cells (i.e., resident macrophages) react quickly and non-specifically after phagocytosis of particular matter with an increase in ROS, while peritoneal and alveolar macrophages (i.e., exudate macrophages) react less strongly[84,85].

Flow cytometry was subsequently used to define cellular subpopulations. Here, it was necessary to use the SSC signal as a basis for PCI, since the fluorescence of the MPPs overlapped with the DCFDA fluorescence signal, which is why we had to use non-fluorescent particles (Fig. 5A). Either way, a higher SSC correlates with the higher fluorescence like higher fluorescence correlates with a higher particle count (Fig. 5B,C). The number of cells in each subpopulation was also taken into consideration for the interpretation of the results. In these experiments, a strong correlation was found between the level of MPP-cell-interaction and ROS response (Fig. 5B,C) for all cell lines, except the epithelial cell line BNL CL.2. However, the percentage of cells above the 100% ROS line (i.e., the ROS level in non-treated cells) corresponded only for ImKC cells to more than 35% of the entire population (Fig. 5C). Either way, an analysis of these small subpopulations might become important when analysing more complex systems or in vivo conditions, in which case cell–cell interactions get more important and small subpopulations might have a higher impact as expected.

For the other cells line, this fraction was much smaller. This explains why an increase in ROS was detectable for the entire ImKC population, while no effects could be observed for the other cell lines. STC-1 cells in particular showed a high ROS response in case of a high PCI, but only a few cells were concerned in their population. Moreover, on the level of the subpopulations, we also observed a decrease in ROS response (below 100% ROS) of cells with low PCI, especially among the macrophages. This response could be explained by an inflammatory response from cells with high PCI also present in the same culture. Such an inflammatory response includes the secretion of antioxidants and has previously only been described for cells challenged with nanoparticles[86]. A secretion of antioxidants would affect cells without or low MPP internalization and would result in a lower baseline ROS production compared to that of the negative control. Interestingly, the highest detected ROS responses were seen in case of small (0.2 and 0.5 µm) and large (6 µm) MPP for all cell lines, except for BNL CL.2. As mentioned in the introduction, small particles (< 0.5 µm) are known to be ROS-inducing. Different uptake mechanisms like phagocytosis for larger particles or less production of antioxidants due to lower uptake rates for the larger particles could explain the high ROS levels induced in the case of 6 µm particles.

MPP effects on cell proliferation. To investigate the effects of MPP on cell proliferation, cells were incubated with MPP of all sizes at low and high concentrations (Table 2). First, resazurin assays were performed to examine the impact of MPP on proliferation at the entire population level. In that case, no significant effects were detected in any of the cell lines (Supplementary Fig. S4). As a result of this finding, we additionally performed a CFSE assay, since effects might only be seen at the subpopulation level. For ImKC cells, proliferation was significantly retarded in presence of particles between 0.5 and 3 µm, when the entire population was considered ("nonapoptotic cells" gate, Fig. 6A). To estimate the MPP effects on cell proliferation at the sub-population level, CFSE dilution assays and flow cytometry analysis were combined, while applying the previously discussed gating strategy (Fig. 5). When analyzing these subpopulations, it became clear that cells with higher PCI also displayed a higher CFSE intensity, indicative of a lower number of cell divisions (Fig. 6B). The correlation between the

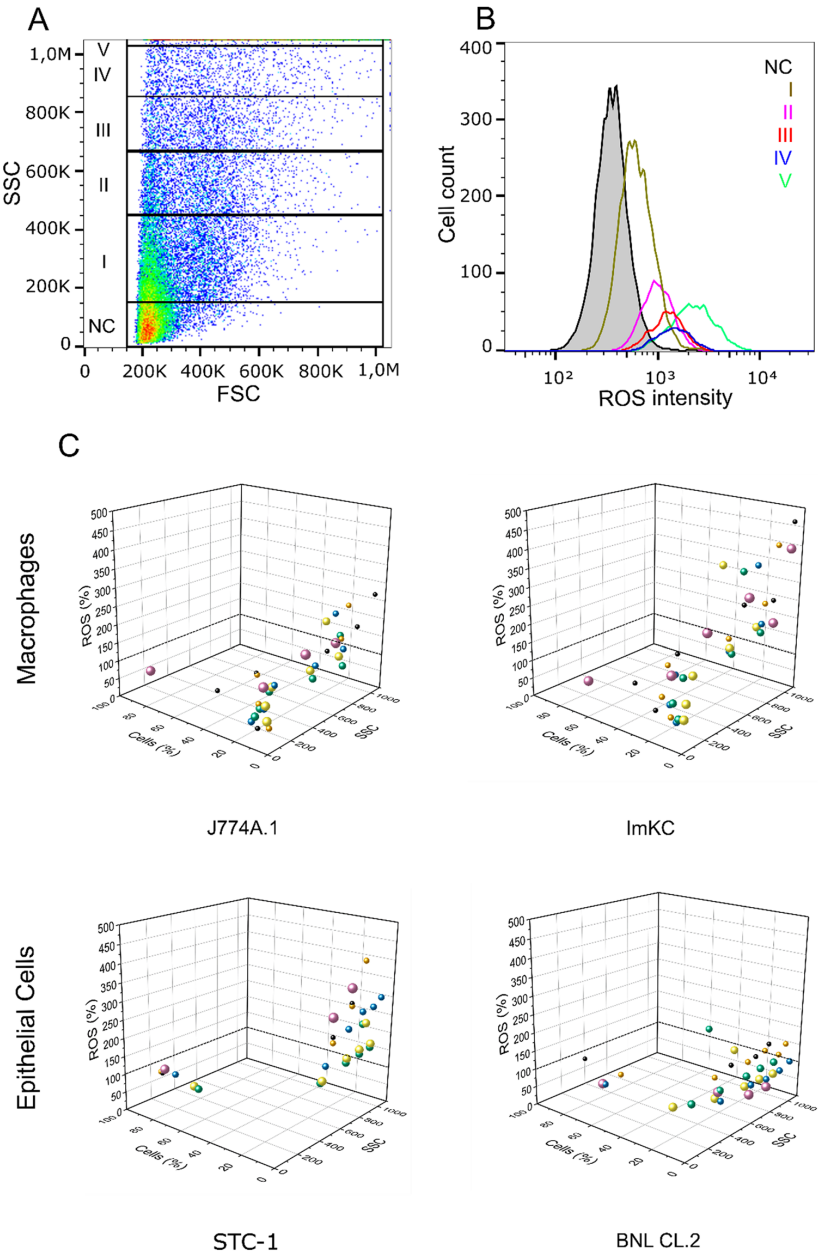

Figure 5. Correlation between ROS generation and intensity of cell-particle interaction. (**A**) Representative gating strategy for rising PCI. Gate NC represents cells with no particle interactions, I–V show increasing PCI (SSC = side scatter, FSC = forward scatter). (**B**) The respective ROS intensity for gated cells shown in (**A**). (**C**) Correlation between PCI, normalized ROS-quantity, and gated cell count. ROS quantity was normalized (control: cells incubated without particles). MFI is the mean SSC value of respectively gated cells. The dashed line highlights the relevant 100% ROS line, the back-ground ROS production determined in non-treated cells cultivated at otherwise similar conditions. Used particle concentration: h_c Table 2 (black circle = 0.2 µm, orange circle = 0.5 µm, blue circle = 1 µm, green circle = 2 µm, yellow circle = 3 µm, purple circle = 6 µm).

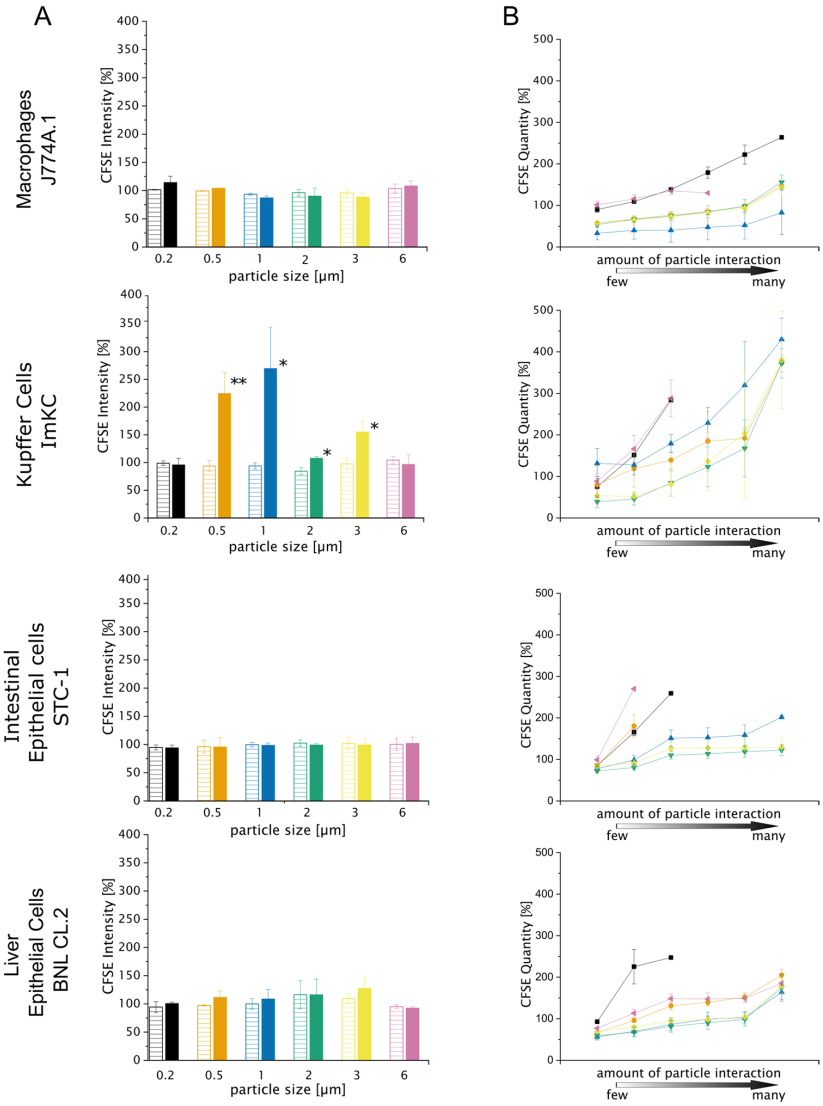

Figure 6. CFSE dilution assay after 72 h. CFSE assay was performed in presence of all particle sizes using all cell lines. Values were normalized (control: cells incubated without particles). As the CFSE intensity per cell is decreasing with every division, higher values for "CFSE intensity" indicate a reduced number of cell division. (**A**) Shows an analysis of the entire population while (**B**) adapts the same gating strategy for subpopulations as in Fig. 4A. Low MPP concentration: striped bars, high MPP concentration: filled bars. Black square = 0.2 µm, orange circle = 0.5 µm, blue triangle = 1 µm, green down-pointed triangle = 2 µm, yellow diamond = 3 µm, purple left-pointed triangle = 6 µm). Data represent mean ± SD, n = 3 biological replicates, *$p < 0.05$, **$p < 0.01$ compared to control.

PCI and the observed effect on proliferation was not as pronounced as for the ROS data, but still statistically significant ($p < 0.05$). As for the ROS assay, these subtle differences between subpopulations were lost when the population was studied as a whole.

The correlation between high PCI and high CFSE is intriguing. It may simply be due to a dilutive effect, i.e. as cells divided, they dilute both the attached/ingested particles and the concentration of the CFSE labeled protein. However, cells with high PCI also tended to show increased ROS production in the above experiment, and increased levels of ROS have been shown to exert an effect on cell proliferation. Oxidative stress induced by microplastic might lead to DNA damage[32]. Hence, the accumulation of ROS in cells displaying high PCI might also influence cell division. A decrease in cell proliferation, has been shown already for high ROS levels in cancer

cells[87]. A decrease in cell division, as seen in the CFSE data, correlates well with the highest ROS accumulation detected in the ImKC cells.

Another possible explanation of the effect of a high PCI on proliferation may again rely on the uptake mechanism. Macrophages need to spend energy on phagocytosing particles. Therefore, less energy is available for cell division. This dynamic energy budget model has been developed for multicellular organisms and was shown recently to be applicable for bacteria as well[88].

Conclusion

Polystyrene microplastic particles (MPP) are well uptaken in the case of exudate and resident macrophages (Kupffer cells) and much less in the case of hepatic and intestinal epithelial cells. Uptake and interaction rates were MPP-size as well as cell-type dependent. Such variations are in line with the cell phenotype. Macrophages are scavenger cells per-se programmed to take-up particulate matter, whereas the material uptake in epithelial cells is mostly limited to molecular transports. Despite the high uptake by the macrophages, a decrease in metabolic activity could only be measured at very high MPP concentrations, while no negative effects were observed for epithelial cells. At the subpopulation level, high particle-cell interactions/uptake tended to correlate with an overproduction of ROS, as well as with a reduction of the proliferative capability for all cell types. Altogether, we can conclude that scavenger cells are more susceptible to noxic effects of MPP ingestion, which are highly correlated to the number of MPP found in the cells. While there is little evidence of acute toxicity caused by the MPP, chronic toxicity due to intracellular accumulation of MPP cannot be excluded at this point and will be clarified by long-term studies. Our results also demonstrate that considering only the whole cellular population for analysis of MPP effects might bias the final results, as correlations involving only small cellular subpopulations may be masked. Hence, for investigations concerning cellular effect of microplastics, there is an urgent need to perform analysis at cell subpopulations or even better at the single-cell level.

Materials and methods

Materials. If not otherwise indicated, Greiner Bio-One (Frickenhausen, Germany) and Thermo Fisher Scientific (Schwerte, Germany) were used as suppliers for cell culture materials. Penicillin, streptomycin, Dulbecco's Phosphate-Buffered Saline without Ca^{2+} and Mg^{2+} (DPBS), RPMI1640 (Roswell Park Memorial Institute), and $DMEM_{Lonza}$ (Dulbecco`s Modified Eagle's Medium; 3.7 g/L $NaHCO_3$, L-glutamine-free) were obtained from Lonza (Lonza Group Ltd, Basel, Switzerland). $DMEM_{ATCC}$ (1.5 g/L $NaHCO_3$, 0.11 mM Na pyruvate, 4 mM L-glutamine) was obtained from ATCC (ATCC LGC Standards GmbH, Wesel, Germany). Modified Eagle Medium without phenol red (MEM) was obtained from Thermo Fisher Scientific (Schwerte, Germany). Fetal calf serum (FCS) was purchased from Sigma Aldrich (Taufkirchen, Germany). Based on the respective standard cell growth media, "conditioned media" were derived as follows: the respective culture supernatant was recovered after 24 h incubation with cells and sterile-filtered using a 0.2 µm cellulose acetate filter before supplementation with 2 mM glutamine. Conditioned media were stored at 4 °C until further use.

Phalloidin-tetramethylrhodamine B isothiocyanate, DAPI, 3-(4,5-dimethyl-2-thiazolyl)-2,5-Diphenyl-2H-tetrazolium bromide (MTT), 2′,7′-dichlorofluorescein diacetate (DCFDA), antimycin A from *Streptomyces* sp., and carboxyfluorescein succinimidyl ester (CFSE) were obtained from Sigma Aldrich (Taufkirchen, Germany). AlamarBlue (CellTiter-Blue Cell Viability Assay) was purchased from Promega (Walldorf, Germany).

Non-functionalized (plain) non-fluorescent and fluorescent polystyrene particles (Yellow Green, PS-YG) were obtained from Polysciences (Polysciences Europe GmbH, Eppenheim, Germany) with the parameter as follows: diameter of 0.2 µm (Cat. # 07304-15 (non-fluorescent), 17151-10 (fluorescent), 5.68×10^{12} particles/mL, size coefficient of variation (CV) ≤ 8%), 0.5 µm (Cat. # 07307-15 (non-fluorescent), 17152-10 (fluorescent), 3.64×10^{11} particles/mL, size CV ≤ 3%), 1 µm (Cat. # 07310-15 (non-fluorescent), 17154-10 (fluorescent), 4.55×10^{10} particles/mL, size CV ≤ 3%), 2 µm (Cat. # 19814-15 (non-fluorescent), 18338-5 (fluorescent), 5.68×10^{9} particles/mL, size CV ≤ 5%), 3 µm (Cat. # 17134-15 (non-fluorescent), 17155-2 (fluorescent), 1.68×10^{9} particles/mL, size CV ≤ 5%) and 6 µm (Cat. # 07312-5 (non-fluorescent), 17156-2 (fluorescent), 2.10×10^{8} particles/mL, size CV ≤ 10%). All MPP were delivered as a sterile aqueous suspension with a concentration of 2.5% (w/v). According to the supplier, all MPP are plain particles with little anionic charge due to residues of sulphate ester groups. Non-fluorescent particles showed no autofluorescence in the ex/em ranges of interest for the intended experiments. Prior to use, MPP stock solutions were diluted to the desired concentration in the respective growth media.

Cell culture. Murine cell lines: Macrophages J774A.1 [from ascites, TIB-67, population doubling time: 17 h (according to supplier information)], intestinal epithelial-like cells STC-1 (CRL3254, population doubling time: 54 h[89]) and hepatic epithelial cells BNL CL.2 [TIB-73, population doubling time: 40 h (according to supplier information)] were obtained from the American Type Culture Collection (ATCC, Manassas, USA). The hepatic macrophage cell line ImKC (Kupffer cells, SCC119, population doubling time: 24 h[73]) was obtained from Merck (Merck KGaA, Darmstadt, Deutschland). ImKC cells were cultivated in RPMI1640 supplemented with 2 mM glutamine. STC-1, BNL CL.2, and J774A.1 cells were cultivated in DMEM ($DMEM_{ATCC}$ for STC-1 and BNL CL.2; $DMEM_{Lonza}$ for J774A.1). For J774A.1 cells, the medium was additionally supplemented with 4 mM glutamine, 24 mM HEPES, and 0.1 mM sodium pyruvate. All media were supplemented with 10% (v/v) FCS and 100 U/mL penicillin/streptomycin, and are referred to as "growth media" throughout the manuscript. The cells were cultivated in a standard cell culture incubator (5% CO_2/95% humidity) at 37 °C. For cell maintenance, all cell lines were passaged three times a week at a starting concentration of about 100,000 cells/mL. For detaching cells, either at 37 °C pre-warmed citric saline buffer (135 mM potassium chloride—15 mM sodium citrate, 5 and 10 min incubation at 37 °C for J774A.1 and ImKC, respectively) or 1× Trypsin/EDTA (for STC-1 and BNL CL.2) was used.

ζ-Potential measurement. The ζ-potential measurements were performed using the LiteSizer 500 (Anton Paar Germany GmbH, Ostfildern-Scharnhausen, Germany) and Omega cuvettes (Anton Paar Germany GmbH, Ostfildern-Scharnhausen, Germany). For ζ-potential measurements, 2.5 µL of the particle solutions were directly diluted in 1 mL of a 1 mM aqueous KCl solution (pH 6) and measured immediately. In some cases, 2.5 µL of the 25 mg/mL particle solutions were incubated in 1 mL growth medium ($DMEM_{ATCC}$, $DMEM_{Lonza}$ and RPMI1640) or a mixture of 10% (v/v) FCS in DPBS overnight at 37 °C. Thereafter, the particles were collected by centrifugation [17,000*g* for 40 min at room temperature (RT)] and resuspended in 1 mL of the 1 mM KCl solution for measurement. Three measurements with at least 100 runs each were performed at 21 °C with an adjusted voltage of 200 V. The ζ-potential was calculated using the Helmholtz-Smoluchowski equation[90].

Flow cytometry. Flow cytometry analyses were performed using a CytoFLEX S or a Cytomics FC500 (Beckman Coulter, Krefeld, Germany). Both devices are equipped with a 488 nm laser. For each sample, at least 30,000 events were measured. For analysis, cells were washed twice with DPBS, detached by trypsinization or by citric acid treatment as described above, and suspended in 1 mL culture medium. Cells were then recovered by centrifugation (200*g*, 5 min), the supernatant was discarded and the cell pellet was resuspended in 0.5–1 mL DPBS. Forward scatter (FSC), side scatter (SSC), and FITC fluorescence (525 nm filter) were recorded. Cells were initially evaluated by scatter properties (FSC/SSC) to select a region ("nonapoptotic cell" gate) representing single, nonapoptotic cells while disregarding debris, and cellular aggregates. Upon uptake or cellular interactions of MPP, the SSC-fluorescence increased, and defined sub-populations become visible in most cases. Taking advantage thereof, we defined additional sub-gates to analyze the response of the sub-populations to non-labeled MPP in terms of production of ROS (ROS assay, DCF fluorescence) and influence on cellular proliferation (CFSE-dilution assay, CFSE fluorescence). Using labeled MPP (PS-YG), the number of particles was also quantified interacting with the cells.

The quantification of microparticles (1–6 µm) is based on the median fluorescence intensity of the particles. The fluorescence intensity of the microparticles was determined in the absence of cells, and this value was assumed to be the fluorescence intensity of one MPP on average. Due to the linear relation of the fluorescence intensity and the number of MPPs (for a plot of the correlation see Supplementary Fig. S1), it was possible to quantify particle numbers per cell. It should be noted that a differentiation between particle uptake and mere particle adhesion to the cells was not possible using flow cytometry. For sub-micron sized particles, no correlation was detectable, since the resolution of fluorescence difference between single particles was too low.

Flow cytometry data were evaluated using FlowJo software v 10.5.0 (Tree Star, Stanford University, CA, USA, 2018).

For ROS assay, both concentrations of non-fluorescent MPPs do not reveal any fluorescence above the autofluorescence of the cells in the DCF channel (Em. 526 nm).

Qualitative analysis of MPP uptake. For the qualitative analysis of the ingestion of the particles by the cells, 15,000 cells were seeded in each well of an 8-well Ibidi slide (µ-Slide 8 Well, ibiTreat, ibidi GmBH, Gräfelfing, Germany). After 24 h in a cell culture incubator, cells were incubated with fluorescent particles (MPP per cell: 0.2 µm: 750,000, 0.5 µm: 48,000, 1 µm: 2000, 2 µm: 700, 3 µm: 200, 6 µm: 25) (total cultivation volume: 300 µL). Thereafter, cells were fixed for 15 min at RT with pre-heated 3.7% (v/v) paraformaldehyde in 1×DPBS. Afterward, the cells were permeabilized with 0.1% (v/v) TritonX-100 for 10 min at RT. Actin filaments and nuclei were stained with 100 nM rhodamine-phalloidin and 100 nM DAPI, respectively. The samples were analyzed using a confocal laser scanning microscope (TCS SP8, 63× oil immersion objective, laser: 408 nm, 488 nm, and 552 nm, Leica Microsystems, Wetzlar, Germany). Z-stacks were taken with a step size of 0.2–0.33 µm.

The MPP uptake was also analyzed using scanning electron microscopy (SEM). Therefore, 100,000 cells per slide were seeded on Ø 13 mm Nunc™ Thermanox™ slides (Thermo Fisher Scientific, Waltham, MA, USA) and incubated for 24 h to allow for cell adhesion (total cultivation volume: 120 µL). Then, 5 µL of a 180 mg/L non-fluorescent particle solution were added to the cells, which corresponds to 20 particles per cell. After another 24 h incubation, the cells were directly fixed using Karnovsky's reagent (4% (v/v) formaldehyde, 5% (v/v) glutaraldehyde, with a final concentration of 32 mM PBS, pH 7.4) for 1 h at RT and afterward dehydrated using an ethanol series 50%, 70%, 80% for 30 min, 90% and absolute ethanol for 1 h. The overnight air-dried samples were sputter-coated with gold, and images were obtained using SEM [FEI Apreo Volumescope, Thermo Fisher Scientific, magnification: 10,000×, 2 kV, Everhart–Thornley detector (ETD)].

Quantitative analysis of MPP uptake. For quantification of the particle-cell-interaction, 700,000 cells per well were seeded in 6-well culture plates and incubated for 24 h for cell adhesion. Afterward, fluorescent particles of various sizes were added at two concentrations, low and high, to the cells. Here, the low and high concentrations range from 2 to 10 MPP (low) and from 25 to 100,000 per cell (high), respectively, depending on the MPP size (Scheme 1, Table 2). Particle concentration was scaled in a logarithmic manner for the smallest particle sizes (0.2, 0.5 µm). For the bigger particles, the added number of particles was roughly scaled to correspond in volume to that added in case of the smaller particles, since otherwise the cells would have been overcrowded. A maximum concentration of 100,000 particles per cell was added in case of 0.2 µm sized particles compared to roughly 100 particles in case of 6 µm ones. After another 24 h of incubation, the cells were collected as described above and analyzed using flow cytometry.

MTT assay. The influence of MPP on the metabolic activity of the cells was analyzed using an MTT assay. This tetrazolium salt-based cell viability assay is a recognized method for the toxicological assessment of PS microparticles[50,73,91]. Briefly, cells were seeded at 10,000 cells/well in 96-well plates (100 µL medium per well).

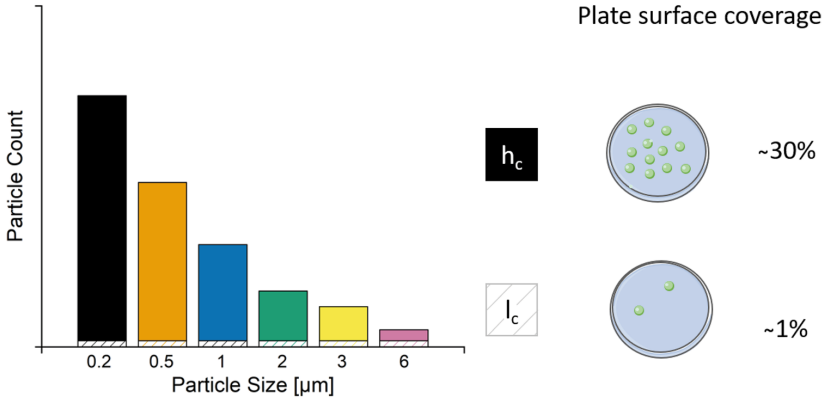

Scheme 1. Relative particle count for low (l_c) and high (h_c) concentration for the respective particle size and the surface coverage per well. Specific values are given in Table 2.

For STC-1 cells, the seeding cell density was increased to 25,000 per well to accommodate for the slower growth rate and metabolism. After 24 h of incubation, the medium was aspirated, and 100 µL of the freshly prepared particle suspension was added. For this purpose, the desired particle concentrations were prepared by diluting the particle stock solution with the respective growth medium. The cells were then incubated for another 24 h. In case of the experiments with 72 h incubation time, the seeding density was reduced, i.e. adapted to the different cellular growth rates, and "conditioned medium" was used. The seeding densities, in this case, were 2000 cells/well (ImKC and BNL CL.2), 4000 cells/well (J774A.1), and 6000 cells/well (STC-1). After 24 h of incubation, the medium was aspirated, and 100 µL of freshly prepared particle dilutions were added for 72 h. After the incubation with the MPP, the medium was aspirated, cells were then washed with DPBS, and 50 µL freshly prepared MTT reagent (1 mg/mL MTT in MEM) was added to each well. After 2 h incubation, the supernatant was removed, and 100 µL of isopropanol were added per well to dissolve the produced formazan crystals. After 5 min shaking at 600 rpm, the absorbance at 570 nm (reference wavelength 650 nm) was measured using a TECAN GENios Pro plate reader (Tecan Austria GmbH, Gröding). Cells incubated without particles or with 0.3% Triton X-100 in the respective cell culture medium, under otherwise identical conditions, were used as negative and positive controls, respectively.

Reactive oxygen species (ROS) assay. Intracellular ROS can be labeled with the non-fluorescent membrane-permeable dye DCFDA[92], which is converted into fluorescent 2′,7′-dichlorofluorescein (DCF) upon oxidation by intracellular ROS. For analysis, 150,000 cells/well were seeded in 12-well plates in 1 mL of the respective culture medium. After 24 h of incubation, the indicated amounts of the freshly prepared particle suspensions (low and high concentration, Scheme 1, Table 2) were added and the plates were further incubated. Cells incubated without particles or in the presence of 50 µM (5 µM for STC-1) antimycin A under otherwise identical conditions were used as negative and positive controls, respectively. After 60 min incubation, 37.5 µM DCFDA was added per well (5 µM for STC-1), followed by another 24 h incubation. For STC-1 cells, the DCFDA concentration was reduced because of concerns regarding the cytotoxicity of the dye, which had manifested itself during the establishment of the assay. Afterward, the DCF fluorescence intensity was measured using flow cytometry.

Resazurin proliferation assay. Resazurin is converted into resorufin, a highly fluorescent dye, by a reduction reaction in the mitochondria. Cells were seeded (15,000 cells for J774A.1 and BNL CL.2; 20,000 cells for ImKC and STC-1, three technical replicates) in 48-well plates. After 24 h of incubation, freshly prepared particle suspensions (20 µL) were added ("treated" cells), final concentrations are given in Table 2 (low and high concentrations). Cells incubated without particles under otherwise identical conditions were used as control ("non-treated" cells). After an additional 24 h incubation, the cell culture medium was removed and 350 µL of a 10% (v/v in the respective cell culture medium) AlamarBlue solution was added. Samples were incubated for 2.5 h. To estimate the background fluorescence of the AlamarBlue solution (F_{Blank}), three wells without cells and particles (i.e., exclusively containing the AlamarBlue solution) were incubated. After incubation, aliquots of the cell culture medium (100 µL) were collected, and the resorufin fluorescence (Ex. 530 nm/Em. 600 nm) was analyzed using a plate reader (Mithras, Berthold Technologies, Bad Wildbad, Germany). The remaining AlamarBlue solution was removed from the wells and fresh cell culture medium was added. After two additional cultivation days, an AlamarBlue assay was performed as described above. For the statistical analysis, the mean value of the AlamarBlue control (F_{blank}) was subtracted from each value of the same well plate. For the determination of the change in fluorescence per hour representing cell proliferation, the fluorescence intensity as detected on day three was subtracted from that of day one (Eq. 1),

$$\Delta_{Fluorescence\ intensity/hour} = \frac{(F_{sample}d3 - F_{blank}d3) - (F_{sample}d1 - F_{blank}d1)}{48h} \quad (1)$$

with F_{sample} being the fluorescence of the sample (either $F_{treated}$ or $F_{non\text{-}treated}$), F_{blank} being the fluorescence of the AlamarBlue control without cells, d3 being the incubation time of three days and d1 the incubation time of one day. Based on these values, the mean value and standard deviation were calculated from three replicates.

CFSE-dilution assay. The CFSE dilution assay was performed as previously described with some modifications[93]. When a CFSE-labeled cell divides, its progeny contains half the number of carboxyfluorescein-tagged proteins, hence each cell division can be assessed by measuring the corresponding decrease in cell fluorescence using flow cytometry. For the assay, cells were washed twice with DPBS, and the cell numbers were adjusted to 5×10^6 cells/mL in DPBS. Then, one volume of CFSE solution (5 µM in DPBS) was added to reach a final concentration of 2.5 µM CFSE and 2.5×10^6 cells/mL. After 5 min incubation at RT in the dark, the labeling was quenched by the addition of one volume of FCS. The cells were washed once with DPBS (200*g*, 5 min) and resuspended in the respective conditioned medium. 150,000 CFSE-stained cells were then seeded per well in 12-well plates (cultivation volume: 1 mL). After 24 h of incubation, a freshly prepared particle suspension (1–10 µL, concentration-dependent) was added, and the cells were incubated for another 72 h. Cells incubated without particles under otherwise identical conditions were used as the negative control.

Statistical analysis. Statistical analysis was performed using Origin software 2019b (Origin, Northampton, MA, USA). All data were tested concerning the homogeneity of variances (Levene test). To investigate differences in MPP interactions with cells and proliferation results, a one-way ANOVA with a Tukey post hoc test was used.

Received: 15 March 2021; Accepted: 9 July 2021
Published online: 03 August 2021

References

1. Mulder, K. & Knot, M. PVC plastic: A history of systems development and entrenchment. *Technol. Soc.* **23**, 265 (2001).
2. Thompson, R. C., Swan, S. H., Moore, C. J. & vom Saal, F. S. Plastics, the environment and human health: Current consensus and future trends. *Philos. Trans. R. Soc. Lond. Ser. B Biol. Sci.* **2009**, 364 (1973).
3. Barnes, D. K. A., Galgani, F., Thompson, R. C. & Barlaz, M. Transport and release of chemicals from plastics to the environment and to wildlife. *Philos. Trans. R. Soc. Lond. Ser. B. Biol. Sci.* **2009**, 364 (1985).
4. Carney Almroth, B. & Eggert, H. Marine plastic pollution: Sources, impacts, and policy issues. *Rev. Environ. Econ. Policy* **13**, 317 (2019).
5. Jambeck, J. R. *et al.* Plastic waste inputs from land into the ocean. *Science (New York, N.Y.)* **347**, 768 (2015).
6. de Souza, M. *et al.* Microplastics as an emerging threat to terrestrial ecosystems. *Glob. Change Biol.* **24**, 1405 (2018).
7. Hurley, R. R. & Nizzetto, L. Fate and occurrence of micro (nano) plastics in soils: Knowledge gaps and possible risks. *Curr. Opin. Environ. Sci. Health* **1**, 6 (2018).
8. Huang, Y., Liu, Q., Jia, W., Yan, C. & Wang, J. Agricultural plastic mulching as a source of microplastics in the terrestrial environment. *Environ. Pollut.* **260**, 114096 (2020).
9. Fotopoulou, K. N. & Karapanagioti, H. K. Degradation of various plastics in the environment. In *Hazardous Chemicals Associated with Plastics in the Marine Environment* (eds. Takada, H. & Karapanagioti, H. K.) 71 (Springer International Publishing, 2019).
10. Vert, M. *et al.* Terminology for biorelated polymers and applications (IUPAC Recommendations 2012). *Pure Appl. Chem.* **84**, 377 (2012).
11. Eriksen, M. *et al.* Plastic pollution in the world's oceans: more than 5 trillion plastic pieces weighing over 250,000 tons afloat at sea. *PLoS ONE* **9**, e111913 (2014).
12. Dris, R. *et al.* Beyond the ocean: Contamination of freshwater ecosystems with (micro-) plastic particles. *Environ. Chem.* **12**, 539 (2015).
13. Piehl, S. *et al.* Identification and quantification of macro-and microplastics on an agricultural farmland. *Sci. Rep.* **8**, 17950 (2018).
14. Gasperi, J. *et al.* Microplastics in air: Are we breathing it in?. *Curr. Opin. Environ. Sci. Health* **1**, 1 (2018).
15. Imhof, H. K. *et al.* Spatial and temporal variation of macro-, meso-and microplastic abundance on a remote coral island of the Maldives, Indian Ocean. *Mar. Pollut. Bull.* **116**, 340 (2017).
16. Schrank, I. *et al.* Effects of microplastic particles and leaching additive on the life history and morphology of *Daphnia magna*. *Environ. Pollut.* **255**, 113233 (2019).
17. Besseling, E., Wegner, A., Foekema, E. M., van den Heuvel-Greve, M. J. & Koelmans, A. A. Effects of microplastic on fitness and PCB bioaccumulation by the lugworm *Arenicola marina* (L.). *Environ. Sci. Technol.* **47**, 593 (2013).
18. Zhang, C., Chen, X., Wang, J. & Tan, L. Toxic effects of microplastic on marine microalgae *Skeletonema costatum*: Interactions between microplastic and algae. *Environ. Pollut.* **220**, 1282 (2017).
19. Yong, C. Q. Y., Valiyaveetill, S. & Tang, B. L. Toxicity of microplastics and nanoplastics in mammalian systems. *Int. J. Environ. Res. Public Health* **17**, 1509 (2020).
20. Toussaint, B. *et al.* Review of micro-and nanoplastic contamination in the food chain. *Food Addit. Contam. Part A Chem. Anal. Control. Expo. Risk. Assess.* **36**, 639 (2019).
21. Revel, M., Châtel, A. & Mouneyrac, C. Micro (nano) plastics: A threat to human health?. *Curr. Opin. Environ. Sci. Health* **1**, 17 (2018).
22. Yang, Y.-F., Chen, C.-Y., Lu, T.-H. & Liao, C.-M. Toxicity-based toxicokinetic/toxicodynamic assessment for bioaccumulation of polystyrene microplastics in mice. *J. Hazard. Mater.* **366**, 703 (2019).
23. Deng, Y., Zhang, Y., Lemos, B. & Ren, H. Tissue accumulation of microplastics in mice and biomarker responses suggest widespread health risks of exposure. *Sci. Rep.* **7**, 1 (2017).
24. Jani, P., Halbert, G. W., Langridge, J. & Florence, A. T. Nanoparticle uptake by the rat gastrointestinal mucosa: Quantitation and particle size dependency. *J. Pharm. Pharmacol.* **42**, 821 (1990).

25. Desai, M. P., Labhasetwar, V., Amidon, G. L. & Levy, R. J. Gastrointestinal uptake of biodegradable microparticles: Effect of particle size. *Pharm. Res.* **13**, 1838 (1996).
26. Wynn, T. A., Chawla, A. & Pollard, J. W. Macrophage biology in development, homeostasis and disease. *Nature* **496**, 445 (2013).
27. Daems, W. T., Koerten, H. K. & Soranzo, M. R. *Differences Between Monocyte-Derived and Tissue Macrophages. The Reticuloendothelial System in Health and Disease* 27–40 (Springer, 1976).
28. Rabinowitz, S. & Gordon, S. Differential expression of membrane sialoglycoproteins in exudate and resident mouse peritoneal macrophages. *J. Cell Sci.* **93**, 623 (1989).
29. Davies, L. C., Jenkins, S. J., Allen, J. E. & Taylor, P. R. Tissue-resident macrophages. *Nat. Immunol.* **14**, 986 (2013).
30. Okabe, Y. & Medzhitov, R. Tissue-specific signals control reversible program of localization and functional polarization of macrophages. *Cell* **157**, 832 (2014).
31. Nathan, C. F. Secretory products of macrophages. *J. Clin. Investig.* **79**, 319 (1987).
32. Hu, M. & Palić, D. Micro-and nano-plastics activation of oxidative and inflammatory adverse outcome pathways. *Redox Biol.* **37**, 101620 (2020).
33. Shekhova, E. Mitochondrial reactive oxygen species as major effectors of antimicrobial immunity. *PLoS Pathog.* **16**, e1008470 (2020).
34. Hume, D. A. The many alternative faces of macrophage activation. *Front. Immunol.* **6**, 370 (2015).
35. van der Goes, A. *et al.* Reactive oxygen species are required for the phagocytosis of myelin by macrophages. *J. Neuroimmunol.* **92**, 67 (1998).
36. Forman, H. J. & Torres, M. Reactive oxygen species and cell signaling: Respiratory burst in macrophage signaling. *Am. J. Respir. Crit. Care Med.* **166**, S4-8 (2002).
37. Trestrail, C., Nugegoda, D. & Shimeta, J. Invertebrate responses to microplastic ingestion: Reviewing the role of the antioxidant system. *Sci. Total Environ.* **734**, 138559 (2020).
38. Gu, L. *et al.* Inhibitory effects of polystyrene microplastics on caudal fin regeneration in zebrafish larvae. *Environ. Pollut.* **266**, 114664 (2020).
39. Schirinzi, G. F. *et al.* Cytotoxic effects of commonly used nanomaterials and microplastics on cerebral and epithelial human cells. *Environ. Res.* **159**, 579 (2017).
40. Wu, B., Wu, X., Liu, S., Wang, Z. & Chen, L. Size-dependent effects of polystyrene microplastics on cytotoxicity and efflux pump inhibition in human Caco-2 cells. *Chemosphere* **221**, 333 (2019).
41. Marchi, S. *et al.* Mitochondria-ros crosstalk in the control of cell death and aging. *J. Signal Transduct.* **2012**, 329635 (2012).
42. Aderem, A. & Underhill, D. M. Mechanisms of phagocytosis in macrophages. *Annu. Rev. Immunol.* **17**, 593 (1999).
43. Champion, J. A., Amanda, W. & Samir, M. Role of particle size in phagocytosis of polymeric microspheres. *Pharm Res* **25**, 1815 (2008).
44. Champion, J. A. & Samir, M. Role of target geometry in phagocytosis. *PNAS* **103**, 4930 (2006).
45. Fröhlich, E. The role of surface charge in cellular uptake and cytotoxicity of medical nanoparticles. *Int. J. Nanomed.* **7**, 5577 (2012).
46. Danaei, M. *et al.* Impact of particle size and polydispersity index on the clinical applications of lipidic nanocarrier systems. *Pharmaceutics* **10**, 57 (2018).
47. Kettler, K., Veltman, K., van de Meent, D., van Wezel, A. & Hendriks, A. J. Cellular uptake of nanoparticles as determined by particle properties, experimental conditions, and cell type. *Environ. Toxicol. Chem.* **33**, 481 (2014).
48. Geiser, M. *et al.* Ultrafine particles cross cellular membranes by nonphagocytic mechanisms in lungs and in cultured cells. *Environ. Health Perspect.* **113**, 1555 (2005).
49. Olivier, V., Duval, J. L., Hindié, M., Pouletaut, P. & Nagel, M. D. Comparative particle-induced cytotoxicity toward macrophages and fibroblasts. *Cell Biol. Toxicol.* **19**, 145 (2003).
50. Hwang, J. *et al.* Potential toxicity of polystyrene microplastic particles. *Sci. Rep.* **10**, 7391 (2020).
51. Stock, V. *et al.* Uptake and effects of orally ingested polystyrene microplastic particles in vitro and in vivo. *Arch. Toxicol.* **2019**, 93 (1817).
52. Cole, M., Lindeque, P., Halsband, C. & Galloway, T. S. Microplastics as contaminants in the marine environment: A review. *Mar. Pollut. Bull.* **62**, 2588 (2011).
53. Hidalgo-Ruz, V., Gutow, L., Thompson, R. C. & Thiel, M. Microplastics in the marine environment: A review of the methods used for identification and quantification. *Environ. Sci. Technol.* **46**, 3060 (2012).
54. Wright, S. L., Thompson, R. C. & Galloway, T. S. The physical impacts of microplastics on marine organisms: A review. *Environ. Pollut.* **178**, 483 (2013).
55. Tabata, Y. & Ikada, Y. Effect of the size and surface charge of polymer microspheres on their phagocytosis by macrophage. *Biomaterials* **9**, 356 (1988).
56. Kurtz-Chalot, A. *et al.* Impact of silica nanoparticle surface chemistry on protein corona formation and consequential interactions with biological cells. *Mater. Sci. Eng. C* **75**, 16 (2017).
57. Ramsperger, A. F. R. M. *et al.* Environmental exposure enhances the internalization of microplastic particles into cells. *Sci. Adv.* **6**, eabd1211 (2020).
58. Patiño, T., Soriano, J., Barrios, L., Ibáñez, E. & Nogués, C. Surface modification of microparticles causes differential uptake responses in normal and tumoral human breast epithelial cells. *Sci. Rep.* **5**, 11371 (2015).
59. Fleischer, C. C. & Payne, C. K. Nanoparticle–cell interactions: Molecular structure of the protein corona and cellular outcomes. *Acc. Chem. Res.* **47**, 2651 (2014).
60. Corbo, C. *et al.* The impact of nanoparticle protein corona on cytotoxicity, immunotoxicity and target drug delivery. *Nanomedicine (Lond.)* **11**, 81 (2016).
61. Weiss, A. C. G. *et al.* Surface modification of spider silk particles to direct biomolecular corona formation. *ACS Appl. Mater. Interfaces.* **12**, 24635 (2020).
62. Walczyk, D., Bombelli, F. B., Monopoli, M. P., Lynch, I. & Dawson, K. A. What the cell "sees" in bionanoscience. *J. Am. Chem. Soc.* **132**, 5761 (2010).
63. Treuel, L. *et al.* Impact of protein modification on the protein corona on nanoparticles and nanoparticle–cell interactions. *ACS Nano* **8**, 503 (2014).
64. Sabbioni, E. *et al.* Interaction with culture medium components, cellular uptake and intracellular distribution of cobalt nanoparticles, microparticles and ions in Balb/3T3 mouse fibroblasts. *Nanotoxicology* **8**, 88 (2014).
65. Moore, T. L. *et al.* Nanoparticle administration method in cell culture alters particle–cell interaction. *Sci. Rep.* **9**, 1 (2019).
66. Lunov, O. *et al.* Differential uptake of functionalized polystyrene nanoparticles by human macrophages and a monocytic cell line. *ACS Nano* **5**, 1657 (2011).
67. Musyanovych, A. *et al.* Criteria impacting the cellular uptake of nanoparticles: A study emphasizing polymer type and surfactant effects. *Acta Biomater.* **7**, 4160 (2011).
68. Kuhn, D. A. *et al.* Different endocytotic uptake mechanisms for nanoparticles in epithelial cells and macrophages. *Beilstein J. Nanotechnol.* **5**, 1625 (2014).
69. Kowalski, W. J., Bahnfleth, W. P. & Whittam, T. S. Filtration of airborne microorganisms: Modeling and prediction. *ASHRAETrans* **105**, 4 (1999).

70. Lam, J., Herant, M., Dembo, M. & Heinrich, V. Baseline mechanical characterization of J774 macrophages. *Biophys. J.* **96**, 248 (2009).
71. Yue, H. *et al.* Particle size affects the cellular response in macrophages. *Eur. J. Pharm. Sci.* **41**, 650 (2010).
72. Mutzke, E., Chomyshyn, E., Nguyen, K. C., Blahoianu, M. & Tayabali, A. F. Phagocytosis-coupled flow cytometry for detection and size discrimination of anionic polystyrene particles. *Anal. Biochem.* **483**, 40 (2015).
73. Wang, Z.-Y., Burlak, C., Klaunig, J. E. & Kamendulis, L. M. Development of a cytokine-producing immortalized murine Kupffer cell line. *Cytokine* **70**, 165 (2014).
74. Sadauskas, E. *et al.* Kupffer cells are central in the removal of nanoparticles from the organism. *Part Fibre Toxicol.* **4**, 1 (2007).
75. Shah, B., Kona, S., Gilbertson, T. A. & Nguyen, K. T. Effects of poly-(lactide-co-glycolide) nanoparticles on electrophysiological properties of enteroendocrine cells. *J. Nanosci. Nanotechnol.* **11**, 3533 (2011).
76. Kamakura, R., Raza, G. S., Prasannan, A., Walkowiak, J. & Herzig, K.-H. Dipeptidyl peptidase 4 and GLP-1 interplay in STC-1 and GLUTag cell lines. *Peptides* **134**, 170419 (2020).
77. Attia, M. F. *et al.* Biodistribution and toxicity of X-ray iodinated contrast agent in nano-emulsions in function of their size. *Pharm. Res.* **33**, 603 (2016).
78. Shang, L., Nienhaus, K. & Nienhaus, G. U. Engineered nanoparticles interacting with cells: Size matters. *J. Nanobiotechnol.* **12**, 1 (2014).
79. Davies, S. P., Reynolds, G. M. & Stamataki, Z. Clearance of apoptotic cells by tissue epithelia: A putative role for hepatocytes in liver efferocytosis. *Front. Immunol.* **9**, 44 (2018).
80. Rejman, J., Oberle, V., Zuhorn, I. S. & Hoekstra, D. Size-dependent internalization of particles via the pathways of clathrin-and caveolae-mediated endocytosis. *Biochem. J.* **377**, 159 (2004).
81. Iyer, G. Y. N., Islam, M. F. & Quastel, J. H. Biochemical aspects of phagocytosis. *Nature* **192**, 535–541 (1961).
82. Calabrese, E. J. Hormesis: Why it is important to toxicology and toxicologists. *Environ. Toxicol. Chem.* **27**, 1451 (2008).
83. Gopi, I. K. & Rattan, S. I. S. Biphasic Dose-response and hormetic effects of stress hormone hydrocortisone on telomerase-immortalized human bone marrow stem cells in vitro. *Dose Response Publ. Int. Hormesis Soc.* **17**, 1559325819889819 (2019).
84. Wang, J. F., Komarov, P. & de Groot, H. Luminol chemiluminescence in rat macrophages and granulocytes: The role of NO, O− 2-/H_2O_2, and HOCl. *Arch. Biochem. Biophys.* **304**, 189 (1993).
85. K. Decker. Biologically active products of stimulated liver macrophages (Kupffer cells). In *EJB Reviews 1990* (eds Christen, P. & Hofmann, E.) 167 (Springer, 1991).
86. Park, E.-J. *et al.* Oxidative stress and apoptosis induced by titanium dioxide nanoparticles in cultured BEAS-2B cells. *Toxicol. Lett.* **180**, 222 (2008).
87. Townley, H. E., Rapa, E., Wakefield, G. & Dobson, P. J. Nanoparticle augmented radiation treatment decreases cancer cell proliferation. *Nanomed. Nanotechnol. Biol. Med.* **8**, 526 (2012).
88. Grossowicz, M., Marques, G. M. & van Voorn, G. A. K. A dynamic energy budget (DEB) model to describe population dynamics of the marine cyanobacterium *Prochlorococcus marinus*. *Ecol. Model.* **359**, 320 (2017).
89. McCarthy, T. *et al.* STC-1 cells. In *The Impact of Food Bioactives on Health* (eds. Verhoeckx K. et al.) 211 (Springer, 2015).
90. von Smoluchowski, M. The kinetic theory of Brownian molecular motion and suspensions. *Ann. Phys.* **326**, 756 (1906).
91. Hesler, M. *et al.* Multi-endpoint toxicological assessment of polystyrene nano-and microparticles in different biological models in vitro. *Toxicol. In Vitro* **61**, 104610 (2019).
92. Chen, X., Zhong, Z., Xu, Z., Chen, L. & Wang, Y. 2′, 7′-Dichlorodihydrofluorescein as a fluorescent probe for reactive oxygen species measurement: Forty years of application and controversy. *Free Radic. Res.* **44**, 587 (2010).
93. Quah, B. J. C. & Parish, C. R. New and improved methods for measuring lymphocyte proliferation in vitro and in vivo using CFSE-like fluorescent dyes. *J. Immunol. Methods* **379**, 1 (2012).

Acknowledgements
We thank Dr. Hendrik Bargel for SEM support. This work was funded by the Deutsche Forschungsgemeinschaft (DFG, German Research Foundation)—project number 391977956—CRC 1357/subproject A05. J.R. was supported by the University of Bayreuth Graduate School. The authors thank Andrea Schott and Juliana Schertel for their technical assistance.

Author contributions
Conceived and designed the experiments: R.F., T.S., V.J., M.V., J.R. Performed the experiments: J.R., M.V. Analysed the data: J.R., M.V., V.J. Wrote the paper: J.R., M.V., V.J., T.S., R.F.

Funding
Open Access funding enabled and organized by Projekt DEAL.

Competing interests
The authors declare no competing interests.

Additional information
Supplementary Information The online version contains supplementary material available at https://doi.org/10.1038/s41598-021-95073-9.

Correspondence and requests for materials should be addressed to T.S. or R.F.

Reprints and permissions information is available at www.nature.com/reprints.

Publisher's note Springer Nature remains neutral with regard to jurisdictional claims in published maps and institutional affiliations.

Noxic Effects of Polystyrene Microparticles on Murine Macrophages and Epithelial Cells

Julia Rudolph*[1], Matthias Völkl*[2], Valérie Jérôme[2], Thomas Scheibel[#1,3,4,5,6], Ruth Freitag[#2,4]

* shared first author
# co-corresponding authors

Supplementary Information

The particle concentration is depending on the number of cells in the used assay, as well as on the total test volume (equation 2),

$$MPP\ concentration\ \left(\frac{\mu g}{mL}\right) = \frac{MPP\ conc.\left(\frac{MPP}{cell}\right) * number\ of\ cells}{total\ test\ volume\ (mL)} * (\rho_{MPP}\ \left(1.05\frac{g}{cm^3}\right) *\ Particle\ volume\ (cm^3)) \quad (2)$$

the density of PS-MPP (ρ_{MPP}) is 1.05 g/cm^3. Particle volume can be calculated using the respective particle size

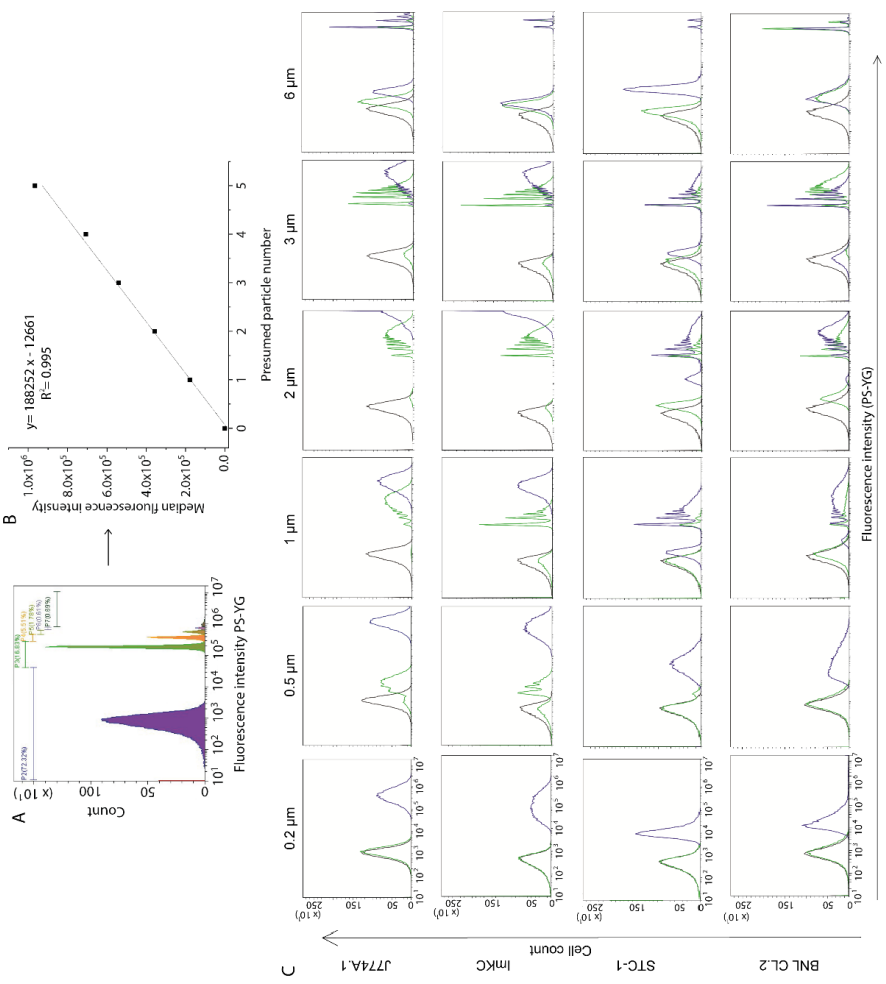

Figure S1. Calculation of particles per cell based on flow cytometry data. Different cell populations were gated using the fluorescence intensity of green fluorescent MPPs. (A) The presumed particle number was plotted based on the mean fluorescence intensity of the populations. (B) There is a linear relationship between fluorescence intensity and presumed particle number (R^2= 0.995). (C) Shown is one replicate of each measurement. Grey: control without particles, green: low MPP concentration, blue: high MPP concentration.

2

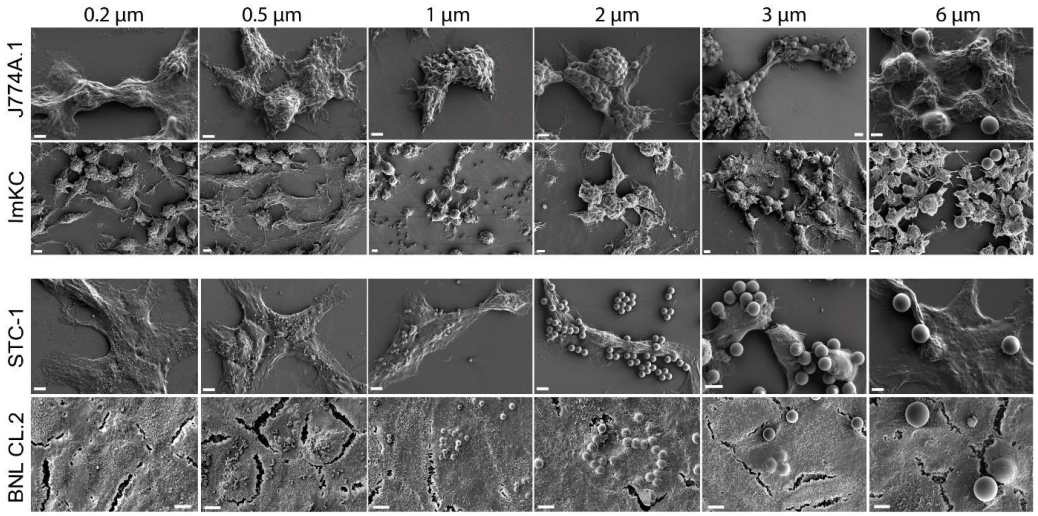

Figure S2. Size-depenent particle uptake analyzed using SEM. All cell lines were incubated in the presence of the differently sized PS-MP for 24 hours. Macrophages cells (J774A.1, ImKC) showed ingested particles, which were surrounded by the cell membrane. For epithelial cell lines (STC-1, BNL CL.2), differences were observed in uptake behavior. STC-1 cells did not show particle ingestion, whereas for BNL CL.2 many particles were found surrounded by the cell membrane. Scale bar: 4 µm.

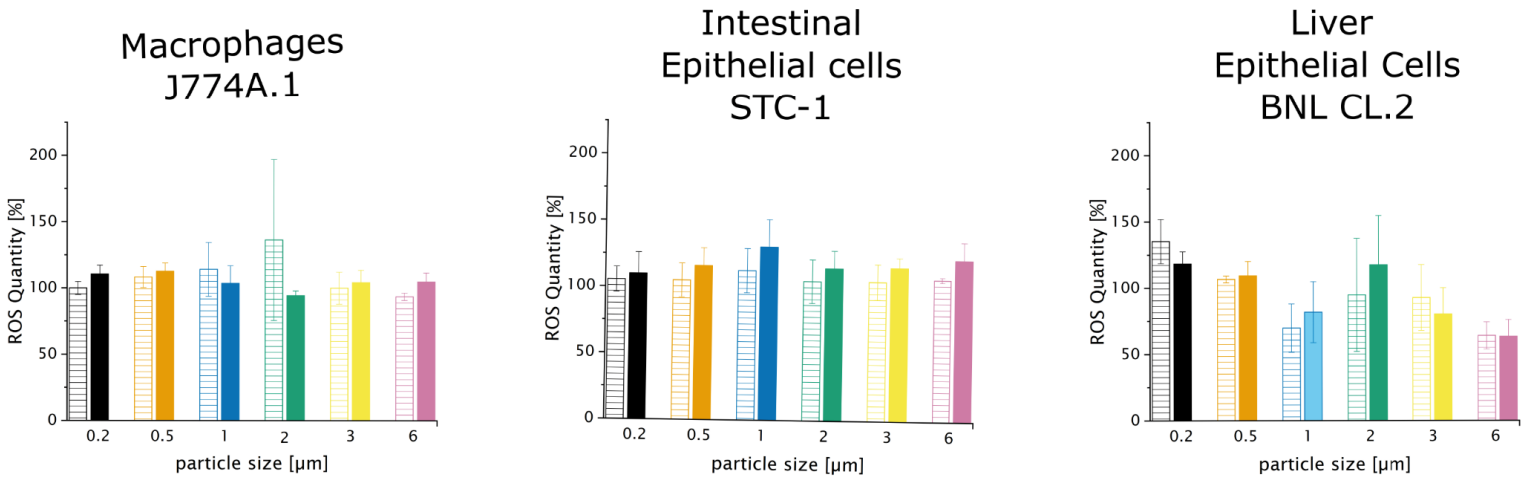

Figure S3. Appearance of reactive oxygen species upon increasing particle concentrations. ROS of the whole cell population treated with an increasing particle concentration (striped bars = low concentration; light bar = medium concentration full bars = high concentration). Quantity is represented in relation to a negative control without particles (100 %). Data represent mean ± SD, n = 3.* = $p < 0.05$, ** = $p < 0.01$ compared to negative control.

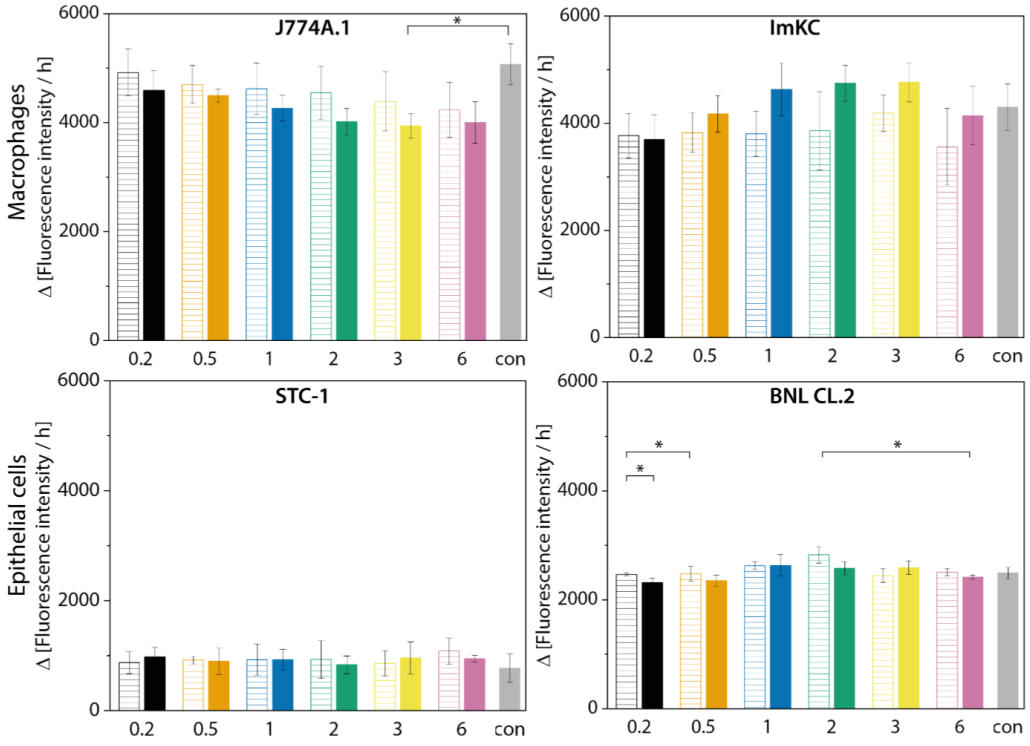

Figure S4. Cellular proliferation detected by the change in fluorescence intensity per hour (resazurin assay). The resazurin assay was performed with all cell lines. Two concentrations of all MPP sizes were used (Table S1, low concentration: striped bars, high concentration: filled bars). Con: control cells without MPP. Significant differences were highlighted (*= $p < 0.05$). Data represent mean ± SD, n = 3.

6.2 Teilarbeit II

Supposedly Identical Microplastic Particles Substantially Differ in Their Material Properties Influencing Particle-Cell Interactions and Cellular Responses

Autoren: Anja F. R. M. Ramsperger*, **Julia Jasinski***, Matthias Völkl*, Thomas Witzmann, Marcel Meinhart, Valérie Jérôme, Winfried P. Kretschmer, Ruth Freitag, Jürgen Senker, Andreas Fery, Holger Kress, Thomas Scheibel und Christian Laforsch
∗ gleichberechtigte Co-Autorenschaft

Das Konzept dieser Teilarbeit stammt zu gleichen Teilen von Anja Ramsperger, Matthias Völkl und mir. Die Experimente wurden von Anja Ramsperger, Matthias Völkl, Thomas Witzmann, Marcel Meinhart und mir durchgeführt. Dabei wurden die Partikel mittels Rasterelektronenmikroskopie, DLS und ζ-Potentialmessungen, sowie die qualitative zelluläre Aufnahme mittels Rasterelektronenmikroskopie von mir analysiert und ausgewertet. Daten zur weiteren Partikelanalyse mittels CP-AFM und GPC sowie NMR wurden von Thomas Witzmann und Marcel Meinhart durchgeführt. Quantitative Daten zur Partikel-Zellinteraktion und Internalisierung mittels Konfokalmikroskopie wurden von Anja Ramsperger erhoben. Matthias Völkl führte die Experimente zur Zytotoxizität durch. Das Manuskript wurde von mir zusammen mit Anja Ramsperger und Matthias Völkl verfasst. Valérie Jérôme, Winfried Kretschmer, Ruth Freitag, Jürgen Senker, Andreas Fery, Holger Kress, Thomas Scheibel und Christian Laforsch waren an der Konzeptionierung, wissenschaftlichen Diskussionen und der Fertigstellung des Manuskripts beteiligt.

Der Artikel wurde am 05.03.2022 im Journal *Journal of Hazardous Materials* veröffentlicht.

Journal of Hazardous Materials 425 (2022) 127961

Contents lists available at ScienceDirect

Journal of Hazardous Materials

journal homepage: www.elsevier.com/locate/jhazmat

Research Paper

Supposedly identical microplastic particles substantially differ in their material properties influencing particle-cell interactions and cellular responses

A.F.R.M. Ramsperger [a,g,1], J. Jasinski [b,1], M. Völkl [c,1], T. Witzmann [d], M. Meinhart [e], V. Jérôme [c], W.P. Kretschmer [f], R. Freitag [c], J. Senker [e], A. Fery [d], H. Kress [g], T. Scheibel [b], C. Laforsch [a,*]

[a] Animal Ecology I and BayCEER, University of Bayreuth, Bayreuth, Germany
[b] Biomaterials, University of Bayreuth, Bayreuth, Germany
[c] Process Biotechnology, University of Bayreuth, Bayreuth, Germany
[d] Leibniz-Institute of Polymer Research e.V., Institute of Physical Chemistry and Polymer Physics & Physical Chemistry of Polymeric Materials, Technical University of Dresden, Dresden, Germany
[e] Inorganic Chemistry III and Northern Bavarian NMR Centre, University of Bayreuth, Bayreuth, Germany
[f] Inorganic Chemistry II and Sustainable Chemistry Centre, University of Bayreuth, Bayreuth, Germany
[g] Biological Physics, University of Bayreuth, Bayreuth, Germany

ARTICLE INFO

Editor: Dr. R Teresa

Keywords:
Microplastic
Cellular internalisation
CP-AFM
NMR
GPC
EDX
ζ-potential
Cytotoxicity
Material properties

ABSTRACT

Microplastics and its putative adverse effects on environmental and human health increasingly gain scientific and public attention. Systematic studies on the effects of microplastics are currently hampered by using rather poorly characterised particles, leading to contradictory results for the same particle type. Here, surface properties and chemical composition of two commercially available nominally identical polystyrene microparticles, frequently used in effect studies, were characterised. We show distinct differences in monomer content, ζ-potentials and surface charge densities. Cells exposed to particles showing a lower ζ-potential and a higher monomer content displayed a higher number of particle-cell-interactions and consequently a decrease in cell metabolism and proliferation, especially at higher particle concentrations. Our study emphasises that no general statements can be made about the effects of microplastics, not even for the same polymer type in the same size class, unless the physicochemical properties are well characterised.

1. Introduction

Microplastics are found in marine (Eriksen et al., 2014; Imhof et al., 2017; Lacerda et al., 2019), limnetic (Imhof et al., 2013; Dris et al., 2015; Klein et al., 2015; Piehl et al., 2019), atmospheric (Dris et al., 2016; Gasperi et al., 2018; Evangeliou et al., 2020) and terrestrial environments including agricultural soils used for food production (Piehl et al., 2018; Rillig and Lehmann, 2020; Rillig, 2012). Due to their worldwide distribution and small sizes (< 5 mm, (Arthur et al., 2008; Frias and Nash, 2019)), they are considered to pose a risk to environmental and human health (Wright and Kelly, 2017; Prata et al., 2020; Campanale et al., 2020). The ingestion of microplastic particles together with food has been shown in a variety of organisms ranging from lower trophic levels up to human beings (Imhof et al., 2013; Wright and Kelly, 2017; Cole and Galloway, 2015; Laist, 1997; Barboza et al., 2020; Mohamed Nor et al., 2021; Schwabl et al., 2019). However, most plastic particles may pass the gastrointestinal system (Schwabl et al., 2019; Nelms et al., 2019), and putative effects, such as inflammation evoked by particles translocated into tissues, may depend on the material's properties. In this context, research on microplastics considered predominantly the size of the particles as a crucial factor responsible for observed effects (Triebskorn et al., 2019). Ingested, larger microplastic particles can induce gut blockage and cause physical tissue damage (Bjorndal et al., 1994; Wright et al., 2013), whereas microplastic particles in the lower micrometre size range can become internalised by cells (Ramsperger et al., 2020; Stock et al., 2019, Rudolph & Völkl et al.,

* Corresponding author.
E-mail address: christian.laforsch@uni-bayreuth.de (C. Laforsch).
[1] These authors contributed equally to this work.

https://doi.org/10.1016/j.jhazmat.2021.127961
Received 9 September 2021; Received in revised form 18 November 2021; Accepted 28 November 2021
Available online 30 November 2021

2021), one pathway that has been described for tissue translocation (Wright and Kelly, 2017). For instance, in zebrafish exposed to 5 and 20 μm polystyrene particles, the 20 μm particles were found in the gastrointestinal tract and the gills, whereas 5 μm particles were also found in liver tissue (Lu et al., 2016; Deng et al., 2017). In mussels, it has been shown that 3.0 and 9.6 μm polystyrene particles were able to translocate from the gastrointestinal tract into the circulatory system with a significantly higher proportion for the smaller particles used in that study (Browne et al., 2008). Microplastics translocated into the circulatory system or tissues can cause inflammation (von Moos et al., 2012) or necrosis (Wright and Kelly, 2017; Triebskorn et al., 2019; Lu et al., 2016; Rahman et al., 2021; Rodriguez-Seijo et al., 2017). In contrast, some studies did not observe tissue translocation or any adverse effects when exposing organisms or their primary cells to microplastics (Elizalde-Velázquez et al., 2020, Riedl et al., 2021). The inconsistency in results may be explained by the fact that different polymer types were used. Given that these different types of microplastic particles differ in many properties, it is likely that they also elucidate different effects in ecotoxicological studies. However, the majority of studies used polystyrene (PS), mostly spherical, microparticles (Brachner et al., 2020; Jacob et al., 2020) as recently stressed by Stock et al. (2021): "all existing studies dealing with microplastic particle uptake and toxicity exclusively used spherical, monodisperse model polystyrene particles". Here, it may be assumed that the outcome of studies using PS microplastics of the same size and shape are comparable with each other.

However, such monodisperse, spherical PS microparticles are often functionalised, for example, with carboxylic or amino groups (Desjardins and Griffiths, 2003; Olivier et al., 2004), which alters their surface properties and renders them chemically activated. Furthermore, Ramsperger et al. (2020) recently showed that also non-functionalised PS microparticles' environmental exposure leads to a surface functionalisation with biomolecules. This so-called eco-corona enhanced the particle's interaction with cells and subsequently their internalisation. In addition, even in commercially available microparticles without intended surface functionalisation, the polymerisation method, often surfactant-free emulsion polymerisation or dispersion polymerisation (Ober et al., 1985; Telford et al., 2013), may alter the surface properties of the synthesised microparticles. Since microplastic particles have a high surface-to-volume ratio, these surface properties can be expected to exert an influence on their effects. In the end, functionalisation, whether intended or inherent, may influence the interaction of such particles with the cellular membranes, potentially even the activation of possible cellular internalisation mechanisms (Lunov et al., 2011; Patiño et al., 2015). Hence, the outcome of studies using microplastics of the same type, size and shape may also not be comparable with each other.

However, to date, microplastic particles used for effect and cellular internalisation studies have mainly been categorised by polymer type, shape, and size (Wright et al., 2013; Stock et al., 2021), while their physicochemical surface properties were hardly considered. A fact highlighted in the comprehensive review of Yong et al. (2020), stating that results from different studies were contradictory, even if the "same type" of microplastic particles were used. For instance, Stock et al. (2019) observed no or only little cytotoxicity for polystyrene particles in the micrometre size range, whereas Dong et al. (2020) did show cytotoxic effects for polystyrene particles in the same size range (Stock et al., 2019; Yong et al., 2020; Di Dong et al., 2020).

We hypothesise that this discrepancy originates from the fact that the supposedly identical microparticles used in the various studies did nevertheless differ concerning some important yet unacknowledged properties. In order to investigate this hypothesis, we used supposedly identical 3 μm plain polystyrene (PS) microplastic particles, both provided with no surface functionalisation, from two different manufacturers (Polysciences and Micromod, referred to as P-MPP and M-MPP, respectively). According to the suppliers, both particle types (P-MPP and M-MPP) used were similar in size, chemistry, and surface conditions ("slight anionic charge due to residues of sulphate ester groups"). To test if both particle types can be regarded as identical, we characterised the particles' surface morphology, ζ-potential, surface charge distribution and further analysed both PS particle types' chemical composition. We correlated the observed surface properties of the microparticles with their interaction and internalisation with two murine macrophage cell lines. To estimate putative cellular responses evoked by different surface properties, we measured cell viability and proliferation after treating the cells with both microplastic particle types.

2. Materials and methods

2.1. Materials

Chemicals were obtained from Merck, Carl Roth, Sigma Aldrich or Biozym, cell culture materials from Greiner bio-one (Greiner Bio-One International GmbH, Frickenhausen, Germany), if not otherwise indicated. Plain polystyrene beads in aqueous solution with a nominal diameter of 3 μm were purchased from Polysciences (Polysciences Inc., Warrington, PA, USA, Cat. # 17134-15, 25 mg/mL, 1.7 * 10^9 particles/mL) and Micromod (Micromod Partikeltechnologie GmbH, Rostock, Germany, Cat. # 01-00-303, 50 mg/mL, 3.4 * 10^9 particles/mL). Both commercial sources state the polydispersity with a coefficient of variation to be < 5%, indicating no relevant size differences between the particle types. Furthermore, the customer services of the two commercial sources declared that both particle types are prepared by emulsion polymerisation using a radical initiator. Polysciences further declared to add 0.05% sodium azide to prevent bacterial growth, whereas the particles from Micromod are solely suspended in water (information obtained by both providers after request). We calculated the concentration of sodium azide used in our experiments to estimate potential interference in the cellular response experiments. Sodium azide has a molecular weight of 65 g/mol resulting in a concentration of 7.7 mM of sodium azide in the stock solution of P-MPP. Since the particles were further diluted (max. dilution: 1:17,000 (particle concentration: 1.5 μg/mL) and min. dilution: 1:17 (particle concentration: 1500 μg/mL)) the concentration of sodium azide in the experiments is further diluted to a range between 0.45 μM and 0.45 mM. The highest sodium azide concentration in our experiments (MTT assay with 1500 μg/mL) corresponds to a final concentration of 0.45 mM sodium azide. Weyermann et al. (2005) described that in MTT assays, a hypertonic concentration of 300 mM sodium azide is required to trigger a cytotoxic reaction. Microplastic particles obtained from Polysciences and Micromod are further abbreviated as P-MPP and M-MPP, respectively.

2.1.1. Cell lines and culture conditions

The murine ImKC cell line was obtained from Merck (SCC119) and cultured in RPMI 1640 medium, the J774A.1 cells (DSMZ GmbH, ACC170) were cultured in Dulbecco's Modified Eagle's Medium (DMEM, Lonza Group Ltd, Basel, Switzerland). To obtain cell culture growth media, DMEM and RPMI were supplemented with 10% (v/v) FCS (Sigma Aldrich, St. Louis, USA), 4 mM L-Glutamine (Gibco, Fisher Scientific, Schwerte, Germany), and 100 U/mL penicillin/streptomycin (Lonza Group Ltd, Basel, Switzerland). Both cell lines were passaged three times a week with a starting cell density of 100,000 cells/mL for cell maintenance. The cells were collected non-enzymatically by incubation (5 min incubation time for J774A.1, 10 min incubation for ImKC) in pre-warmed (37 °C) citric saline buffer (135 mM potassium chloride, 15 mM sodium citrate) or by scraping.

2.2. Methods

2.2.1. ζ-potential and dynamic lights scattering (DLS) measurements

The ζ-potential was measured before (stock solution, from manufacturer), after washing the particles with Milli-Q water, and after incubating the particles in two cell culture media (DMEM or RPMI). All

ζ-potential measurements were performed in 1 mM KCl to ensure equimolar salt concentrations and conductivity. For each treatment, 4 μL of a 25 mg/mL particle solution was diluted in 1 mL of the appropriate medium (described below) to a final concentration of 0.1 mg/mL. For the stock solution samples, the particles were diluted in freshly prepared 1 mM KCl and immediately measured. No further preparation of the particles originating from the stock solution was performed. For washed samples, loosely bound surfactants had to be removed. Therefore, the particles were washed with Mili-Q water. The washing procedure consisted of a washing step followed by centrifugation at 17,000*g* for 20 min at room temperature. The washing procedure was repeated three times. After the third wash, the pellet was then resuspended in freshly prepared 1 mM KCl and immediately measured. Compared to the stock solution and washed samples, a more realistic situation at cell culture conditions was tested. The particles were incubated in cell culture growth medium (DMEM or RPMI) overnight at 37 °C. Since the ionic strength of the cell culture medium is too high for the ζ-potential measurement, a medium change to 1 mM KCl using centrifugation was necessary. One centrifugation step at 17,000 *g* for 20 min at room temperature was performed to avoid removing a possible protein corona from the particle surface. The pellet was resuspended in freshly prepared 1 mM KCl and immediately measured.

The ζ-potential measurements were performed using Omega cuvettes (Mat.No.: 155765, Anton Paar Germany GmbH, Ostfildern-Scharnhausen, Germany) and a LiteSizer 500 (Anton Paar Germany GmbH, Ostfildern-Scharnhausen, Germany). Three measurements with at least 100 runs each were performed at 21 °C with an adjusted voltage of 200 V, and the ζ-potential was calculated using the Helmholtz-Smoluchowski equation (Drechsler et al., 2020; Smoluchowski, 1916). For the stock solution particles, the ζ-potentials were additionally measured at different pH values using a pH titration. The pH value was adjusted automatically by the Methrom dosing system (Metrohm GmbH & Co.KG, Filderstadt, Germany) with 0.1 M HCl or 0.1 M KOH in pH steps of ± 0.5. P-MPP and M-MPP were measured within a pH range from 2.5 to 10.5 and 2.5 to 11, respectively. Starting at pH 6, HCl was added to measure at the acidic pH range (pH 6–2.5), or KOH was added to measure the ζ-potential at the basic pH range (pH 6–11). For both pH ranges, separate samples of particles originating from the stock solution were used. The pH 6 in the 1 mM KCl is stable for at least 1 h, and since the measurement at one specific pH were performed within 5 min, we can be sure that the pH values are correct during the measurements. During this time, no precipitation of surfactants was observed.

For DLS measurements, 2 μL of the corresponding particle solution was diluted in 1 mL 1 mM KCl, resulting in a final particle concentration of 0.05 mg/mL. The measurements with at least 10 runs each were performed at 21 °C using the backscatter (angle 175°) using a LiteSizer 500 (Anton Paar Germany GmbH, Ostfildern-Scharnhausen, Germany).

2.2.2. Colloidal probe atomic force microscopy (CP-AFM)

Prior to the AFM measurements, tipless cantilevers (CSC38, Mikro-Masch, Sofia, Bulgaria) were calibrated via thermal noise (Hutter and Bechhoefer, 1993) and had a spring constant between 0.03 and 0.4 N/m. Cantilevers were cleaned in Milli-Q water, ethanol, Milli-Q water, and acetone and treated with air-plasma for 10 min (SmartPlasma, plasma technology GmbH, Herrenberg-Gülstein, Germany). Silica colloidal particles (nominal diameter of 4.8 μm, microParticles GmbH, Berlin, Germany) were attached to the cantilevers with 2-components epoxide glue (UHU Plus Endfest, UHU GmbH & Co. KG, Bühl/Baden, Germany). Glass slides were cleaned with acetone, isopropanol, ethanol, ethanol/Milli-Q water (50:50) and Milli-Q water for 10 min each in an ultrasonic bath at room temperature. After drying with nitrogen, the substrates were treated in air-plasma for 10 min. One-half of the substrate was covered with 1 g/L polyethyleneimine for an hour before rinsing with Milli-Q water and drying with argon. Microplastic particles were washed 3 times with Milli-Q water, and droplets of the suspension were placed onto the polyethyleneimine-covered side of the substrates until the water evaporated. Thereafter, the substrate with particles was mounted into a liquid cell and rinsed three times with 0.1 mM NaCl to remove not immobilised microplastic particles.

CP-AFM measurements were performed in a 0.1 mM NaCl-solution and at slightly acidic pH due to dissolved CO_2 using an MFP-3D Bio (Asylum Research Inc., Santa Barbara, USA) mounted on an inverted optical microscope (Axio Observer Z1, Zeiss, Oberkochen, Germany). After a first optical alignment, force maps for P-MPP (500 nm^2, 10 × 10 pts) and M-MPP (300 nm^2, 6 × 7 pts) were conducted to determine the apex of each particle. This allows a precision of nearly 50 nm in the XY direction. 15–20 particles were evaluated, and each particle was measured three times with feedback of the lateral deflection. The precision was sufficient, as there were no significant differences in lateral deflection between measurements with centred spheres and spheres with an offset of up to 100 nm. After the alignment of the colloidal probe and microplastic particle, the measurements were executed with a tip velocity of 1 μm/s and a scan rate of 0.5 Hz.

2.2.3. Gel permeation chromatography (GPC)

Gel permeation chromatography (GPC) was carried out on an Agilent (Polymer Laboratories Ltd., Church Stretton, UK) PL-GPC 220 high-temperature chromatographic unit equipped with DP and RI detectors and three linear mixed beds with guard columns (Olexis). GPC analysis was performed at 150 °C using 1,2,4-trichlorobenzene as the mobile phase. Both particle types were centrifuged and subsequently dried. Afterwards, the particles were dissolved (0.1 wt%) in the mobile phase in an external oven (150 °C) and the solutions were chromatographed without filtration. The molecular weights of the samples were referenced to polystyrene standards (Mw = 518–2,500,000 g/mol, K = 12.100 and Alpha = 0.707).

2.2.4. Nuclear magnetic resonance (NMR)

Both particle types were centrifuged and subsequently dried. For NMR, both particle types were dissolved in $CDCl_3$. ^1H and ^{13}C liquid-state NMR spectra were acquired on an Avance III HD spectrometer (Bruker, Massachusetts, USA) operating at a B_0 field of 16.4 T. The spectrometer is equipped with a helium-cooled TCI-CryoProbe. The ^1H NMR spectra (ν_0 (^1H) = 700.2 MHz) were obtained with a single pulse (SP) excitation with a pulse length of 3.0 μs corresponding to 30° tip angle and a recycle delay of 1 s to allow for quantitative analysis of the spectral intensities. The ^{13}C NMR spectra (ν_0 (^{13}C) = 176.0 MHz) were acquired with an SP sequence, a 6 μs pulse length corresponding to a 45° tip angle and a recycle delay of 3 s. During ^{13}C acquisition, proton broadband decoupling was applied using a waltz-16 sequence with ν_{nut} = 3.6 kHz. Both, the ^{13}C and ^1H NMR spectra are referenced to tetramethylsilane (TMS).

2.2.5. Energy-dispersive X-ray spectroscopy (EDX)

Both particle types were dried after recovery by centrifugation and applied on graphite. EDX spectroscopy was carried out using a Zeiss Ultraplus (Carl Zeiss AG, Oberkochen, Germany) equipped with a 30 mm^2 Thermo Scientific UltraDry EDS Detector using a beam voltage of 20 kV.

2.2.6. Scanning electron microscopy (SEM)

100,000 cells per slide were seeded on Ø 13 mm Nunc™ Thermanox™ slides (Thermo Fisher Scientific, Waltham, MA, USA) and incubated for 24 h under cell culture conditions in cell culture growth medium. 5 μL of a 180 μg/mL particle solution in cell culture growth medium was added to the cells (≙ 20 particles per cell). After 24 h incubation, the cells were directly fixed using Karnovsky's reagent (4% (v/v) formaldehyde, 5% (v/v) glutaraldehyde, with a final concentration of 32 mM PBS, pH 7.4) for 1 h at room temperature and afterwards dehydrated using an ethanol series 50%, 70%, 80% for 30 min, 90% and absolute ethanol for 1 h. The overnight air-dried samples were sputter-coated with platin and depicted using SEM (FEI Apreo Volumescope,

Thermo Fisher Scientific, magnification 8000, 2 kV, Everhart-Thornley detector). A 1 mg/mL aqueous particle suspension was dried overnight on a silicon wafer for the particle characterisation. The samples were sputter-coated with platin and imaged using SEM (FEI Apreo Volumescope, Thermo Fisher Scientific, magnification 20,000 and 150,000, 1.5 kV, T2 detector).

2.2.7. Confocal microscopy

The cells were prepared as described in Ramsperger et al. (2020). In brief, for each particle type and cell line three coverslips (Ø 18 mm) with 5×10^4 cells per mL were cultivated for 24 h at cell culture conditions in 12 well plates before incubation with the microplastic particles. For the experimental procedure, the microplastic particle stock solutions were diluted in Dulbecco's phosphate buffer saline (DPBS, Merck) to obtain the same number of particles (P-MPP 1:50; M-MPP: 1:100; microplastic particles: DPBS, concentration: 500 μg/mL). 100 μL of each microplastic particle dilution was directly added to pre-cultured cells in cell culture growth media resulting in a final microplastic particle concentration of 5 μg/mL, corresponding to 340,000 particles per mL or seven particles per cell. After 1 h incubation on ice to allow particle sedimentation, the well plates were incubated at 37 °C and 5% CO_2 for 2 h to activate the cellular metabolism and allow the internalisation of the particles. The coverslips were washed three times with DPBS to remove unattached particles. Cells were fixed with 4% PFA and fluorescently labelled with Alexa Fluor™ Phalloidin 488 (Invitrogen, Carlsbad, USA) as described in Ramsperger et al. (2020).

To determine the total number of particle-cell-interactions (PCI), which is defined as a particle in close proximity to a cell, five randomly chosen regions of interest (ROI) (0.29 mm^2 each) were selected and imaged by using a DMI 6000 microscope (LEICA, Wetzlar, Germany, HCX PL APO 63 ×/1.30 oil objective) including a spinning disc unit (CSU X1, YOKOGAWA, Musashino, Japan) with an EMCCD camera (Evolve 512, PHOTOMETRICS, Tucson, Arizona, including an additional 1.2 × magnification lens). Procedures were adapted from Ramsperger et al. (2020). A differential interference contrast (DIC) microscopy image was acquired from each ROI to quantify the PCI and confocal stacks of fluorescently labelled cells were acquired using a 488 nm laser (50 mW, Sapphire 488, COHERENT, Santa Clara, California) at a spinning disc speed of 5000 rpm to excite fluorescence. Axial stacks of the cells were acquired with a vertical distance of 0.2 μm. As the ImKC cells are smaller than the J774A.1 cells, the confocal stacks were used to calculate the area covered by cells within an ROI using the algorithm described in.

To quantify the number of microplastic particles internalised by the cells, we screened each sample for 100 PCI, to distinguish between particles attached to cell membranes or internalised as described in Ramsperger et al. (2020). The coverslips were screened in the DIC-channel until 100 particle-cell-interactions were detected, or until the whole coverslip was screened entirely (e.g., in the case of ImKC cells treated with M-MPP, where less than 100 particle-cell-interactions were detected).

For better comparability between P-MPP and M-MPP treatments and different cell lines, a standardisation was performed to the same area covered by cells on a coverslip (17.7 mm^2, which corresponds to 7% coverage of a coverslip resulting in a mean of 20,000 cells per coverslip). This has been performed as the two cell lines showed different areas covered with cells due to the different sizes of the cells (mean individual cell size J774A.1: 810 ± 190 μm^2 and ImKC: 350 ± 20 μm^2, calculated from ROI images of the fluorescent channel). The number of PCI were extrapolated to a whole coverslip. As the areas on the coverslips covered by cells differ between replicates and cell lines each coverslip was standardised (Mean cell area ± SE: J774A 0.1 P-MPP: 18.4 ± 0.25 mm^2, M-MPP: 32.6 ± 1.5 mm^2; ImKC P-MPP: 3.6 ± 0.03 mm^2, M-MPP: 6.4 ± 0.26 mm^2).

2.2.8. Metabolic activity assay (MTT)

J774A.1 and ImKC cells were detached with citrate buffer as described above and 10,000 cells in 100 μL were seeded per well in a 96-well plate and cultured at cell culture conditions for 24 h. Afterwards, freshly prepared particle dilutions (1.5, 15, 37.5, 75, 112.5, 150, 750–1500 μg/mL in the corresponding cell culture growth medium, concentrations are correlating to used concentrations in the literature (Stock et al., 2019; Harvilchuck and Carlson, 2006) were added for another 24 h. Additionally, two control treatments were performed. Cells that were not exposed to microplastic particles are defined as non-treated cells representing 100% metabolic activity ('negative control'), and cells treated with 0.3% Triton X-100 are defined as cells representing 0% metabolic activity ('positive control'). During experimental setting of the assay we analysed (under cell-free conditions) the influence of the microplastic particles on the absorbance measurement. We showed that even the highest amount of microplastic particles used does not interfere with the absorption measurement. After 24 h incubation, the cells were washed with DPBS and 50 μL freshly prepared MTT reagent (1 mg/mL 3-(4,5-dimethyl-2-thiazolyl)-2,5-Diphenyl-2H-tetrazolium bromide (MTT) in serum-free Modified Eagle Medium without phenol red) was added to each well. After 2 h incubation, the MTT reagent was removed, and 100 μL isopropanol were added per well. After 5 min rotating at 600 rpm, the absorbance at 570 nm (reference wavelength 650 nm) was measured using a TECAN GENios Pro plate reader (Tecan Austria GmbH, Gröding). Each cell line – MPP type and concentration was run in triplicate (except for ImKC, where 6 biological replicates were used for 0–150 μg/mL microplastic particle concentrations), and each experiment was run in 6 technical replicates.

2.2.9. Proliferation assay

100,000 cells were seeded in 1 mL growth medium per well in a 12-well plate and left to settle for 3 h at cell culture conditions. Afterwards, the cells were treated with 37.5, 150 and 1500 μg/mL of either particle suspension (≙ 25, 100, 1000 particles per cell). The cells were collected after 0, 24, 48 and 72 h with citric saline buffer as described above and resuspended in 1 mL cell growth medium. Cell number was evaluated using the automated fluorescence cell counter Luna II (Logos Biosystems, Gyeonggi-do, Korea). A 2 μL sample of the cell suspension was mixed with 18 μL Staining-Mix (Acridine Orange and Propidium iodide, proprietary concentrations, Logos Biosystems) and loaded into the chamber of a PhotonSlide (Logos Biosystems). Cells incubated without particles at otherwise identical conditions were used as reference.

2.3. Statistical analysis

Statistical analysis was conducted either using Origin software 2019b (Origin, Northampton, MA, USA) or R studio software (Version 1.2.5019, R Core Team 2020). All data were tested for normal distribution (Shapiro-Wilk test) and homogeneity of variances (Levene test). To investigate differences between the particle types in the ζ-potential-measurements a one-way ANOVA with a Tukey post hoc test was used. For PCI and internalisation experiments and MTT, a Kruskal-Wallis test with a Games Howell post hoc test (p-adjust method for multiple nesting: Bonferroni Holm) was conducted to check for differences between treatments. For the MTT assay, outliers of > 15% of the overall mean were excluded from the statistical analysis. For the proliferation experiments, a one-way ANOVA with a Tukey post hoc test was used.

3. Results

3.1. Surface structures and size distributions of P-MPP and M-MPP

Scanning electron microscopy (SEM) analysis revealed that the morphological surface structures of the P-MPP and the M-MPP differed (Fig. 1A). Apart from that, both particle types showed a highly monodisperse size distribution in the SEM images, which we further

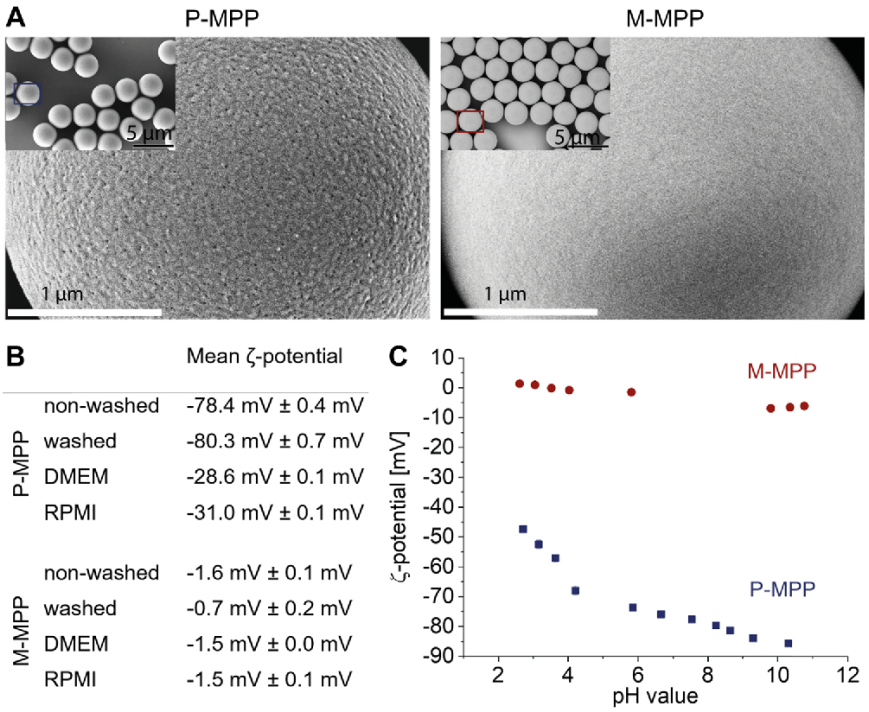

Fig. 1. (A) SEM images show differences in surface morphology of both particle types. (B and C) ζ-potential measurements of P-MPP (blue) and M-MPP (red) particles. The ζ-potential measurements were performed in 1 mM KCl at pH 6 (B) and selected pH values during a pH titration (C). (B) Both particles were measured in stock solution and after incubation in MilliQ water as well as after incubation in two cell culture media (DMEM and RPMI) supplemented with 10% (v/v) FCS. (C) For the titration, stock particles were used. Data points represent mean ± SD, n 3. The surface charge of P-MPP was significantly more negative than that of M-MPP, regardless of the pH of the medium used. (For interpretation of the references to color in this figure legend, the reader is referred to the web version of this article.)

confirmed by using dynamic light scattering (DLS). Here, the diameter of P-MPP was 3.1 ± 0.4 µm and that of M-MPP 3.0 ± 0.5 µm, showing that P-MPP and M-MPP did not differ significantly in size.

3.2. Differences in particles' ζ-potentials

We measured the ζ-potentials at pH 6 of both particle types after the incubation in three different media (Milli Q-water and two cell culture media DMEM and RPMI) (Fig. 1B). The initial ζ-potentials of both particle types were slightly altered by incubation in Milli Q-water from −78.4 ± 0.4 mV (initial) to −80.3 ± 0.7 mV for P-MPP ($p < 0.01$) and from −1.6 ± 0.1 mV (initial) to −0.7 ± 0.2 mV for M-MPP ($p < 0.05$). The incubation of P-MPP in both cell culture media supplemented with 10% v/v FCS showed a significant change in ζ-potential from −78.4 ± 0.4 mV (initial) to −28.6 ± 0.1 mV in DMEM and −31.0 ± 0.1 mV in RPMI ($p < 0.01$). For M-MPP no significant changes in ζ-potential were observed after incubation in both cell culture media (from −1.6 ± 0.1 mV to −1.5 ± 0.0 mV in DMEM and from −1.6 ± 0.1 mV to −1.5 ± 0.1 mV in RPMI) (Fig. 1B). This shows that a considerable difference in the ζ-potentials of both particle types remains under cell culture conditions. To investigate the effect of pH on the ζ-potentials, a pH titration was performed. Here, the ζ-potential of the P-MPP taken from the stock solution of the supplier decreased from −47 mV at pH 2.5 to −85 mV at pH 10.5, whereas the ζ-potential of the M-MPP changed from + 1.5 mV at pH 2.5 to −6.9 mV at pH 11 (Fig. 1C). Overall, the surface charge of P-MPP was significantly more negative than that of M-MPP, regardless of the pH of the medium used.

3.3. Particles' chemical composition and surface charge distribution

For a better understanding of where the differences of the ζ-potential of both particle types may originate from, we measured the particles' chemical compositions and average PS chain lengths by using liquid-state nuclear magnetic resonance (NMR), energy dispersive X-ray (EDX) spectroscopy, and gel permeation chromatography (GPC) (Fig. 2 and Table 1). The NMR spectroscopic analysis showed that both particle types display a similar and small number of carboxylic groups on their surfaces. For P-MPP, we found no characteristic NMR signals for co-monomers and surfactants. However, P-MPP exhibits a content of 3‰ of negatively charged chain-terminating sulphate (-SO_4^-) units with a number-averaged molecular weight (M_n) of 38,100 g/mol and a polydispersity of 5.0, indicating a higher molecular weight distribution compared to M-MPP. The negative ζ-potential of P-MPP indicates that the sulphate groups are preferentially exposed on the particles` surfaces. EDX analysis confirmed the presence of sulphur on the P-MPP surface, which was absent on the M-MPP. We further analysed surface charge distribution by colloidal probe atomic force microscopy (CP-AFM). We deduced the effective Debye length from this method, which describes the range of the electrostatic repulsive forces for like-charged surfaces. We found a constant effective Debye length of about 24 nm in multiple P-MPP given by the curves' slope (Fig. 3A and B) as well as on one and the same particle (Fig. S1B). This indicates a homogeneously distributed negative surface charge of P-MPP.

The significantly smaller ζ-potentials for M-MPP suggest that fewer charged groups are assembled on the particle surfaces compared to P-MPP. Chemical composition analysis of M-MPP revealed a content of 1% charge-neutral chain-terminating benzoic acid ester units which confirms the measured low ζ-potential. The smaller number-averaged molecular weight (M_n) of 9500 g/mol corresponds to shorter polymer chains with a polydispersity of 2.3, resulting in more end groups. One might assume that considering the higher molecular weight distribution of P-MPP compared to M-MPP, the density of two beads should be different. However, the difference in density is defined by the difference in defects (functional groups), in the present case, essentially end groups resulting from the initiator. Despite the difference in the molecular weight distribution of P-MPP and M-MPP, the number of end groups is too small to cause significant differences in density. More importantly, the radical polymerisation mechanism in styrene droplets leads to a preferred accumulation of defects on the surface of the resulting particles, but to a lesser extent, in the bulk material. Thus, we focused on the

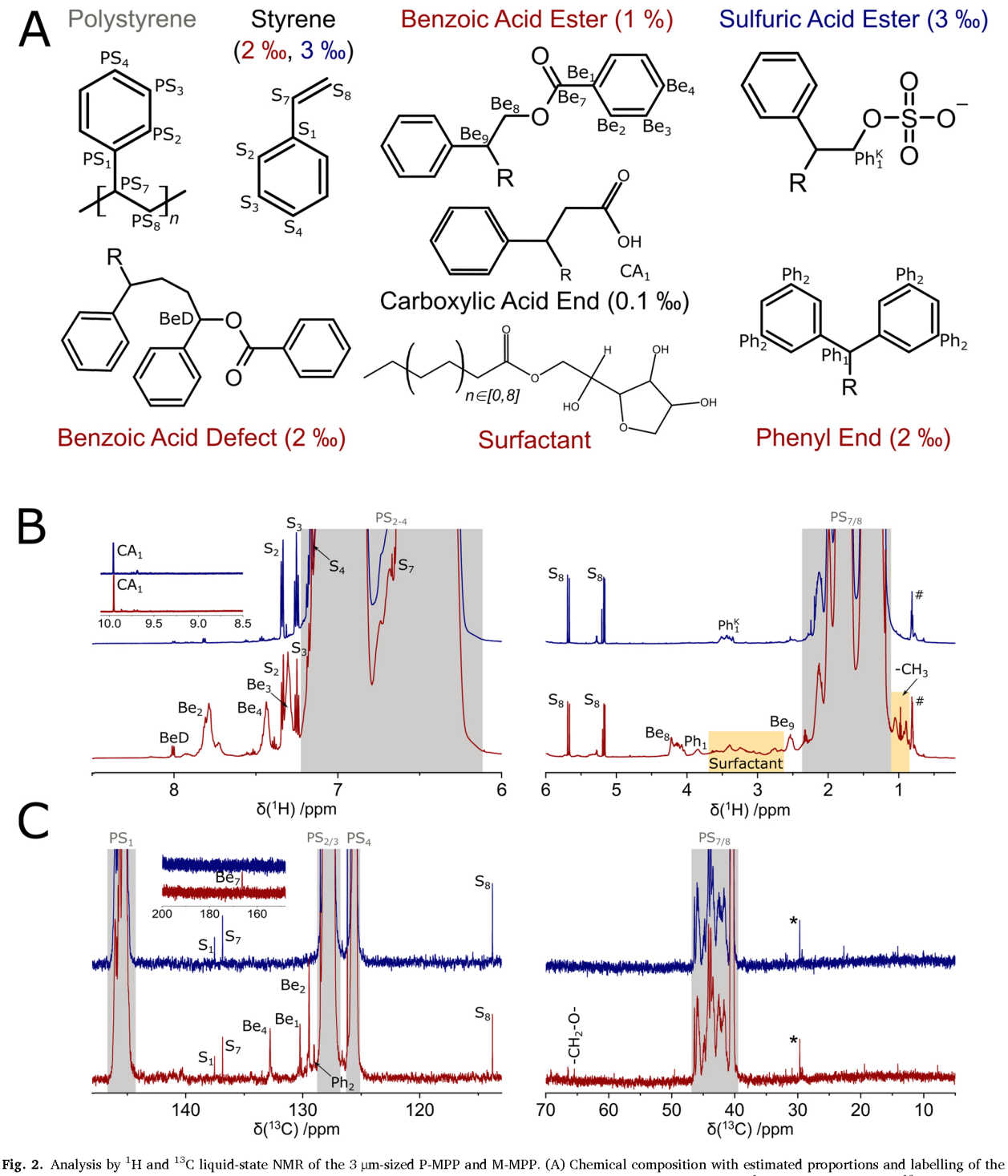

Fig. 2. Analysis by ^{1}H and ^{13}C liquid-state NMR of the 3 µm-sized P-MPP and M-MPP. (A) Chemical composition with estimated proportions and labelling of the characteristic units. The chemical structure of the surfactant is exemplarily expressing observed ester and sugar groups. (B) ^{1}H NMR spectra and (C) ^{13}C NMR spectra including assignment of characteristic resonances. Spectra, proportions and characteristic chemical units are given in a colour code (black refers to both particle types, blue refers to P-MPP, red represents M-MPP). Resonances within the grey regions are assigned to the repeating unit of PS and the other region represents the surfactant.

Table 1
Results of the GPC Measurement. M_n number average molecular weight, M_w weight average molecular weight, Polydispersity molecular weight distribution. Each sample was measured twice and averaged.

	M_n (g/mol)	M_w (g/mol)	Polydispersity
P-MPP	38,072	190,385	5.04
M-MPP	9462	22,145	2.34

physicochemical properties of the particles' surfaces. Small characteristic resonances for ether and sugar groups containing surfactants were observed for M-MPP. They might provide sufficient charges to match the observed low ζ-potentials and prevent self-aggregation of the particles. The force curves for M-MPP gained by AFM differed strongly between measurements on different particles (Fig. 3C). Moreover, only weak attractive van-der-Waals forces were observed compared to P-MPP, and the effective Debye length of the electrostatic repulsive forces differed between 9 nm and 22 nm. These varying effective Debye lengths suggest that the surface charge is heterogeneously distributed on the M-MPP's surfaces, which was subsequently verified by measuring four different spots on the same M-MPP (Fig. S1A). For two spots, electrostatic repulsive forces and attractive van-der-Waals forces were found, whereas the other two spots showed only slightly repulsive electrostatic forces. Therefore, M-MPP showed not only surface charge heterogeneities between single particles but on the very same particle.

Next to differences in surface charge, P-MPP and M-MPP also differ in their residual monomer content as shown by the ^{1}H- and ^{13}C NMR spectra. In P-MPP, 3‰ of residual styrene monomers were dissolved within the PS particles, whereas in M-MPP 2‰ were found (Fig. 2B and C).

3.4. Particle-cell interactions and subsequent internalisation

Our results show, that although both particle types are sold as plain polystyrene microplastic particles of similar size and surface characteristics, distinct differences exist, in particular, regarding the surface properties and monomer content. Both properties may alter the interaction with cells which we investigated by using two murine macrophage cell lines (J774A.1 and ImKC). In this context, SEM analysis revealed a qualitative difference on the type of particle-cell-interactions (PCI). A PCI consists of particles being solely attached to cellular membranes (Fig. 4, indicated by white arrows) or particles being covered by cellular membranes and, therefore, internalised (Fig. 4, indicated by orange arrows). For both analysed cell lines, the SEM images depicted that P-MPP were more often internalised than M-MPP.

Subsequently, this qualitative observation was confirmed by spinning disc confocal microscopy (Fig. 5). In cell line J774A.1, the observed PCI were 150 times more frequent for P-MPP than for M-MPP, and P-MPP were significantly internalised 80 times as often. Similarly, the ImKC cells, significantly more often interacted (factor of 260) with P-MPP than with M-MPP, and P-MPP were by a factor of 360 more often internalised than M-MPP (all differences for both cell lines were highly significant $p \leq 0.001$) (Fig. 6; factors rounded to the nearest integer).

3.5. Cellular responses MTT results

To test if differences in PCI and internalisation are affecting the cells, we measured the metabolic activity (Fig. 7) and proliferation (Fig. 8) of both macrophage cell lines upon exposure to both particle types. ImKC cells showed a significant increase in metabolic activity after treatment with 15 and 37.5 μg/mL P-MPP ($p < 0.05$) and a significant decrease for 1500 μg/mL P-MPP compared to the negative control ($p < 0.05$). For the J774A.1 cell line, we did observe a trend towards a lower metabolic activity with a rising P-MPP concentration, but the differences compared to non-treated (100% metabolic activity, negative control) were not statistically significant. The M-MPP did not significantly affect the metabolic activity from either cell line at particle concentrations tested.

Furthermore, we analysed possible effects on cell proliferation upon exposure to a low, medium, and high concentration (37.5 μg/mL, 150 μg/mL, 1500 μg/mL) for both particle types. In the case of cells incubated with P-MPP cell counts showed a dependence on the particle concentration for both cell lines. For the ImKC cell line, 150 μg/mL yielded a significant lower cell count after 72 h compared to the control ($p < 0.05$) and a slight increase at 37.5 μg/mL. J774A.1 was not affected by the latter concentrations. The highest concentration of P-MPP significantly inhibited the proliferation for both cell lines ($p < 0.001$). Growth rates and cell counts for M-MPP did not show significant differences ($p > 0.05$) for both cell types (Fig. 8) at any used concentration.

4. Discussion

Overall, our findings show that chemical composition and surface

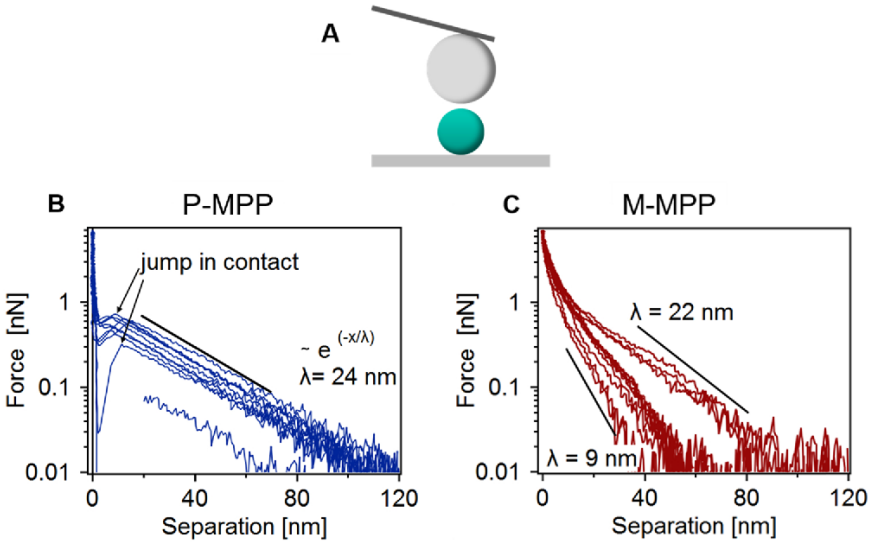

Fig. 3. Scheme of a CP-AFM measurement (A) of P-MPP (B) and M-MPP (C). (A) CP-AFM measurements were performed with a silica colloidal probe (grey, 4.8 μm) attached to a cantilever on polystyrene beads (green, 3 μm, P-MPP and M-MPP) and obtained in an aqueous solution of 0.1 mM NaCl (calculated Debye length λ 30 nm) and pH 5–6. Semi-logarithmic force-separation curves of more than ten particles are plotted and the straight solid lines indicate exponential Debye fits. Force curves in (B) show a constant effective Debye length of 24 nm indicating a homogeneously distributed surface charge for P-MPP. In contrast, the effective Debye length differs (9–22 nm) for each of the particles seen in (C) suggesting a heterogeneously distributed surface charge for M-MPP. The M-MPP also show an additional slowly increasing force below 10 nm separation. This indicates a steric repulsive force. Whereas the curves of P-MPP show a jump in contact at the same separation induced by attractive van-der-Waals forces. (For interpretation of the references to color in this figure legend, the reader is referred to the web version of this article.)

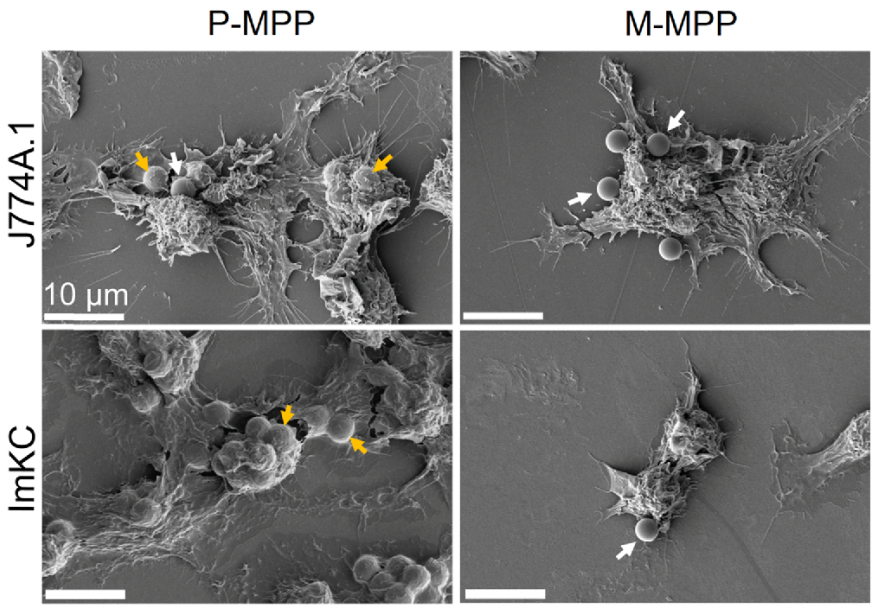

Fig. 4. Qualitative study on particle-cell-interaction (PCI) and internalised microplastic particles via SEM of J774A.1 and ImKC macrophages incubated with the two different microplastic particle types. The cells were incubated with 20 particles per cell for 24 h. The P-MPP are more often covered by cellular membranes and therefore internalised (orange arrows) by both cell lines compared to the M-MPP, being solely attached to membranes of both cell lines (white arrows). Scale bar: 10 µm. (For interpretation of the references to color in this figure legend, the reader is referred to the web version of this article.)

characteristics of nominally identical microplastic particles from different suppliers significantly differ and suggest that these differences influence PCI and cellular responses on two murine macrophage cell lines.

The differences in the surface properties of P-MPP and M-MPP particles most likely originate from the differences in the synthesis conditions. Our results indicate that different radical initiators were used, affecting surface morphology, surface charge, and chemical composition. The pronounced difference in the ζ-potentials of P-MPP and M-MPP was surprising since the supplier described both particle types as bearing a slightly negative surface charge due to the presence of sulphate ester groups. However, whereas in the case of P-MPP, we did observe anionic sulphate groups on the surface, most likely originating from the chosen initiator (Moad et al., 1982; Van Berkel et al., 2003), we did not find such evidence for M-MPP. In M-MPP, the heterogeneously distributed slightly negative ζ-potential on the surface is most likely caused by a small portion of carboxyl groups probably formed by oxidation reactions during the polymerisation process (Beachell and Smiley, 1967; Yousif and Haddad, 2013; Arráez et al., 2019). The NMR spectroscopic data indicate that a similar process was presumably active in the synthesis of P-MPP, but the contribution to the P-MPP surface net charge and charge distribution is negligible compared to the anionic groups from the used initiator. Moreover, whereas the highly charged P-MPP show a homogeneously distributed surface charge, the much lower surface charge of M-MPP is widely and heterogeneously distributed over the surface. Since they cannot rely on electrostatic repulsion for colloidal stabilisation, M-MPP seem to be stabilised by charge-neutral surfactants. In contrast, in P-MPP the absence of characteristic NMR signals for co-monomers and surfactants indicates that the interaction with sister particles and, therefore, also cell membranes is predominantly electrostatic. Given the high surface-to-volume ratio of microplastic particles, not only the overall charge but also the charge distribution may affect how cellular membranes and particles interact, since our findings show that the homogeneously charged P-MPP show significantly higher PCI compared to the heterogeneously and significantly less charged M-MPP.

Fröhlich (2012) describe in their comprehensive review that, amongst other properties, the surface morphology of a particle can play a role in how the particles interact with cells. Our SEM analysis depicts that the surface structure was slightly more pronounced in P-MPP compared to M-MPP, which might affect PCI and the propensity for internalisation. For human epithelial cells, a correlation of the surface roughness with the likelihood of internalisation has been shown, with a rougher surface of a nanoparticle leading to a higher internalisation compared to smooth particles (Niu et al., 2015). This is consistent with our results, where P-MPP become internalised more often than the smoother M-MPP. In contrast, other studies showed a decreased cellular internalisation of rougher compared to smoother nanoparticles (Piloni et al., 2019; Kim et al., 2021), indicating that the surface roughness is not the dominant factor triggering PCI and internalisation. This has already been highlighted by Schrade et al. (2012), suggesting that surface charge is more important for internalisation than surface morphology. For instance, Musyanovych et al. (2011), e.g. showed that PS nanoparticles with an anionic surfactant with a ζ-potential of −60 mV (in KCl, −28 mV in cell culture medium with 10% FCS) were internalised by HeLa cells more often than nanoparticles stabilised with a non-ionic surfactant and having a ζ-potential of −5 mV (in KCl, −12 mV in cell culture medium with 10% FCS). This is in concordance with our findings that both murine macrophage cell lines showed a higher number of PCI and internalised particles for the more negatively charged P-MPP compared to M-MPP. This may be explained by the main biological function of macrophages, which is the internalisation of negatively charged bacteria via phagocytosis (Fröhlich, 2012). Gebicki and James (1962) described the ζ-potential of bacteria with −22 mV at pH 7.0, which is in the range of the P-MPPs ζ-potential in cell culture media. Besides, with 3 µm in diameter the PS particles used in our experiments are within the size range of bacteria (Levin and Angert, 2015).

Another aspect of potential relevance for PCI and internalisation is the formation of a corona on the surface of the particles altering their initial surface properties (Lundqvist et al., 2008; Tenzer et al., 2013; Monopoli et al., 2012). The changes in ζ-potential recorded after incubating the particles in cell culture media are highly indicative of the formation of a protein corona (Partikel et al., 2019). It has already been shown that the protein corona formation is influenced by the surface properties like modification with chemical groups or surface charge (Lundqvist et al., 2008; Tenzer et al., 2013; Shannahan et al., 2013; Cao et al., 2019; Saavedra et al., 2019). Our results show that the initially higher negative ζ-potential of P-MPP seems to be more altered by the incubation in cell culture media than that of M-MPP, although the

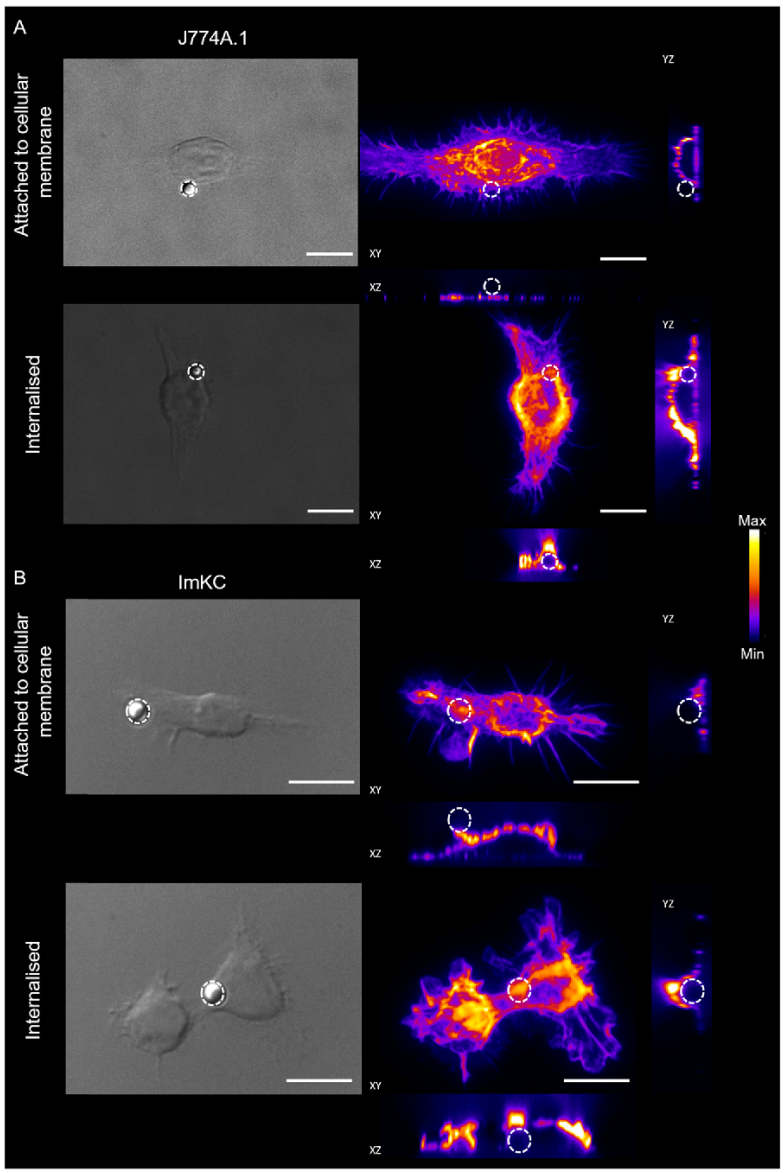

Fig. 5. Representative images for the differentiation of microplastic particles attached to cellular membranes and internalised particles. Differential interference contrast (DIC) microscopy images (left column) of M-MPP-cell interactions with cells from the J774A.1 (A) cell line and cells from the ImKC cell line (B). Fluorescence images were acquired by spinning disc confocal microscopy (right side) of the same cells from DIC images with fluorescently labelled filamentous actin (false colour maximum intensity projection, arbitrary units). XY-, YZ- and XZ-projections of three-dimensional confocal stacks allow the differentiation of microplastic particles attached to cell membranes from internalised microplastic particles. Circles indicate microplastic particle positions. Only those particles being completely covered by the filamentous actin were considered to be internalised (A and B lower panel), whereas the other particles were only attached to cellular membranes. Scale bars: 10 μm.

difference in ζ-potential between the particles remain after the incubation. This indicates the formation of a more pronounced protein corona on P-MPP, which may additionally explain the distinctly higher numbers of PCI and internalised particles. However, most of the findings of protein corona formation were reported for nanoparticles (Lundqvist et al., 2008; Tenzer et al., 2013; Monopoli et al., 2012; Shannahan et al., 2013). It has to be noted that care must be taken when comparing nano- and microparticles, as the particles reactivity is much higher for smaller particles (Buzea et al., 2007) and the internalisation mechanisms by macrophages may be different depending on the particle size (Koval et al., 1998). Nevertheless, it has been shown that the internalisation of 3 μm PS particles coated with biomolecules forming an eco-corona into cells is enhanced compared to uncoated microplastic particles (Ramsperger et al., 2020), indicating that the coating of a particle is an important factor for PCI and internalisation.

Distinct differences between P-MPP and M-MPP in ζ-potential, surface charge distribution and residual monomer content may also explain the observed differences in cell metabolism and cell proliferation.

No cellular responses were observed for M-MPP in any of the experiments. In contrast, P-MPP induced a significant reduced metabolic response in both cell lines in the highest used concentration (1500 μg/mL). The lower metabolic activity is reflected by an inhibited cell proliferation in both cell lines, indicating that the properties of the used PS particles interfere with the viability of the cells. Further, the ImKC cells showed an increase in metabolic activity for the lowest concentrations (15 μg/mL and 37.5 μg/mL) only when exposed to P-MPP. This is characteristic for a hormesis effect, showing an increase in metabolic activity at low concentrations of a contaminant with a continuous drop at higher concentrations (Calabrese and Why, 2008; Gopi and Rattan, 2019). The higher sensitivity observed by the ImKC compared to the J774A.1 cells may arise from the fact that the cell lines originate from different body compartments. The J774A.1 cell line was derived from a murine reticulum cell carcinoma (Ralph and Nakoinz, 1975), whereas the ImKC cell line was established from murine resident liver Kupffer

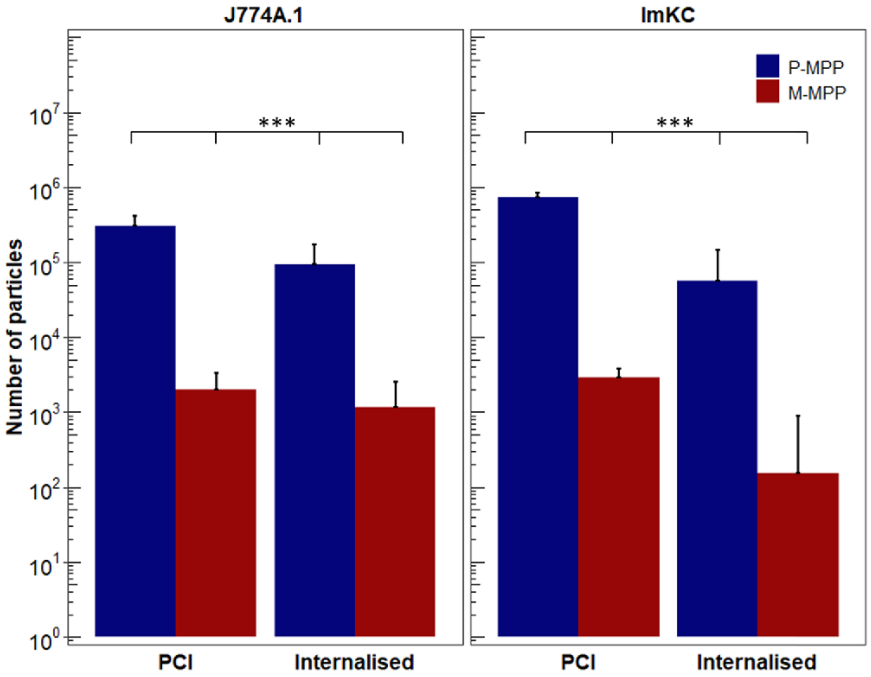

Fig. 6. Comparison of P-MPP and M-MPP with two macrophage cell lines concerning their particle-cell interactions and number of internalised particles. The cells were incubated with 5 μg/mL microplastic particles for 2 h. The numbers of particle-cell interactions and internalised microplastic particles were standardised to coverslips with 20,000 cells for better comparison, as the relative cell area on a coverslip for both cell lines differed. Data points represent mean + SD, n 300 images (P-MPP & M-MPP J774A.1, P-MPP ImKC), n 41 images (M-MPP, ImKC), significance level: *** $p \leq 0.001$.

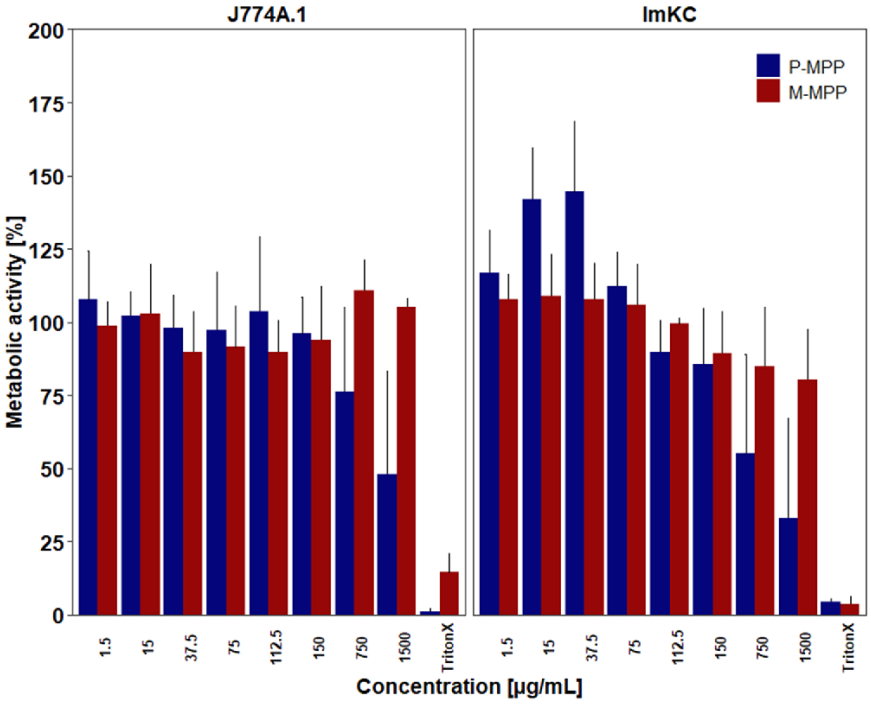

Fig. 7. MTT cell metabolism measurements with both cell lines after 24 h incubation with the respective particles. Results are shown as mean + SD. Data are given as the percentage of the particular experiment to the viability of the negative control (cells without particles). While there is no cytotoxicity for concentrations below 150 μg/mL, cytotoxicity at higher concentrations was dependent on particle type as well as on the cell line. Triton X-100 was used as a cell toxic positive control. Data points represent mean + SD, independent experimental replicates: n 3–9.

cells (Wang et al., 2014). Kupffer cells were described to be more sensitive to stress factors than some other macrophage cell lines (Tanifum et al., 2018), whereas J774A.1 cells have generally been described as less sensitive to particle exposure. For instance, J774A.1 cells exposed to similar concentrations of 2 μm carboxylated-PS particles (Mutzke et al., 2015) or sulphate-functionalised 4 μm PS particles (Stock et al., 2019) did not show cytotoxicity.

The observed cellular responses of the P-MPP compared to the M-MPP may originate from the higher amount of residual styrene monomers in P-MPP. It has been shown that styrene monomers induce particularly hepatotoxic effects (Harvilchuck and Carlson, 2006; Withey, 1976), which could explain the stronger cellular response of

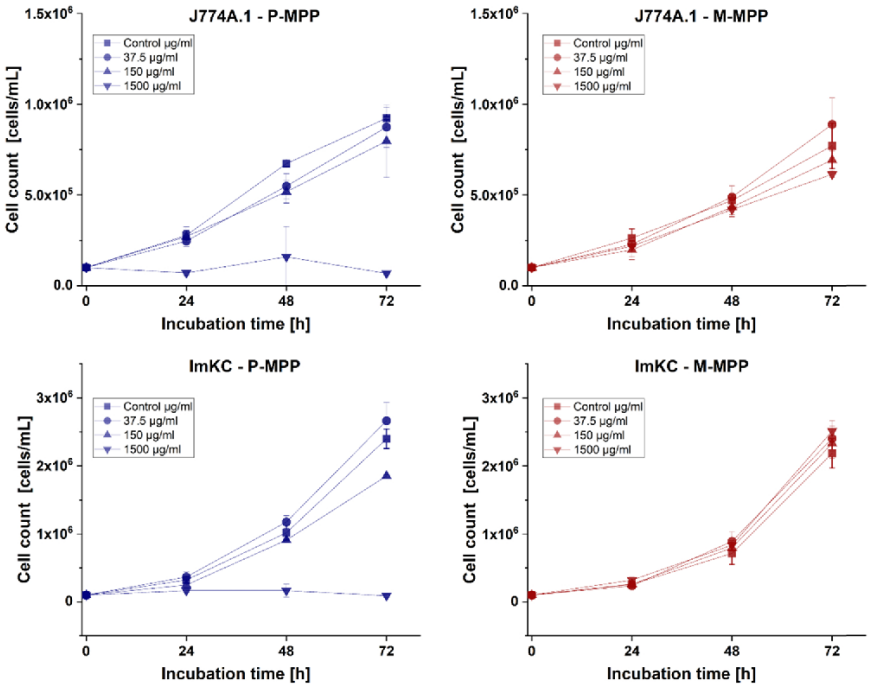

Fig. 8. Cell proliferation of J774A.1 and ImKC cell lines in a time and concentration-dependent manner for P-MPP and M-MPP. Each experiment was performed in 12–well tissue culture plates. M-MPP did not significantly influence cell proliferation independent of the concentration. Cells incubated with P-MPP showed almost no proliferation at 1500 µg/mL and a significantly lower cell count for ImKC at 150 µg/mL after 72 h. Data represent mean ± SD, n 3 and were slightly offset.

ImKC cells. Upon cellular internalisation, these monomers might leach into the cytoplasm. Leaching of residual monomers is a known problem in biomedical applications e.g., dental braces (Kloukos et al., 2013). Furthermore, the higher number of internalised P-MPP could induce cell damage, leading to reduced cell proliferation. Recently, Goodman et al. (2021) showed a reduced proliferation ability for a human lung epithelial cell line after the exposure to 1 and 10 µm PS particles. An increase in particle internalisation has been shown to induce oxidative stress (Schirinzi et al., 2017; Hwang et al., 2019), which is known to damage DNA (Townley et al., 2012) and leads to bioenergetic failure (Fang and Maldonado, 2018) and, therefore, might lower the proliferation rate as well. In addition, the internalisation of particles occurs most probably by an energy-dependent mechanism like phagocytosis (Hirsch, 1965). The higher internalisation rate of P-MPP might therefore result in less energy available for cell proliferation compared to M-MPP, which are internalised less frequently. Hence, various particle properties may act synergistically in causing adverse effects. Surface charge and morphology enhance particle internalisation, and residual monomers and increased numbers of internalised particles may affect the viability of the cells. However, since these effects occurred only at higher concentrations, the relevance for exposure to animals and humans is still debatable. Nevertheless, microplastic particles occurring in nature may exhibit a huge variety of chemical and physical properties, which may alter particle cell interaction even at lower concentrations. Further, microplastic contamination in nature is expected to distinctly rise in the future (Lebreton and Andrady, 2019), enhancing the number of ingested or inhaled microplastic particles and might lead to chronic exposure to particles having properties that potentially cause adverse effects.

5. Conclusion

Overall, our results show that nominally "identical" plain polystyrene microparticles from different manufacturers differ highly in their chemical composition and surface properties resulting in pronounced differences in PCI and the proportion of internalised particles by murine macrophages. Particles showing a more negative ζ-potential and a higher residual monomer content induced a significant metabolic response in a sensitive cell line and altered cell proliferation, especially at higher particle concentrations. Our study paves the way to explain the discrepancy in the results of previously published effect studies while highlighting the need for well-characterised microplastic particles in hazard assessment studies as particles from different manufacturers lead to non-comparable results. It further emphasises that no general conclusions can be drawn concerning the toxicity of microplastics per se, even for the same type of polymer in the same size range having the same shape. Hence, only a detailed characterisation of microplastics' chemical composition and surface properties allows for comparability between toxicological studies and enables unravelling those properties that may render specific types of microplastics hazardous.

Funding

This work was supported by the Deutsche Forschungsgemeinschaft (DFG, German Research Foundation) – project number 391977956 – SFB 1357, DFG (INST 91/289-1 FUGG), Research and Innovation programme, P A.F.R.M.R. was supported by a scholarship of the elite network of Bavaria (BayEFG) and the University of Bayreuth Graduate School.

CRediT authorship contribution statement

A.F.R.M. Ramsperger: Conceptualization, Methodology, Investigation, Writing – original draft, Writing – review & editing, Formal analysis, Visualization, Project administration, Validation. **J. Jasinski:** Conceptualization, Methodology, Investigation, Writing – original draft, Writing – review & editing, Formal analysis, Visualization, Project administration, Validation. **M. Völkl:** Conceptualization, Methodology,

Investigation, Writing – original draft, Writing – review & editing, Formal analysis, Visualization, Project administration, Validation. **T. Witzmann:** Conceptualization, Methodology, Investigation, Writing – original draft, Writing – review & editing, Formal analysis, Visualization, Validation. **M. Meinhart:** Conceptualization, Methodology, Investigation, Writing – original draft, Writing – review & editing, Formal analysis, Visualization, Validation. **V. Jerome:** Conceptualization, Methodology, Writing – original draft, Writing – review & editing, Formal analysis, Validation, Supervision. **W. Kretschmer:** Methodology, Investigation, Formal analysis, Validation, Supervision. **R. Freitag:** Conceptualization, Methodology, Writing – original draft, Writing – review & editing, Formal analysis, Validation, Resources, Supervision, Project administration, Funding acquisition. **J. Senker:** Conceptualization, Methodology, Writing – original draft, Writing – review & editing, Formal analysis, Validation, Resources, Supervision, Project administration, Funding acquisition. **A. Fery:** Conceptualization, Methodology, Writing – original draft, Writing – review & editing, Formal analysis, Validation, Resources, Supervision, Project administration, Funding acquisition. **H. Kress:** Conceptualization, Methodology, Writing – original draft, Writing – review & editing, Formal analysis, Validation, Resources, Supervision, Project administration, Funding acquisition. **T. Scheibel:** Conceptualization, Methodology, Writing – original draft, Writing – review & editing, Formal analysis, Validation, Resources, Supervision, Project administration, Funding acquisition. **C. Laforsch:** Conceptualization, Methodology, Writing – original draft, Writing – review & editing, Formal analysis, Validation, Resources, Supervision, Project administration, Funding acquisition.

Declaration of Competing Interest

The authors declare that they have no known competing financial interests or personal relationships that could have appeared to influence the work reported in this paper.

Data availability

All data are available in the main text or the supplementary materials.

Acknowledgements

The authors would like to acknowledge K. Schweimer, G. Auernhammer, H. Bargel, J. Schertel, Ulrich Mansfeld and all the technicians from the different departments for their excellent technical support. We thank M. Weiss for the support with the confocal spinning disc microscope.

Author contributions

AFRM.R., J.J., M.V., V.J., R.F., J.S., A.F., H.K., T.S. and C.L. designed the experiment. AFRM.R., J.J., M.V., T.W., M.M., V.J., WP.K., R.F., J.S., A.F., H.K., T.S., and C.L. wrote the manuscript. All authors contributed to the interpretation and discussion of the results. J.J. conducted the ζ-potential measurements, DLS measurements and SEM analysis of the cells and particles. M.M. and WP.K. conducted the GPC, EDX and NMR experiments. T.W. conducted the CP-AFM measurements. AFRM.R. conducted the cellular internalisation experiments. M.V. conducted the MTT and cell proliferation experiments.

Appendix A. Supplementary material

Supplementary data associated with this article can be found in the online version at doi:10.1016/j.jhazmat.2021.127961.

References

Arráez, F.J., Arnal, M.L., Müller, A.J., 2019. Thermal degradation of high-impact polystyrene with pro-oxidant additives. Polym. Bull. 76, 1489–1515. https://doi.org/10.1007/s00289-018-2453-4.

Arthur, C., Baker, J., Bamford, H., 2008. In: Proceedings of the International Research Workshop on the Occurrence, Effects, and Fate of Microplastic Marine Debris, 9–11 September 2008. NOAA Technical Memorandum NOS-OR&R-30. (https://repository.library.noaa.gov/view/noaa/2509).

Barboza, L.G.A., Lopes, C., Oliveira, P., Bessa, F., Otero, V., Henriques, B., Raimundo, J., Caetano, M., Vale, C., Guilhermino, L., 2020. Microplastics in wild fish from North East Atlantic Ocean and its potential for causing neurotoxic effects, lipid oxidative damage, and human health risks associated with ingestion exposure. Sci. Total Environ. 717, 134625 https://doi.org/10.1016/j.scitotenv.2019.134625.

Beachell, H.C., Smiley, L.H., 1967. Oxidative degradation of polystyrene. J. Polym. Sci. Part A-1 Polym. Chem. 5, 1635–1643. https://doi.org/10.1002/pol.1967.150050713.

Bjorndal, K.A., Bolten, A.B., Lagueux, C.J., 1994. Ingestion of marine debris by juvenile sea turtles in coastal Florida habitats. Mar. Pollut. Bull. 28, 154–158. https://doi.org/10.1016/0025-326X(94)90391-3.

Brachner, A., Fragouli, D., Duarte, I.F., Farias, P.M.A., Dembski, S., Ghosh, M., Barisic, I., Zdzieblo, D., Vanoirbeek, J., Schwabl, P., Neuhaus, W., 2020. Assessment of human health risks posed by nano-and microplastics is currently not feasible. Int. J. Environ. Res. Public Health 17, 1–10. https://doi.org/10.3390/ijerph17238832.

Browne, M.A., Dissanayake, A., Galloway, T.S., Lowe, D.M., Thompson, R.C., 2008. Ingested microscopic plastic translocates to the circulatory system of the mussel, Mytilus edulis (L.). Environ. Sci. Technol. 42, 5026–5031. https://doi.org/10.1021/es800249a.

Buzea, C., Pacheco, I.I., Robbie, K., 2007. Nanomaterials and nanoparticles: Sources and toxicity. Biointerphases 2, MR17–MR71. https://doi.org/10.1116/1.2815690.

Calabrese, E.J., 2008. Hormesis. Why it is importantto toxicology and toxicologists. Edited by Foxit Reader. Toxicol. Chem. 27, 1451–1474.

Campanale, C., Massarelli, C., Savino, I., Locaputo, V., Uricchio, V.F., 2020. A detailed review study on potential effects of microplastics and additives of concern on human health. Int. J. Environ. Res. Public Health 17. https://doi.org/10.3390/ijerph17041212.

Cao, X., Han, Y., Li, F., Li, Z., McClements, D.J., He, L., Decker, E.A., Xing, B., Xiao, H., 2019. Impact of protein-nanoparticle interactions on gastrointestinal fate of ingested nanoparticles: not just simple protein corona effects. NanoImpact 13, 37–43. https://doi.org/10.1016/j.impact.2018.12.002.

Cole, M., Galloway, T.S., 2015. Ingestion of nanoplastics and microplastics by pacific oyster larvae. Environ. Sci. Technol. 49, 14625–14632. https://doi.org/10.1021/acs.est.5b04099.

Deng, Y., Zhang, Y., Lemos, B., Ren, H., 2017. Tissue accumulation of microplastics in mice and biomarker responses suggest widespread health risks of exposure. Sci. Rep. 7, 1–10. https://doi.org/10.1038/srep46687.

Desjardins, M., Griffiths, G., 2003. Phagocytosis: latex leads the way. Curr. Opin. Cell Biol. 15, 498–503. https://doi.org/10.1016/S0955-0674(03)00083-8.

Di Dong, C., Chen, C.W., Chen, Y.C., Chen, H.H., Lee, J.S., Lin, C.H., 2020. Polystyrene microplastic particles: in vitro pulmonary toxicity assessment. J. Hazard. Mater. 385, 121575 https://doi.org/10.1016/j.jhazmat.2019.121575.

Drechsler, A., Caspari, A., Synytska, A., 2020. Influence of roughness and capillary size on the zeta potential values obtained by streaming potential measurements. Surf. Interface Anal. 52, 991–995. https://doi.org/10.1002/sia.6792.

Dris, R., Gasperi, J., Rocher, V., Saad, M., Renault, N., Tassin, B., 2015. Microplastic in urban sources and receiving water within an urban area: a case study in Greater Paris. Environ. Chem. 12, 592–599. https://doi.org/10.1071/EN14167.

Dris, R., Gasperi, J., Saad, M., Mirande, C., Tassin, B., 2016. Synthetic fibers in atmospheric fallout: a source of microplastics in the environment? Mar. Pollut. Bull. 4–7. https://doi.org/10.1016/j.marpolbul.2016.01.006.

Elizalde-Velázquez, A., Carcano, A.M., Crago, J., Green, M.J., Shah, S.A., Cañas-Carrell, J.E., 2020. Translocation, trophic transfer, accumulation and depuration of polystyrene microplastics in Daphnia magna and Pimephales promelas. Environ. Pollut. 259, 113937 https://doi.org/10.1016/j.envpol.2020.113937.

Eriksen, M., Lebreton, L.C.M., Carson, H.S., Thiel, M., Moore, C.J., Borerro, J.C., Galgani, F., Ryan, P.G., Reisser, J., 2014. Plastic pollution in the world's oceans: more than 5 trillion plastic pieces weighing over 250,000 tons afloat at sea. PLoS One 9, 1–15. https://doi.org/10.1371/journal.pone.0111913.

Evangeliou, N., Grythe, H., Klimont, Z., Heyes, C., Eckhardt, S., Lopez-Aparicio, S., Stohl, A., 2020. Atmospheric transport is a major pathway of microplastics to remote regions. Nat. Commun. 11 https://doi.org/10.1038/s41467-020-17201-9.

Fang, D., Maldonado, E.N., 2018. VDAC regulation: a mitochondrial target to stop. Cell Proliferation, first ed. Elsevier Inc. https://doi.org/10.1016/bs.acr.2018.02.002.

Frias, J.P.G.L., Nash, R., 2019. Microplastics: finding a consensus on the definition. Mar. Pollut. Bull. 138, 145–147. https://doi.org/10.1016/j.marpolbul.2018.11.022.

Fröhlich, E., 2012. The role of surface charge in cellular uptake and cytotoxicity of medical nanoparticles. Int. J. Nanomed. 7, 5577–5591. https://doi.org/10.2147/IJN.S36111.

Gasperi, J., Wright, S.L., Dris, R., Collard, F., Mandin, C., Guerrouache, M., Langlois, V., Kelly, F.J., Tassin, B., 2018. Microplastics in air: are we breathing it in? Curr. Opin. Environ. Sci. Health 1, 1–5. https://doi.org/10.1016/j.coesh.2017.10.002.

Gebicki, J.M., James, A.M., 1962. The Electrokinetic Properties of the Spheroplasts of Aerobacter Arogenes, pp. 158–167.

Goodman, K.E., Hare, J.T., Khamis, Z.I., Hua, T., Sang, Q.X.A., 2021. Exposure of human lung cells to polystyrene microplastics significantly retards cell proliferation and

triggers morphological changes. Chem. Res. Toxicol. https://doi.org/10.1021/acs.chemrestox.0c00486.
Gopi, I.K., Rattan, S.I.S., 2019. Biphasic dose–response and hormetic effects of stress hormone hydrocortisone on telomerase-immortalized human bone marrow stem cells in vitro. Dose-Response 17, 1–9. https://doi.org/10.1177/1559325819889819.
Harvil chuck, J.A., Carlson, G.P., 2006. Comparison of styrene and its metabolites styrene oxide and 4-vinylphenol on cytotoxicity and glutathione depletion in Clara cells of mice and rats. Toxicology 227, 165–172. https://doi.org/10.1016/j.tox.2006.08.001.
Hirsch, J.G., 1965. Phagocytosis. Annu. Rev. Microbiol. 339–350. https://doi.org/10.1038/179290c0.
Hutter, J.L., Bechhoefer, J., 1993. Calibration of atomic-force microscope tips. Rev. Sci. Instrum. 64, 1868–1873. https://doi.org/10.1063/1.1143970.
Hwang, J., Choi, D., Han, S., Choi, J., Hong, J., 2019. An assessment of the toxicity of polypropylene microplastics in human derived cells. Sci. Total Environ. 684, 657–669. https://doi.org/10.1016/j.scitotenv.2019.05.071.
Imhof, H.K., Ivleva, N.P., Schmid, J., Niessner, R., Laforsch, C., 2013. Contamination of beach sediments of a subalpine lake with microplastic particles. Curr. Biol. 23, R867–R868. https://doi.org/10.1016/j.cub.2013.09.001.
Imhof, H.K., Sigl, R., Brauer, E., Feyl, S., Giesemann, P., Klink, S., Leupolz, K., Löder, M. G.J., Löschel, L.A., Missun, J., Muszynski, S., Ramsperger, A.F.R.M., Schrank, I., Speck, S., Steibl, S., Trotter, B., Winter, I., Laforsch, C., 2017. Spatial and temporal variation of macro-, meso- and microplastic abundance on a remote coral island of the Maldives, Indian Ocean. Mar. Pollut. Bull. 116, 340–347. https://doi.org/10.1016/j.marpolbul.2017.01.010.
Jacob, H., Besson, M., Swarzenski, P.W., Lecchini, D., Metian, M., 2020. Effects of virgin micro- and nanoplastics on fish: trends, meta-analysis, and perspectives. Environ. Sci. Technol. 54, 4733–4745. https://doi.org/10.1021/acs.est.9b05995.
Kim, H.J., Kim, S.H., Kim, H.M., Kim, Y.S., Oh, J.M., 2021. Surface roughness effect on the cellular uptake of layered double hydroxide nanoparticles. Appl. Clay Sci. 202, 105992 https://doi.org/10.1016/j.clay.2021.105992.
Klein, S., Worch, E., Knepper, T.P., 2015. Occurrence and spatial distribution of microplastics in river shore sediments of the rhine-main area in Germany. Environ. Sci. Technol. 49, 6070–6076. https://doi.org/10.1021/acs.est.5b00492.
Kloukos, D., Pandis, N., Eliades, T., 2013. Bisphenol-A and residual monomer leaching from orthodontic adhesive resins and polycarbonate brackets: a systematic review. Am. J. Orthod. Dentofac. Orthop. 143, S104–S112. https://doi.org/10.1016/j.ajodo.2012.11.015 e2.
Koval, M., Preiter, K., Adles, C., Stahl, P.D., Steinberg, T.H., 1998. Size of IgG-opsonized particles determines macrophage response during internalization. Exp. Cell Res. 242, 265–273. https://doi.org/10.1006/excr.1998.4110.
Lacerda, A.L.d.F., dos, L., Rodrigues, S., van Sebille, E., Rodrigues, F.L., Ribeiro, L., Secchi, E.R., Kessler, F., Proietti, M.C., 2019. Plastics in sea surface waters around the Antarctic Peninsula. Sci. Rep. 9, 1–12. https://doi.org/10.1038/s41598-019-40311-4.
Laist, D., 1997. Impacts of marine debris: entanglement of marine life in marine debris including a comprehensive list of species with entanglement and ingestion records. In: Coe, J.M., Rogers, D.B. (Eds.), Marine Debris & Plastics: Environmental Concerns, Sources, Impacts and Solutions. Springer-Verlag, New York, pp. 99–139. https://doi.org/10.1007/978-1-4613-8486-1_10.
Lebreton, L., Andrady, A., 2019. Future scenarios of global plastic waste generation and disposal. Palgrave Commun. 5, 1–11. https://doi.org/10.1057/s41599-018-0212-7.
Levin, P.A., Angert, E.R., 2015. Small but mighty: cell size and bacteria. Cold Spring Harb. Perspect. Biol. 7, 1–11. https://doi.org/10.1101/cshperspect.a019216.
Lu, Y., Zhang, Y., Deng, Y., Jiang, W., Zhao, Y., Geng, J., Ding, L., Ren, H., 2016. Uptake and accumulation of polystyrene microplastics in zebrafish (Danio rerio) and toxic effects in liver. Environ. Sci. Technol. 50, 4054–4060. https://doi.org/10.1021/acs.est.6b00183.
Lundqvist, M., Stigler, J., Elia, G., Lynch, I., Cedervall, T., Dawson, K.A., 2008. Nanoparticle size and surface properties determine the protein corona with possible implications for biological impacts. Proc. Natl. Acad. Sci. USA 105. https://doi.org/10.1073/pnas.0805135105, 14265–70.
Lunov, O., Syrovets, T., Loos, C., Beil, J., Delacher, M., Tron, K., Nienhaus, G.U., Musyanovych, A., Mailänder, V., Landfester, K., Simmet, T., 2011. Differential uptake of functionalized polystyrene nanoparticles by human macrophages and a monocytic cell line. ACS Nano 5, 1657–1669. https://doi.org/10.1021/nn2000756.
Moad, G., Solomon, D.H., Johns, S.R., Willing, R.I., 1982. Structure of benzoyl peroxide initiated polystyrene: determination of the initiator-derived functionality by ^{13}C NMR. Macromolecules 15, 1188–1191. https://doi.org/10.1021/ma00232a045.
Mohamed Nor, N.H., Koelmans, A., Kooi, M., Diepens, N., 2021. Lifetime accumulation of microplastic in children and adults. Environ. Sci. Technol. 55, 5084–5096. https://doi.org/10.1021/acs.est.0c07384.
Monopoli, M.P., Åberg, C., Salvati, A., Dawson, K.A., 2012. Biomolecular coronas provide the biological identity of nanosized materials. Nat. Nanotechnol. 7, 779–786. https://doi.org/10.1038/nnano.2012.207.
von Moos, N., Burkhardt-Holm, P., Koehler, A., 2012. Uptake and effects of microplastics on cells and tissue of the blue mussel Mytilus edulis L. after an experimental exposure. Environ. Sci. Technol. 46, 327–335. https://doi.org/10.1021/es302332w.
Musyanovych, A., Dausend, J., Dass, M., Walther, P., Mailänder, V., Landfester, K., 2011. Criteria impacting the cellular uptake of nanoparticles: a study emphasizing polymer type and surfactant effects. Acta Biomater. 7, 4160–4168. https://doi.org/10.1016/j.actbio.2011.07.033.
Mutzke, E., Chomyshyn, E., Nguyen, K.C., Blahoianu, M., Tayabali, A.F., 2015. Phagocytosis-coupled flow cytometry for detection and size discrimination of anionic polystyrene particles. Anal. Biochem. 483, 40–46. https://doi.org/10.1016/j.ab.2015.04.034.
Nelms, S.E., Parry, H.E., Bennett, K.A., Galloway, T.S., Godley, B.J., Santillo, D., Lindeque, P.K., 2019. What goes in, must come out: combining scat-based molecular diet analysis and quantification of ingested microplastics in a marine top predator. Methods Ecol. Evol. 10, 1712–1722. https://doi.org/10.1111/2041-210X.13271.
Niu, Y., Yu, M., Meka, A., Liu, Y., Zhang, J., Yang, Y., Yu, C., 2015. Understanding the contribution of surface roughness and hydrophobic modification of silica nanoparticles to enhanced therapeutic protein delivery. J. Mater. Chem. B 4, 212–219. https://doi.org/10.1039/c5tb01911g.
Ober, C.K., Lok, K.P., Hair, M.L., 1985. Monodispersed, micron-sized polystyrene particles by dispersion polymerization. J. Polym. Sci. Polym. Lett. Ed. 23, 103–108. https://doi.org/10.1002/pol.1985.130230209.
Olivier, V., Rivière, C., Hindié, M., Duval, J.-L., Bomila-Koradjim, G., Nagel, M.-D., 2004. Uptake of polystyrene beads bearing functional groups by macrophages and fibroblasts. Colloids Surf. B Biointerfaces 33, 23–31. https://doi.org/10.1016/j.colsurfb.2003.08.008.
Partikel, K., Korte, R., Mulac, D., Humpf, H.U., Langer, K., 2019. Serum type and concentration both affect the protein-corona composition of PLGA nanoparticles. Beilstein J. Nanotechnol. 10, 1002–1015. https://doi.org/10.3762/BJNANO.10.101.
Patiño, T., Soriano, J., Barrios, L., Ibáñez, E., Nogués, C., 2015. Surface modification of microparticles causes differential uptake responses in normal and tumoral human breast epithelial cells. Sci. Rep. 5, 11371. https://doi.org/10.1038/srep11371.
Piehl, S., Leibner, A., Löder, M.G.J., Dris, R., Bogner, C., Laforsch, C., 2018. Identification and quantification of macro- and microplastics on an agricultural farmland. Sci. Rep. 8, 1–9. https://doi.org/10.1038/s41598-018-36172-y.
Piehl, S., Mitterwallner, V., Atwood, E.C., Bochow, M., Laforsch, C., 2019. Abundance and distribution of large microplastics (1–5 mm) within beach sediments at the Po River Delta, northeast Italy. Mar. Pollut. Bull. 149, 110515 https://doi.org/10.1016/j.marpolbul.2019.110515.
Piloni, A., Wong, C.K., Chen, F., Lord, M., Walther, A., Stenzel, M.H., 2019. Surface roughness influences the protein corona formation of glycosylated nanoparticles and alter their cellular uptake. Nanoscale 11, 23259–23267. https://doi.org/10.1039/c9nr06835j.
Prata, J.C., da Costa, J.P., Lopes, I., Duarte, A.C., Rocha-Santos, T., 2020. Environmental exposure to microplastics: an overview on possible human health effects. Sci. Total Environ. 702, 134455 https://doi.org/10.1016/j.scitotenv.2019.134455.
Rahman, A., Sarkar, A., Yadav, O.P., Achari, G., Slobodnik, J., 2021. Potential human health risks due to environmental exposure to nano- and microplastics and knowledge gaps: a scoping review. Sci. Total Environ. 757, 143872 https://doi.org/10.1016/j.scitotenv.2020.143872.
Ralph, P., Nakoinz, I., 1975. Phagocytosis and cytolysis by a macrophage tumour and its cloned cell line MACROPHAGES. Nature 257, 393–394.
Ramsperger, A.F.R.M., Narayana, V.K.B., Gross, W., Mohanraj, J., Thelakkat, M., Greiner, A., Schmalz, H., Kress, H., Laforsch, C., 2020. Environmental exposure enhances the internalization of microplastic particles into cells. Sci. Adv. 6, 1–10. https://doi.org/10.1126/sciadv.abd1211.
Rillig, M.C., 2012. Microplastic in terrestrial ecosystems and the soil? Environ. Sci. Technol. 46, 6453–6454 https://doi.org/dx.doi.org/10.1021/es302011r.
Rillig, M.C., Lehmann, A., 2020. Microplastic in terrestrial ecosystems. Science 368. https://doi.org/10.1126/science.abb5979 (80-.).
Rodriguez-Seijo, A., Lourenço, J., Rocha-Santos, T.A.P., da Costa, J., Duarte, A.C., Vala, H., Pereira, R., 2017. Histopathological and molecular effects of microplastics in Eisenia andrei Bouché. Environ. Pollut. 220, 495–503. https://doi.org/10.1016/j.envpol.2016.09.092.
Rudolph, J., Völkl, M., Jérôme, V., Scheibel, T., Freitag, R., 2021. Noxic effects of polystyrene microparticles on murine macrophages and epithelial cells. Sci. Rep. 11 (1), 15702 https://doi.org/10.1038/s41598-021-95073.
Riedl, S.A.B., Völkl, M., Holzinger, A., 2021. In vitro cultivation of primary intestinal cells from Eisenia fetida as basis for ecotoxicological studies. Ecotoxicology. https://doi.org/10.1007/s10646-021. https://doi.org/10.1007/s10646-021.
Saavedra, J., Stoll, S., Slaveykova, V.I., 2019. Influence of nanoplastic surface charge on eco-corona formation, aggregation and toxicity to freshwater zooplankton. Environ. Pollut. 252, 715–722. https://doi.org/10.1016/j.envpol.2019.05.135.
Schirinzi, G.F., Pérez-Pomeda, I., Sanchís, J., Rossini, C., Farré, M., Barceló, D., 2017. Cytotoxic effects of commonly used nanomaterials and microplastics on cerebral and epithelial human cells. Environ. Res. 159, 579–587. https://doi.org/10.1016/j.envres.2017.08.043.
Schrade, A., Mailänder, V., Ritz, S., Landfester, K., Ziener, U., 2012. Surface roughness and charge influence the uptake of nanoparticles: fluorescently labeled pickering-type versus surfactant-stabilized nanoparticles. Macromol. Biosci. 12, 1459–1471. https://doi.org/10.1002/mabi.201200166.
Schwabl, P., Koppel, S., Konigshofer, P., Bucsics, T., Trauner, M., Reiberger, T., Liebmann, B., 2019. Detection of various microplastics in human stool: a prospective case series. Ann. Intern. Med. 171, 453–457. https://doi.org/10.7326/M19-0618.
Shannahan, J.H., Lai, X., Ke, P.C., Podila, R., Brown, J.M., Witzmann, F.A., 2013. Silver nanoparticle protein corona composition in cell culture media. PLoS One 8, e74001. https://doi.org/10.1371/journal.pone.0074001.
Smoluchowski, M.V., 1916. Drei vortage uber diffusuin, brwonsche bewegung und koagulation von kolloidteilchen. Z. Phys. 17, 557–585.
Stock, V., Böhmert, L., Lisicki, E., Block, R., Cara-Carmona, J., Pack, L.K., Selb, R., Lichtenstein, D., Voss, L., Henderson, C.J., Zabinsky, E., Sieg, H., Braeuning, A., Lampen, A., 2019. Uptake and effects of orally ingested polystyrene microplastic particles in vitro and in vivo. Arch. Toxicol. 93, 1817–1833. https://doi.org/10.1007/s00204-019-02478-7.
Stock, V., Laurisch, C., Franke, J., Dönmez, M.H., Voss, L., Böhmert, L., Braeuning, A., Sieg, H., 2021. Uptake and cellular effects of PE, PP, PET and PVC microplastic particles. Toxicol. Vitr. 70, 105021 https://doi.org/10.1016/j.tiv.2020.105021.

Tanifum, E.A., Devkota, L., Ngwa, C., Badachhape, A.A., Ghaghada, K.B., Romero, J., Pautler, R.G., Annapragada, A.V., 2018. A hyperfluorinated hydrophilic molecule for aqueous 19 F MRI contrast media. Contrast Media Mol. Imaging (2018). https://doi.org/10.1155/2018/1693513.

Telford, A.M., Pham, B.T.T., Neto, C., Hawkett, B.S., 2013. Micron-sized polystyrene particles by surfactant-free emulsion polymerization in air: synthesis and mechanism. J. Polym. Sci. Part A Polym. Chem. 51, 3997–4002. https://doi.org/10.1002/pola.26841.

Tenzer, S., Docter, D., Kuharev, J., Musyanovych, A., Fetz, V., Hecht, R., Schlenk, F., Fischer, D., Kiouptsi, K., Reinhardt, C., Landfester, K., Schild, H., Maskos, M., Knauer, S.K., Stauber, R.H., 2013. Rapid formation of plasma protein corona critically affects nanoparticle pathophysiology. Nat. Nanotechnol. 8 https://doi.org/10.1038/nnano.2013.181, 772–81.

Townley, H.E., Rapa, E., Wakefield, G., Dobson, P.J., 2012. Nanoparticle augmented radiation treatment decreases cancer cell proliferation. Nanomed. Nanotechnol. Biol. Med. 8, 526–536. https://doi.org/10.1016/j.nano.2011.08.003.

Triebskorn, R., Braunbeck, T., Grummt, T., Hanslik, L., Huppertsberg, S., Jekel, M., Knepper, T.P., Krais, S., Müller, Y.K., Pittroff, M., Ruhl, A.S., Schmieg, H., Schür, C., Strobel, C., Wagner, M., Zumbülte, N., Köhler, H.R., 2019. Relevance of nano- and microplastics for freshwater ecosystems: a critical review. TrAC Trends Anal. Chem. 110, 375–392. https://doi.org/10.1016/j.trac.2018.11.023.

Van Berkel, K.Y., Russell, G.T., Gilbert, R.G., 2003. Entry in emulsion polymerization: effects of initiator and particle surface charge. Macromolecules 36, 3921–3931. https://doi.org/10.1021/ma025695y.

Wang, Z.Y., Butlak, C., Klaunig, J.E., Kamendulis, L.M., 2014. Development of a cytokine-producing immortalized murine Kupffer cell line. Cytokine 70, 165–172. https://doi.org/10.1016/j.cyto.2014.07.251.

Weyermann, J., Lochmann, D., Zimmer, A., 2005. A practical note on the use of cytotoxicity assays. Int. J. Pharm. 288, 369–376. https://doi.org/10.1016/j.ijpharm.2004.09.018.

Withey, J.R., 1976. Quantitative analysis of styrene monomer in polystyrene and foods including some preliminary studies of the uptake and pharmacodynamics of the monomer in rats. Environ. Health Perspect. 17, 125–133. https://doi.org/10.1289/ehp.7617125.

Wright, S.L., Kelly, F.J., 2017. Plastic and human health: a micro issue? Environ. Sci. Technol. 51, 6634–6647. https://doi.org/10.1021/acs.est.7b00423.

Wright, S.L., Thompson, R.C., Galloway, T.S., 2013. The physical impacts of microplastics on marine organisms: a review. Environ. Pollut. 178, 483–492. https://doi.org/10.1016/j.envpol.2013.02.031.

Yong, C.Q.Y., Valiyaveetill, S., Tang, B.L., 2020. Toxicity of microplastics and nanoplastics in Mammalian systems. Int. J. Environ. Res. Public Health 17. https://doi.org/10.3390/ijerph17051509.

Yousif, E., Haddad, R., 2013. Photodegradation and photostabilization of polymers, especially polystyrene: review. SpringerPlus 2, 1–32. https://doi.org/10.1186/2193-1801-2-398.

Supplementary Materials

Figs. S1

Supplementary Information

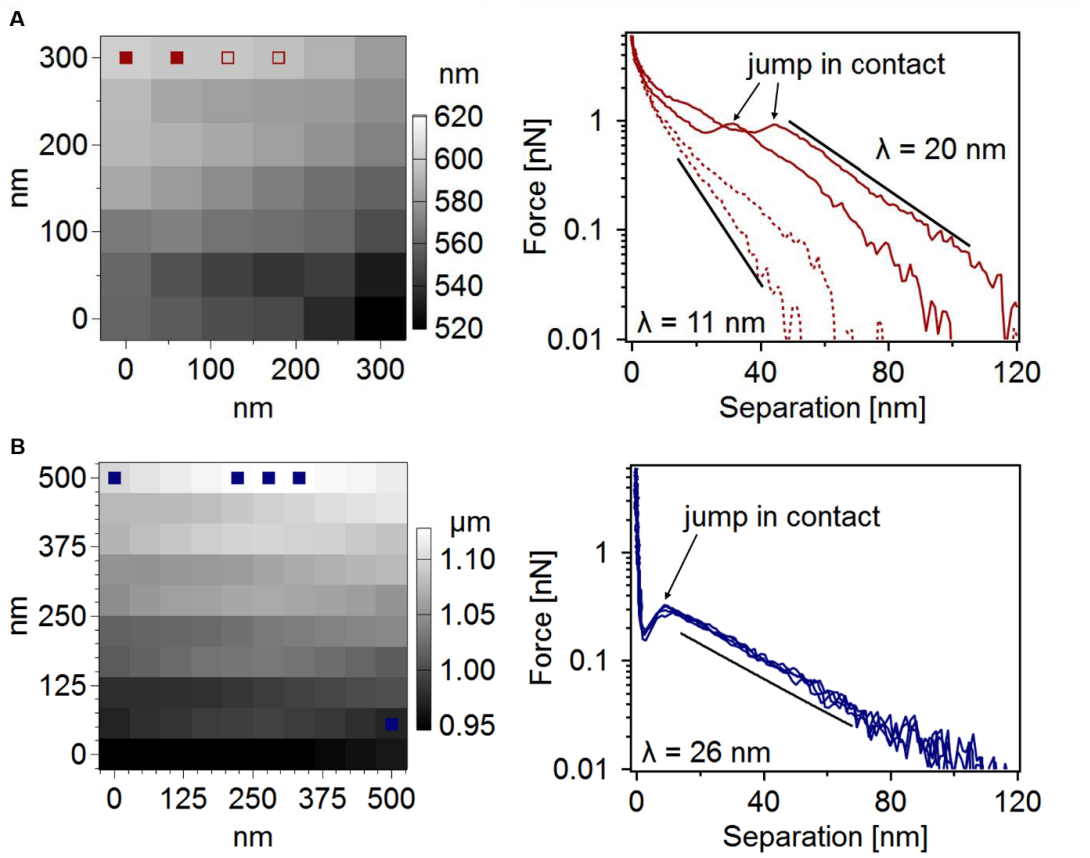

Fig. S1. Force map (left) of a M-MPP, and the corresponding semi-logarithmic force-separation curves (right) (B) and of a P-MPP (C). *Obtained in an aqueous solution of 0.1 mM NaCl (λ = 30 nm) in a slightly acidic pH 5 -6 through dissolved CO_2, which also reduces the calculated Debye length. The straight solid lines resemble the exponential Debye fit. Force Maps show the relative height in XY-direction close to the apex of a particle. Colored pixels show the measurement locations of the force curves displayed right. The brighter the pixel the closer is the measurement location to the apex. Varying attractive van-der-Waals and repulsive electrostatic forces (measured Debye length 11 nm – 20 nm) with measurement location are visible for M-MPP in A. For 2 spots (solid squares & curves) we found van-der-Waals and stronger electrostatic forces than for the other 2 spots (open squares & dashed curves) In contrast, P-MPP show constant attractive van-der-Waals and repulsive electrostatic forces (measured Debye length 26 nm) for every measurement location. The jump into contact is also always visible.*

6.3 Teilarbeit III

Tailor-Made Protein Corona Formation on Polystyrene Microparticles and Its Effect on Epithelial Cell Uptake

Autoren: **Julia Jasinski**, Magdalena V. Wilde, Matthias Völkl, Valérie Jérôme, Thomas Fröhlich, Ruth Freitag und Thomas Scheibel

Die Konzeptionierung sowie alle Experimente dieser Teilarbeit wurden von Matthias Völkl, Magdalena Wilde und mir durchgeführt. Dabei wurde die Beschichtung der Partikel mit Modellproteinen, die Protein-Corona Analyse mittels ζ-Potentialmessungen, SDS-PAGE und Rasterelektronenmikroskopie, sowie quantitative Analyse der Proteinadsorption mittels Quarzkristallmikrowaage (QCM-D) von mir durchgeführt und ausgewertet. Zusätzlich wurde die zelluläre Interaktion qualitativ mittels Konfokalmikroskopie und quantitativ mittels Durchflusszytometrie von mir analysiert und ausgewertet. Magdalena Wilde führte die Analyse der Protein-Corona mittels LC-MS/MS durch und wertete die Daten aus. Daten zu den zellulären Effekten (Zytotoxizität) wurden von Matthias Völkl erhoben. Das Manuskript wurde von mir verfasst. Valérie Jérôme, Thomas Fröhlich, Ruth Freitag und Thomas Scheibel waren an der Konzeptionierung, wissenschaftlichen Diskussionen und der Fertigstellung des Manuskripts beteiligt.

Der Artikel wurde am 04.10.2022 im Journal *ACS Applied Materials & Interfaces* veröffentlicht.

Nachdruck unter freundlicher Genehmigung des Verlags. Jasinski, J., Wilde, M. V., Völkl, M., Jérôme, V., Fröhlich, T., Freitag, R. & Scheibel, T. Tailor-Made Protein Corona Formation on Polystyrene Microparticles and Its Effect on Epithelial Cell Uptake. *ACS Applied Materials & Interfaces*, **14**, 47277-47287 (2022).

ACS APPLIED MATERIALS & INTERFACES

www.acsami.org Research Article

Tailor-Made Protein Corona Formation on Polystyrene Microparticles and its Effect on Epithelial Cell Uptake

Julia Jasinski, Magdalena V. Wilde, Matthias Voelkl, Valérie Jérôme, Thomas Fröhlich, Ruth Freitag, and Thomas Scheibel*

Cite This: ACS Appl. Mater. Interfaces 2022, 14, 47277−47287 Read Online

ACCESS | Metrics & More | Article Recommendations | Supporting Information

ABSTRACT: Microplastic particles are pollutants in the environment with a potential impact on ecology and human health. As soon as microplastic particles get in contact with complex (biological) environments, they will be covered by an eco- and/or protein corona. In this contribution, protein corona formation was conducted under defined laboratory conditions on polystyrene (PS) microparticles to investigate the influence on surface properties, protein corona evolution, particle−cell interactions, and uptake in two murine epithelial cells. To direct protein corona formation, PS particles were preincubated with five model proteins, namely, bovine serum albumin (BSA), myoglobin, β-lactoglobulin, lysozyme, and fibrinogen. Subsequently, the single-protein-coated particles were incubated in a cell culture medium containing a cocktail of serum proteins to analyze changes in the protein corona profile as well as in the binding kinetics of the model proteins. Therein, we could show that the precoating step has a critical impact on the final composition of the protein corona. Yet, since proteins building the primary corona were still detectable after additional incubations in a protein-containing medium, backtracking of the particle's history is possible. Interestingly, whereas the precoating history significantly disturbs particle−cell interactions (PCIs), the cellular response (i.e., metabolic activity, MTT assay) stays unaffected. Of note, lysozyme precoating revealed one of the highest rates in PCI for both epithelial cell lines. Taken together, we could show that particle history has a significant impact on protein corona formation and subsequently on the interaction of particles with murine intestinal epithelial-like cells. However, as this study was limited to one cell type, further work is needed to assess if these observations can be generalized to other cell types.

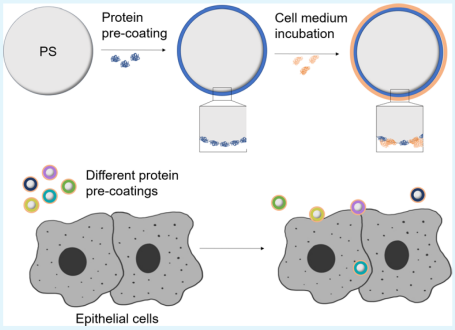

KEYWORDS: *microplastic, particle history, particle−cell interaction, particle ingestion, cytotoxicity, LC−MS/MS, QCM-D*

INTRODUCTION

Microplastic particles (MPs), defined in a size range of 0.1 μm to 5 mm,[1] can nowadays be found in all environmental compartments.[2−4] It is known that MP also enters the food chain and evokes several effects on various species.[5−9] When MP gets in contact with various (biological) environments, biomolecules and microorganisms adsorb on several particles' surface and form a so-called eco-corona, which can severely change the particle properties, for instance, the bioavailability.[10−13]

In case particles get in contact with proteins, a so-called protein corona will be formed covering the particles,[14−17] described by the so-called Vroman effect. The protein corona is hereby a highly dynamic protein layer, where proteins adsorb within seconds, though the proteins will be displaced over time by proteins with a higher affinity for the particle surface.[18−21] However, recent studies have shown that the protein corona is more complex and less dynamic than originally thought. In particular, protein−protein interactions play a more important role than those described by Vroman.[22,23] Hence, it can be stated that the mechanism of protein corona formation is still not fully understood. So far, protein corona formation has been mainly investigated in the case of nanoparticles (i.e., diameter < 0.1 μm[24]).[14,16,19,23,25,26] Besides particle size,[27,28] surface modifications like carboxy or amine groups influence protein corona formation and composition.[14,16,29−31] Noteworthy, it has been shown that protein corona composition can influence the cellular uptake of particles. In the case of a protein corona containing immunoglobulins and complement factors from human plasma on pristine particles, a stealth effect was observed where cells did not recognize the particles anymore,[17] but this is dependent on cell type. In previous studies, the uptake of small pristine poly(lactic acid) (PLA) and polystyrene (PS) particles (<0.5 μm) could be shown with intestinal epithelial cell lines (e.g., STC-1) after incubation in cell culture medium (ccm) with serum.[32,33] Hepatic epithelial cells (e.g., BNL CL.2) ingested

Received: August 4, 2022
Accepted: September 20, 2022
Published: October 4, 2022

large PS particles (PSPs) with up to 3 μm in diameter.[33] The focus was on whether and how the history of a particle, i.e., the environment in which it has been incubated first, influences protein corona evolution and, therefore, the particles' interaction with cells (PCI). Therefore, PS particles (PSPs) were precoated with five different model proteins (bovine serum albumin, BSA, myoglobin, β-lactoglobulin, lysozyme, and fibrinogen) followed by a subsequent incubation in cell culture medium containing a cocktail of serum protein (i.e., fetal calf serum). Changes in particle charges in correlation with the protein corona were assessed by ζ-potential measurements. The adsorption/desorption of proteins (i.e., binding kinetics) was measured by quartz crystal microbalance with dissipation monitoring (QCM-D). An in-depth analysis of changes in protein corona composition was performed using liquid chromatography−mass spectrometry (LC−MS)/MS analysis. Finally, the impact thereof on cellular uptake and cytotoxicity was investigated in murine epithelial cells.

MATERIALS AND METHODS

If not otherwise stated, cell culture materials were purchased from Thermo Fisher Scientific (Schwerte, Germany) and Greiner Bio-One (Frickenhausen, Germany). Dulbecco's phosphate-buffered saline without Ca^{2+} and Mg^{2+} (DPBS), fetal calf serum (FCS), penicillin, and streptomycin were obtained from Sigma-Aldrich (Taufkirchen, Germany). Dulbecco's modified Eagle's medium (DMEM, 1.5 g/L $NaHCO_3$, 0.11 mM Na pyruvate, 4 mM L-glutamine) was obtained from ATCC (ATCC LGC Standards GmbH, Wesel, Germany). Modified Eagle's medium without phenol red (MEM) was obtained from Thermo Fisher Scientific (Schwerte, Germany).

Phalloidin-tetramethylrhodamine B isothiocyanate, 4′,6-diamidino-2-phenylindole (DAPI), and 3-(4,5-dimethyl-2-thiazolyl)-2,5-diphenyl-2*H*-tetrazolium bromide (MTT) were obtained from Sigma-Aldrich (Taufkirchen, Germany).

As polystyrene particles, nonfunctionalized fluorescent particles (Yellow Green, PS-YG) were received from Polysciences (Polysciences Europe GmbH, Eppenheim, Germany) with the parameter as follows: diameter of 0.2 μm (Cat. #17151-10, 5.68×10^{12} particles/mL, size coefficient of variation (CV) $\leq$ 8%) and 3 μm (Cat. #17155-2, 1.68×10^{9} particles/mL, size CV $\leq$ 5%). All PS particles (PSPs) were plain particles in a sterile aqueous suspension (2.5% (w/v)) with a slight anionic charge. Before use, PSP stock solutions were diluted to the required concentration in cell culture medium supplemented with 10% FCS (ccm_{FCS}).

The model proteins bovine serum albumin (BSA fraction V), myoglobin (from the equine heart), β-lactoglobulin (from bovine milk), lysozyme (from chicken egg white), and fibrinogen (from bovine plasma) were obtained from Sigma-Aldrich (Taufkirchen, Germany). Molecular weight and net charge (according to the database) are shown in Table 1.

Table 1. Proteins Used in This Study with Abbreviations, Molecular Weight, Net Charge (=Difference between Positively and Negatively Charged Amino Acids at pH 7.0), and Theoretical pI According to the ProtParam Database

protein name	abbreviation	molecular weight (kDa)	charge	theoretical pI
BSA	BSA	66.4	−17	5.60
myoglobin	myo	16.9	±0	7.36
β-lactoglobulin	lac	18.3	−8	4.38
lysozyme	lys	14.3	+8	9.32
fibrinogen	fib	α-chain: 63.1	+1	7.73
		β-chain: 50.9	+7	8.66
		γ-chain: 47.6	−11	5.46

Protein Coating of PS Particles. The particles (3 μL of the 25 mg/mL aqueous solution) were incubated overnight at 37 °C in the cell culture incubator (37 °C, 5% CO_2, 95% humidity) in 1 mL of a 15 mg/mL solution of the respective proteins. Afterward, the particles were centrifuged at 17,000*g* for 30 min at room temperature (RT). The resulting pellet was washed 3× with Milli-Q (MQ) water (17,000*g*, 30 min, RT). If necessary, the particles were incubated in cell culture medium (ccm) or in ccm supplemented with 10% FCS (ccm_{FCS}) overnight in the cell culture incubator. The particles were again centrifuged and washed with water, as described.

Sodium Dodecyl-Sulfate Polyacrylamide Gel Electrophoresis (SDS-PAGE). Discontinuous polyacrylamide gel electrophoresis (PAGE) was performed using 12.5% SDS gels. Laemmli loading buffer with β-mercaptoethanol was added to the particles after preincubation with model proteins or incubation in ccm_{FCS}. The particles were heated up to 95 °C for 10 min and afterward centrifuged (17,000*g*, 3 min, RT). The resulting supernatant was applied to the gel. Finally, the gel was silver-stained.

ζ-Potential Measurement. The ζ-potential measurements were performed, as described previously.[33,34] In brief, for the ζ-potential measurements of the control, 3 μL of the particle solutions was diluted in 1 mL of a 1 mM aqueous KCl solution (pH 6). The precoated or ccm_{FCS}-incubated particles were centrifuged (17,000*g* for 30 min, RT) and afterward resuspended in 1 mL of the 1 mM KCl solution. To determine the ζ-potential, a LiteSizer 500 (Anton Paar Germany GmbH, Ostfildern-Scharnhausen, Germany) was used. Here, three measurements with at least 100 runs each were performed at 21 °C with an adjusted voltage of 200 V, and for calculation, the Helmholtz−Smoluchowski equation was used.[35]

Sample Preparation for Analysis of the Protein Corona Composition. For proteome analysis, the treated microplastic particles (200−1000 μL) were centrifuged for 10 min (29,000*g*). The supernatant was discarded, and the resulting pellet was resuspended with 2× Laemmli buffer (0.5 M tris−HCl, pH 6.8, 20% glycerol (v/v), 40 g/L SDS, 10% 2-mercaptoethanol (V/V), 0,002% bromophenol blue), vortexed shortly, and incubated for 5 min at 95 °C. Afterward, the samples were vortexed again and centrifuged for 5 min at 30,000*g*. Samples were then transferred to polyacrylamide gradient gels (mini-PROTEAN TGX 4−20%, Biorad, Germany), which were run until gel pockets were drained. By using Roti Blue staining solution (Roth, Germany), gels were stained overnight. Protein-containing areas were excised and destained. Before enzymatic digestion, proteins in the gel pieces were reduced with 45 mM dithiothreitol (DTT) (30 min, 55 °C) and alkylated with 100 mM iodoacetamide in the dark (2× for 15 min each, RT). Gel pieces were washed twice for 15 min with 50 mM NH_4HCO_3, and sequential in-gel digestion was performed, first using Lys-C (4 h, 37 °C, 70 ng lysyl endopeptidase, Mass Spectrometry Grade (FUJIFILM Wako Pure Chemical Corporation)) followed by trypsin (incubation overnight, 37 °C, 70 ng trypsin (sequencing grade modified trypsin, Promega, Germany)). Supernatants were collected, pooled, and dried using a vacuum centrifuge (Vacuum concentrator, Bachofer, Germany). Peptides were extracted using 70% acetonitrile (ACN).

LC−MS/MS Analysis for Analysis of the Protein Corona Composition. LC−MS/MS was performed using an EASY-nLC 1000 (Thermo Fisher Scientific) connected to an LTQ Orbitrap XL (Thermo Scientific). Samples were dissolved in solvent A (0.1% formic acid), loaded on a trap column (PEP-Map100 C18, 75 μm × 2 cm, 3 μm particles (Thermo Fisher Scientific)), and separated using a reversed-phase column (PepMap RSLC C18, 75 μm × 50 cm, 2 μm particles, Thermo Scientific) at a flow rate of 200 nL/min. A 30 min gradient was applied from 2 to 50% solvent B (0.1% formic acid in ACN), followed by a washing step with 85% solvent B for 10 min. For data acquisition, a top-five data-dependent collision-induced dissociation (CID) method was used. The proteomic data were processed as follows: spectra were analyzed using MASCOT V2.6.2 (Matrix Science Limited, U.K.),[36] and the different subsets of the Uniprot/Swissprot databases (see Table S1) were used. Identified proteins were filtered for an FDR < 1%, a MASCOT score above 50, and a minimum of two significant sequences.

Scanning Electron Microscopy (SEM). Seventy microliters of the precoated and ccm_{FCS}-incubated particles were dried overnight on a

https://doi.org/10.1021/acsami.2c13987
ACS Appl. Mater. Interfaces 2022, 14, 47277−47287

ACS Applied Materials & Interfaces www.acsami.org Research Article

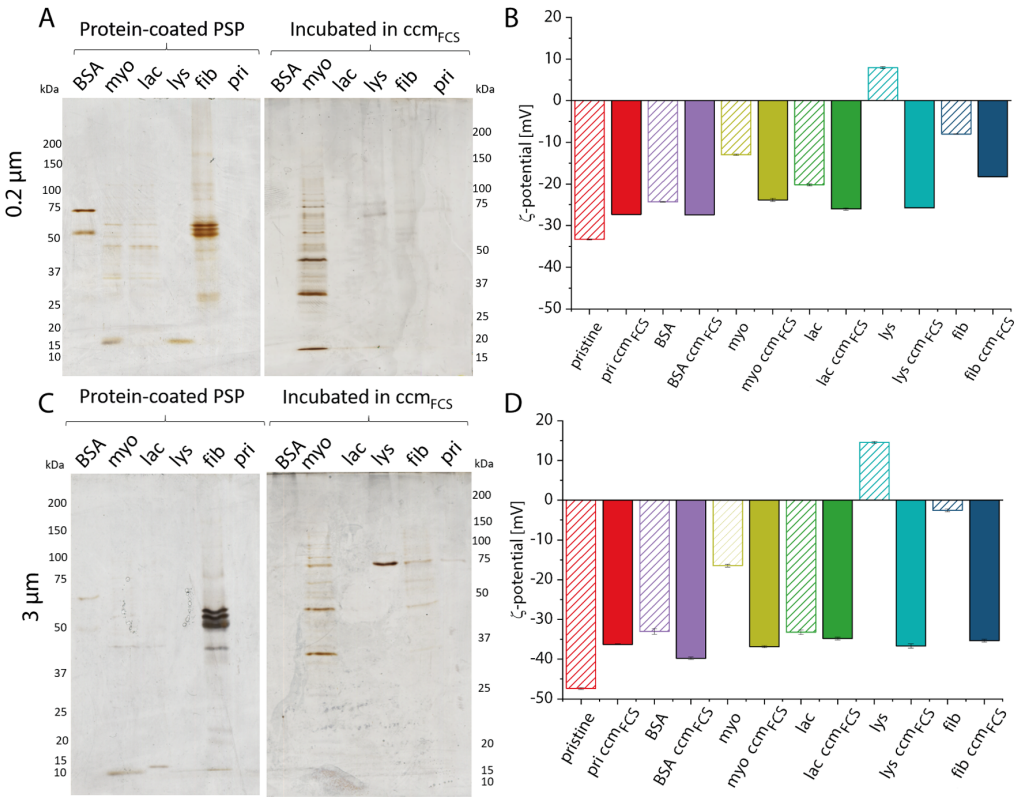

Figure 1. Protein corona analysis using silver-stained SDS-PAGE (A, C) and ζ-potential measurements (B, D). 0.2 (A, B) and 3 µm (C, D) PS particles (PSPs) were analyzed after customized protein coating (first round of coating, striped bars) using pristine particles (pri), BSA, myoglobin (myo), β-lactoglobulin (lac), lysozyme (lys), and fibrinogen (fib) and after further incubation in cell culture medium containing a cocktail of serum proteins (ccm$_{FCS}$, second round of coating, filled bars).

silicon wafer. Two nanometer platin sputter-coated samples were imaged using SEM (FEI Apreo Volumescope, Thermo Fisher Scientific, magnifications 80,000× and 150,000×, 1.5 kV, ETD or T2 detector).

Quartz Crystal Microbalance with Dissipation Monitoring (QCM-D). QCM-D is known to be a determination method for film thickness and, therefore, for the adsorption or desorption of molecules or binding kinetics.[37−39] The QCM-D experiments were performed using a Q-Sense A3 system (Q-Sense, Göteborg, Sweden). For adsorption reactions onto Au chips (5 MHz, QuarztPro, Jarfalla, Sweden), we did not use beads, which might not have led to a homogeneous spreading, hence leaving the naked surface area exposed. Instead, the chips were spin-coated with a 5% (w/v) PS solution (in ethyl acetate), as liquid PS allows for full coverage of the chip surface. For the measurements, 15 mg/mL of the respective aqueous protein solutions was applied to the chips and incubated for 4 h (at RT, "precoating"). Afterward, cell culture medium without (ccm) and with 10% FCS (ccm$_{FCS}$) was applied and the chips were incubated overnight at room temperature. Then, the chips were rinsed with Milli-Q water.

For calculation of the adsorbed mass (Δm), the Sauerbrey equation was used[40]

$$\Delta m = -C\Delta F_n/n \quad (1)$$

C is the mass sensitivity constant (here: C = 17.7 ng/cm^{-2}*Hz^{-1}), ΔF is the frequency shift, and n is the overtone number. The presented data show the values of the third overtone ($\Delta F_3/3$).

Cell Culture. The murine intestinal epithelial-like cells STC-1 (CRL 3254) and hepatic epithelial cells BNL CL.2 (TIB-73) were obtained from the American Type Culture Collection (ATCC, Manassas). Cells were cultivated in DMEM supplemented with 10% (v/v) FCS and 100 U/mL penicillin/streptomycin in a standard cell culture incubator (5% CO_2/95% humidity) at 37 °C. Both cell lines were passaged three times a week at a starting concentration of about 100,000 cells/mL. For detaching cells, 0.05% (for STC-1) or 0.25% (for BNL CL.2) trypsin/EDTA was used.

Qualitative Analysis of PSP Uptake. For qualitative analysis of the cellular uptake of PSP, 15,000 cells/well were seeded in an 8-well Ibidi slide (µ-Slide 8 Well, ibiTreat, ibidi GmBH, Gräfelfing, Germany). After a 24 h incubation under cell culture conditions, fluorescent particles were added (0.2 µm: 15,000 PSP per cell; 3 µm: 20 PSP per cell) (total cultivation volume: 300 µL) for a further 24 h incubation. Thereafter, cells were fixed for 15 min at RT with preheated paraformaldehyde (3.7% (v/v) in 1× DPBS). Cells were then permeabilized with 0.1% (v/v) Triton X-100 for 10 min at RT. By using 100 nM rhodamine-phalloidin and 100 nM DAPI, actin filaments and nuclei were stained, respectively. Samples were investigated using a confocal laser scanning microscope (CLSM) (TCS SP8, 63× oil immersion objective, laser: 408, 488, and 552 nm, Leica Microsystems, Wetzlar, Germany). Z-stacks were recorded with a step size of 0.2−0.33 µm.

Quantitative Analysis of Particle−Cell Interaction (PCI). As recently described, the quantification of particle−cell interactions was performed using flow cytometry.[33] In brief, 800,000 cells per well were seeded in 6-well culture plates and incubated for 24 h. Thereafter, fluorescent particles were added at a density of 12,000 PSP per cell (0.2 µm) or 4 PSP per cell (3 µm). After a further 24 h incubation, cells were collected by trypsinization and recovered using centrifugation (200g, 5 min). After resuspension in 0.5 mL DPBS, samples were analyzed using flow cytometry. Flow cytometry analyses were performed using a CytoFLEX S (Beckman Coulter, Krefeld, Germany). At least 30,000 events were measured for each sample. Forward scattering (FSC), side

https://doi.org/10.1021/acsami.2c13987
ACS Appl. Mater. Interfaces 2022, 14, 47277−47287

scattering (SSC), and FITC fluorescence (525 nm filter) were recorded. The calculation of interacting particles per cell was performed, as previously described.[33]

MTT Assay. The influence of coated PSP on the metabolic activity of the cells was analyzed using an MTT assay, as a well-established method for the toxicological assessment of PS microparticles.[41−43] The experiments were performed, as previously described.[33] Briefly, BNL CL.2 cells were seeded at 10,000 cells in 100 μL/well in 96-well plates. For STC-1 cells, the seeding density was 25,000 cells/well. After 24 h of incubation, the medium was aspirated and 100 μL of particle suspension freshly prepared in the growth medium was added. The cells were then incubated for another 24 h, and afterward, cells were washed with DPBS, and 50 μL of freshly prepared MTT reagent (1 mg/mL MTT in MEM) was added. After 2 h of incubation, the supernatant was replaced by 100 μL of isopropanol. After shaking at 600 rpm for 5 min, absorbance was measured at 570 nm (reference wavelength 650 nm) using a TECAN GENios Pro plate reader (Tecan Austria GmbH, Gröding). Cells incubated without particles or with 0.3% Triton X-100 in the respective cell culture medium, under otherwise identical conditions, were used as negative and positive controls, respectively.

Statistical Analysis. For statistical analysis, Origin software, 2019b (Origin, Northampton, MA) was used. All data were tested concerning the homogeneity of variances (Levene test), and to investigate differences in PSP interactions with cells, a one-way analysis of variance (ANOVA) with a Tukey post hoc test was used.

RESULTS

Protein Corona Formation on Polystyrene Particles Depends on the Incubation Conditions. The protein corona of PSP was first analyzed using SDS-PAGE and measuring the ζ-potential (Figure 1). To customize the corona formation, five different model proteins (BSA, myoglobin, lactoglobulin, lysozyme, and fibrinogen) were preincubated with 0.2 and 3 μm particles. The coating was confirmed for all model proteins using SDS-PAGE (Figure 1A,C). After a subsequent incubation in cell culture medium (ccm_{FCS}), additional proteins were detectable, originating from FCS. In comparison to pristine particles ("pri"), customized protein corona formation induced a change in the ζ-potential of the particle surface. Lysozyme-coated PSP showed a positive potential, which coincides with the positive protein net charge (Table 1). PSPs coated with the other model proteins showed a slightly lower ζ-potential in comparison to uncoated ones (i.e., pristine PSP). Upon further incubation in cell culture medium containing a cocktail of serum proteins (ccm_{FCS}, filled bars), the differences between the groups were leveled and the ζ-potentials became akin independently of the underlying first-layer model protein.

The composition of the protein corona after the second round of coating was further analyzed using LC−MS/MS. For comparison, pristine PSPs only subjected to incubation in the cell culture medium containing a cocktail of serum proteins (ccm_{FCS}) were used ("pristine"). The top-five binding proteins are presented in Table 2. After precoating with BSA and lysozyme, these model proteins were still detected in a high quantity, indicating that these proteins still constituted the main component of the protein corona after incubation in ccm_{FCS}. In the case of myoglobin, lactoglobulin, and fibrinogen as well as for the pristine PSP, the main component after incubation in ccm_{FCS} was hemoglobin subunit β. In the case of the pristine PSP, the second major component of the corona is BSA, which incidentally is the main component of FCS. Noteworthily, the emPAI values,[44] which allow the estimation of the protein abundance, were higher for the precoated particles than for those solely incubated in ccm_{FCS}. This indicated that more proteins adsorbed when PSPs were subjected to two rounds of coating. This suggests that the presence of a protein film on the polystyrene material conditioned the surface and favored subsequent binding of additional proteins when available from the environment. Importantly, the final protein corona composition seemed to be highly dependent on the model protein used for precoating. Likely, particles got a "signature" or "history" depending on the surrounding medium they experienced.

Table 2. Quantitative Analysis of Protein Corona Composition Using LC−MS/MS[a]

pristine	BSA-coated	myoglobin-coated
hemoglobin fetal subunit β (2.99)	BSA (4.74)	hemoglobin fetal subunit β (3.04)
BSA (2.76)	hemoglobin fetal subunit β (3.13)	BSA (2.08)
serotransferrin (1.34)	globin C1 (1.7)	myoglobin (0.86)
hemoglobin subunit α (1.08)	apolipoprotein A-I (0.66)	hemoglobin subunit α (0.64)
β-lactoglobulin-coated	lysozyme-coated	fibrinogen-coated
α-2-HS-glycoprotein (0.96)	α-2-HS-glycoprotein (0.64)	secreted phosphoprotein 24 (0.38)
hemoglobin fetal subunit β (5.47)	**lysozyme (8.19)**	hemoglobin fetal subunit β (12.03)
BSA (3.05)	hemoglobin fetal subunit β (7.09)	fibrinogen β chain (6.69)
globin C1 (2.4)	fibrinogen β chain (4.13)	fibrinogen γ-B chain (3.85)
β-lactoglobulin (1.1)	fibrinogen γ-B chain (2.31)	fibrinogen α chain (2.93)
peptidoglycan recognition protein 1 (1.02)	BSA (2.07)	apolipoprotein A-I (1.72)

[a]3 μm PSPs were preincubated with model proteins (BSA, myoglobin, β-lactoglobulin, lysozyme, and fibrinogen) and afterward incubated in cell culture medium containing 10% FCS (ccm_{FCS}). The respective preincubated protein is highlighted in **bold fonts**. Pristine PSPs (i.e., without preincubation) incubated in ccm_{FCS} were included for comparison. The emPAI value, which allows estimating protein abundance, is given in parentheses. Only the five most abundant proteins are shown. The complete list can be found in Table S2.

Incubation of protein-coated particles in ccm_{FCS} did not show apparent differences between the respective model proteins when analyzing the particles using SEM, so myoglobin-coated particles were chosen exemplarily (Figure 2). For 0.2 μm PSPS, the further incubation in ccm_{FCS} led to a thicker-looking layer around the particles. Differences in the particle size according to the protein layer could be provoked by either the size of the protein corona or the magnification. The smaller particles needed a higher magnification, which allowed us to identify the thin protein layer around the particles' surface. The amount of adsorbed protein on PS was further quantified using a quartz crystal microbalance with dissipation monitoring (QCM-D; Figure 3). QCM-D can be used as a method to determine the layer thickness on films and thus the adsorption or desorption of molecules on the surface.[37−39] In our experimental settings, we used a PS solution (5% (w/v)) rather than a bead suspension to achieve a homogeneous coverage of the chip surface.

Here, all proteins, except lysozyme, adsorbed indistinguishably on the surface (PS). Lysozyme showed significantly lower adsorption to PS. For BSA, a small amount of protein seemed to be washed off or displaced by proteins of the FCS, and the overall adsorbed mass increased upon the follow-up coating. The additional protein adsorption out of the FCS-containing medium (ccm_{FCS}) was in total less compared to the adsorption

https://doi.org/10.1021/acsami.2c13987
ACS Appl. Mater. Interfaces 2022, 14, 47277−47287

ACS Applied Materials & Interfaces www.acsami.org Research Article

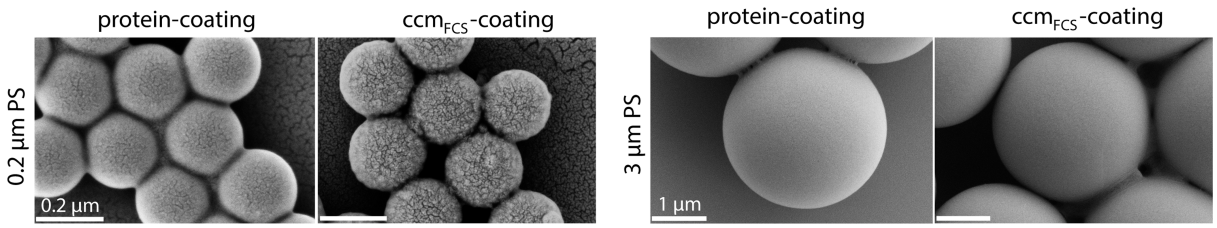

Figure 2. Surface morphological changes upon protein coating of PS particles. Exemplary SEM images of myoglobin-coated PSP, which were in some cases further incubated in ccm$_{FCS}$, as indicated. The SEM images of pristine and PSP coated with the other model proteins are shown in Figure S1. Scale bars: 0.2 μm PS: 0.2 μm, 3 μm PS: 1 μm.

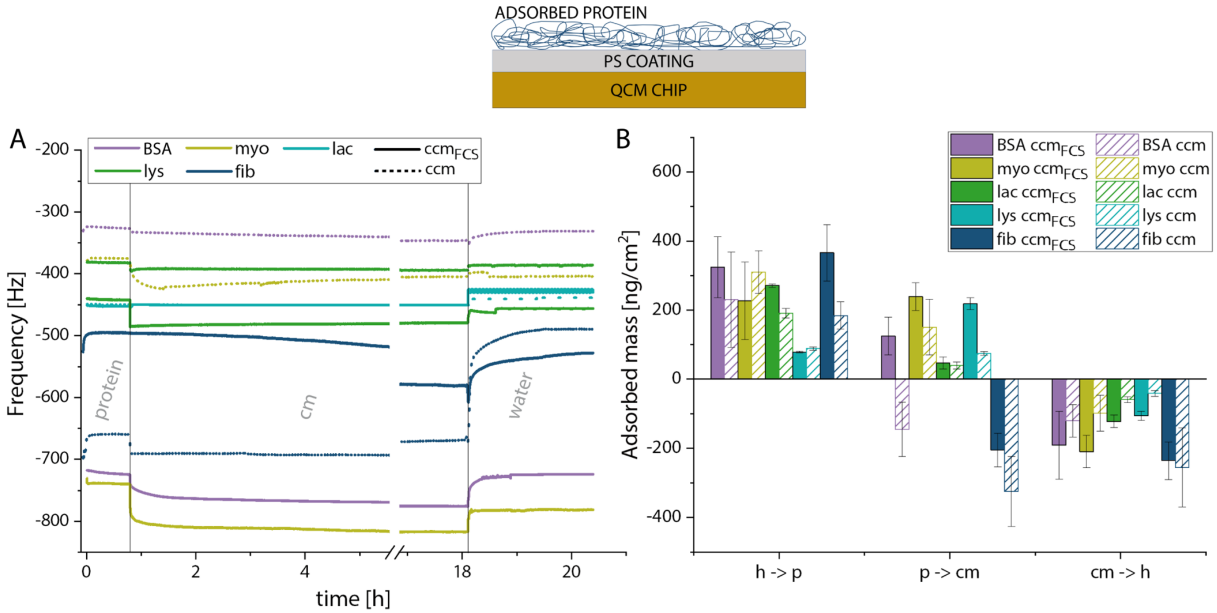

Figure 3. Interaction between protein-coated PS surfaces and fetal calf serum was measured using a quartz crystal microbalance. Frequency shift was plotted as a function of time (A) and the resulting adsorbed mass according to the Sauerbrey equation (eq 1, B). Gold chips were coated with PS and incubated with 15 mg/mL of the appropriate protein (p). Afterward, cell culture medium (cm) with (ccm$_{FCS}$, filled line) or without (ccm, dashed line) FCS was added and everything was incubated overnight. PSPs were washed with water (h). In panel B, "h -> p", "p - > cm", and "cm -> h" depict the differences in the mass adsorption when changing the medium from water (h) to aqueous protein solution (p), to cell culture medium (cm), and finally to water (h). Data mean ± standard deviation (SD), n = 3 replicates.

of the BSA precoating. In contrast, after the incubation with ccm, the total mass of adsorbed protein (BSA) decreased over time. In the case of myoglobin and lysozyme precoating, additional protein adsorption was detected upon incubation in cell culture media (ccm$_{FCS}$ and ccm). This additional adsorption was in a similar size range compared to the first adsorption during precoating. When adding cell culture medium (with and without FCS), fibrinogen was washed off to a small amount, and during the incubation in ccm$_{FCS}$, there was a small increase in adsorbed mass. When adding medium without FCS, the protein mass decreased slowly over time, indicating washing-off effects. When washing with water, a lot of protein was washed off, indicating the presence of loosely bound proteins.

Particle–Cell Interactions (PCIs) and Cellular Effects of Protein-Coated PSPs. To investigate the influence of the protein corona on the particle–cell interaction, we used murine epithelial cells (hepatic BNL CL.2 and intestinal STC-1), which are not specialized for particle ingestion or removal of pathogens unlike macrophages.[45−47] Both cell types have shown cell line-dependent differences in the particle uptake of pristine PS particles, as published previously.[33] BNL CL.2 cells are known to engulf PS particles up to 3 μm, whereas STC-1 cells only internalized particles below 0.5 μm. Particle–cell interaction (PCI) using protein-precoated PSPs was analyzed using confocal laser scanning microscopy (CLSM) and showed differences compared to pristine ones (Figure 4). STC-1 cells took up myoglobin-coated 3 μm PSP, which was not the case for pristine particles. In addition, 0.2 μm myoglobin-coated PSP showed higher PCI compared to pristine particles, indicating that the particles got stuck on the cell surface. The BSA- and fibrinogen-coated PSPs interacted with the cell surface but were not found inside the cells. For BNL Cl.2 cells, no significant differences were found since all particle types were ingested. Compared to STC-1 cells, BNL Cl.2 cells showed higher PCI.

While CLSM could distinguish between internalized particles and particles interacting with the cell surface, it only provided qualitative data. Flow cytometry was used to quantify the PCI (Figure 5).

BSA-coated particles showed a similar interaction as the pristine ones in the case of 0.2 μm PSP with STC-1 cells.

https://doi.org/10.1021/acsami.2c13987
ACS Appl. Mater. Interfaces 2022, 14, 47277−47287

ACS Applied Materials & Interfaces www.acsami.org Research Article

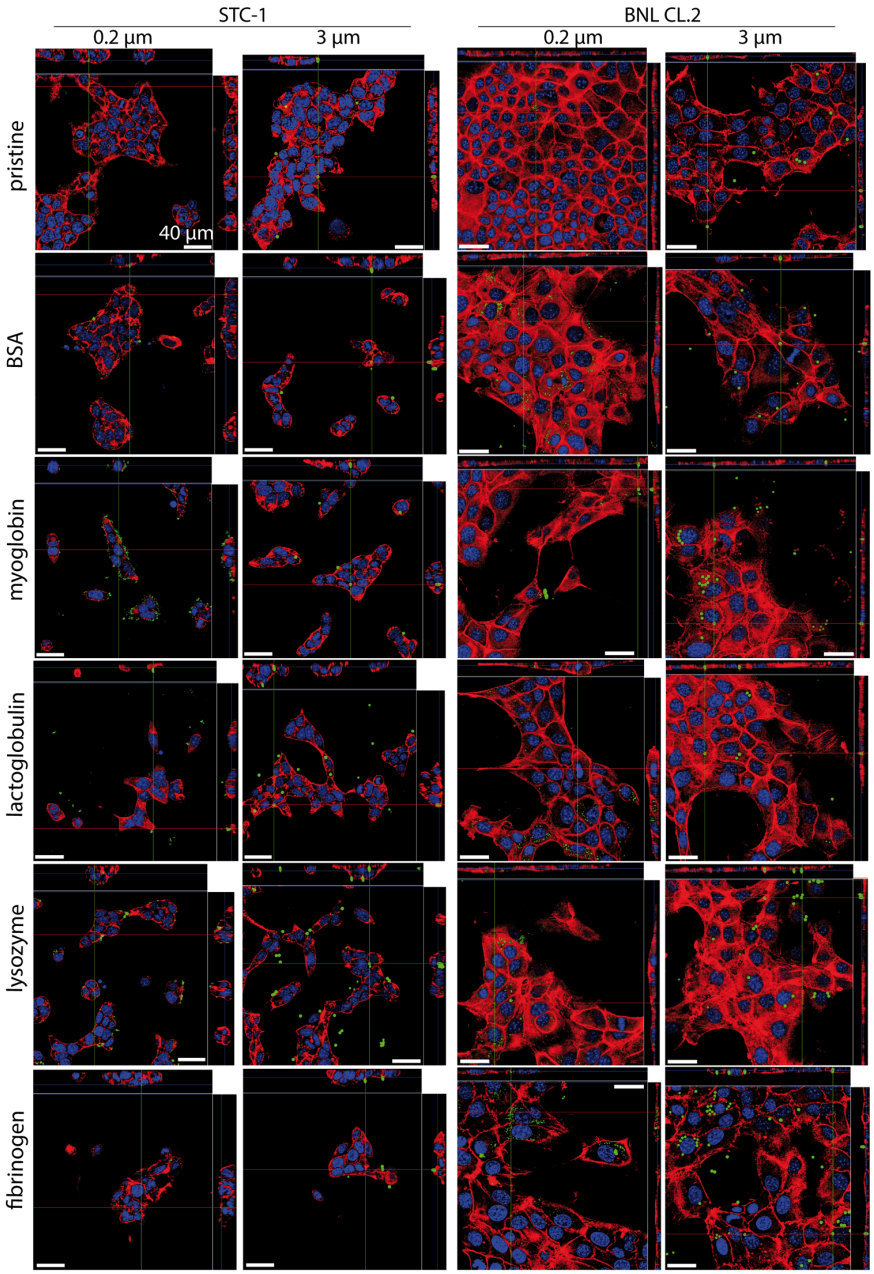

Figure 4. Particle uptake by epithelial cells (intestinal epithelial cells: STC-1 and hepatic epithelial cells: BNL CL.2) in the presence of green-fluorescent protein-coated particles was analyzed using CLSM. As a control, noncoated and water-washed particles (pristine) were used. Actin filaments were stained with rhodamine-phalloidin (red), nuclei were stained with DAPI (blue); FITC-fluorescent PSPs are shown in green. Scale bar: 40 μm.

Fibrinogen-coated PSP showed a lower PCI (lower fluorescence signal) compared to the pristine particles, whereas lysozyme-coated ones showed the highest PCI (highest fluorescence signal). For the 3 μm particles, the quantification of PCI showed significant differences in the case of lactoglobulin- and fibrinogen-coated particles (compared to the other precoated and pristine particles). Lactoglobulin-coated particles showed less interaction (65% of the cell population with no particle interaction). Fibrinogen-coated particles showed almost no interaction (85% of cell population without interaction). BSA-coated particles (0.2 μm) showed a similar interaction in comparison to pristine ones with BNL CL.2 cells. Myoglobin- and lysozyme-coated particles showed higher PCI compared to pristine ones, with lysozyme-coated particles revealing the highest cell interaction. Using 0.2 μm fibrinogen-coated particles, two cell populations were detected. The population with the lower fluorescence signal showed lower PCI and more cells compared to the population with a higher fluorescence

https://doi.org/10.1021/acsami.2c13987
ACS Appl. Mater. Interfaces 2022, 14, 47277−47287

ACS Applied Materials & Interfaces www.acsami.org Research Article

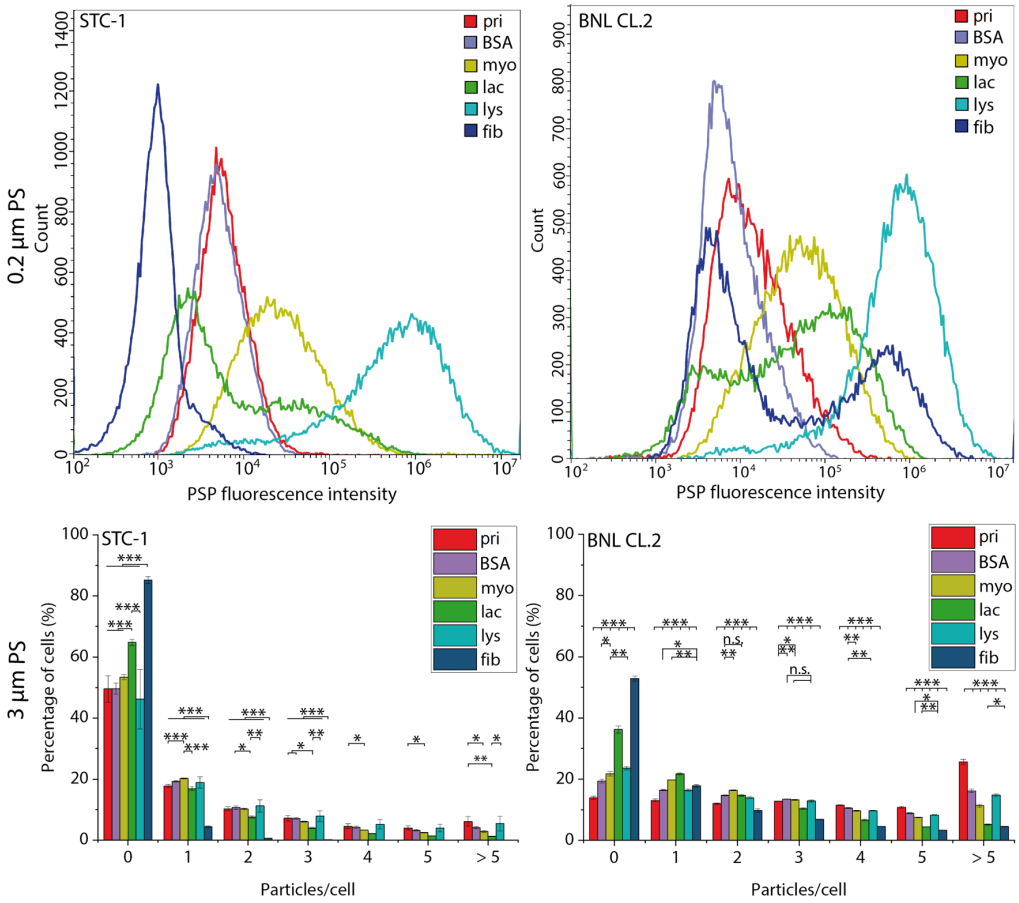

Figure 5. Flow cytometry analysis to quantify particle−cell interactions of pristine (pri) and protein-coated 3 μm PSP with intestinal (STC-1) and hepatic (BNL CL.2) epithelial cells (lower panel, bar charts). Data mean ± SD, n = 3 biological replicates. For 0.2 μm particles (upper panel), no quantification of PCI was possible. ns, nonsignificant, * <0.05, ** <0.01, *** <0.001.

signal (=higher PCI). This indicated that some cells interacted with more particles than with pristine ones, whereas the main cell population interacted with fewer particles. The quantification in the case of 3 μm particles showed, in general, a lower PCI of protein-coated particles upon incubation with BNL CL.2 cells, compared to pristine PSP. Here, BSA-, myoglobin-, and lysozyme-coated particles showed similar interaction rates. In contrast, lactoglobulin- and fibrinogen-coated particles showed significantly less PCIs. Like, with STC-1 cells, fibrinogen-coated particles interacted least with BNL CL.2 (53% of cell population without particle interaction).

To finally analyze cellular effects caused by the protein coating, an MTT assay was performed for all particle−cell combinations (Figure S2). No cytotoxic effects were detected, even at high particle concentrations (100,000 μg/mL and 100 μg/mL for 0.2 and 3 μm PSP, respectively). Only myoglobin-coated particles with 0.2 μm diameter induced in BNL CL.2 cells a slightly reduced, nonsignificant metabolic activity compared to the other precoated particles.

DISCUSSION

According to the Vroman effect, some proteins form a protein corona upon contact with particle surfaces and will be replaced over time by other proteins with a higher affinity to the particles' surface.[18,20] Here, we observed differences in protein corona composition, depending on protein precoating, i.e., the composition of the first protein corona, which is in accordance with the model from Docter et al., in which proteins build a multilayer protein corona involving different protein−protein interactions.[22,23] Therefore, it is assumed that the protein corona on particles is quite complex but at the same time quite stable.

In our study, proteins building the first corona were still detectable after additional incubations in protein-containing medium allowing backtracking of the particle's history. Comparing the results gained from QCM-D and LC−MS/MS measurements showed significant differences in the case of lysozyme and fibrinogen pretreatment. In the case of lysozyme precoating, lysozyme was identified as the most abundant protein in the protein corona, using LC−MS/MS as an analytical tool. In contrast, using QCM-D, lysozyme showed the lowest protein adsorption on the PS surface. In addition, the adsorbed protein mass increased significantly when incubated with an FCS-containing medium. Based thereon, lysozyme was expected to be found way less abundant than was the case. For fibrinogen, there was a lot of protein desorption after incubation in cell culture medium. Here, it was also expected to find less fibrinogen than detected using LC−MS/MS. This can be

https://doi.org/10.1021/acsami.2c13987
ACS Appl. Mater. Interfaces 2022, 14, 47277−47287

explained by the high sensitivity of LC−MS/MS, allowing the identification of proteins down to the attomole range. As a result, especially QCM-D data should be interpreted carefully. Further, PS was applied as a small film on the gold chip, which could lead to effects of different surface curvatures and topographies. Additionally, the QCM-D measurements were performed at room temperature since there was no temperature control possible during this time point of analysis. These results revealed that there is no one-to-one data transfer possible from one experimental setup to another, comparing the protein adsorption to a film (QCM-D) versus to a particle (LC−MS/MS), as reported previously.[48,49] Browne et al. reported differences in BSA adsorption to a PS surface when comparing an oxidized and untreated PS film, underlying that the pure PS film surface may not be comparable with a PS particle surface, which can include traces of additives.[21,34] As reported recently, protein conformation experienced substantial changes when adsorbing on a surface in a protein-type-, particle size-, and charge-dependent manner. In particular, whereas BSA and myoglobin adopted a conformation state different from the native one (i.e., α-helix content was decreased and random coil content increased) after binding on gold nanoparticles, this was not the case for lysozyme.[50] However, the reported conformational changes were observed for nanosurface. Whether such structural changes are responsible for the differences in protein interactions observed in our case can only be speculated upon, especially since we investigated particles in the micro- to submicrometer range. Additional experiments, beyond the scope of this contribution, will be required to investigate this in detail.

Comparing the amount of PCI using flow cytometry revealed differences depending on particle size and model proteins used for coating. In general, the influence of the protein precoating tends to be more visible for the submicron particles than for the larger ones. In detail, for 0.2 μm PSP, lysozyme-coated particles showed a higher PCI compared to the pristine MP, whereas this was not true for 3 μm PSP. This might be related to the previously described size difference influence on the protein corona composition.[27,28,51] It is known that fewer proteins can interact with the surface of smaller particles.[27,28] Additionally, we cannot exclude that during incubation with the cells some aggregation of the coated particles might occur. In this context, it can be expected that for smaller particles a broader variety of aggregates displaying various sizes will form, which can then influence the bioavailability (i.e., cellular uptake). Interestingly, using human epithelial cells, Wen et al. observed that the coating of gold nanoparticles with BSA, myoglobin, or lysozyme significantly decreased the cellular uptake efficiency in a protein-type-dependent manner but was not related to any aggregation of the protein-coated nanoparticles.[50]

Taking together the results of the ζ-potential measurement, the LC−MS/MS data, and the particle−cell interaction analysis, the precoating with lysozyme is noteworthy. As lysozyme is the only positively charged (at neutral pH) used model protein with the highest theoretical pI, the precoating with lysozyme and PSP leads to the only positive ζ-potential, which is following the protein charge.[52] Even though no differences in the ζ-potential were found after the incubation in cell culture medium (ccm_{FCS}) compared to those in the other model proteins, lysozyme precoating revealed one of the highest rates in PCI for both epithelial cell lines. Using LC−MS/MS showed a high affinity of lysozyme for PS compared to serum proteins and a high particle−protein interaction compared to the other, neutral or negatively charged, model proteins. It has been reported that lysozyme-coated gold nanoparticles are internalized by murine fibroblasts via clathrin-dependent endocytosis,[53,54] confirming the cellular interaction with lysozyme-coated particles. On the other hand, particles with a precoating leading to the enrichment of hemoglobin subunit β in the protein corona showed a lower PCI. Based on that, we assume that (i) hemoglobin has a high affinity for PS and (ii) hemoglobin could slightly hinder the interaction with the cellular membrane. A decreased cellular internalization of hemoglobin-coated nanoparticles in alveolar lung cells was described previously,[55] which is in line with our results. The precoating had no significant effect on the cellular response (i.e., metabolic activity, MTT assay) of the two tested cell lines. Since no cytotoxic effects were found in previous studies when using a comparable particle concentration with pristine particles,[33,34,56,57] and none of the used proteins are known to be toxic to cells, this result was anticipated.

In a greater perspective, the effects of environmentally treated particles cannot be excluded though since the protein adsorption seems to depend on the history of the particles. Possible toxic components from the environment might be present on an MP surface and also accumulate.[58−61] In terms of protein corona, every ingestion by an organism will lead to additional protein adsorption, e.g., by proteins present in saliva, gastrointestinal bowels, or blood.[29,62−64] At each stage, which is designated by a change in the environment (e.g., pH), proteins might ad- and desorb or proteins will be substituted. In particular, a decrease in pH, e.g., due to gastric acid, could lead to changes in the particles' surface charge and protein adsorption.[65] Based thereon, evolving protein compositions dependent on a particle's history will be presented on the surface, similar to stamps in a passport. Considering the impact of the particle's history on the PCI, it is reasonable to assume that excretion mechanisms and/or accumulation in organs (e.g., liver and spleen) will also be influenced.[66−69] Taken together, it is possible to backtrack a microparticle's history, which will enable to understand protein corona formation in more complex systems, like seawater, terrestrial environment, or digestive tracts of organisms.

CONCLUSIONS

In summary, differences in the protein−particle interaction and based thereon particle−cell interaction in murine epithelial cells were detected after covering differently sized PS microparticles with model proteins. Based on the first protein layer (model proteins), differences in the protein corona composition were detected when incubating the particles further in cell culture medium containing a cocktail of serum proteins. Using proteomic analysis, it was possible to trace the particles' history. We hypothesize that based on the present proteins on the particles' surface, the interaction with the cellular surface may change. Our results allow a deeper understanding of the behavior of proteins of the protein corona when introducing the particles to a second environmental system and emphasize the need for further analyzing the particles' environmental history, especially for toxicological studies.

ASSOCIATED CONTENT

Supporting Information

The Supporting Information is available free of charge at https://pubs.acs.org/doi/10.1021/acsami.2c13987.

https://doi.org/10.1021/acsami.2c13987
ACS Appl. Mater. Interfaces 2022, 14, 47277−47287

Overview of the databases used in the proteomic analysis for all samples (Table S1); complete list of identified proteins in the corona using LC−MS/MS (Table S2); SEM images of different protein-coated PS particles (Figure S1); and metabolic activity of cells incubated in the presence of protein-coated particles (Figure S2) (PDF)

AUTHOR INFORMATION

Corresponding Author

Thomas Scheibel − *Biomaterials, University of Bayreuth, D-95447 Bayreuth, Germany; Bayreuth Center for Colloids and Interfaces (BZKG), Bayreuth Center for Molecular Biosciences (BZMB), Bayreuth Center for Material Science (BayMAT), and Bavarian Polymer Institute (BPI), University of Bayreuth, D-95447 Bayreuth, Germany;* orcid.org/0000-0002-0457-2423; Email: Thomas.scheibel@bm.uni-bayreuth.de

Authors

Julia Jasinski − *Biomaterials, University of Bayreuth, D-95447 Bayreuth, Germany;* orcid.org/0000-0003-1093-5857

Magdalena V. Wilde − *Gene Center Munich, Laboratory for Functional Genome Analysis (LAFUGA), LMU München, D-81377 Munich, Germany*

Matthias Voelkl − *Process Biotechnology, University of Bayreuth, D-95447 Bayreuth, Germany;* orcid.org/0000-0002-8750-8733

Valérie Jérôme − *Process Biotechnology, University of Bayreuth, D-95447 Bayreuth, Germany;* orcid.org/0000-0001-6492-2168

Thomas Fröhlich − *Gene Center Munich, Laboratory for Functional Genome Analysis (LAFUGA), LMU München, D-81377 Munich, Germany*

Ruth Freitag − *Process Biotechnology, University of Bayreuth, D-95447 Bayreuth, Germany;* orcid.org/0000-0002-6569-9137

Complete contact information is available at: https://pubs.acs.org/10.1021/acsami.2c13987

Author Contributions

J.J., M.W., M.V., V.J., T.F., R.F., and T.S. designed the experiments and wrote the manuscript. J.J., M.W., and M.V. analyzed the data. V.J., T.F., R.F., and T.S. reviewed and edited the manuscript and supervised it during the experiments. J.J. performed the experiments. M.W. performed the LC−MS/MS experiments and analysis of the data. M.V. provided MTT analysis.

Funding

This work was supported by the Deutsche Forschungsgemeinschaft (DFG, German Research Foundation)—project number 391977956—SFB 1357/A05 and A01.

Notes

The authors declare no competing financial interest.

ACKNOWLEDGMENTS

The authors thank Sarah Lentz for her support with QCM-D measurements and data analysis.

REFERENCES

(1) Vert, M.; Doi, Y.; Hellwich, K. H.; et al. Terminology for Biorelated Polymers and Applications (IUPAC Recommendations 2012). *Pure Appl. Chem.* **2012**, *84*, 377−410.

(2) Imhof, H. K.; Rusek, J.; Thiel, M.; Wolinska, J.; Laforsch, C. Do Microplastic Particles Affect *Daphnia magna* at the Morphological, Life History and Molecular Level? *PLoS One* **2017**, *12*, No. e0187590.

(3) Eriksen, M.; Lebreton, L. C. M.; Carson, H. S.; et al. Plastic Pollution in the World's Oceans: More than 5 Trillion Plastic Pieces Weighing over 250,000 Tons Afloat at Sea. *PLoS One* **2014**, *9*, No. e111913.

(4) Lacerda, A. L. d. F.; Rodrigues, L. d. S.; van Sebille, E.; et al. Plastics in Sea Surface Waters Around the Antarctic Peninsula. *Sci. Rep.* **2019**, *9*, No. 3977.

(5) von Moos, N.; Burkhardt-Holm, P.; Köhler, A. Uptake and Effects of Microplastics on Cells and Tissue of the Blue Mussel Mytilus edulis L. after an Experimental Exposure. *Environ. Sci. Technol.* **2012**, *46*, 11327−11335.

(6) Yang, Y.-F.; Chen, C.-Y.; Lu, T.-H.; Liao, C.-M. Toxicity-Based Toxicokinetic/Toxicodynamic Assessment for Bioaccumulation of Polystyrene Microplastics in Mice. *J. Hazard. Mater.* **2019**, *366*, 703−713.

(7) Yong, C.Q.Y.; Valiyaveetill, S.; Tang, B. L. Toxicity of Microplastics and Nanoplastics in Mammalian Systems. *Int. J. Environ. Res. Public Health* **2020**, *17*, No. 1509.

(8) Schwarzer, M.; Brehm, J.; Vollmer, M.; et al. Shape, Size, and Polymer Dependent Effects of Microplastics on *Daphnia magna*. *J. Hazard. Mater.* **2022**, *426*, No. 128136.

(9) Trotter, B.; Wilde, M. V.; Brehm, J.; et al. Long-term Exposure of *Daphnia magna* to Polystyrene Microplastic (PS-MP) Leads to Alterations of the Proteome, Morphology and Life-history. *Sci. Total Environ.* **2021**, *795*, No. 148822.

(10) Galloway, T. S.; Cole, M.; Lewis, C. Interactions of microplastic debris throughout the marine ecosystem. *Nat. Ecol. Evol.* **2017**, *1*, No. 0116.

(11) Saavedra, J.; Stoll, S.; Slaveykova, V. I. Influence of Nanoplastic Surface Charge on Eco-Corona Formation, Aggregation and Toxicity to Freshwater Zooplankton. *Environ. Pollut.* **2019**, *252*, 715−722.

(12) Fadare, O. O.; Wan, B.; Liu, K.; et al. Eco-Corona vs Protein Corona: Effects of Humic Substances on Corona Formation and Nanoplastic Particle Toxicity in *Daphnia magna*. *Environ. Sci. Technol.* **2020**, *54*, 8001−8009.

(13) Witzmann, T.; Ramsperger, A. F. R. M.; Wieland, S.; et al. Repulsive Interactions of Eco-Corona-Covered Microplastic Particles Quantitatively Follow Modeling of Polymer Brushes. *Langmuir* **2022**, *38*, 8748−8756.

(14) Cedervall, T.; Lynch, I.; Lindman, S.; et al. Understanding the Nanoparticle−Protein Corona using Methods to Quantify Exchange Rates and Affinities of Proteins for Nanoparticles. *Proc. Natl. Acad. Sci.* **2007**, *104*, 2050−2055.

(15) Lynch, I.; Dawson, K. A. Protein-Nanoparticle Interactions. *Nano Today* **2008**, *3*, 40−47.

(16) Walczyk, D.; Bombelli, F. B.; Monopoli, M. P.; Lynch, I.; Dawson, K. A. What the Cell "Sees" in Bionanoscience. *J. Am. Chem. Soc.* **2010**, *132*, 5761−5768.

(17) Caracciolo, G.; Palchetti, S.; Colapicchioni, V.; et al. Stealth Effect of Biomolecular Corona on Nanoparticle Uptake by Immune Cells. *Langmuir* **2015**, *31*, 10764−10773.

(18) Vroman, L. Effect of Adsorbed Proteins on the Wettability of Hydrophilic and Hydrophobic Solids. *Nature* **1962**, *196*, 476−477.

(19) Casals, E.; Pfaller, T.; Duschl, A.; Oostingh, G. J.; Puntes, V. Time Evolution of the Nanoparticle Protein Corona. *ACS Nano* **2010**, *4*, 3623−3632.

(20) Nierenberg, D.; Khaled, A. R.; Flores, O. Formation of a Protein Corona Influences the Biological Identity of Nanomaterials. *Rep. Pract. Oncol. Radiother.* **2018**, *23*, 300−308.

(21) Browne, M.; Lubarsky, G.; Davidson, M.; Bradley, R. Protein Adsorption onto Polystyrene Surfaces Studied by XPS and AFM. *Surf. Sci.* **2004**, *553*, 155−167.

(22) Docter, D.; Westmeier, D.; Markiewicz, M.; et al. The Nanoparticle Biomolecule Corona: Lessons Learned−Challenge Accepted? *Chem. Soc. Rev.* **2015**, *44*, 6094−6121.

https://doi.org/10.1021/acsami.2c13987
ACS Appl. Mater. Interfaces 2022, 14, 47277−47287

(23) Corbo, C.; Molinaro, R.; Parodi, A.; et al. The Impact of Nanoparticle Protein Corona on Cytotoxicity, Immunotoxicity and Target Drug Delivery. *Nanomedicine* **2016**, *11*, 81−100.
(24) Biswas, P.; Wu, C.-Y. Nanoparticles and the Environment. *J. Air Waste Manage. Assoc.* **2005**, *55*, 708−746.
(25) Fleischer, C. C.; Payne, C. K. Nanoparticle−Cell Interactions: Molecular Structure of the Protein Corona and Cellular Outcomes. *Acc. Chem. Res.* **2014**, *47*, 2651−2659.
(26) Kihara, S.; Ashenden, A.; Kaur, M.; et al. Cellular Interactions with Polystyrene Nanoplastics—The Role of Particle Size and Protein Corona. *Biointerphases* **2021**, *16*, No. 041001.
(27) Gebauer, J. S.; Malissek, M.; Simon, S.; et al. Impact of the Nanoparticle−Protein Corona on Colloidal Stability and Protein Structure. *Langmuir* **2012**, *28*, 9673−9679.
(28) Piella, J.; Bastús, N. G.; Puntes, V. Size-Dependent Protein−Nanoparticle Interactions in Citrate-Stabilized Gold Nanoparticles: the Emergence of the Protein Corona. *Bioconjugate Chem.* **2017**, *28*, 88−97.
(29) Lundqvist, M.; Stigler, J.; Elia, G.; et al. Nanoparticle size and surface properties determine the protein corona with possible implications for biological impacts. *Proc. Natl. Acad. Sci.* **2008**, *105*, 14265−14270.
(30) García-Álvarez, R.; Hadjidemetriou, M.; Sánchez-Iglesias, A.; Liz-Marzán, L. M.; Kostarelos, K. In vivo Formation of Protein Corona on Gold Nanoparticles. The Effect of their Size and Shape. *Nanoscale* **2018**, *10*, 1256−1264.
(31) Akhter, M. H.; Khalilullah, H.; Gupta, M.; et al. Impact of Protein Corona on the Biological Identity of Nanomedicine: Understanding the Fate of Nanomaterials in the Biological Milieu. *Biomedicines* **2021**, *9*, No. 1496.
(32) Shah, B.; Kona, S.; Gilbertson, T. A.; Nguyen, K. T. Effects of Poly-(Lactide-Co-Glycolide) Nanoparticles on Electrophysiological Properties of Enteroendocrine Cells. *J. Nanosci. Nanotechnol.* **2011**, *11*, 3533−3542.
(33) Rudolph, J.; Völkl, M.; Jérôme, V.; Scheibel, T.; Freitag, R. Noxic Effects of Polystyrene Microparticles on Murine Macrophages and Epithelial Cells. *Sci. Rep.* **2021**, *11*, No. 15702.
(34) Ramsperger, A.; Jasinski, J.; Völkl, M.; et al. Supposedly Identical Microplastic Particles Substantially Differ in their Material Properties Influencing Particle-Cell Interactions and Cellular Responses. *J. Hazard. Mater.* **2022**, *425*, No. 127961.
(35) Von Smoluchowski, M. Zur Kinetischen Theorie der Brownschen Molekularbewegung und der Suspensionen. *Ann. Phys.* **1906**, *326*, 756−780.
(36) Perkins, D. N.; Pappin, D. J.; Creasy, D. M.; Cottrell, J. S. Probability-Based Protein Identification by Searching Sequence Databases using Mass Spectrometry Data. *Electrophoresis* **1999**, *20*, 3551−3567.
(37) Dolatshahi-Pirouz, A.; Rechendorff, K.; Hovgaard, M.; et al. Bovine Serum Albumin Adsorption on Nano-Rough Platinum Surfaces Studied by QCM-D. *Colloids Surf., B* **2008**, *66*, 53−59.
(38) Reimhult, K.; Petersson, K.; Krozer, A. QCM-D Analysis of the Performance of Blocking Agents on Gold and Polystyrene Surfaces. *Langmuir* **2008**, *24*, 8695−8700.
(39) Molino, P. J.; Higgins, M. J.; Innis, P. C.; Kapsa, R. M.; Wallace, G. G. Fibronectin and Bovine Serum Albumin Adsorption and Conformational Dynamics on Inherently Conducting Polymers: a QCM-D Study. *Langmuir* **2012**, *28*, 8433−8445.
(40) Sauerbrey, G. Use a Quartz Vibration Form Weigh Thin Films on a Microbalance. *Z. Phys.* **1959**, *155*, 206−222.
(41) Wang, B.; Li, K.; Jin, W.; et al. Properties and Inflammatory Effects of Various Size Fractions of Ambient Particulate Matter from Beijing on A549 and J774A.1 Cells. *Environ. Sci. Technol.* **2013**, *47*, 10583−10590.
(42) Hesler, M.; Aengenheister, L.; Ellinger, B.; et al. Multi-Endpoint Toxicological Assessment of Polystyrene Nano-and Microparticles in Different Biological Models in vitro. *Toxicol. In Vitro* **2019**, *61*, No. 104610.
(43) Hwang, J.; Choi, D.; Han, S.; et al. Potential Toxicity of Polystyrene Microplastic Particles. *Sci. Rep.* **2020**, *10*, No. 7391.
(44) Ishihama, Y.; et al. Exponentially Modified Protein Abundance Index (emPAI) for Estimation of Absolute Protein Amount in Proteomics by the Number of Sequenced Peptides per Proteins. *Mol. Cell. Proteomics* **2005**, *4*, 1265−1272.
(45) Aderem, A.; Underhill, D. M. Mechanisms of Phagocytosis in Macrophages. *Annu. Rev. Immunol.* **1999**, *17*, 593−623.
(46) Champion, J. A.; Mitragotri, S. Role of Target Geometry in Phagocytosis. *Proc. Natl. Acad. Sci.* **2006**, *103*, 4930−4934.
(47) Wynn, T. A.; Chawla, A.; Pollard, J. W. Macrophage Biology in Development, Homeostasis and Disease. *Nature* **2013**, *496*, 445−455.
(48) Aguilar, K. C.; Tello, F.; Bierhalz, A. C.; et al. Protein Adsorption onto Alginate-Pectin Microparticles and Films Produced by Ionic Gelation. *J. Food Eng.* **2015**, *154*, 17−24.
(49) Rahmati, M.; Mozafari, M. Protein Adsorption on Polymers. *Mater. Today Commun.* **2018**, *17*, 527−540.
(50) Wen, M.; Li, Y.; Zhong, W.; et al. Interactions of Cationic Gold Nanoclusters with Serum Proteins and Effects on their Cellular Responses. *J. Colloid Interface Sci.* **2022**, *610*, 116−125.
(51) Contado, C.; Mehn, D.; Gilliland, D.; Calzolai, L. Characterization Methods for Studying Protein Adsorption on Nano-Polystyrene Beads. *J. Chromatogr. A* **1606**, *1606*, No. 460383.
(52) Cai, C.; Bakowsky, U.; Rytting, E.; Schaper, A. K.; Kissel, T. Charged Nanoparticles as Protein Delivery Systems: a Feasibility Study using Lysozyme as Model Protein. *Eur. J. Pharm. Biopharm.* **2008**, *69*, 31−42.
(53) De Campos, A. M.; Diebold, Y.; Carvalho, E. L.; Sánchez, A.; José Alonso, M. Chitosan Nanoparticles as New Ocular Drug Delivery Systems: in vitro Stability, in vivo Fate, and Cellular Toxicity. *Pharm. Res.* **2004**, *21*, 803−810.
(54) Lee, Y.; Geckeler, K. E. Cytotoxicity and Cellular Uptake of Lysozyme-Stabilized Gold Nanoparticles. *J. Biomed. Mater. Res., Part A* **2012**, *100*, 848−855.
(55) Stayton, I.; Winiarz, J.; Shannon, K.; Ma, Y. Study of Uptake and Loss of Silica Nanoparticles in Living Human Lung Epithelial Cells at Single Cell Level. *Anal. Bioanal. Chem.* **2009**, *394*, 1595−1608.
(56) Fröhlich, E. The role of surface charge in cellular uptake and cytotoxicity of medical nanoparticles. *Int. J. Nanomed.* **2012**, *7*, 5577−5591.
(57) Stock, V.; Böhmert, L.; Lisicki, E.; et al. Uptake and effects of orally ingested polystyrene microplastic particles in vitro and in vivo. *Archiv. Toxicol.* **2019**, *93*, 1−17.
(58) Li, J.; Liu, H.; Chen, J. P. Microplastics in Freshwater Systems: A Review on Occurrence, Environmental Effects, and Methods for Microplastics Detection. *Water Res.* **2018**, *137*, 362−374.
(59) Wang, F.; Wong, C. S.; Chen, D.; et al. Interaction of Toxic Chemicals with Microplastics: a Critical Review. *Water Res.* **2018**, *139*, 208−219.
(60) Verla, A. W.; Enyoh, C. E.; Verla, E. N.; Nwarnorh, K. O. Microplastic−Toxic Chemical Interaction: a Review Study on Quantified Levels, Mechanism and Implication. *SN Appl. Sci.* **2019**, *1*, 1−30.
(61) Fu, L.; Li, J.; Wang, G.; Luan, Y.; Dai, W. Adsorption Behavior of Organic Pollutants on Microplastics. *Ecotoxicol. Environ. Saf.* **2021**, *217*, No. 112207.
(62) Ma, Z.; Bai, J.; Jiang, X. Monitoring of the Enzymatic Degradation of Protein Corona and Evaluating the Accompanying Cytotoxicity of Nanoparticles. *ACS Appl. Mater. Interfaces* **2015**, *7*, 17614−17622.
(63) Lundqvist, M.; Augustsson, C.; Lilja, M.; et al. The Nanoparticle Protein Corona Formed in Human Blood or Human Blood Fractions. *PLoS One* **2017**, *12*, No. e0175871.
(64) Weiss, A. C. G.; Herold, H. M.; Lentz, S.; et al. Surface Modification of Spider Silk Particles to Direct Biomolecular Corona Formation. *ACS Appl. Mater. Interfaces* **2020**, *12*, 24635−24643.
(65) Stock, V.; Fahrenson, C.; Thuenemann, A.; et al. Impact of Artificial Digestion on the Sizes and Shapes of Microplastic Particles. *Food Chem. Toxicol.* **2020**, *135*, No. 111010.

https://doi.org/10.1021/acsami.2c13987
ACS Appl. Mater. Interfaces 2022, 14, 47277−47287

(66) Hirn, S.; Semmler-Behnke, M.; Schleh, C.; et al. Particle Size-Dependent and Surface Charge-Dependent Biodistribution of Gold Nanoparticles after Intravenous Administration. *Eur. J. Pharm. Biopharm.* **2011**, *77*, 407−416.
(67) Schleh, C.; Semmler-Behnke, M.; Lipka, J.; et al. Size and Surface Charge of Gold Nanoparticles Determine Absorption across Intestinal Barriers and Accumulation in Secondary Target Organs after Oral Administration. *Nanotoxicology* **2012**, *6*, 36−46.
(68) Wang, B.; He, X.; Zhang, Z.; Zhao, Y.; Feng, W. Metabolism of Nanomaterials in vivo: Blood Circulation and Organ Clearance. *Acc. Chem. Res.* **2013**, *46*, 761−769.
(69) Dai, Q.; Bertleff-Zieschang, N.; Braunger, J. A.; et al. Particle Targeting in Complex Biological Media. *Adv. Healthcare Mater.* **2018**, *7*, No. 1700575.

https://doi.org/10.1021/acsami.2c13987
ACS Appl. Mater. Interfaces 2022, 14, 47277−47287

"Supporting Information"

Tailor-made protein corona formation on polystyrene microparticles and its effect on epithelial cell uptake

Julia Jasinski[1], Magdalena V. Wilde[2], Matthias Voelkl[3], Valérie Jérôme[3], Thomas Fröhlich[2], Ruth Freitag[3], Thomas Scheibel[1,4,5,6,7,*]

[1] Biomaterials, University of Bayreuth, D-95447 Bayreuth, Germany
[2] Gene Center Munich, Laboratory for Functional Genome Analysis (LAFUGA), LMU München, D-81377 Munich, Germany
[3] Process Biotechnology, University of Bayreuth, D-95447 Bayreuth, Germany
[4] Bayreuth Center for Colloids and Interfaces (BZKG), University of Bayreuth, D-95447 Bayreuth, Germany
[5] Bayreuth Center for Molecular Biosciences (BZMB), University of Bayreuth, D-95447 Bayreuth, Germany
[6] Bayreuth Center for Material Science (BayMAT), University of Bayreuth, D-95447 Bayreuth, Germany
[7] Bavarian Polymer Institute (BPI), University of Bayreuth, D-95447 Bayreuth, Germany

* Corresponding author. E-Mail address: Thomas.scheibel@bm.uni-bayreuth.de

Table S1. Overview of the databases used in the proteomic analysis for all samples.

Pre-coating	Database	Subset
Pristine	SwissProt	-
BSA	UniProt	*Bos taurus*
Myoglobin	UniProt	*Equus caballus*
β-Lactoglobulin	UniProt	*Bos taurus*
Lysozyme	UniProt	*Gallus gallus*
Fibrinogen	UniProt	*Bos taurus*

Table S2. Complete list of identified proteins in the corona using LC-MS/MS. 3 µm PS particles were pre-incubated in model proteins (BSA, myoglobin, β-lactoglobulin, lysozyme, and fibrinogen) and afterward incubated in ccm_{FCS}. The respective model protein is highlighted in **bold fonts**. Pristine PSP (i.e., without pre-incubation) incubated in ccm_{FCS} were included for comparison. The emPAI value, which allows the estimation of protein abundance, is given in brackets.

Pristine	BSA-coated	Myoglobin-coated
Hemoglobin fetal subunit β (2.99)	**BSA (4.74)**	Hemoglobin fetal subunit β (3.04)
BSA (2.76)	Hemoglobin fetal subunit β (3.13)	BSA (2.08)
Serotransferrin (1.34)	Globin C1 (1.7)	**Myoglobin (0.86)**
Hemoglobin subunit α (1.08)	Apolipoprotein A-I (0.66)	Hemoglobin subunit α (0.64)
α-2-HS-glycoprotein (0.96)	α-2-HS-glycoprotein (0.64)	Secreted phosphoprotein 24 (0.38)
Cathelicidin-2 (0.73)	Keratin, type I cytoskeletal (0.33)	α-2-HS-glycoprotein (0.34)
Apolipoprotein A-I (0.45)	Vitronectin (0.33)	Vitronectin (0.15)
α-1-antiproteinase (0.38)	Keratin 1 (0.28)	C4b-binding protein α chain (0.11)
Fetuin-B (0.3)	Apolipoprotein E (0.23)	Gelsolin (0.1)
Gelsolin (0.21)	Antithrombin-III (0.15)	Complement factor B (0.09)
α-fetoprotein (0.11)	Serotransferrin (0.1)	Plasminogen (0.08)
Lactotransferrin (0.1)		
α-2-macroglobulin (0.09)		
Complement factor B (0.09)		
Complement C3 (0.08)		

β-Lactoglobulin-coated	Lysozyme-coated	Fibrinogen-coated
Hemoglobin fetal subunit β (5.47)	**Lysozyme (8.19)**	Hemoglobin fetal subunit β (12.03)
BSA (3.05)	Hemoglobin fetal subunit β (7.09)	**Fibrinogen β chain (6.69)**
Globin C1 (2.4)	Fibrinogen β chain (4.13)	**Fibrinogen γ-B chain (3.85)**
β-lactoglobulin (1.1)	Fibrinogen γ-B chain (2.31)	**Fibrinogen α chain (2.93)**
Peptidoglycan recognition protein 1 (1.02)	BSA (2.07)	Apolipoprotein A-I (1.72)
α-2-HS-glycoprotein (0.97)	Globin C1 (1.65)	Globin C1 (1.66)
Vitronectin (0.75)	Fibrinogen α chain (1.14)	Plasminogen (1.18)
Apolipoprotein E (0.66)	α-2-HS-glycoprotein (0.97)	Vitronectin (0.75)
Antithrombin-III (0.22)	Apolipoprotein E (0.84)	Complement component C9 (0.3)
α-1-antiproteinase (0.18)	Vitronectin (0.63)	BSA (0.24)
Prothrombin (0.11)	α-1-antiproteinase (0.63)	α-2-HS-glycoprotein (0.21)
Coagulation factor V (0.03)	Apolipoprotein A-I (0.48)	Coagulation factor XIII B chain (0.18)
	SERPIN domain-containing protein (0.3)	Coagulation factor XIII A chain (0.16)
	Plasminogen (0.23)	Complement component 3 (0.15)
	Keratin, type I cytoskeletal 10 (0.23)	Uncharacterized protein (0.08)
	Uncharacterized protein (0.2)	Complement component C6 (0.07)
	Complement component C9 (0.14)	Complement component 5 (0.04)
	Complement component 3 (0.13)	
	Keratin 1 (0.13)	
	C4b-binding protein α chain (0.11)	
	Gelsolin (0.09)	
	Uncharacterized protein (0.04)	
	Coagulation factor V (0.03)	

ccm_{FCS}: cell culture medium supplemented with 10% fetal calf serum

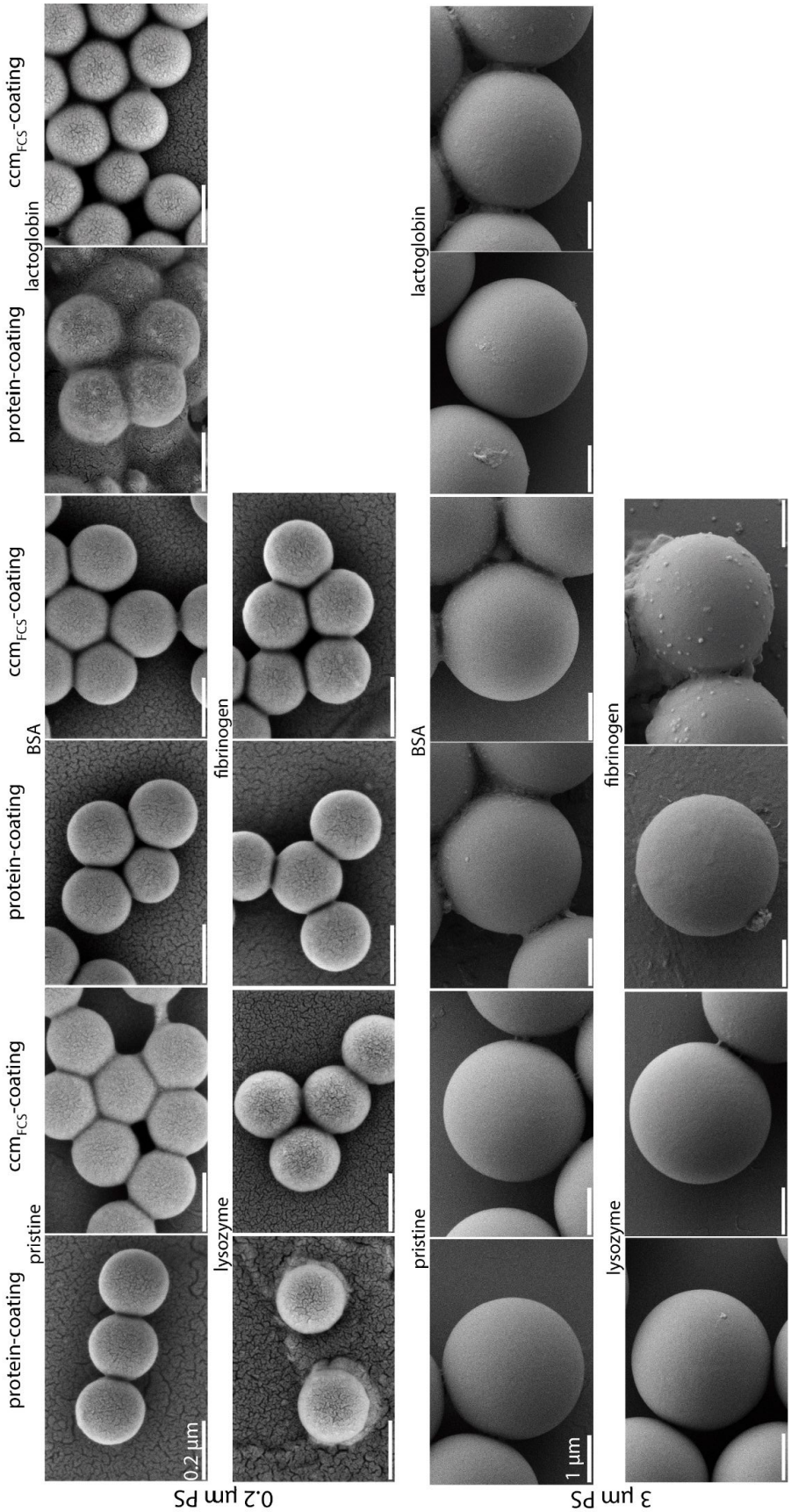

Figure S1. SEM images of pristine and different protein-coated PS-particles (analyzed directly after protein-coating and washing steps, "protein-coating"). The particles were additionally incubated in cell culture medium supplemented with 10 % FCS ("ccm$_{FCS}$"). Pristine PSP were only incubated in ccm$_{FCS}$ (i.e., without pre-incubation). Scale bar: 0.2 µm PSP: 0.2 µm. 3 µm PSP: 1 µm.

4

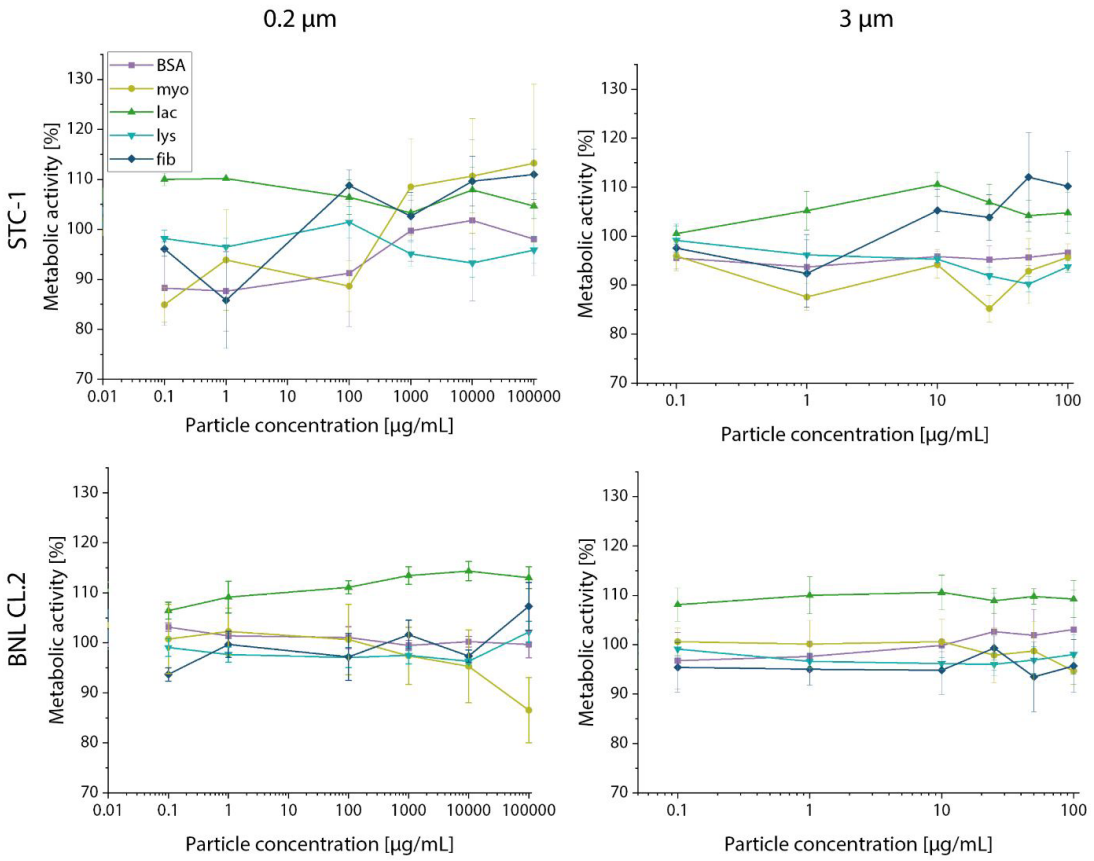

Figure S2. Metabolic activity of cells incubated in the presence of protein-coated particles. The metabolic activity was determined using the MTT assay. Data represent mean ± SD, n = 3 biological replicates.

6.4 Teilarbeit IV

Influence of the Polymer Type of a Microplastic Challenge on the Reaction of Murine Cells

Autoren: **Julia Jasinski**, Matthias Völkl, Magdalena V. Wilde, Valérie Jérôme, Thomas Fröhlich, Ruth Freitag und Thomas Scheibel

Die Konzeptionierung sowie alle Experimente dieser Teilarbeit wurden von Matthias Völkl, Magdalena Wilde und mir durchgeführt. Die verwendeten Celluloseacetat Mikropartikel wurden von mir hergestellt. Die Partikelanalyse mittels DLS, ζ-Potentialmessungen und Rasterelektronenmikroskopie, sowie die qualitative Analyse der zellulären Aufnahme mittels Rasterelektronenmikroskopie und Konfokalmikroskopie wurde von mir durchgeführt und ausgewertet. Zusätzlich wurde der Resazurin Assay und eine Lebend-/Totfärbung der Zellen von mir durchgeführt und ausgewertet. Daten zu den zellulären Effekten (Zytotoxizität) wurden von Matthias Völkl erhoben. Magdalena Wilde analysierte die Protein-Corona mittels LC-MS/MS durch und analysierte die Daten. Das Manuskript wurde von mir verfasst. Valérie Jérôme, Thomas Fröhlich, Ruth Freitag und Thomas Scheibel waren an der Konzeptionierung, wissenschaftlichen Diskussionen und der Fertigstellung des Manuskripts beteiligt.

Der Artikel wurde am 05.03.2024 im Journal *Journal of Hazardous Materials* veröffentlicht.

Journal of Hazardous Materials 465 (2024) 133280

Contents lists available at ScienceDirect

Journal of Hazardous Materials

journal homepage: www.elsevier.com/locate/jhazmat

Research Paper

Influence of the polymer type of a microplastic challenge on the reaction of murine cells

Julia Jasinski [a,1], Matthias Völkl [b,2], Magdalena V. Wilde [c,d,3], Valérie Jérôme [b,4], Thomas Fröhlich [c,5], Ruth Freitag [b,f,6], Thomas Scheibel [a,e,f,g,h,*,7]

[a] Biomaterials, Faculty of Engineering Sciences, University of Bayreuth, Bayreuth, Germany
[b] Process Biotechnology, Faculty of Engineering Sciences, University of Bayreuth, Bayreuth, Germany
[c] Gene Center Munich, Laboratory for Functional Genome Analysis (LAFUGA), LMU München, Munich, Germany
[d] Department of Earth and Environmental Sciences, Paleontology & Geobiology, LMU München, Munich, Germany
[e] Bayreuth Center for Colloids and Interfaces (BZKG), University of Bayreuth, Bayreuth, Germany
[f] Bayreuth Center for Molecular Biosciences (BZMB), University of Bayreuth, Bayreuth, Germany
[g] Bayreuth Center for Material Science (BayMAT), University of Bayreuth, Bayreuth, Germany
[h] Bavarian Polymer Institute (BPI), University of Bayreuth, Bayreuth, Germany

HIGHLIGHTS

- Microparticles of PE, PS, PVC, PLA, CA differ in their particle surface properties.
- Protein corona and cellular interaction differences are based on the polymer used.
- Microparticles show no immediate toxicity in macrophages and epithelial cells.

GRAPHICAL ABSTRACT

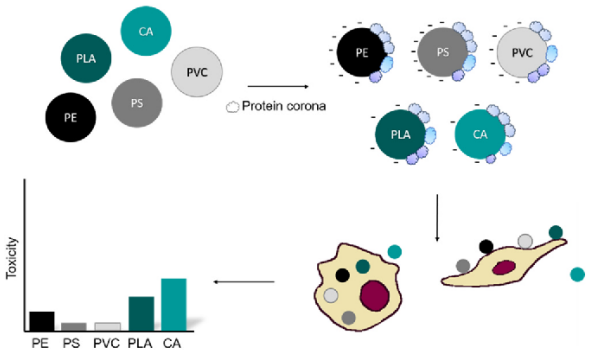

ARTICLE INFO

Editor: Joao Pinto da Costa

ABSTRACT

Due to global pollution derived from plastic waste, the research on microplastics is of increasing public interest. Until now, most studies addressing the effect of microplastic particles on vertebrate cells have primarily utilized

* Corresponding author at: Biomaterials, Faculty of Engineering Sciences, University of Bayreuth, Bayreuth, Germany.
E-mail address: thomas.scheibel@bm.uni-bayreuth.de (T. Scheibel).
[1] 0000–0003-1093–5857
[2] 0000–0002-8750–8733
[3] 0000–0002-1997–8768
[4] 0000–0001-6492–2168
[5] 0000–0002-4709–3211
[6] 0000–0002-6569–9137
[7] 0000–0002-0457–2423

https://doi.org/10.1016/j.jhazmat.2023.133280
Received 18 September 2023; Received in revised form 9 December 2023; Accepted 13 December 2023
Available online 16 December 2023

Keywords:
Polymer particles
Cellulose acetate microparticles
Particle-cell interaction
Protein corona
Reactive oxygen species

polystyrene particles (PS). Other studies on polymer microparticles made, e.g., of polyethylene (PE), polyvinyl chloride (PVC), polypropylene (PP), or poly (ethylene terephthalate) (PET), cannot easily be directly compared to these PS studies, since the used microparticles differ widely in size and surface features. Here, effects caused by pristine microparticles of a narrow size range between 1 - 4 μm from selected conventional polymers including PS, PE, and PVC, were compared to those of particles made of polymers derived from biological sources like polylactic acid (PLA), and cellulose acetate (CA). The microparticles were used to investigate cellular uptake and assess cytotoxic effects on murine macrophages and epithelial cells. Despite differences in the particles' properties (e.g. ζ-potential and surface morphology), macrophages were able to ingest all tested particles, whereas epithelial cells ingested only the PS-based particles, which had a strong negative ζ-potential. Most importantly, none of the used model polymer particles exhibited significant short-time cytotoxicity, although the general effect of environmentally relevant microplastic particles on organisms requires further investigation.

1. Introduction

Plastics are, per definition, made out of petroleum-based polymers, like polyethylene (PE), polystyrene (PS), or polypropylene (PP), often supplemented with additives, such as pigments, surfactants or plasticizers [1–3]. Commodity plastics have advantageous properties and the list of their applications is long, including inter alia use as package material and foils, in textiles, or as pipes [4–6]. Nevertheless, plastic recycling rates are low, leading to increasing environmental pollution [4,6–8].

Once in the environment, large plastic pieces can disintegrate, e.g. by photodegradation (UV irradiation), into smaller fragments until they reach the micrometer size range [9–11]. Plastic particles < 5 mm are defined as microplastic [2,12,13]. Over the past decade, there has been a notable rise in attention towards microplastics, with instances of their global dispersion even reaching uninhabited areas [14–17]. One potential solution being explored to address this issue involves the investigation of biodegradable polymers. These polymers can be degraded and catabolized in the presence of microorganisms, such as bacteria or fungi, and disappear within a reasonable amount of time from the environment [18–22].

Due to their ubiquitous presence, microplastics inevitably interact with organisms of all kinds causing different types of stress. In animal studies using mussels, daphnids, fish, or mice, the exposition to larger microplastics (5–80 μm) leads to physical tissue damage and blockage of the gastrointestinal tract, and in consequence to metabolic perturbations [23–27]. Smaller microparticles can reach the circulatory system and accumulate in different tissues like the liver, gut, and spleen, where they induce inflammation, oxidative stress, or necrosis [28–30]. Once ingested by cells, microparticles can induce different noxic effects, such as inflammatory cytokine release, loss of phenotypical cellular behaviors, oxidative stress reactions (ROS production), or DNA damage [31–34].

Regarding the in vitro experiments, the most investigated polymer type is PS [29,35–38], even though this is not the most abundant polymer found as plastic waste in the environment [14,39,40]. However, PS particles are commercially available in a wide size range with different modifications like chemical groups, magnetic, or fluorescent properties [32,41]. Much less is known about other polymer microparticles such as PE, poly (vinyl chloride) (PVC), and the biologically degradable poly (lactic acid) (PLA) [8,29,33]. Previously published works analyzed cellular effects using different polymer microparticles (e.g. PVC, PET, PP, and PE), the particles were, in most cases, comparatively large (10 - 100 μm in diameter) and polydisperse, making a direct comparison between the different polymer types difficult [29,31,33,42]. As a consequence, the impact of varying polymer types on the environmental and cellular effects of microplastic particles remains insufficiently explored. Differences between the polymer types could include varying surface properties such as the surface charge, the hydrophobicity, and potential surface modifications with chemical groups, which, in return, influence the formation of a protein corona within a biological environment [43,44]. These parameters are further crucial when cellular interactions are investigated [45–53]. In addition, the particle size is important for particle-cell interactions [32,45,46,54,55]. Macrophages are a cell type that specializes in the ingestion of pathogens (and particles) via phagocytosis, of foreign matter of up to a size of about 10 μm [32,56,57]. Other cell types, such as epithelial cells, do not show phagocytosis. However, these cells have been shown to engulf particles up to 0.5 μm via pinocytosis [32,48,54,55].

Here, we used commercially available, pristine polymer microparticles (MP), made of PS, PE, PVC, and PLA, within a comparable size range of 1 – 4 μm to study cellular responses. In addition, we used in-house generated cellulose acetate (CA) microparticles as bio-based controls. We assessed particle surface properties (using techniques such as Scanning Electron Microscopy (SEM), ζ-potential, and Dynamic Light Scattering (DLS) measurements), explored the formation of protein corona (analyzed through LC-MS/MS), and examined particle-cell interactions (utilizing Confocal Laser Scanning Microscopy). These investigations aimed to pinpoint distinctive effects resulting from the polymer type on particle-induced cellular responses. This was achieved by employing complementary assays that scrutinized cytotoxicity, metabolic activity, and oxidative stress.

2. Materials and methods

2.1. Materials

If not otherwise stated, Greiner Bio-One (Frickenhausen, Germany) and Thermo Fisher Scientific (Schwerte, Germany) were used as suppliers for cell culture materials. Penicillin, streptomycin, Dulbecco's Phosphate-Buffered Saline without Ca^{2+} and Mg^{2+} (DPBS), $DMEM_{Lonza}$ (Dulbecco`s Modified Eagle's Medium; high glucose, 3.7 g/L $NaHCO_3$, L-glutamine-free) and RPMI1640 (Roswell Park Memorial Institute) were obtained from Lonza (Lonza Group Ltd, Basel, Switzerland). $DMEM_{ATCC}$ (high glucose, 1.5 g/L $NaHCO_3$, 0.11 mM Na pyruvate, 4 mM L-glutamine) was obtained from ATCC (ATCC LGC Standards GmbH, Wesel, Germany). Modified Eagle Medium without phenol red (MEM) was obtained from Thermo Fisher Scientific (Schwerte, Germany). Fetal calf serum (FCS) was purchased from Sigma Aldrich (Taufkirchen, Germany).

3-(4,5-dimethyl-2-thiazolyl)− 2,5-Diphenyl-2 H-tetrazolium bromide (MTT), was obtained from Sigma Aldrich (Taufkirchen, Germany). AlamarBlue (CellTiter-Blue Cell Viability Assay) was purchased from Promega (Walldorf, Germany). For fluorescence staining of cells, CellTracker Red CMTPX Dye (Cat. # C34552) and Hoechst 33342 (Cat. # H-3570) were obtained from Thermo Fisher Scientific (Schwerte, Germany).

Dichloromethane (DCM) was obtained from Thermo Fisher Scientific (Schwerte, Germany). Polyvinyl alcohol (PVA), and cellulose acetate (CA) were obtained from Sigma Aldrich (Taufkirchen, Germany).

Non-functionalized (plain) non-fluorescent 2 μm polystyrene (PS) particles (Cat. # 19814–15, 5.68 $\times 10^9$ particles/mL) were obtained from Polysciences (Polysciences Europe GmbH, Eppenheim, Germany). They were delivered as a sterile aqueous suspension with a concentration of 2.5% (w/v). According to the supplier, the plain particles have a slight anionic charge due to residues of sulfate ester groups. Plain

polylactic acid (PLA) particles with a size of 2 μm (Cat. # 11–00-203, 2.4 $\times 10^9$ particles/mL) were obtained from Micromod (Micromod Partikeltechnologie GmBH, Rostock, Germany). The PLA particles were delivered as a sterile aqueous suspension with a concentration of 1% (w/v). Plain polyethylene (low-density polyethylene, LDPE) particles with a size of 1- 4 μm (Cat. # CPMS-0.96 1–4 μm - 0.2 g, size CV ≤ 10%) were purchased from Cospheric (Cospheric LLC, Santa Babara, CA, USA). The LDPE particles were delivered as a powder (0.2 g) and were resuspended in 3 mL of a sterile aqueous solution with 0.1% (w/v) Tween 20, resulting in a 1.5% (w/v) PE suspension (5.4 $\times 10^7$ particles/mL, based on particle size analysis using a camsizer (Microtrac Retsch GmbH, Haan, Germany)). Sterile plain polyvinylchloride (PVC) particles with a size of 1.4 μm (8.3 $\times 10^7$ particles/mL, size CV ≤ 10%) were purchased from Quantum Design (Quantum Design GmBH, Darmstadt, Germany). All particles showed no autofluorescence in the excitation/emission wavelength ranges of interest for the intended experiments. Before use, MP stock solutions were diluted to the desired concentration in the respective growth media.

2.2. Production of cellulose acetate (CA) particles

To produce cellulose acetate (CA) microparticles, a pre-mix matrix emulsification setup according to Sawalha *et al.*, 2008 was used [58]. As introduced for PLA according to Sawalha *et al.*, CA was dissolved in dichloromethane (DCM) to gain a stock solution of 5% (w/w). PVA was dissolved in MilliQ water (1% w/v) to prepare an aqueous stock solution. 11 mL of a non-solvent solution (comprising 8 mL 30% (w/w) methanol-water and 3 mL of the 1% aqueous PVA solution) was prepared. Then, 0.5 mL of the CA solution and 1.15 mL DCM were added to the non-solvent solution. The solution was stirred for 1 min in a closed glass vessel (700 rpm). This pre-mix was passed approximately 10 times through a sterile filter (Whatman® Puradisc 13, PFTE filter) with a 1 μm pore size. The filter was exchanged after 3 filtrations. The resulting suspension was left overnight under gentle stirring (70 rpm) to evaporate the DCM. The microparticles were washed five times in MilliQ water by centrifugation (17,000 *g*, 30 min, RT) and then stored in sterile MilliQ water until further usage.

2.3. ζ-potential and DLS measurement

The ζ-potential and dynamic light scattering (DLS) measurements were performed using the LiteSizer 500 (Anton Paar Germany GmbH, Ostfildern-Scharnhausen, Germany) and Omega cuvettes (Anton Paar Germany GmbH, Ostfildern-Scharnhausen, Germany). The particle suspensions were diluted in 1 mL of a 1 mM aqueous KCl solution (pH 6.0) yielding a concentration of 0.05 mg/mL particles and were measured immediately. In some cases, 0.05 mg/mL of the particle suspensions were incubated in 1 mL cell medium ($DMEM_{ATCC}$, containing 10% (v/v) FCS) overnight at 37 °C. Thereafter, the particles were collected by centrifugation (17,000 *g* for 30 min at room temperature (RT)) and resuspended in 1 mL of the 1 mM KCl solution for measurement. Three measurements with at least 100 runs each were performed at 21 °C with an adjusted voltage of 200 V. The ζ-potential was calculated using the Helmholtz-Smoluchowski equation [59]. The DLS measurements were performed at 21 °C with at least 10 runs each using the backscatter angle (175°).

2.4. Scanning electron microscopy (SEM) particle characterization

A 0.5 mg/mL pristine aqueous particle suspension was dried overnight on a silicon wafer for particle characterization. The samples were sputter-coated with platin and imaged using SEM (FEI Apreo Volumescope, Thermo Fisher Scientific, magnification 50,000x, 2 kV, Everhart-Thornley detector).

2.5. Sample preparation for analysis of the protein corona composition

To perform proteome analysis, pristine microplastic particles were placed in a cell culture medium (DMEM) containing 10% (v/v) FCS and incubated overnight at 37 °C in a standard cell culture incubator (5% CO_2/ 95% humidity). The resulting samples were then processed for LC-MS/MS analysis, using previously described methods [26,60]. Briefly, the microplastic particles were centrifuged at 20,000 *g* for 30 min and the supernatant was removed. The resulting pellet was resuspended in 2x Laemmli buffer (0.5 M tris−HCl, pH 6.8, 20% glycerol (v/v), 40 g/L SDS, 10% 2-mercaptoethanol (V/V), 0.002% bromophenol blue), briefly vortexed, and incubated at 95 °C for 5 min. Samples were transferred to denaturing polyacrylamide gradient gels (NuPAGE™ 4 to 12%, Bis-Tris, Mini-Protein-Gel, Thermo Fisher Scientific, U.S.A), and run at 200 V for 5 min. The gels were stained overnight with ROTI Blue staining solution (Roth, Germany), subsequently the protein-containing areas were cut out and destained using acetonitrile (ACN) diluted 1:1 with 50 mM NH_4HCO_3. Before enzymatic digestion, proteins in the gel pieces were reduced with 45 mM dithiothreitol (DTT) at 55 °C for 30 min and alkylated with 100 mM iodoacetamide in the dark (2x for 15 min each at room temperature). The gel pieces were then washed twice with 50 mM ammonium bicarbonate for 15 min, and a sequential in-gel digestion was performed. Starting with lysyl endopeptidase Lys-C (4 h, 37 °C, 70 ng, mass spectrometry grade, FUJIFILM Wako Pure Chemical Corporation, USA), followed by trypsin (37 °C, overnight incubation, 70 ng modified porcine trypsin, sequencing grade, Promega, Germany) per gel piece (ca. 0.5 ×1.0 cm). Peptides were extracted using 70% ACN, their supernatants were collected and dried with a vacuum centrifuge (vacuum concentrator, Bachofer, Germany).

2.6. LC-MS/MS analysis for determination of the protein corona composition

The LC-MS/MS analysis was conducted using an Ultimate 3000 RSLC (Thermo Fisher Scientific, U.S.A) connected to a Q Exactive HF-X mass spectrometer (Thermo Scientific, U.S.A), following previously described procedures [26]. In summary, the samples were dissolved in solvent A (0.1% formic acid), loaded onto a trap column (PEP-Map100 C18, 75 μm x 2 cm, 3 μm particles, Thermo Fisher Scientific, U.S.A), and separated using a reversed-phase column (PepMap RSLC C18, 75 μm × 50 cm, 2 μm particles, Thermo Scientific, U.S.A) at a flow rate of 250 nL/min. A 30-minute gradient was applied from 3 to 25% solvent B (0.1% formic acid in ACN), followed by a 5-min increase to 40% solvent B. Subsequently, a washing step with 85% solvent B was performed. For data acquisition, a top-fifteen data-dependent method was used. The following proteomic data process was applied: spectra were analyzed using MASCOT V2.6.2 (Matrix Science Limited, UK), using a *Bos taurus* subset of the Uniprot database [61]. Identified proteins were subsequently filtered for an FDR < 1%, a MASCOT score above 50, and a minimum of 2 significant sequences. The resulting proteins were then categorized based on their biological or molecular function according to the UniProt database. The abundance of the categorized proteins was determined by dividing the sum of the emPAI score of the specific category by the sum of the emPAI scores of all found proteins for the distinct polymer particle [62].

2.7. Cell culture

The hepatic macrophage cell line ImKC (Kupffer cells, SCC119) was obtained from Merck (Merck KGaA, Darmstadt, Deutschland) and was cultivated in RPMI1640 supplemented with 2 mM glutamine. Murine macrophages J774A.1 (from ascites, TIB-67), intestinal epithelial-like cells STC − 1 (CRL-3254), and hepatic epithelial cells BNL CL.2 (TIB-73) were obtained from the American Type Culture Collection (ATCC, Manassas, USA). These cells were cultivated in DMEM (J774A.1 in $DMEM_{Lonza}$, STC-1, and BNL CL.2 in $DMEM_{ATCC}$). For J774A.1 cells, the

medium was additionally supplemented with 4 mM glutamine, 24 mM HEPES, and 0.1 mM sodium pyruvate. All media were supplemented with 10% (v/v) FCS and 100 U/mL penicillin/streptomycin, and are referred to as "complete cell medium" throughout the manuscript. The cells were cultivated in a standard cell culture incubator (5% CO_2/ 95% humidity) at 37 °C. For cell maintenance, all cell lines were passaged three times a week. For detaching cells, either at 37 °C pre-warmed citric saline buffer (135 mM potassium chloride - 15 mM sodium citrate, 5- and 10-min incubation at 37 °C for J774A.1 and ImKC, respectively) or 1x Trypsin/EDTA (for STC −1 and BNL CL.2) was used.

2.8. Scanning electron microscopy for particle-cell interaction

The analysis of particle-cell interaction using SEM was performed as described previously [32,63]. In brief, 100,000 cells per slide were seeded on Ø 13 mm NuncTM Thermanox™ slides (Thermo Fisher Scientific, Waltham, MA, USA) and were incubated overnight in complete cell medium at cell culture conditions. Afterward, particle suspensions were added to the cells, corresponding to 30 particles per cell. After an additional 24 h incubation at cell culture conditions, the cells were fixed using Karnovsky's reagent (4% v/v formaldehyde, 5% v/v glutaraldehyde, 32 mM PBS, pH 7.4) for 1 h at RT and afterward dehydrated using an ethanol series of 50%, 70%, 80% for 30 min, 90% and absolute ethanol for 1 h. The overnight air-dried samples were then sputtered with platin, and analyzed using SEM (FEI Apreo Volumescope, Thermo Fisher Scientific, magnification 20,000x, 2 kV, Everhart-Thornley detector).

2.9. Confocal laser scanning microscopy

Cells were seeded with 15,000 cells/well in Ibidi slides (µ-Slide 8 Well, ibiTreat, ibidi GmBH, Gräfelfing, Germany) and incubated for 5 h at cell culture conditions. Afterward, polymer microparticles were added (to a density of 10 particles/cell), and further incubation occurred overnight. For localization of non-fluorescent particles using confocal laser scanning microscopy (CLSM), the cytoplasm of the cells was fluorescence stained using a CellTracker (2 µM in serum-free cell culture medium) for 30 min at 37 °C. In addition, nuclei were stained using Hoechst 33342 (1.5 µg/mL in complete cell medium) for 10 min at 37 °C. After the incubation time, the staining solution was removed and 250 µL of fresh pre-warmed complete cell medium was added. The analysis of the particle-cell interaction at living, non-fixed cells was performed using CSLM with an environmental control chamber (TCS SP8, 63x oil immersion objective, with 3x software zoom, laser: 408 nm, and 552 nm, at 37 °C, 5% CO_2, Leica Microsystems, Wetzlar, Germany). Z-stacks were made with a step size of 0.33 µm.

2.10. Resazurin assay

The resazurin assay was performed as previously described [32]. In brief, the cells were seeded (15,000 cells for J774A.1, ImKC, and BNL CL.2; 20,000 cells for STC-1, three technical replicates) in 48-well plates. After 24 h of incubation, freshly prepared particle suspensions were added ("treated" cells) to yield final concentrations of 20 particles/ cell. As a control, cells were incubated without particles at otherwise identical conditions ("control" cells). After an additional 24 h of incubation, the cell medium was removed, and 350 µL of a 10% (v/v in the respective complete cell culture medium) AlamarBlue solution was added. The samples were incubated for 2.5 h. To estimate the background fluorescence of the AlamarBlue solution (F_{blank}), three wells without cells and particles (i.e., exclusively containing the AlamarBlue solution) were incubated. After incubation, aliquots of the cell culture medium (100 µL) were collected, and the resorufin fluorescence (Ex. 530 nm / Em. 600 nm) was analyzed using a plate reader (Mithras, Berthold Technologies, Bad Wildbad, Germany). The remaining AlamarBlue solution was removed from the wells, and fresh cell culture medium was added. After two, four, and six additional cultivation days, the assay was repeated as described. For the analysis, the mean value of the AlamarBlue control (F_{blank}) was subtracted from each value of the same well plate. The conversion of AlamarBlue of each day (day n) was determined using Eq. (1),

$$AlamarBlue\quad conversion_{day\quad n} = \frac{(F_{sample\quad dn} - F_{blank\quad dn})}{(F_{control\quad d7} - F_{blank\,d7})} \tag{1}$$

With F_{sample} being the fluorescence of the sample (either $F_{treated}$ or $F_{control}$), F_{blank} being the fluorescence of the AlamarBlue control without cells, dn being the incubation of the distinct days (1, 3, 5, and 7 days). Based on these values, the mean value and standard deviation were calculated from three replicates.

2.11. Live/dead staining

To observe potential cytotoxic effects, live/dead staining was performed. Here, the cells were seeded in 48 well plates (50,000 cells/well). The samples were incubated for 24 h under cell culture conditions before adding the particles (at a particle concentration of 30 particles/ cell). Cells in the absence of particles acted as a control. After overnight incubation, the cells were washed twice with 1x DPBS and were stained afterward with calcein-AM (live, 2 µM) and ethidium-homodimer (dead, 4 µM) for 30 min at RT. After washing with 1x DPBS, the samples were analyzed using fluorescence microscopy.

2.12. MTT assay

The influence of MP on the metabolic activity of the cells was analyzed using an MTT assay. This tetrazolium salt-based cell assay is a well-established method for the toxicological assessment of PS microparticles [64–66]. The experiments were performed as previously described [32]. Briefly, cells were seeded at 10,000 cells/well in 96-well plates (100 µL medium per well). For STC-1 cells, the seeding cell density was increased to 25,000 per well to accommodate for the slower growth rate and metabolism. After 24 h of incubation, the medium was aspirated, and 100 µL of the freshly prepared particle suspension was added. The desired particle concentrations were prepared by diluting the particle stock solution with the respective growth medium (1:100 – 1:10000). The cells were then incubated for another 24 h. After the incubation with MP, the medium was aspirated, cells were then washed with DPBS, and 50 µL freshly prepared MTT reagent (1 mg/mL MTT in MEM) was added to each well. After 2 h incubation, the supernatant was removed, and 100 µL of isopropanol were added per well to dissolve the produced formazan crystals. After 5 min of shaking at 600 rpm, the absorbance at 570 nm (reference wavelength 650 nm) was measured using a TECAN GENios Pro plate reader (Tecan Austria GmbH, Gröding). Cells incubated without particles or with 0.3% Triton X-100 in the respective cell culture medium, at otherwise identical conditions, were used as negative and positive controls, respectively.

$$metabolic\quad activity\quad [\%] = \frac{Abs570_{sample}}{Abs570_{blank}} x100 \tag{2}$$

With $Abs_{570\text{-sample}}$ being the mean value of the measured absorption of the test sample, and $Abs_{570\text{-blank}}$ being the mean value of the measured absorption of the negative control.

2.13. Reactive Oxygen species

Reactive oxygen species (ROS) were measured with the membrane-permeable but non-fluorescent dye 2′,7′-dichlorofluorescein diacetate (DCFDA). DCFDA is oxidated inside the cells by ROS to the fluorescent 2′, 7′-dichlorofluorescein (DCF). The fluorescence intensity can be correlated to the amount of ROS inside the cells. Briefly, 150,000 cells per well were seeded in a 12-well plate in 1 mL growth medium and

incubated for 24 h (37 °C, 5% CO_2, 95% humidity). Afterwards, freshly prepared particle suspensions in complete growth medium were added using the respective concentration. 50 μM Antimycin A (5 μM for STC-1) was added in the case of the positive control. After 60 min, 37.5 μM DCFDA (5 μM for STC-1), was added per well, and the cells were incubated for another 24 h. For STC-1, the Antimycin A and DCFDA concentration was lower, since the pre-test showed a reduction in viability at higher concentrations. Cells were then collected, washed in DPBS, and measured using flow cytometry at 525 nm (Cytomics FC500, Beckman Coulter, Krefeld, Germany). The ROS amount was calculated according to Eq. (3).

$$ROS \quad amount \quad [\%] = \frac{MFI_{sample}}{MFI_{NC}} x100 \tag{3}$$

With MFI_{sample} being the mean fluorescence intensity of the green fluorescence of the test sample, MFI_{NC} being the mean fluorescence intensity of the green fluorescence of the negative control (i.e., cells incubated without MP).

2.14. Statistical analysis

Statistical analysis was performed using Origin software 2019b (Origin, Northampton, MA, USA). All data were tested referring to the homogeneity of variances (Levene test). To investigate differences in the size and the proliferation results, a one-way ANOVA with a Tukey post hoc test was used.

3. Results

3.1. Particle properties differ based on the underlying polymer material

Since particle characteristics like surface chemistry, surface charge, or particle size are known to be important for their uptake by cells [45,47–49,51–53], the properties of the used particles were analyzed regarding their surface morphology (scanning electron microscopy (SEM)), size (dynamic light scattering (DLS)), and charge (ζ-potential) (Fig. 1). CA, PE, and PLA showed a more irregular and rough-looking surface morphology compared to PS and PVC particles. Both, biological-derived and potentially biodegradable synthetic polymer types (PLA and CA) further showed a larger size distribution (Fig. 1 A). Nevertheless, all particle diameters were below 3 μm (between 1 - 2.5 μm) according to DLS measurements (Fig. 1 B) and, therefore, in a size range suitable for cellular particle ingestion [32,56,57]. DLS data showed a non-significant trend for particle aggregation after incubation in cell culture medium supplemented with 10% fetal calf serum (FCS), more or less pronounced depending on the polymer type (Fig. 1 B). The

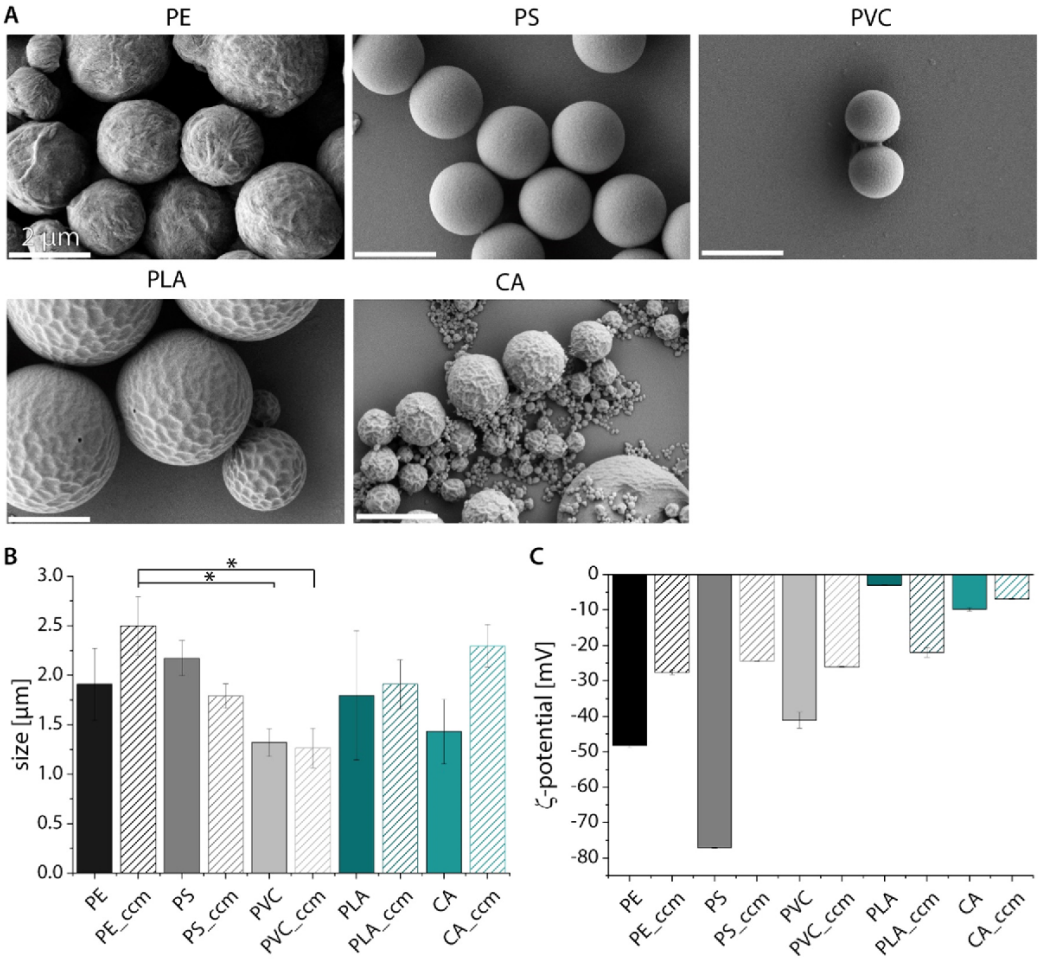

Fig. 1. Particle characterization using scanning electron microscopy (SEM, A; pristine particles), dynamic light scattering (DLS, B; grey: petroleum-based microparticles, green: bio-based microparticles), and ζ-potential (C) measurements. DLS and ζ-potentials were measured directly or after incubation in cell culture medium ("ccm") in 1 mM KCl. DLS and ζ-potential. Data represent mean ± SD, n 3. * $p < 0.05$. Scale bar (SEM): 2 μm.

ζ-potential of the MP differed widely in 1 mM KCl (i.e., PS > PE ≈ PVC > CA > PLA). After incubation in cell culture medium (ccm), the ζ-potential of all MPs aligned around − 25 mV (Fig. 1 C), except for CA particles showing a significantly lower ζ-potential of about − 7 mV. In detail, after ccm treatment, the ζ-potential decreased by approximately 1.5-fold for PE, PVC, and CA and 3.2-fold for PS. In contrast, for PLA, it increased by 7.3-fold. This observed trend in the ζ-potential arises from the interaction involving a comparable composition of serum proteins binding to the surface of the particles [32,60,67]. In most cases (except for CA), the material type does not play an important role in terms of MP surface charge after incubation in cell culture medium.

LC-MS/MS was subsequently used to identify the serum proteins from the medium bound on the particles' surface [60] (Table 1, Fig. 2). For all polymer microparticles, BSA was the most abundant protein in the protein corona according to the emPAI score [68], and only few differences were seen when looking at the next four most abundant proteins (Table 1).

To compare the proteins in the protein corona, they were classified according to the biological process they are involved in or their molecular function. Here, significant differences were identified (Fig. 2).

The protein corona covering PE and PS microparticles showed a similar protein composition regarding proteins that are involved in oxygen transport (PE: 22%, PS: 20%), cell adhesion or cellular mobility (PE and PS: 8%), but differed in the abundance of transporter proteins, which are more often found in the corona of PE (41%, PS: 27%), and uncharacterized proteins, which are more abundant in the corona of PS particles (11%, PE: 2%). Noteworthy, proteins involved in the immune system and the activation of the immune response were mainly found in the corona of PS particles (15%, PE: 8%, PVC: 10%, PLA: 6%), whereas the corona of CA microparticles showed the lowest amount of these proteins in the protein corona (5%). In contrast, the corona of CA particles revealed the highest abundance of ion and metal transporter proteins (39%). PVC and PLA particle coronae showed a high abundance of proteins involved in cellular adhesion and cellular mobility (18% and 16%, respectively). In consequence, whereas the ζ-potential analysis displayed similar values for almost all materials (except CA) after incubation in ccm, the composition of the protein corona apparently depends on the underlying polymer material and, hence, can influence the way MPs interact with cells.

3.2. *Differential analysis of particle uptake as a function of polymer type and cell line*

To investigate the polymer-dependent particle-cell interactions, an analysis of the qualitative cellular uptake was done as previously described for comparable PS particles [32] for chosen four murine cell lines (macrophages (J774A.1 and ImKC) and epithelial cells (STC-1 and BNL CL.2)). The qualitative uptake analysis was done as previously described for comparable PS particles. The MP ingestion was analyzed using scanning electron microscopy (SEM, Fig. 3) and confocal laser scanning microscopy (CLSM, Fig. 4). PS particles were additionally used for comparison.

Both macrophage cell lines took up PS particles (Figs. 3, 4),

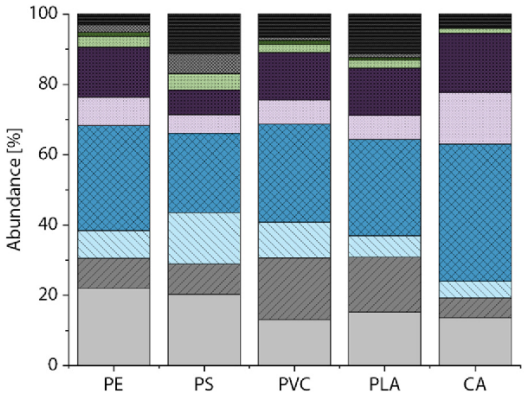

Fig. 2. Classification of identified proteins after quantitative analysis of the protein corona composition after incubation in cell culture medium using LC-MS/MS. The proteins were categorized according to the biological process they are involved in or their molecular function, namely oxygen transport, cell adhesion/ cytoskeleton/ cell mobility, immunity/ immune system, ion or metal transport, lipid transport/ lipid metabolism, protease inhibitor, protease/ hydrolase/ peroxidase, protein transport, transport proteins (vitamins, hormones) and other.

consistent with previously published data, where PS particles with a diameter < 10 μm were ingested by macrophage cell lines [32,55–57]. Additionally, macrophage cell lines (J774A.1 and ImkC, Fig. 3) ingested PLA particles. In case of polymer particles made of CA, PE, and PVC, the ingestion by macrophages (J774A.1 and ImKC) could only be indicated using SEM (Fig. 3). CLSM analysis was performed to confirm MP engulfment, i.e., by getting a virtual cross-section through the cells by fluorescent staining the cytoplasm and nuclei (Fig. 4). With this method, MP ingestion could be verified for all MP types, and the ingested particles could be identified as grey and white spots in the red-stained cytoplasm (Fig. 4, white arrows). Multiple CA particles were detected near macrophage cells, suggesting that their ingestion was comparatively less effective or preferred when compared to the other types of microplastic particles analyzed.

Hepatic epithelial cells (BNL CL.2) ingested PS particles (Fig. 3), as reported previously [32]. Using CLSM, the ingestion of CA particles was also observed (Fig. 4), but not the uptake of other MP (PE, PLA, PVC). In case of intestinal epithelial cells (STC-1), no particle ingestion was observed at all using SEM (Fig. 3) and CLSM (Fig. 4). Nevertheless, particle-cell interactions could be seen for all MP types, whereby the interaction with CA particles was less frequent than for the other MPs (Fig. 4). The lack of microparticle ingestion in STC-1 cells coincides with the lack of appropriate uptake mechanisms for macrometer-sized material, like phagocytosis or macropinocytosis as previously reported [32, 69,70].

Table 1
Quantitative analysis of the protein corona composition after incubation in cell culture medium using LC-MS/MS. Listing of the five most abundant proteins found in the protein corona for each polymer type. The complete list can be found in Table S1. The emPAI value, given in brackets, allows estimation of the protein abundance.

PE	PS	PVC	PLA	CA
BSA (13.12)	BSA (7.32)	BSA (3.18)	BSA (2.38)	BSA (1.88)
Hemoglobin fetal subunit β (9.02)	Hemoglobin fetal subunit β (5.32)	Hemoglobin fetal subunit β (1.51)	Hemoglobin fetal subunit β (1.51)	Apolipoprotein A-I (1.68)
Apolipoprotein A-I (3.97)	Globin A1 (2.99)	Keratin, type I cytoskeletal 14 (1.28)	Uncharacterized protein (1.20)	Serotransferrin (1.13)
Serotransferrin (3.33)	Hemoglobin β (2.17)	Globin C1 (1.07)	Globin C1 (1.07)	Hemoglobin fetal subunit β (1.00)
Globin C1 (2.35)	α-2-HS-glycoprotein (1.61)	Serotransferrin (1.03)	α-2-HS-glycoprotein (0.95)	Globin C1 (0.62)

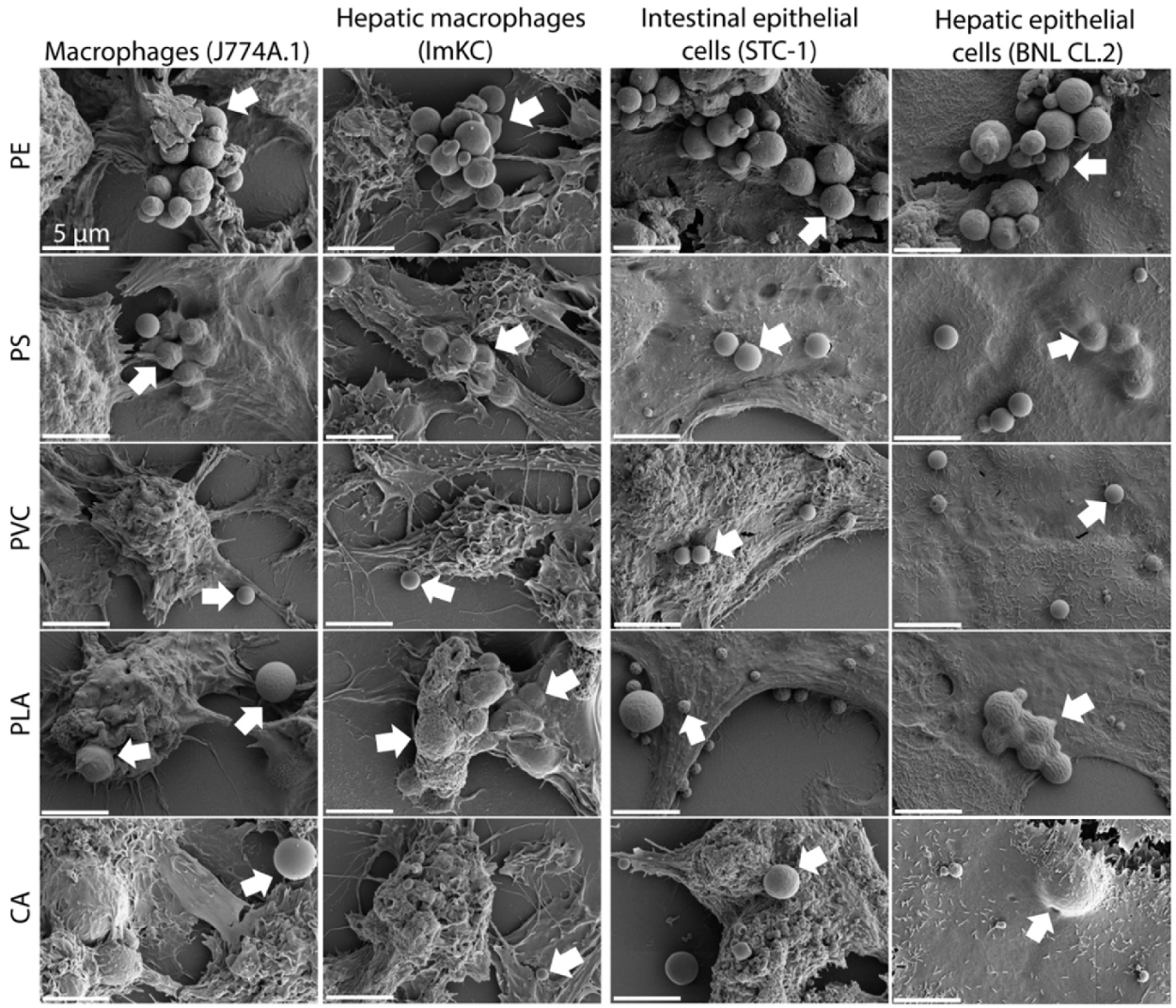

Fig. 3. Particle uptake by macrophages (J774A.1 and ImKC) and epithelial cells (intestinal: STC-1 and hepatic: BNL CL.2) analyzed using scanning electron microscopy (SEM). White arrows point to polymer particles as an example. For each polymer particle type, 30 particles per cell were added. Scale bars: 5 µm.

3.3. *Influence of polymer particles on cellular reactions*

Putative cellular effects caused by the interaction with MP were analyzed using live/dead staining, as well as the resazurin, MTT, and ROS assays. This allowed us to identify different noxic effects such as immediate toxicity (live/dead staining), the effect on the proliferative capacity of the cells (resazurin assay), the effect of MP on metabolic activity (MTT assay), and the impact on the amount of intracellular reactive oxygen species (ROS assay). For all MP types, no cytotoxicity was observed using live/dead staining (Fig. S2), and the resazurin assay (Fig. S3). The MTT assay revealed a marginal reduction in metabolic activity following PVC incubation at the highest concentration (100 MP/cell) for J774A.1, ImKC, and STC-1 cells, as opposed to the metabolic activity observed with PS or the control group without particles (referred to as "mock") (Table S2). ImKC cells showed additionally slightly reduced metabolic activity for PE particles at the highest concentration. For PLA particles, a slightly reduced metabolic activity was detected in BNL CL.2 cells at the highest particle concentration. Overall, MTT results also indicate low toxicity (metabolic activity always > 80%). However, no general clear trend could be identified regarding cell line or polymer type-specific cellular stress response. For example, BNL CL.2 cells did not show a decreased metabolic activity at the highest concentration of PVC particles, whereas this was the case in the other cell lines. The observed decrease in metabolic activity was minor and specifically evident only at the highest particle concentration. This might be indicative of mechanical stress on the cells, likely resulting from an excess of particles within the system.

In the case of macrophage cell lines (J774A.1 and ImKC), incubation with PLA particles led to a noteworthy elevation in ROS levels (Fig. 5). This increase in ROS levels was not apparent in epithelial cells, possibly due to the absence of particle ingestion by these cells. Moreover, the augmented ROS levels were more pronounced at higher particle concentrations compared to lower ones, suggesting a cellular response linked to the ingestion of particles. Noteworthy, an incubation with CA particles showed a statistically significant increase in the amount of ROS in all cell lines at higher particle concentrations. In this context, the lowest increase was observed for STC-1 epithelial cells and the highest for J774A.1 macrophage cells. This again correlates with the ingestion

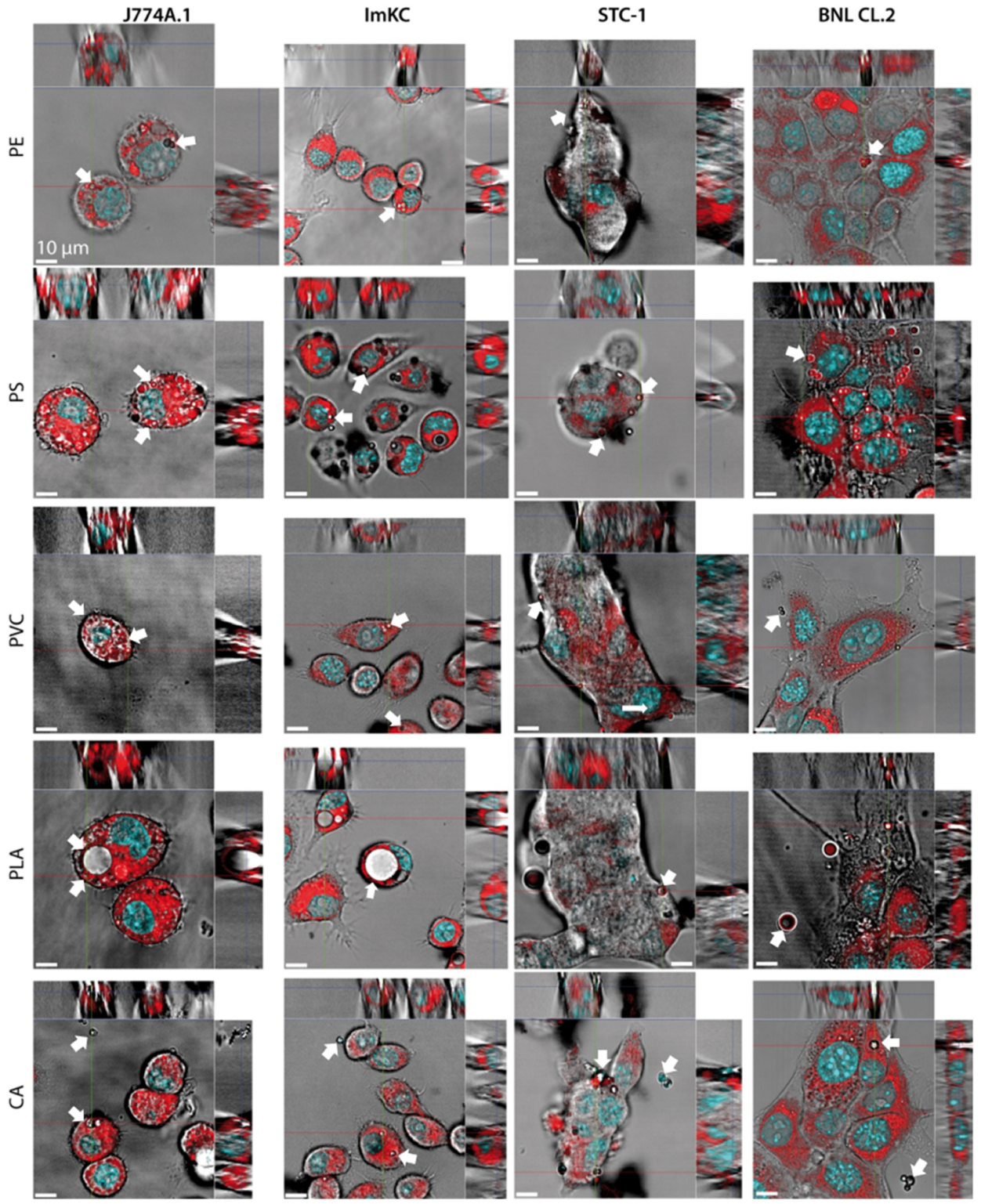

Fig. 4. Particle ingestion analysis in macrophage (J774A.1, ImKC) and epithelial cells (STC-1, BNL CL.2) using confocal laser scanning microscopy (CLSM). 10 non-fluorescent particles per cell were added. The cytoplasm (CellTracker, red) and nuclei (Hoechst, blue) were fluorescently stained. White arrows show exemplary microparticles. Scale bars: 10 µm. The corresponding fluorescence images (without brightfield) are shown in Fig. S1.

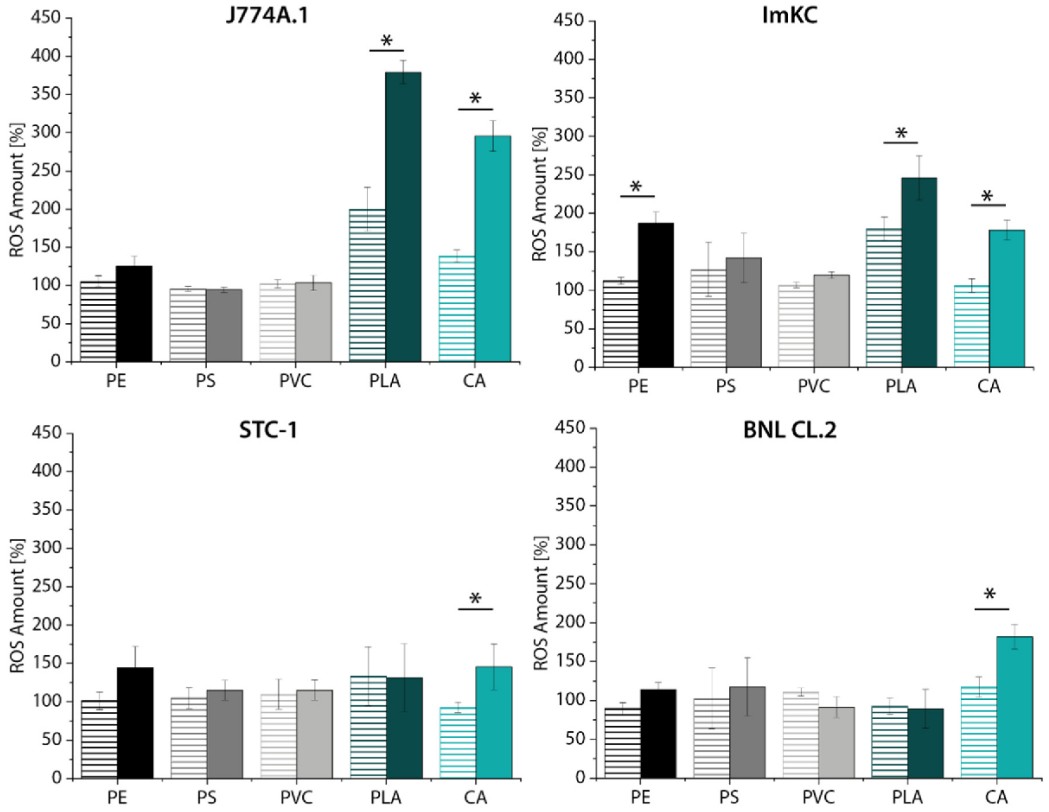

Fig. 5. ROS assays for all cell lines incubated with different polymer microparticles. ROS of the whole cell population was induced with two different particle concentrations (striped bars: low concentration, filled bars: high concentration). 100% ROS amount is depicted from a negative control without particles. Data represent mean ± SD, n 3. * $p < 0.05$. Data for PS particles are taken from [32].

rate of the CA particles.

No cell line showed a significant change in ROS amount upon the incubation with PS and PVC particles. In case of PE particle incubation, all cell lines showed a higher ROS amount at higher particle concentrations compared to low concentrations.

4. Discussion

This work analyzed the uptake and cytotoxic effects of pristine microparticles from synthetic polymers (PS, PE, PVC) and polymers derived from biological sources (PLA and CA) with a narrow size range between 1 - 4 μm. The investigated polymer microparticles showed polymer-specific particle properties and cellular interaction, as well as distinct cellular effects (Fig. 6).

The ζ-potential of the pristine particles varied between − 77 mV (PS) and − 3 mV (PLA). The variation was toned down after the incubation in serum-containing medium. While the ζ-potential after incubation in cell culture medium and the ingestion rate were indistinguishable for most particles, CA showed lower values in both. Both parameters, the ζ-potential, and the ingestion rate are highly coherent, explaining this observation. The ζ-potential influences the particle-cell interaction, and, therefore, enhances the ingestion by cells [47,63]. The surface charge further influences the protein corona formation, which is expected to have an additional influence on particle-cell interactions [47,50,63,71]. The formation of a protein corona on the surface of particles is primarily governed by the interplay of protein-particle interactions and protein-protein interactions [50,72,73]. Several factors influence this process, including the individual protein's abundance in the surrounding medium (meaning that highly abundant proteins tend to be more prevalent in the protein corona), the secondary structure of the proteins, and the hydrophobicity of the polymer particles [50,72,73]. It is important to note that since all polymer particles were exposed to the same cell culture medium (i.e., same protein cocktails), any discrepancies in the composition of the protein corona are predominantly driven by the varying hydrophobic nature of the polymer particles, which, in turn, impacts the proteins' affinity for binding to the particle's surface. In this context, few immune proteins were found in the CA protein corona. In contrast, PS showed a high abundance of immune system-related proteins, correlating with the high number of immunoglobulins in the serum (the cell culture medium contained 10% (v/v) fetal calf serum). The protein composition could influence particle ingestion, as macrophages are recognized for their phagocytic capabilities, a process governed by receptor-mediated endocytosis mechanisms [32,56,57]. Proteins like fetuin or complement c3, i.e. opsonins, which were found in the protein coronae, interact with cell membrane receptors and initiate phagocytosis in macrophages [74–76]. As a result, polymer particles with elevated levels of opsonin proteins within the protein corona, such as PS, PE, and PVC, may exhibit greater recognition and ease of internalization compared to polymer particles with fewer opsonin proteins, as seen with CA. Furthermore, polymer-specific surface groups can interact uniquely with the cellular membrane. Recently, Kuroiwa *et al.* showed an aromatic-aromatic interaction between a macrophage receptor (TIM-4) and the aromatic side chain of polystyrene particles [77].

Regarding the particle toxicity, no acute cytotoxic effects were observed at the concentrations employed for any of the tested particles. Nevertheless, distinct cellular reactions were found when analyzing the ROS amount. This corroborates previously published results, where no

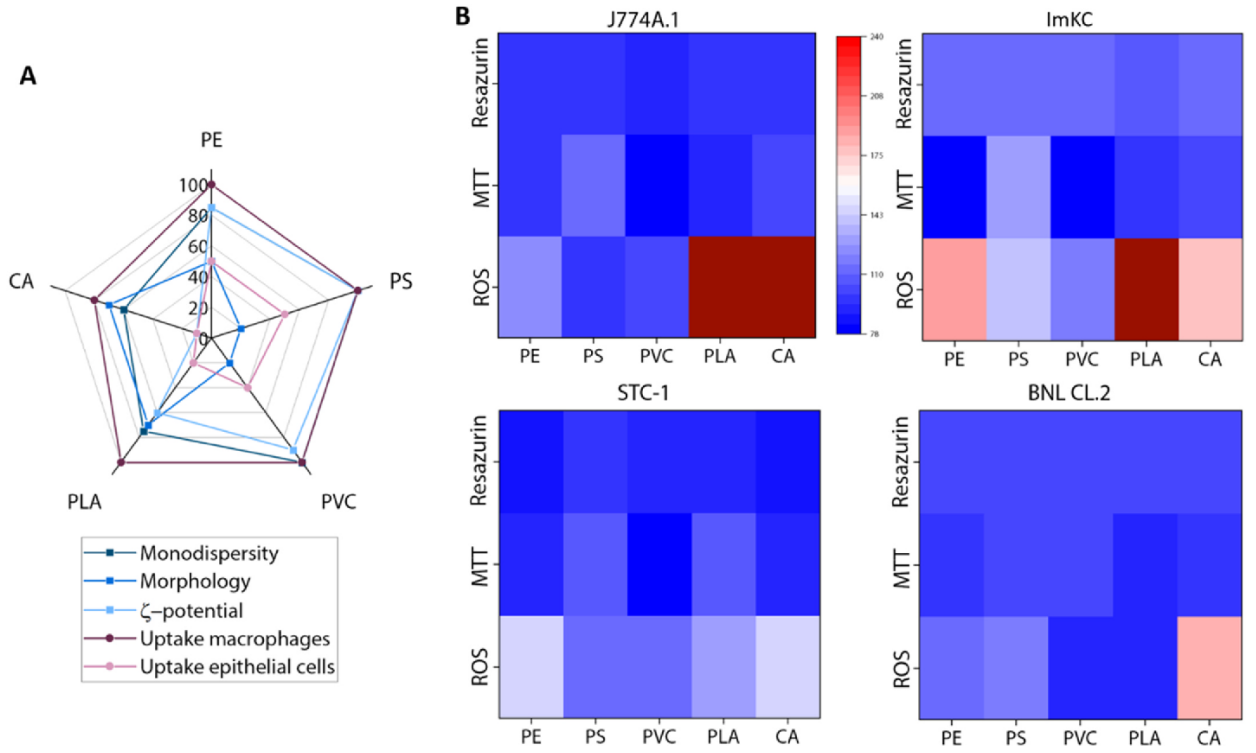

Fig. 6. Overview of particle properties, ingestion behavior (A), and cellular response (B) of all polymer particles. A: Particle properties: monodispersity based on SEM images, surface morphology ("Morphology, prominent surface morphology, based on SEM images), ζ-potential in cell culture medium ("ζ-potential" in the same range as for the other MPs). Uptake in macrophages and epithelial cells: ingestion based on SEM and CLSM. B: Heat maps for the three different used cytotoxicity assays (Resazurin day 7, MTT, and ROS: highest used concentrations).

immediate cytotoxicity and low changes in the metabolic activity were found, but significant effects regarding the intracellular ROS or cytokine production [32,34]. However, all of these increases were solely evident at the highest particle concentration employed. Notably, the most substantial rise in ROS levels was elicited by both bio-based particles ($CA_{1.5\,\mu m}$, $PLA_{2\,\mu m}$). These ROS levels (380% at J774A.1% and 250% at ImKC) are of some concern and must be addressed in further studies. This contradicts the common use of biopolymers as antioxidant coating agents in applications like food packaging or medical implants [78]. However, since the biopolymers are often used as coating agents rather than in particulate form in these applications, the observed differences could be due to this difference in the polymers' shape. For CA particles, the SEM images showed a less monodisperse particle size distribution, and it should be kept in mind, that the combination of micro- and nanoparticles already showed a higher toxicity in mice than the usage of homogeneous particle sizes, which could additionally influence the cytotoxicity of CA particles [79]. Additionally, the potential impact of biological and intracellular degradation should be considered when working with biopolymers, even though the incubation period (24 h) in the utilized setup was relatively short. [80,81]. For PE particles, a low cellular response was found in all cell lines using the ROS assay, in accordance with the fact that these particles were not ingested by all cells. On the other hand, the tendency of PE particles to aggregate (Fig. 3) could induce mechanical stress on the cells. Such aggregation behavior was already previously described for PE, and cellular effects like increased cytokine release were observed [40,82].

Taken all the results together, we were able to show that microparticles made of PE, PS, PVC, PLA, and CA, differ in their pristine particle properties, where especially the respective particle surface, i.e. the ζ-potential and the resulting protein corona composition, proved to be highly relevant for particle-cell interaction. However, no induced cellular toxicity could be observed at environmentally relevant particle concentrations. Naturally, these model particles do not reflect a picture of effects that might occur within a natural environment, where particles will be weathered, contain additives, or have an eco-corona [34,82,83]. Different polymers will not only be covered by unique protein coronae (as shown above) but will also be differently influenced by weathering. It is therefore highly recommended that more studies with different polymer types than PS are conducted to unravel their distinct cellular responses.

Funding

This work was supported by the Deutsche Forschungsgemeinschaft (DFG, German Research Foundation) - project number 391977956 - SFB 1357/A05 (T.S., R.F.) and A01 (T.F.).

Declaration of Competing Interest

The authors declare that they have no known competing financial interests or personal relationships that could have appeared to influence the work reported in this paper.

Data Availability

Data will be made available on request.

Acknowledgments

We thank Daniel Wagner for the measurement of the particle size

distribution of PE particles.

Authors' contributions

JJ, MV, MVW, VJ, RF, TF, and TS designed the experiments. JJ performed the particle analysis and cell ingestion experiments, as well as the live-dead staining and resazurin assay. MVW performed the LC-MS/MS analysis and editing of the data. MV provided MTT and ROS cell assays. VJ, RF, TF, and TS supervised the experiments. JJ analyzed the data and created the figures. JJ, MV, MVW, VJ, RF, TF, and TS wrote the manuscript. VJ, RF, TF, and TS reviewed and edited the manuscript and supervised it during the experiments.

Environmental Implication

Our study contributes to a better understanding of microplastics toxicology, which appears to be dependent on cell type . This information is essential, as sound knowledge on the characteristics driving microplastic toxicity on organisms may explain the often contradictory results observed in effect studies on microplastics and will help to advance risk assessment for microplastic particles.

Appendix A. Supporting information

Supplementary data associated with this article can be found in the online version at doi:10.1016/j.jhazmat.2023.133280.

References

[1] Andrews, S., 2010. Additives. Encyclopedia of Polymer Science and Technology. Wiley.
[2] Hartmann, N.B., et al., 2019. Are we speaking the same language? Recommendations for a Definition And Categorization Framework For Plastic Debris. ACS Publications,.
[3] Wiesinger, H., Wang, Z., Hellweg, S., 2021. Deep dive into plastic monomers, additives, and processing aids. Environ Sci Technol 55, 9339–9351.
[4] Cole, M., et al., 2013. Microplastic ingestion by zooplankton. Environ Sci Technol 47, 6646–6655.
[5] Luijsterburg, B., Goossens, H., 2014. Assessment of plastic packaging waste: material origin, methods, properties. Resour, Conserv Recycl 85, 88–97.
[6] Aljaibachi, R., Callaghan, A., 2018. Impact of polystyrene microplastics on Daphnia magna mortality and reproduction in relation to food availability. PeerJ 6, e4601.
[7] Campanale, C., Massarelli, C., Savino, I., Locaputo, V., Uricchio, V.F., 2020. A detailed review study on potential effects of microplastics and additives of concern on human health. Int J Environ Res Public Health 17, 1212.
[8] Brachner, A., et al., 2020. Assessment of human health risks posed by nano-and microplastics is currently not feasible. Int J Environ Res Public Health 17, 8832.
[9] Andrady, A.L., 1998. Biodegradation of plastics: monitoring what happens. Plastics Additives. Springer, pp. 32–40.
[10] Julienne, F., Delorme, N., Lagarde, F., 2019. From macroplastics to microplastics: role of water in the fragmentation of polyethylene. Chemosphere 236, 124409.
[11] Meides, N., et al., 2021. Reconstructing the environmental degradation of polystyrene by accelerated weathering. Environ Sci Technol 55, 7930–7938.
[12] Frias, J.P.G.L., Nash, R., 2019. Microplastics: finding a consensus on the definition. Mar Pollut Bull 138, 145–147.
[13] Fred-Ahmadu, O.H., et al., 2020. Interaction of chemical contaminants with microplastics: principles and perspectives. Sci Total Environ 706, 135978.
[14] Klein, S., Worch, E., Knepper, T.P., 2015. Occurrence and spatial distribution of microplastics in river shore sediments of the rhine-main area in Germany. Environ Sci Technol 49, 6070–6076.
[15] Dris, R., Gasperi, J., Saad, M., Mirande, C., Tassin, B., 2016. Synthetic fibers in atmospheric fallout: a source of microplastics in the environment? Mar Pollut Bull 104, 290–293.
[16] Rillig, M.C., Lehmann, A., 2020. Microplastic in terrestrial ecosystems. Science 368, 1430–1431.
[17] Wang, F., et al., 2021. Microplastic abundance and distribution in a Central Asian desert. Sci Total Environ 800, 149529.
[18] Havstad, M.R., 2020. Biodegradable plastics. Plastic Waste and Recycling. Elsevier, pp. 97–129.
[19] Filiciotto, L., Rothenberg, G., 2021. Biodegradable plastics: standards, policies, and impacts. ChemSusChem 14, 56–72.
[20] Ghosh, K., Jones, B.H., 2021. Roadmap to biodegradable plastics—current state and research needs. ACS Sustain Chem Eng 9, 6170–6187.
[21] Leitner, L.C., et al., 2023. Efficient synthesis and wetting characteristics of amphiphilic galactose–PLA block copolymers: a potential additive for the accelerated biodegradation of micro-and nanoplastics. Macromol Chem Phys 224, 2100431.
[22] Rohrl, M., et al., 2023. New functional polymer materials via click chemistry-based modification of cellulose acetate. ACS Omega.
[23] von Moos, N., Burkhardt-Holm, P., Köhler, A., 2012. Uptake and effects of microplastics on cells and tissue of the Blue Mussel Mytilus edulis L. after an experimental exposure. Environ Sci Technol 46, 11327–11335.
[24] Wright, S.L., Thompson, R.C., Galloway, T.S., 2013. The physical impacts of microplastics on marine organisms: a review. Environ Pollut 178, 483–492.
[25] Jin, Y., Lu, L., Tu, W., Luo, T., Fu, Z., 2019. Impacts of polystyrene microplastic on the gut barrier, microbiota and metabolism of mice. Sci Total Environ 649, 308–317.
[26] Trotter, B., et al., 2021. Long-term exposure of *Daphnia magna* to polystyrene microplastic (PS-MP) leads to alterations of the proteome, morphology and life-history. Sci Total Environ 795, 148822.
[27] Brehm, J., et al., 2022. In-depth characterization revealed polymer type and chemical content specific effects of microplastic on Dreissena bugensis. J Hazard Mater 437, 129351.
[28] Lu, L., Wan, Z., Luo, T., Fu, Z., Jin, Y., 2018. Polystyrene microplastics induce gut microbiota dysbiosis and hepatic lipid metabolism disorder in mice. Sci Total Environ 631-632, 449–458.
[29] Yong, C.Q.Y., Valiyaveetill, S., Tang, B.L., 2020. Toxicity of microplastics and nanoplastics in mammalian systems. Int J Environ Res Public Health 17, 1509.
[30] Rahman, A., Sarkar, A., Yadav, O.P., Achari, G., Slobodnik, J., 2021. Potential human health risks due to environmental exposure to nano-and microplastics and knowledge gaps: a scoping review. Sci Total Environ 757, 143872.
[31] Schirinzi, G.F., et al., 2017. Cytotoxic effects of commonly used nanomaterials and microplastics on cerebral and epithelial human cells. Environ Res 159, 579–587.
[32] Rudolph, J., Völkl, M., Jérôme, V., Scheibel, T., Freitag, R., 2021. Noxic effects of polystyrene microparticles on murine macrophages and epithelial cells. Sci Rep 11, 1–16.
[33] Palaniappan, S., Sadacharan, C.M., Rostama, B., 2022. Polystyrene and polyethylene microplastics decrease cell viability and dysregulate inflammatory and oxidative stress markers of MDCK and L929 cells in vitro. Expo Health 14, 75–85.
[34] Völkl, M., et al., 2022. Pristine and artificially-aged polystyrene microplastic particles differ in regard to cellular response. J Hazard Mater 435, 128955.
[35] Stock, V., et al., 2019. Uptake and effects of orally ingested polystyrene microplastic particles in vitro and in vivo. Arch Toxicol 93, 1817–1833.
[36] Goodman, K.E., Hare, J.T., Khamis, Z.I., Hua, T., Sang, Q.-X.A., 2021. Exposure of human lung cells to polystyrene microplastics significantly retards cell proliferation and triggers morphological changes. Chem Res Toxicol 34, 1069–1081.
[37] Jeon, S., et al., 2021. The reactive oxygen species as pathogenic factors of fragmented microplastics to macrophages. Environ Pollut 281, 117006.
[38] Jeon, S., et al., 2023. Size- and oxidative potential-dependent toxicity of environmentally relevant expanded polystyrene styrofoam microplastics to macrophages. J Hazard Mater 459, 132295.
[39] Kor, K., Mehdinia, A., 2020. Neustonic microplastic pollution in the Persian Gulf. Mar Pollut Bull 150, 110665.
[40] Busch, M., Kämpfer, A.A., Schins, R.P., 2021. An inverted in vitro triple culture model of the healthy and inflamed intestine: adverse effects of polyethylene particles. Chemosphere 284, 131345.
[41] Olivier, V., Duval, J.-L., Hindie, M., Pouletaut, P., Nagel, M.-D., 2003. Comparative particle-induced cytotoxicity toward macrophages and fibroblasts. Cell Biol Toxicol 19, 145–159.
[42] Stock, V., et al., 2021. Uptake and cellular effects of PE, PP, PET and PVC microplastic particles. *Toxicol* Vitr 70, 105021.
[43] Lundqvist, M., et al., 2008. Nanoparticle size and surface properties determine the protein corona with possible implications for biological impacts. Proc Natl Acad Sci 105, 14265.
[44] Bilardo, R., Traldi, F., Vdovchenko, A., Resmini, M., 2022. Influence of surface chemistry and morphology of nanoparticles on protein corona formation. WIREs Nanomed Nanobiotechnol 14, e1788.
[45] Tabata, Y., Ikada, Y., 1988. Effect of the size and surface charge of polymer microspheres on their phagocytosis by macrophage. Biomaterials 9, 356–362.
[46] Gaumet, M., Gurny, R., Delie, F., 2009. Localization and quantification of biodegradable particles in an intestinal cell model: the influence of particle size. Eur J Pharm Sci 36, 465–473.
[47] Fröhlich, E., 2012. The role of surface charge in cellular uptake and cytotoxicity of medical nanoparticles. Int J Nanomed 7, 5577.
[48] Kettler, K., Veltman, K., van de Meent, D., van Wezel, A., Hendriks, A.J., 2014. Cellular uptake of nanoparticles as determined by particle properties, experimental conditions, and cell type. Environ Toxicol Chem 33, 481–492.
[49] Caracciolo, G., et al., 2015. Stealth effect of biomolecular corona on nanoparticle uptake by immune cells. Langmuir 31, 10764–10773.
[50] Tenzer, S., et al., 2013. Rapid formation of plasma protein corona critically affects nanoparticle pathophysiology. Nat Nanotechnol 8, 772.
[51] Corbo, C., et al., 2016. The impact of nanoparticle protein corona on cytotoxicity, immunotoxicity and target drug delivery. Nanomedicine 11, 81–100.
[52] Kurtz-Chalot, A., et al., 2017. Impact of silica nanoparticle surface chemistry on protein corona formation and consequential interactions with biological cells. Mater Sci Eng: C 75, 16–24.
[53] Kihara, S., et al., 2021. Cellular interactions with polystyrene nanoplastics—the role of particle size and protein corona. Biointerphases 16, 041001.
[54] Aderem, A., Underhill, D.M., 1999. Mechanisms of phagocytosis in macrophages. Annu Rev Immunol 17, 593–623.

[55] Champion, J.A., Mitragotri, S., 2006. Role of target geometry in phagocytosis. Proc Natl Acad Sci 103, 4930–4934.
[56] Bruinink, A., Wang, J., Wick, P., 2015. Effect of particle agglomeration in nanotoxicology. Arch Toxicol 89, 659–675.
[57] Stock, V., et al., 2020. Impact of artificial digestion on the sizes and shapes of microplastic particles. Food Chem Toxicol 135, 111010.
[58] Sawalha, H., Purwanti, N., Rinzema, A., Schroën, K., Boom, R., 2008. Polylactide microspheres prepared by premix membrane emulsification—effects of solvent removal rate. J Membr Sci 310, 484–493.
[59] Von Smoluchowski, M., 1906. Zur kinetischen theorie der brownschen molekularbewegung und der suspensionen. Ann der Phys 326, 756–780.
[60] Jasinski, J., et al., 2022. Tailor-made protein corona formation on polystyrene microparticles and its effect on epithelial cell uptake. ACS Appl Mater Interfaces 14, 47277–47287.
[61] Consortium, T.U., 2022. UniProt: the universal protein knowledgebase in 2023. Nucleic Acids Res 51, D523–D531.
[62] Ishihama, Y., et al., 2005. Exponentially modified protein abundance index (emPAI) for estimation of absolute protein amount in proteomics by the number of sequenced peptides per protein*s. Mol Cell Proteom 4, 1265–1272.
[63] Ramsperger, A., et al., 2022. Supposedly identical microplastic particles substantially differ in their material properties influencing particle-cell interactions and cellular responses. J Hazard Mater 425, 127961.
[64] Wang, Z.-Y., Burlak, C., Klaunig, J.E., Kamendulis, L.M., 2014. Development of a cytokine-producing immortalized murine Kupffer cell line. Cytokine 70, 165–172.
[65] Hester, M., et al., 2019. Multi-endpoint toxicological assessment of polystyrene nano-and microparticles in different biological models in vitro. Toxicol Vitr 61, 104610.
[66] Hwang, J., et al., 2020. Potential toxicity of polystyrene microplastic particles. Sci Rep 10 (1), 12.
[67] Riedl, S.A., et al., 2022. In vitro cultivation of primary intestinal cells from Eisenia fetida as basis for ecotoxicological studies. Ecotoxicology 31, 221–233.
[68] Ishihama, Y., et al., 2005. Exponentially modified protein abundance index (emPAI) for estimation of absolute protein amount in proteomics by the number of sequenced peptides per protein*s. Mol Cell Proteom 4, 1265–1272.
[69] Shah, B., Kona, S., Gilbertson, T.A., Nguyen, K.T., 2011. Effects of poly-(Lactide-Co-Glycolide) nanoparticles on electrophysiological properties of enteroendocrine cells. J Nanosci Nanotechnol 11, 3533–3542.
[70] Kamakura, R., Raza, G.S., Prasannan, A., Walkowiak, J., Herzig, K.-H., 2020. Dipeptidyl peptidase 4 and GLP-1 interplay in STC-1 and GLUTag cell lines. Peptides 170419 (().
[71] Partikel, K., Korte, R., Mulac, D., Humpf, H.-U., Langer, K., 2019. Serum type and concentration both affect the protein-corona composition of PLGA nanoparticles. Beilstein J Nanotechnol 10, 1002–1015.
[72] Nguyen, V.H., Lee, B.-J., 2017. Protein corona: a new approach for nanomedicine design. Int J Nanomed 3137–3151.
[73] Gorshkov, V., Bubis, J.A., Solovyeva, E.M., Gorshkov, M.V., Kjeldsen, F., 2019. Protein corona formed on silver nanoparticles in blood plasma is highly selective and resistant to physicochemical changes of the solution. Environ Sci: Nano 6, 1089–1098.
[74] Wang, H., et al., 1998. Fetuin (α2-HS-glycoprotein) opsonizes cationic macrophagedeactivating molecules. Proc Natl Acad Sci 95, 14429–14434.
[75] Lausen, M., et al., 2018. Complement C3 opsonization of Chlamydia trachomatis facilitates uptake in human monocytes. Microbes Infect 20, 328–336.
[76] Brown, E.J., 1992. Complement receptors, adhesion, and phagocytosis. Infect Agents Dis 1, 63–70.
[77] Kuroiwa, M., et al., 2023. Tim4, a macrophage receptor for apoptotic cells, binds polystyrene microplastics via aromatic-aromatic interactions. Sci Total Environ 875, 162586.
[78] Sivakanthan, S., Rajendran, S., Gamage, A., Madhujith, T., Mani, S., 2020. Antioxidant and antimicrobial applications of biopolymers: a review. Food Res Int 136, 109327.
[79] Liang, B., et al., 2021. Underestimated health risks: polystyrene micro- and nanoplastics jointly induce intestinal barrier dysfunction by ROS-mediated epithelial cell apoptosis. Part Fibre Toxicol 18, 20.
[80] Da Silva, D., et al., 2018. Biocompatibility, biodegradation and excretion of polylactic acid (PLA) in medical implants and theranostic systems. Chem Eng J 340, 9–14.
[81] Zielhuis, S.W., et al., 2007. Long-term toxicity of holmium-loaded poly (L-lactic acid) microspheres in rats. Biomaterials 28, 4591–4599.
[82] Deng, J., et al., 2022. Microplastics released from food containers can suppress lysosomal activity in mouse macrophages. J Hazard Mater, 128980.
[83] Barrick, A., et al., 2021. Plastic additives: challenges in ecotox hazard assessment. PeerJ 9, e11300.

Supplement Information

Influence of the polymer type of a microplastic challenge on the reaction of murine cells

Julia Jasinski[1], Matthias Völkl[2], Magdalena V. Wilde[3], Valérie Jérôme[2], Thomas Fröhlich[3], Ruth Freitag[2,5], Thomas Scheibel[1,4,5,6,7]

[1] Biomaterials, Faculty of Engineering Sciences, University of Bayreuth, Bayreuth, Germany
[2] Process Biotechnology, Faculty of Engineering Sciences, University of Bayreuth, Bayreuth, Germany
[3] Gene Center Munich, Laboratory for Functional Genome Analysis (LAFUGA), LMU München, Munich, Germany
[4] Bayreuth Center for Colloids and Interfaces (BZKG), University of Bayreuth, Bayreuth, Germany
[5] Bayreuth Center for Molecular Biosciences (BZMB), University of Bayreuth, Bayreuth, Germany
[6] Bayreuth Center for Material Science (BayMAT), University of Bayreuth, Bayreuth, Germany
[7] Bavarian Polymer Institute (BPI), University of Bayreuth, Bayreuth, Germany

Table S1. Complete list of identified proteins in the corona using LC-MS/MS. Pristine polymer particles were incubated in the serum-containing cell culture medium. The emPAI value, which allows the estimation of protein abundance, is given in brackets.

PS	PE	PVC	PLA	CA
BSA (7.32)	BSA (13.12)	BSA (3.18)	BSA (2.38)	BSA (1.88)
Hemoglobin fetal subunit β (5.32)	Hemoglobin fetal subunit β (9.02)	Hemoglobin fetal subunit β (1.51)	Hemoglobin fetal subunit β (1.51)	Apolipoprotein A-I (1.68)
Globin A1 (2.99)	Apolipoprotein A-I (3.97)	Keratin, type I cytoskeletal 14 (1.28)	Uncharacterized protein OS=Bos taurus OX=9913 PE=4 SV=1 (1.20)	Serotransferrin (1.13)
Hemoglobin β (2.17)	Serotransferrin (3.33)	Globin C1 (1.07)	Globin C1 (1.07)	Hemoglobin fetal subunit β (1.00)
α-2-HS-glycoprotein (1.61)	Globin C1 (2.35)	Serotransferrin (1.03)	α -2-HS-glycoprotein (0.95)	Globin C1 (0.62)
Serotransferrin (1.45)	Globin A1 (2.17)	α -2-HS-glycoprotein (0.95)	Apolipoprotein A-I (0.85)	α -2-HS-glycoprotein (0.61)
Pancreatic adenocarcinoma upregulated factor-like (1.38)	α -2-HS-glycoprotein (2.16)	Actin, cytoplasmic 1 (0.71)	Keratin 3 (0.80)	Actin, cytoplasmic 1 (0.43)
Apolipoprotein A-I (1.37)	Actin, cytoplasmic 1 (1.67)	Uncharacterized protein OS=Bos taurus OX=9913 PE=4 SV=1 (0.68)	Actin, cytoplasmic 1 (0.71)	α -2-macroglobulin variant 4 (0.42)
Uncharacterized protein OS=Bos taurus OX=9913 PE=4 SV=1 (1.18)	α -1-antiproteinase (1.64)	α -1-antiproteinase (0.63)	Serotransferrin (0.60)	α -2-macroglobulin variant 20 (0.41)
Actin, cytoplasmic 1 (1.04)	Hemoglobin β (1.51)	Keratin 1 (0.61)	α -1-antiproteinase (0.50)	α -1-antiproteinase (0.38)
Peptidoglycan recognition protein 1 (1.00)	Vitamin D-binding protein (1.44)	α -fetoprotein (0.54)	14-3-3 protein sigma (0.49)	Immunoglobulin light chain, λ gene cluster (0.35)
Tetranectin (0.93)	Tetranectin (1.27)	Apolipoprotein E (0.49)	Keratin 77 (0.43)	α -2-macroglobulin (0.34)
α -1-antiproteinase (0.91)	β -2-glycoprotein 1 (1.14)	Apolipoprotein A-I (0.45)	α -fetoprotein (0.38)	α -fetoprotein (0.31)

Cathelicidin 6 (0.85)	α -2-macroglobulin variant 23 (1.10)	Complement component 3 (0.44)	Plasminogen (0.38)	Vitamin D-binding protein (0.31)
Cathelicidin-7 (0.79)	Serpin A3-2 (1.08)	Tetranectin (0.39)	α -2-macroglobulin variant 20 (0.36)	Fetuin-B (0.30)
Transthyretin (0.74)	α -fetoprotein (1.02)	Pigment epithelium-derived factor (0.38)	α -2-antiplasmin (0.32)	Complement component 3 (0.22)
Plasminogen (0.69)	α -2-macroglobulin (0.92)	α -2-macroglobulin variant 20 (0.36)	Inter- α -trypsin inhibitor heavy chain H2 (0.31)	Uncharacterized protein OS=Bos taurus OX=9913 PE=1 SV=1 (0.20)
Apolipoprotein E (0.65)	α -2-macroglobulin variant 4 (0.85)	Immunoglobulin light chain, λ gene cluster (0.35)	Vitamin D-binding protein (0.31)	Pigment epithelium-derived factor (0.18)
Prothrombin (0.60)	Keratin 3 (0.80)	Vitamin D-binding protein (0.32)	Fibrinogen β chain (0.30)	Plasminogen (0.17)
Insulin-like growth factor-binding protein 2 (0.60)	Complement component 3 (0.79)	α -2-antiplasmin (0.32)	α -2-macroglobulin (0.28)	Isocitrate dehydrogenase [NADP], mitochondrial (0.16)
Complement component 3 (0.59)	Angiotensinogen (0.79)	α -2-macroglobulin (0.31)	Hemopexin (0.24)	Angiotensinogen (0.16)
Immunoglobulin light chain, λ gene cluster (0.57)	α -1-acid glycoprotein (0.67)	Inter- α -trypsin inhibitor heavy chain H2 (0.31)	Complement component 3 (0.22)	Serpin A3-1 (0.15)
Uncharacterized protein OS=Bos taurus OX=9913 PE=1 SV=1 (0.55)	Serpin A3-3 (0.63)	α -2-macroglobulin variant 4 (0.30)	Apolipoprotein E (0.22)	ATP synthase subunit β (0.13)
α -fetoprotein (0.54)	Kininogen-1 (0.62)	Fetuin-B (0.30)	Antithrombin-III (0.22)	ATP synthase subunit α, mitochondrial (0.13)
Lactotransferrin (0.53)	α -2-antiplasmin (0.62)	Apolipoprotein A-IV (0.30)	Inter- α -trypsin inhibitor heavy chain H4 (0.21)	Uncharacterized protein OS=Bos taurus OX=9913 GN=LOC107131209 PE=4 SV=3 (0.10)
Vitronectin (0.51)	Annexin A2 (0.62)	Complement factor I (0.25)	Junction plakoglobin (0.20)	Gelsolin (0.09)
Complement factor B (0.51)	Kininogen-2 (0.54)	Apolipoprotein B (0.24)	α -1B-glycoprotein (0.20)	Apolipoprotein B (0.08)
Vitamin D-binding protein (0.50)	Adiponectin D (0.53)	Hemopexin (0.24)	Fetuin-B (0.19)	Inter- α -trypsin inhibitor heavy chain H2 (0.08)
Retinol-binding protein 4 (0.47)	α -1B-glycoprotein (0.52)	Inter- α -trypsin inhibitor heavy chain H4 (0.21)	Complement factor I (0.18)	Inter- α -trypsin inhibitor heavy chain (0.08)
α -2-macroglobulin variant 20 (0.46)	Uncharacterized protein OS=Bos taurus OX=9913 GN=CALM2 PE=3 SV=1 (0.52)	Fibrinogen β chain (0.21)	Plakophilin-1 (0.15)	
Uncharacterized protein OS=Bos taurus OX=9913 GN=C4A PE=1 SV=3 (0.45)	Complement factor B (0.51)	Annexin A2 (0.21)	Vinculin (0.15)	
Inter- α -trypsin inhibitor heavy chain H2 (0.42)	KRT4 protein (0.47)	Leucine-rich α -2-glycoprotein 1 (0.21)	Complement factor H (0.14)	
α -2-antiplasmin (0.41)	Retinol-binding protein 4 (0.47)	Fructose-bisphosphate aldolase (0.21)	Desmoplakin (0.13)	
α -2-macroglobulin (0.40)	Protein AMBP (0.45)	α -1B-glycoprotein (0.20)	Uncharacterized protein OS=Bos	

			taurus OX=9913 GN=C4A PE=1 SV=3 (0.12)
Uncharacterized protein OS=Bos taurus OX=9913 PE=4 SV=1 (0.38)	Transthyretin (0.45)	Uncharacterized protein OS=Bos taurus OX=9913 GN=C4A PE=1 SV=3 (0.19)	Afamin (0.11)
LOC790886 protein (0.38)	Serpin family G member 1 (0.44)	Kininogen-1 (0.18)	Kininogen-2 (0.11)
Fibrinogen β chain (0.38)	Plasminogen (0.44)	Kininogen-2 (0.18)	Apolipoprotein B (0.10)
Uncharacterized protein OS=Bos taurus OX=9913 GN=LOC107131209 PE=4 SV=3 (0.37)	Prothrombin (0.44)	Uncharacterized protein OS=Bos taurus OX=9913 GN=LOC784932 PE=1 SV=1 (0.17)	Uncharacterized protein OS=Bos taurus OX=9913 GN=LOC506828 PE=4 SV=1 (0.10)
Uncharacterized protein OS=Bos taurus OX=9913 PE=1 SV=1 (0.36)	Uncharacterized protein OS=Bos taurus OX=9913 PE=1 SV=1 (0.44)	Prothrombin (0.17)	Complement factor B (0.10)
L-lactate dehydrogenase (0.36)	Hemopexin (0.43)	Fibulin-1 (0.16)	Inter- α -trypsin inhibitor heavy chain H1 (0.08)
Immunoglobulin light chain, λ gene cluster (0.35)	RAB1A, member RAS oncogene family (0.40)	Angiotensinogen (0.16)	Desmoglein-1 (0.07)
Leucine-rich α -2-glycoprotein 1 (0.34)	Pantetheinase (0.39)	Complement factor B (0.15)	
β -2-glycoprotein 1 (0.33)	Antithrombin-III (0.39)	Complement component C9 (0.14)	
Four and a half LIM domains 1 (0.33)	Peroxiredoxin-1 (0.39)	Pyruvate kinase (Fragment) (0.13)	
Complement factor I (0.33)	Uncharacterized protein OS=Bos taurus OX=9913 GN=LOC784932 PE=1 SV=1 (0.38)	Plasminogen (0.13)	
Uncharacterized protein OS=Bos taurus OX=9913 PE=1 SV=3 (0.32)	Serpin A3-7 (0.38)	Afamin (0.11)	
Glyceraldehyde-3-phosphate dehydrogenase (0.32)	Immunoglobulin light chain, λ gene cluster (0.35)	Periostin (0.09)	
Kininogen-1 (0.31)	Apolipoprotein B (0.33)	Gelsolin (0.09)	
Fructose-bisphosphate aldolase (0.31)	Uncharacterized protein OS=Bos taurus OX=9913 GN=C4A PE=1 SV=3 (0.31)	Inter- α -trypsin inhibitor heavy chain H1 (0.08)	
α -2-macroglobulin variant 4 (0.30)	SERPIND1 protein (0.31)	Complement factor H (0.08)	
Pigment epithelium-derived factor (0.28)	Heat shock cognate 71 kDa protein (0.30)	Inter- α -trypsin inhibitor heavy chain H3 (0.08)	
Uncharacterized protein OS=Bos taurus OX=9913 GN=LOC525947 PE=1 SV=1 (0.27)	Gelsolin (0.28)	Desmoplakin (0.05)	

Insulin-like growth factor-binding protein 5 (0.27)	Serpin A3-7 (0.27)	Talin 1 (0.03)
Apolipoprotein B (0.26)	Inter- α -trypsin inhibitor heavy chain H2 (0.27)	
Serpin family G member 1 (0.24)	Heat shock 70 kDa protein 1A (0.24)	
Hemopexin (0.24)	Afamin (0.24)	
Angiotensinogen (0.24)	Lymphocyte cytosolic protein 1 (0.24)	
Gelsolin (0.23)	Glyceraldehyde-3-phosphate dehydrogenase (0.23)	
Kinesin family member 12 (0.22)	Vitronectin (0.23)	
Complement component C9 (0.21)	Uncharacterized protein OS=Bos taurus OX=9913 GN=LOC506828 PE=4 SV=1 (0.22)	
Fructose-bisphosphate aldolase (0.21)	Apolipoprotein E (0.22)	
Histidine-rich glycoprotein (0.20)	Inter- α -trypsin inhibitor heavy chain H4 (0.21)	
α -1B-glycoprotein (0.20)	Complement component C9 (0.21)	
Pyruvate kinase (Fragment) (0.20)	Leucine-rich α -2-glycoprotein 1 (0.21)	
Complement factor properdin (0.19)	Fetuin-B (0.19)	
Apolipoprotein A-IV (0.19)	Elongation factor 1- α (0.17)	
Hyaluronan-binding protein 2 (0.19)	Fibrinogen γ-B chain (0.17)	
Periostin (0.18)	Uncharacterized protein OS=Bos taurus OX=9913 GN=LOC525947 PE=1 SV=1 (0.15)	
Thyroxine-binding globulin (0.18)	Vinculin (0.15)	
Complement factor H (0.17)	Fibrinogen β chain (0.14)	
Complement component C7 (0.17)	Inter- α -trypsin inhibitor heavy chain H1 (0.12)	
Fibrinogen γ-B chain (0.17)	Inter- α -trypsin inhibitor heavy chain H3 (0.12)	
Serpin A3-7 (0.17)	Insulin-like growth factor binding protein, acid labile subunit (0.12)	
Inter- α -trypsin inhibitor heavy chain H3 (0.16)	Plasma kallikrein (0.11)	
Fibulin-1 (0.16)	Complement component 5 (0.10)	

Inter- α -trypsin inhibitor heavy chain H4 (0.16)	Desmoplakin (0.09)
Vitamin K-dependent protein C (0.16)	Fibrinogen α chain (0.09)
Vinculin (0.15)	Complement component C7 (0.08)
Cartilage oligomeric matrix protein (0.14)	Complement factor H (0.08)
Coagulation factor V (0.13)	Talin 1 (0.06)
Complement component 5 (0.13)	
Kininogen-2 (0.11)	
Thrombospondin-4 (0.11)	
Afamin (0.11)	
Hepatocyte growth factor-like protein (0.10)	
Sulfhydryl oxidase (0.09)	
Collagen type VI α 3 chain (0.08)	
Fibronectin (0.08)	
Inter- α -trypsin inhibitor heavy chain H1 (0.08)	
Collagen type XVIII α 1 chain (0.08)	
Phosphatidylinositol-glycan-specific phospholipase (0.08)	
Anion exchange protein (0.08)	
Uncharacterized protein OS=Bos taurus OX=9913 GN=LOC506828 PE=4 SV=1 (0.05)	

18

19

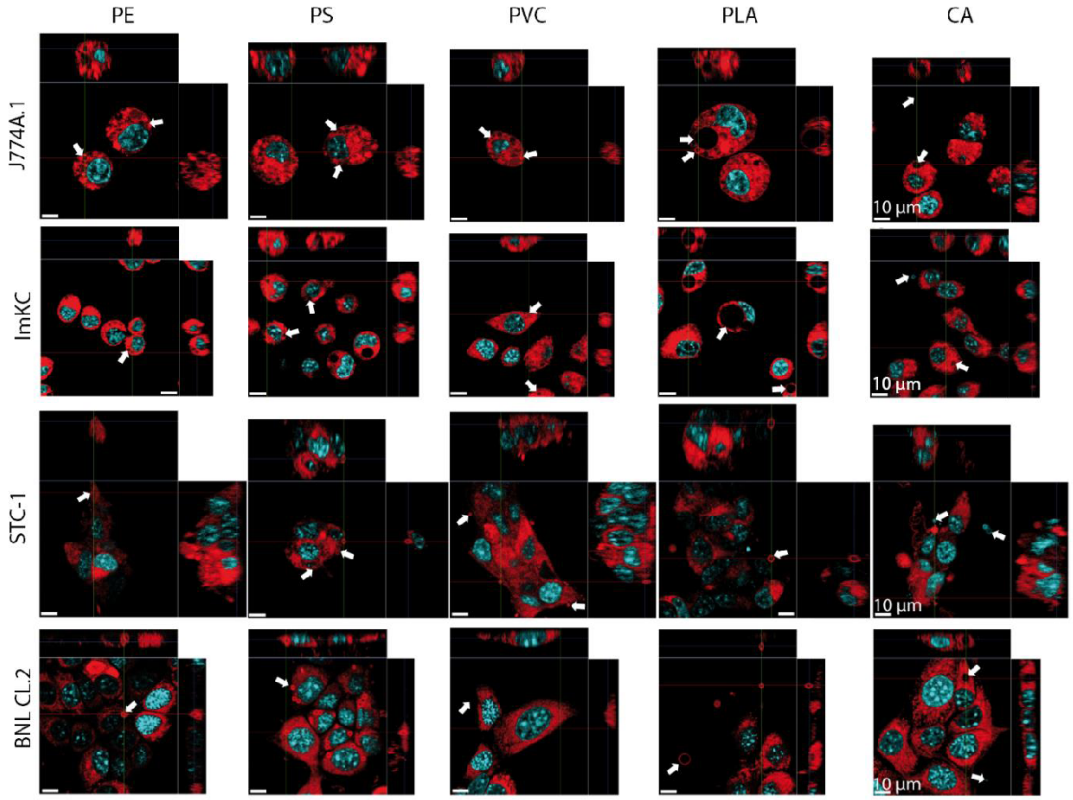

20

21 Figure S1. Analysis of particle ingestion in murine cells using confocal laser scanning microscopy (CLSM). 10 non-fluorescent
22 particles per cell were added to murine macrophages (J774A.1, ImKC) and epithelial cells (STC-1, BNL CL.2). White arrows
23 show exemplary microparticles. Fluorescence staining of cytoplasm (CytoTracker, red) and nuclei (Hoechst, blue). Scale bars:
24 10 µm.

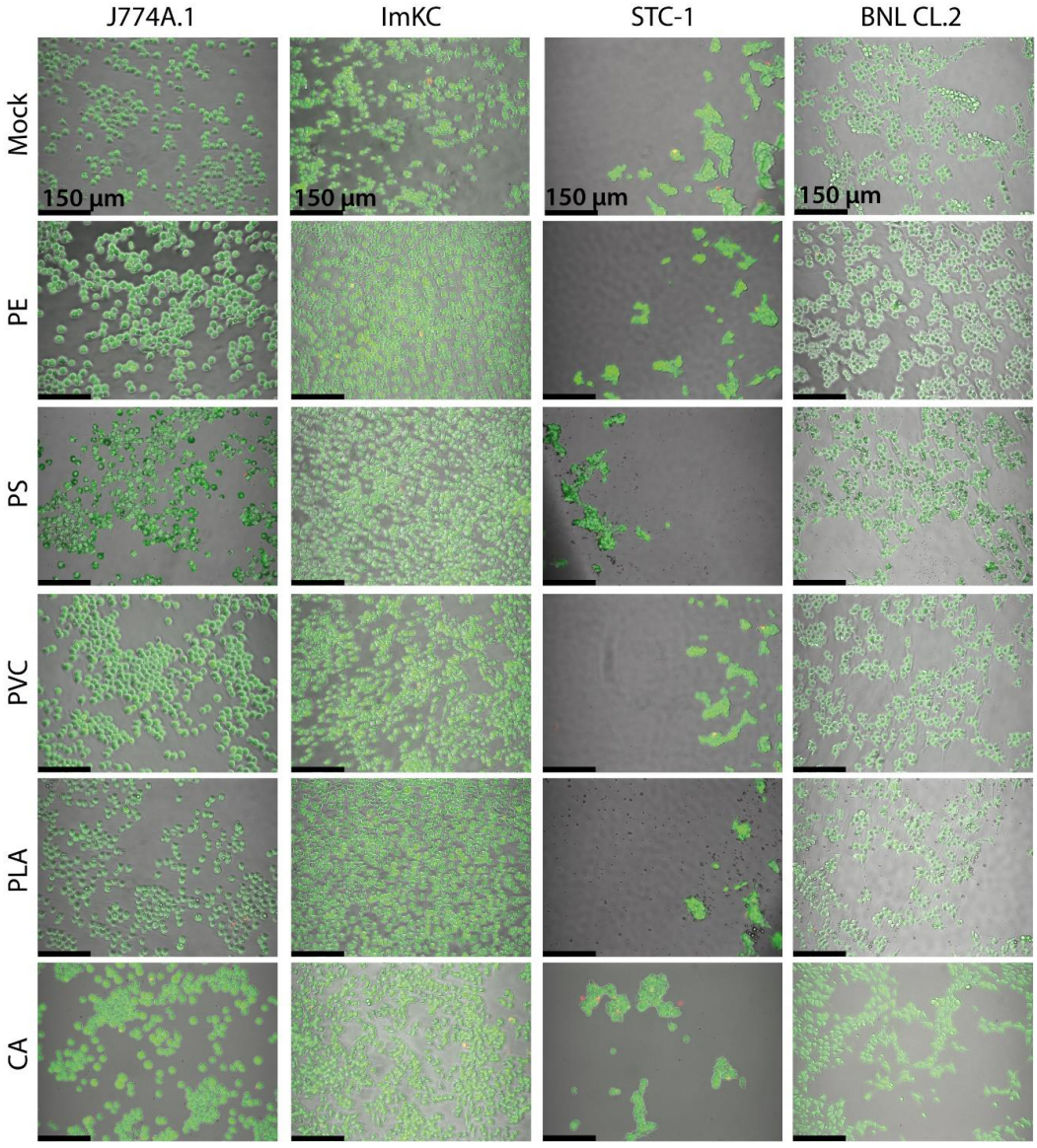

Figure S2. Live/dead staining after a 1-day incubation with polymer particles (MP concentration: 30 particles per cell). Green: live cells, red: dead cells. Mock= cells without particles (control).

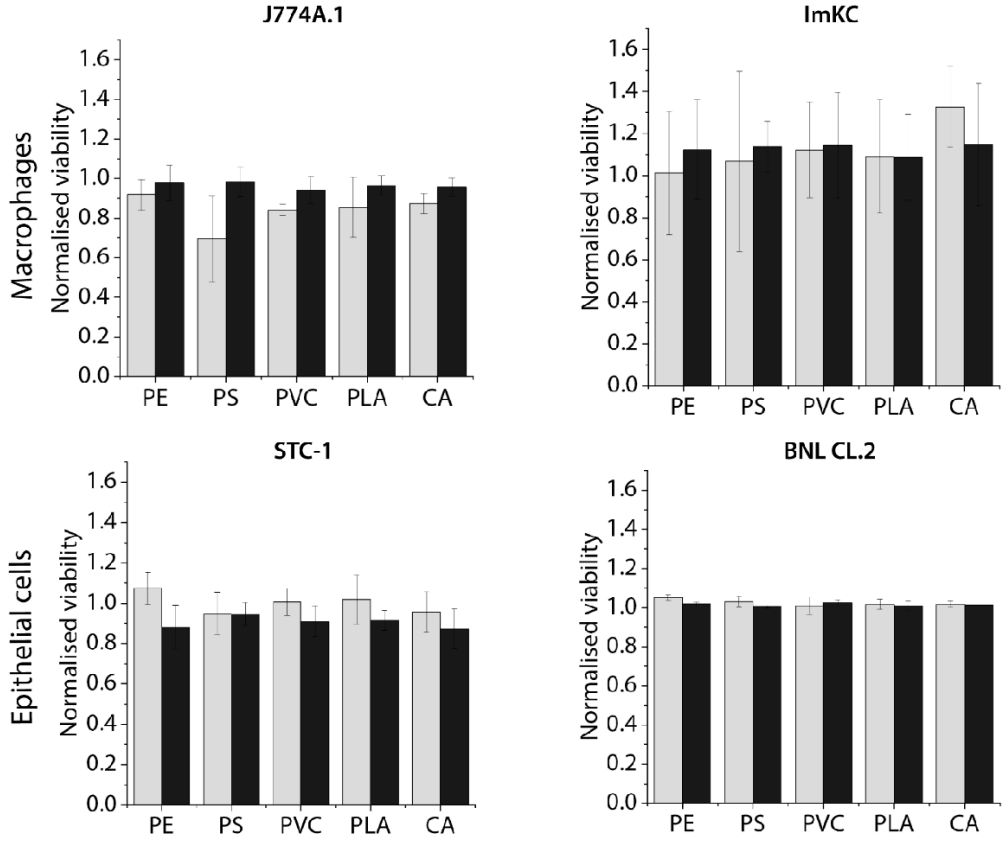

Figure S3. Resazurin assay after 1 and 7 days of incubation with different polymer microparticles (MP concentration: 20 particles per cell). The data were normalized to the respective mean value of the control. As a control, cells without microparticle incubation were used. ■ = day 1, ■ = day 7. The data do not differ significantly ($p > 0.05$). n=3 biological replicates.

Table S2. Cell metabolic activity after 24 h in the presence of polymer microparticles. The metabolic activity was determined using the MTT assay in correlation to cells without particles acting as negative control ("mock"). The cells were incubated with different particle concentrations (1, 10, and 100 particles per cell). Data represent mean ± SD, n = 3 biological replicates. † data taken from [1].

		Metabolic activity (%)				
	# MP/cells	PE	PS†	PVC	PLA	CA
J774A.1	Mock	97.5 ± 2.7	105.8 ± 4.1	101.8 ± 1.9	95.6 ± 0.6	101.8 ± 1.9
	1	96.0 ± 5.1	131.6 ± 8.7	92.8 ± 3.8	112.3 ± 9.0	100.1 ± 5.3
	10	99.2 ± 8.1	128.8 ± 9.1	88.7 ± 4.9	106.0 ± 5.1	104.3 ±6.1
	100	97.5 ± 7.4	114.8 ± 9.8	81.2 ± 6.3	90.9 ± 5.3	100.9 ± 3.0
ImKC	Mock	103.1 ± 3.0	98.8 ± 5.0	99.8 ± 4.6	104.3 ± 5.6	103.3 ± 3.2
	1	100.3 ± 4.2	129.1 ± 8.9	95.9 ± 4.5	111.0 ± 5.4	93.7 ± 4.8
	10	86.7 ± 5.8	131.7 ± 6.7	86.4 ± 8.5	105.0 ± 7.9	103.4 ± 6.8
	100	81.5 ± 6.9	128.4 ± 8.9	81.8 ± 3.1	95.3 ± 6.3	100.7 ± 8.7
STC-1	Mock	98.8 ± 4.3	111.5 ± 6.9	98.1 ± 5.5	99.4 ± 4.5	98.1 ± 5.5
	1	97.8 ± 5.6	106.9 ± 6.2	98.5 ± 2.6	94.3 ± 8.6	108.6 ± 11.9
	10	101.7 ± 13.9	109.8 ± 7.9	99.0 ± 4.7	98.9 ± 9.5	102.8 ± 7.8
	100	90.3 ± 8.6	109.6 ± 8.4	78.6 ± 4.2	107.7 ± 2.2	93.4 ± 1.7
BNL CL.2	Mock	100.7 ± 2.3	104.8 ± 5.3	98.1 ± 2.2	106.1 ± 2.1	98.1 ± 2.2
	1	106.4 ± 6.0	104.7 ± 6.1	99.6 ± 4.7	105.7 ± 5.7	95.7 ± 3.9
	10	96.5 ± 2.7	103.3 ± 4.0	100.7 ± 5.8	99.1 ± 2.9	98.1 ± 2.1
	100	96.4 ± 5.6	102.2 ± 4.9	102.8 ± 5.7	88.9 ± 6.2	96.5 ± 1.1

1. Rudolph, J., Völkl, M., Jérôme, V., Scheibel, T. & Freitag, R. Noxic Effects of Polystyrene Microparticles on Murine Macrophages and Epithelial Cells. *Scientific Reports* **11**, 1-16 (2021).

6.5 Teilarbeit V

Polystyrene Microparticle Distribution After Ingestion by Murine Macrophages

Autoren: **Julia Jasinski***, Matthias Völkl*, Jonas Hahn, Valérie Jérôme, Ruth Freitag und Thomas Scheibel

∗ gleichberechtigte Co-Autorenschaft

Die Konzeptionierung sowie alle Experimente dieser Teilarbeit wurden zu gleichen Teilen von Matthias Völkl und mir durchgeführt. Die Analyse der Kolokalisierung der Partikel mit zellulären Organellen mittels Konfokalmikroskopie wurde von mir durchgeführt und ausgewertet. Zusätzlich wurden die Experimente mittels time-lapse live cell microscopy von mir durchgeführt und ausgewertet. Das Zelltracking und die Auswertung der Daten wurden von Jonas Hahn durchgeführt. Daten zur Exkretion und Verteilung der Partikel während der Zellteilung wurden von Matthias Völkl erhoben und ausgewertet. Das Manuskript wurde von mir zusammen mit Matthias Völkl verfasst. Valérie Jérôme, Ruth Freitag und Thomas Scheibel waren an der Konzeptionierung, wissenschaftlichen Diskussionen und der Fertigstellung des Manuskripts beteiligt.

Der Artikel wurde am 07.06.2024 im Journal *Journal of Hazardous Materials* veröffentlicht.

Journal of Hazardous Materials 457 (2023) 131796

Contents lists available at ScienceDirect

Journal of Hazardous Materials

journal homepage: www.elsevier.com/locate/jhazmat

Polystyrene microparticle distribution after ingestion by murine macrophages

Julia Jasinski [a,1], Matthias Völkl [b,1], Jonas Hahn [a], Valérie Jérôme [b], Ruth Freitag [b,d], Thomas Scheibel [a,c,d,e,f,*]

[a] Biomaterials, Faculty of Engineering Sciences, University of Bayreuth, Bayreuth, Germany
[b] Process Biotechnology, Faculty of Engineering Sciences, University of Bayreuth, Bayreuth, Germany
[c] Bayreuth Center for Colloids and Interfaces (BZKG), University of Bayreuth, Bayreuth, Germany
[d] Bayreuth Center for Molecular Biosciences (BZMB), University of Bayreuth, Bayreuth, Germany
[e] Bayreuth Center for Material Science (BayMAT), University of Bayreuth, Bayreuth, Germany
[f] Bavarian Polymer Institute (BPI), University of Bayreuth, Bayreuth, Germany

HIGHLIGHTS

- Macrophage polarization status and phenotype influenced response to microplastic.
- Macrophage phenotype influenced microplastic distribution during cell division.
- Particles were mainly located in the cytoplasm, to a lesser extend in the ER and endosomes.
- No active execretion was detected in vital macrophages.

GRAPHICAL ABSTRACT

Parts of the figure were drawn using pictures from Servier Medical Art. Servier Medical Art by Servier is licensed under a Creative Commons Attribution 3.0 Unported License (https://creativecommons.org/licenses/by/3.0/).

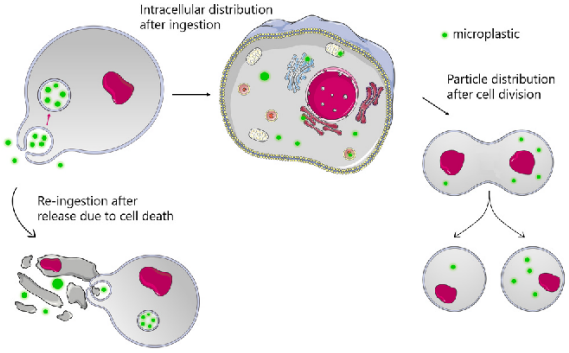

ARTICLE INFO

Editor: Teresa Rocha-Santos

Keywords:
Microplastic
Polarization
Excretion
Cell division

ABSTRACT

The impact of microplastic particles on organisms is currently intensely researched. Although it is well established that macrophages ingest polystyrene (PS) microparticles, little is known about the subsequent fate of the particles, such as entrapment in organelles, distribution during cell division, as well as possible mechanisms of excretion. Here, submicrometer (0.2 and 0.5 μm) and micron-sized (3 μm) particles were used to analyze particle fate upon ingestion of murine macrophages (J774A.1 and ImKC). Distribution and excretion of PS particles was investigated over cycles of cellular division. The distribution during cell division seems cell-specific upon comparing two different macrophage cell lines, and no apparent active excretion of microplastic particles could

* Corresponding author at: Biomaterials, Faculty of Engineering Sciences, University of Bayreuth, Bayreuth, Germany.
E-mail address: scheibel@bm.uni-bayreuth.de (T. Scheibel).
[1] Both authors contributed equally.

https://doi.org/10.1016/j.jhazmat.2023.131796
Received 13 April 2023; Received in revised form 28 May 2023; Accepted 5 June 2023
Available online 7 June 2023

Intracellular allocation
Endosomes

be observed. Using polarized cells, M1 polarized macrophages show higher phagocytic activity and particle uptake than M2 polarized ones or M0 cells. While particles with all tested diameters were found in the cytoplasm, submicron particles were additionally co-localized with the endoplasmic reticulum. Further, 0.5 μm particles were occasionally found in endosomes. Our results indicate that a possible reason for the previously described low cytotoxicity upon uptake of pristine PS microparticles by macrophages may be due to the preferential localization in the cytoplasm.

1. Introduction

Macrophages are specialized immune cells that possess the remarkable ability of phagocytosis allowing to engulf particles larger than 0.5 μm in diameter [1,2]. They ingest pathogens and dead cells to clear them from the body, initially wrapping them in a vesicular system called phagosome [3,4]. Subsequently, the phagosomes are fused with lysosomes to form phagolysosomes [4,5]. Lysosomes are vesicles defined by a low pH and the presence of digestive enzymes, which allows the digestion of organic matter (e.g., removal of pathogens or dead cells) and the recycling of intracellular materials [5–7]. Besides forming phagolysosomes, lysosomes can also fuse with endosomes, forming so-called recycling endosomes or endolysosomes [8,9]. Endosomes are less specialized vesicles for molecular transport and are found in all cell types [10,11]. They follow a hierarchical maturation after endocytosis via early, late, and recycling endosomes [11,12]. During the maturation process of endosomes and phagosomes, the presence of specific, such as Ras-related (Rab), proteins is observed. Notably, early endosomes are characterized by the presence of Rab5, while late endosomes are marked by the presence of Rab7 [4,13]. Proteins like Rab7 are also found in late phagosomes as well as in late macropinosomes [4,13,14]. The endoplasmic reticulum (ER) generally is known to be involved in protein transport, folding, and secretion [15]. The to-be-secreted proteins reach the Golgi apparatus, where they are packed into vesicles for transport by endosomes to their next intended destination inside the cells, or alternatively, by the exocytosis pathway to be secreted [16,17].

Macrophages are capable of ingesting a wide range of substances, including microplastic particles (MPP) [18–20]. The abundance of microplastic, usually classified as plastic particles/fragments within a size range of 0.1 – 5000 μm [21], is a global problem, as microplastic is found everywhere in the environment such as in water, air, and soil [22–24]. For a wide range of organisms, microplastic ingestion, e.g., via their diet, has been described [22,25]. While it is likely that the majority of plastic particles transit through the gastrointestinal tract, there have been reports of their accumulation in various tissues, leading to inflammation and other detrimental effects [26,27]. The particle uptake hereby depends on various particle properties, including size, shape, surface charge, and surface chemistry [3,28,29]. Especially in vitro, various effects of MPP on cells could be observed. Several publications have described a reduction in metabolic activity, albeit typically observed only at high concentrations of the MPP under investigation [19]. The uptake of the particles, though, seems to be of high importance for possible effects on murine macrophages, as shown by Ramsperger et al. [29]. In studies involving murine macrophages, it has been observed that aged particles tend to induce higher levels of cytotoxicity, increased oxidative stress, and genotoxicity [18,20]. In some studies, researchers have reported the occurrence of mitochondrial, lysosomal, or endoplasmic reticulum (ER)-associated stress responses following particle exposure in both rat blood cells and human lung cells. However, it remains unexplored whether these effects are dependent on the localization of the particles inside or on the membrane of these specific organelles [30,31]. In consequence, the mechanisms underlying these effects, which probably arise intracellularly, are not yet understood.

For tissue translocation of particles, the ingestion by specialized immune cells, e.g., macrophages, is thought to be crucial [32,33]. As previously reported, microplastic particles have been detected in human blood and tissues, exposing them to various immune cells, including both exudate and resident macrophages [34]. Exudate macrophages are found patrolling in the bloodstream to reach local sites of inflammation [35,36], whereas resident macrophages are permanently localized at a specific tissue and show a specialized cell morphology and function [35,36]. Additionally, particles seem to be capable of inducing diverse cytotoxic effects in macrophages potentially leading to alterations in cell polarization, i.e., the propensity to acquire a pro-inflammatory (M1) or an anti-inflammatory (M2) phenotype [37–39]. However, contrasting reports have emerged where no significant change in polarization was observed upon incubation with polymer microparticles [18,39]. Macrophages that undergo polarization into the M1 type are pro-inflammatory accompanied by an increased phagocytic activity, as evidenced by the secretion of cytokines like tumor necrosis factor (TNF)-α [37,38,40,41]. The polarization of M1 macrophages can be induced by bacterial lipopolysaccharides (LPS), which bind to cellular membrane receptors, namely integrins of the cluster of differentiation (CD) 11b or CD18, and induce phagocytosis [1]. In contrast, M2 polarization, usually induced by interleukin (IL)-4, IL-10, or IL-13 [42], was described as anti-inflammatory state [38,40,41]. M2 macrophages are characterized by the secretion of anti-inflammatory cytokines, like IL–10, as well as transforming growth factor (TGF)-β, collagen IV, and other growth factors [40,41]. The polarization state of macrophages (M1 or M2) can be distinguished using specific CD markers, such as CD80 for M1 and CD206 for M2. The impact of macrophage polarization on MP ingestion, however, has received limited research attention thus far [43,44]. Collin-Faure et al. showed that the incubation with 0.1 and 10 μm PS particles induced a small and not significant M1 polarization in J774A.1 cells, which was not the case for 1 μm particles [45]. In contrast, Stock et al. analyzed human macrophages (THP-1) and claimed no effects on macrophage activation and polarization after incubation with 1 μm, 4 μm, and 10 μm PS particles [18].

Importantly, a release of previously ingested particles by macrophages has to date only been described for nanoparticles, i.e. particles ≤ 100 nm [33,46]. The phenomenon of particle release has not been observed with larger PS microparticles (5 μm) [47].

In this study, our objective was to examine the potential impact of a macrophage's phenotype and polarization status on its interaction with PS MPP. Therefore, we investigated the fate of ingested PS particles of varying diameters (0.2, 0.5, and 3 μm) in two murine macrophage cell lines derived from ascites and liver tissue. To assess the cellular uptake of the particles, we employed time-lapse video microscopy, allowing us to monitor the internalization process. Additionally, we made use of specific (immuno)staining techniques targeting organelles and performed confocal microscopy analysis to investigate the subcellular localization of the ingested particles. This approach enabled us to examine the precise compartments within the macrophages where the particles were located. We also investigated the distribution of the particles during cell division and their subsequent release from macrophages. For this purpose, flow cytometry was employed, providing quantitative data on the partitioning of particles in dividing cells. By employing these comprehensive experimental techniques, we aimed to gain insights into the complex interplay between macrophage phenotype, polarization status, and the interactions with PS MPP.

2. Materials and methods

Cell culture materials were obtained from Greiner Bio-One

(Frickenhausen, Germany) and Thermo Fisher Scientific (Schwerte, Germany) if not otherwise indicated. Dulbecco's Phosphate-Buffered Saline without Ca^{2+} and Mg^{2+} (DPBS), penicillin, streptomycin, and fetal calf serum (FCS) were purchased from Sigma Aldrich (Taufkirchen, Germany). DMEM (Dulbecco's Modified Eagle's Medium; 3.7 g/L $NaHCO_3$, L-glutamine-free) and RPMI1640 (Roswell Park Memorial Institute) were obtained from Lonza (Lonza Group Ltd, Basel, Switzerland).

For the fluorescence staining, CellTracker Red CMTPX Dye, MitoTracker Red FM, BODIPY TR Ceramide, ER-Tracker Red, Acridine Orange, and HOECHST 33342 were obtained from Thermo Fisher Scientific (Schwerte, Germany).

The monoclonal rabbit anti-early endosome antibody 1 (EEA1, Cat. # 3288 S) and polyclonal rabbit anti-Ras-related protein 7 (Rab7, Cat. #2094 S) primary antibodies were obtained from Cell Signaling Technology. The polyclonal goat anti-rabbit-TRITC secondary antibody was from Sigma Aldrich (Taufkirchen, Germany, Cat. # T6778).

Polystyrene particles (PS) were obtained from Polysciences (Polysciences Europe GmbH, Eppenheim, Germany) either non-functionalized or fluorescent (PS_{green}, Yellow Green, Ex/Em green particles: 441/486 nm; PS_{red}, Polychromatic Red, Ex/Em red particles: 512/565 nm) in sterile aqueous suspensions (2.5% (w/v)). MP properties: diameter of 0.2 μm (5.68 $\times 10^{12}$ particles/mL, size coefficient of variation (CV) ≤ 8%), 0.5 μm (3.64 $\times 10^{11}$ particles/mL, size CV ≤ 3%), and 3 μm (1.68 $\times 10^{9}$ particles/mL, size CV ≤ 5%). The particles' properties, including size, surface charge, protein corona formation, fluorescence intensity, and stability, have been thoroughly investigated in prior studies conducted by our group [19,20,29].

2.1. Cell culture

Macrophages from ascites (J774A.1), obtained from the American Type Culture Collection (ATCC, Manassas, USA, TIB-67), and hepatic macrophages (ImKC, Kupffer cells), obtained from Merck (Merck KGaA, Darmstadt, Germany, SCC119) were used. The cells were cultivated as previously described [19,29]. In brief, all cell media were supplemented with 10% (v/v) FCS and 100 U/mL penicillin/streptomycin. J774A.1 cells were cultivated in DMEM, supplemented with 4 mM glutamine, 24 mM HEPES, and 0.1 mM sodium pyruvate. ImKC cells were cultivated in RPMI1640 supplemented with 2 mM glutamine. These media are further referred to as growth media. Cells were cultivated in a standard cell culture incubator (5% CO_2/95% humidity) at 37 °C. For cell maintenance, both cell lines were passaged three times a week, and for detaching cells, pre-warmed citric saline buffer (135 mM potassium chloride, 15 mM sodium citrate, incubation at 37 °C for 5 min (J774A.1) or 10 min (ImKC)) was used.

2.2. Macrophage polarization

Macrophages were polarized to analyze whether MPP uptake depends on the respective polarization. Suitable substance concentrations were chosen based on previously published studies [50]. 150,000 cells/well were seeded in a 12-well plate and incubated for 24 h. Afterwards, *E. coli* O111:B4 derived LPS (Sigma Aldrich, Taufkirchen, #L2630 – #Lot 112732) or recombinant mouse IL-4 (BioLegend, San Diego, USA) were added for 24 h at the respective concentration for M1 (100 ng/mL) or M2 (20 ng/mL) polarization. M1 cell polarization was verified by antibody staining (Biolegend, San Diego, CA, FITC anti-mouse CD80, Item 105005) of the CD80 surface marker (Fig. S1), and M2 polarization by antibody staining (Biolegend, San Diego, CA, FITC anti-mouse CD206, Item 141719) of the CD206 surface marker. Isotype control was done according to the manufacturer's instructions (PE/Cyanine7 Rat IgG2a, κ Isotype Ctrl Antibody for CD206, Item 400521; FITC Rat IgG2a, κ Isotype Ctrl Antibody for CD80, Item 400505). Briefly, cells were collected after incubation with the polarizing substance, centrifuged (200x g, 5 min), washed with DPBS, resuspended in 100 μL DPBS and counted. For every 10^6 cells, 0.5 μg/mL antibody was added, and the mixture was incubated for 20 min in the dark. Afterwards, 900 μL DPBS was added, and cells were centrifuged (200x g, 5 min), washed with DPBS and resuspended in 750 μL DPBS. The staining was evaluated using flow cytometry (Excitation 488 nm, Emission 570 nm, Cytomics FC500, Beckman Coulter, Krefeld, Germany). Analysis of the results was done using the FlowJo software v 10.5.0 (Tree Star, Stanford University, CA, USA, 2018).

For uptake analysis, 3.41 × 10^6 fluorescent particles (PS_{red}) were added per well, which is equivalent to a concentration of approximately 50 μg/mL PSred, and incubated for the respective amount of time with the polarized cells. Comparable in vivo studies have reported MPP concentrations between 1.6 and 99.4 μg/mL in human blood (Lee et al., 2021, Leslie et al., 2022).

Afterwards, cells were detached and washed twice with DPBS, and the particle cell interaction (PCI) was analyzed using flow cytometry as described previously [19].

2.3. Analysis of particle distribution during cell division

For a possible, specific distribution of engulfed MPP during cell division, cells were first stained with CellTrace Violet (CTV) dye, which binds covalently to intracellular amines [51,52]. Each cellular division dilutes the dye by a factor of two. Analysis of the level of fluorescence in the cell populations using flow cytometry permits determining the number of generations through which a cell has progressed, since the label was applied. Cells were first stained using a CTV Proliferation Kit (CTV, Ex/Em CTV: 405/450 nm, Invitrogen, Carlsbad, CA, USA) according to the manufacturer's instructions, followed by incubation with PS_{red} particles to measure the particle distribution in the daughter cells during cell division. Briefly, cells were detached, counted, and adjusted to 10^6 cells/mL. Cells were centrifuged (200 × g, 5 min), washed with DPBS, and resuspended in 1 mL DPBS. 1 μL of CTV stock solution per 1 mL cell suspension was added for a working concentration of 5 μM CTV. Cells were then incubated for 20 min at room temperature, and protected from light. Afterwards, cells were centrifuged (200 × g, 5 min), the supernatant was discarded, and the pellet was resuspended in a volume of complete growth medium corresponding to five times the original staining volume to remove the free staining dye. After five minutes of incubation, cells were centrifuged (200 × g, 5 min), resuspended in growth medium, seeded in 12-well plates at 150,000 cells/-well, and incubated for 24 h to allow for cell adhesion. Cells were then loaded with particles (1.68 × 10^6 PS_{red} particles/well) for 24 h. After incubation, cells were washed thoroughly with DPBS to remove unbound particles. Then, cells were detached, washed twice with DPBS, and analyzed using flow cytometry (data corresponding to day 0). Cells were subsequently analyzed every other day to track the particle distribution. The supplementary information provides a detailed explanation of how the corresponding approximation was calculated (Fig. S2, Eq. S1).

2.4. Analysis of particle excretion after ingestion

To analyze if cells are excreting and potentially re-ingesting particles, cells incubated with PS_{green} or PS_{red} were pooled, and possible mixing of the different fluorescent particles was tracked. Briefly, cells were detached, counted, and seeded at 150,000 cells per well in a 12-well plate. After 24 h of incubation, cells were loaded with PS_{green} or PS_{red} particles (1.68 × 10^6 particles/well) for 24 h. Afterwards, cells were washed intensively to remove the free (i.e., not ingested) particles. Cells were then detached, counted, and a mixture containing 75,000 PS_{green} loaded cells/75,000 PS_{red} loaded cells were seeded in 12 well plates. Control wells only contained cells pre-loaded with either PS_{green} or PS_{red} particles (150,000 cells/well each). Cells were washed, detached, and analyzed every other day using a flow cytometer (Ex/Em PS_{green}: 441/486 nm, Ex/Em PS_{red}: 512/565 nm).

2.5. Co-localization with organelles

0.2 μm, 0.5 μm, and 3 μm PS_{green} were used to explore the co-localization of MPP with specific organelles. The cells were seeded at 20,000 cells/well and incubated in Ibidi slides (μ-Slide 8 Well, ibiTreat, ibidi GmBH, Gräfelfing, Germany) for 7 h under cell culture conditions. Afterwards, PS_{green} (0.2 μm: 5.6×10^8 particles/well, 0.5 μm: 3.6×10^7 particles/well, 3 μm: 1.6×10^5 particles/well) were added to the cells, followed by a 15-hour incubation. Thereafter, cytoplasm (CellTracker), nuclei (HOECHST 33342), mitochondria (MitoTracker red), ER (ER-Tracker red), Golgi apparatus (BODIPY TR), and lysosomes (acridine orange) were stained in the living cells according to the manufacturer's instructions. For organelle staining, the following conditions were chosen: CellTracker: 2 μM in serum-free medium for 30 min at 37 °C; HOECHST 33342 staining: 1.5 μg/mL in complete cell culture medium for 10 min at 37 °C, Mito-Tracker red: 300 nM in serum-free medium for 30 min at 37 °C; ER-Tracker: 1.5 μM in DPBS for 30 min at 37 °C; BODiPY TR: 0.5–10 μM in complete cell culture medium for 30 min at 4 °C; acridine orange: 10 μg/mL in complete cell culture medium for 10 min at 37 °C.

Endosomes were immunostained with specific antibodies after cell fixation and permeabilization. For cell fixation, cells were incubated with 3.7% paraformaldehyde (PFA) for 20 min at room temperature (RT). After three washing steps with DPBS, the cells were permeabilized using ice-cold 100% methanol at − 20 °C for 10 min, followed by 3 washing steps with DPBS. Blocking buffer (0.5% (v/v) Tween 20, 1% (w/v) BSA in DPBS) was applied for 30 min at 37 °C and rinsed off afterwards. Then, the samples were incubated for 90 min at 37 °C with rabbit anti-early endosome antibody 1 (EEA1) and rabbit anti-Ras-related protein 7 (Rab7) primary antibodies diluted 1:200 and 1:160, respectively. After three further washing steps with DPBS, the samples were incubated for 90 min at 37 °C with a secondary goat anti-rabbit-TRITC antibody diluted 1:100 in blocking buffer. After 3 washing steps with DPBS, nuclei were stained as described above. The samples were then analyzed using confocal laser scanning microscopy (TCS SP8, 63x oil immersion objective, with 3x software zoom, laser: 408 nm, 488 nm, and 552 nm, Leica Microsystems, Software: Leica Application Suite X (LAS X), v.3.5.7.23225, Wetzlar, Germany). Z-stacks were made with 0.2 or 0.3 μm step size.

2.6. Live cell microscopy (time-lapse microscopy)

For time-lapse microscopy, J774A.1 and ImKC macrophages were seeded into 35 mm^2 Petri dishes (300,000 cells/ dish) and incubated overnight under cell culture conditions. A confocal laser scanning microscope (TCS SP8, 20x objective with 2x software zoom) with environmental control (37 °C, 5% CO2) was used for microscopy. The imaging process was started by adding 3 μm PS particles (5×10^6 particles/ dish). Images were taken every 1.5 min for a total duration of 25 h. Image stacks and particle tracking videos were generated using ImageJ (National Institutes of Health, Bethesda, MD, USA, v1.53i). For cellular tracking, the detection of 60 cell positions was performed manually [53]. Deterministic circle detection using the circle Hough transform and Canny edge detection could identify the positions of the cells reasonably well [54,55]. Tracking was performed using Trackpy, a python package based on the Crocker-Grier algorithm [56,57]. This algorithm calculates the track of individual cells. Tracks were eventually improved by the same algorithm, subtracting drift and filtering detection and affiliation errors. A custom-written Python program was used to calculate ensemble mean square displacement (emsd) from given tracks for each video. The calculation of the mean square displacement (msd) serves as a first test to distinguish between different undirected migration rates and is interpreted as a measure of viability.

2.7. Statistical analysis

Origin software 2019b (Origin, Northampton, MA, USA) was used for statistical analysis. A test for equal variance was additionally performed using Levene|| (level of significance 0.05). A factorial ANOVA (level of significance 0.05) with a Tukey post hoc test was performed to investigate differences in the particle-cell interaction after macrophage polarization.

3. Results

Live-cell time-lapse microscopy was used to get insights into the fate of ingested 3 μm MPP during a 25-h incubation. Particle-cell interaction (PCI) and possible release of the PS particles by the two investigated macrophage cell lines were followed in real-time (Fig. 1 (ImKC), Fig. S4 (J774A.1), videos S1–6). J774A.1 cells were used as exudate macrophages, whereas ImKC cells are resident in the liver. In general, differences could be detected in cellular movement between the two investigated cell lines. Specifically, J774A.1 cells exhibited higher motility and greater cellular activity, as evidenced by increased movement, as depicted in Fig. S5. Throughout the 25-hour incubation period, we did not observe any active particle release in either of the cell lines studied. The sole observed release occurred from dead cells, which were visibly necrotic as indicated by the presence of blue circles in Fig. 1. In such cases, the particles pass through the compromised cell membrane due to cellular damage. Additionally, we noticed instances where neighboring cells not only ingested the membrane fragments released by dead cells but also engulfed the particles originating from those cells (Fig. 1, blue arrows). Furthermore, several cells exhibited more frequent and active interactions with the particles, as evidenced by their high degree of movement. This phenomenon was observed across both cell lines used in the study, as depicted in Video S2 and S4. Further analysis of the videos revealed that the allocation of particles during cell division appeared to lack a discernible pattern in terms of distribution among the daughter cells (Fig. 1, Fig. S4, red circles). This suggests a random or stochastic distribution during the division process.

3.1. Macrophage polarization influences particle ingestion

The live-cell time-lapse microscopy analysis revealed differences in terms of cellular movement and PCI. Since it is known that the polarization of macrophages influences their phagocytotic activity, we hypothesized that the observed differences in the cellular activity might be related to the polarization status of the macrophages. To investigate this further, M1 polarization was induced using LPS and M2 polarization using IL-4. The success of polarization was verified through immunostaining with surface marker antibodies (Fig. S2) [37–39]. Subsequently, the polarized macrophages were challenged with 3 μm PS_{green} (25 μg/mL) particles for 6 h. The PCI was quantified using flow cytometry (Fig. 2). To facilitate the interpretation of the results, we categorized the PCI into three groups based on the number of particles in contact with each cell. These groups were defined as follows: cells in contact with more than four particles (">4"), cells in contact with one to four particles ("1–4"), and cells without detectable PCI ("0").

Upon polarization to the M1 state, macrophages of both cell lines exhibited higher PCI compared to non-polarized (M0) macrophages. Of note, compared to J774A.1 cell, where only a non-significant trend towards a PCI increase was measured, ImKC cells showed a significantly higher tendency for PCI following M1 polarization (no particle interaction: $p < 0.05$, 1–4 and > 4 interacting particles: $p > 0.001$). Conversely, in J774A.1 macrophages polarized to the M2 state, fewer particle interactions were observed (i.e., the percentage of cells not displaying any PCI was slightly increased) compared to the M0 control cells (Fig. 2, no particle interaction: $p < 0.05$, 1–4 and > 4 interacting particles: not significant). In ImKC cells polarized to M2 the PCI remained comparable to that of the M0 ImKC controls.

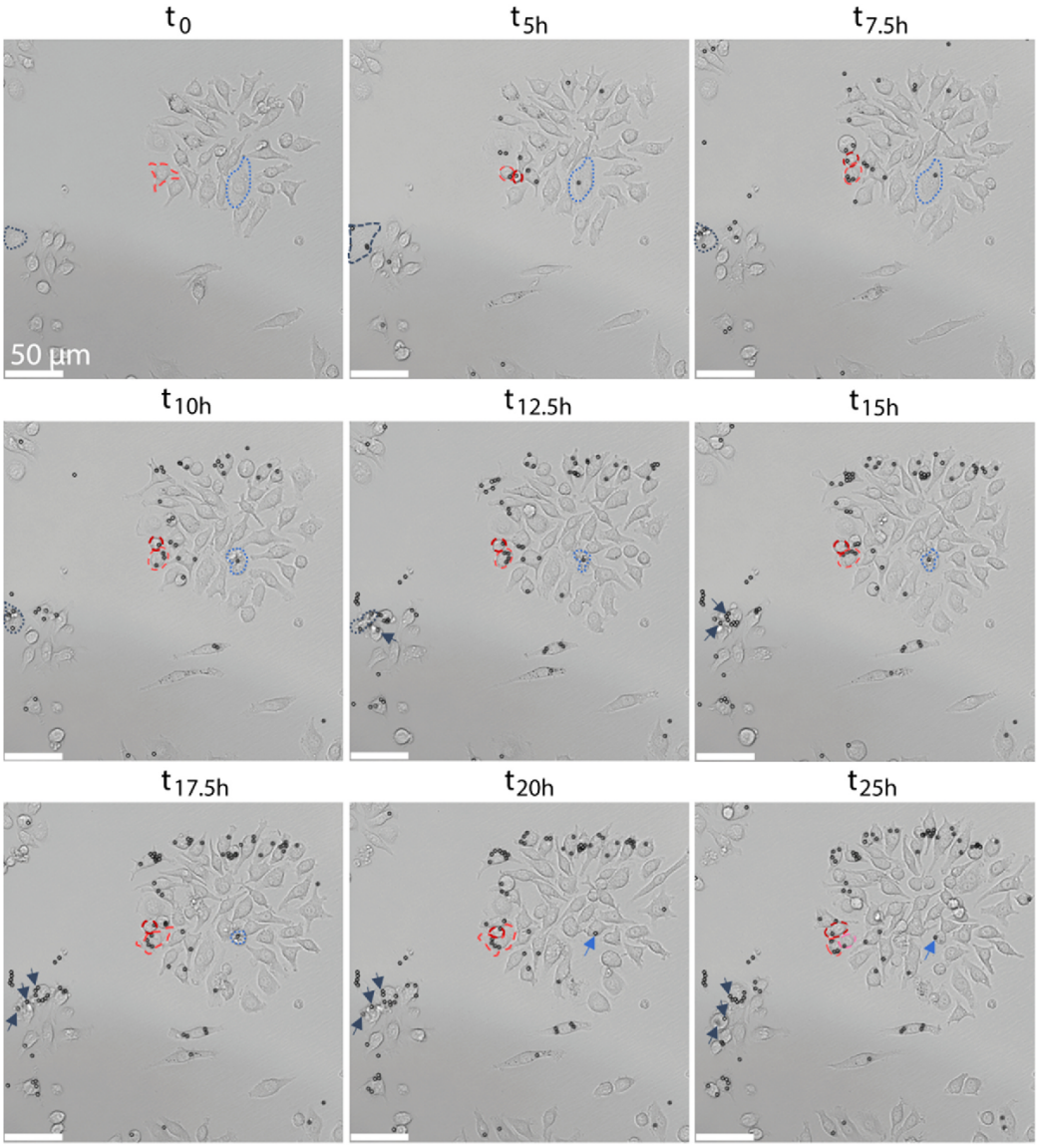

Fig. 1. Sample sections from live-cell microscopy of ImKC incubated with 3 µm PS for 25 h. Blue markings show the interaction of particles with apoptotic cells (blue circles) and the re-ingestion of particles by their neighbor cells (blue arrows). Red circles indicate the particle distribution during cell division. The two different shades of blue and red indicate two examples per event. Scale bar: 50 µm. The complete video is shown in Supplementary Information (video S3).

3.2. *Symmetrical distribution of MP during cell division*

Time-lapse videos indicated a random, i.e., asymmetrical distribution of MPP during cell division (i.e., to the daughter cells). To investigate this further, both cell lines were loaded with 3 µm PS_{red} particles and subsequently stained with the CTV dye to track the respective cell divisions. Flow cytometry was employed to investigate the percentage of cells exhibiting a specific number of (PCI over a period of three days, and respective cell populations were compared with calculated values, approximating a symmetrical distribution of particles to the daughter cells (Table 1). The actual number of PCI observed in J774A.1 cells was found to be closer to the estimated or approximated number, as compared to ImKC cells. Not surprisingly, for both cell lines, the difference between the calculated values and the measured distribution was more pronounced for cells with low PCI. Interestingly, a fraction (12.5%) of cells with ≥ 4 particles per cell persisted at day 2 in case of ImKC cells, which deviates from the expectation of a symmetrical distribution. This was not observed for J774A.1 cells. This result was not attributed to a reduced number of cell divisions, as assessed by the CTV dye.

3.3. *Qualitative and quantitative analysis of particle release revealed no active excretion*

Time-lapse videos did not reveal any apparent particle release by living cells. Furthermore, as shown above, in case of ImKC cells a relatively high number of cells with > 4 particles was still present 48 h after loading with 3 µm PS_{red}. Such observations suggest that a particle release/detachment is a rare event. To quantitatively determine the release or detachment of PS particles by murine macrophages, one batch

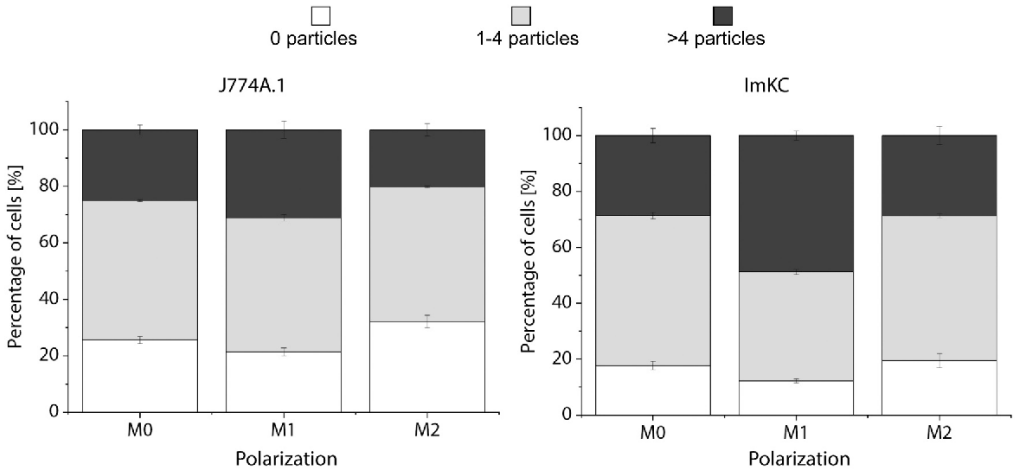

Fig. 2. Interaction frequency of 3 μm PS particles and macrophages in dependence on the macrophage polarization state. Polarization to M1 macrophages was obtained using lipopolysaccharide (LPS), and polarization to M2 macrophages by using IL 4. Cells were polarized for 24 h, particles were incubated for 6 h hours. Data representing mean value ± SD, n 3.

Table 1
Percentage of cells interacting with a given number of particles after cell division measured by flow cytometry (Fig. S3). Corresponding values were calculated assuming a symmetrical distribution of PCI in the daughter cells.

	Cells [%]					
	J774A.1			**ImKC**		
Number of PCI	Day 0[a]	Day 1	Day 2	Day 0	Day 1	Day 2
0	47.7 (n.a.)	73.7 (65.7)	79.2 (84.9)	15.9 (n. a.)	37.3 (29.8)	59.2 (56.5)
1	22.6 (n.a.)	16.4 (26.2)	14.6 (14.4)	13. 8 (n.a.)	19.6 (31.1)	18.5 (38.3)
2	12.2 (n.a.)	5.4 (5.2)	3.4 (0.7)	11.8 (n. a.)	12.8 (18.0)	9.1 (5.2)
3	6.6 (n. a.)	1.9 (1.4)	0.9 (0)	9.9 (n. a.)	8.7 (9.6)	4.9 (0)
4	3.6 (n. a.)	0.8 (0.9)	0.3 (0)	8.1 (n. a.)	5.7 (7.3)	2.6 (0)
> 4	6.8 (n. a.)	0.9 (0.6)	0.2 (0)	37.9 (n. a.)	16.8 (4.1)	5.0 (0)

[a] Day 0 corresponds to cells that have been incubated for 24 h with ten 3 μm PS_{red} per cell. Given are the measured cell populations at the respective time. The calculated theoretical values are given in brackets. The materials and methods section provides a detailed description of the calculation of the theoretical values.

of cells was incubated with 3 μm PS_{green} particles, while another batch was incubated with 3 μm PS_{red} particles. After 24 h incubation, the cells were washed extensively to remove unbound and weakly interacting particles, and both cell fractions were pooled. The pooled cells were incubated for up to 72 h to allow for cell division, putative particle release, and *de novo* ingestion of particles. Flow cytometry was employed to analyze the cells and identify the presence of a "Mixed" population, characterized by the detection of fluorescence signals from both particle types yet indicating interaction with both (Fig. 3 and Fig. 4). The analysis involved examining the cytograms to observe potential instances of particle release by a cell batch initially challenged with one particle type, followed by the re-attachment of those released particles to cells from the batch that had been exposed to the other particle type.

During the course of incubation, starting from 24 h onwards, there was an increase in the percentage of cells without interacting particles. This observation can be attributed to cell division of cells initially without PCI as well as to an asymmetric distribution of particles during division of cells with a lower number of PCI. This is in line with the decrease described above at incubation times ≥ 24 h. However, a small but well-discernable population of cells interacting with both particle types (Gate "Mixed") was visible for both cell lines. This population arose between 0 h and 2–6 h, but did not expand over 72 h of incubation time. Instead, a slight decrease was observed at longer incubation times. This indicates that some particles must have been released at early points after the pooling process and that at least some of these particles were re-ingested by cells from the other batch. Since this fraction did not grow over the time of incubation, an active release by the living cells is unlikely. This phenomenon can be at least partly attributed to the release of particles from dead cells followed by their subsequent ingestion by neighboring cells, as demonstrated in the time-lapse video (e.g., Fig. 1).

3.4. *Localization of submicron particles in the endoplasmic reticulum and endosomes*

Previous studies have reported various cytotoxic effects following particle uptake, which have been attributed to processes occurring within the nuclei, i.e. the disturbance of gDNA integrity, as well as stress responses related to functions of mitochondria, lysosomes, or ER [19,20,30,31]. Here, we analyzed the intracellular distribution of PS particles after cellular uptake by staining specifically selected organelles and analyzing putative particle co-localization using confocal microscopy. These experiments aimed to elucidate, whether the observed effects coincide with the physical presence of the particles (also dependent on particle size) in the presumably affected organelles.

Cells were incubated with fluorescent particles (0.2 μm, 0.5 μm, 3 μm) for 15 h followed by specific staining of the cellular compartments in the living cells. The cytoplasmic proteins were stained using a non-toxic cell permeable fluorescence dye (i.e., CellTracker fluorescent probe) reacting with thiol groups in a glutathione S transferase-mediated reaction. After conversion, the fluorescent dye is, according to the manufacturer's information, retained in living cells for at least 72 h. Selected organelles playing a crucial role in cell physiology, namely lysosomes, nuclei, mitochondria, endoplasmic reticulum (ER), and Golgi apparatus, were identified using specific fluorescence staining. A co-localization of 3 μm particles with organelles, which are usually much smaller, is improbable, but these larger particles were included in the experimental settings because they have been used for

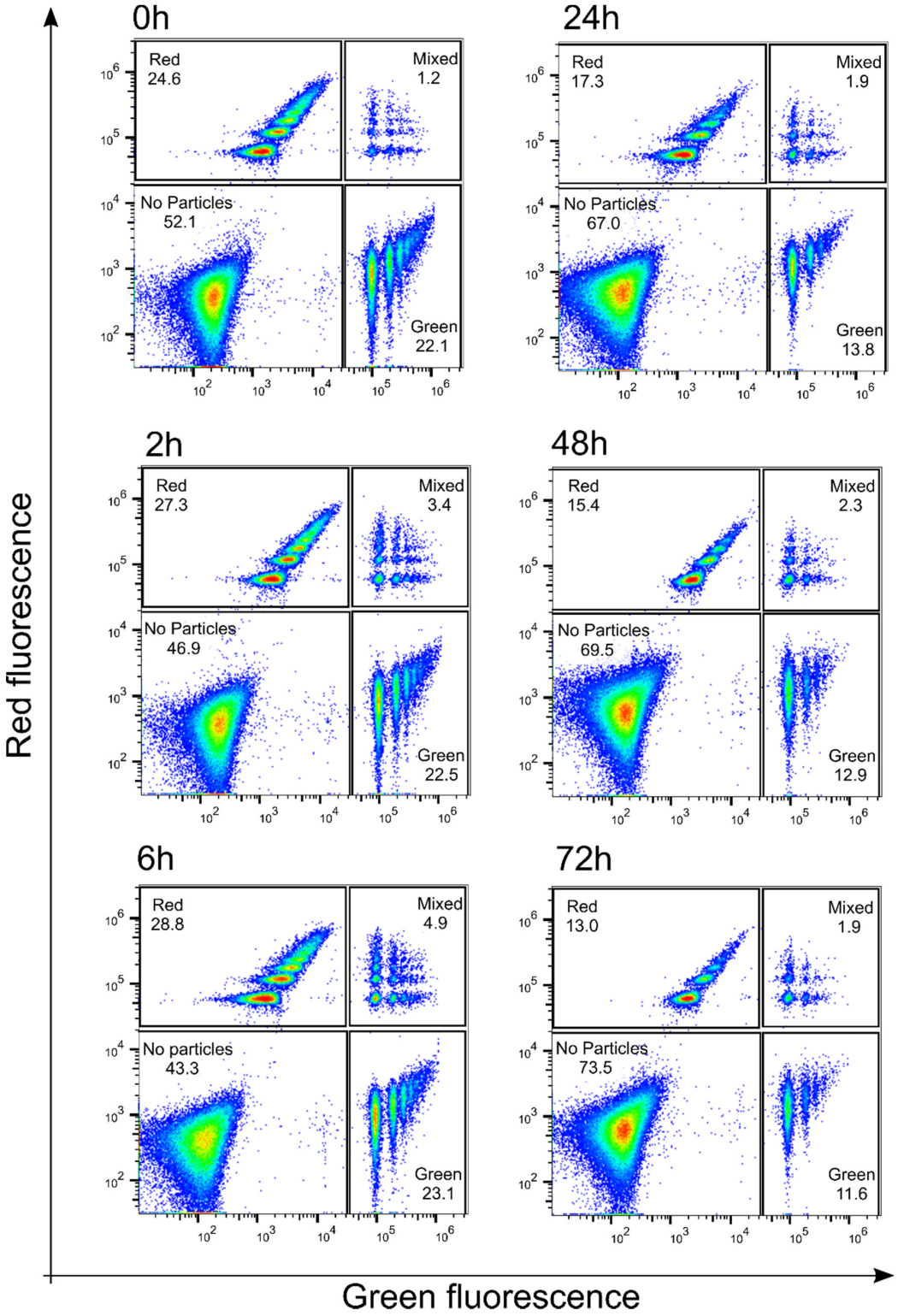

Fig. 3. Putative particle release over time in case of ImKC cells. One batch of cells was incubated with 3 μm PS_{green} particles another batch was incubated with 3 μm PS_{red} for 24 h. 150,000 cells were seeded per well, and 1.68 × 106 particles/well were added. Cells were then pooled (0 h), and the particle distribution was measured for 72 h using flow cytometry. "Red" gate = only PS_{red}, "Green" gate = only PS_{green}, "Mixed" gate = at least 1 particle of PS_{red} and PS_{green}.

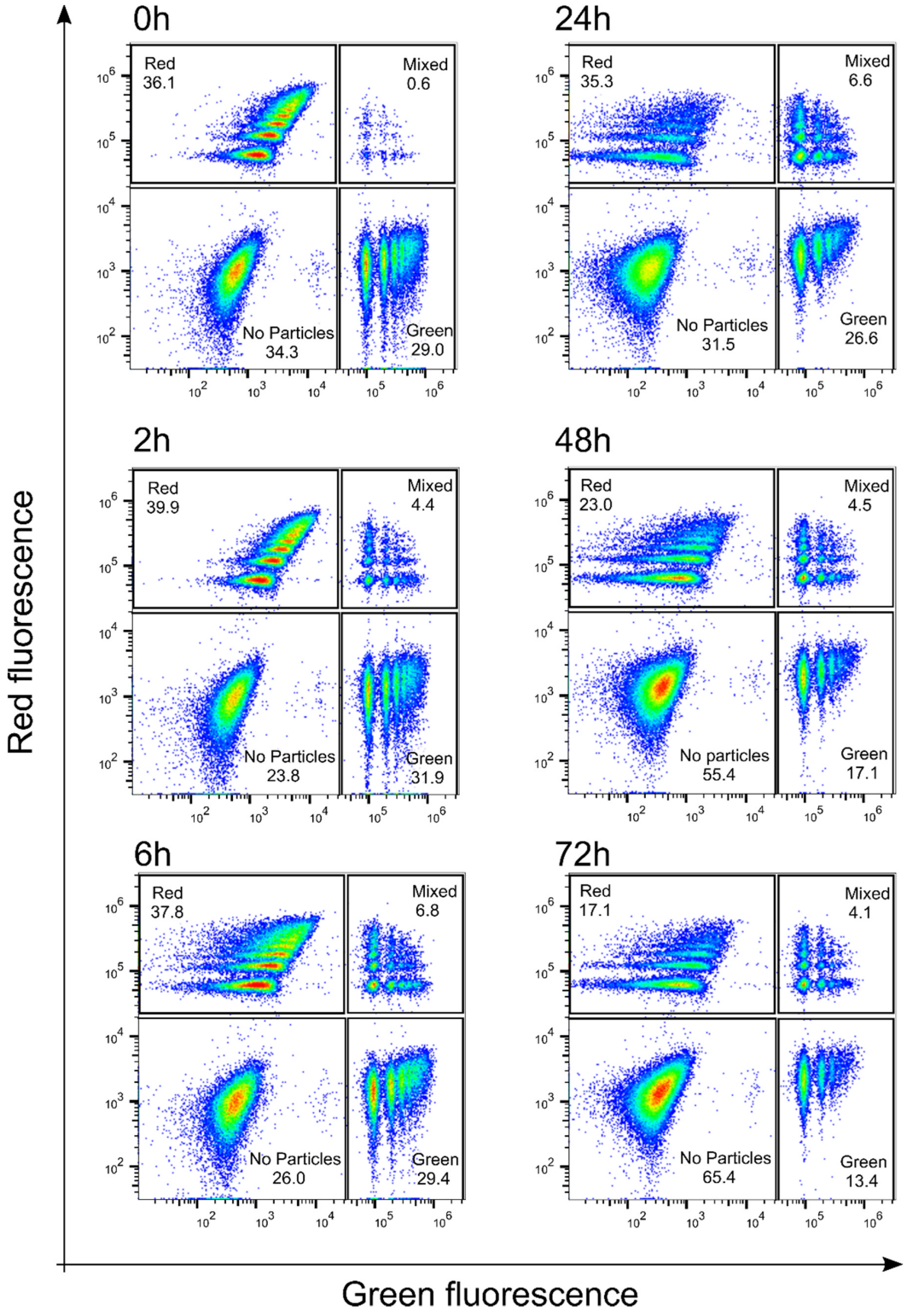

Fig. 4. Putative particle release over time in case of J774A.1 cells. One batch of cells was incubated with 3 μm PS_{green} particles another batch was incubated with 3 μm PS_{red} for 24 h. 150,000 cells were seeded per well, and 1.68 × 106 particles/well were added. Cells were then pooled (0 h), and the particle distribution was measured for 72 h using flow cytometry. "Red" gate = only PS_{red}, "Green" gate = only PS_{green}, "Mixed" gate = at least 1 particle of PS_{red} and PS_{green}.

the particle release analysis as mentioned above.

Independent of their size, the particles were mainly found in the cytoplasm, implying that the particles had been ingested, yet not merely attached to the cells. Consequently, the PCI interactions, measured in flow cytometry experiments are likely representative of particle uptake and not only particles binding to the cell membrane. Regardless of the cell line used, particles with a size of 3 μm were not found in any of the organelles (Fig. S6, S7). However, the smaller particles (0.2 and 0.5 μm) were partly found in the ER of both macrophage cell lines (Fig. 5A). No particles were ever found in or in contact with the nuclei, mitochondria, Golgi apparatus, or lysosomes (Fig. S6, S7). These findings indicate a size-dependent distribution pattern, suggesting that smaller particles have the capability to access and reside within the ER of macrophages.

To further investigate the observations made during cytoplasm staining, particularly the presence of green spots indicating the absence of co-localization, additional staining with endosome antibodies was performed. This step was undertaken because endosomes are known to play a role in the exocytosis process [11,12,16,17]. In detail, early and late endosomes were stained using EEA-1 or Rab7, respectively ; Fig. 5B and 0.2 μm PS_{green}: Figure S8). Only 0.5 μm particles were found in the endosomes. While J774A.1 cells contained particles only in the late endosomes, in ImKC cells they were found in both, early and late endosomes.

4. Discussion

Even though various previous studies addressed the cytotoxic effects of MPP [18–20,25,26], the intracellular fate of the particles after ingestion and a possible contribution of a directed distribution/-organelle co-localization to these effects has not been studied in depth so far.

According to the current understanding, ingested foreign matter may be distributed randomly, symmetrically or even one-sidedly during cellular division, while organelles are distributed in a symmetrical manner [58–60]. For nanoparticles, random distribution has been shown in previous studies [48,49]. While the data obtained for J774A.1 aligned reasonably well with the approximation derived from the assumption of a random (non-symmetrical) distribution, ImKC cells showed a higher deviation from the symmetrical distribution. These cell-specific differences could be related to the natural function of the two macrophage types; J774A.1 are exudate macrophages from blood, while ImKC cells are descendants of liver-resident macrophages. ImKC cells, thus, may be expected to react to foreign particles as to intruding bacteria, whereas the reaction of the J774A.1 cells is more indifferent, leading to a more equal distribution.

Throughout the 72-hour incubation period, no significant release of ingested particles was observed. The occasionally observed mixing of particles during the first 6 h of the experiment was most likely due to non-ingested particles washed off during the pooling process, since this fraction did not increase after 6 h but decreased in a similar pattern as the other PCI populations. A minor addition to the observed mixing of particles was probably due to a re-ingestion of particles released after cell death. Excretion of particles has been reported for nanoparticles. However, this process typically involves their incorporation into lysosomes for active excretion [46,61]. In the case of micrometer-sized MPP, it appears that active excretion does not occur. Consistent with the findings of this study, particles larger than 1 μm in diameter were not detected within endosomes or lysosomes. This observation suggests that the most common cellular pathway for excretion, which involves the incorporation of particles into endosomes and subsequent lysosomal degradation, may not be applicable to particles measuring 3 μm in size [14,62].

The intracellular distribution of MPP after cellular ingestion is not well understood but may be relevant to understand possible cytotoxic effects of MP. Here, all investigated particles were localized in the cytosol, i.e., truly ingested, not merely attached to the cells. The observation of 3 μm particles as distinct green dots, while submicron particles exhibited a pronounced yellow color in the cytoplasm, is most likely an artifact resulting from the size of the 3 μm particles. The larger size of these particles might cause a displacement of the cytoplasm, leading to the formation of a cavity within the cell.

The changes in mitochondrial activity and genomic DNA integrity observed previously after challenging cells (macrophages) with PS particles [19,20] have unlikely been due to physical presence, i.e. a co-localization of particles with either mitochondria or nuclei, as co-localization of particles with these organelles could not be observed in this study. Therefore, the previously described mitochondrial damage is not necessarily based on ingestion of the MPP in mitochondria or interaction with chromosomes. Instead, the observed effects could be attributed to, e.g., oxidative stress. Increased ROS, which was described previously, conceivably contributes to reduced mitochondrial activity as well as to genotoxicity [63,64].

Furthermore, no co-localization of MPP with the Golgi apparatus was observed. The absence of co-localization between the submicrometer-sized particles (0.2 and 0.5 μm) and organelles such as mitochondria and the Golgi apparatus could be attributed to the relatively large size of the particles in comparison to these organelles [65,66]. In contrast, cells from both investigated cell lines exhibited co-localization of 0.2 μm and 0.5 μm particles with the ER. The ER is responsible for many protein-related processes, including translation, folding, post-translational modifications, and transport [67,68]. Whether these functions are altered by the presence of submicron particles and whether this may contribute to the observed noxic effects needs further study. For ER staining, the ER-Tracker™ was used, which binds to sulphonylurea receptors prominent in the ER [69,70]. Nevertheless, Ashcroft et al. reported a variable sulphonylurea receptor expression by some cells, possibly leading to non-specific labelling [69]. Even though a variable sulphonylurea receptor expression was not previously reported for macrophage cell lines, non-specific labelling could still be an alternative explanation.

Lysosomes are known for their contribution to clearance of pathogens as well as particles ≤ 0.2 μm from cells, therefore a co-localization of at least the smaller PS particles was expected with these organelles after ingestion [5–7]. The lack of evidence for a general co-localization may to some extent be due to the chosen staining method, since it could not be fully excluded that acridine orange clusters in lysosomes leading to high fluorescence intensity, which eventually quenched or overlaid the particles' fluorescence [71,72]. Identifying early and late endosomes using antibody staining (early: EEA1, late: Rab7) showed that only 0.5 μm PS particles in ImKC macrophages co-localized with endosomes. Importantly, the proteins chosen as endosome markers, namely EEA-1 and Rab7, are also expressed in macropinosomes and phagosomes [4,13,14]. Since cellular ingestion is mainly based on phagocytosis for both cell lines [73], this could indicate that 0.5 μm particles may actually be localized in the early and/or late phagosome. Any particle reaching the late endosome in the hierarchal endocytic pathway should be found in lysosomes as well [14]. This, however, was not the case in our experiments. Together with the lack of localization in lysosomes, this could mean that particle-containing phagosomes for some reason are not capable of forming phagolysosomes.

Following the assumption of staining phagosomes rather than endosomes in our case may explain the observed differences in localization of 0.2 μm and 0.5 μm particles. 0.2 μm PS particles presumably are ingested by different endocytic pathways (i.e., clathrin- or caveolae-mediated endocytosis) compared to 0.5 μm particles, which more likely have been ingested by phagocytosis or macropinocytosis [1,73] and, therefore, have become engulfed in a phagosome or macropinosome. In case of 0.2 μm particles, no phagosome/macropinosome will be formed, and no co-localization will be observed in such vesicles [1,73]. Just as for pathogens, the size of the particles may influence uptake and intracellular processing by determining the rate of endosomal maturation [74].

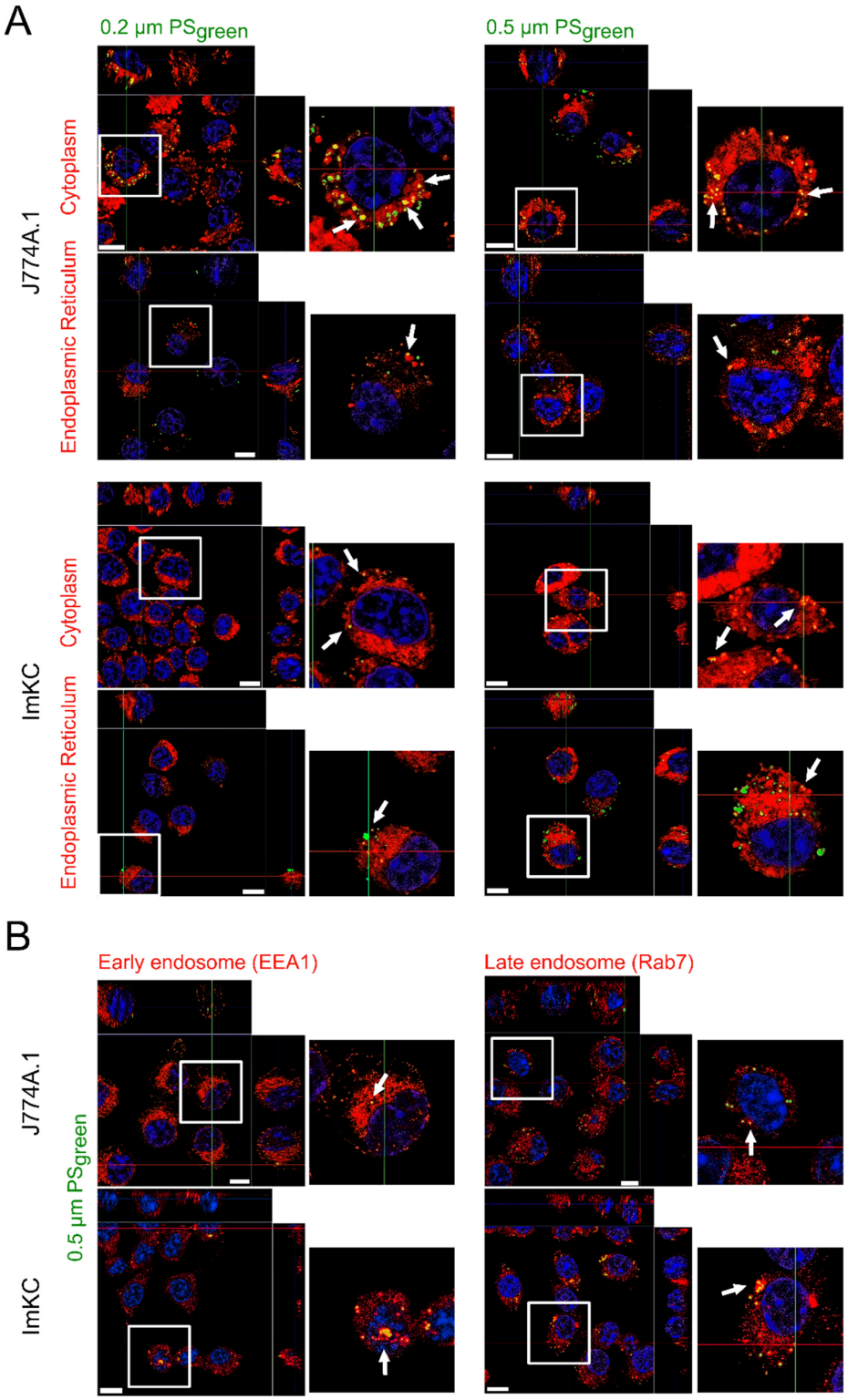

Fig. 5. Particle co-localization with organelles as indicated in J774A.1 and ImKC macrophages. 0.2 and 0.5 µm PS_{green} particles were used, and the particle incubation occurred for 15 h. A: Co-localization with the cytoplasm and the ER. The images of mitochondria, Golgi apparatus, and lysosomes are shown in Figs. S6 and S7. B: Co-localization of 0.5 µm particles with endosomes. Early and late endosomes were stained using antibody staining (EEA-1 and Rab7, respectively). The corresponding picture on the right side displays an enlarged view of the specific cell, which is highlighted by a white square. The images of 0.2 µm particles are shown in Fig. S8. Red: cytoplasm or organelles, blue: nuclei (Hoechst), green: fluorescent particles. A yellow color indicates a co-localization of the particle with the stained cellular compartment, and white arrows show exemplary co-localized particles. Scale bar: 10 µm.

Since only a few 0.5 μm particles were found in late endosomes/phagosomes in J774A.1 cells and none in early endosomes/phagosomes, but 0.5 μm particles were found in both early and late endosomes/phagosomes of the ImKC cells, a correlation between the activation status of the two cell lines and the intracellular processing can be postulated. The speed of phagosome maturation depends on the macrophage activation status, and M1 macrophages have been shown to have slower phagosome maturation than M0 and M2 macrophages [75]. The activation status of ImKC cells, as indicated by CD80 (M1 marker), exhibits slower kinetics compared to that of other cells. Therefore, co-localization of MP in the early and late endosomes/phagosomes is still observable. In J774A.1 cells, the phagosomes mature more quickly, and no co-localization with the early endosome/early phagosome is observed at the point of measurement (after 15 h). However, the co-localization results must be interpreted with caution, since only one-time point (after 15 h) was analyzed, and there is the possibility that the particles either had not yet reached the organelles or had already passed them.

Finally, we could show that activation (M1/M2 status) affects MPP uptake. In particular, M1 cells are significantly more likely to ingest particles than the non-committed control cells (M0 or M2 macrophage). In vivo, M1 macrophages are responsible for maintaining a pro-inflammatory state and show highly active phagocytic behavior, fitting with the here-found results. The significant interaction of M1 macrophages with MPP might be highly synergistic with an induced polarization due to the presence of the particles, contributing to the pro-inflammatory response to MPP detected in various in vitro and in vivo studies [20,45].

Gaining valuable insights into the influence of a macrophage's phenotype and polarization status on its interaction with PS MPP was obtained by employing a variety of experimental approaches. Our observations revealed a diverse response of macrophages to MPP, which was dependent on the specific cell type and the degree of polarization. These findings underscore the critical importance of considering these cellular factors when investigating cellular responses to microplastics. Our results further show that the distribution patterns of engulfed MPP did not exhibit any discernible trends during cell division.

Despite the repeatedly observed effects of nano- and microparticles on cells, only a limited number of particles have been identified within specific organelles, namely the endoplasmic reticulum and endosomes. Finally, it should be noted that while particles were released by cells after cell death, no active excretion process was observed for living macrophages. Since pathogens are typically rendered harmless by macrophages through lysosomal digestion, it is anticipated that ingested particles will persist within macrophages for as long as the cells remain viable, potentially leading to their accumulation. This raises concerns regarding the potential long-term effects of microplastic exposure. Our results enhance our understanding of the cellular mechanisms involved in the fate and behavior of microplastics within macrophage populations and provide valuable insights for assessing potential health and environmental implications associated with exposure to microplastics.

Environmental implication

Our study contributes to a better understanding of microplastics' toxicology, which appears to be dependent on cell type and also on the polarization state of such cells. This information is essential, as sound knowledge on the characteristics driving microplastic toxicity on organisms may explain the often contradictory results observed in effect studies on microplastics and will help to advance risk assessment for microplastic particles.

Funding

This work was supported by the Deutsche Forschungsgemeinschaft (DFG, German Research Foundation) - project number 391977956 - SFB 1357/A05.

CRediT authorship contribution statement

JJ, MV, JH, VJ, RF, and TS designed the experiments. MV provided mixed particle experiments, excretion analysis, and macrophage polarization experiments. JJ performed organelle staining as well as time-lapse experiments. JH supported the cellular movement analysis. VJ, RF, and TS supervised the experiments. JJ, MV and JH analyzed the data. JJ, MV, VJ, RF, and TS wrote the manuscript. VJ, RF, and TS reviewed and edited the manuscript.

Declaration of Competing Interest

The authors declare no competing interest.

Data Availability

Data will be made available on request.

Acknowledgments

We thank Johanna Fritsche for supporting the experiments with polarized macrophages.

Appendix A. Supporting information

Supplementary data associated with this article can be found in the online version at doi:10.1016/j.jhazmat.2023.131796.

References

[1] Aderem, A., Underhill, D.M., 1999. Mechanisms of phagocytosis in macrophages. Annu Rev Immunol 17, 593–623.
[2] Mylvaganam, S., Freeman, S.A., Grinstein, S., 2021. The cytoskeleton in phagocytosis and macropinocytosis. Curr Biol 31, R619–R632.
[3] Champion, J.A., Mitragotri, S., 2006. Role of target geometry in phagocytosis. Proc Natl Acad Sci 103, 4930–4934.
[4] Lee, H.-J., Woo, Y., Hahn, T.-W., Jung, Y.M., Jung, Y.-J., 2020. Formation and maturation of the phagosome: a key mechanism in innate immunity against intracellular bacterial infection. Microorganisms 8, 1298.
[5] Settembre, C., Fraldi, A., Medina, D.L., Ballabio, A., 2013. Signals from the lysosome: a control centre for cellular clearance and energy metabolism. Nat Rev Mol Cell Biol 14, 283–296.
[6] Luzio, J.P., Pryor, P.R., Bright, N.A., 2007. Lysosomes: fusion and function. Nat Rev Mol Cell Biol 8, 622–632.
[7] Zhang, Z., et al., 2021. Role of lysosomes in physiological activities, diseases, and therapy. J Hematol Oncol 14, 1–39.
[8] Hesketh, G.G., Wartosch, L., Davis, L.J., Bright, N.A., Luzio, J.P., 2018. The lysosome and intracellular signalling. Endocytosis Signal 151–180.
[9] Jeger, J.L., 2020. Endosomes, lysosomes, and the role of endosomal and lysosomal biogenesis in cancer development. Mol Biol Rep 47, 9801–9810.
[10] Helenius, A., Mellman, I., Wall, D., Hubbard, A., 1983. Endosomes. Trends Biochem Sci 8, 245–250.
[11] Scott, C.C., Vacca, F., Gruenberg, J., 2014. Endosome maturation, transport and functions. In: Seminars in cell & developmental biology, Vol. 31. Elsevier, pp. 2–10.
[12] Podinovskaia, M., Spang, A., 2018. The endosomal network: mediators and regulators of endosome maturation. Endocytosis Signal 1–38.
[13] Mukherjee, K., Khatua, B., Mandal, C., 2020. Sialic acid-siglec-E interactions during Pseudomonas aeruginosa infection of macrophages interferes with phagosome maturation by altering intracellular calcium concentrations. Front Immunol 11, 332.
[14] Vieira, O.V., Botelho, R.J., Grinstein, S., 2002. Phagosome maturation: aging gracefully. Biochem J 366, 689–704.
[15] Chen, X., Cubillos-Ruiz, J.R., 2021. Endoplasmic reticulum stress signals in the tumour and its microenvironment. Nat Rev Cancer 21, 71–88.
[16] Jahn, R., Südhof, T.C., 1999. Membrane fusion and exocytosis. Annu Rev Biochem 68, 863–911.
[17] Wu, L.-G., Hamid, E., Shin, W., Chiang, H.-C., 2014. Exocytosis and endocytosis: modes, functions, and coupling mechanisms. Annu Rev Physiol 76, 301.
[18] Stock, V., et al., 2019. Uptake and effects of orally ingested polystyrene microplastic particles in vitro and in vivo. Arch Toxicol 1–17.
[19] Rudolph, J., Völkl, M., Jérôme, V., Scheibel, T., Freitag, R., 2021. Noxic effects of polystyrene microparticles on murine macrophages and epithelial cells. Sci Rep 11, 1–16.

[20] Völkl, M., et al., 2022. Pristine and artificially-aged polystyrene microplastic particles differ in regard to cellular response. J Hazard Mater 435, 128955.
[21] Frias, J.P.G.L., Nash, R., 2019. Microplastics: finding a consensus on the definition. Mar Pollut Bull 138, 145–147.
[22] Imhof, H.K., Ivleva, N.P., Schmid, J., Niessner, R., Laforsch, C., 2013. Contamination of beach sediments of a subalpine lake with microplastic particles. Curr Biol 23, R867–R868.
[23] Dris, R., Gasperi, J., Saad, M., Mirande, C., Tassin, B., 2016. Synthetic fibers in atmospheric fallout: a source of microplastics in the environment? Mar Pollut Bull 104, 290–293.
[24] Evangeliou, N., et al., 2020. Atmospheric transport is a major pathway of microplastics to remote regions. Nat Commun 11, 1–11.
[25] Toussaint, B., et al., 2019. Review of micro-and nanoplastic contamination in the food chain. Food Addit Contam: Part A 36, 639–673.
[26] Lu, Y., et al., 2016. Uptake and accumulation of polystyrene microplastics in zebrafish (danio rerio) and toxic effects in liver. Environ Sci Technol 50, 4054–4060.
[27] Schwabl, P., et al., 2019. Detection of various microplastics in human stool: a prospective case series. Ann Intern Med 171, 453–457.
[28] Fröhlich, E., 2012. The role of surface charge in cellular uptake and cytotoxicity of medical nanoparticles. Int J Nanomed 7, 5577.
[29] Ramsperger, A., et al., 2022. Supposedly identical microplastic particles substantially differ in their material properties influencing particle-cell interactions and cellular responses. J Hazard Mater 425, 127961.
[30] Lim, S.L., et al., 2019. Targeted metabolomics reveals differential biological effects of nanoplastics and nanoZnO in human lung cells. Nanotoxicology 13, 1117–1132.
[31] Liu, L., Liu, B., Zhang, B., Ye, Y., Jiang, W., 2022. Polystyrene micro (nano) plastics damage the organelles of RBL-2H3 cells and promote MOAP-1 to induce apoptosis. J Hazard Mater 438, 129550.
[32] von Moos, N., Burkhardt-Holm, P., Köhler, A., 2012. Uptake and Effects of Microplastics on Cells and Tissue of the Blue Mussel Mytilus edulis L. after an Experimental Exposure. Environ Sci Technol 46, 11327–11335.
[33] Jenkins, J.T., et al., 2013. Excretion and toxicity of gold–iron nanoparticles. Nanomed: Nanotechnol, Biol Med 9, 356–365.
[34] Leslie, H.A., et al., 2022. Discovery and quantification of plastic particle pollution in human blood. Environ Int 163, 107199.
[35] Haldar, M., Murphy, K.M., 2014. Origin, development, and homeostasis of tissue-resident macrophages. Immunol Rev 262, 25–35.
[36] Guillot, A., Tacke, F., 2019. Liver macrophages: old dogmas and new insights. Hepatol Commun 3, 730–743.
[37] Reichard, A.C., Cheemarla, N.R., Bigley, N.J., 2015. SOCS1/3 expression levels in HSV-1-infected, cytokine-polarized and-unpolarized macrophages. J Interferon Cytokine Res 35, 32–41.
[38] Shapouri-Moghaddam, A., et al., 2018. Macrophage plasticity, polarization, and function in health and disease. J Cell Physiol 233, 6425–6440.
[39] Feito, M., et al., 2021. Response of RAW 264.7 and J774A. 1 macrophages to particles and nanoparticles of a mesoporous bioactive glass: a comparative study. Colloids Surf B: Biointerfaces 208, 112110.
[40] Mills, C., 2012. M1 and M2 macrophages: oracles of health and disease. Crit Reviews™ Immunol 32.
[41] Italiani, P., Boraschi, D., 2014. From monocytes to M1/M2 macrophages: phenotypical vs. functional differentiation. Front Immunol 5, 514.
[42] Gordon, S., 2003. Alternative activation of macrophages. Nat Rev Immunol 3, 23–35.
[43] Mills, C.D., 2015. Anatomy of a discovery: m1 and m2 macrophages. Front Immunol 6, 212.
[44] Seyedizade, S.S., et al., 2020. Current status of M1 and M2 macrophages pathway as drug targets for inflammatory bowel disease. Arch Immunol Et Ther Exp 68, 1–24.
[45] Collin-Faure, V., et al., 2022. Does size matter? A proteomics-informed comparison of the effects of polystyrene beads of different sizes on macrophages. Environ Sci: Nano 9, 2827–2840.
[46] Oh, N., Park, J.-H., 2014. Surface chemistry of gold nanoparticles mediates their exocytosis in macrophages. ACS Nano 8, 6232–6241.
[47] Liu, L., et al., 2021. Cellular internalization and release of polystyrene microplastics and nanoplastics. Sci Total Environ 779, 146523.
[48] Walczak, P., Kedziorek, D., Gilad, A., Barnett, B., Bulte, J.W., 2007. Applicability and limitations of MR tracking of neural stem cells with asymmetric cell division and rapid turnover: the case of the shiverer dysmyelinated mouse brain. Magn Reson Med: J Int Soc Magn Reson Med 58, 261–269.
[49] Lijster, T., Åberg, C., 2020. Asymmetry of nanoparticle inheritance upon cell division: effect on the coefficient of variation. Plos One 15, e0242547.
[50] Orihuela, R., McPherson, C.A., Harry, G.J., 2016. Microglial M1/M2 polarization and metabolic states. Br J Pharmacol 173, 649–665.
[51] Tempany, J.C., Zhou, J.H., Hodgkin, P.D., Bryant, V.L., 2018. Superior properties of CellTrace Yellow™ as a division tracking dye for human and murine lymphocytes. Immunol Cell Biol 96, 149–159.
[52] Lemieszek, M.B., Findlay, S.D., Siegers, G.M., 2022. CellTrace™ violet flow cytometric assay to assess cell proliferation. Cancer Cell Biology. Springer, pp. 101–114.
[53] Schindelin, J., et al., 2012. Fiji: an open-source platform for biological-image analysis. Nat Methods 9, 676–682.
[54] Canny, J., 1986. A computational approach to edge detection. IEEE Trans Pattern Anal Mach Intell 679–698.
[55] Yuen, H., Princen, J., Illingworth, J., Kittler, J., 1990. Comparative study of Hough transform methods for circle finding. Image Vis Comput 8, 71–77.
[56] Crocker, J.C., Grier, D.G., 1996. Methods of digital video microscopy for colloidal studies. J Colloid Interface Sci 179, 298–310.
[57] Allan, D.B., Caswell, Thomas, Keim, Nathan, C., van der Wel, Casper, M., et al., 2021. Ruben W. soft-matter/trackpy: Trackpy v0.5.0 (v0.5.0). Zenodo.
[58] Zhao, W., et al., 2015. The Salmonella effector protein SifA plays a dual role in virulence. Sci Rep 5, 1–10.
[59] Thyberg, J., Moskalewski, S., 1998. Partitioning of cytoplasmic organelles during mitosis with special reference to the Golgi complex. Microsc Res Tech 40, 354–368.
[60] Carlton, J.G., Jones, H., Eggert, U.S., 2020. Membrane and organelle dynamics during cell division. Nat Rev Mol Cell Biol 21, 151–166.
[61] Sadauskas, E., et al., 2007. Kupffer cells are central in the removal of nanoparticles from the organism. Part Fibre Toxicol 4, 1–7.
[62] De Chastellier, C., Thilo, L., 1997. Phagosome maturation and fusion with lysosomes in relation to surface property and size of the phagocytic particle. Eur J Cell Biol 74, 49–62.
[63] Visalli, G., et al., 2021. Acute and sub-chronic effects of microplastics (3 and 10 μm) on the human intestinal cells HT-29. Int J Environ Res Public Health 18, 5833.
[64] Hu, M., Palić, D., 2020. Micro-and nano-plastics activation of oxidative and inflammatory adverse outcome pathways. Redox Biol 37, 101620.
[65] Kühnel, W., 2003. Color atlas of cytology, histology, and microscopic anatomy. Thieme Medical Publishers.
[66] Wiemerslage, L., Lee, D., 2016. Quantification of mitochondrial morphology in neurites of dopaminergic neurons using multiple parameters. J Neurosci Methods 262, 56–65.
[67] Berridge, M.J., 2002. The endoplasmic reticulum: a multifunctional signaling organelle. Cell Calcium 32, 235–249.
[68] Maruri-Avidal, L., López, S., Arias, C.F., 2008. Endoplasmic reticulum chaperones are involved in the morphogenesis of rotavirus infectious particles. J Virol 82, 5368–5380.
[69] Ashcroft, S.J., Ashcroft, F.M., 1992. The sulfonylurea receptor. Biochim Et Biophys Acta (BBA)-Mol Cell Res 1175, 45–59.
[70] Don, A.S., et al., 2007. Essential requirement for sphingosine kinase 2 in a sphingolipid apoptosis pathway activated by FTY720 analogues. J Biol Chem 282, 15833–15842.
[71] Wang, F., et al., 2006. Study on the formation and depolymerization of acridine orange dimer in acridine orange–sodium dodecyl benzene sulfonate–protein system. J Colloid Interface Sci 298, 757–764.
[72] Qi, J., et al., 2019. Towards more accurate bioimaging of drug nanocarriers: turning aggregation-caused quenching into a useful tool. Adv Drug Deliv Rev 143, 206–225.
[73] Uribe-Querol, E., Rosales, C., 2020. Phagocytosis: our current understanding of a universal biological process. Front Immunol 11, 1066.
[74] Baranov, M.V., Kumar, M., Sacanna, S., Thutupalli, S., 2021. Modulation of immune responses by particle size and shape. Front Immunol 3854.
[75] Canton, J., 2014. Phagosome maturation in polarized macrophages. J Leukoc Biol 96, 729–738.

Supplementary Information

Polystyrene microparticle distribution after ingestion by murine macrophages

Julia Jasinski[1†], Matthias Völkl[2†], Jonas Hahn[1], Valérie Jérôme[2], Ruth Freitag[2,4], Thomas Scheibel[1,3,4,5,6]

[1] Biomaterials, Faculty of Engineering Sciences, University of Bayreuth, Bayreuth, Germany
[2] Process Biotechnology, Faculty of Engineering Sciences, University of Bayreuth, Bayreuth, Germany
[3] Bayreuth Center for Colloids and Interfaces (BZKG), Universität Bayreuth, Bayreuth, Germany
[4] Bayreuth Center for Molecular Biosciences (BZMB), Universität Bayreuth, Bayreuth, Germany
[5] Bayreuth Center for Material Science (BayMAT), Universität Bayreuth, Bayreuth, Germany
[6] Bavarian Polymer Institute (BPI), Universität Bayreuth, Bayreuth, Germany

† both authors contributed equally

Videos

Video S1. Movement of J774A.1 macrophages with no added particles (=control) over 25 h.

Video S2. Movement of J774A.1 macrophages and their interaction with 3 µm PSPs over 25 h.

Video S3. Movement of ImKC macrophages with no added particles (=control) over 25 h.

Video S5. Movement of ImKC macrophages and their interaction with 3 µm PSPs over 26 h.

21 **Figures**

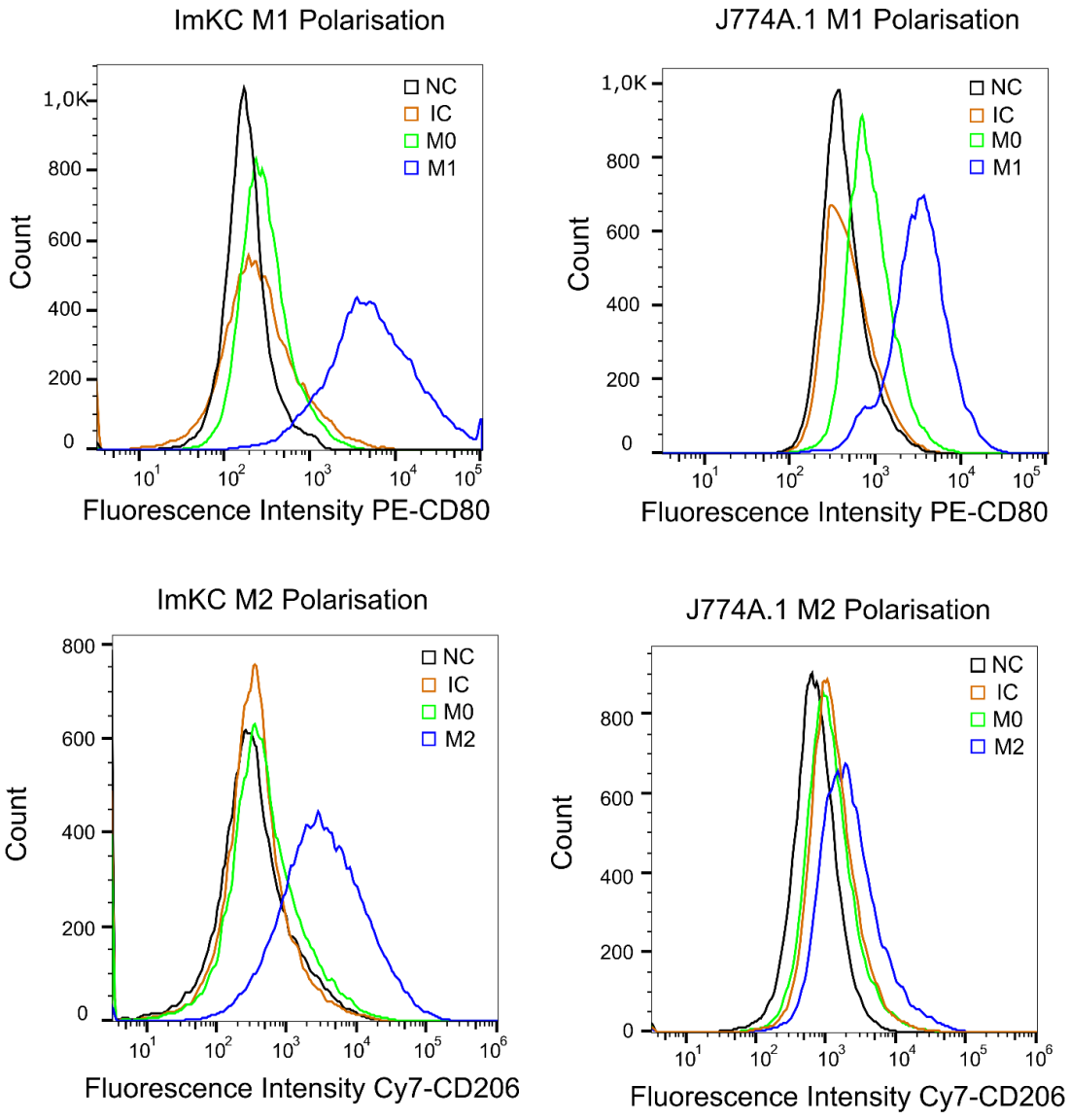

22

23

24 Figure S1. Antibody staining of polarized macrophages. The CD80 and CD206 surface marker of polarized and non-polarized
25 cells were stained, respectively. Polarization was induced by adding 100 ng LPS for 24 h to the growth medium in the case of
26 M1 polarization and 20 ng/mL IL-4 in the case of M2 polarization. NC = unstained and untreated negative control, IC = isotype
27 control, M0 = untreated and stained, M1 = M1 polarized and stained, M2 = M2 polarized and stained

28

29

Calculation of the approximation

This approximation was calculated as follows:

- The number of particles per cell at day 0 (P_{n,t_0}) was measured for the respective cell populations.
- Cell division was calculated by measuring the CTV fluorescence every other day.
- In the case of ImKC, the CTV intensity was only 1/3 on day 1 compared to day 0, indicating three times the number of cells or approximately 3 cells out of 1.
- A symmetrical distribution was assumed.
- Particles per cell were calculated on the assumed Day 1, counted, summarised (P_{all,t_1}) and normalized to 100% (P_{n,t_1}).
- Same procedure was obtained for the following days (P_{n,t_m}).
- The calculated numbers were used as an approximation for a symmetrical distribution and compared to the measured data.

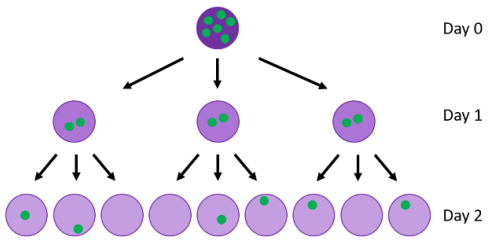

Figure S2. Exemplary process scheme for the calculation of the approximation considering a symmetrical distribution.

Equation 1. Mathematical equation for the calculation of the approximation.

$$P_{all,t_0} = P_{0,t_0} + P_{1,t_0} + P_{2,t_0} + \cdots + P_{n,t_0}$$

$$P_{all,t_1} = \left(3 * P_{0,t_0} + 2 * P_{1,t_0} + 3 * P_{2,t_0}\right) + \left(1 * P_{1,t_0} + 2 * P_{2,t_0} + 3 * P_{3,t_0}\right) + \cdots + \left(1 * P_{n,t_0} + 2 * P_{n+1,t_0} + 3 * P_{n+2,t_0}\right)$$

$$P_{0,t_1} = \frac{\left(3 * P_{0,t_0} + 2 * P_{1,t_0} + 3 * P_{2,t_0}\right) * 100\%}{P_{all,t_1}}$$

$$P_{1,t_1} = \frac{\left(1 * P_{1,t_0} + 2 * P_{2,t_0} + 3 * P_{3,t_0}\right) * 100\%}{P_{all,t_1}}$$

$$P_{2,t_1} = \frac{\left(1 * P_{4,t_0} + 2 * P_{5,t_0} + 3 * P_{6,t_0}\right) * 100\%}{P_{all,t_1}}$$

$$P_{m,t_1} = \frac{\left(1 * P_{n,t_0} + 2 * P_{n+1,t_0} + 3 * P_{n+2,t_0}\right) * 100\%}{P_{all,t_1}}$$

$$P_{all,t_2} = \left(3 * P_{0,t_1} + 2 * P_{1,t_1} + 3 * P_{2,t_1}\right) + \left(1 * P_{1,t_1} + 2 * P_{2,t_1} + 3 * P_{3,t_1}\right) + \cdots + \left(1 * P_{n,t_1} + 2 * P_{n+1,t_1} + 3 * P_{n+2,t_1}\right)$$

$$P_{all,t_m} = \left(3 * P_{0,t_m} + 2 * P_{1,t_m} + 3 * P_{2,t_m}\right) + \left(1 * P_{1,t_m} + 2 * P_{2,t_m} + 3 * P_{3,t_m}\right) + \cdots + \left(1 * P_{n,t_m} + 2 * P_{n+1,t_m} + 3 * P_{n+2,t_m}\right)$$

$$P_{all,t_0} = Combined\ cell\ population\ at\ t_0\ [\%]$$

$$P_{all,t_1} = Combined\ cell\ population\ at\ t_1\ [\%]$$

$$P_{0,t_0} = cell\ population\ with\ 0\ PCI\ at\ t_0\ [\%]$$

$$P_{1,t_0} = cell\ population\ with\ 1\ PCI\ at\ t_0\ [\%]$$

$$P_{2,t_0} = cell\ population\ with\ 2\ PCI\ at\ t_0\ [\%]$$

$$P_{n,t_0} = cell\ population\ with\ n\ PCI\ at\ t_0\ [\%]$$

$$m \in \mathbb{N}$$

$$n = 1 + (3 * m)$$

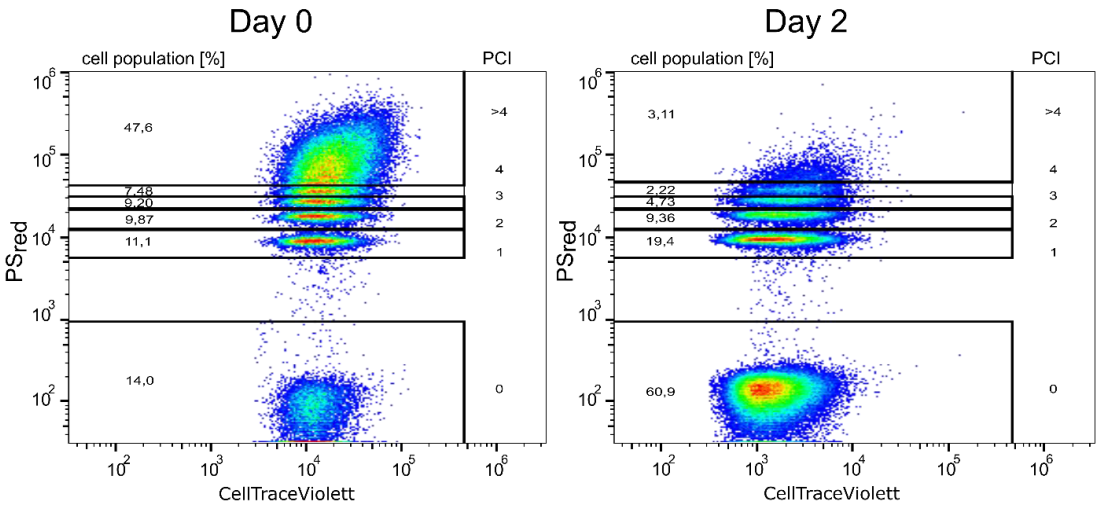

Figure S3. Gating strategy of the particle distribution during cell division measured using flow cytometry. Representative dot plot of the time-dependent distribution of the 3 µm PS_{red} (1.68 *10^6 particles per mL) in ImKC (150,000 cells seeding density) on the y-axis and the corresponding dilution of the CTV dye.

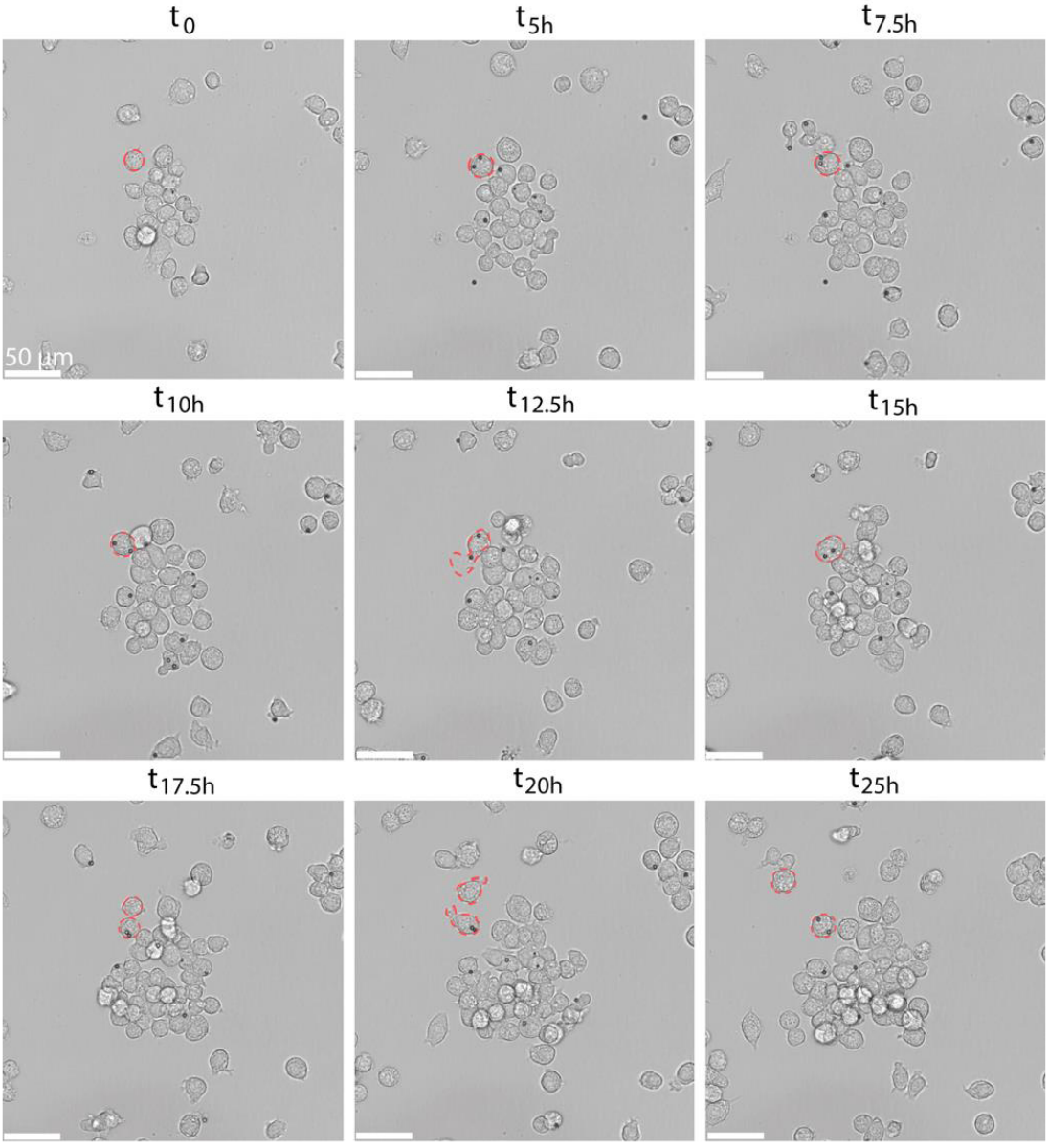

Figure S4. Sample sections from live-cell microscopy of J774A.1 incubated with 3 µm PS for 25h. Scale bar: 50 µm. The complete video is shown in Video S2.

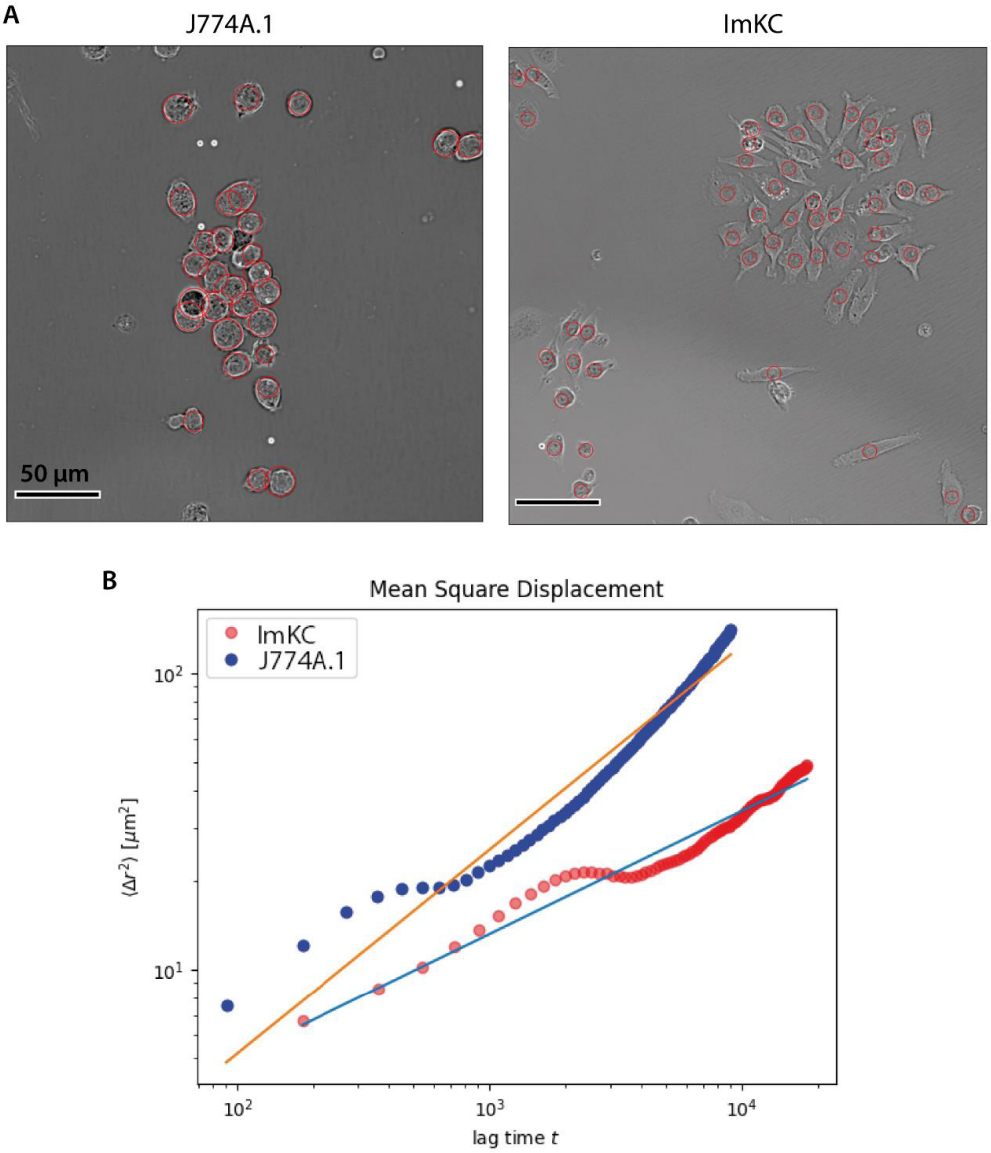

Figure S5. Cellular movement tracking after 25h incubation. A: Tracking of single cell movement for both cell lines, J774A.1 and ImKC, respectively. Circular cell detection is performed via a python script using Canny edge detection and circle Hough transform [53,54]. Performance was evaluated to work reasonably well. Detection error was improved when tracking dismisses artefacts. B: The ensemble mean square displacement (emsd) was displayed, and its fit is given as A*t^n with A: displacement, t: time, n: number of positions. For J77A.1 (blue dots), the fit is represented as an orange line with A= 0.22 and n= 0.69. For ImKC (red dots), the fit is given as a blue line with A= 0.75 and n= 0.42.

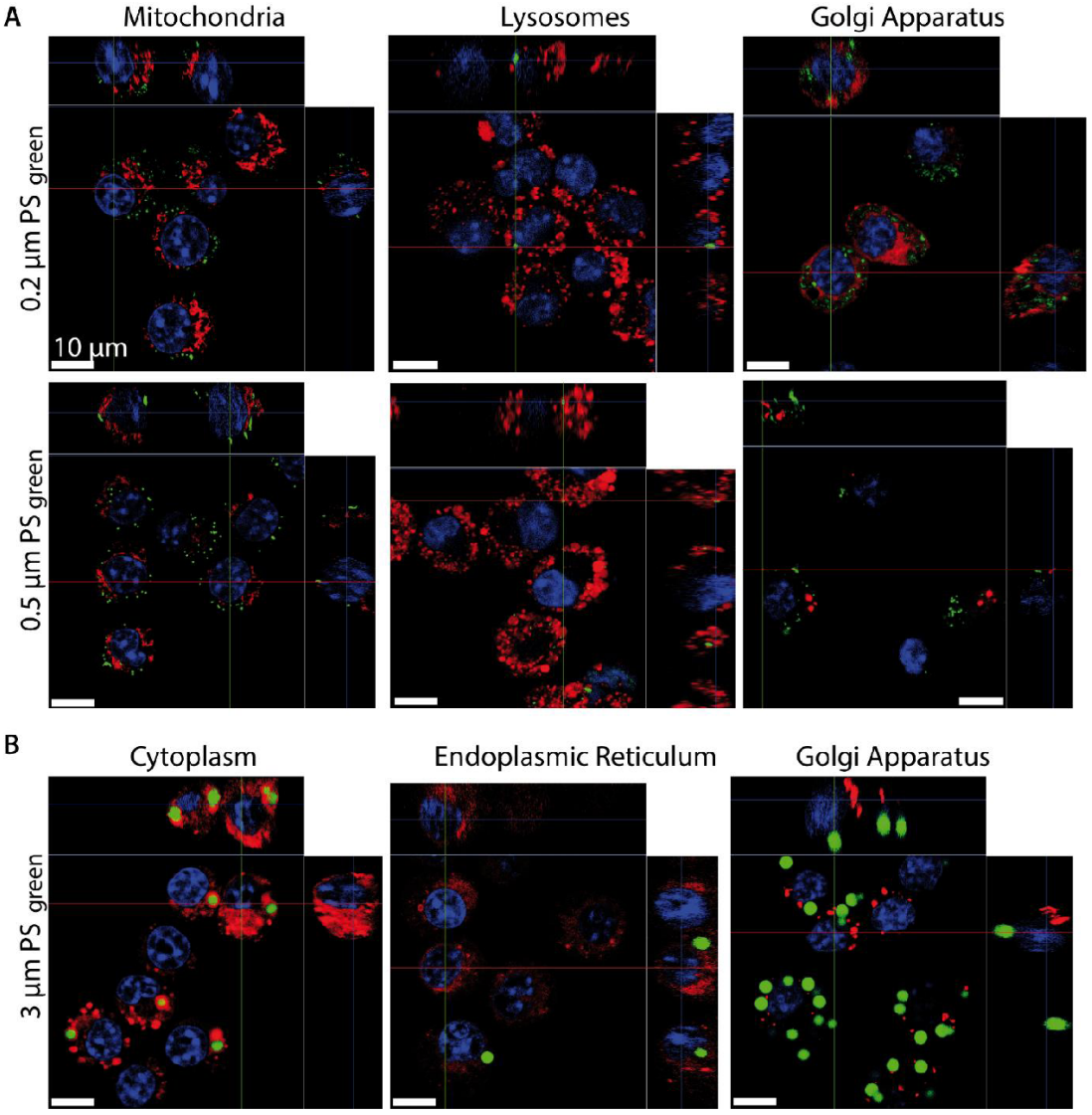

Figure S6. PS particle co-localisation with organelles as indicated in J774A.1 macrophages. The PS_{green} particles are differently sized (0.2 and 0.5 µm (A), 3 µm (B)) and the particle incubation occurred for 15 h. Images are representative examples of confocal microscopy analysis. Red: organelles, blue: nuclei (Hoechst), green: fluorescent particles. Scale bar: 10 µm.

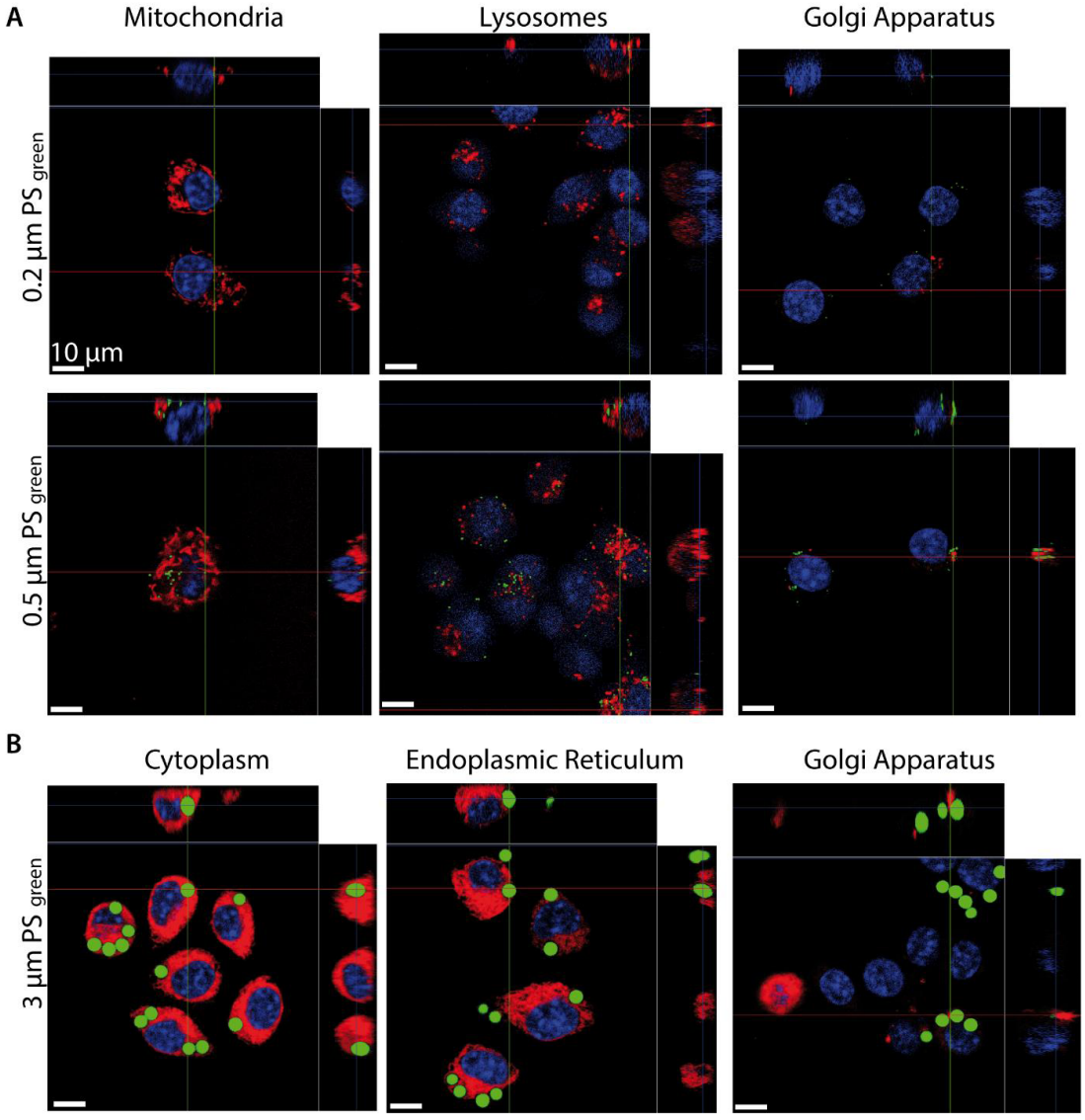

Figure S7. PS particle co-localization with organelles as indicated in ImKC macrophages. The PS_{green} particles are differently sized (0.2 and 0.5 µm (A), and 3 µm (B)) and the particle incubation occurred for 15 h. Images are representative examples of confocal microscopy analysis. Red: organelles, blue: nuclei (Hoechst), green: fluorescent particles. Scale bar: 10 µm.

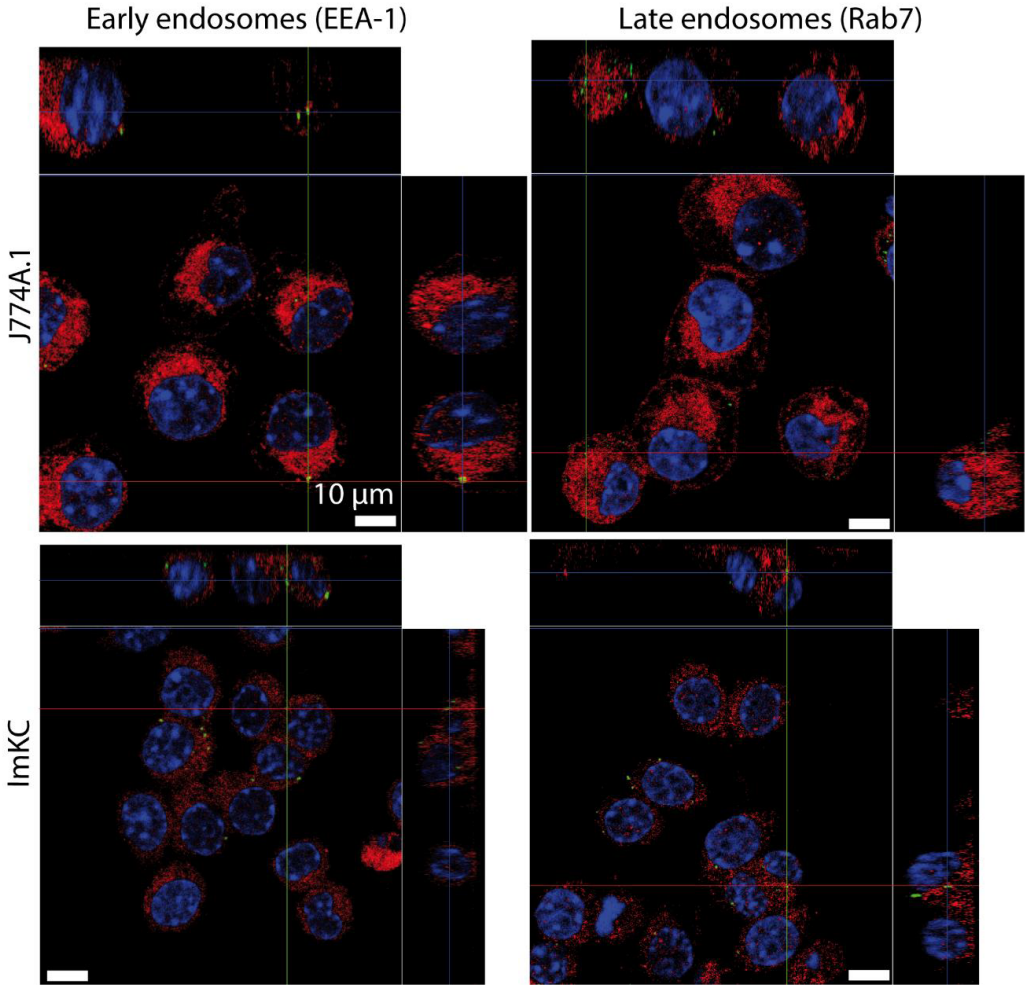

Figure S8. Endosome and 0.2 µm PS particle co-localization in J774A.1 and ImKC macrophages. The particle incubation occurred for 15 h. These images are representative examples of confocal microscopy analysis. Red: endosomes (anti-EEA1 or anti-Rab7), blue: nuclei (Hoechst), green: fluorescent particles. A yellow color indicates a co-localization of the particle with an endosome. Scale bar: 10 µm.

Danksagung

Während meiner Promotion durfte ich nicht nur mit verschiedenen Menschen zusammenarbeiten und einige Kaffeepausen genießen, sondern auch eine unvergessliche Zeit in Bayreuth verbringen. Das Abschließen einer Promotion erfordert nicht nur fachliche, sondern auch menschliche Unterstützung und an dieser Stelle möchte ich die Gelegenheit nutzen, mich bei allen Personen zu bedanken, die mich auf diesem Weg begleitet haben und eine große Hilfe waren.

Zuerst und insbesondere möchte ich mich bei meinem Doktorvater, Prof. Dr. Thomas Scheibel, bedanken. Neben der Möglichkeit am Lehrstuhl Biomaterialien mit diesem, für den Lehrstuhl ungewöhnlichen aber sehr spannenden Thema zu promovieren, konnte ich durch das entgegengebrachte Vertrauen und die Freiheiten nicht nur wissenschaftlich, sondern besonders auch persönlich Wachsen. Dabei möchte ich mich auch für die Gelegenheit des Aufenthaltes an der Queensland University of Queensland (QUT) in Brisbane bedanken, welcher mir unheimlich viel bedeutet hat.

Im Zuge dessen möchte ich mich auch bei allen KooperationspartnerInnen in den Arbeitsgruppen von Prof. Dr. Ruth Freitag (Universität Bayreuth), Dr. Thomas Fröhlich (LMU München), und Prof. Dr. Christian Laforsch (Universität Bayreuth), sowie dem gesamten SFB 1357 Mikroplastik für die stets gute Zusammenarbeit und den sehr guten Austausch bedanken. Besonderer Dank geht auch an Prof. Dr. Christopher Barner-Kowollik, Dr. Laura Delafresnaye und allen *bin chicken* an der QUT, die meine Zeit in Australien durch ihre Unterstützung in allen Bereichen unvergesslich gemacht haben.

Ein großer Dank auch an Matthias Völkl, mit dem ich nicht nur an einem sehr spannenden Thema eng zusammenarbeiten durfte, sondern auch das Glück hatte, einen kommunikativen Kooperationspartner an meiner Seite zu haben. Tiefsten Dank möchte ich an Dr. Valérie Jérôme aussprechen, die mich während meiner Promotion wissenschaftlich sehr stark unterstützte, Manuskripte Korrektur las und uns immer wieder Mut zugesprochen und angespornt hat.

Für die Hilfe im Kampf mit und gegen kaputte Laborgeräte, nicht-wachsenden Zellen oder Bestellungen möchte ich unseren TA's Alexandra Pellert, Andreas Schmidt, Claudia Stemmann, Nicole Pittel und Johannes Diehl danken. Auch vielen Dank an die Sekretärinnen, Andrea Bodner und Sabrina Schwägerl, für das Lösen kleiner und großer Probleme. Allen ehemaligen und aktuellen *Fibers* möchte ich ebenfalls für das stets angenehme Arbeitsklima,

interdisziplinäre Diskussionen, immer ein offenes Ohr und neue Blickwinkel bedanken. Vielen Dank auch an meine Studentinnen, Elisabeth Ranze und Julia Bechthold, für ihre motivierte Bearbeitung der Aufgaben.

Besonderer Dank geht an Stephen Strassburg, Shakir Bin Zainuddin, Julia Claussen und natürlich Kai Mayer, auf die ich mich immer verlassen konnte und kann, sei es eine wissenschaftliche Diskussion oder einfach ein offenes Ohr. Vielen Dank geht auch an Claudia Müller für alle zusammen gearbeiteten Wochenenden, Joggingrunden, getrockneten Tränen und Telefonate. Diese Unterstützung war eine der wichtigsten Stützen während meiner Zeit am Lehrstuhl.

Ein unendlich großer Dank von Herzen gilt meiner Familie und meinen Freunden. Durch Anne Raasch und Eva Kluge habe ich das Vertrauen für ein Studium, sowie eine anschließende Promotion gefasst. Wir können Stolz auf alles sein, was wir geschafft haben. Für die riesige Unterstützung in allen Lebenslagen durch meine Eltern Katrin und Steffen, sowie meinen Schwestern Luise, Theres und Saskia, kann ich mich nicht genug bedanken. Ihr Glaube an mich hat mir immer Motivation und Kraft gegeben. Der größte Dank geht an meinen Ehemann, besten Freund und größte Stütze, Richard. Durch seine tägliche Unterstützung voller Verständnis und Liebe kann ich mir keinen besseren Begleiter für mein Leben vorstellen.

Eidesstattliche Versicherungen und Erklärungen

(§9 Satz 2 Nr. 3 PromO BayNAT)
Hiermit versichere ich eidesstattlich, dass ich die Arbeit selbstständig verfasst und keine anderen als die von mir angegebenen Quellen und Hilfsmittel benutzt habe (vgl. Art. 64 Abs. 1 Satz 6 BayHSchG).

(§9 Satz 2 Nr. 3 PromO BayNAT)
Hiermit erkläre ich, dass ich die Dissertation nicht bereits zur Erlangung eines akademischen Grades eingereicht habe und dass ich nicht bereits diese oder eine gleichartige Doktorprüfung endgültig nicht bestanden habe.

(§9 Satz 2 Nr. 4 PromO BayNAT)
Hiermit erkläre ich, dass ich Hilfe von gewerblichen Promotionsberatern bzw. -vermittlern oder ähnlichen Dienstleistern weder bisher in Anspruch genommen habe noch künftig in Anspruch nehmen werde.

(§9 Satz 2 Nr. 7 PromO BayNAT)
Hiermit erkläre ich mein Einverständnis, dass die elektronische Fassung meiner Dissertation unter Wahrung meiner Urheberrechte und des Datenschutzes einer gesonderten Überprüfung unterzogen werden kann.

(§9 Satz 2 Nr. 8 PromO BayNAT)
Hiermit erkläre ich mein Einverständnis, dass bei Verdacht wissenschaftlichen Fehlverhaltens Ermittlungen durch universitätsinterne Organe der wissenschaftlichen Selbstkontrolle stattfinden können.

Bayreuth,_____ _____

Julia Jasiński